THE UNIVERSITY OF WARWICK

Library Declaration and Deposit Agreement

1. STUDENT DETAILS

Please complete the following:

Full name: ……

University ID number: ……

2. THESIS DEPOSIT

2.1 I understand that under my registration at the University, I am required to deposit my thesis with the University in BOTH hard copy and in digital format. The digital version should normally be saved as a single pdf file.

2.2 The hard copy will be housed in the University Library. The digital version will be deposited in the University's Institutional Repository (WRAP). Unless otherwise indicated (see 2.3 below) this will be made openly accessible on the Internet and will be supplied to the British Library to be made available online via its Electronic Theses Online Service (EThOS) service.
[At present, theses submitted for a Master's degree by Research (MA, MSc, LLM, MS or MMedSci) are not being deposited in WRAP and not being made available via EthOS. This may change in future.]

2.3 In exceptional circumstances, the Chair of the Board of Graduate Studies may grant permission for an embargo to be placed on public access to the hard copy thesis for a limited period. It is also possible to apply separately for an embargo on the digital version. (Further information is available in the *Guide to Examinations for Higher Degrees by Research*.)

2.4 *If you are depositing a thesis for a Master's degree by Research, please complete section (a) below. For all other research degrees, please complete both sections (a) and (b) below:*

(a) Hard Copy

I hereby deposit a hard copy of my thesis in the University Library to be made publicly available to readers (please delete as appropriate) EITHER immediately OR after an embargo period of ……..... months/years as agreed by the Chair of the Board of Graduate Studies.

I agree that my thesis may be photocopied. YES / NO (*Please delete as appropriate*)

(b) Digital Copy

I hereby deposit a digital copy of my thesis to be held in WRAP and made available via EThOS.

Please choose one of the following options:

EITHER My thesis can be made publicly available online. YES / NO (*Please delete as appropriate*)

OR My thesis can be made publicly available only after…..[date] (Please give date)
YES / NO (*Please delete as appropriate*)

OR My full thesis cannot be made publicly available online but I am submitting a separately identified additional, abridged version that can be made available online.
YES / NO (*Please delete as appropriate*)

OR My thesis cannot be made publicly available online. YES / NO (*Please delete as appropriate*)

3. GRANTING OF NON-EXCLUSIVE RIGHTS

Whether I deposit my Work personally or through an assistant or other agent, I agree to the following:

Rights granted to the University of Warwick and the British Library and the user of the thesis through this agreement are non-exclusive. I retain all rights in the thesis in its present version or future versions. I agree that the institutional repository administrators and the British Library or their agents may, without changing content, digitise and migrate the thesis to any medium or format for the purpose of future preservation and accessibility.

4. DECLARATIONS

(a) I DECLARE THAT:

- I am the author and owner of the copyright in the thesis and/or I have the authority of the authors and owners of the copyright in the thesis to make this agreement. Reproduction of any part of this thesis for teaching or in academic or other forms of publication is subject to the normal limitations on the use of copyrighted materials and to the proper and full acknowledgement of its source.
- The digital version of the thesis I am supplying is the same version as the final, hard-bound copy submitted in completion of my degree, once any minor corrections have been completed.
- I have exercised reasonable care to ensure that the thesis is original, and does not to the best of my knowledge break any UK law or other Intellectual Property Right, or contain any confidential material.
- I understand that, through the medium of the Internet, files will be available to automated agents, and may be searched and copied by, for example, text mining and plagiarism detection software.

(b) IF I HAVE AGREED (in Section 2 above) TO MAKE MY THESIS PUBLICLY AVAILABLE DIGITALLY, I ALSO DECLARE THAT:

- I grant the University of Warwick and the British Library a licence to make available on the Internet the thesis in digitised format through the Institutional Repository and through the British Library via the EThOS service.
- If my thesis does include any substantial subsidiary material owned by third-party copyright holders, I have sought and obtained permission to include it in any version of my thesis available in digital format and that this permission encompasses the rights that I have granted to the University of Warwick and to the British Library.

5. LEGAL INFRINGEMENTS

I understand that neither the University of Warwick nor the British Library have any obligation to take legal action on behalf of myself, or other rights holders, in the event of infringement of intellectual property rights, breach of contract or of any other right, in the thesis.

Please sign this agreement and return it to the Graduate School Office when you submit your thesis.

Student's signature: ..... Date: .....

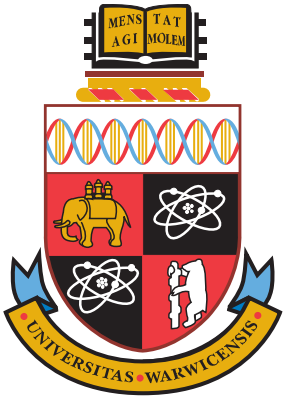

Mechanisms of GPCR signal regulation in fission yeast

by

Kathryn Jane Richardson

A thesis submitted to the University of Warwick
for the degree of
Doctor of Philosophy in Systems Biology

Systems Biology Doctoral Training Centre

July 2014

Supervisors: Dr Graham Ladds and Professor David Rand

Contents

List of Figures

List of Tables

List of videos

Video 6.1 - related to Figure 5.15 and Appendix F. Time-lapse images of *Δmam2 S. pombe* strains expressing Mam2^{4K}mCh. Images were obtained every 15 minutes following four hours of treatment with 10 µM P-factor using a DeltaVision wide-field confocal microscope. The time-lapse video was loaded into ImageJ, maximal projections were taken and the video was set to gray scale. The images were exported as a video with a frame rate of two frames per second. This video was also used to determining the percentage of lysed cells in each frame following treatment with P-factor.

Video 6.2 - related to Figure 5.15. Time-lapse images of *Δmam2 S. pombe* strains expressing Mam2^{4K}mCh. Images were obtained every 15 minutes following 30 minutes of treatment with 10 µM P-factor using a DeltaVision wide-field confocal microscope. The time-lapse video was loaded into ImageJ, maximal projections were taken and the video was set to gray scale. The images were exported as a video with a frame rate of two frames per second.

Video 6.3 - related to Figure 5.19. Time-lapse images of *Δmam2 S. pombe* strains expressing Mam2mCh. Images were obtained every 15 minutes following 30 minutes of treatment with 10 µM P-factor using an SP5 confocal microscope in the bright field channel. The time-lapse video was loaded into ImageJ and maximal projections were taken over the 2 middle slices of the Z-stack. The images were exported as a video with a frame rate of 3 frames per second. The video illustrates that cells expressing Mam2mCh form conjugation tubes from a single tip.

Video 6.4 - related to Figure 5.19 Time-lapse images of *Δmam2 S. pombe* strains expressing Mam2^{4K}mCh. Images were obtained every 15 minutes following 30 minutes of treatment with 10 µM P-factor using a DeltaVision wide-field confocal microscope in the DIC channel. The time-lapse video was loaded into ImageJ and maximal projections were taken over the middle two slices of the Z-stack. The images were changed to gray scale and exported as a video with a frame rate of two frames per second. The video illustrates that some cells expressing Mam2^{4K}mCh form conjugation tubes for both tips.

Video 6.5 - related to Figure 5.20. Time-lapse images of *mam2*$^{+}$ strains containing CRIB-GFP marker for Cdc42-GTP and expressing Mam2^{4K}mCh. Images were obtained every 15 minutes following six hours of treatment with 10 µM P-factor using a DeltaVision wide-field confocal microscope in the GFP channel. The time-lapse video was loaded into ImageJ and maximal projections were taken over the Z-stack. The images were changed to gray scale and exported as a video with a frame rate of two frames per second. The video illustrates that in some cells that elongate to form conjugation tubes from both tips, CRIB-GFP is observed at both tips.

Abbreviations and acronyms

1C	One complement of DNA content (G_1 phase)
2C	Two complements of DNA content (G_2 phase)
ABC	**A**TP-**B**inding **C**assette
AD	**A**ctivating **D**omain
AP	**A**daptor **P**rotein
ARF	**A**DP-**R**ibosylation **F**actor
AT_1	**A**ngio**T**ensin II type **1**
ATP	**A**denosine **T**ri**P**hosphate
BD	**B**inding **D**omain
bp	**b**ase **p**air
cAMP	**c**yclic **A**denosine **M**ono**P**hosphate
CCPs	**C**lathrin-**C**oated **P**it**s**
CCVs	**C**lathrin-**C**oated **V**esicle**s**
CFP	**C**yan **F**luorescent **P**rotein
CFU	**C**olony **F**orming **U**nit
CK1	**C**asein **K**inase 1
CK2	**C**asein **K**inase 2
CNS	**C**entral **N**ervous **S**ystem
COOH	**C**-terminus
CRIB	**C**dc42/**R**ac **I**nteractive-**B**inding
D_1	**D**opamine 1
DAG	**D**i**A**cyl**G**lycerol
DAPI	4',6-Diamidino-2-Phenylindole, Dihydrochloride
DMM	**D**efined **M**inimal **M**edium
DNA	**D**eoxy**Ribose** **N**ucleic **A**cid

DPP-4	**D**i**P**eptidyl **P**eptidase-**4**
Dsh	**Dish**evelled
DT	**D**oubling **T**ime
DYRK	**D**ual-specificity **Y**ak-**R**elated **K**inase
EC	**E**xtra**C**ellular
E. coli	***E**scherichia **coli***
$\mathbf{EC_{50}}$	p**E**ffective **C**oncentration$_{50}$
ESCRT	**E**ndosomal **S**orting **C**omplex **R**equired for **T**ransport
$\mathbf{EDT_2}$	**E**thane**D**i**T**hiol$_2$
EDTA	**E**thylene**D**iamine**T**etraacetic **A**cid
ER	**E**ndoplasmic **R**eticulum
ERK	**E**xtracellular signal-**R**egulated **K**inase
fbp1	**f**ructose-1,6-**bis**p**h**osphatase
FOA	5-**F**luoro-**O**rotic **A**cid
FRET	**F**luorescent **R**esonance **E**nergy **T**ransfer
FSC	**F**orward **SC**atter
FSH	**F**ollicle-**S**timulating **H**ormone
GAP	**G**TPase **A**ccelerating **P**rotein
GABA	**G**amma-**A**mino**B**utyric **A**cid
GDI	**G** Protein **D**issociation **I**nhibitor
GDP	**G**uanosine **D**i**P**hosphate
GEF	**G**uanosine Nucleotide **E**xchange **F**actor
GFP	**G**reen **F**luorescent **P**rotein
GIP	**G**lucose-dependent **I**nsulin-releasing **P**olypeptide
GIRK	**G** protein-gated **I**nwardly **R**ectifying potassium ($\mathbf{K^+}$)
GLP-1	**G**lucagon-**L**ike **P**eptide-**1**
GnRH	**G**onadotropi**n**-**R**eleasing **H**ormone
GPCR	**G** **P**rotein-**C**oupled **R**eceptor
GRK	**G** protein **R**eceptor **K**inase
GSK-3β	**G**lycogen **S**ynthase **K**inase-**3β**
GTP	**G**uanosine **T**ri**P**hosphate
HPLC	**H**igh-**P**erformance **L**iquid **C**hromatography
IC	**I**ntra**C**ellular

IGF-I	**I**nsulin-like **G**rowth **F**actor-I
Incretin	**In**testine se**cret**ion **in**sulin
IP_3	**I**nositol tri**p**hosphate
JNK	c-**J**un **N**-terminal **K**inase
kDa	**k**ilo **Da**lton
LH	**L**uteinizing **H**ormone
LRP5/6	**L**ipoprotein receptor-**R**elated **P**rotein
M_1	**M**uscarinic **1**
M_3	**M**uscarinic **3**
MAPK	**M**itogen **A**ctivated **P**rotein **K**inase
MAP2K	**M**itogen **A**ctivated **P**rotein **K**inase **K**inase
MAP3K	**M**itogen **A**ctivated **P**rotein **K**inase **K**inase **K**inase
mCherry	**m**onomeric **Cherry**
MVBs	**M**ulti**V**esicular **B**ody
NH_2	**N**-terminus
nmt1	**N**o **M**essage in **T**hiamine
OD	**O**ptical **D**ensity
ODE	**O**rdinary **D**ifferential **E**quation
ONPG	**O**-**N**itro**P**henyl-D-**G**alactoside
ORF	**O**pen **R**eading **F**rame
P-factor	**P**heromone
P-loop	**P**hosphate binding loop
pEC_{50}	Negative Natural Logarithm of Median **E**ffective **C**oncentration
RACK1	**R**eceptor for **A**ctivated **C** **K**inase **1**
PAR_1	**P**rotease-**A**ctivated **R**eceptor **1**
PAR_2	**P**rotease-**A**ctivated **R**eceptor **2**
PBS	**P**hosphate **B**uffered **S**aline
PCR	**P**olymerase **C**hain **R**eaction
PDE	**P**artial **D**ifferential **E**quation
PDGF	**P**latelet **D**erived **G**rowth **F**actor
PI_3K	**P**hospho**I**nositide **3**-**K**inase
PIP_2	**P**hosphatidyl**I**nositol 4,5-bis**p**hosphate
PIP_5K	**P**hosphatidyl**I**nositol 4-**P**hosphate 5-**K**inase

PKA	**P**rotein **K**inase **A**
PKB	**P**rotein **K**inase **B**
PKC	**P**rotein **K**inase **C**
pKS	**p**Bluscript**KS**
PLC	**P**hospho**L**ipase **C**
RBD	R**R**as **B**inding **D**omain
RO	**R**everse **O**smotically
RGS	**R**egulator of **G** Protein **S**ignalling
RTK	**R**eceptor **T**yrosine **K**inase
S. cerevisiae	***S****accharomyces* ***cerevisiae***
S.E.M	**S**tandard **E**rror of the **M**ean
SD	**S**ingle **D**rop-out minimal medium
SDS	**S**odium **D**odecyle **S**ulphate
S. pombe	***S****chizosaccharomyces* ***pombe***
SSC	**S**ide **SC**atter
TE	**T**ris-HCl-**E**DTA
Tiam$_1$	T-cell lymphoma invasion and metastasis-inducing protein 1
TM	**T**rans-**M**embrane
TRH	**T**hyrotropin-**R**eleasing **H**ormone
WT	**W**ild **T**ype
Ub	**Ub**iquitin
UBDs	Ubiquitin-binding domains
UTR	**U**n**T**ranslated **R**egion
V$_2$R	**V**asopressin type-**2** **R**eceptor
VALAP	**VA**seline, **LA**nolin and **P**araffin
YE	**Y**east **E**xtract
YFP	**Y**ellow **F**luorescent **P**rotein

Acknowledgements

I would like to express my gratitude to Graham Ladds and David Rand for supporting me during my studies, especially Graham for his unfaltering guidance. Next, I would like to thank all of the Ladds lab without whom the PhD would not have been as memorable and enjoyable. In particular, Cathryn Weston, Michael Bond, Wayne Croft, Ingrid Tigges, Anthony Knight, Robert Lockely and Manuel Alejandro Esparza-Franco and special thanks to Jeanette Bennett and Magdalena Mos who were not only great friends and counsellors throughout but made me smile constantly. Special thanks to the Systems Biology DTC members for all of their great help and support, particularly Vicky Buchanan-Wollaston, Sarah Shute and Anne Maynard.

A very special thanks to Jason Piper, that light in my life without whom the first two pages of each chapter would not have been so well proofread. Next, I wish to thank my beautiful friends Karis, Steph, Lucy, Ryan, Emma and Elliot who have kept me sane throughout the process.

Finally, and most importantly I would like to thank my amazing family without them I would not have progressed to this point. My parents Anthony and Evelyn, my sister and best friend Anna, my brother Mark, my grandmother Grace and brother-in-law Nathan. You have all encouraged and guided me through the last 25 years. I love you all.

Declaration of authorship

I, Kathryn Jane Richardson, declare that this thesis titled, 'Mechanisms of GPCR signal regulation in fission yeast' and the work presented in it are my own. I confirm that:

- This work was done wholly or mainly while in candidature for a research degree at this University.
- Where any part of this thesis has previously been submitted for a degree or any other qualification at this University or any other institution, this has been clearly stated.
- Where I have consulted the published work of others, this is always clearly attributed.
- Where I have quoted from the work of others, the source is always given. With the exception of such quotations, this thesis is entirely my own work.
- I have acknowledged all main sources of help.
- Where the thesis is based on work done by myself jointly with others, I have made clear exactly what was done by others and what I have contributed myself.

Signed:

Date:

UNIVERSITY OF WARWICK

Abstract

Systems Biology Doctoral Training Centre

Doctor of Philosophy

by

Kathryn Jane Richardson

Cells communicate with each other and respond to environmental cues by sending and receiving signals. Many external signals (ligands) are detected through G protein-coupled receptors (GPCRs), a major class of transmembrane proteins. GPCRs transduce these external signals into appropriate intracellular responses, enabling the cell to adapt to its environment. Malfunctions in these signalling pathways can lead to a range of human diseases and hence GPCRs have become attractive candidates for pharmacological design.

The activation of a single receptor has the ability to induce numerous intracellular responses. Coupling this with the great number of different GPCR-types expressed in human cells means that understanding the basic principles of signal transduction and termination in humans is complicated. This study utilises the more simplistic eukaryotic yeast *Schizosaccharomyces pombe* (*S. pombe*) to overcome this complexity, as it contains only two GPCR types and hence the cross-talk between pathways is greatly reduced, whilst the structure and signalling functions of GPCRs are often evolutionarily conserved between yeast and humans.

Mathematical modelling was used to aid the understanding of GPCR signalling in *S. pombe* and to inform experimental design. Specifically, an ordinary differential equation model first developed by Croft et al. (2013) was extended to include all known downstream signal transduction, regulation and termination events. This model is the first of its kind to describe a whole GPCR signalling pathway within *S. pombe*. Although it accurately predicts the cellular response to GPCR signalling it could only reproduce the biological plateau in temporal response with the addition of a 'yet unknown mechanism' GPCR degradation term. This motivated the investigation of how GPCRs in *S. pombe* are internalised from the plasma membrane in response to ligand stimulation.

The primary mechanism for signal termination is via internalisation of the GPCR. This study identified three potential casein kinases (Cki1, Cki2 and Cki3) that promote internalisation of the *S. pombe* GPCR Mam2. Microscopy analyses in combination with quantitative transcriptional, cell growth and cell cycle position assays uncovered a novel role for these kinases: that Cki2 regulates cell size during vegetative growth, Cki1 and Cki3 regulate the GPCR-response pathway and that Cki3 is essential for completing cytokinesis in *S. pombe* that have already undergone formation of a conjugation tube in response to ligand. Confocal microscopy of fluorescent labelled Mam2 indicated a role for Cki2 in the internalisation and hence termination of the GPCR-response pathway. These findings add to the growing body of evidence that casein kinases are implicated in GPCR desensitisation.

Chapter 1

Introduction

1.1 Cellular signalling

Cells communicate with each other and respond to environmental cues by sending and receiving signals. These signals are translated into appropriate intracellular responses to enable the cells to adapt to their environment. Lipophilic signalling molecules such as testosterone, progesterone and derivatives of vitamins A and D are able to cross the cell membrane and activate cytosolic or nuclear receptors. However, the majority of signalling molecules are lipophobic, and often require a mechanism of signal transduction to transfer the message across the cell membrane. Transmembrane (TM) receptors transduce external signals into complex but co-ordinated intracellular pathways, leading to changes in gene expression, ion balance and enzyme activity.

The largest family of TM receptors are the G protein-coupled receptors (GPCRs). In 2001, the completion of the human genome project identified approximately 23,000 genes [1], and subsequent analysis uncovered over 800 potential GPCR coding regions [2]. These receptors are activated by a myriad of ligands, which include ions, proteins, lipids, sugars, nucleotides and photons (reviewed in [3]). Receptors can couple to an equally wide array of intracellular signalling molecules to induce a diverse range of signalling outcomes.

The sheer volume of signalling responses that are governed by GPCRs means that malfunctions in the receptors or their associated signalling pathways are responsible for a wide array of human disorders, including allergic rhinitis, pain, hypertension, addiction, schizophrenia and cancer to name a few [4]. Unsurprisingly, GPCRs are estimated to constitute $\sim$35% of pharmaceutical drug targets world wide (reviewed in [5]). Central to the detection and treatment of such GPCR-related disorders is an understanding of the core principles and underlying mechanisms of GPCR signal transduction and termination.

1.1.1 Yeast as a model organism for understanding cell signalling

In higher eukaryotes such as humans, the diverse range of GPCRs that are expressed on the cell-surface at any one time and their ability to couple to and activate a number of different pathways in response to ligand-binding can result in multiple cellular responses. This makes it difficult to fully dissect the role of individual components and processes of GPCR signal transduction and termination. For this reason, lower eukaryotes such as yeast are an attractive system for studying signalling responses in isolation, mainly due to the reduced number of signalling components present in each cell and hence, the integration of responses to different stimuli and cross-talk between separate pathways can be greatly reduced.

In addition to the reduction in complexity, yeast has been used as a model organism because many of the signalling components and mechanisms are conserved in higher eukaryotes [6]. For example, the observation that cell viability could be restored by expressing the oncogenic mammalian *H-ras* sequence in the budding yeast *Saccharomyces cerevisiae* (*S. cerevisiae*) strains lacking the equivalent homologs (*RAS1* and *RAS2*) illustrated that both sequence and biological function was evolutionarily conserved [7].

Another important example using the fission yeast *Schizosaccharomyces pombe* (*S. pombe*) was not only the discovery of genes that controlled cell cycle progression, but the observation that the mechanism of cell division including the concept of 'checkpoints' (which are specific points during the cell cycle at which a cell evaluates whether it should progress to the next stage) were conserved between yeast and humans [8, 9]. These studies provided an insight into the cell division process, which lead to a greater understanding of the human cell cycle and as a result, the development of treatments for diseases such as cancer [10].

Yeast are regarded as genetically tractable simple eukaryotes because it is relatively straightforward to create mutant strains, overexpress gene products in excess and generate auxotrophic and enzymatic reporter strains with which to monitor signal transduction. One such example is the *S. pombe* pheromone-responsive β-galactosidase reporter strains [11]. These strains have been modified to include the bacterial *lacZ* gene in place of the pheromone-responsive *sxa2* gene enabling quantification of pheromone-induced signalling. This study utilises the fission yeast *S. pombe* reporter strains to help understand the basic principles of GPCR signal transduction, regulation and termination.

1.2 An introduction to GPCRs

1.2.1 GPCR structure

GPCRs have been identified in every eukaryotic organism [12] and share a common structure comprising seven TM α-helical regions connected by alternating intracellular and extracellular loops (IC/EC). These structures are combined with an extracellular N-terminal and intracellular C-terminal domain, which differ in length and function (Figure 1.1). The EC loops and N-terminus have functional roles in ligand recognition, whilst the intracellular regions are implicated in signalling and scaffolding roles by interacting with downstream signalling machinery.

The intracellular C-terminal domains of GPCRs are thought to form an eighth helical coiled-coil region oriented in parallel to the cell membrane [13, 14], which can undergo palmitoylation (the covalent attachment of a 16-carbon fatty acid group) and consequently associate with the plasma membrane forming an 'IC_4' region [15] (Figure 1.1). In response to ligand-binding, the receptor can activate heterotrimeric guanine-nucleotide-binding proteins (G proteins) (reviewed in [3]).

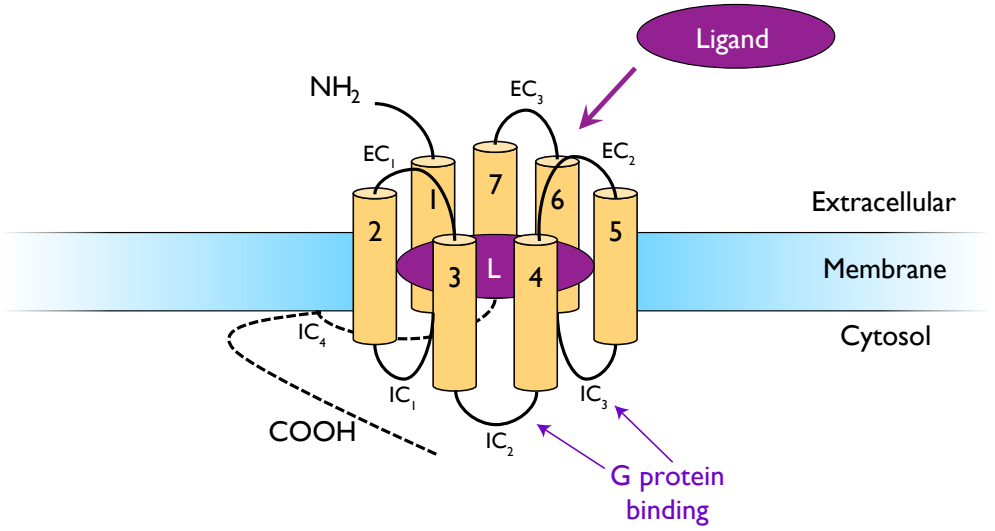

FIGURE 1.1: **GPCR structure.** GPCRs are composed of seven transmembrane-spanning α-helical domains (labelled 1-7). Each TM is connected by alternating intracellular and extracellular loop regions (denoted IC_1-IC_3 and EC_1-EC_3). GPCRs contain an extracellular N-terminus (NH_2) and an intracellular C-terminal tail (COOH), which is thought to form an eighth helical region oriented along the plasma membrane, creating a potential intracellular loop region (IC_4). The receptor is coupled to a G protein via the IC_2 and IC_3 loops. Activation occurs when an appropriate ligand binds the receptor.

1.2.2 GPCR families

Although all GPCRs share a common structure they can be can be grouped into six families (A-F or I-VI) based upon structural similarities, function and ligand-binding [12] (Table 1.1). Class D, the fungal mating-pheromone receptors will be the focus of this study.

Family	Name
A	Rhodopsin-like receptors
B	Secretin-like receptors
C	Metabotrophic glutamate receptors
D	Fungal mating-pheromone receptors
E	cAMP receptors
F	Frizzled/smoothened receptors

Table 1.1: **Types of GPCR families.** The classification of six GPCR families.

1.3 Signal transduction via GPCRs

Despite the large range of ligands that bind to activate GPCRs, most receptors share a common signalling mechanism of coupling to heterotrimeric G proteins (reviewed in [3]). G proteins belong to a highly conserved superfamily that are structurally identified by the presence of a phosphate-binding loop (P-loop) [16].

1.3.1 Signalling via G proteins

G proteins are binary switches that are 'off' when bound to guanosine diphosphate (GDP) and 'on' when bound to guanosine triphosphate (GTP). The P-loop is responsible for the correct positioning of the triphosphate moiety of the bound nucleotide [16]. Activation of the G protein stabilises the effector binding site via an interaction with a conserved threonine residue in switch I and a glycine residue in the switch II region, which form hydrogen bonds with the γ-phosphate of GTP in combination with a Mg^{2+} cofactor (reviewed in [17]) (Figure 1.2a). This functionality is conferred by an ∼20 kDa G domain that is conserved across all G proteins [18].

G protein activation occurs spontaneously, but can be accelerated by interactions with guanine nucleotide-exchange factors (GEFs). GEFs function to reduce the affinity of the G protein for guanine nucleotides by altering the phosphate binding site, favouring the release of GDP for the more cellularly abundant GTP molecule [19]. Similarly, all G proteins contain a weak intrinsic GTP-hydrolysis activity, which can be accelerated by GTPase accelerating proteins (GAPs), switching the G protein from a GTP 'on' state to a GDP 'off' state (Figure 1.2b). G proteins exist in two forms, as either monomeric or

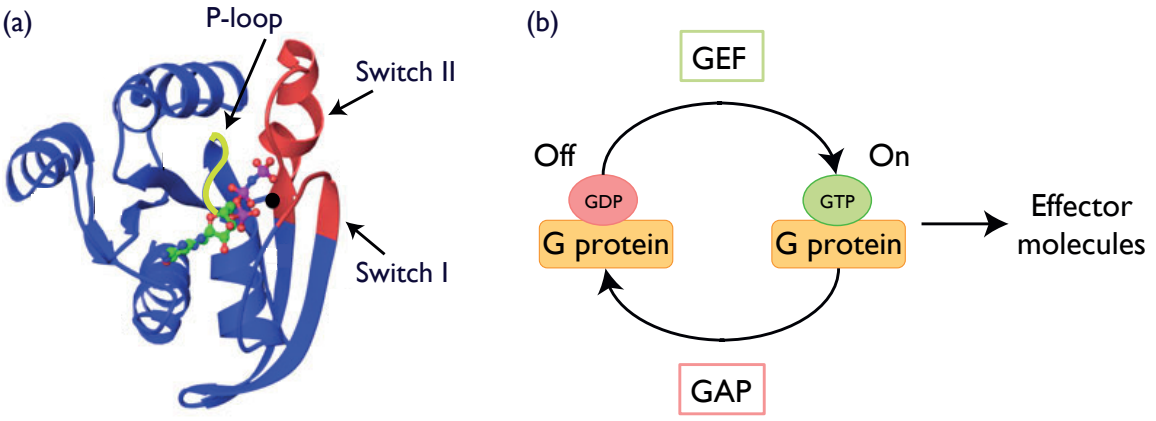

FIGURE 1.2: **Nucleotide binding and hydrolysis on G proteins.** (a) Ribbon diagram of RAS, the archetypical GTPase, with bound GTP shown in a ball-and-stick model, the Mg^{2+} ion as a black sphere and the P-loop in yellow (constructed in Swiss-PDB viewer, PDB code 121P). The Switch I and II regions are coloured red. (b) G proteins become activated when GDP is released and a molecule of GTP binds. This process is catalysed by guanine nucleotide-exchange factors (GEFs). The cycle is reset through the intrinsic GTPase activity of the G protein, however, this can be accelerated through interaction with a GTPase-activating protein (GAP). GTP bound G proteins transduce the signalling via an interaction with an effector protein.

heterotrimeric, and control a myriad of signalling pathways such as cell growth, vesicle and protein transport and cytoskeleton assembly [20].

1.3.2 Monomeric G proteins

One of the earliest identified monomeric G proteins was the p21 Ras oncogenes: a 21 kDa family of proteins that were found to be activated in many human cancers ([21] and reviewed in [22]). A vast number of Ras-like proteins are now known and the family is often referred to as the Ras family of small G proteins [23, 24]. Within this family it is possible to recognise five subfamilies: Ras, Rho, Rab, Ran and ADP-ribosylation factor (Arf) [25]; the Ran family plays a role in nuclear transport, whereas the Arf and large Rab family of proteins function in membrane trafficking [26].

Ras and Rho families are involved in cell signalling [26]. Ras proteins are typically activated through receptor tyrosine kinases (RTKs) and have been shown to play a key role in transducing extracellular growth factor signals via mitogen activated protein kinase (MAPK) cascades to promote cell growth [27]. In addition to activation of MAPK cascades, Ras proteins can mediate signal transduction via other G proteins. In particular, members of the Rho family of GTPases, which can be subdivided into six classes, with the most well characterised being the Rho, Rac and Cdc42 groups [28]. One important discovery involving G protein activation by other G proteins, was Ras activation of Rac with the aid of the Rho GEF T-cell lymphoma invasion and metastasis-inducing protein 1 ($Tiam_1$) [29].

$Tiam_1$/Rac signalling affects cell migration, invasion and tumour metastasis and as such these proteins have been implicated in many humans cancers [30].

1.3.3 Heterotrimeric G proteins

G proteins can also exist as dissociable heterotrimeric complexes consisting of a Gα, Gβ and Gγ subunit [31], which couple to the intracellular regions of the GPCR. A ligand binding to the extracellular site of the receptor causes an ∼30% rotation in TM_6 [32], which separates it from TM_3 exposing the IC_2 and IC_3 regions of the receptor [33]. This conformational change promotes the release of GDP on the Gα subunit and subsequent binding of GTP, thereby activating the G protein. In this manner, the activated GPCR acts as a GEF for the heterotrimeric G protein by promoting the release of GDP. As a consequence of G protein activation, a hydrophobic binding pocket necessary for the association of the Gβγ dimer is lost [18] and as a result the Gα and Gβγ subunits can dissociate. Both subunits are able to interact with a range of effector molecules (reviewed in [3], described in greater detail below and summarised in Figure 1.3).

1.3.3.1 Signalling through the Gα subunit

The type of Gα subunit generally classifies the G protein heterotrimer and is more commonly the signal transducer [35]. Four G protein families exist: $G\alpha_s$, $G\alpha_i$, $G\alpha_q$ and $G\alpha_{12}$ and are classified by their target proteins ([36, 37] and reviewed in [38]).

Active receptors that couple via $G\alpha_s$ stimulate adenylyl cyclase, a membrane-bound enzyme that catalyses the conversion of adenosine triphosphate (ATP) to cyclic adenosine monophosphate (cAMP). The rise in cAMP levels activates protein kinase A (PKA) and initiates a cascade of phosphorylation reactions within the cell thereby transducing signalling [39] (Figure 1.3). Classical physiological effects of PKA activation in skeletal muscle and liver cells promotes glycolysis to produce glucose, whilst activation in kidney cells promotes exocytosis of aquaporin 2, thereby regulating water secretion in the urine.

Receptors that couple via $G\alpha_q$, once activated, stimulate the activity of the plasma membrane-bound enzyme phospholipase C (PLC) [40]. PLC cleaves the membrane lipid phosphatidylinositol 4,5-bisphosphate (PIP_2) into inositol 1,4,5-trisphosphate (IP_3) and diacylglycerol (DAG). IP_3 diffuses from the plasma membrane to the endoplasmic reticulum (ER) where it binds IP_3-gated calcium (Ca^{2+})-release channels. As a consequence, the cytosolic concentration of Ca^{2+} increases, influencing the activity of proteins, such as PKC by promoting its translocation from the cytosol to the plasma membrane [35]. PKC can then be activated by a combination of Ca^{2+}, DAG and a negatively charged membrane phospholipid phosphatidylserine [41]. Once activated, the second messenger PKC initiates

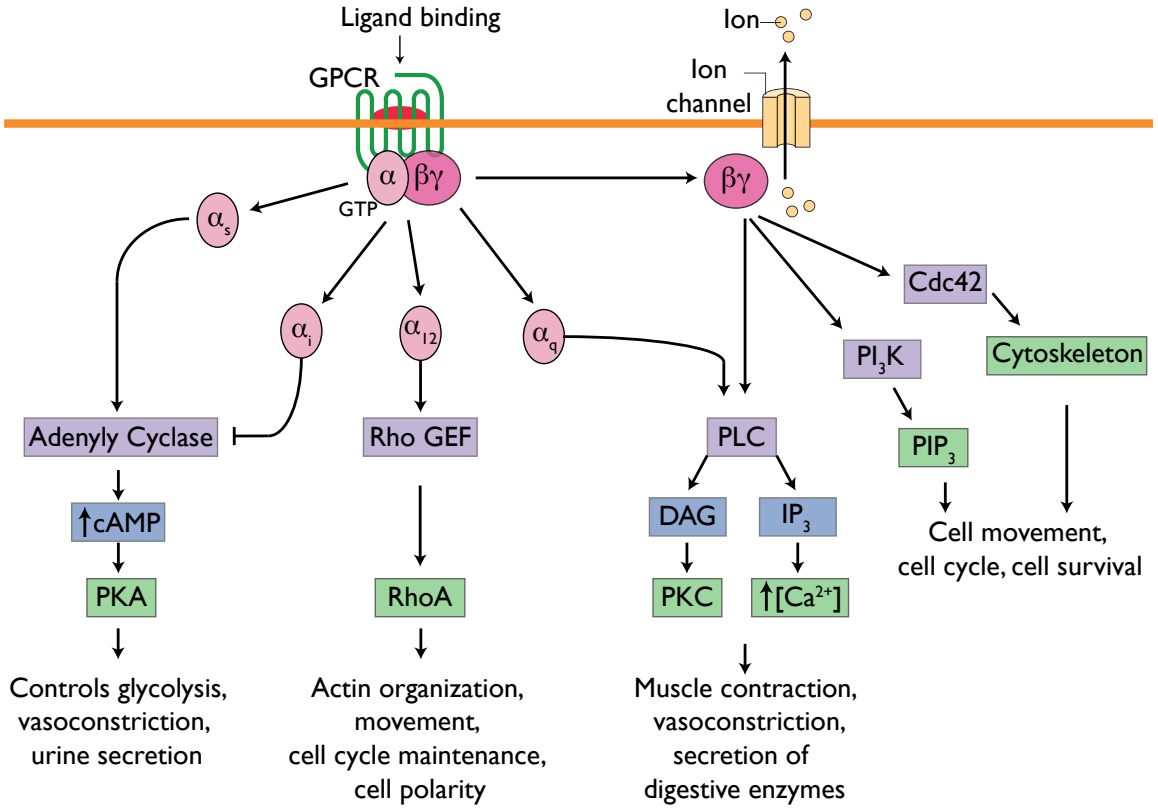

FIGURE 1.3: **Heterotrimeric G proteins activate many signalling pathways.** The binding of a ligand favours the release of GDP for GTP on the Gα subunit and as such the GPCR acts as a GEF for the G protein. Following activation, the Gα and Gβγ subunit dissociate activating many signalling responses. Subtypes of Gα such as $G\alpha_s$, $G\alpha_i$, $G\alpha_{12}$ and $G\alpha_q$, subsequently bind to and regulate the activity of effectors such as adenylyl cyclase, RhoGEF and phospholipase C (PLC). These modulate downstream effectors directly or by generating second messengers (such as cyclic AMP (cAMP), diacylglycerol (DAG) and inositol-1,4,5-trisphosphate (IP_3) that modulate further downstream effectors, such as protein kinase A (PKA) and protein kinase C (PKC). Following release the Gβγ dimer subunit can also bind to and regulate certain downstream effectors, such as ion channels, PLC, the Rho G protein Cdc42 and phosphoinositide 3-kinase (PI_3K). Figure is adapted from [34] and incorporates some resulting physiological responses following activation.

a cascade of phosphorylation reactions to transduce signalling inside the cell with one typical physiological role being contraction in smooth muscle cells (Figure 1.3).

GPCRs that couple via $G\alpha_i$ inhibit adenylyl cyclase and have additional roles in the PLC pathway. Their associated Gβγ subunits can bind and activate ion channels, for example potassium (K^+)-channels [37]. Finally, $G\alpha_{12}$ proteins activate the family of monomeric Rho GTPases (via activation of Rho GEFs) to regulate the actin cytoskeleton (reviewed in [38]) (Figure 1.3).

1.3.3.2 The Gβγ subunit as the signal transducer

The Gβγ dimer can also activate a host of downstream effectors including Ca^{2+}-channels, MAPKs, phospholipases, phosphoinositide 3-kinase (PI_3K), G protein-coupled receptor kinases (GRKs) and the essential Rho G protein Cdc42 (reviewed by [42]). Gβγ dimers also have important roles in mediating the opening of inwardly rectifying K^+-channels, primarily in neurons of the central nervous system (CNS) [43, 44] (Figure 1.3).

1.3.4 Signal transduction via MAPKs

As stated earlier, mitogenic cascades transduce signalling inside the cell. The signal is transferred via sequential phosphorylation, typically beginning with activation of a MAP kinase kinase kinase (MAP3K), which activates a MAP kinase kinase (MAP2K) and finally, a MAP kinase (MAPK) (Figure 1.4). Phosphorylation occurs within the activation loop on serine, threonine and on occasions tyrosine residues. Mitogenic pathways are often used for transmitting cytoplasmic signalling to the nucleus to activate transcription factors altering gene expression. In mammalian cells there are three canonical MAPK signalling cascades: the extracellular signal-regulated kinases (ERK), c-Jun N-terminal kinase/stress-activated protein kinases (JNK/SAPK) and p38 kinases, the activation of these results in a variety of cellular responses including: proliferation, apoptosis, cell cycle arrest, cytokine release and embryonic development [45, 46] (Figure 1.4).

GPCRs can activate MAPKs via several distinct mechanisms: via their Gβγ subunits, β-arrestin/endocytotic pathways (discussed later), transactivating RTKs [47], which classically signal via Ras to activate the ERK pathway, or via second messengers following activation of there associated Gα subunits. Some receptors, such as the gonadotropin-releasing hormone (GnRH) receptor can activate the three canonical MAPK cascades, depending on which Gα subunit it is associated with. Specifically, activation of GnRH receptor (by GnRH) when coupled to $G\alpha_q$ (depending on the cell type) can activate the ERK, JNK and p38 MAPK pathways to regulate biosynthesis and secretion of gonadotropins such as follicle-stimulating hormone (FSH) and luteinizing hormone (LH) [48, 49].

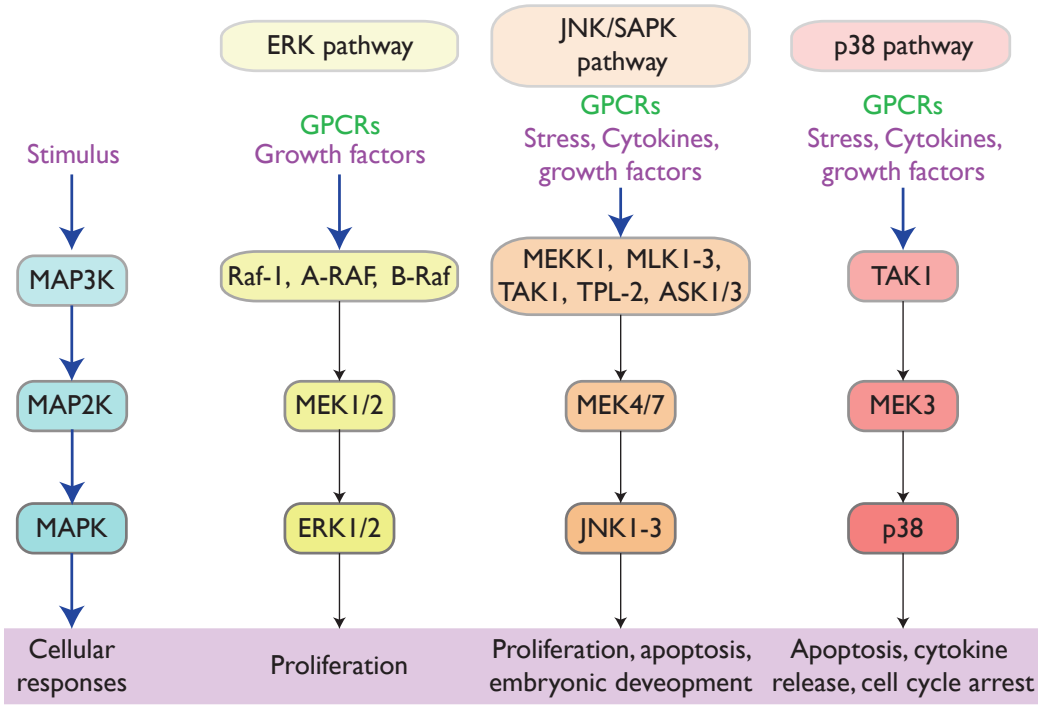

Figure 1.4: **Three canonical mammalian MAPK cascades.** Extracellular stimuli such as growth factors and environmental stress can induce the activation of MAPK cascades. There are three canonical members of the MAPK family: extracellular signal-regulated kinase 1/2 (ERK1/2), c-Jun N-terminal kinase 1-3 (JNK 1-3) and p38, which regulate a host of cellular processes. In addition, GPCRs can also activate these MAPK cascades via activation of the heterotrimeric G protein subunits.

1.3.5 GPCR signalling in *S. pombe*

Contrary to humans where over 800 GPCRs have been identified [1], the *S. cerevisiae* and *S. pombe* yeasts both contain only two GPCR-mediated signal transduction pathways: one to sense the availability of nutrients and the second to detect and respond to the presence of mating-pheromones [50]. *S. cerevisiae* propagates pheromone signalling via the Gβγ subunit, whereas in *S. pombe* signalling is transduced via the Gα subunit. As the Gα subunit is more commonly the signal transducer in mammalian systems, this study investigates GPCR signalling in *S. pombe* as this is more relevant to higher eukaryotes.

Haploid *S. pombe* cells proliferate via mitosis when carbon and nitrogen sources are plentiful. The detection of extracellular glucose via the GPCR Git3 results in the activation of Gpa2 (a Gα-subunit) [51]. GTP-bound Gpa2 activates Cyr1, an adenylyl cyclase, which increases the cellular concentration of cAMP [52], resulting in activation of PKA. There are at least two pathways downstream of PKA, one leading to sexual development and the other to gluconeogenesis (reviewed in [50]). Both pathways are regulated by PKA but can be activated to different extents: for example, nitrogen depletion enhances transcription

of *ste11*, a gene that encodes a transcription factor (TF) required for mating and meiosis [53, 54] whereas, glucose depletion promotes gluconeogenesis through induction of *fbp1* (fructose-1,6-bisphosphatase) [55] (Figure 1.5).

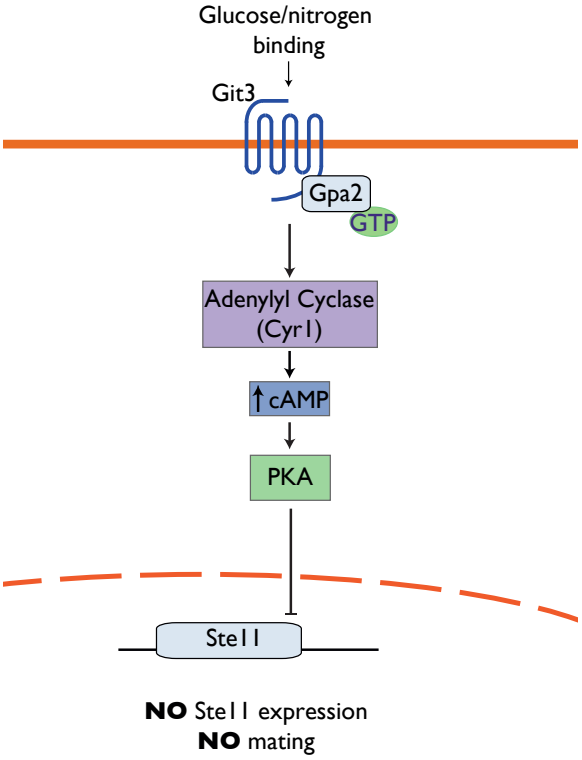

FIGURE 1.5: **When nutrients are plentiful Ste11 is not expressed.** When glucose and nitrogen are available they bind to activate the GPCR Git3, which activates the Gα protein Gpa2 via GDP for GTP exchange. GTP-bound Gpa2 activates adenylyl cyclase (Cyr1) resulting in an increase in cAMP levels, which activates PKA, resulting in the inhibition of *Ste11* a gene that encodes the transcription factor Ste11, which is required to up-regulate genes required for mating and meiosis [53, 54].

Under conditions of starvation, signal transduction along the PKA pathway is reduced. As a result, intracellular cAMP levels fall facilitated by the action of the phosphodiesterase Cgs2, which converts cAMP to AMP [56]. Only under conditions of starvation do *S. pombe* cells prepare to mate with an opposite mating-type partner. The reduction in nutrients increases expression of the TF Ste11, which prepares the cells for mating by up regulating and expressing cell-specific GPCRs on the plasma membrane and promoting the release of pheromones to attract a partner [57].

1.3.5.1 *S. pombe* cells arrest in G_1 phase when nutrients are low

When nutrients are scarce *S. pombe* cells arrest in the G_1 phase of the cell cycle to ensure that in the event of meeting a mating partner, the cells contain only one complement of

DNA. During mitotic growth the cyclins Cdc13 and Cig2 form complexes with a cyclin-dependent kinase Cdc2, to regulate the G_2/M and G_1/S phase transition of the cell cycle, respectively [58]. To exit mitosis and progress to G_1 phase, Cdc13 is degraded by the Anaphase-promoting complex/cyclosome [59]. In response to starvation the cAMP/PKA pathway is inhibited. This enhances the formation and activation of the cyclosome [60] and thus increases degradation of Cdc13, effectively down regulating Cdc2 and preventing an adequate signal to progress from G_1 into S phase. A G_1 arrest is maintained during the mating process through additional destruction of the cyclin Cdc13 by Rum1, a protein upregulated by Ste11 in response to pheromone stimulation.

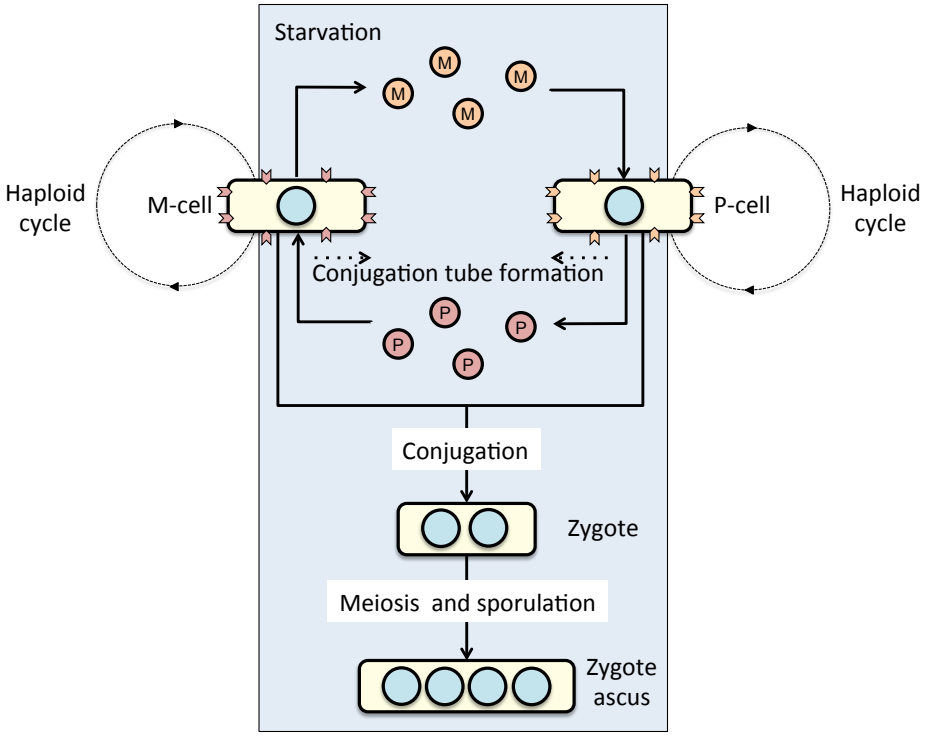

FIGURE 1.6: **The processes involved in mating in *S. pombe*.** *S. pombe* cells exist as either **M** or **P**-type cells, which proliferate via mitosis when nutrients are plentiful. Under conditions of starvation mating-pheromones are secreted (**M**-cells release M-factor and **P**-cells release P-factor), which bind the opposite mating type receptor to elicit a number of responses, including elongation from a single tip (forming conjugation tubes) towards cells of the opposite mating type (dotted arrow indicates direction of growth). Upon meeting, cells conjugate to form a diploid zygote, which sporulates to form ascospores.

1.3.5.2 The mating-response in *S. pombe*

M-cells (h^-) express the GPCR Mam2 and release M-factor [61], whereas **P**-cells (h^+) express the GPCR Map3 and release P-factor [62]. When the appropriate pheromone binds an opposite mating type receptor, an intracellular signalling cascade is initiated [63]. The activation of this pathway leads to potentiation through the morphological pathway (where cells form conjugation tubes in the direction of the pheromone) and up regulation of mating-responsive genes, including genes that are required to maintain the cells in G_1 arrest, *rum1* [64], and *sxa2*, a serine carboxypeptidase that is secreted exogenously to cleave pheromone [65, 66]. Once two heterothallic cells meet, this promotes conjugation and karyogamy, leading to sporulation [67] (Figure 1.6).

1.3.5.3 GPCR signal transduction in the *S. pombe* pheromone-response

Initiation of the mating-response signalling pathway is via the binding of either P-factor or M-factor pheromone to Mam2 and Map3, respectively. As with mammalian GPCRs the ligand-binding event triggers activation of Gpa1 (a Gα subunit) through nucleotide (GDP to GTP) exchange [63]. GTP-bound Gpa1 activates the downstream monomeric G protein Ras1, most likely via the GEF Ste6 [68]. Ras1 provides a branching point in the pathway, with GTP-bound Ras1 being able to activate two distinct effectors. One pathway involves activation of a MAP kinase cascade via sequential phosphorylation of Byr2, Byr1 and Spk1 [69]. The activation of the MAPK Spk1 is thought to promote phosphorylation of Ste11 inducing genes required for mating [70] (Figure 1.7).

The second pathway controls the morphology response (the growth towards the mating partner); this occurs via the activation of Scd1, one of two GEFs for the Rho-like monomeric G protein Cdc42 [71, 72], the second is Scd2, which facilitates Scd1's interaction with Cdc42 [73]. GTP-bound Cdc42 can then activate a number of downstream effectors. One of these effectors is the protein kinase Shk1 [74], which targets Tea1 (a protein that regulates microtubule dynamics and recruits actin) to the cell tips, thereby promoting cell elongation [75]. Shk1 also interacts with the MAP3K Byr2 by promoting its active conformation [76].

Another effector of Cdc42 is the Boi-like protein Pob1 (Boi-like meaning that is resembles the function of the BOI proteins in *S. cerevisiae*, which are involved in polar growth [77]), which is targeted to the cell tips to promote an interaction between the formin For3 and Cdc42. This interaction removes the autoinhibition of For3 and the resulting Cdc42 activation of For3 assembles actin cables for myosin V-directed transport, which guides a multi-protein exocyst complex, which directs vesicles to the plasma membrane [78–81]. Pheromone-induced activation of this pathway therefore results in both a transcriptional and morphological response in the form of elongation of the cell towards its mating partner (Figure 1.7).

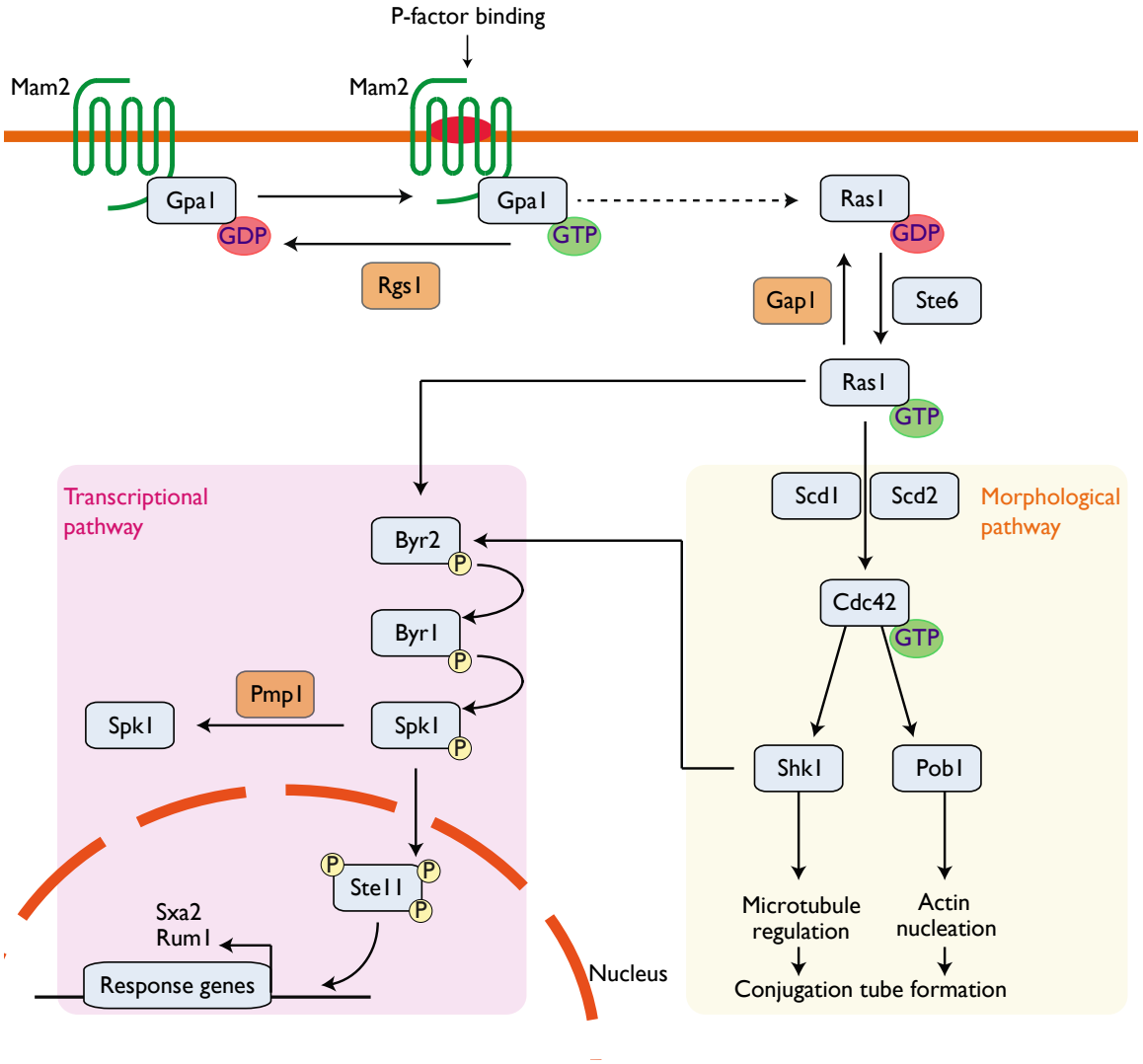

Figure 1.7: **M-type *S. pombe* pheromone-response pathway.** Activation of Mam2, the GPCR in response to P-factor promotes GDP for GTP exchange on the G protein Gpa1. GTP-bound Gpa1 activates another G protein Ras1 via an interaction with Ste6. Ras1 can then activate two pathways: The transcriptional pathway, which transduces signalling via a MAPK cascade consisting of Byr2, Byr1 and Spk1, which then phosphorylates the TF Ste11 promoting transcription of a number of mating-responsive genes such as *sxa2* and *rum1*. The morphological pathway, resulting in activation of the essential G protein Cdc42 via two GEFs Scd1 and Scd2. Active Cdc42 regulates the organisation of microtubules (via Shk1) and actin nucleation (through Pob1-mediated For3 activation, For3 not shown). Shk1 also phosphorylates Byr2 (a MAP3K), which modulates pheromone responsive gene transcription. The G proteins Gpa1 and Ras1 are negatively regulated by Gap1 and Rgs1 and Spk1 is dephosphorylated by the phosphatase Pmp1.

1.4 Regulation of GPCR signal transduction

All cells have developed mechanisms for detecting the change in stimulus through a reversible process of adaptation or signal termination, where a prolonged exposure to the signal decreases the cells response to that level of stimulus. Switching off activated receptors and G proteins and by returning the levels of second messengers, protein phosphorylation and other changed metabolites to their original values, returns the cells to a 'normal' state, which primes the cell ready to respond to other stimuli. There are various modes of signal regulation within GPCR signal transduction pathways, such as removing the source of stimulus, removing or inactivating the GPCR, deactivating the G protein or regulating signal transduction of downstream signalling components.

Simple eukaryotic organisms such as the fission yeast *S. pombe* use highly conserved signal transduction mechanisms to regulate cell behaviour and as such, have been utilised to understand fundamental cell signalling processes in mammalian cells [72, 82–85]. However, few studies have focused on the regulation of signal transduction [86, 87] and to date no studies have investigated receptor inactivation within the pheromone-response pathway of *S. pombe*.

The pharmaceutical industry invest billions of dollars each year to discover therapeutic compounds for GPCRs that give desired physiological effects (reviewed in [5]). Many long-term treatments that target these receptors result in the patient becoming tolerant to the drug. This tolerance often results in having to increase the dosage to deliver the same physiological outcome, which can be debilitating for the patient and lead to undesirable side effects. Understanding how these receptors are regulated at the plasma membrane is key to developing appropriate treatments for diseases. This thesis therefore aims to elucidate the mechanisms of GPCR signal regulation and termination of *S. pombe* in greater depth with a particular emphasis on how the GPCR is regulated in response to P-factor stimulation.

1.4.1 Regulation of GPCR signal transduction via ligand depletion

Some cells have developed mechanisms for attenuating GPCR signalling responses by depleting the extracellular ligand. The process of degrading extracellular ligand to attenuate and desensitise the signalling response is conserved from humans to yeast. In human pancreatic β-cells, two intestine secretion insulin (incretin) peptide hormones: glucose-dependent insulin-releasing polypeptide (GIP) and glucagon-like peptide-1 (GLP-1), are both secreted in response to food ingestion and bind to activate the GIP and GLP-1 GPCRs, respectively [88]. Activation of these receptors stimulates the secretion of insulin from pancreatic β-cells to stimulate glucose uptake. Following GIP and GLP-1 peptide secretion these hormones are rapidly (<4 mins) degraded by the enzyme dipeptidyl peptidase-4 (DPP-4) [89], which

is expressed on the cells' surface [90]. As a result, the majority of GIP and GLP-1 is inactivated before reaching the systemic circulation. By degrading the ligand this prevents continuous stimulation of the pathway and therefore, regulates insulin secretion [91].

In *S. cerevisiae* BAR1, an aspartyl protease, is released by **a**-type cells of the *S. cerevisiae* following stimulation by α-factor mating-pheromone [92]. α-factor is a tridecapeptide (13-residue oligopeptide) [93] that is inactivated by BAR1 through cleavage of the protein between a leucine residue at position six and lysine residue at position seven [94]. Inactivation of the extracellular pheromone plays an important role in the cells' recovery from pheromone stimulation [95].

Following this discovery, a similar mechanism in *S. pombe* was also discovered. In response to the pheromone (P-factor) *S. pombe* **M**-cells produce and secrete Sxa2, a carboxypeptidase which cleaves P-factor at the C-terminal leucine residue. The secretion of Sxa2 reduces the extracellular concentration of P-factor allowing the cells that have not yet mated to return to mitotic growth [96–98].

S. pombe **P**-cells on the other hand that secrete M-factor do not possess the ability to degrade extracellular M-factor [99]. M-factor is a hydrophobic nonapeptide with a C-terminal cysteine residue that is both carboxyl-methylated and S-farnesylated on the thiol group to become active [100, 101]. Following its synthesis and modification M-factor is transported across the cell membrane by Mam1, an ATP-dependent peptide transporter belonging to the ATP-binding cassette (ABC) superfamily of proteins [102]. To date, no protein has been identified that degrades exogenous M-factor.

1.4.2 Regulating signalling response via GPCR desensitisation

Many GPCR signalling pathways do not degrade extracellular ligand but instead use a variety of other mechanisms for attenuating signalling response. One of these is regulating the localisation and activity of key signalling molecules such as the GPCR, G protein and regulatory proteins ([103] and reviewed in [104]). In particular, many cells control the level of signal transduction by regulating the GPCR. In some fields this is defined as receptor desensitisation, in which there exist three modes (reviewed in [105]):

1. Receptor inactivation by preventing an interaction with the G protein and thus, signal transduction.
2. Receptor sequestration, typically by internalising the receptor from the cell membrane preventing further activation by a ligand.
3. Receptor down-regulation, where the GPCRs are degraded following internalisation.

In each case, receptor desensitisation requires phosphorylation by specific protein kinases to initiate these processes. The time frames over which these processes occur range from seconds (phosphorylation) to minutes (internalisation) and hours (down-regulation).

1.4.3 Receptor phosphorylation promotes GPCR desensitisation

The most rapid mechanism by which GPCRs are uncoupled from heterotrimeric G proteins is via covalent modification on the intracellular receptor domains as a consequence of phosphorylation by specific kinases, typically on serine and threonine residues. Human GPCRs are the targets of many kinases including second messenger kinases such as PKA and PKC, casein kinases, receptor tyrosine kinases (RTKs) including the second messengers Akt/protein kinase B (PKB) and most notably G protein-coupled receptor kinases (GRKs) (summarised in Figure 1.8 and discussed in detail below).

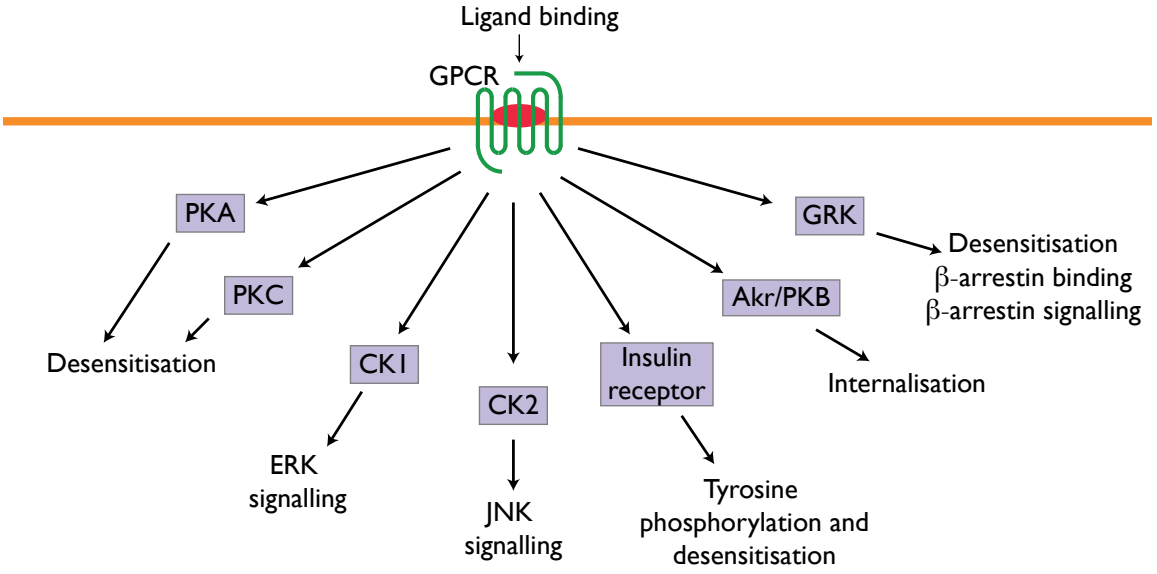

FIGURE 1.8: **Protein kinases that phosphorylate GPCRs.** The schematic shows protein kinases (purple box) that have been shown to phosphorylate GPCRs and the main functional consequences.

1.4.3.1 GPCR phosphorylation by second messengers

GPCR phosphorylation can result from a feedback mechanism where the receptor is phosphorylated to prevent G protein activation by the second messenger kinase it activates, which consequently reduces the activity of the kinase. GPCRs that signal via $G\alpha_s$ increase cAMP levels within the cell which activates PKA. One of PKAs targets is the upstream receptor, where phosphorylation of the IC_3 loop or C-terminal domain sterically inhibits an interaction with the G protein [106, 107]. One classic example of GPCR phosphorylation by PKA is the β_2-adrenergic receptor [108].

In a similar fashion, signalling via $G\alpha_q$ activates PKC, and sometimes one of PKC's targets is the upstream receptor, where phosphorylation of the intracellular regions prevents G protein-coupling. A well studied example of this is the angiotensin II type 1 (AT_1)

receptor, which couples to a $G\alpha_q$ that when activated results in the activation of PKC, which subsequently phosphorylates the C-terminal AT_1 receptor domains [109].

Although *S. pombe* contains both PKA and PKC, when nutrients are scarce and the cells initiate a mating response, as a direct result these kinases' activity is significantly reduced (Figure 1.5). It is therefore unlikely that PKA or PKC are active and able to phosphorylate the GPCR Mam2 in response to pheromone stimulation. This suggests that Mam2 may be phosphorylated by other kinases.

1.4.3.2 GPCR phosphorylation by casein kinases

Multiple studies within yeast and mammalians cells have highlighted a role for casein kinases in phosphorylating GPCRs in response to ligand-binding. Casein kinases are highly conserved ubiquitous serine/threonine protein kinases that can be grouped into two major families based upon structural similarities: casein kinase 1 (CK1), a family of monomeric proteins that can be further classified into seven isoforms (α, β, γ_1, γ_2, γ_3, δ, ε), and casein kinase 2 (CK2), a group of tetrameric proteins that consist of two α catalytic and two β regulatory subunits [110].

Studies on the mating-pheromone receptors of *S. cerevisiae* have demonstrated an essential role for two CK1 homologs, YCK1 and YCK2 in the phosphorylation of specific serine residues in the C-terminal domain of STE2 (a GPCR), promoting its internalisation from the plasma membrane [111–114]. Although the pheromone-induced mating response pathway in *S. pombe* has been studied for over 25 years and casein kinases have been identified, however, no studies have suggested a possible role for these kinases in phosphorylation of GPCRs.

In mammalian cells, CK1α was first shown to phosphorylate human photoactivated rhodopsin [115] and later was demonstrated to phosphorylate the muscarinic 1 (M_1) [116, 117] and muscarinic 3 (M_3) receptors [118, 119]. In addition to phosphorylation of the C-terminal tail region, CK1α appeared to regulate the ability of the M_3 receptor to favour coupling to the ERK mitogenic pathway [119, 120], suggesting that GPCR phosphorylation by casein kinases may direct signalling to other pathways than G proteins.

The CK2 family has also been shown to phosphorylate GPCRs. The first example of this came from studies of the thyrotropin-releasing hormone (TRH) receptor where mutation of potential CK2 phosphorylation sites in the C-terminal tail resulted in a reduction in receptor phosphorylation and loss of internalisation [121]. Later, CK2 was identified in phosphorylating residues in the IC_3 loop of the M_3 receptor [122]. Interestingly, phosphorylation of the M_3 receptor by CK2 did not result in receptor internalisation but enhanced coupling of the receptor to the JNK pathway [122]. Further evidence for the involvement of CK2 in GPCR phosphorylation was illustrated with the dopamine 1 (D_1) and adenosine

A_{2A} receptors. This study suggested a potential mechanism of the phosphorylation event uncoupling the G proteins from their cognate receptors following ligand-binding [123].

It should be noted that both CK1 and CK2 have been shown to have roles within GPCR signal transduction pathways that do not involve phosphorylating the ligand-bound GPCR but regulate other signal transduction machinery. A good example of this is the involvement of CK1α and CK1γ in Wnt signalling, a crucial pathway for activating gene transcription to control processes during embryonic development and in regeneration of tissues in adult organisms [110, 124–128].

1.4.3.3 GPCR phosphorylation by the insulin receptor and second messenger Akt/PKB

Ligand-induced GPCR phosphorylation has been shown to occur via other plasma membrane receptors and their downstream effectors. Specifically, the insulin-like growth factor 1 (IGF_1) receptor (a RTK) was shown to stimulate the phosphorylation and internalisation of the β_2-adrenergic receptor in response to insulin [129, 130]. Further studies suggested a mechanism whereby insulin receptor activation of PIP_3K drives the activity of Akt/PKB, which directly phosphorylates the β_2-adrenergic receptor in its C-terminal domain [131]. To date there have been no RTKs identified in yeast and therefore unlikely to promote phosphorylation of the GPCR Mam2.

1.4.3.4 GPCR phosphorylation by G protein-coupled receptor kinases

The most characterised of the kinases that phosphorylate ligand-bound GPCRs are GRKs. There are seven GRKs in humans that share a similar residue assembly: including an ∼25 residue N-terminal tail (implicated in GPCR binding), followed by a regulators of G protein signalling (RGS) homology domain (RGS proteins act as GAPs for Gα subunits, this region therefore provides specificity for a GRK interaction with a particular Gα subunit [132]), which is disrupted by the protein kinase domain and finally, a C-terminal region containing structural elements responsible for membrane or Gβγ targeting [133].

Unlike other kinases, GRKs do not require phosphorylation in their activation loop to achieve an activated state, instead they are directly activated by docking with ligand-bound GPCRs [134, 135]. Once activate, the GRK is able to multi-phosphorylate the ligand-bound receptor enabling high-affinity binding of β-arrestin, which uncouples the G protein from the receptor, preventing further G protein-mediated signal transduction [136]. It should be noted that to date, no GRK or β-arrestin homologs have been identified in yeast.

β-arrestins are ubiquitously expressed in all cell types, and function not only to inhibit GPCR/G protein-coupling but also promote receptor internalisation and β-arrestin-mediated signalling, serving as scaffolds for numerous signalling pathways. These pathways

include the Src family of tyrosine kinases (that are recruited to β-arrestin bound GPCRs) and in particular MAPK cascades such as ERK, JNK and p38 pathways ([137] and reviewed in [138, 139]).

1.4.4 Receptor internalisation

Many different types of kinases have been shown to phosphorylate GPCRs (summarised in Figure 1.8). In addition to phosphorylation of the intracellular receptor domains preventing G protein activation, phosphorylation can also promote endocytosis (internalisation) of the receptor from the plasma membrane. Although β-arrestins were initially discovered as proteins that prevent receptor/G protein-coupling, later they were associated with facilitating receptor endocytosis via clathrin-coated pits (CCPs).

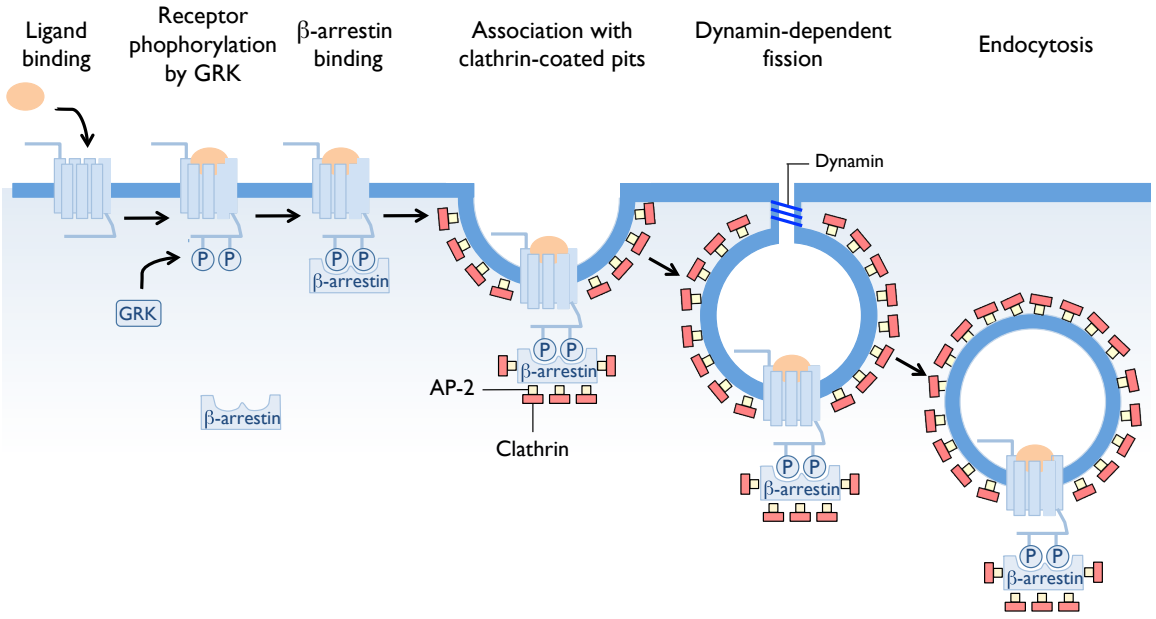

FIGURE 1.9: **β-arrestin dependent GPCR internalisation.** GPCRs are phosphorylated by GRKs on their C-terminal tail and IC_3 residues following ligand-binding and activating the extracellular binding pocket. This phosphorylation event promotes the binding of β-arrestin and prevents further G protein activation (thereby terminating G protein signalling). The arrestin protein is recognised by clathrin-coated machinery (AP-2 and clathrin), which binds and envelopes the GPCR. finally the GTPase dynamin helps pinch off the clathrin-coated vesicle resulting in endoyctosis of the GPCR into the cytosol.

Mammalian β-arrestins exist in a constitutively phosphorylated state in the cytosol and are dephosphorylated upon binding activated GPCRs at the plasma membrane (reviewed in [139]). Dephosphorylation of the arrestin molecule upon binding the active receptor results in a conformational change in the C-terminal domain of the arrestin protein revealing residues that bind the endocytotic machinery; specifically clathrin and the clathrin adaptor

complex AP-2 [140–142]. Once bound, invagination of the plasma membrane with the GPCR and β-arrestin protein occurs, enveloped with clathrin and AP-2 complexes, which guide the formation of intracellular vesicles. The release of the vesicle from the plasma membrane is aided by the activity of the GTPase dynamin, which helps pinch off the clathrin-coated vesicles (CCVs) resulting in the internalisation of the cell-surface receptor into the cytosol (Figure 1.9). The two best characterised receptors that are endocytosed following GRK phosphorylation are the β_2-adrenergic receptor and rhodopsin [133].

Several GPCRs are internalised in an β-arrestin-independent manner. The β_1-adrenergic receptor for example is guided by GRK2 to clathrin-coated pits (CCPs) via an interaction between clathrin and a clathrin box present on the C-terminus of GRK2 and is subsequently endocytosed [143]. Active GPCRs can also be internalised in a clathrin-independent manner via interactions with planar lipid rafts and caveolae that internalise cell-surface receptors into vesicles (reviewed in [144]).

1.4.5 Down-regulation of GPCRs by degradation

Another important observation that lead to our present view of GPCR regulatory mechanisms came form classical studies of the β_2-adrenergic receptor [106, 145, 146]. It was shown that phosphorylation of the intracellular receptor domains by GRKs occurs when the GPCR forms an active conformation (ligand-bound) and that these receptors are subsequently internalised and trafficked to the degradation pathway (down-regulated) [145]. This type of GPCR regulation is termed homologous, as the ligand-binding event on that type of receptor promotes down-regulation of those receptors only. This selective property of GRKs to phosphorylate only active receptor conformations infers that GRK-mediated phosphorylation is generally considered a paradigm for homologous desensitisation.

It was also observed that phosphorylation of the β_2-adrenergic receptor by activated PKA is not preferential to whether the GPCR is bound to ligand [147]. Activation of any receptor that stimulates adenylyl cyclase within the cell can activate PKA and thus, PKA can potentially activate other receptors that are active or inactive. Down-regulation of an non ligand-bound GPCR as the result of activation of a different type of GPCR is generally known as heterologous desensitisation [148]. Phosphorylation of the β_2-adrenergic receptor by PKA is considered a classical example of heterologous down-regulation [149].

Following endocytosis, the receptor can be trafficked to recycling endosomes and (following dephosphorylation, removal of the ligand and removal of other associated proteins such as arrestins) subsequently recycled back to the plasma membrane (reviewed in [104]). However, most often the receptor is trafficked to the lysosome for degradation thereby reducing its expression levels on the cell-surface and hence, is down-regulated (reviewed in [104]). What controls the fate of the receptor following its internalisation is still not entirely known. Some studies have shown that cytoplasmic sequences present in certain

GPCRs promote sorting of internalised receptors to lysosomes [150], as well as sequences that promote [151] or prevent [152] rapid recycling of endosomes (vesicles) to the plasma membrane.

1.4.6 GPCR sorting following ubiquitination

In addition to phosphorylation of the GPCR initiating the process of receptor internalisation, another post-translational modification process for sorting GPCRs has been observed. Ubiquitination is the process of covalently attaching a protein of ubiquitin (a highly conserved polypeptide of 76 amino acids) to a substrate lysine residue (ubiquitination) [153], which acts as a sorting signal for the protein. The process of ubiquitination is mediated by the concerted action of three enzymes. First ubiquitin is activated in an ATP-dependent process by an activating enzyme E1, second a conjugating enzyme E2 accepts ubiquitin from E1 and finally, a ubiquitin protein ligase E3 transfers the activated ubiquitin from E2 to the substrate lysine residue (Figure 1.10). Other amino acids such as cysteine, serine and threonine can be ubiquitinated, however this has only been shown to occur on proteins lacking available lysines [154].

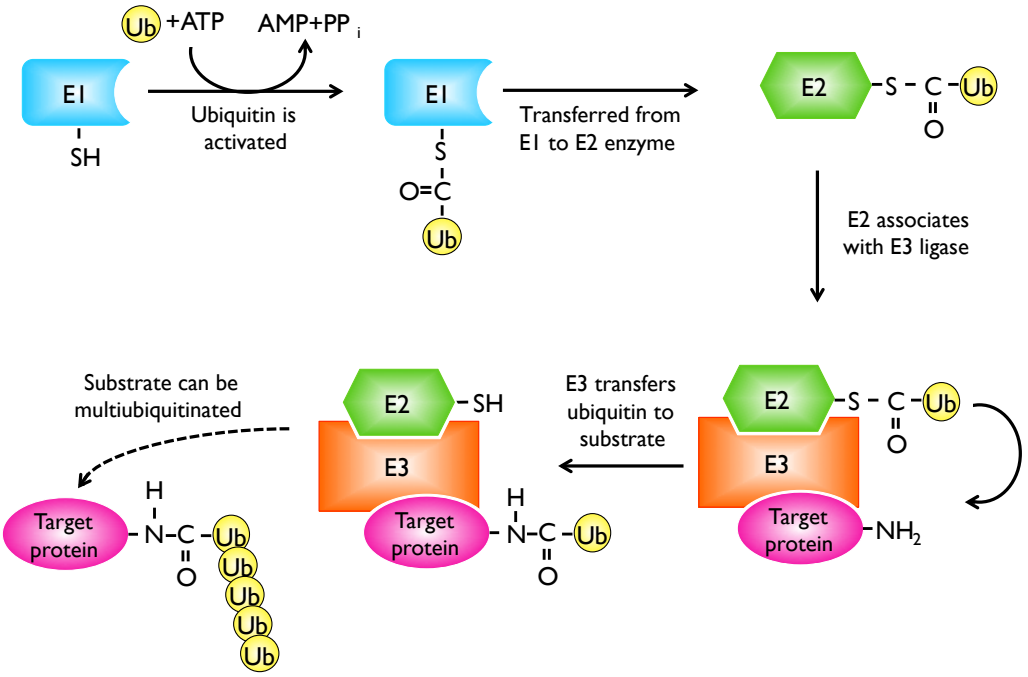

FIGURE 1.10: **Ubiquitination of target protein.** Ubiquitin (Ub) is activated by covalent attachment to E1 enzyme in an ATP-dependent reaction and is subsequently transferred to an E2 (ubiquitin-conjugating) enzyme. Ubiquitin is transferred from E2 to the lysine residue of the target protein with the assistance of an E3 (ubiquitin ligase) enzyme. After several cycles of ubiquitination, the target protein can become multiubiquitinated (forming a chain of ubiquitin molecules on the substrate).

Ubiquitin molecules can either be ligated onto substrate lysine residues or other ubiquitin proteins forming polyubiquitin chains. Depending on whether the substrate is monoubiquitinated (one ubiquitin polypeptide on a single lysine), multimonoubiquitinated (several single ubiquitin molecules to different lysine residues in a protein) or polyubiquitinated (forming a polymeric chain of ubiquitin molecules from a single lysine residue) can determine the fate of the target protein [155]. For example, ubiquitination of proteins can either signal for their degradation via the proteasome or lysosome, alter their cellular location, affect their functional activity or promote/prevent protein interactions ([156, 157] and reviewed in [158]).

Ligand-promoted ubiquitination of GPCRs typically initiates its internalisation and trafficking to the lysosome for degradation [159]. Following endocytosis into endosomes the receptors are sorted into the multivesicular body (MVB); a distinct endosomal compartment containing intracellular vesicles associated with endosomal degradation. The ubiquitin tags on the receptors are recognised by proteins of the endosomal sorting complex required for transport (ESCRT) machinery, many components of which contain ubiquitin-binding domains (UBDs), which provide a framework for a network of ubiquitin interactions that lead to the sorting and degradation of the cargo by the lysosome [160] (Figure 1.11).

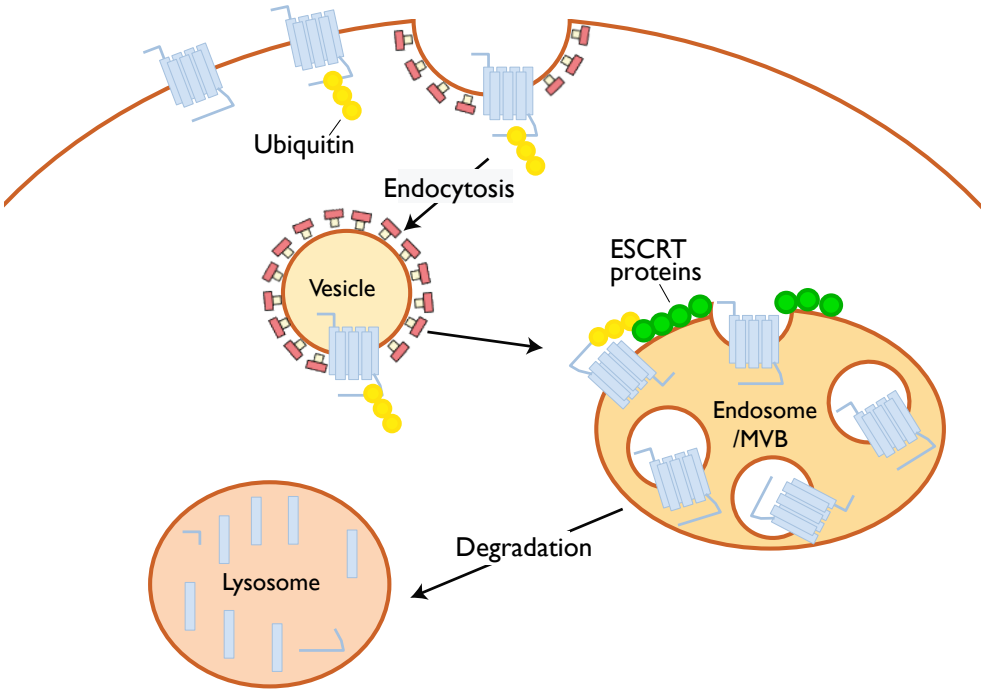

FIGURE 1.11: **Degradation by ubiquitination of GPCRs.** Following ubiquitination of the GPCR it is internalised into vesicles in a clathrin-dependent manner. The early vesicles fuse with early endosomes and develop into the multivesicular body (MVB). The ubiquitinated receptors (with yellow tags) are recognised by ubiquitin-binding domains of ESCRT proteins (green), which help invaginate the GPCRs into intracellular lumens. The MVB then fuses with the lysosome where the GPCRs are degraded.

Some GPCRs such as the vasopressin type-2 receptor (V_2R) [161] and protease-activated receptor 2 (PAR_2) [162] are only ubiquitinated following GRK phosphorylation and the subsequent binding of β-arrestin. One supposition for this requirement is that the β-arrestins may serve as adaptors to bring as yet unidentified E3 ligases to the receptors in a ligand-dependent manner [163].

1.4.7 Constitutive internalisation of GPCRs

GPCRs also internalise independently of ligand stimulation (constitutive internalisation), however a conserved mechanism for how this occurs is still unknown (reviewed in [164]). Some GPCRs, for example the β_2-adrenergic and M_3 receptor have been shown to constitutively internalise via clathrin-independent mechanisms and following internalisation are recycled back to the plasma membrane [165]. In response to ligand activation the β_2-adrenergic and M_3 receptors were shown to switch from a clathrin-independent to clathrin-dependent endocytosis mechanisms, resulting in these receptors being trafficked to the lysosome for degradation [165]. What initiates the internalisation of these receptors via the clathrin-independent mechanism is unknown. Some studies suggest that constitutive internalisation occurs when the receptor momentarily forms an active complex, resulting in a conformation that mimics the ligand-bound state, which is then phosphorylated and endocytosed in a clathrin-dependent manner [166].

Ubiquitination of the *S. cerevisiae* receptor STE2 is essential for its constitutive and ligand-induced internalisation [112]. For some GPCRs such as the protease-activated receptor-1 (PAR1) [167] and the chemokine CXCR7 [168], ubiquitination of these receptors in fact enhances rather then reduces the concentration of the GPCR at the membrane. These studies showed that mutating lysine residues in the C-terminal domain of the GPCR resulted in an increase in constitutive internalisation. These studies illustrate that conserved mechanisms of how ubiquitination controls GPCR internalisation are still unknown.

1.4.8 The role of GPCR C-terminal domains

The C-terminus of GPCRs are not only important targets of post-translational modification such as phosphorylation and ubiquitination, but also act as scaffolds around which other signalling components can organise. Receptor function and trafficking is regulated by a variety of GPCR interacting proteins (GIPs) that interact with the C-terminal domain of GPCRs [169]. One example is the intracellular protein dishevelled (Dsh) described earlier. The Dsh protein is required to interact with the PDZ-domain (a conserved binding motif that plays a role in the organisation of protein complexes on the membrane through binding to consensus C-terminal motifs in target proteins [170]) of the frizzled receptors C-terminal domain in order to initiate a signalling cascade [171].

RGS proteins are another classic group of proteins that have been shown to interact with the C-terminal tail of GPCRs to enhance their localisation at the plasma membrane [172, 173] and to promote selectivity of RGS function [172, 174–176]. Examples of these are the μ-opioid and δ-opioid receptors, in which there C-terminal domains provide a scaffold that RGS4 can bind and as a result can regulate signalling [177].

Key features within the C-terminal domain of GPCRs regulate their localisation and sorting. For example, the presynaptic terminal localisation of metabotropic glutamate receptors has been shown to be dependent on the presence of a PDZ motif in its C-terminus, which interacts with an intracellular kinase to regulate function and localisation [178]. The C-terminal tail of the calcitonin receptor was show to interact with filamin an actin-binding protein to enhance its recycling to the membrane following ligand-induced endocytosis [179]. The *S. cerevisiae* pheromone-receptor STE2 was shown to be present in greater quantities at the cell surface when mutated to lack the C-terminal tail, illustrating that the C-terminal tail is required for receptor sorting [180].

Another important example, is the essential interaction between the two neurotransmitters gamma-aminobutyric acid (GABA) B1 and GABA B2 receptors via their C-terminal domains to confer signal transduction. GABA B1 contains the GABA-binding site, but expressed alone is not trafficked to the cell-surface [181]. In contrast, the GABA B2 subunit is sequestered to the cell-surface but does not contain a GABA-binding site [181]. Only when co-expressed together do these subunits interact via their C-terminus creating a coiled-coil region and hence, transduce signalling inside the cell [182, 183].

1.4.9 Internalisation of the M-type receptor Mam2

The mechanisms or proteins that promote receptor internalisation/desensitisation in *S. pombe* have not yet been described, but GPCRs in general are known to internalise following phosphorylation (by specific kinases on serine and threonine residues) of the C-terminal tail and intracellular loops of the receptor. A number of possible sites for phosphorylation have been identified on the C-terminus of Mam2, which appear to be required for pheromone-dependent internalisation. Specifically, the removal of an 8-residue sequence (YSISDESE) from the C-terminal tail (Figure 1.12), increased both the potency of pheromone and plasma membrane localisation of the receptor ([173]; E. McCann, PhD thesis, 2010). These three serine residues were therefore considered potential targets of ligand promoted phosphorylation and internalisation of Mam2.

FIGURE 1.12: **Sequence of the predicted C-terminal tail of Mam2.** Possible sites of phosphorylation (by serine and threonine kinases) are highlighted in blue and possible sites of ubiquitination (on lysine residues) are highlighted in red. The YSISDESE sequence is highlighted in bold with a dashed border and includes the three serine residues, which are suggested to have a role in Mam2 internalisation (E. McCann, PhD thesis, 2010).

In other yeast, GPCR phosphorylation on serine residues is involved in receptor internalisation [112]. Specifically, the three serines within the SINNDAKSS sequence (a region of the C-terminal tail) of the *S. cerevisiae* α-factor receptor STE2 have been shown to be hyperphosphorylated following treatment with α-factor, which is a prerequisite for monoubiquitination of the neighbouring lysine (K) residue to mediate ligand-stimulated endocytosis [111–114]. Phosphorylation of the SINNDAKSS sequence is also a requirement of constitutive internalisation [112].

Like STE2, Mam2 displays both constitutive and ligand-induced internalisation. Fluorescent labelled Mam2 was shown to reside in the yeast vacuole (equivalent to the mammalian lysosome) and the plasma membrane of untreated cells [184], which then internalised from the plasma membrane following treatment with P-factor [173]. There is no evidence for the recycling of Mam2 or STE2 following their internalisation from the plasma membrane in response to ligand-binding [185, 186]. Given serine phosphorylation is essential for receptor internalisation and ubiquitination of the neighbouring lysine residue in *S. cerevisiae*, a potentially similar mechanism may occur in *S. pombe*, however no lysine residues neighbour any serines within the C-terminal tail of Mam2, which suggests that the mechanisms for internalisation may be different between the two yeast species (Figure 1.12).

Neither *S. pombe* or *S. cerevisiae* carry homologues of GRKs or β-arrestin proteins, which traditionally phosphorylate and promote endocytosis via clathrin-coated vesicles of mammalian GPCRs. However, two *S. cerevisiae* casein kinases YCK1 and YCK2 have been shown to promote phosphorylation and internalisation of STE2 [112]. To date, there have been no proteins identified in *S. pombe* that phosphorylate the C-terminal tail or intracellular loops of Mam2 to promote its internalisation.

1.4.10 Regulators of G protein signalling

The heterotrimeric Gα subunit contains two catalytic residues required for GTP hydrolysis; a glutamate in switch II which correctly orientates the water molecule, to enable transfer of the γ-phosphate and an arginine in switch I, which stabilises the transition state for the Gα-subunit to have an intrinsic GTPase activity [17]. Gα subunits contain all the required catalytic residues to perform the GTPase function required for the termination of signalling.

However, the intrinsic GTPase rate can be enhanced by a class of GAP proteins known RGS proteins. RGS proteins act allosterically to stabilise the transition state, increasing the rate of GTP hydrolysis [187]. A study using RGS4 from rats showed it stabilises the flexible regions of the $G\alpha_i$ subunit into a conformation resembling the transition state and as a result, was assumed to lower the activation energy required for GTP hydrolysis [188]. Therefore, RGS proteins typically promote signal desensitisation by increasing the rate of GTP hydrolysis on the G protein.

S. pombe, contains only one RGS species, Rgs1, which targets the Gα subunit Gpa1 by catalysing its hydrolysis from a GTP to GDP [87]. Cells deficient in Rgs1 are hypersensitive to pheromone and are unable to mate despite undergoing a G_1 arrest and conjugation tube formation [87, 189]. Counter-intuitively, Rgs1 was shown to confer both negative and positive regulation of pheromone signalling depending on the cellular concentration of Rgs1 and pheromone stimulation [190]. In addition, the localisation of Rgs1 and its ability to regulate Gpa1 has been shown to be dependent on a physical interaction between the C-terminal domain of Mam2. Fluorescent labelled Rgs1 was observed in the nucleus rather than the plasma membrane following the removal of the C-terminal tail of Mam2 and was localised to the plasma membrane when co-expressed with full length Mam2 [173].

1.4.11 G protein regulation by GAPs

Like Gα subunits, monomeric G proteins contain a conserved glutamate on the switch II region which is required for the coordination of the water molecule during GTP hydrolysis [17]. However, monomeric G proteins do not contain the catalytic arginine which is required for GTPase activity. In the case of monomeric G proteins, GAPs donate the catalytic arginine residue and therefore, aid the termination of the G protein response [19, 191].

In the *S. pombe* mating response pathway the monomeric G protein Ras1 is regulated via the GAP, Gap1. Loss of Gap1, results in hypersensitivity to pheromone and a reduced ability for the S. pombe to mate with an opposite mating type partner [86]. Unlike Rgs1, which has been shown to have both a positive and negative regulatory role on signalling in *S. pombe*, Gap1 has only been shown to negatively regulate Ras1 [96] (Figure 1.7).

1.4.12 MAPK regulation by phosphatases

Signal transduction via MAPK cascades typically requires the addition of phosphate groups on tyrosine, serine and threonine residues of the target protein. Protein phosphatases act to remove these regulatory phosphate groups and typically aim to terminate signal transduction [192]. Protein phosphatases can be divided into three groups: the protein tyrosine phosphatases, serine/threonine phosphatases and dual specificity phosphatases,

which as the name suggest can remove the phosphate group from phosphotyrosine and phosphoserine/phosphothreonine residues (reviewed in [193]).

In addition to GPCR signal activation via directly or indirectly activating MAPK cascades, GPCRs have been shown to regulate MAPK phosphatases that deactivate MAPKs. For example, $G\alpha_{12}$ has been shown to directly stimulate PP5 [194] as well as PP2A [195] phosphatases, which have been suggested to play a role in attenuating p38 (a MAPK) (reviewed in [196]).

Recovery from pheromone stimulation in *S. pombe* can be enhanced by phosphatases which regulate the MAPK cascades. The key site for regulation of the pheromone-induced MAPK cascade is Spk1, which when phosphorylated activates the transcription factor, Ste11. A dual-specificity phosphatase Pmp1 is thought to dephosphorylate Spk1 in order to reduce pheromone-dependent gene transcription [11].

Like kinases, phosphatases act on several substrates within the cell [197]. Other phosphatases that target MAPKs in *S. pombe* are the Pyp1 and Pyp2 phosphatases. These have been shown to dephosphorylate the stress-activated Sty1 MAPK [198, 199]. Pmp1 has also been shown to dephosphorylate Pmk1, the MAPK of the cell integrity MAPK cascade [200]. The cell integrity MAPK pathway is thought to be involved in cell wall construction, morphogenesis, cytokinesis and ion homeostasis as deletion of either member of the cascades causes hyperosmotic stress or elevated temperatures and morphological defects with cells displaying septa [201–204].

1.5 Mathematical modelling of GPCRs

Many studies have employed computational modelling approaches to understand the complex behaviour of signalling networks, such as those initiated from GPCRs (reviewed extensively in [205]). Mathematical models can be used as tools to hypothesise mechanisms and infer parameters such as reaction rates and species concentrations, often with the aim of guiding experimental design and thus reducing the time in the laboratory.

1.5.1 Equilibrium models

Existing GPCR signalling models focus on the pharmacology of different equilibrium states of the receptor. These types of models describe how the addition of ligand and/or G protein changes the equilibrium between two distinct receptor conformations, inactive receptor (R) and active receptor (R^*) (reviewed in [206, 207]). These models include terms for describing affinity, the effectiveness of how a ligand binds the receptor and efficacy, the ability of a ligand to induce an intracellular response; two important quantities which are key in drug design.

Two of the most influential equilibrium models to date are the cubic ternary complex model of GPCR signalling [208] (Figure 1.13) and the operational model of pharmacological agonism [209] (reviewed in [210]). The cubic ternary model accounts for constitutive activity of the receptor and was the first to model and explain inverse agonism (a ligand that binds to the receptor to reduce its activity below the basal level). Whereas, the operational model of pharmacological agonism was the first to describe how GPCR activity can be modulated in either a positive or negative fashion, by the binding of ligands to sites that were topographically distinct from the ligand-binding site [211].

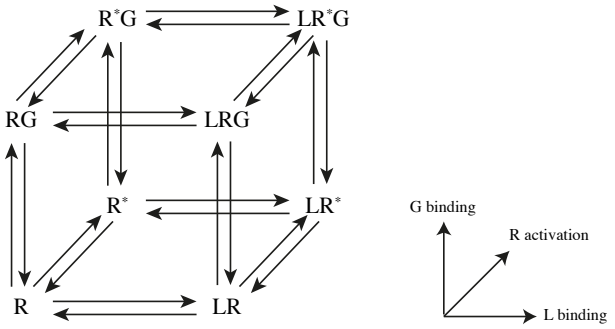

FIGURE 1.13: **Cubic ternary complex model of GPCR signalling.** The receptor can exist in two states: inactive (R) and active (R*). The equilibrium between these two states can depend on Ligand (L) and or G protein (G) binding (figure adapted from [212]).

1.5.2 Kinetic models

Another type of GPCR signalling network approach is a kinetic model, which aims to link time-course data of GPCR binding with the kinetics of early (such as G protein activation) and later (for example, effector activation, MAPK activation and GPCR desensitisation) downstream signalling events (which are not captured in equilibrium models). Kinetic models of this type are generally formulated as ordinary differential equations (ODEs), which describe how the concentration of each species evolves with time. Other types of kinetic models also exist: ones that use partial differential equations (PDEs) to describe spatial information and also stochastic models, which unlike the previously discussed deterministic models assume that events are probabilistic and therefore, multiple simulations must be run to obtain statistical power (which can be computationally heavy depending on the of signalling components).

Kinetic models are based on interactions through collisions (the basis of mass action kinetics) whereby proteins are assumed to move by diffusion. The law of mass action states that the rate of a chemical reaction is proportional to the product of the concentrations of the reactants, where a rate parameter is used to define the probability of a reaction to

occur if two molecules approach each other. A simple example of mass action kinetics can be described by considering that two species A and B collide forming a complex AB.

$$\mathrm{A} + \mathrm{B} \underset{k_2}{\overset{k_1}{\rightleftharpoons}} \mathrm{AB}$$

where k_1 is the forward reaction rate of unit $[time]^{-1}[conc]^{-1}$, while k_2 is the backward reaction rate of unit $[time]^{-1}$. Note that reaction rate units are not uniquely defined but rather depend on the reaction. Three ODEs can be formulated for each species:

$$\frac{d[A]}{dt} = -k_1[A][B] + k_2[AB] \tag{1.1}$$

$$\frac{d[B]}{dt} = -k_1[A][B] + k_2[AB] \tag{1.2}$$

$$\frac{d[AB]}{dt} = k_1[A][B] - k_2[AB] \tag{1.3}$$

which has an equilibrium point for $\frac{[C]}{[A][B]} = \frac{k_1}{k_2}$, at this point the concentrations of each species reaction do not change with time. By formulating a network of biochemical reactions in this way, the dynamics of biological system can be investigated, specifically with the goal of analysing the behaviour of the individual variables and also of the complete system at the same time. Kinetic models of this type can be tested for perturbations where molecules or interactions are removed from the system, which then can be compared with knock-out experiments, or provide biological predictions.

The most extensively modelled GPCR system that has been described using kinetic models of this form, is the pheromone-response pathway of *S. cerevisiae*. The earlier models focused on STE2 (the mating-type GPCR), which is activated via α-factor pheromone, signalling through the Gβγ subunit and included reactions for describing signal desensitisation by the RGS species (SST2) [213]. A kinetic model describing these species was developed and demonstrated that transcriptional induction of the RGS protein SST2, was caused by free (active) Gβγ subunits that produces a negative feedback loop, leading to desensitisation of the pathway [213]. A similar model based upon data measuring the time and dose-dependent loss of fluorescence resonance energy transfer (FRET) between the cyan fluorescent protein (CFP)-tagged Gα and the yellow fluorescent protein (YFP)-tagged Gβγ subunits suggested a relationship between G protein activation and transcriptional induction of mating-response genes [214].

Most GPCR models aim to understand how drugs bind and activate the receptor and G protein. Often these mathematical models are based on components of the pathway that are located at the plasma membrane and do not include the intracellular signalling cascades. Only one model of an entire GPCR signalling pathway has been developed; the pheromone-response pathway in *S. cerevisiae* [215]. This mathematical model was

developed to include the additional filamentous growth pathway in *S. cerevisiae* [216] and by varying the parameters to investigate the model reactions, new hypotheses regarding the contribution of distinct mechanisms to overall crosstalk between the two pathways were described.

1.5.3 Modelling the pheromone-response pathway in *S. pombe*

The mating process of *S. pombe* involves both extracellular and intracellular mechanisms that transduce signalling using a combination of fast (seconds) responses, such as protein modifications and slow (minutes to hours) responses such as transcriptional regulation, cell migration and cell cycle arrest. Mathematical analysis of large-scale signalling networks such as the *S. pombe* mating-response requires the integration of several events that happen at diverse spatial and temporal scales.

Previous modelling efforts of the *S. pombe* mating-response have focused on pheromone binding the GPCR and signal transduction via the G protein. Smith *et al.* (2009) produced the first kinetic model of GPCR signalling of the mating-response in *S. pombe*. They were able to reproduce experimental data with the existence of an inactive GTP-bound state of the G protein [190]. This novel idea placed significant importance on rapid GTP-hydrolysis, rather than retention of a GTP-bound state to produce a maximal signalling response and as such was termed the 'inert state hypothesis'. They suggested that the RGS protein could act as both a positive regulator, accelerating the conversion of bound-GTP to GDP on the G protein (thus allowing the GDP-bound G protein to associate with ligand-occupied receptors for reactivation) and a negative regulator, by hydrolysing GTP prior to the interaction of a GTP-bound G protein with its effector [190].

Croft *et al.* (2013) developed the kinetic model further to include an additional spatial regulation of the RGS species in transducing signalling in the mating-response pathway of *S. pombe* [173]. Using a combination of confocal imaging and quantitative β-galactosidase assays they showed that a physical interaction between the RGS species and the C-terminal domain of Mam2 was essential for RGS plasma membrane localisation and consequent hydrolysis of the G protein [173]. These results highlighted the importance of the receptor tail in transducing and regulating the signalling response.

The previous mathematical models of the *S. pombe* pheromone-response pathway can not reproduce some transcriptional end-point data such as deleting the proteins Gpa1 and Pmp1 because these species are not contained within in the model. Activation of Gpa1 promotes GDP for GTP exchange on the monomeric G protein Ras1 and this in turn signals via a MAPK cascade to phosphorylate the transcription factor Ste11 to up-regulate genes required for mating.

1.6 Aims of the project

This study aims to investigate, identify and describe the underlying mechanisms involved in GPCR internalisation in response to ligand stimulation in the fission yeast *S. pombe*.

By critiquing the literature of the regulatory mechanisms of GPCR signalling in *S. pombe*, gaps in the current state of knowledge in this field seemed evident. First, the currently accepted mathematical model of GPCR signalling in *S. pombe* lacked known signalling species and regulatory mechanisms. To gain a more in depth understanding of how regulatory components in *S. pombe* maintain and control signalling response the mathematical model will be extended to include all known mechanisms. And finally, there is no literature describing how GPCRs are internalised in response to ligand stimulation in *S. pombe* and specifically, what proteins initiate this process. Interestingly *S. pombe* does not contain homologs of GRKs or β-arrestins (the canonical apparatus which initiate GPCR desensitisation mechanisms in mammalian cells). Therefore, an investigation to identify the kinases that initiate GPCR internalisation and their roles within *S. pombe* should be performed. Below are the objectives for each chapter:

- Chapter 3 extends the current mathematical model of GPCR signalling to include all known points of signal regulation. Although the mechanisms for receptor internalisation in response to ligand stimulation are unknown in *S. pombe*, the simulations from Chapter 3 emphasise that internalisation is a key mechanism for modelling the experimental data which motivates Chapter 4.
- Chapter 4 identifies protein kinases that may promote internalisation and investigates their role within the pheromone-signalling response in *S. pombe*.
- Finally, Chapter 5 seeks to understand the different mechanisms of receptor internalisation and investigates how the kinases identified in Chapter 4 influence GPCR internalisation.

The following chapter, Materials, methods and constructs, contains details of experimental and theoretical approaches used throughout this study. References to sections within Materials, methods and constructs are quoted throughout this document; hence the reader may continue reading from Chapter 3.

Chapter 2

Materials, methods and constructs

2.1 Materials

2.1.1 General laboratory reagents

Laboratory reagents were supplied by Sigma-Aldrich Co. Ltd. (Poole, Dorset, UK) and were of analytical grade, unless otherwise stated.

2.1.2 Molecular biology reagents

Restriction enzymes, T4 deoxyribonucleic acid (DNA) ligase and *Taq* DNA polymerase (from *Thermus aquaticus*) were supplied by Invitrogen Ltd (Paisley, Scotland, UK). Thermosensitive alkaline phosphatase was supplied by Promega (Southampton, UK). FastStart high fidelity DNA polymerase blend was purchased from Roche Diagnostics Ltd (Lewes, East Sussex, UK). All oligonucleotides were synthesised by Invitrogen Ltd.

2.1.3 Photographic supplies

DNA gels were visualised using a G:Box iChemi gel documentation system with GeneTool analysis software (Syngene, Cambridge, UK).

2.1.4 P-factor (pheromone)

High-performance liquid chromatography (HPLC) purified P-factor (pheromone) was synthesised by AltaBioscience (University of Birmingham, Birmingham, UK) using Biotech Instruments BT7300 Peptide Synthesiser.

2.1.5 Growth medium

Yeast extract, luria broth and select agar were supplied by Invitrogen Ltd. Plates and liquid medium for the selective growth of *S. pombe* were made using Amino Acid selective medium

(AA) and for *S. cerevisiae* were made using Single Drop-out minimal medium (SD). Rich (Yeast Extract) medium was used with appropriate amino acid supplements (250 µg/ml) as required. For example, YEALU was YE medium supplemented with adenine, leucine and uracil. Plates were made with 1.5% (w/v) select agar. The following medium are made by dissolving the reagents in reverse osmotically filtered (RO) water.

Table 2.1: Defined Minimal Medium (DMM) (Per litre)

NH_4CL	5 g
Na_2HPO_4	2.2 g
Phthalic acid	3 g
Glucose	20 g
L-adenine (add as required for selective medium)	0.5 g
L-leucine (add as required for selective medium)	0.5 g
L-uracil (add as required for selective medium)	0.5 g
Salts (50x Stock)	10 ml
Vitamins (1,000x Stock)	1 ml
Minerals (10,000x Stock)	100 µl

Table 2.2: Stock solution of salts (50x) (Per litre)

$MgCl_2.6H_2O$	52.5 g
$CaCl_2.2H_2O$	735 mg
KCl	50 g
Na_2SO_4	2 g

Table 2.3: Stock solution of vitamins (1,000x) (Per 100 ml)

Nicotinic acid	1 g
Inositol	1 g
Pantothenic acid	500mg
Biotin	400 mg

Table 2.4: Stock solution of minerals (10,000x) (Per litre)

Citric acid	1 g
Boric acid	500 mg
$MnSO_4.H_2O$	500 mg
$ZnSO_4.7H_2O$	400 mg
Molybdic acid	305 mg
$FeCl_3.6H_2O$	200 mg
KI	100 mg
$CuSO_4.5H_2O$	40 mg

Table 2.5: Yeast extract medium (YE) (Per litre)

Yeast extract	5 g
Glucose	30 g

Table 2.6: Selective medium (AA) (Per litre)

Yeast nitrogen base (without amino acids)	6.7 g
Glucose	20 g
Amino acid mix	1.5 g
Select amino acid mix	0.5 g

Table 2.7: Amino acid mix

L-alanine	2 g
L-arginine	2 g
L-asparagine	2 g
L-cysteine	2 g
L-glutamine	2 g
L-glutamate	2 g
L-glycine	2 g
L-isoleucine	2 g
L-lysine	2 g
L-phenylalanine	2 g
L-proline	2 g
L-serine	2 g
L-threonine	2 g
L-tryptophan	2 g
L-tyrosine	2 g
L-valine	2 g
myo-inositol	2 g
para-amino benzoic acid	0.4 g

Table 2.8: Select amino acid mix (components as required)

Adenine	2 g
L-histidine	2 g
L-leucine	4 g
Uracil	2 g
L-methionine	2 g

Table 2.9: YPDA medium (Per litre)

Peptone	20 g
Yeast extract	10 g
20% glucose (w/v)	100 ml
L-adenine	0.1 g

Table 2.10: SD (Single Drop-out minimal medium) (Per litre)

Yeast Nitrogen base w/o a.a containing $(NH_4)_2SO_4$	6.7 g
Drop-out solution	100 ml
20% glucose (w/v)	100 ml

Table 2.11: Drop-out solution

L-adenine	0.2 g
L-arginine	0.2 g
L-histidine	0.2 g
L-isoleucine	0.2 g
L-leucine	1 g
L-lysine	0.3 g
L-methionine	0.2 g
L-phenylalanine	0.5 g
L-threonine	2 g
L-tryptophan	0.2 g
L-tyrosine	0.3 g
L-uracil	0.2 g
L-valine	1.5 g

2.1.6 Bacterial strain

Plasmid amplification was performed using *Escherichia coli (E. coli)* strain DH5α supplied by Stratagene (Cambridge, UK). *E. coli* strain DH5α genotype: *supE44 hsdR17 endA96 thi-1 relA1 recA1 gyrA96.*

2.1.7 Yeast strains

To differentiate between genes and protein from two species of yeast: *S. pombe* genes are denoted *yfg1* and proteins Yfg1, whereas *S. cerevisiae* genes are denoted *YFG1* and proteins YFG1.

2.1.7.1 *S. cerevisiae* strain

The yeast strain AH109 was used in the yeast 2-hybrid system (supplied by BD Biosciences Clontech (Oxford, UK)) and has the following genotype: *MAT**a**, TRP-901, LEU2-3, 112,*

URA3-52, HIS3-200, GAL4Δ, GAL80Δ, LYS2::GAL1$_{UAS}$-GAL1$_{TATA}$-HIS3, MEL1, GAL2$_{UAS}$- GAL2$_{TATA}$-ADE2, URA3::MEL1$_{UAS}$-MEL1$_{TATA}$-lacZ

2.1.7.2 *S. pombe* strains

Standard nomenclature was used to describe the *S. pombe* strains used in this study (Table 2.12). Deletions of genes are referred to as *yfg1-D10* in which 1,000 base pairs (bp) of the *yfg1* locus had been deleted. Gene disruption using the selectable *ura4* or kanamycin-resistance (kan^R) are denoted as *yfg1*::*ura4*$^+$ and *yfg1*::*kan*^{R}, respectively and gene replacement as *yfg1::yfg2*. Creation of reporter strains in which expression of a reporter gene is linked to the promoter of an endogenous gene at the original locus are referred to as *pro1>rep1*.

All strains are mating type stable with deletion of the *mat2* and *mat3* [217]. Therefore *mat1-M, Δmat2/3* strains encode **M**-cells that are incapable of switching mating type. The majority of strains used in this study contain mutations of the *ade6* gene and deletions of the *leu1* and *ura4* genes, which encode enzymes involved in the biosynthesis of adenine, leucine and uracil, respectively. The product of the *cyr1* gene is adenylate cyclase and disruption of this ORF allows *S. pombe* to undergo sexual differentiation during mitotic growth [53].

The *sxa2* gene encodes an extracellular serine carboxypeptidase, which degrades exogenous P-factor [218]. Disruption of this ORF prolongs the response to P-factor stimulation and increases the functionality of reporter strains [11]. To create the reporter strain JY544 (*sxa2>lacZ*) the *sxa2* ORF was replaced with bacterial *lacZ* genes thereby enabling P-factor induction of β-galactosidase under the control of the transcription factor Ste11. *lacZ* encodes β-galactosidase an enzyme that converts ONPG into galactose and o-nitrophenol, which absorbs visible light at 420 nm and therefore, provides an indirect measure of signal amplification through the pathway.

The Cdc42/Rac interactive-binding (CRIB) domain binds specifically to GTP-bound Cdc42 [219]. A plasmid containing the CRIB domain fused to three tandem repeats of GFP under the control of the *shk1* promoter was integrated into *S. pombe* strains containing a *ura4* point mutation [83]. These strains enabled the localisation of Cdc42-GTP to be visualised using confocal microscopy.

Strain	Genotype	Source
JY444	*mat1-M*, *Δmat2/3::LEU2*$^-$, *leu1-32*, *ura4-D18*	[220]
JY448	*mat1-M*, *Δmat2/3::LEU2*$^-$, *leu1-32*, *ura4-D18*, *sxa2>lacZ*	[221]
JY544	*mat1-M*, *Δmat2/3::LEU2*$^-$, *leu1-32*, *ade6-M216*, *ura4-D18*, *cyr1-D51*, *sxa2>lacZ*	[11]
JY630	*mat1-M*, *Δmat2/3::LEU2*$^-$, *leu1-32*, *ade6-M216*, *ura4-D18*, *cyr1-D51*, rgs1::ura4$^+$, *sxa2>lacZ*	[190]
JY949	*mat1-M*, *Δmat2/3::LEU2*$^-$, *leu1-32*, *ade6-M216*, *ura4-D18*, *cyr1-D51*, *pmp1::ura4*$^+$, *sxa2>lacZ*	[11]
JY1025	*mat1-P*, *Δmat2/3::LEU2*$^-$, *leu1-32*, *ura4-D18*	[11]
JY1169	*mat1-M*, *Δmat2/3::LEU2*$^-$, *leu1-32*,*ade6-M216*, *ura4-D18*, *cyr1-D51*, *mam2-D10*, *sxa2>lacZ*	[222]
JY1285	*mat1-M*, *Δmat2/3::LEU2*$^-$, *leu1-32*, *ade6-M216*, *ura4-D18*, *cyr1-D51*, *gpa1-D12*	[82]
JY1291	*mat1-M*, *Δmat2/3::LEU2*$^-$, *leu1-32*, *ade6-M216*, *ura4-D18*, *cyr1-D51*, *mam2-D10*, *rgs1-D14*, *sxa2>lacZ*	[11]
JY1353	*mat1-M*, *Δmat2/3::LEU2*$^-$, *leu1-32*, *ade6-M216*, *ura4-D18*, *mam2::ura4*$^+$	[173]
JY1538	*mat1-M*, *Δmat2/3::LEU2*$^-$, *leu1-32*, *ade6-M216*, *ura4-D18*, *cyr1-D51*, *gap1::ura4*$^-$, *sxa2>lacZ*	[223]
JY1600	*mat1-M*, *Δmat2/3::LEU2*$^-$, *leu1-32*, *ade6-M216*, *ura4-D18*, *cyr1-D51*, *cki3::ura4*$^+$, *sxa2>lacZ*	TS
JY1601	*mat1-M*, *Δmat2/3::LEU2*$^-$, *leu1-32*, *ade6-M216*, *ura4-D18*, *cyr1-D51*, *ste6::ura4*$^-$, *sxa2>lacZ*	[223]
JY1618	*mat1-M*, *Δmat2/3::LEU2*$^-$, *leu1-32*, *ade6-M216*, *ura4-D18*, *cyr1-D51*, *gap1::ura4*$^-$, *rgs1::ura4*$^-$, *sxa2>lacZ*	CW
JY1622	*mat1-M*, *Δmat2/3::LEU2*$^-$, *leu1-32*, *ade6-M216*, *ura4-D18*, *cyr1-D51*, *efc25::ura4*$^-$, *ste6::ura4*$^-$, *sxa2>lacZ*	TS
JY1673	*mat1-M*, *Δmat2/3::LEU2*$^-$, *leu1-32*, *ade6-M216*, *ura4-D18*, *cyr1-D51*, *scd1::Kan*^{R}, *sxa2>lacZ*	[223]
JY1674	*mat1-M*, *Δmat2/3::LEU2*$^-$, *leu1-32*, *ade6-M216*, *ura4-D18*, *cyr1-D51*, *gap1::ura4*$^-$, *scd1::Kan*^{R}, *sxa2>lacZ*	[223]
JY1689	*mat1-M*, *Δmat2/3::LEU2*$^-$, *leu1-32*, *ade6-M216*, *ura4-D18*, *cyr1-D51*, *ura4*$^-$*::*[*shk1* promoter: ScGIC2 CRIB domain:3xGFP:*Ura4*$^+$], *sxa2>lacZ*	WC
JY1718	*mat1-M*, *Δmat2/3::LEU2*$^-$, *leu1-32*, *ade6-M216*, *ura4-D18*, *cyr1-D51*, *gap1::ura4*$^-$, *rgs1::ura4*$^-$, *sxa2>lacZ*	TS
JY1720	*mat1-M*, *Δmat2/3::LEU2*$^-$, *leu1-32*, *ade6-M216*, *ura4-D18*, *cyr1-D51*, *mam2-D10*, *cki3::ura*$^+$, *sxa2>lacZ*	TS
JY1722	*mat1-M*, *Δmat2/3::LEU2*$^-$, *leu1-32*, *ade6-M216*, *ura4-D18*, *cyr1-D51*, *cki2::ura4*$^+$, *sxa2>lacZ*	TS
JY1727	*mat1-M*, *Δmat2/3::LEU2*$^-$, *leu1-32*,*ade6-M216*, *ura4-D18*, *cyr1-D51*, *mam2-D10*, *cki1::ura*$^+$, *sxa2>lacZ*	TS
JY1730	*mat1-M*, *Δmat2/3::LEU2*$^-$, *leu1-32*, *ura4-D18*, *cki3::ura*$^+$ *sxa2>lacz*	TS
JY1731	*mat1-M*, *Δmat2/3::LEU2*$^-$, *leu1-32*, *ade6-M216*, *ura4-D18*, *cyr1-D51*, *cki1::ura4*$^+$, *sxa2>lacZ*	TS
JY1734	*mat1-M*, *Δmat2/3::LEU2*$^-$, *leu1-32*,*ade6-M216*, *ura4-D18*, *cyr1-D51*, *mam2-D10*, *cki2::ura*$^+$, *sxa2>lacZ*	TS

Table 2.12: ***S. pombe* strains used in this study**. The strain name, genotype and source is displayed. TS refers to strains produced in this study, WC refers to strains created by Wayne Croft (University of Warwick, UK) and CW refers to strains created by Cathryn Weston (University of Warwick, UK).

2.2 Methods

2.2.1 Cloning techniques

DNA preparation and manipulations were performed using standard methods [224] or QIAGEN DNA Mini / QIAGEN Plasmid Maxi Kits (Qiagen, West Sussex, UK). Restriction endonucleases were used according to manufacturers' recommendations. DNA fragments were analysed by electrophoresis on 1-2% (w/v) agarose gels containing 0.5 µg/ml ethidium bromide. Purification of DNA from agarose gels were performed using the QIAquick Gel Extraction Kit (Qiagen, West Sussex, UK).

2.2.2 Transformation of *E. coli*

Chemically competent *E. coli* DH5α cells were prepared and transformed with plasmid DNA using a heat shock approach described by Sambrook *et al.* (1989) [224].

2.2.3 Transformation of *S. pombe*

S. pombe was transformed with circularised plasmid DNA or linear DNA fragments using a lithium acetate method as described by Okazaki *et al.* (1990) [225], with a heat shock approach.

2.2.4 Polymerase chain reaction

Taq DNA polymerase (Invitrogen Ltd) was used to screen bacterial colonies and yeast strains for insertion or deletion of DNA fragments. FastStart high fidelity polymerase blend (Roche Diagnostics Ltd) was used for amplifying DNA fragments for cloning. Reactions were performed according to manufacturers' recommendations.

2.2.4.1 Screening plasmid DNA from bacterial cells

A single bacterial colony was suspended in 100 µl water and stored at 4°C. 1 µl of this suspension was used as the template in a 10 µl PCR reaction.

2.2.4.2 Screening yeast genomic DNA

1 µl of yeast genomic DNA (200 - 400 ng) was used as the template in a 10 µl PCR reaction.

2.2.5 Double stranded DNA sequencing

All plasmid DNA was sequenced with oligonucleotides that bind specific regions within the plasmid to confirm no mutations were added during amplification in bacteria or the PCR

reaction. Sequencing was performed by the Molecular Biology Service at the University of Warwick or Source BioScience LifeSciences (Nottingham, UK).

2.2.6 Preparation of yeast genomic DNA

Genomic DNA was isolated from yeast using the protocol from Hoffman and Winston (1987) [226]. Briefly, 10 ml of yeast culture was grown to a density of ~1x10^7 cells/ml and harvested at 2000 rpm for 5 min. Cells were washed in distilled water and 200 µl Blue Buffer (2% (w/v) Triton X-100, 1% (w/v) sodium dodecyle sulphate (SDS), 100 mM NaCl, 10 mM Tris-HCl, pH 8.0 and 1 mM ethylene-diaminetetraacetic acid (EDTA)) was used to resuspend the yeast. 200 µl of a 1:1 phenol:chloroform and 400 µl acid-washed glass beads (425-600 µm diameter) were added and the tube was vortexed for 3 min to promote cell lysis. 200 µl Tris-HCl-EDTA (TE) (pH 7.5) was added immediately and the solid and aqueous phase separated at 13500 rpm for 5 min at 4°C. The aqueous phase was transferred to 1 ml ice-cold ethanol, mixed by inversion and genomic DNA was harvested at 13500 rpm for 5 min at 4°C. The pellet was washed with 70% (v/v) ethanol, dried and resuspended in 50 µl TE (pH 7.5). Preparation of genomic DNA by this method typically yields 10-20 µg DNA.

2.2.7 Cell number and size analysis

Cell densities and median cell volumes were determined using a Z2 Coulter® Particle counter with Isoton II azide-free electrolyte, both supplied by Beckman Coulter (Luton, Bedfordshire, UK).

2.2.8 β-galactosidase assays

2.2.8.1 *S. pombe*

β-galactosidase assays of *S. pombe* cultures were performed using a method modified from Dohlman *et al.* (1995) [227]. Cells were cultured to a density of ~5x10^6 cells/ml in DMM (lacking thiamine unless stated) and 500 µl aliquots transferred to 2 ml Safe-Lock Eppendorf tubes containing varying concentrations of P-factor diluted in HPLC-grade methanol (and dried to remove the methanol). Tubes were incubated at 29°C for the length of the assay on a rotating wheel and 50 µl transferred to 750 µl Z-buffer (Table 2.13) containing 2.25 mM o-nitrophenyl-D-galactoside and incubated on a rotating wheel at 29°C for a further 90 min. Reactions were halted by addition of 200 µl 2M Na_2CO_3 and β-galactosidase production calculated as the ratio of ONPG product formed (detected by optical density (OD) measurement at 420 nm using an Ultrospec 3000; Pharmacia Biotech, Uppsala, Sweden) to assayed cells (determined using a Coulter Channelyser; Beckman Coulter, Luton, Bedfordshire, UK) using the formula $OD_{420}/10^6$ assayed cells.

Table 2.13: Z-buffer

$NaPO_4$ (pH 7.0)	0.1 M
KCl	10 mM
$MgSO_4$	1 mM
β-mercaptoethanol	50 mM
(v/v) chloroform	0.5%
(w/v) SDS	0.005%

2.2.8.2 *S. cerevisiae*

S. cerevisiae cells were cultured to a density of ∼5 x 10^5 cells/ml in SD with 2 ml transferred to 8 ml YPDA medium and incubated at 29°C for 3 h. 1.5 ml aliquots were transferred to 1.7 ml Eppendorf tubes and centrifuged with pellets resuspended in 300 µl Z-buffer lacking β-mercaptoethanol. Tubes underwent 3 rounds of freeze-thawing in liquid nitrogen and 100 µl was transferred to 700 µl Z-buffer and 160 µl Z-buffer containing 13.28 mM ONPG, followed by incubation on a rotating wheel at 29°C until development of yellow colouration. Reactions were halted by addition of 400 µl 1M Na_2CO_3 and β-galactosidase production calculated as the ratio of ONPG product formed (OD at 420 nm) per min to assayed cells (determined with OD600) using the formula OD420/(t x OD600).

2.2.8.3 Analysis of data from β-galactosidase assays

Non-linear regression of dose-response data and statistical analysis was completed using GraphPad Prism software version 6.0 for Mac OS X (GraphPad Software Inc., San Diego, CA, USA). Where possible, sigmoidal dose response curves using the log(agonist)vs response-variable slope (four parameter) were fit to dose-response data and a bell-shaped curve was fitted to non-monotonic responses.

2.2.9 Calculating doubling time

S. pombe cells were cultured in liquid DMM to a density of ∼2x10^6 cells/ml and their cell density measured three times (as described in section 2.2.7). The average of the three densities were taken (N_0). The cultures were then grown for a further 8 h and the cell densities were measured again three times and the average was calculated (N_8). During exponential growth phase cell cultures grow according to cell density with N_t:

$$N_t = N_0 \exp(kt) \tag{2.1}$$

after defining the initial density, N_0, where t is the time between cell density measurements (t = 8 h in our case) and k is a growth constant or frequency (number of times it has grown

per unit time) where in the case of doubling $k = \frac{ln(2)}{DT}$, where DT is the doubling time in hours. Therefore DT can be calculated by:

$$DT = \frac{8ln(2)}{ln\left(\frac{N_8}{N_0}\right)} \tag{2.2}$$

2.2.10 Yeast 2-hybrid assay

AH109 was co-transformed with the vectors pGBKT7 and pGADT7 (BD Biosciences) expressing proteins of interest. The two plasmids were selected by growth on SD medium lacking leucine and tryptophan. Upon protein interaction, the GAL4 transcription factor is reconstituted and the appropriate reporter genes are activated, resulting in growth on medium also lacking histidine and adenine.

2.2.11 Yeast mating assays

Cells were cultured in liquid DMM to a density of ∼5x10^6 cells/ml. 400 µl of each mating type strain were mixed and harvested at 2000 rpm for 3 min. Cells were resuspended in 20 µl of sterile water and 10 µl spotted onto 2xDMM plates containing 100-fold lower NH_4Cl than detailed in section 2.1.5. Non-mixed controls were also spotted onto the plates. Following 72 h incubation at 29°C the first plate was used to perform an Iodine staining assay as described in section 2.2.11.1 and the second plate was used to determine CFU recovery (section 2.2.11.2).

2.2.11.1 Iodine staining

The plate was exposed to iodine crystals for 10 min or until staining was observed. Brown/Black colony colouration occurred from iodine staining of the starch contained within spore cell walls and indicated a successful mating [220].

2.2.11.2 CFU recovery assay

Each colony from the plate was collected and suspended in 1 ml of sterile water. Two separate 1 in 100 dilutions were then made from each 1 ml culture. One of these was plated onto separate YE plates at final dilution factors of 1 in 1,000 and 1 in 10,000 respectively. The other was placed in a 55°C heat block for 10 min to lyse the yeast cells but retain the spores formed from mating. This heat-treated sample was then plated onto separate YE plates at final dilution factors of 1 in 1,000 and 1 in 10,000. Following 72 h incubation, the number of colonies on each plate were counted using a G:Box iChemi gel documentation system with GeneTool analysis software (Syngene, Cambridge, UK). The number of colony

forming units (CFU) as a percentage of the total (colony survival) was calculated using the following equation:

$$\text{CFU recovery (\%)} = \frac{\text{Number of colonies formed after heat treatment}}{\text{Number of colonies formed before heat treatment}} \text{ x } 100$$

The CFU recovery assay was developed by Michael Bond, University of Warwick, 2010 [228].

2.2.12 Visualisation of cell wall and septa

1 ml of cultured cells were harvested and resuspended in 20 µl sterile water containing 0.1 mg/ml calcofluor white (Sigma-Aldrich Co. Ltd.). 4 µl of cell suspension was transferred to a solid DMM (2% (w/v) agarose) pad on a glass slide and imaged using the microscopes described in section 2.2.14.

2.2.13 Visualisation of nuclei

90 µl of *S. pombe* cells were fixed by adding 10 µl of 36.5% (v/v) formaldehyde solution and incubating at 21°C for 10 mins. After this time harvest the cells and wash twice with phosphate buffered saline (PBS) to remove the formaldehyde and resuspended in 10 µl of PBS. 2.5 µl of this culture to a microscope slide and dry in a fume hood for 5 mins. 2 µl of cells was mixed with 2 µl 4',6-Diamidino-2-Phenylindole, Dihydrochloride (DAPI) (Vecta shield mounting medium with DAPI; Vector Lab, Inc.) on a slide immediately before imaging as described in section 2.2.14.

2.2.14 Fluorescence microscopy

Strains were cultured in the appropriate medium to a density of ~5x10^6 cells/ml. 2 µl of cell culture was transferred directly to a solid DMM (2% (w/v) agarose) pad made on a glass microscope slide (by pipetting 50 µl of liquid agarose onto one slide and compressing the agarose with second slide allowing the agarose pad to solidify, thereby creating a flat surface) and the residual medium was allowed to dry. A coverslip was placed over the cells on the agar pad and sealed with a Vaseline, Lanolin and Paraffin (VALAP) mixture (made by equal parts by weight) to prevent drying of the sample. Images were then obtained using either a True Confocal Scanner Leica TCS SP5 microscope (Leica Microsystems Ltd., Milton Keynes, UK) (section 2.2.14.2) or DeltaVision system wide-field deconvolution microscope (section 2.2.14.3). Image acquisition and subsequent deconvolution of images from the DeltaVision system was performed with softWoRx (applied precision) software. Deconvolution was performed with the following settings; Ratio = conservative, Number of cycles = 8 and Noise filtering = high.

2.2.14.1 Time-series live-cell imaging

Microscope slides for time-series imaging of live cells were prepared as in section 2.2.14. P-factor was added at the desired concentration to the DMM (2% (w/v) agarose) pad and imaged with either of the microscopes described in section 2.2.14.

2.2.14.2 Leica SP5 microscope

Cells were imaged by taking a Z-stack at time = 0 h and subsequently every 15 min for a period of 16 h, unless otherwise stated in the experiment. The imaging procedure was set up such that cells were focused at 0 h and the Z position noted (Z_{focus}). The Z-stack was then defined such that 20 Z-slice images would be obtained from Z_{focus} - 10 µm to Z_{focus} + 10 µm to allow for drift in the focal plane over the course of the experiment. The time-series experiment was setup such that both light-field and fluorescence images were generated.

Table 2.14: List of figures taken using Leica SP5

Figure 4.2a
Figure 4.5
Figure 4.7
Figure 4.7
Figure 4.8
Figure 4.12b
Figure 4.14
Figure 4.15
Figure 4.17
Figure 4.22
Figure 4.24
Figure 4.26
Figure 4.28
Figure D.1

2.2.14.3 DeltaVision wide-field microscope

Cells were imaged by taking Z-stacks from time = 0 h and subsequently every 15 min for a period of 16 h, unless stated otherwise in the experiment. The imaging procedure was set up such the bottom of the cell was focused at 0 h and the distance between that Z position and the coverslip was measured (Zdistance). At each time point in the series the Zdistance was kept constant before taking 20 Z-stacks of 0.3 µm.

Table 2.15: List of figures taken using DeltaVision

Figure 5.3
Figure 5.6
Figure 5.7b
Figure 5.8a
Figure 5.10
Figure 5.11
Figure 5.15
Figure 5.20
Figure 5.21
Figure 5.22a
Figure E.1
Figure E.2

2.2.15 Flow cytometry

Flow cytometry was performed using a Becton, Dickinson and Company (BD) LSR II flow cytometer (BD Biosciences, Oxford, UK).

2.2.15.1 Flow cytometry analysis of cell DNA content

Cells were grown in minimal medium to a density of $\sim$1x10^7 cells/ml (unless otherwise stated). 1 ml of culture was sonicated, harvested at 2000 rpm for 5 min and fixed in 1 ml of ice cold 70% (v/v) ethanol overnight. 300 µl of fixed cells were then washed in 3 ml of 50 mM sodium citrate and resuspended in 500 µl of 50 mM sodium citrate containing 0.1 mg/ml RNase A. Cells were incubated at 37°C for 2 h before the addition of 500 µl of 50 mM sodium citrate containing 8 g/ml propidium iodide. Up to 30,000 particles per sample were then analysed using the flow cytometer, measuring the intensities of staining with propidium iodide. Excitation was achieved using a 488 nm laser and emission detected using a 575/26 nm band pass filter with a 550 nm long pass filter. Protocol described by Sazer and Sherwood (1990) [229].

2.2.16 Cell viability assay

Analysis of cell viability was performed using the LIVE/DEAD® *Funga* Light™ yeast viability kit (Invitrogen Ltd.), which utilises two nucleic acid stains, propidium iodide and SYTO®9, which differ in ability to translocate across the cell membrane. Viable cells will only contain SYTO®9 whereas non-available cells that have a comprised cell membrane, will contain both dies. The reduction in SYTO®9 signal in non-viable cells caused by the

förster resonance energy transfer (FRET) between the two fluorophores is detected using flow cytometry and provides a quantitative measure of the percentage of non-viable cells within a population [230].

Cells were cultured to a density of $\sim 5x10^5$ cells/ml in DMM and 500 µl aliquots transferred to 2 ml Safe-lock tubes (Eppendorf Ltd.) containing P-factor pheromone (diluted in HPLC-grade methanol and dried to remove methanol). Following 16 h incubation at 29^oC on a rotating wheel, cells were washed twice in 1 ml PBS and stained in 1 ml PBS containing 1 µl SYTO®9 (3.34 mM in dimethyl sulfoxide) and 1 µl propidium iodide (20 mM in dimethyl sulfoxide). The percentage of cells containing both dyes was evaluated using a BD LSR II flow cytometer. Both dyes were excited using a 488 nm laser and emission detected using a 550 nm long pass filter with a 575/26 nm band pass filter for propidium iodide and a 505 nm long pass filter with a 530/30 nm band pass filter for SYTO®9.

2.2.17 Statistical significance

All statistical significance was calculated using pairwise comparisons with either one-way or two-way ANOVA with a Dunnet's multiple comparison test.

2.2.18 Image analysis

All image processing was performed using the open source software ImageJ (http://rsb.info.nih.gov/ij/). Cell segmentation and tracking was performed using the Quantitative Imaging of Membrane Proteins (QuimP) plugin for ImageJ, first described by Dormann *et al.* (2002) [231] and further developed to quantify spatio-temporal patterns of fluorescently labelled proteins in the cortex of moving cells [232–234]. All images to be analysed with QuimP were processed by creating maximal projections from Z-stacks and subtracting background pixel intensity prior to analysis unless otherwise stated in the experiment.

2.2.18.1 Cell segmentation and tracking

QuimP software was used to segment individual cells within an image. Cell selection was where possible, randomised by using a random number generator to obtain a coordinate on the image and subsequently selecting the closest cell to this co-ordinate (based on distance to the closest cell edge).

2.2.18.2 Single cell quantification

The image analysis software QuimP calculates fluorescence measurements from pixel intensities and cell size measurements based on the cell outline for each single time point image or for each frame of a given time-series set of images. Statistical significance of the data

generated from QuimP was analysed using GraphPad Prism software version 6.0 for Mac OS X (GraphPad Software Inc., San Diego, CA, USA).

2.2.19 Computational methods

Modelling and simulation were performed using code written and implemented within Mathematica 9.0.1.0 (Wolfram Research Inc., USA). The *xCellerator* (California Institute of Technology, USA, 2005) package for Mathematica was used to facilitate *in silico* experimentation and hypothesis modification. The package takes a reaction scheme as input and produces an equivalent system of ordinary differential equations (ODEs).

2.2.19.1 Numerical differential equation Solver

Systems of ODEs were solved using the in-built *Mathematica* function `NDSolve` with the default options. This function has a range of available algorithms at its disposal and selects the most appropriate depending on the type of system being solved. It automatically adjusts step-size to achieve the specified accuracy and precision, which in all cases were set to `Automatic` and found to function without introducing any significant numerical errors.

2.2.19.2 Simulation of dose-response Curves

To simulate the addition of pheromone after a certain time, the ligand concentration was increased from zero up to a range of concentrations (1 nM - 100 µM) corresponding approximately to the concentrations seen by cells in an assay. The system was allowed to reach steady state in the absence of ligand before it was added. The increase in ligand concentration was not quite instantaneous, instead a *tanh* function was used to avoid numerical errors that can occur at discontinuities during the solving process. It is assumed that binding of ligand to receptor depletes the local availability of ligand. The output is taken to be the number of active effector complexes and is integrated over the duration of the simulated assay to mimic the accumulation of the reporter gene β-galactosidase, which in *S. pombe* is very stable. The accumulated quantity is plotted against the stimulating quantity of ligand to produce a simulated dose-response curve.

2.2.19.3 Simulated modified strains

Modifications to the simulated wild type (WT) strain were achieved by altering the values used for reaction rate constants, usually setting some of them to zero to prevent the required reactions from occurring, or by altering the initial concentrations of some species to simulate additional plasmid-borne expression or gene deletions.

2.3 Constructs

2.3.1 Creation of constructs for gene disruption

This section describes the generation of constructs to allow insertion of exogenous DNA (such as the *ura4* cassette) in place of the endogenous gene through homologous recombination. All constructs were created in the pBluscriptKS (pKS, Stratagene) vector (JD1776). Table 2.16 details all integration constructs used in this study.

Name	Description	source
JD3535	pKS-*gap1::ura4*	C. Weston, PhD thesis, 2013
JD3903	pKS-*cki1::ura4*	This study
JD3905	pKS-*cki3::ura4*	This study
JD3908	pKS-*cki2::ura4*	This study

Table 2.16: **Plasmids used for gene integration**

2.3.1.1 Disruption of *cki1*

The *cki1* open reading frame (ORF) was disrupted by insertion of the *ura4* cassette into a 9 base pair (bp) region from position 1 from the ATG start codon. To drive the integration of the *ura4* cassette, a 452 bp 5' untranslated region (UTR), together with the first 419 bp of the *cki1* ORF was amplified from *S. pombe* genomic DNA using sense (JO3125) and antisense (JO3126) oligonucleotide, which introduced an *Xba*I and *Eco*RI site at each end of the PCR product, respectively. The 971 bp PCR product and the pKS vector (JD1776) was digested with *Xba*I and *Eco*RI before ligating.

Inverse PCR amplification was performed with a sense oligonucleotide (JO3078) starting from position 10 relative to position 1 from the ATG codon and an antisense oligonucleotide (JO3075) starting from position -1 relative to the ATG codon. These oligonucleotides contained half a *Bam*HI site, such that when the PCR product was ligated to re-circularise the vector this introduced a full *Bam*HI site and removed the first 9 bp of the *cki1* ORF.

Finally, the *ura4* cassette was inserted as a *Bam*HI fragment into the *Bam*HI digested integration construct described above to produce JD3903 (Figure A.1). This construct was used to produce *Δcki1* strains (containing the *ura4*$^+$ cassette running antisense relative to the direction of the *cki1* ORF) through homologous recombination, using a lithium acetate transformation [225] of *S. pombe* with *Xba*I and *Eco*RI digested JD3903.

2.3.1.2 Disruption of *cki2*

The *cki2* ORF was disrupted through insertion of the *ura4* cassette into a 8 bp region relative to position 1 from the ATG codon. To drive the integration of the *ura4* cassette a 469 bp 5' UTR together with the first 435 bp of the *cki2* ORF was amplified from *S. pombe* genomic DNA using a sense (JO3127) and antisense (JO3128) oligonucleotide, which introduced an *Xba*I and *Hind*III site, respectively. The 904 bp PCR product and pKS vector (JD1776) was digested with *Xba*I and *Hind*III before ligating.

Inverse PCR amplification was performed vector described above with a sense oligonucleotide (JO3088) starting from position 9 relative to position 1 from the ATG codon and an antisense oligonucleotide (JO3082) starting from position -1 relative to the ATG codon. These oligonucleotides contained half a *Bam*HI site, such that when the PCR product was ligated to re-circularise the vector. This introduced a full *Bam*HI site in place of the first 8 bp of the *cki2* ORF.

Finally, the *ura4* cassette was inserted as a *Bam*HI fragment into *Bam*HI digested integration construct to produce JD3908 (Figure A.2). This construct can be used to produce *Δcki2* strains (containing the *ura4*$^+$ cassette running antisense relative to the direction of the *cki2* open reading frame) through homologous recombination, using a lithium acetate transformation [225] of *S. pombe* with *Xba*I and *Hind*III digested JD3908.

2.3.1.3 Disruption of *cki3*

The *cki3* ORF was disrupted through insertion of the *ura4* cassette into a 9 bp region relative to position 1 from the ATG codon. To drive the integration of the *ura4* cassette a 480 bp 5' UTR together with the first 422 bp of the *cki3* ORF was amplified from *S. pombe* genomic DNA using a sense (JO3129) and antisense (JO3130) oligonucleotide, which introduced an *Xba*I and *Hind*III site respectively. The PCR product and pKS vector (JD1776) was digested with *Xba*I and *Hind*III before ligating.

Inverse PCR amplification was performed on the resulting vector with a sense oligonucleotide (JO3132) starting from position 10 relative to position 1 from the ATG codon and an antisense oligonucleotide (JO3131) starting from position -1 relative to the ATG codon. These oligonucleotides contained half a *Bam*HI site, such that when the PCR product was ligated to re-circularise the vector. This introduced a full *Bam*HI site in place of the first 9 bp of the *cki3* ORF.

Finally, the *ura4* cassette was inserted as a *Bam*HI fragment into *Bam*HI digested integration construct to produce JD3905 (Figure A.3). This construct can be used to produce *Δcki3* strains (containing the *ura4*$^+$ cassette running antisense relative to the direction of the *cki3* open reading frame) through homologous recombination, using a lithium acetate transformation [225] of *S. pombe* with *Xba*I and *Hind*III digested JD3905.

2.3.2 Constructs for constitutive gene expression

This section describes the generation of constructs to allow expression of genes from the pREP3x or pREP4x vectors. The pREP vectors, which contain the inducible *nmt1* (no message in thiamine) promoter allow the control of gene expression through the addition or removal of thiamine from the growth medium and are used to control the expression of the exogenous genes in *S. pombe* [235].

Yeast strains used in this study are auxotrophic in the *S. pombe* gene *leu1*, which encodes β-isopropylmalate dehydrogenase, a protein required for leucine biogenesis [236]. pREP3x constructs exploit this auxotropic phenotype by using the *leu1* for selection. pREP3x plasmids contain the *S. cerevisiae LEU2* gene, which complements for the loss of *leu1* [235]. Similarly, pREP4x constructs use the *S. pombe* gene *ura4* for selection, as these plasmids contain the *ura4* gene [237]. *ura4* encodes orotidine-5'-phosphate decarboxylase, which is essential for biogenesis of uracil. *ura4* can be used for both positive and negative selection. Growth in the presence of 5' fluoroorotic acid (FOA) causes cytotoxicity, whilst the absence of uracil leads to auxotrophy for *ura4* disruptants [238].

It should be noted that throughout this study a modified version of pREP3x was used, which contains an *Eco*RV site directly before the *Bam*HI site in the pREP multiple cloning site (MCS). Table 2.17 lists all vectors used in this study to generate constructs for controlled gene expression and Table 2.18 lists all the vectors used to express exogenous genes throughout this study.

The following nomenclature has been used to describe the expression of genes and binding domains etc. in this study. *S. pombe* cells transformed with pREP3x-Yfg1 and abbreviated to pYfg1 for example, implies that cells express Yfg1.

Name	Description	source
JD1776	pKS	Stratagene
JD2320	pGADT7	BD clontech
JD2935	pREP3x-Mam2Δ5	[173]
JD3374	pKS-Mam2Δtail	E. McCann, PhD thesis, 2010
JD3386	pREP3x	[235]
JD3453	pKS-mCherry	M. Bond, PhD thesis, 2012
JD3590	pREP3x-Mam2-mCherry	[173]

Table 2.17: **Plasmids used to generate constructs for increased gene expression**

2.3.2.1 Creation of pREP3x-Cki constructs

These constructs were used in section 4.5.9 to elucidate the effect of constitutive expression of either Cki1, Cki2 and Cki3 in *S. pombe* cells. The ORFs of Cki1, Cki2 and Cki3 were amplified by PCR from an *S. pombe* cDNA library (created by Dr. Stephen J. Elledge [239] and kindly provided by Professor Jonathan Millar, University of Warwick) using a sense and antisense oligonucleotide, which introduced a full *Bam*HI site at either end of the PCR fragment (for oligonucleotides see Figure A.4). The PCR product was then digested with *Bam*HI and cloned into *Bam*HI digested pREP3x (JD3386) to create pREP3x-Cki1 (JD3893), pREP3x-Cki2 (JD3766) and pREP3x-Cki3 (JD3782) (Figure A.4), which enables expression of Cki1, Cki2 and Cki3 respectively in *S. pombe* under the control of the inducible *nmt1* promoter.

2.3.2.2 Creation of pGADT7-Cki1/Cki2/Cki3 constructs

These constructs were used in section 5.2 to elucidate a possible protein-protein interaction between Cki1/ Cki2/ Cki3 with either the C-terminal tail of Mam2 or Rgs1. The pGADT7 vector (JD2320) was designed, such that when a protein of interest is fused to the GAL4 transcriptional activation domain (AD) and when co-transformed with a protein of interest expressed from pGBKT7 vector fused to the GAL4 DNA-binding domain (BD), induces transcription of the reporter gene *lacZ*. Expression of β-galactosidase will only occur if these two proteins of interest interact and bind to the GAL4-responsive promoter, indicating a possible protein-protein interaction.

The ORFs of Cki1, Cki2 and Cki3 were amplified by PCR from an *S. pombe* cDNA library (created by Dr. Stephen J. Elledge [239] and kindly provided by Professor Jonathan Millar, University of Warwick) using a sense and antisense oligonucleotide, which introduced a full *Bam*HI site at either end of the PCR fragment (for oligonucleotides see Figure A.5). The PCR product was then digested with *Bam*HI and cloned into the *Bam*HI digested MCS of pGADT7 (JD2320) to create pGADT7-Cki1 (JD3770), pGADT7-Cki2 (JD3771) and pGADT7-Cki3 (JD3763) (Figure A.5), which enables expression of Cki1, Cki2 and Cki3 respectively in *S. cerevisiae* under the control of the T7 promoter.

2.3.2.3 Creation of pREP3x-Mam2^{2K}-mCherry

Ubiquitination typically occurs on lysine residues. There are four lysine residues in the C-terminal tail of Mam2: at position 307, 329, 345 and 346 from codon 1 from the ATG. This construct was used in Chapter 5 to elucidate the effect of removing the two lysine codons 307 and 329 on the signalling behaviour and localisation of Mam2.

Mam2 tagged mCherry was amplified on pREP3x-Mam2-mCherry (JD3590) (a plasmid where the glutamine at position 304 (Q304) relative to position 1 (ATG) has been altered

from CAA to CAg so that this residue forms the front half of a *Pvu*II restriction site), using a mutagenic sense oligonucleotide (JO2955), initiated directly downstream of Q304 and an antisense oligonucleotide (REP2). Amplification with JO2955 introduced a mutation at the 307^{th} and 329^{th} codons of Mam2, changing the lysine codon (AAA) to arginine (AgA) by a single base mutation. The PCR product (Figure A.6, highlighted in grey) was ligated into *Pvu*II digested pKS-Mam2Δtail. The small fragment produced from a digest with *Xho*I and*Bam*HI digested pKS-Mam2^{2K}-mCherry was ligated into *Xho*I/*Bam*HI digested pREP3x (JD3386) to produce pREP3x-Mam2^{2K}-mCherry (JD3802), which enables expression of the mutated receptor in *S. pombe* cells under the control of the inducible *nmt1* promoter (Figure A.6).

2.3.2.4 Creation of pREP3x-Mam2^{4K}-mCherry

To abolish ubiquitination of the C-terminal tail of Mam2, all four lysine residues (at codon positions 307, 329, 345 and 346 from codon 1 from the ATG) were either mutated or removed to elucidate their influence on the localisation and signalling behaviour of Mam2 (Chapter 5).

pREP3x-Mam2Δ5 (JD2935) (where the last 5 amino acid residues of Mam2 have been removed, which include lysine residues 345 and 346 and this plasmid has also been altered at Q304 from CAA to CAg so that this residue forms the front half of a *Pvu*II restriction site) was amplified with sense (JO2955) and antisense (REP2) oligonucleotide to create a PCR product that changed the 307^{th} and 329^{th} lysine (AAA) codons to arginines (AgA). The PCR product (Figure A.7, highlighted in grey) was ligated into *Pvu*II digested pKS-Mam2Δtail to create pKS-Mam2^{4K}. A second PCR amplification was performed on pKS-Mam2^{4K} with sense (REP1) and antisense (JO3038) oligonucleotides. This produces a DNA fragment (Figure A.7, boxed by a red dotted line) that includes an *Xba*I site upstream of the Mam2 ATG codon and excludes the Stop codon, such that when the fragment is digested with *Xba*I and ligated into *Xba*I/ *Pvu*II digested pKS-mCherry it creates a vector that lacks any of the lysine residues in the C-terminal tail of Mam2 and is tagged with mCherry (pKS-Mam2^{4K}-mCherry).

Finally, the small fragment produced when digesting pKS-Mam2^{4K}-mCherry with *Xho*I and *Bam*HI was ligated into *Xho*I/*Bam*HI digested pREP3x (JD3386) to produce pREP3x-Mam2^{4K}-mCherry (JD3804), which enables expression of the mutated receptor in *S. pombe* under the control of the inducible *nmt1* promoter (Figure A.7).

Name	Description	Source
JD557	pREP41x	[98]
JD636	pREP41x-Sxa2	[98]
JD1170	pGBKT7	BD Clontech
JD1627	pREP3x-Mam2	[184]
JD2261	pREP3x-GFP	[222]
JD2320	pGADT7	BD Clontech
JD2332	pREP3x-Gpa1	[82]
JD2388	pREP4x-Rgs1	[82]
JD2555	pREP3x-Rgs1	[87]
JD2673	pREP3x-Gpa1^{G223S}	[82]
JD2880	pREP3x-Mam2Δtail	[173]
JD2885	pREP3x-Mam2-GFP	[184]
JD2999	pREP3x-Mam2Δ5-GFP	[173]
JD3001	pREP3x-Mam2Δ13-GFP	[173]
JD3003	pREP3x-Mam2Δ21-GFP	[173]
JD3007	pREP3x-Mam2Δ37-GFP	[173]
JD3180	pGADT7-Rgs1	[173]
JD3182	pGBKT7-Rgs1	[173]
JD3221	pGBKT7-Mam2tail	[173]
JD3280	pGBKT7-Map3tail	E. McCann, PhD thesis, 2010
JD3284	pGBKT7-STE2tail	E. McCann, PhD thesis, 2010
JD3317	pREP3x-Mam2Δtail-GFP	[173]
JD3386	pREP3x	[235]
JD3514	pREP3x-mCherry	[228]
JD3590	pREP3x-Mam2-mCherry	[173]
JD2621	pREP3x-Mam2Δtail-mCherry	[173]
JD3681	pREP-RBD	M. Bond, University of Warwick
JD3763	pGADT7-Cki3	This study
JD3766	pREP3x-Cki2	This study
JD3770	pGADT7-Cki1	This study
JD3771	pGADT7-Cki2	This study
JD3782	pREP3x-Cki3	This study
JD3893	pREP3x-Cki1	This study
JD3802	pREP3x-Mam2^{2K}-mCherry	This study
JD3804	pREP3x-Mam2^{4K}-mCherry	This study

Table 2.18: **Inducible plasmids** The name, description and source of the plasmids used in this study.

Chapter 3

Extending the mathematical model

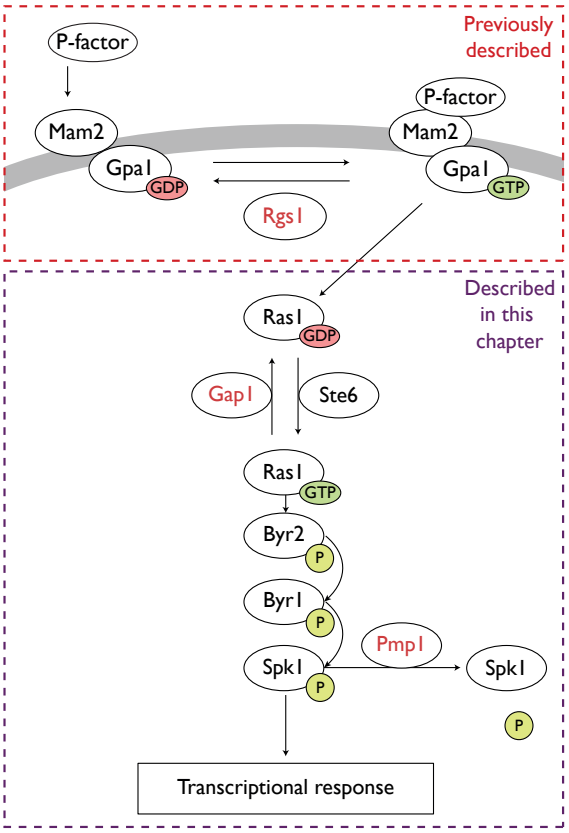

FIGURE 3.1: **The current *S. pombe* model**. P-factor binds the GPCR Mam2 promoting GDP/GTP exchange on the G protein Gpa1. GTP-bound Gpa1 activates Ras1 via the GEF Ste6, transducing signalling via sequential phosphorylation of a MAPK cascade (Byr2, Byr1 and Spk1), resulting in activation of Ste11 (not included), which induces transcription of mating-responsive genes. There are various points of regulation through the pathway (highlighted with red text) including: Rgs1, which catalyses the hydrolysis of Gpa1. Gap1, which hydrolyses Ras1 and Pmp1 a phosphatase that regulates the action of Spk1 (Figure adapted form [50]). The red dashed box highlights components described in the previous models and the purple box contains components that are incorporated into the model in this chapter.

3.1 Chapter aim

This chapter extends the previously discussed mathematical models of the *S. pombe* mating-response pathway to include all known components, including known points of adaptation (signal regulation) (Figure 3.1).

3.2 Background

The first kinetic model of the *S. pombe* mating-response pathway by Smith *et al.* (2009) was developed on quantitative data via the use of *lacZ* reporter strains [190]. These types of assays will henceforth be referred to as end-point data, as the assay is performed following 16 h of pheromone treatment (for details on how these reporter strains are used as an indirect measure of pheromone activation see section 2.1.7.2). The first mathematical model could only reproduce the end-point data with the existence of a novel inactive GTP-bound state of the G protein [190]. The inactive-GTP bound state placed significant importance on rapid GTP-hydrolysis rather than retention of a GTP-bound state to induce a maximal transcriptional response. They suggested that the RGS protein could act as both a positive regulator, accelerating the conversion of inactive-GTP to GDP on the G protein (thus increasing the pool of GDP-bound G protein to associate with ligand-occupied receptors for reactivation) and a negative regulator, by hydrolysing GTP prior to effector activation via the G protein (Figure 3.2).

The second model by Croft *et al.* (2013) was an extension of the first and imposed spatial regulation of the RGS species [173]. A combination of confocal imaging and end-point data demonstrated that a physical interaction between the RGS species and the C-terminal domain of Mam2 (the GPCR) was essential for RGS plasma membrane localisation and consequent hydrolysis of the G protein. These findings highlighted the importance of the receptor tail in transducing and regulating signalling response in *S. pombe*.

Previous modelling efforts were incapable of recapitulating all end-point data as only terms for describing pheromone binding Mam2 (a GPCR), signal transduction via Gpa1 (a G protein) and signal regulation by Rgs1 (the RGS species) were described (Figure 3.1). The signal transduction pathway is more complex than this. GTP-bound Gpa1 promotes GDP/GTP exchange on the monomeric G protein Ras1, signals via a MAPK cascade to phosphorylate the transcription factor Ste11, which then up-regulates mating responsive

genes (including *sxa2*) (reviewed in [50]). Therefore, a complete model that incorporates all known components of the pathway will be described in this chapter.

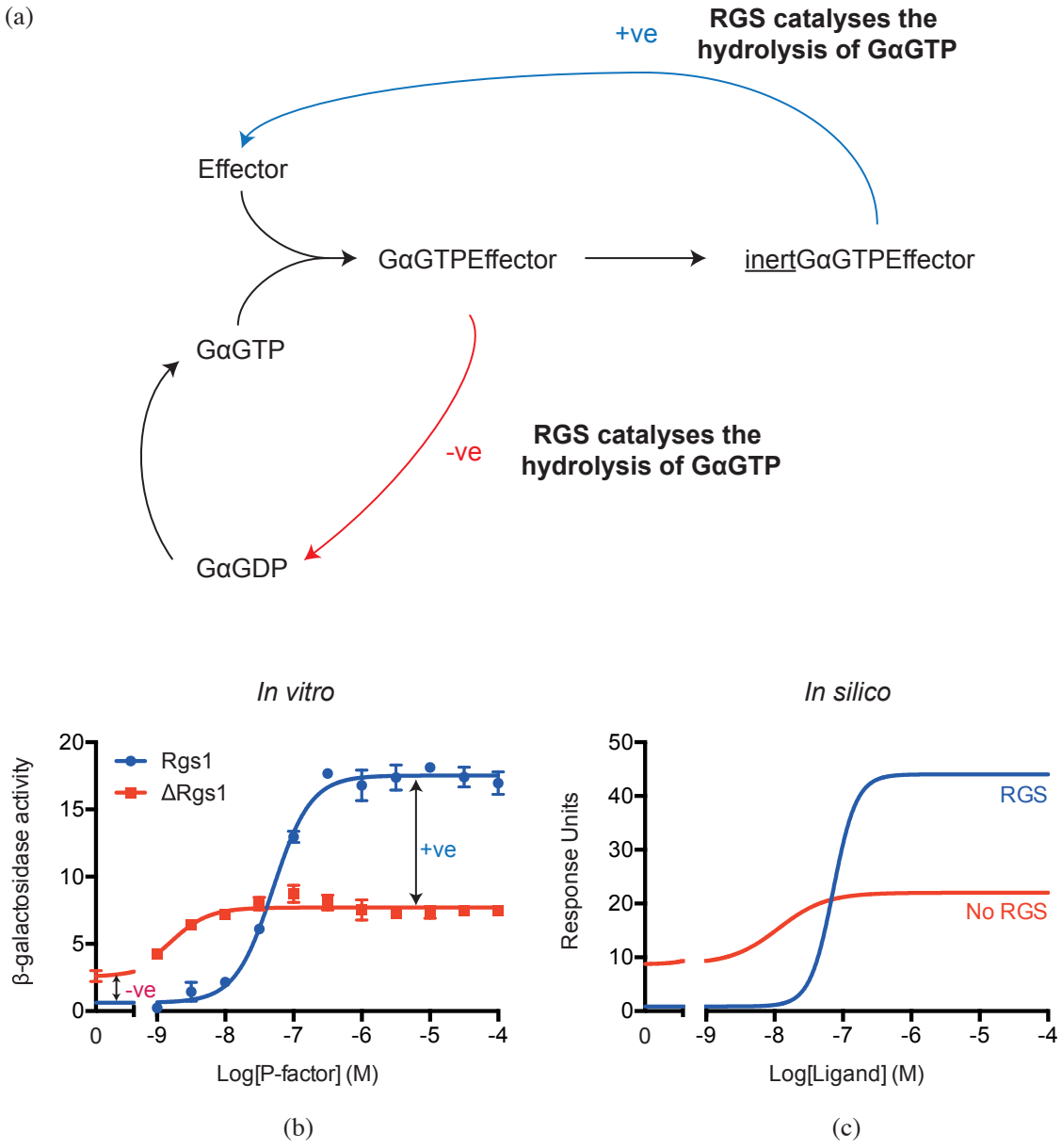

FIGURE 3.2: **Rgs1 can both negatively and positively regulate signalling.** (a) A model of the inert state hypothesis. The GTP-bound Gα-subunit enters an inert state while remaining associated with an effector molecule following activation of downstream signalling. GTP-hydrolysis is the only exit from the inert state and an RGS protein can both positively and negatively regulate signalling through acceleration of GTP-hydrolysis. (b) *In vitro* end-point data adapted from Smith *et al.* (2009) [190], which highlights the negative (-ve) and positive (+ve) role of Rgs1. (c) Smith *et al.* (2009) *in silico* output showing that simulating the deletion of RGS recapitulates the experimental data.

3.3 Implementation of model

The implementation of the Croft *et al.* (2013) model [173], which included the inert state hypothesis and spatial regulation of Rgs1 is summarised below to illustrate how the models described in this chapter were simulated and to set a benchmark for extending the model.

3.3.1 The addition of ligand

In the *in vitro* experiments *S. pombe* strains were grown to mid-exponential growth phase prior to treatment with pheromone. To simulate this *in silico*, the initial ligand concentration, L(0), was set to zero for a simulated period of 14 h (t_0=14 h). This enabled the system of ODEs to equilibrate before the addition of ligand. The concentration of ligand was then rapidly but not discontinuously increased to the specified concentration L(t_0) using Equation 3.1 (Figure 3.3).

$$L(t) = \frac{L(t_0)}{2}\Big(tanh\big(b(t-t_0)\big) + tanh\big(bt_0\big)\Big) \tag{3.1}$$

Increasing the constant b alters the sharpness of the transition, i.e. closer to a step-function. The value of b used in the simulations was 100 as this was found to be sufficiently sharp to allow the application of ligand close to instantaneous and yet smooth enough that the numerical differential equation solving algorithm remained accurate in this region [173, 190].

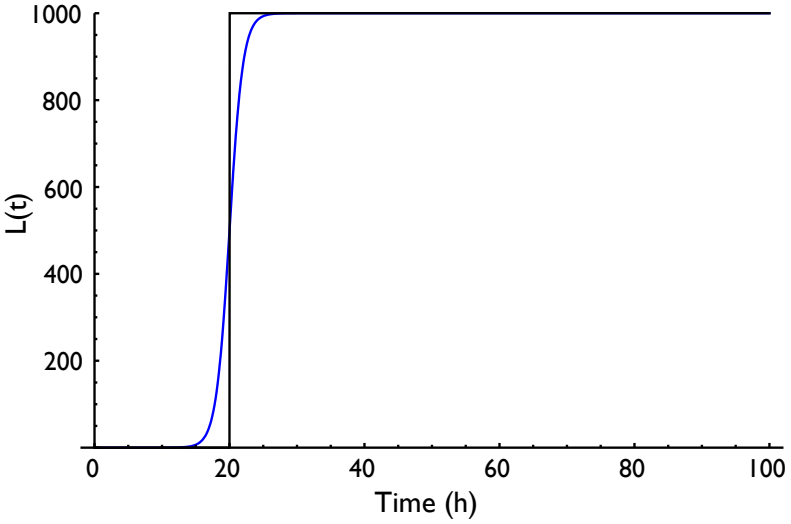

FIGURE 3.3: **Ligand application.** Comparison between ligand application using a discontinuous step function (black) and the smooth tanh function described in Equation 3.1 (blue), with L(t_0)=1000 and b=0.5 for visualisation.

3.3.2 Measuring the response

The *S. pombe* pheromone-response was measured by determining the β-galactosidase activity following a period of treatment with pheromone (typically 16 h). Measuring β-galactosidase activity per cell is a proxy for the concentration of β-galactosidase. This therefore provides an indirect measure of *sxa2* transcription and hence, signal transduction through the pathway. This can be simulated in *silico* by an integral from t=0 h up to a short time after the system reaches a new equilibrium t_{assay} (following treatment with ligand) [11]. A cascade of linear relaxation elements (z1(t), z2(t) and z3(t)) was applied to the number of active effector molecules (in the case of the Croft *et al.* (2013) model this is GαGTPEffector however, as the model was extended this species changed) and $\int_0^{t_{\text{assay}}} z3(t)$ was the quantity measured. The cascade was applied by augmenting the system of differential equations with Equations 3.2 - 3.4.

$$z1'(t) = \gamma G\alpha\text{GTPEffector} - \gamma z1(t) \tag{3.2}$$

$$z2'(t) = \gamma z1(t) - \gamma z2(t) \tag{3.3}$$

$$z3'(t) = \gamma z2(t) - \gamma z3(t) \tag{3.4}$$

These equations empirically and simplistically model the components downstream of the G protein and reflects the time difference between the dynamics of the G protein cycle and expression of β-galactosidase. A value of $\gamma=\frac{3}{2}$ was used to stretch the response time to that observed in time-course data [190]; induction of β-galactosidase in response to pheromone becomes detectable between 2 h and 4 h [11]. It should be noted that as the model was extended the cascade of relaxation elements were removed.

3.3.2.1 The model output

When reaction rates (k) were unknown, these were assigned an arbitrary value and heuristically determined to best fit the experimental data. This technique was implemented in the previous mathematical models of the *S. pombe* mating-response and is a technique employed to extend the model in this chapter. The Croft *et al.* (2013) model reaction scheme with the corresponding reaction rates k (Table 3.2) was transformed into a systems of ODEs (as detailed in 2.2.19). The resulting systems of ODEs can be simulated with the initial species concentrations as described in Table 3.1 and solved using the in-built Mathematica function NDSolve with the default options.

Species	Concentration (nM)	Assumptions	Source
L	0 - 100,000		
R	205	Calculated	[184]
GαGDP	205	Assumed 1:1 ratio with R	[213, 215, 240–242]
Gβγ	205	1:1 ratio with GαGDP	[213, 215, 240–242]
RGSc	60	Same as *S. cerevisiae* RGS species	[241]
Effector	205	1:1 ratio with GαGDP	[190]
All other species concentraions were set to 0 nM			

TABLE 3.1: **Initial species concentrations used to simulate the wild type *S. pombe* response.** Initial (when t=0 h) concentrations of species before the system is equilibrated and source/or justification for using these concentrations are described.

Ligand / G protein signalling			
L + R → LR	k_1	0.0025	$nM^{-1}h^{-1}$
Gαβγ+ R → RGαβγ	k_2	0.005	$nM^{-1}h^{-1}$
Gαβγ + LR → LRGαβγ	k_3	0.02	$nM^{-1}h^{-1}$
L + RGαβγ → LRGαβγ	k_4	0.005	$nM^{-1}h^{-1}$
L + RRGSm → LRRGSm	k_5	0.005	$nM^{-1}h^{-1}$
Gαβγ + RRGSm → RRGSmGαβγ	k_6	0.005	$nM^{-1}h^{-1}$
Gαβγ + LRRGSm → LRRGSmGαβγ	k_7	0.02	$nM^{-1}h^{-1}$
L + RRGSmGαβγ→ LRRGSmGαβγ	k_8	0.005	$nM^{-1}h^{-1}$
G protein activation			
LRGαβγ → GαGTP + Gβγ + LR	k_9	50	h^{-1}
Gαβγ → GαGTP + Gβγ	k_{10}	0.2	h^{-1}
LRRGSmGαβγ → GαGTP + Gβγ + LRRGSm	k_{11}	40	h^{-1}
Effector + GαGTP → GαGTPEffector	k_{12}	10	$nM^{-1}h^{-1}$
RGS trafficking			
RRGSc → RRGSm	k_{13}	0.0005	h^{-1}
RRGSm → RRGSc	k_{14}	0.005	h^{-1}
R + RRGSc → RRGSm	k_{15}	0.1	$nM^{-1}h^{-1}$
RRGSm → R + RRGSm	k_{16}	100	h^{-1}
LR + RRGSc → LRRGSm	k_{17}	0.1	$nM^{-1}h^{-1}$
LRRGSm → LR + RRGSm	k_{18}	100	h^{-1}
RGαbg + RRGSc → RRGSmGαβγ	k_{19}	0.1	$nM^{-1}h^{-1}$
RRGSmGαβγ → RGαβγ + RRGSm	k_{20}	0.1	h^{-1}
LRGαβγ + RRGSc → LRRGSmGαβγ	k_{21}	0.1	$nM^{-1}h^{-1}$
GαGTP + RRGSc → RRGSmGαGTP	k_{22}	60	$nM^{-1}h^{-1}$
RRGSmGαGTP → GαGTP + RRGSc	k_{23}	0.05	h^{-1}
inertGαGTPEffector + RRGSc → RRGSminertGαGTPEffector	k_{24}	0.0001	$nM^{-1}h^{-1}$
Switching off / recycling G protein			
GαGTPEffector → Effector + inertGαGTP	k_{25}	1	h^{-1}
GαGTP → GαGDP	k_{26}	0.005	h^{-1}
GαGTP + RRGSm → RRGSmGαGTP	k_{27}	500	$nM^{-1}h^{-1}$
RRGSmGαGTP → GαGDPP + RRGSc	k_{28}	2.5	h^{-1}
GαGTP + LRRGSm → LRRGSmGαGTP	k_{29}	100	$nM^{-1}h^{-1}$
LRRGSmGαGTP → GαGDPP + LRRGSm	k_{30}	2.5	h^{-1}
GαGTP + RRGSm → RRGSmGαGTP	k_{31}	0.5	$nM^{-1}h^{-1}$
RRGSmGαGTP → GαGDPP + RRGSm	k_{32}	0.5	h^{-1}
inertGαGTPEffector → GαGDPP + Effector	k_{33}	0.005	h^{-1}
inertGαGTPEffector + RRGSm → RRGSminertGαGTPEffector	k_{34}	50	$nM^{-1}h^{-1}$
RGSminertGαGTPEffector → GαGDPP + RRGSc + Effector	k_{35}	0.3	h_{-1}
inertGαGTPEffector + LRRGSm → LRRGSminertGαGTPEffector	k_{36}	50	$nM^{-1}h^{-1}$
LRRGSminertGαGTPEffector → GαGDPP + LRRGSm + Effector	k_{37}	0.3	h^{-1}
GαGDPP → GαGDP + P	k_{38}	1000	h^{-1}
GαGDP + Gβγ → Gαβγ	k_{39}	1000	$nM^{-1}h^{-1}$
P → ∅	k_{40}	10	h^{-1}

TABLE 3.2: **The Croft *et al.* (2013) model reaction scheme.** 40 reactions are described each with an associated rate constant (k). Reactions included terms for the inert state hypothesis of the Gα species (inertGαGTP) and the spatial regulation of RGS, with separate cytoplasmic (RGSc) and membrane bound RGS (RGSm) species [173].

Effector	$Effector'(t) = -k_{12}Effector(t)G\alpha GTP(t) + k_{25}G\alpha GTPEffector(t)$
$G\alpha\beta\gamma$	$G\alpha bg'(t) = -k_{10}G\alpha\beta\gamma(t) - k_3G\alpha\beta\gamma(t)LR(t) - k_2G\alpha\beta\gamma(t)R(t) + k_{39}G\beta\gamma(t)G\alpha GDP(t) - k_7G\alpha\beta\gamma(t)LRRGSm(t) - k_6G\alpha\beta\gamma(t)RRGSm(t)$
$G\beta\gamma$	$G\beta\gamma'(t) = k_{10}G\alpha\beta\gamma(t) + k_9LRG\alpha\beta\gamma(t) - k_{39}G\beta\gamma(t)G\alpha GDP(t) + k_{11}LRRGSmG\alpha\beta\gamma(t)$
L	$L'(t) = -\frac{1}{2}k_1L(t)R(t)(Tanh(t_0b) - Tanh(b(t_0-t))) - \frac{1}{2}k_4L(t)RG\alpha\beta\gamma(t)(Tanh(t_0b) - Tanh(b(t_0-t))) - \frac{1}{2}k_5L(t)(Tanh(t_0b) - Tanh(b(t_0-t)))RRGSm(t) - \frac{1}{2}k_8L(t)(Tanh(t_0b) - Tanh(b(t_0-t)))RRGSmG\alpha\beta\gamma(t)$
LR	$LR'(t) = -k_3G\alpha\beta\gamma(t)LR(t) + k_9LRG\alpha\beta\gamma(t) + \frac{1}{2}k_1L(t)R(t)(Tanh(t_0b) - Tanh(b(t_0-t))) + k_{18}LRRGSm(t) - k_{17}LR(t)RRGSc(t)$
$LRG\alpha\beta\gamma$	$LRG\alpha\beta\gamma'(t) = k_3G\alpha\beta\gamma(t)LR(t) - k_9LRG\alpha\beta\gamma(t) + \frac{1}{2}k_4L(t)RG\alpha\beta\gamma(t)(Tanh(t_0b) - Tanh(b(t_0-t))) - k_{21}LRG\alpha\beta\gamma(t)RRGSc(t)$
P	$P'(t) = -k_{40}P(t) + k_{38}G\alpha GDPP(t)$
R	$R'(t) = -k_2G\alpha\beta\gamma(t)R(t) - \frac{1}{2}k_1L(t)R(t)(Tanh(t_0b) - Tanh(b(t_0-t))) - k_{15}R(t)RRGSc(t) + k_{16}RRGSm(t)$
$RG\alpha\beta\gamma$	$RG\alpha bg'(t) = k_2G\alpha\beta\gamma(t)R(t) - \frac{1}{2}k_4L(t)RG\alpha\beta\gamma(t)(Tanh(t_0b) - Tanh(b(t_0-t))) - k_{19}RG\alpha\beta\gamma(t)RRGSc(t) + k_{20}RRGSmG\alpha\beta\gamma(t)$
$G\alpha GDP$	$G\alpha GDP'(t) = -k_{39}G\beta\gamma(t)G\alpha GDP(t) + k_{38}G\alpha GDPP(t)$
$G\alpha GDPP$	$G\alpha GDPP'(t) = -k_{38}G\alpha GDPP(t) + k_{26}G\alpha GTP(t) + k_{33}inertG\alpha GTP(t) + k_{30}LRRGSmG\alpha GTP(t) + k_{37}LRRGSminertG\alpha GTP(t) + k_{28}RRGSmG\alpha GTP(t) + k_{35}RRGSminertG\alpha GTP(t) + k_{32}RRGSmG\alpha GTP(t)$
$G\alpha GTP$	$G\alpha GTP'(t) = k_{10}G\alpha\beta\gamma(t) + k_9LRG\alpha\beta\gamma(t) - k_{26}G\alpha GTP(t) - k_{12}Effector(t)G\alpha GTP(t) - k_{29}G\alpha GTP(t)LRRGSm + k_{11}LRRGSmG\alpha\beta\gamma(t) - k_{22}G\alpha GTP(t)RRGSc(t) - k_{27}G\alpha GTP(t)RRGSm(t) + k_{23}RRGSmG\alpha GTP(t) - k_{31}G\alpha GTP(t)RRGSm(t)$
$G\alpha GTPEffector$	$G\alpha GTPEffector'(t) = k_{12}Effector(t)G\alpha GTP(t) - k_{25}G\alpha GTPEffector(t)$
inertGαGTP	$inertG\alpha GTP'(t) = k_{25}G\alpha GTPEffector(t) - k_{33}inertG\alpha GTP(t) - k_{36}inertG\alpha GTP(t)LRRGSm(t) - k_{24}inertG\alpha GTP(t)RRGSc(t) - k_{34}inertG\alpha GTP(t)RRGSm(t)$
LRRGSm	$LRRGSm'(t) = -k_{18}LRRGSm(t) - k_7G\alpha\beta\gamma(t)LRRGSm(t) - k_{29}G\alpha GTP(t)LRRGSm(t) - k_{36}inertG\alpha GTP(t)LRRGSm(t) + k_{11}LRRGSmG\alpha\beta\gamma(t) + k_{30}LRRSmG\alpha GTP(t) + k_{37}LRRGSminertG\alpha GTP(t) + k_{17}LR(t)RRGSc(t) + \frac{1}{2}k_5L(t)(Tanh(t_0b) - Tanh(b(t_0-t)))RRGSm(t)$
$LRRGSmG\alpha\beta\gamma$	$LRRGSmG\alpha\beta\gamma'(t) = k_7G\alpha\beta\gamma(t)LRRGSm(t) - k_{11}LRRGSmG\alpha\beta\gamma(t) + k_{21}LRG\alpha\beta\gamma(t)RRGSc(t) + \frac{1}{2}k_8L(t)(Tanh(t_0b) - Tanh(b(t_0-t)))RRGSmG\alpha\beta\gamma(t)$
$LRRGSmG\alpha GTP$	$LRRGSmG\alpha GTP'(t) = k_{29}G\alpha GTP(t)LRRGSm(t) - k_{30}LRRGSminertG\alpha GTP(t)$
$LRRGSminertG\alpha GTP$	$LRRGSminertG\alpha GTP'(t) = k_{36}inertG\alpha GTP(t)LRRGSm(t) - k_{37}LRRGSminertG\alpha GTP(t)$
RRGSc	$RRGSc'(t) = -k_{13}RRGSc(t) - k_{17}LR(t)RRGSc(t) - k_{21}LRG\alpha\beta\gamma(t)RRGSc(t) - k_{15}R(t)RRGSc(t) - k_{19}RG\alpha\beta\gamma(t)RRGSc(t) - k_{22}G\alpha GTP(t)RRGSc(t) - k_{24}inertG\alpha GTP(t)RRGSc(t) + k_{14}RRGSm(t) + k_{23}RRGSmG\alpha GTP(t) + k_{28}RRGSmG\alpha GTP(t) + k_{35}RRGSminertG\alpha GTP(t)$
RRGSm	$RRGSm'(t) = k_{18}LRRGSm(t) + k_{13}RRGSc(t) - k_{14}RRGSm(t) - k_{27}G\alpha GTP(t)RRGSm(t) - k_{34}inertG\alpha GTP(t)RRGSm(t) + k_{16}RRGSm(t) + k_{20}RRGSmG\alpha\beta\gamma(t)$
$RRGSmG\alpha GTP$	$RRGSmG\alpha GTP'(t) = k_{22}G\alpha GTP(t)RRGSc(t) + k_{27}G\alpha GTP(t)RRGSm(t) - k_{23}RRGSmG\alpha GTP(t) - k_{28}RRGSmG\alpha GTP(t)$
$RRGSminertG\alpha GTP$	$RRGSminertG\alpha GTP'(t) = k_{24}inertG\alpha GTP(t)RRGSc(t) + k_{34}inertG\alpha GTP(t)RRGSm(t) - k_{35}RRGSminertG\alpha GTP(t)$
RRGSm	$RRGSm'(t) = k_{15}R(t)RRGSc(t) - k_{16}RRGSm(t) - k_6G\alpha\beta\gamma(t)RRGSm(t) - \frac{1}{2}k_5L(t)(Tanh(t_0b) - Tanh(b(t_0-t)))RRGSm(t) - k_{31}G\alpha GTP(t)RRGSm(t) + k_{32}RRGSmG\alpha GTP(t)$
$RRGSmG\alpha\beta\gamma$	$RRGSmG\alpha\beta\gamma'(t) = k_{19}RG\alpha\beta\gamma(t)RRGSc(t) + k_6G\alpha\beta\gamma(t)RRGSm(t) - k_{20}RRGSmG\alpha\beta\gamma(t) - \frac{1}{2}k_8L(t)(Tanh(t_0b) - Tanh(b(t_0-t)))RRGSmG\alpha\beta\gamma(t)$
$RRGSmG\alpha GTP$	$RRGSmG\alpha GTP'(t) = k_{31}G\alpha GTP(t)RRGSm(t) - k_{32}RRGSmG\alpha GTP(t)$
z1	$z1'(t) = \frac{3}{2}Effector(t)G\alpha GTP - \frac{3}{2}z1(t)$
z2	$z2'(t) = \frac{3}{2}z1(t) - \frac{3}{2}z2(t)$
z3	$z3'(t) = \frac{3}{2}z2(t) - \frac{3}{2}z3(t)$

TABLE 3.3: **Croft *et al.* (2013) system of ODEs.** Each species associated differential equation describes the rate of change of that species concentration with respect to time. The ODEs are generated with the reactions rates k described in the Croft *et al.* 2013 reaction scheme (Table 3.2). b=100 (constant for ligand addition) and t_0=14 (equilibration time before ligand application).

3.4 Extending the model

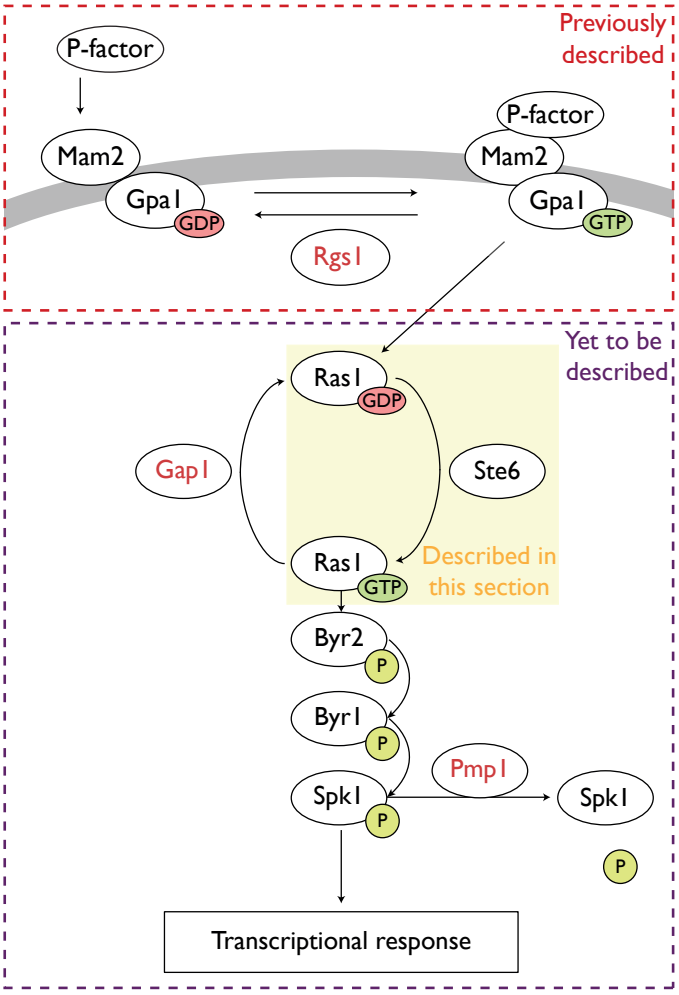

Figure 3.4: **Modelling Ras1 activation.** P-factor binds the GPCR Mam2 promoting GDP/GTP exchange on the G protein Gpa1. GTP-bound Gpa1 activates Ras1 via the GEF Ste6, transducing signalling via sequential phosphorylation of a MAPK cascade (Byr2, Byr1 and Spk1), resulting in activation of Ste11 (not included), which induces transcription of mating-responsive genes. There are various points of regulation through the pathway (highlighted with red text) including: Rgs1, which catalyses the hydrolysis of Gpa1. Gap1, which hydrolyses Ras1 and Pmp1 a phosphatase that regulates the action of Spk1 (Figure adapted form [50]). The red dashed box highlights components described in the previous models, the purple dashed box contains components that are yet to be described in this chapter and the yellow box highlights species that will be described in this section.

3.4.1 The Ras model: Part 1 - activation of Ras1 via Gpa1

During the development of the model, generic terms have been used to describe the components of the pheromone-induced pathway of *S. pombe* and these are listed in Table 3.4.

Protein species	Modelling species
P-factor	L
Mam2	R
Gpa1	Gα
-	Gβγ
Rgs1	RGS
Ste6	Gef
Ras1	Ras
Gap1	Gap
Byr2	MAP3K
Byr1	MAP2K
Spk1	MAPK
Pmp1	PhTase

Table 3.4: **Species terms used in the models.** General species terms used to describe components of the pheromone-response pathway.

P-factor binds and activates Mam2 promoting nucleotide exchange on Gpa1 [63]. Active GTP-bound Gpa1 promotes nucleotide exchange on the monomeric G protein Ras1. Like other monomeric G proteins, Ras1 requires an interaction with a GEF to enhance the release of GDP and thus, enable G protein activation through the binding of GTP [19]. *S. pombe* contains two known GEFs for Ras1: Ste6 and Efc25 [68, 243]. In addition to promoting GDP disassociation on Ras1, these activating proteins direct Ras1 signalling to different downstream effectors by potentiating either the transcriptional or morphological pathway [244] (Figure 1.7).

Strains lacking *ste6* prevents mating in *S. pombe* but does not affect the cells' morphology, i.e. cells retain a typical barrel shape during mitotic growth and form conjugation tubes following treatment with P-factor [68]. Conversely, strains lacking *efc25* mate like WT cells but display a spherical rather than a barrel shape morphology. Spherical shaped *S. pombe* have been observed in other studies, typically when proteins required for cell polarity are mutated or removed [73, 243]. These studies suggest that Ste6 directs Ras1 signalling via the transcriptional pathway and Efc25 directs Ras1 signalling via the morphological pathway (Figure 3.5).

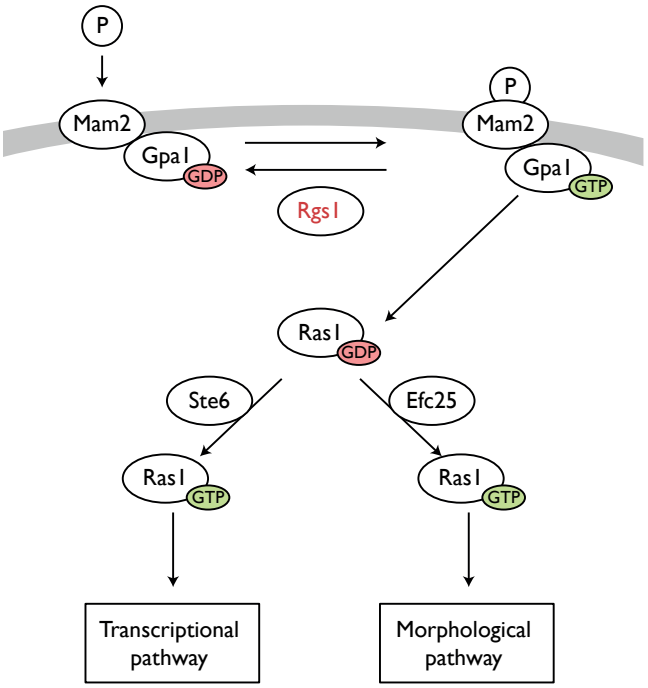

FIGURE 3.5: **Ras1 has two known downstream targets.** P-factor binding the GPCR Mam2, promotes nucleotide exchange on Gpa1. GTP-bound Gpa1 activates the G protein Ras1 via an interaction with either Ste6 or Efc25, which directs Ras1 signalling to either the transcriptional or morphological pathway, respectively. Rgs1 regulates signalling by catalysing the hydrolysis of GTP on Gpa1 (Figure adapted from [223]).

Overexpression of Efc25 in *Δste6* strains rescues pheromone-induced transcription, whereas overexpression of Ste6 in mitotically growing untreated *Δefc25* cells does not rescue the defects in cell morphology (C. Weston, PhD thesis, 2013) (i.e. cells maintain a spherical shape). These data along with the knowledge that Ste6 is pheromone-inducible [68], suggests that Ste6 requires an interaction with another protein to activate Ras1. It seems plausible that this interaction could be the G protein subunit Gpa1, as its self is pheromone-inducible and G proteins have been shown to enhance GEF activity in other systems [245]. Therefore, it was assumed that Gpa1 binds Ste6 prior to activation of Ras1.

To include the binding of Gpa1 to Ste6 prior to Ras1 activation in the model, the Effector species from the Croft *et al.* (2013) model (Table 3.2) was replaced with a generic GEF term to represent Ste6. Following this, the Croft *et al.* (2013) model including the Effector species replaced with GEF is referred to as the 'RAS model'.

To simulate Ras1 activation, two reactions were included in the RAS model. One describing the binding of GDP-bound RAS to GαGTPGEF to form an inert-trimeric complex consisting of Gα, GEF and RAS and a second equation describing the dissociation of the trimeric complex, releasing GTP-bound RAS and inertGαGTPGEF (reaction 41 and 42,

respectively from Figure 3.6a). These reactions satisfy the inert state hypothesis proposed by Smith *et al.* (2009), which suggests that following activation of one Effector molecule (for this model, RAS), the Gα complex enters an inert state that can be recycled back to GDP-bound Gα via an interaction with RGSm (Figure 3.6b).

GEF + GαGTP → GαGTPGEF	k_{33}=13 $nM^{-1}h^{-1}$
GαGTPGEF + RASGDP → inertGαGTPGEFRASGTP	k_{41}=50 $nM^{-1}h^{-1}$
inertGαGTPGEFRASGTP → inertGαGTPGEF + RASGTP	k_{42}=4 h^{-1}

(a)

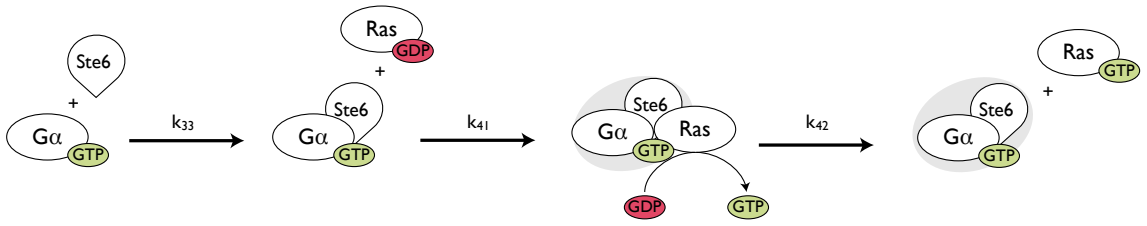

(b)

FIGURE 3.6: **RAS activation.** (a) Reactions describing the activation of RAS activation with associated rate constants and a (b) schematic describing the reactions from part (a); the inert state is highlighted in grey.

Overexpression of Ste6 or Ras1 in wild type (WT) *S. pombe* strains does not affect P-factor induced transcription (C. Weston, PhD thesis, 2013, [228]). Therefore, the concentration of Ste6 and Ras1 was assumed to not be a limiting factor during signal transduction in response to P-factor. Thus the initial concentration of the GEF and RASGDP in the RAS model was assumed to equal the concentration of the G protein ([GαGDP]=[GEF]=[RASGDP]=205 nM).

The previous mathematical models of the *S. pombe* mating-response pathway impose the inertGαGTP as a separate physical state [173, 190]. In the RAS model, GαGTP is bound in complex with GEF and the GαGTPGEFRASGTP trimeric-complex becomes inert following the binding and subsequent activation of a single RAS species. Recycling of the inertGαGTPGEF complex was assumed to occur with the same mechanisms as proposed for inertGαGTP in the previous models [173, 190], i.e. inertGαGTPGEF binds RGSm and LRRGSm with the same affinity as inertGαGTP in the Croft *et al.* (2013) model. In addition, inertGαGTPGEF binds RGSc with a slower affinity and thus maintains the importance of spatial regulation of the RGS species in transducing signalling response.

3.4.1.1 Partial activation of RAS by GαGTP

Loss of the G proteins, Gpa1 or Ras1, prevents mating in *S. pombe* [63, 246]. This was verified by performing a β-galactosidase assay (as described in section 2.2.8.1) with WT (JY544), *Δgpa1* (JY1285) and *Δras1* (JY630) strains, as no β-galactosidase activity was observed following 16 h of treatment (Figure 3.7a). The equivalent *in silico* experiment recapitulated the lack of transcriptional response when removing Gpa1 and Ras1 (Figure 3.7b). Specifically, the RAS model with reactions 41 and 42 (Figure 3.6) was simulated with initial species concentrations described in Table 3.5, following successive changes of [GαGDP]=0 nM to reflect *Δgpa1* cells and [RASGDP]=0 nM to reflect *Δras1* cells and measuring the accumulation of RASGTP after 16 h simulated induction.

Species	Initial concentration (nM)
L	0 - 100,000
R	205
GαGDP	205
Gβγ	205
RGSc	60
GEF	205
RASGDP	205
All other species were set to 0 nM	

TABLE 3.5: **Initial concentrations for species in the RAS model.** For simulation of wild-type cells.

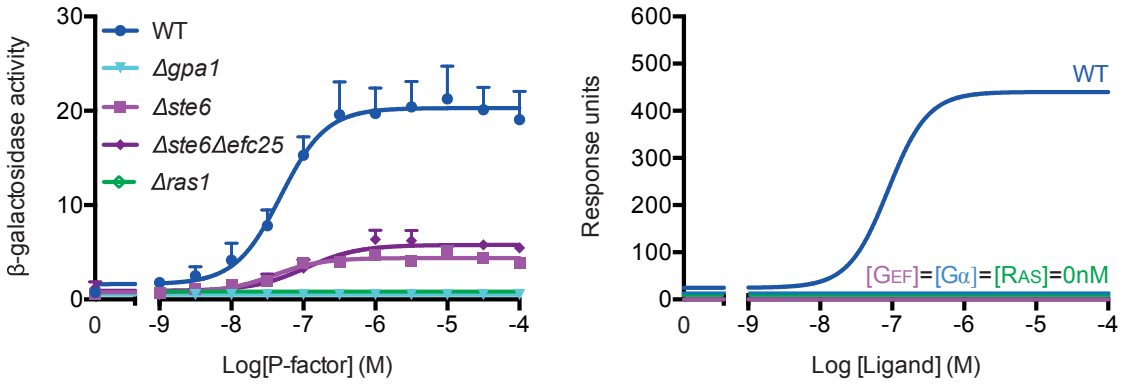

(a) (b)

FIGURE 3.7: **The simulation was unable to recapitulate the β-galactosidase activity observed in *Δste6* cells.** (a) Figure adapted from C. Weston, PhD thesis, 2013. (b) Deletion of Ste6, Gap1 and Ras1 can be simulated *in silico* by running the RAS model with reactions 41 and 42 (Figure 3.6) with species concentrations described in Table 3.5, following successive changes of [GEF]=[GαGDP]=[RASGDP]=0 nM and measuring the accumulation of RASGTP after 16 h simulated induction.

Deletion of *ste6* reduces maximal transcriptional expression but does not prevent β-galactosidase activity (Figure 3.7a). This suggested that Ras1 could be partially activated by another protein in response to P-factor. The equivalent *in silico* experiment [GEF]=0 nM did not produce any response (Figure 3.7b) as no Ste6-independent mechanisms for RAS activation had been included in the model.

The most likely candidate to activate Ras1 was the other Ras1 GEF Efc25. However, a dose-dependent increase in β-galactosidase activity was also observed in the double *ste6* and *efc25* deletion strain (Figure 3.7a). Therefore, Ras1 can be activated in P-factor-dependent manner by another protein. The only known P-factor-dependent signalling species upstream of Ras1 is Mam2 (a GPCR) and Gpa1 (a G protein). If the receptor directly activated Ras1 then β-galactosidase activity would have been observed in the *Δgpa1* β-galactosidase assay, yet no such response was observed (Figure 3.7a). This suggests that Ras1 could be activated by Gpa1 or another protein that has yet to be identified.

As *S. pombe* Ras1 has been studied extensively over the last 20 years and no such protein has been identified in activating Ras1 in a pheromone-dependent manner, Gpa1 was assumed to partially activate Ras1. This activation of Ras1 via Gpa1 was included in the model by the following equation:

$$G\alpha GTP + RasGDP \rightarrow G\alpha GTP + RasGTP \quad k_{50}=0.00034\ nM^{-1}h^{-1}$$

The rate at which GαGTP promotes nucleotide exchange on RAS (k_{50}) was chosen to be 0.00034 $nM^{-1}h^{-1}$ as this displayed a ∼75% reduction in the model output when [GEF]=0 nM, which is qualitatively similar reduction as observed *in vitro* (Figure 3.8).

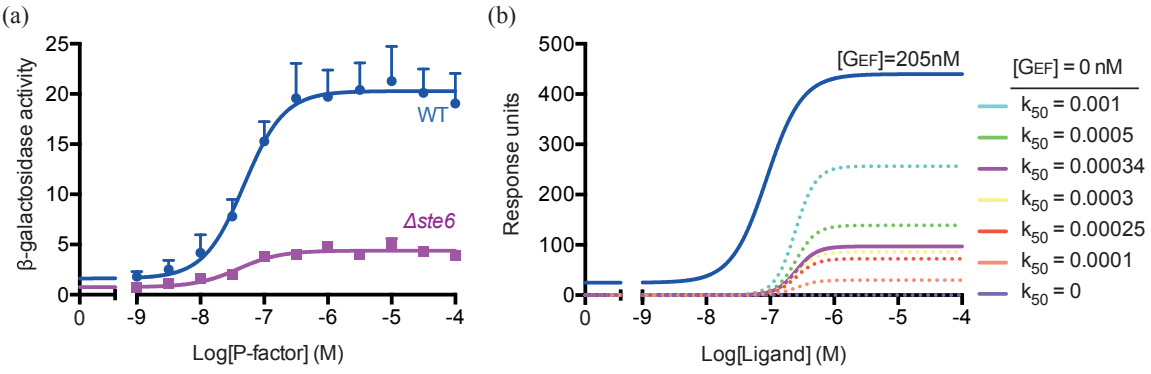

FIGURE 3.8: **Perturbation of rate k_{50} (GαGTP activating RAS).** (a) Figure adapted from C. Weston, PhD thesis, 2013. (b) The RAS model plus reactions 41, 42 and 50 including species concentrations described in Table 3.5 were simulated with reaction rates k_{50} when [GEF]=0 nM. Response units were measured by the accumulation of RasGTP after 16 h simulated induction. k_{50}=0.00034 $nM^{-1}h^{-1}$ showed an ∼75% reduction (as seen *in vitro*) when [GEF]=0 nM in comparison to simulations with [GEF]=205 nM.

3.4.2 The Ras model: Part 2 - regulation of Ras1 via Gap1

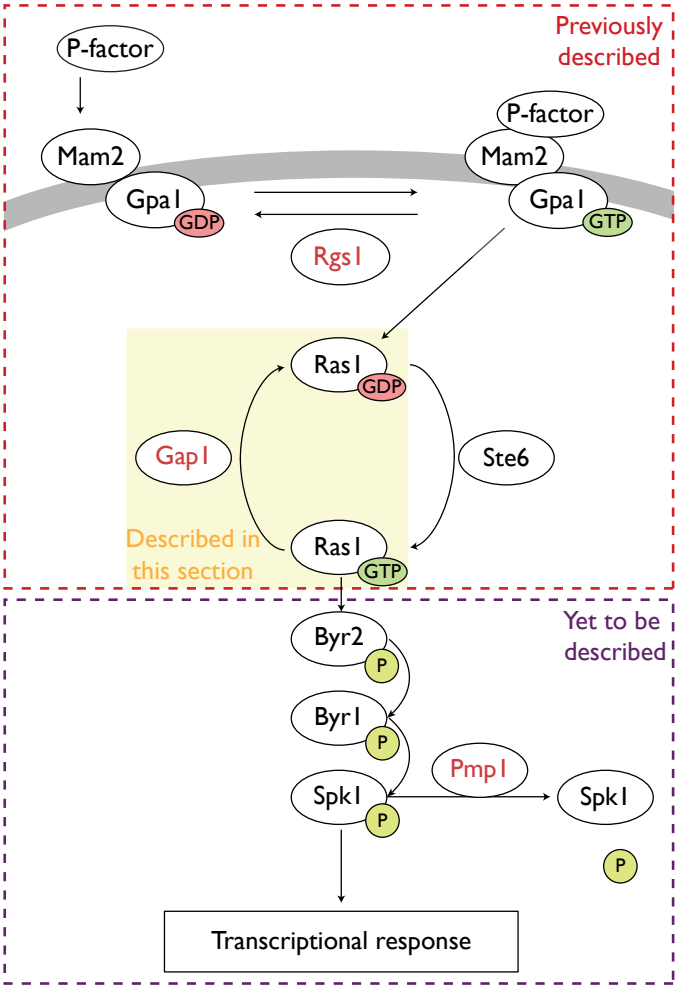

Figure 3.9: **Modelling Ras1 inactivation via Gap1.** P-factor binds the GPCR Mam2 promoting GDP/GTP exchange on the G protein Gpa1. GTP-bound Gpa1 activates Ras1 via the GEF Ste6, transducing signalling via sequential phosphorylation of a MAPK cascade (Byr2, Byr1 and Spk1), resulting in activation of Ste11 (not included), which induces transcription of mating-responsive genes. There are various points of regulation through the pathway (highlighted with red text) including: Rgs1, which catalyses the hydrolysis of Gpa1. Gap1, which hydrolyses Ras1 and Pmp1 a phosphatase that regulates the action of Spk1 (Figure adapted form [50]). The red dashed box highlights components described in the previous models, the purple dashed box contains components that are yet to be described in this chapter and the yellow box highlights species that will be described in this section.

Ras proteins contain a weak intrinsic GTPase activity, which is greatly enhanced through interaction with GAPs [247]. Ras1 is regulated through interaction with Gap1 (a GAP) [86]. A previous study has shown that Ras1 binds Gap1 via the second glycine residue within the P-loop of Ras1 [223], analogous to mammalian systems [248]. Therefore, regulation of Ras1 was included in the model by assuming RASGTP binds a generic species GAP to promote GTP hydrolysis (Table 3.6).

RASGTP + GAP → RASGTPGAP	k_{44}=0.00075 $nM^{-1}h^{-1}$
RASGTPGAP → RASGDPP + GAP	k_{45}=10 $nM^{-1}h^{-1}$
RASGTP → RASGDPP	k_{48}=10 $nM^{-1}h^{-1}$
RASGDPP → RASGDP + P	k_{49}=1000 $nM^{-1}h^{-1}$

TABLE 3.6: **Reactions for inactivation of RAS via GAP.** RASGTP forms a complex with GAP to create a RASGTPGAP complex, which disassociates to release GAP and RASGDP (reactions 45, 48 and 49).

The initial concentration of GAP was not assumed to be a limiting factor for signal transduction and therefore the concentration of [GAP]=205 nM, equivalent to the concentration of RAS (Table B.1). The RAS model including reactions describing the activation of RAS (reactions 41, 42 and 48) and reactions describing regulation of RAS via GAP (reactions 44, 45, 48 and 49) were collated and from this point on referred to as the 'RAS model' (for the full RAS model reaction scheme and initial conditions see Appendix B).

Species	Initial concentration (nM)
L	0 - 100,000
R	205
GαGDP	205
Gβγ	205
RGSc	60
Ste6	205
RASGDP	205
GAP	205
All other species were set to 0 nM	

TABLE 3.7: **Initial concentrations for species in the RAS model.** For simulation of wild-type cells.

It seems counterintuitive that a regulator of signalling such as Rgs1 increases maximal signalling when overexpressed and reduces maximal signalling when removed *in vivo* (Figure 3.10a, see 2xRgs1 for overexpression and *Δrgs1* for deletion of Rgs1). The Ras model was able to recapitulate the changes in maximal expression displayed *in vitro* (Figure 3.10b), as it included reactions which maintained the inert state hypothesis of the GαGTP species.

The RAS model was simulated with species concentrations described in Table B.1, but varying RGSc concentration in succession from 0 nM, 60 nM, 120 nM and 180 nM with the output measuring the accumulation of RASGTP after 16 h simulated induction.

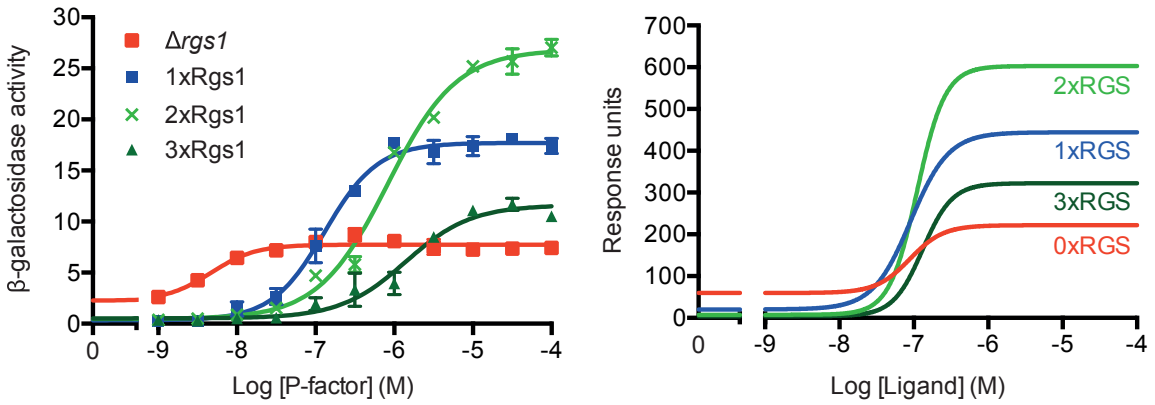

(a) (b)

FIGURE 3.10: **Ras model reproduces the positive and negative role on signalling.** (a) Experimental data adapted from Smith *et al.* (2009) [190]. Error bars represents ±SEM. (b) Simulations of the Ras model (Appendix B) with initial concentrations described in Table B.1 but by varying RGSc concentration from [RGSc]=0 nM (0xRGS), [RGSc]=60 nM (1xRGS), [RGSc]=120 nM (2xRGS) to [RGSc]=180 nM (3xRGS) were created by measuring the accumulation of RASGTP after 16 h simulated induction.

Contrary to Rgs1, overexpression of Gap1 in WT *S. pombe* strains reduces maximal signalling response (C. Weston, PhD thesis, 2013). This suggests that Gap1 negatively regulates P-factor signalling. To elucidate whether Gap1 is a sole negative regulator of signalling and to determine whether the reactions described in the RAS model for inactivation of RAS via GAP accurately describe the mechanism of Ras1 activation, a β-galactosidase assay was performed with WT (*gap1*$^{+}$) and *Δgap1* (JY1538) strains. Cells were grown to mid-exponential growth phase before treatment with a range of P-factor concentrations (from 0 µM to 100 µM).

After 16 h strains were assayed for β-galactosidase activity (as described in section 2.2.8.1). *Δgap1* cells displayed an increase in basal signalling at 4±1 *lacZ* units in comparison to WT strains at 1±1 *lacZ* units (however, this was not considered statistically significant, as p=0.1502 when n=5 (where n represents the number of independent experiments) calculated using a Student's t-test) and a non-monotonic response peaking at ∼100 nM was observed (Figure 3.11a).

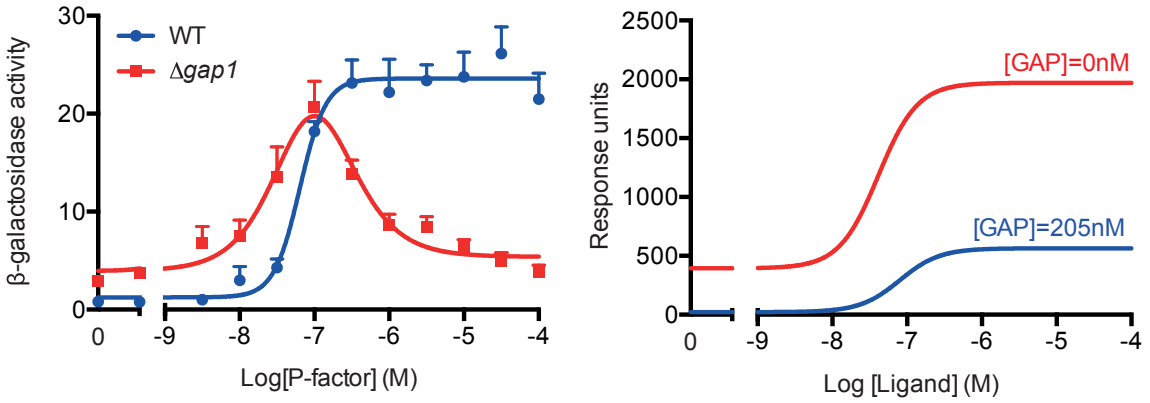

(a) (b)

FIGURE 3.11: **The Ras model did not recapitulate the non-monotonic response.** (a) WT (JY544) and *Δgap1* (JY1538) strains were grown to mid-exponential growth phase before treatment with a range of P-factor concentrations (from 0 µM to 100 µM). After 16 h strains were assayed for β-galactosidase activity (as described in section 2.2.8.1). Data shown is the average of five independent experiments±SEM. The results are in agreement with previously published work [223]. (b) Simulations of the RAS model with initial concentrations described in Table B.1 with [GAP]=205 nM and [GAP]=0 nM to simulate WT and *Δgap1* cells *in vitro*, were performed by measuring the accumulation of RASGTP complexes following 16 h simulated induction.

The equivalent *in silico* experiment for strains lacking *gap1* did not capture the non-monotonic response displayed *in vitro* (Figure 3.11). Instead an increase in basal signalling (also observed *in vitro*) and maximal transcriptional response was observed (Figure 3.11b). Simulations of the RAS model with initial concentrations described in Table B.1 were performed with [GAP]=205 nM to simulate WT cells and [GAP]=0 nM to simulate *Δgap1* cells, by measuring the accumulation of RASGTP complexes following 16 h simulated induction.

S. pombe cells lacking *gap1* were shown to increase cell lysis following prolonged treatment with P-factor [223]. These observations could explain the non-monotonic response of *Δgap1* cells observed *in vitro* (Figure 3.11a). To determine whether cells became increasingly non-viable in response to treatment with P-factor, a cell viability assay (as described in section 2.2.16) was performed with WT (*gap1*$^+$) and *Δgap1* strains that were grown to mid-exponential growth phase before treatment with a range of P-factor concentrations (from 0 µM to 100 µM) for 16 h.

A P-factor-dependent increase in non-viable cells was observed in both *gap1*$^+$ cells (WT strains) and *Δgap1* cells (Figure 3.12). However, a significant increase in the percentage of non-viable cells was observed following 10 µM P-factor treatment (as WT displayed 12±2% whereas *Δgap1* cells displayed 85±3% of cells were non-viable, $p<0.0001$ when

n=3, Student's t-test). The P-factor-dependent increase in cell lysis corresponded with the loss of β-galactosidase activity observed in *Δgap1* strains (Figure 3.11). These data therefore suggested that *Δgap1* cells are less likely to survive, following treatment with P-factor in the absence of Ras1-GTP hydrolysis thus, indicating that Gap1 is essential during the *S. pombe* mating-response to induce a maximal signalling response [223].

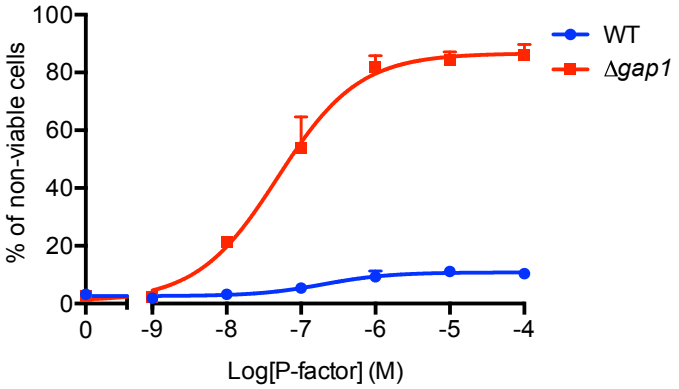

FIGURE 3.12: ***Δgap1* became non-viable with increasing P-factor concentration.** WT (JY544) and *Δgap1* (JY1538) strains were grown to mid-exponential growth phase before treatment with a range of P-factor concentrations (from 0 µM to 100 µM). After 16 h a cell viability assay was performed (as described in section2.2.16), which indicates the percentage of non-viable cells within a population. Data shown is the average of three independent experiments ±SEM. The results are in agreement with previously published work [223].

GTP-bound Ras1 transduces signalling via Byr2 (a MAP3K) to enhance gene transcription and Scd1 (a GEF for the essential G protein Cdc42) to initiate conjugation tube formation [249] (Figure 3.13). Rga4 is a GAP for Cdc42 [250]. Increasing Rga4's concentration in *Δgap1* strains does not prevent P-factor-induced cell lysis, whereas increasing Cdc42 concentration in *Δgap1* strains partially rescues cell viability [223]. Together, with the knowledge that deletion of Cdc42 or its downstream effectors is lethal to the cell [74, 77], these data suggest that a reduction rather than an increase in Cdc42 activation promotes cell lysis in *Δgap1* strains. These data also suggest that Cdc42 becomes activated via forming a complex with Ras1; and therefore, loss of Gap1 renders Cdc42 in complex and thus is less likely to active its downstream effectors; mimicking a strain lacking Cdc42, which is lethal (Figure 3.13).

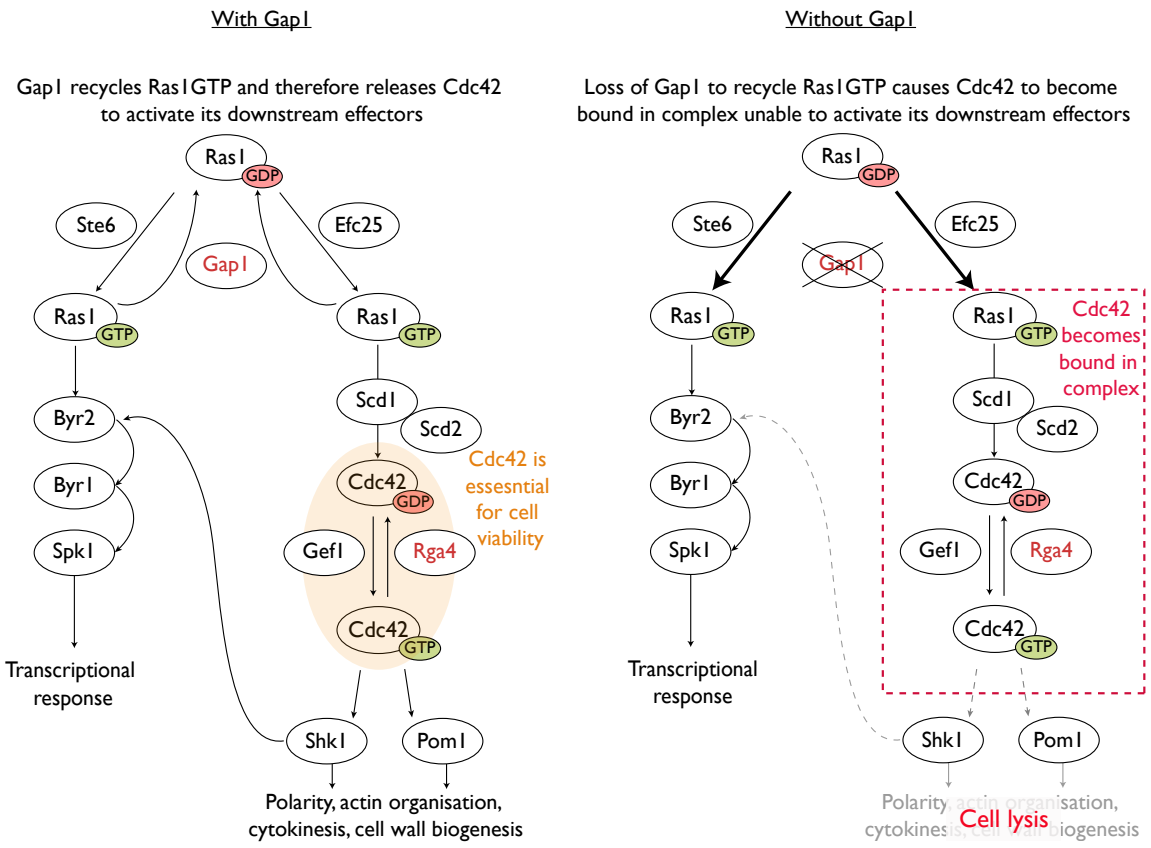

FIGURE 3.13: **Loss of Gap1 reduces Cdc42 activation promoting cell lysis.** Ras1 activation via Ste6 directs signalling to the MAPK cascade (Byr2, Byr1 and Spk1) resulting in transcription of mating-responsive genes. Activation of Ras1 via Efc25, directs Ras1 to activate Cdc42 (an essential G protein) via an interaction with Scd1 (and Scd2). GTP-bound Cdc42 activates Shk1 and Pom1, proteins required for polarised cell growth (conjugation tube formation). The two pathways are linked as Shk1 facilitates Byr2 activation. Gap1 promotes GDP for GTP exchange on Ras1 and Rga4 acts as a GAP for Cdc42. When Gap1 is present, Cdc42 is released from a Ras1/Scd1/Scd2/Cdc42/Gef1 complex (red dashed box), by Ras1 hydrolysis. However, when Gap1 is removed Cdc42 becomes stuck in complex and is therefore less likely to activate its downstream effectors (illustrated by the grey arrows).

The RAS model did not contain terms for Ras1 activation of the morphological (conjugation tube formation) pathway and was therefore unable to replicate the non-monotonic β-galactosidase response caused by cell lysis (Figure 3.11). Creating an *in vivo* system, which prevents P-factor-dependent cell lysis whilst simultaneously increases maximal β-galactosidase activity when *gap1* is deleted, would suggest that Gap1 acts as a sole negative regulator and that the reactions described in the RAS model were plausible.

S. pombe strains lacking Scd1 have not been shown to signal significantly different to strains containing endogenous *scd1* [223]. This was confirmed by performing a β-galactosidase assay (as described in section 2.2.8.1) with WT (JY544) and *Δscd1* (JY1673)

cells following growth to mid-exponential growth phase and treatment with varying P-factor concentrations (0 µM to 100 µM) for 16 h (Figure 3.14). A reduction in maximal response and pEC_{50} was observed in *Δscd1* strains, however, these were not considered significant (for p-values see Figure 3.14c).

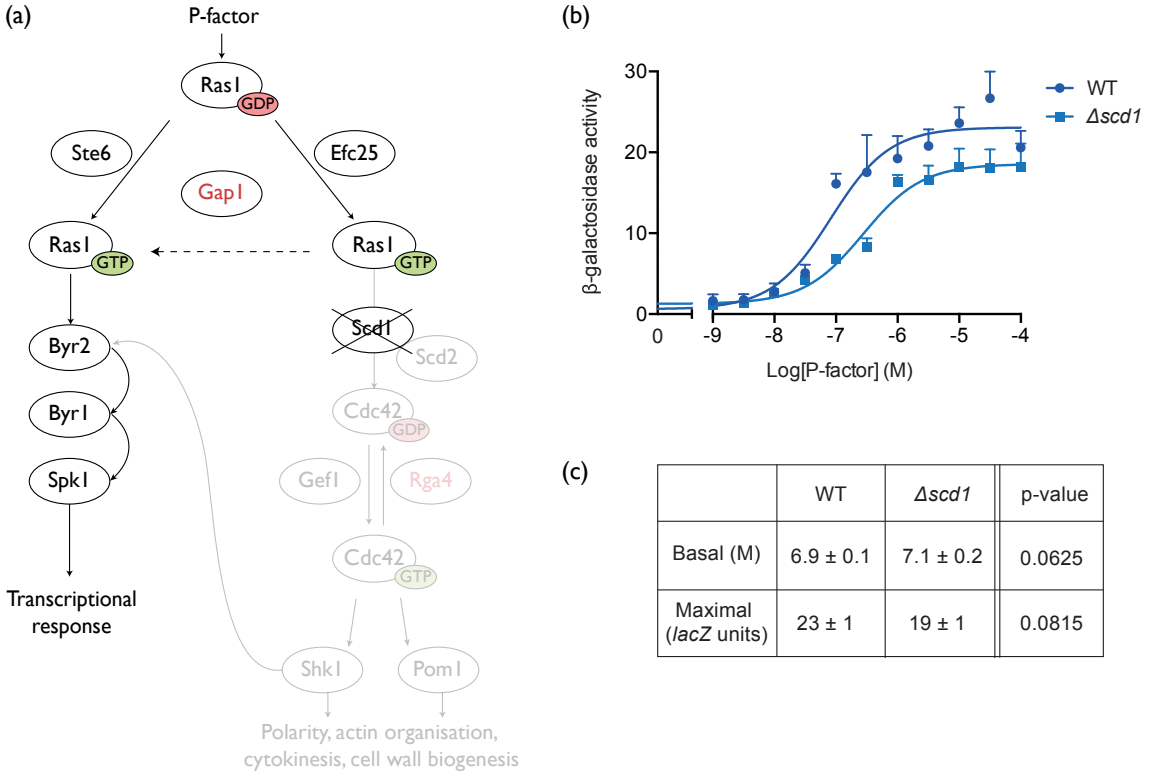

	WT	*Δscd1*	p-value
Basal (M)	6.9 ± 0.1	7.1 ± 0.2	0.0625
Maximal (*lacZ* units)	23 ± 1	19 ± 1	0.0815

FIGURE 3.14: **Scd1 is not required for pheromone-induced gene transcription.** (a) Deletion of Scd1 directs Ras1 signalling via Byr2. (b) β-galactosidase assay (as described in section 2.2.8.1) with WT (JY544) and *Δscd1* (JY1673) strains following growth to mid-exponential growth phase and treatment with varying P-factor concentrations (0 µM to 100 µM) for 16 h. The results are in agreement with previously published work [223]. (c) The table displays basal, maximal and corresponding p-values determined using a Student's t-test. Data shown is the average of three independent experiments ±SEM.

These data, together with the knowledge that deletion of Scd1 causes spherical cells that do not form conjugation tubes in response to P-factor, indicated that the transcriptional and morphological pathways could be separated via removal of Scd1 [73, 223]. Therefore, deletion of both *scd1* and *gap1* would provide a system to measure the transcriptional effect due to loss of *gap1* in *S. pombe* by preventing cell lysis (Figure 3.15a). Hence, WT (JY544), *Δgap1* (JY1538), *Δscd1* (JY1673) and *Δscd1Δgap1* (JY1674) cells were grown to mid-exponential growth phase, treated with a range of P-factor concentrations (from 0 µM and 100 µM) for 16 h and assayed for β-galactosidase activity to assess the effect of

removing *gap1* on maximal response and cell viability (as described in section 2.2.8.1 and 2.2.16, respectively).

Maximal β-galactosidase activity was significantly increased in strains lacking *gap1* and *scd1* in comparison to *Δscd1* cells (Figure 3.15b: from 18±12 *lacZ* units to 53±7 *lacZ* units, p=0.0148 when n=3 using a Student's t-test). A significant reduction in the percentage of non-viable cells (from 90±2% to 41±3%) was exhibited upon deletion of *scd1* in *Δgap1* strains (Figure 3.15c: p=0.0001 when n=3, Student's t-test). These data suggest that when cell lysis is prevented in strains lacking Gap1, maximal response is increased. Therefore, Gap1 most likely acts as a negative regulator of signalling when cell lysis is prevented.

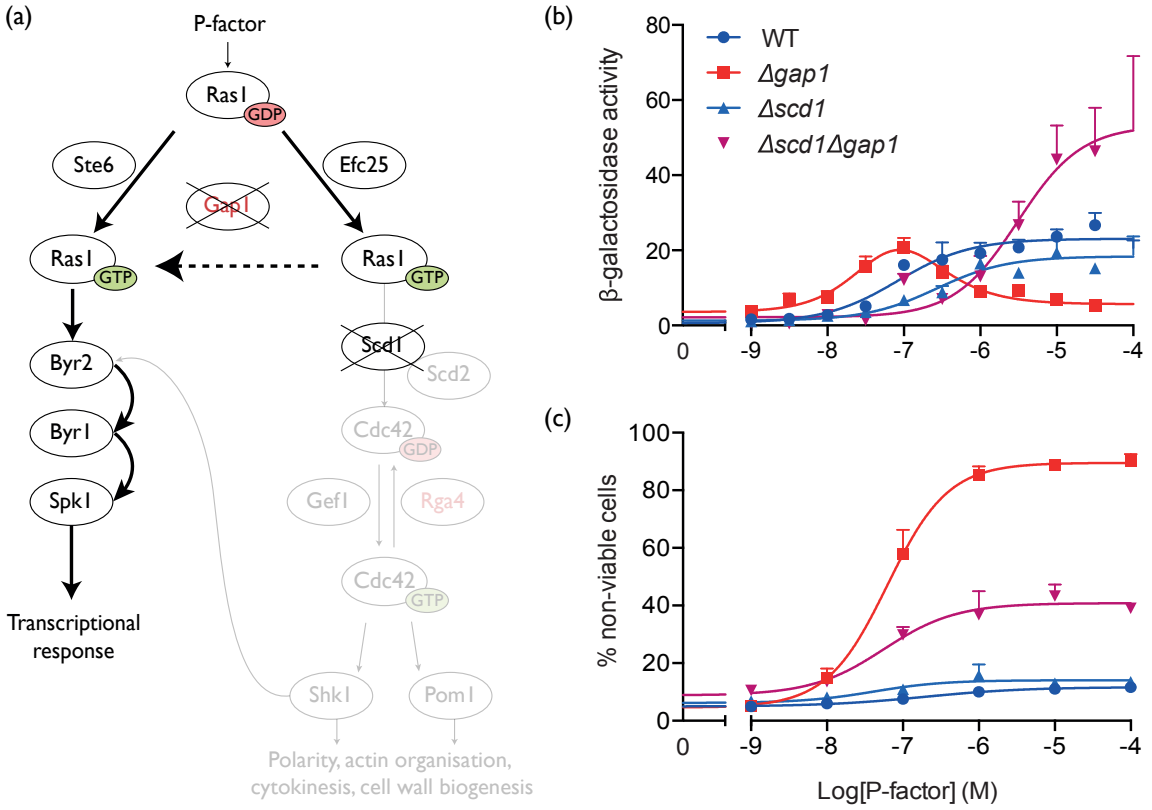

FIGURE 3.15: **Scd1 depletion facilitated quantification of removing *gap1*.** (a) Loss of Scd1 and Gap1 amplifies signalling of Ras1 via Byr2. WT (JY544), *Δgap1* (JY1538), *Δscd1* (JY1673) and *Δscd1Δgap1* (JY1674) strains were grown to mid-exponential growth phase before treatment with a range of P-factor concentrations (from 0 µM to 100 µM). After 16 h strains were assayed for (b) β-galactosidase activity (as described in section 2.2.8.1) and (c) cell viability assay (as described in section 2.2.16) to determine the percentage of non-viable. Data shown is the average of three independent experiments ±SEM.

3.4.3 The MAPK cascade

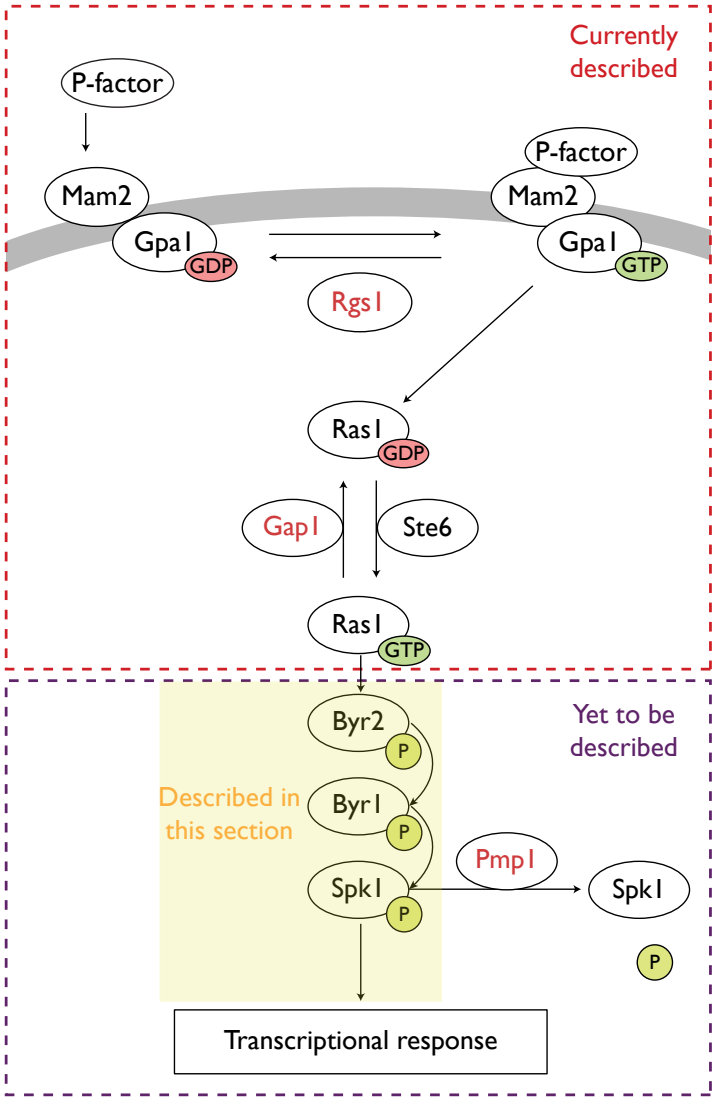

Figure 3.16: **Modelling the MAPK cascade.** P-factor binds the GPCR Mam2 promoting GDP/GTP exchange on the G protein Gpa1. GTP-bound Gpa1 activates Ras1 via the GEF Ste6, transducing signalling via sequential phosphorylation of a MAPK cascade (Byr2, Byr1 and Spk1), resulting in activation of Ste11 (not included), which induces transcription of mating-responsive genes. There are various points of regulation through the pathway (highlighted with red text) including: Rgs1, which catalyses the hydrolysis of Gpa1. Gap1, which hydrolyses Ras1 and Pmp1 a phosphatase that regulates the action of Spk1 (Figure adapted form [50]). The red dashed box highlights components described in the previous models, the purple dashed box contains components that are yet to be described in this chapter and the yellow box highlights species that will be described in this section.

3.4.3.1 Ras1GTP forms a complex with Byr2

The mitogen-activated protein kinase Byr2 acts downstream of Ras1 and is required for pheromone-induced sexual differentiation in *S. pombe* [76]. Byr2 contains a Ras-binding domain (RBD) in its N-terminal 230 amino acid region [251] and is recruited to the plasma membrane in a P-factor-dependent manner via binding Ras1 [252]. Despite this, it is unclear whether the binding of Ras1 to Byr2 transduces signalling. To answer this question, the RBD of Byr2 that had previously been cloned (by M. Bond at the University of Warwick, 2012) into the pREP3x vector (JD3681, pRBD) and the vector alone control (JD3386) were transformed into WT strains (JY544; *sxa2>lacZ*) and assayed for β-galactosidase activity following growth to mid-exponential growth phase and treatment with varying concentrations of P-factor for 16 h (as described in section 2.2.8.1), to quantify the affect on transcription.

Expression of RBD significantly reduced maximal transcriptional response from 23±1 *lacZ* units to 2±0.3 *lacZ* in comparison to WT strains ($p<0.0001$, Student's t-test) (Figure 3.17a). This suggests that RBD sequesters endogenous Ras1 thereby inhibiting the binding of Ras1 with Byr2. These data indicated that signal transduction is only successful when Ras1 forms a complex with Byr2.

The RAS model was extended to include the binding of Ras1 to Byr2, described by the following reaction:

$$\text{RASGTP} + \text{MAP3K} \rightarrow \text{RASGTPMAP3K} \qquad k_{43}=9\ \text{nM}^{-1}\text{h}^{-1}$$

This reaction was simulated with the RAS model using initial concentration [MAP3K]=205 nM and measuring the accumulation of RASGTPMAP3K complexes after 16 h simulated induction (Figure 3.17, WT).

The competitive sequestration of Ras1 between Byr2 and RBD was simulated *in silico* using the RAS model with reaction 43 and an additional reaction which described RASGTP binding RBD with the same rate ($k_{43}=k_{RBD}=9\ \text{nM}^{-1}\text{h}^{-1}$). The initial concentrations of all species are described in Table B.1 but with [MAP3K]=205 nM and [RBD]=1000 nM. The accumulation of RASGTPMAP3K complexes was then measured *in silico* following 16 h simulated induction. Simulated expression with the RBD results in a reduction in maximal response similar to the *in vitro* data (Figure 3.17), suggesting that reactions and rates used to describe the *S. pombe* mating-response could be plausible.

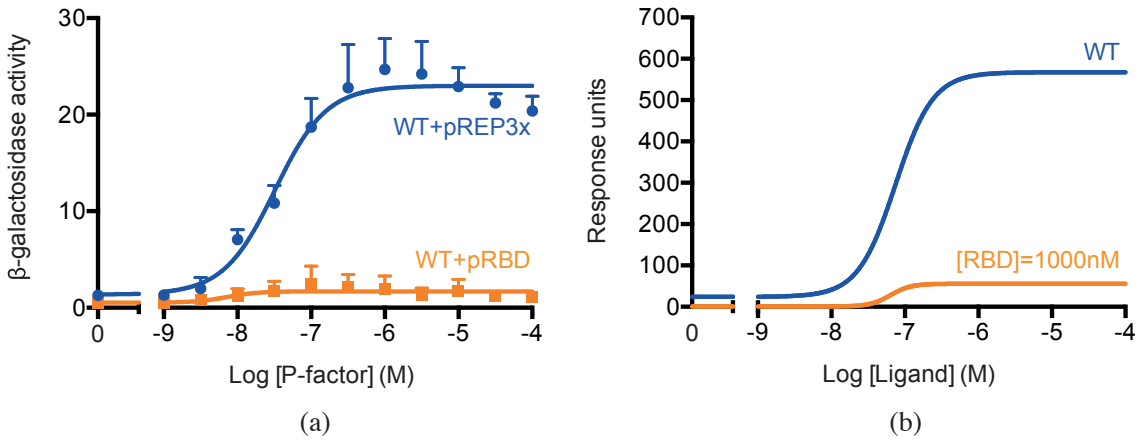

FIGURE 3.17: **Expression of the RBD in WT cells reduces transcription.** (a) The WT strain JY544 was transformed with pREP3x (JD3386) and pRBD (JD3681) and grown to mid-exponential growth phase before treatment with a range of P-factor concentrations (from 0 µM to 100 µM). After 16 h cells were assayed for β-galactosidase (as described in section 2.2.8.1). Data shown is the average of three independent experiments ±SEM. (b) Competitive sequestration of Ras1 between Byr2 and RBD was simulated *in silico* using the Ras model including two reactions that described RASGTP binding RBD and Byr2 with the same rate (k) but with differing initial concentrations ([Byr2]=205nM and [RBD]=1000 nM) and all other initial species concentrations as described in Table B.1; the output was the accumulation of RASGTPMAP3K complexes following 16 h simulated induction.

3.4.3.2 Sequential activation of Byr2, Byr1 and Spk1

MAPK cascades relay information typically from the membrane into the nucleus promoting changes in gene expression. Cascades consists of three kinases: MAP3K, MAP2K and MAPK, which transmit signalling from one component to another by sequential phosphorylation [253].

In *S. pombe*, the binding of Ras1 to the N-terminus of Byr2 (a MAP3K) prevents autoinhibition of the Byr2 kinase catalytic domain (CD) [76], which promotes kinase activation. The CD of Byr2 then phosphorylates Byr1 (a MAP2K), which in turn phosphorylates Spk1, a MAPK that has been suggested to promote phosphorylation of the transcription factor Ste11 [69, 70, 254–258].

Byr2, Byr1 and Spk1 are structurally and functionally related to the *S. cerevisiae* MAPK proteins STE11, STE7 and FUS3, respectively [259]. However, the *S. cerevisiae* mitogenic cascade requires the scaffold protein *STE5* to sequester all three components of the cascade, insulating the mating-response MAPK kinases from other signalling pathways, such as the starvation response, which also requires STE7 and STE11, but activates KSS1 (a MAPK) to promote a growth response [260–264]. To date no *STE5* homologue has been identified

in *S. pombe*. Therefore, Byr2, Byr1 and Spk1 were not assumed to bind in complex to promote signal transduction (Figure 3.18a).

MAPK signal transduction was incorporated into the RAS model (with reactions 43, 44, 45, 48 and 49) by the addition of reactions 51-54 (Figure 3.18b), which describe the phosphorylation of MAP2K by RASGTPMAP3K and subsequent phosphorylation of MAPK. Dissociation of the complexes are also included. The initial concentrations of the MAPK cascade were unknown and therefore assumed to be equivalent to other species concentrations, as not to be a limiting factor during the response Table 3.8.

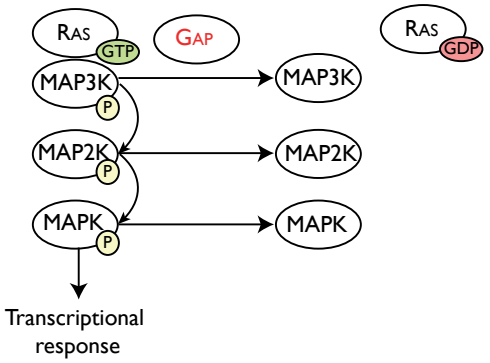

MAP2K + RASGTPMAP3K→MAP2KP + RASGTPMAP3K	k_{51}	0.005	$nM^{-1}h^{-1}$
MAP2KP + MAPK → MAP2KP + MAPKP	k_{52}	1	$nM^{-1}h^{-1}$
MAP2KP → MAP2K	k_{53}	8	h^{-1}
MAPKP → MAPK	k_{54}	8	h^{-1}

FIGURE 3.18: **MAPK signalling in the *S. pombe* mating-response pathway.** The complex RASGTPMAP3K promotes phosphorylation of MAP2K, which in turn phosphorylates MAPK. The negative regulator GAP promotes nucleotide exchange on RAS.

Species	Initial concentration (nM)
L	0 - 100,000
R	205
GαGDP	205
Gβγ	205
RGSc	60
GEF	205
RASGDP	205
GAP	205
MAP3K	205
MAP2K	205
MAPK	205
All other species were set to 0 nM	

TABLE 3.8: **Initial concentrations for species in the RAS model including negative regulation by GAP and the MARK.** For simulation of wild-type cells.

Phosphorylation of the transcription factor (Ste11) by MAPKp was not included in this version of the model because there was insufficient evidence to suggest a mechanism for how and in which cellular compartment (i.e. cytoplasm or nucleus) Spk1 promotes phosphorylation of Ste11.

3.4.4 Regulation of Spk1 by Pmp1

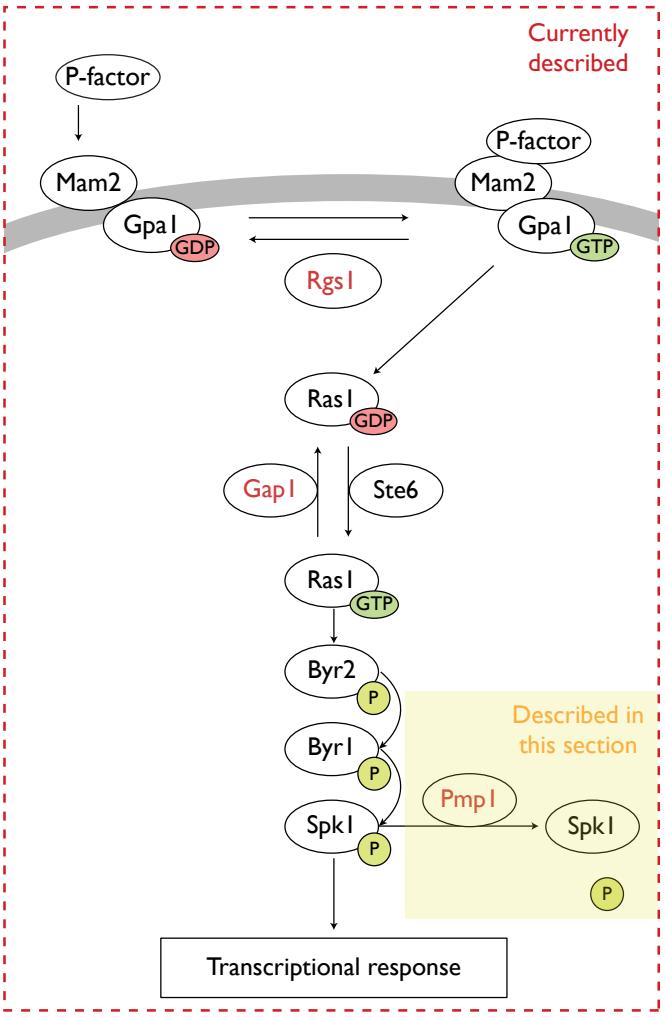

Figure 3.19: **Modelling deactivation of Scd1 via Pmp1.** P-factor binds Mam2 promoting GDP/GTP exchange on the G protein Gpa1. GTP-bound Gpa1 activates Ras1 via the GEF Ste6, transducing signalling via sequential phosphorylation of a MAPK cascade (Byr2, Byr1 and Spk1), resulting in activation of Ste11 (not included), which induces transcription of mating-responsive genes. There are various points of regulation through the pathway (highlighted with red text) including: Rgs1, which catalyses the hydrolysis of Gpa1. Gap1, which hydrolyses Ras1 and Pmp1 a phosphatase that regulates the action of Spk1 (Figure adapted form [50]). The red box highlight components that have been described and the yellow box highlights species that will be described in this section.

MAPK cascades are deactivated by negative regulators that modulate the intensity and duration of the signal. To date, only Pmp1 a dual-specificity phosphatase has been suggested to negatively regulate the action of the MAPK cascade, specifically Spk1 [11][221]. The action of Pmp1 negatively regulating Spk1 was included in the model reaction scheme by the following reaction, where PhTase represents the PhTase Pmp1:

$$\text{PhTase} + \text{MAPK}_\text{P} \rightarrow \text{PhTase} + \text{MAPK} \quad k_{55} \quad 0.04 \quad \text{nM}^{-1}\text{h}^{-1}$$

The RAS model equations including reactions that describe regulation by GAP (reactions 44,45,48,49), signal transduction via the MAPK (reactions 43,51-54) and regulation of the MAPK by PhTase (reaction 55) were collated and termed the KR model (see section 3.5).

The deletion of *pmp1 in vivo* resulted in an increase in β-galactosidase activity in comparison to WT cells (Figure 3.20a, the experimental data collected in this study was published in Mos *et al.* (2013) [221], please see Appendix G). The equivalent *in silico* experiment recapitulated the *in vitro* assay (Figure 3.20b). Simulations of the KR model with initial concentrations described in Table 3.8, alternating [PhTase]=205 nM and [PhTase]=0 nM and measuring the accumulation of MAPKP complexes following 16 h simulated induction.

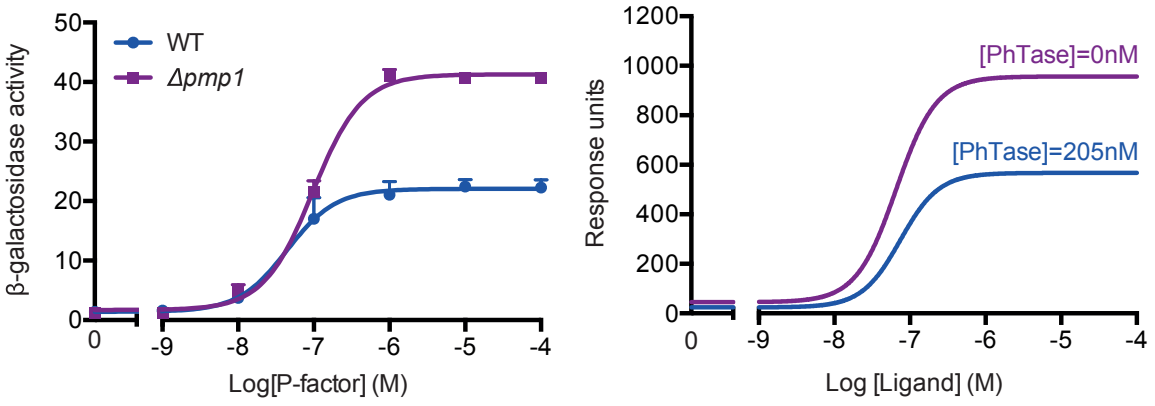

(a) (b)

FIGURE 3.20: **The KR model recapitulated the increase in maximal response observed *in vitro*.** (a) WT (JY544) and *Δpmp1* (JY949) strains were grown to mid-exponential growth phase and treated with a range of P-factor concentrations from 0 µM to 100 µM for 16 h before being assayed for β-galactosidase activity (as described in section 2.2.8.1). Data shown is the average of three independent experiments ±SEM. This data has been published in [221]. (b) simulations of the KR model with initial concentrations described in Table 3.8 but alternating [PhTase]=205 nM and [PhTase]=0 nM and measuring the accumulation of MAPKP complexes following 16 h simulated induction.

3.5 KR model: includes all known signalling components

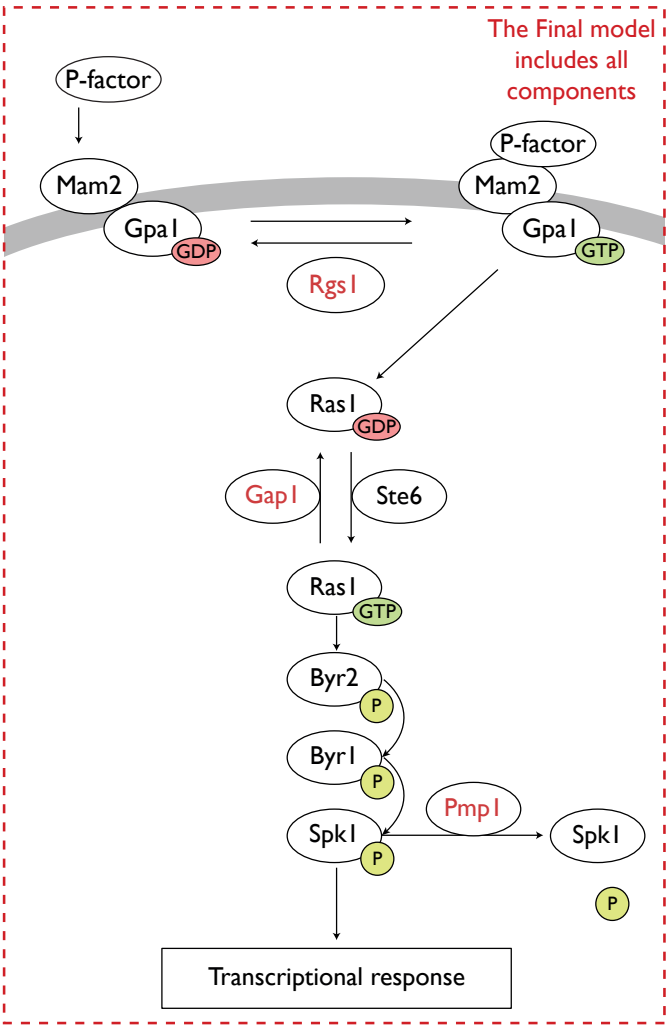

Figure 3.21: **The KR model.** P-factor binds the GPCR Mam2 promoting GDP/GTP exchange on the G protein Gpa1. GTP-bound Gpa1 activates Ras1 via the GEF Ste6, transducing signalling via sequential phosphorylation of a MAPK cascade (Byr2, Byr1 and Spk1), resulting in activation of Ste11 (not included), which induces transcription of mating-responsive genes. There are various points of regulation through the pathway (highlighted with red text) including: Rgs1, which catalyses the hydrolysis of Gpa1. Gap1, which hydrolyses Ras1 and Pmp1 a phosphatase that regulates the action of Spk1 (Figure adapted form [50]). The red dashed box highlights components that have been described in the KR model.

The previous model by Croft *et al.* (2013) [173] was extended to include the downstream signalling components of the *S. pombe* mating-response pathway up to and including the activation of the MAPK Spk1. The KR model reaction scheme displayed by Table 3.9 was developed on our current understanding of the system based on experimental data collected in this study and from the literature.

Ligand / G protein signalling			
L + R → LR	k_1	0.0025	$nM^{-1}h^{-1}$
Gαβγ + R → RGαβγ	k_2	0.005	$nM^{-1}h^{-1}$
Gαβγ + LR → LRGαβγ	k_3	0.02	$nM^{-1}h^{-1}$
L + RGαβγ → LRGαβγ	k_4	0.005	$nM^{-1}h^{-1}$
L + RRGSm → LRRGSm	k_5	0.005	$nM^{-1}h^{-1}$
Gαβγ + RRGSm → RRGSmGαβγ	k_6	0.005	$nM^{-1}h^{-1}$
Gαβγ + LRRGSm → LRRGSmGαβγ	k_7	0.02	$nM^{-1}h^{-1}$
L + RRGSmGαβγ → LRRGSmGαβγ	k_8	0.005	$nM^{-1}h^{-1}$
G protein activation			
LRGαβγ → GαGTP + Gβγ + LR	k_9	50	h^{-1}
Gαβγ → GαGTP + Gβγ	k_{10}	0.2	h^{-1}
LRRGSmGαβγ → GαGTP + Gβγ + LRRGSm	k_{11}	40	h^{-1}
RGS trafficking			
RRGSc → RRGSm	k_{12}	0.0005	h^{-1}
RRGSm → RRGSc	k_{13}	0.005	h^{-1}
R + RRGSc → RRGSm	k_{14}	0.1	$nM^{-1}h^{-1}$
RRGSm → R + RRGSm	k_{15}	100	h^{-1}
LR + RRGSc → LRRGSm	k_{16}	0.1	$nM^{-1}h^{-1}$
LRRGSm → LR + RRGSm	k_{17}	100	h^{-1}
RGαβγ + RRGSc → RRGSmGαβγ	k_{18}	0.1	$nM^{-1}h^{-1}$
RRGSmGαβγ → RGαβγ + RRGSm	k_{19}	0.1	h^{-1}
LRGαβγ + RRGSc → LRRGSmGαβγ	k_{20}	0.1	$nM^{-1}h^{-1}$
GαGTP + RRGSc → RRGSmGαGTP	k_{21}	60	$nM^{-1}h^{-1}$
RRGSmGαGTP → GαGTP + RRGSc	k_{22}	0.05	h^{-1}
Switching off / recycling G protein			
GαGTP → GαGDP	k_{23}	0.005	h^{-1}
GαGTP + RRGSm → RRGSmGαGTP	k_{24}	500	$nM^{-1}h^{-1}$
RRGSmGαGTP → GαGDPP + RRGSc	k_{25}	2.5	h^{-1}
GαGTP + LRRGSm → LRRGSmGαGTP	k_{26}	100	$nM^{-1}h^{-1}$
LRRGSmGαGTP → GαGDPP + LRRGSm	k_{27}	2.5	h^{-1}
GαGTP + RRGSm → RRGSmGαGTP	k_{28}	0.5	$nM^{-1}h^{-1}$
RRGSmGαGTP → GαGDPP + RRGSm	k_{29}	0.5	h^{-1}
GαGDPP → GαGDP + P	k_{30}	1000	h^{-1}
GαGDP + G*bg* → Gαβγ	k_{31}	1000	$nM^{-1}h^{-1}$
P → ∅	k_{32}	10	h^{-1}
Ras1 activation			
GEF + GαGTP → GαGTPGEF	k_{33}	13	$nM^{-1}h^{-1}$
GαGTPGEF + RASGDP → inertGαGTPGEFRASGTP	k_{41}	50	$nM^{-1}h^{-1}$
inertGαGTPGEFRASGTP → inertGαGTPGEF + RASGTP	k_{42}	4	h^{-1}
Activation of Byr2			
RASGTP + MAP3K → RASGTPMAP3K	k_{43}	9	$nM^{-1}h^{-1}$
GαGTP + RASGDP → GαGTP + RASGTP	k_{50}	0.00034	$nM^{-1}h^{-1}$
Recycling of Gpa1 / Ste6 complex			
inertGαGTPGEF + RRGSc → RRGSminertGαGTPGEF	k_{34}	0.0001	$nM^{-1}h^{-1}$
inertGαGTPGEF → GαGDPP + GEF	k_{36}	0.005	h^{-1}
inertGαGTPGEF + RRGSm → RRGSminertGαGTPGEF	k_{37}	0.3	$nM^{-1}h^{-1}$
RRGSminertGαGTPGEF → RGαGDPP + RRGSc + Ste6	k_{38}	0.3	h^{-1}
inertGαGTPGEF + LRRGSm → LRRGSminertGαGTPGEF	k_{39}	50	$nM^{-1}h^{-1}$
LRRGSm inertGαGTPGEF → GαGDPP + LRRGSm + GEF	k_{40}	0.3	h^{-1}
Regulation of Ras1 by Gap1			
RASGTP + GAP → RASGTPGAP	k_{44}	4.2	$nM^{-1}h^{-1}$
RASGTPGAP → RASGDPP + GAP	k_{45}	8	h^{-1}
RASGTPMAP3K + GAP → RASGDPPMAP3KGAP	k_{46}	0.00075	$nM^{-1}h^{-1}$
RASGTPMAP3KGAP → RASGDPP + MAP3K + GAP	k_{47}	10	h^{-1}
RASGTP → RASGDPP	k_{48}	10	h^{-1}
RASGDPP → RASGDP + P	k_{49}	1000	h^{-1}
MAPK activation and deactivation			
MAP2K + RASGTPMAP3K→MAP2KP + RASGTPMAP3K	k_{51}	0.005	$nM^{-1}h^{-1}$
MAP2KP + MAPK → MAP2KP + MAPKP	k_{52}	1	$nM^{-1}h^{-1}$
MAP2KP → MAP2K	k_{53}	8	h^{-1}
MAPKP → MAPK	k_{54}	8	h^{-1}
PhTase + MAPKP → PhTase + MAPK	k_{55}	0.04	$nM^{-1}h^{-1}$

TABLE 3.9: **Reaction scheme for the KR model.**

3.6 Validation of the KR model

The development of the mathematical model to include downstream signalling components has resulted in significant changes to the reaction scheme (although not compromising the key elements of G protein cycling, GPCR-RGS interactions and spatial regulation of the RGS). As a result, validation of the KR model was performed to ensure the new model remains able to reproduce the biological data that the original model could simulate. Validation should provide a greater confidence in the core hypotheses built into the model and subsequently in using the KR model as a predictive tool.

Unless stated otherwise the KR model reaction scheme (Table 3.9) was simulated with initial species concentrations described in Table 3.10 by measuring the accumulation of MAPKp complexes following 16 h simulated induction.

Species	Initial concentration (nM)
L	0 - 100,000
R	205
GαGDP	205
Gβγ	205
RGSc	60
Gef	205
RasGDP	205
Gap	205
MAP3K	205
MAP2K	205
MAPK	205
PhTase	205
All other species were set to 0 nM	

Table 3.10: **Initial concentrations for species for simulating the KR model.** For simulation of wild-type cells.

3.6.1 Blocking the GPCR-RGS interaction

It has been shown that deletion of *rgs1* or removal the C-terminal domain of Mam2 results in a two-fold decrease in maximal transcriptional response, an increase in basal signalling and an increase in potency of P-factor, when compared to WT ($rgs1^+$) cells with full length Mam2 [173] (Figure 3.22a). These findings highlighted that an interaction between Rgs1 and the C-terminal domain of the Mam2 was essential for a WT signalling response. The KR model recapitulated the signalling characteristics of the *in vitro* assay i.e. an increase in basal and decrease in maximal signalling response was observed. This was achieved

in silico by removing all RGS species ([RGSc]=0 nM) and blocking interactions between the receptor (R) and RGS (k_{14}=k_{16}=k_{18}=k_{20}=0) however, the KR model was unable to reproduce the increase in potency (Figure 3.22b).

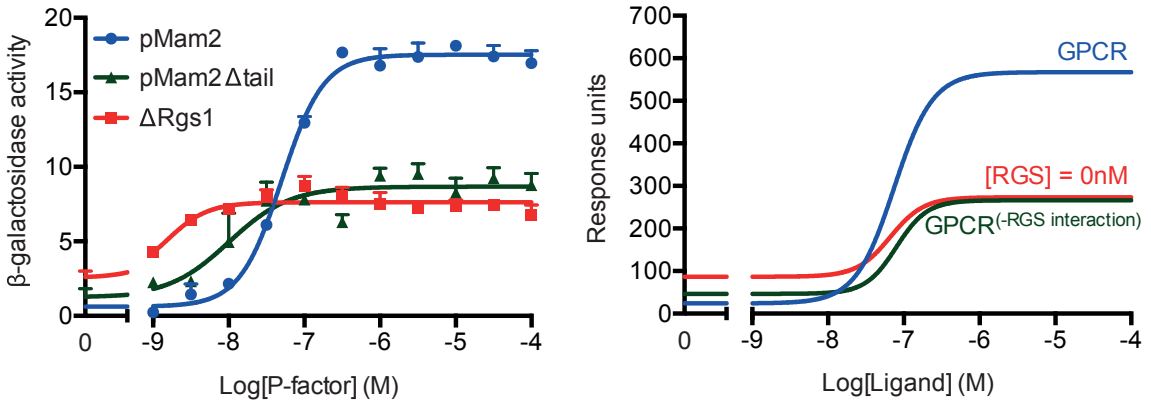

FIGURE 3.22: **Model testing: Removal of the receptor tail.** (a) *Δrgs1* (JY630) and *Δmam2* (JY1169) transformed with pREP3x-Mam2 (pMam2, JD1627) and pREP3x-Mam2Δtail (pMam2Δtail, JD2880) *S. pombe* cells were grown to mid-exponential growth phase before treatment with a range of P-factor concentrations (from 0 µM to 100 µM)for 16 h and then assayed for β-galactosidase activity (figure adapted from [173]). (b) Simulations are of the KR model in an unmodified system (GPCR), when all GPCR-RGS interaction reactions are blocked (k_{14}=k_{16}=k_{18}=k_{20}=0) in Table 3.9 ($GPCR^{-RGSinteraction}$) and when [RGS]=0 nM (No RGS).

3.6.2 Negative role of RGS in the absence of a GPCR-RGS interaction

It has been shown that in strains lacking Mam2 sequential increases in Rgs1 concentration reduces basal signalling response, suggesting that in this environment Rgs1 acts as a sole negative regulator, contrary to its role when Mam2 is present [173] (Figure 3.23a). The KR model reproduced the reduction in signalling response with increasing RGSc concentration ([RGSc]=0 nM, [RGSc]=60 nM, [RGSc]=120 nM and [RGSc]=180 nM) (Figure 3.23b), suggesting that the reactions used to extend the model still captured the signalling behaviours.

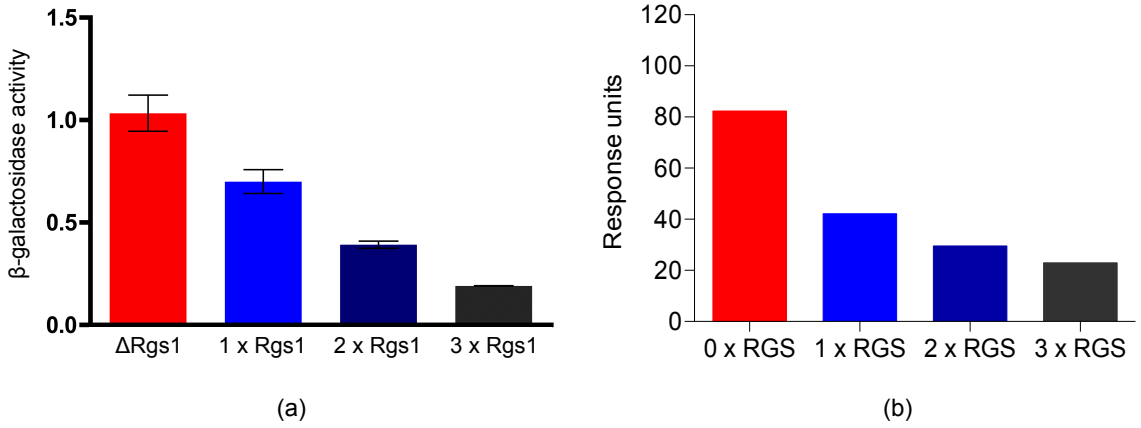

FIGURE 3.23: **Model testing: RGS influence in the absence of a receptor.** (a) *Δmam2 S. pombe* (JY1169) transformed with pREP3x (JD3386, 1xRgs1), pREP3x-Rgs1 (JD2555, 2xRgs1) and both pREP3x-Rgs1 and pREP4x-Rgs1 (JD2555 + JD2388, 3xRgs1) and *Δmam2Δrgs1* (JY1291), which lacks endogenous Rgs1 (ΔRgs1) were grown to mid-exponential growth phase and treated with a range of P-factor concentrations from 0 µM to 100 µM for 16 h before being assayed for β-galactosidase activity (as described in section 2.2.8.1). Data shown is the average of three independent experiments ±SEM. Experimental data adapted from [190]. (b) Simulations were with [R]=0 nM and varying RGS concentration from [RGSc]=0 nM, [RGSc]=60 nM, [RGSc]=120 nM and [RGSc]=180 nM.

3.6.3 Dependence on RGS concentration

The concentration of GαGTP is likely to be a critical control point in a system where GαGTP is the signal transducer. In the model, the RGS species accelerates the hydrolysis of GαGTP and therefore, these RGS species are key regulators of signal transduction. As a consequence, signal output should be sensitive to the concentration of RGS and this has been shown *in vitro* by Smith *et al.* (2009) [190].

To validate if the KR model is sensitive to RGS concentration WT *S. pombe* cells (JY544) were transformed with pREP3x (JD3386, 1xRgs1), pREP3x-Rgs1 (JD2555, 2xRgs1) and both pREP3x-Rgs1 and pREP4x-Rgs1 (JD2555 and JD2388, 3xRgs1) and these strains along with *Δrgs1* (JY630) cells were grown to mid-exponential growth phase before treatment with a range of P-factor concentrations (from 0 µM to 100 µM) for 16 h and assayed for β-galactosidase activity (as described in section 2.2.8.1).

The experiment showed that increasing Rgs1 concentration *in vitro* increased maximal signalling response and reduced the potency of P-factor (Figure 3.24a, 2xRgs1), whereas further increasing the cellular concentration of Rgs1 caused a reduction in maximal signalling response and even further reduction in potency in comparison to cells containing

endogenous levels of Rgs1 (Figure 3.24 a, 3xRgs1). These data illustrated the dual positive and negative role that Rgs1 can have one signalling response [190]. The KR model was able to replicated the positive and negative signalling characteristics of Rgs1 *in silico* by increasing the concentration from [RGSc]=0 nM (0xRGS), [RGSc]=60 nM (1xRGS), [RGSc]=120 nM (2xRGS) and [RGSc]=180 nM (3xRGS) (Figure 3.24b).

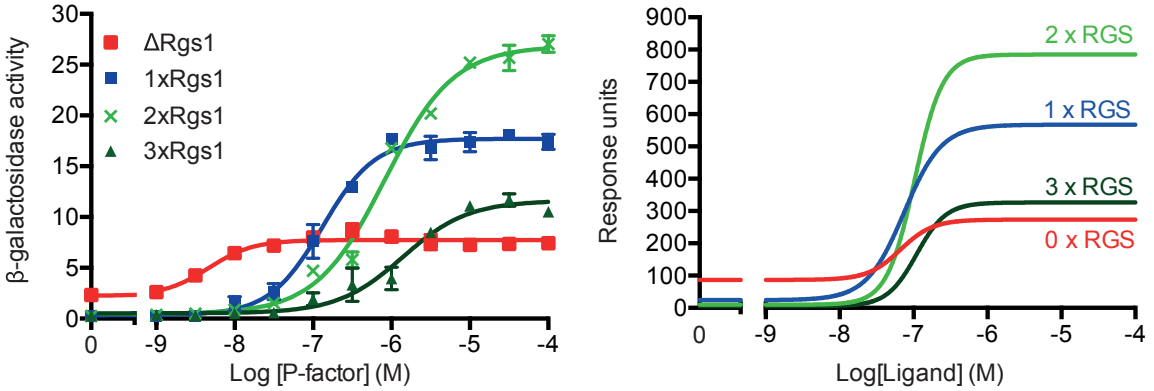

(a) (b)

FIGURE 3.24: **Model testing: dependence of Rgs1 concentration.** (a) WT *S. pombe* cells (JY544) that were transformed with pREP3x (JD3386, 1xRgs1), pREP3x-Rgs1 (JD2555, 2xRgs1) and both pREP3x-Rgs1 and pREP4x-Rgs1 (JD2555 + JD2388, 3xRgs1) and *Δrgs1* (JY630) cells (ΔRgs1) were grown to mid-exponential growth phase before treatment with a range of P-factor concentrations (from 0 µM to 100 µM). After 16 h cells were assayed for β-galactosidase activity (as described in section 2.2.8.1). Data shown is the average of three independent experiments ±SEM. Experimental data adapted from [190]. (b) Simulations of the KR model with [RGSc]=60 nM (1xRGS), [RGSc]=120 nM (2xRGS) and [RGSc]=180 nM (3xRGS).

Additional validations of the KR model were conducted against previously determined experimental data. The model was found to qualitatively agree with experimental data from a range of experiments including conditions of Gpa1 overexpression, Mam2 overexpression and when expressing an Rgs1 insensitive Gpa1 mutant (Appendix C).

3.6.4 Gβγ as the signal transducer

In some GPCR signalling systems such as the pheromone-response pathway in *S. cerevisiae*, Gβγ rather than the Gα is the signal transducer [265]. The previous models of the *S. pombe* mating-response pathway were able to recapitulate the *S. cerevisiae* transcriptional mating-response data (B. Smith, PhD thesis, 2009 and W. Croft, PhD thesis, 2012). However, these models only included reactions up to and including the G protein binding and activating an Effector species, which in the case of the *S. cerevisiae* system would be the MAP3K STE20. The *S. pombe* system is more complex than this as Gpa1 activates another G protein Ras1 via the GEF Ste6 prior to signal transduction to a mitogenic cascade.

In *S. cerevisiae*, loss of SST2 (a RGS protein) increases basal, maximal transcriptional response and the potency of α-factor, whereas overexpression of SST2 reduces maximal transcriptional response and potency, characteristics typical of a negative regulator [266]. The model developed in this thesis was able to simulate a system where Gβγ was the signal transducer by some basic modifications, mainly that Ste6 was activated by Gβγ rather than GαGTP (Table 3.11, reaction k_{33}) and all reactions involving inertGαGTP (k_{37} - k_{42}) were removed (Table 3.11).

The equivalent *in silico* experiment was simulated using the version of the model that signals via the Gβγ (Table 3.11); specifically, simulations were of an unmodified system (RGS), when no RGS species was present [RGS]=0 nM (No RGS) and when RGS concentration was doubled ([RGS]=120 nM, 2xRGS) (Figure 3.25).

Although the No RGS simulation displayed an elevated basal response, it was unable to capture the increase in potency and maximal transcriptional response observed *in vitro* [266], instead a constant elevated signalling profile, which did not display a dose-dependent change in response units was observed. In addition, the Gβγ model was unable to capture the reduction in maximal transcriptional response and potency observed when overexpressing the RGS protein SST2 and there was no difference in dose-response profiles between 1xRGS and 2xRGS (Figure 3.25). Only now that the KR model includes downstream components of the Gα could it discriminate between the two yeast systems.

Ligand / G protein signalling			
L + R → LR	k_1	0.0025	$nM^{-1}h^{-1}$
Gαβγ + R → RGαβγ	k_2	0.005	$nM^{-1}h^{-1}$
Gαβγ + LR → LRGαβγ	k_3	0.02	$nM^{-1}h^{-1}$
L + RGαβγ → LRGαβγ	k_4	0.005	$nM^{-1}h^{-1}$
L + RRGSm → LRRGSm	k_5	0.005	$nM^{-1}h^{-1}$
Gαβγ + RRGSm → RRGSmGαβγ	k_6	0.005	$nM^{-1}h^{-1}$
Gαβγ + LRRGSm → LRRGSmGαβγ	k_7	0.02	$nM^{-1}h^{-1}$
L + RRGSmGαβγ → LRRGSmGαβγ	k_8	0.005	$nM^{-1}h^{-1}$
G protein activation			
LRGαβγ → GαGTP + Gβγ + LR	k_9	50	h^{-1}
Gαβγ → GαGTP + Gβγ	k_{10}	0.2	h^{-1}
LRRGSmGαβγ → GαGTP + Gβγ + LRRGSm	k_{11}	40	h^{-1}
RGS trafficking			
RRGSc → RRGSm	k_{12}	0.0005	h^{-1}
RRGSm → RRGSc	k_{13}	0.005	h^{-1}
R + RRGSc → RRGSm	k_{14}	0.1	$nM^{-1}h^{-1}$
RRGSm → R + RRGSm	k_{15}	100	h^{-1}
LR + RRGSc → LRRGSm	k_{16}	0.1	$nM^{-1}h^{-1}$
LRRGSm → LR + RRGSm	k_{17}	100	h^{-1}
RGαβγ + RRGSc → RRGSmGαβγ	k_{18}	0.1	$nM^{-1}h^{-1}$
RRGSmGαβγ → RGαβγ + RRGSm	k_{19}	0.1	h^{-1}
LRGαβγ + RRGSc → LRRGSmGαβγ	k_{20}	0.1	$nM^{-1}h^{-1}$
GαGTP + RRGSc → RRGSmGαGTP	k_{21}	60	$nM^{-1}h^{-1}$
RRGSmGαGTP → GαGTP + RRGSc	k_{22}	0.05	h^{-1}
Switching off / recycling G protein			
GαGTP → GαGDP	k_{23}	0.005	h^{-1}
GαGTP + RRGSm → RRGSmGαGTP	k_{24}	500	$nM^{-1}h^{-1}$
RRGSmGαGTP → GαGDPP + RRGSc	k_{25}	2.5	h^{-1}
GαGTP + LRRGSm → LRRGSmGαGTP	k_{26}	100	$nM^{-1}h^{-1}$
LRRGSmGαGTP → GαGDPP + LRRGSm	k_{27}	2.5	h^{-1}
GαGTP + RRGSm → RRGSmGαGTP	k_{28}	0.5	$nM^{-1}h^{-1}$
RRGSmGαGTP → GαGDPP + RRGSm	k_{29}	0.5	h^{-1}
GαGDPP → GαGDP + P	k_{30}	1000	h^{-1}
GαGDP + Gβγ → Gαβγ	k_{31}	1000	$nM^{-1}h^{-1}$
P → ∅	k_{32}	10	h^{-1}
Ras1 activation			
Ste6 + Gβγ → Gβγ Ste6	k_{33}	13	$nM^{-1}h^{-1}$
Gβγ Ste6 + RASGDP → Gβγ Ste6RASGTP	k_{34}	50	$nM^{-1}h^{-1}$
Gβγ Ste6RASGTP → Gβγ Ste6 + RASGTP	k_{35}	4	h^{-1}
Activation of Byr2			
RASGTP + Byr2 → RASGTPMAP3K	k_{36}	9	$nM^{-1}h^{-1}$
Gβγ + RASGDP → Gβγ + RASGTP	k_{49}	0.00034	$nM^{-1}h^{-1}$
Regulation of RAS by GAP			
RASGTP + GAP → RASGTPGAP	k_{43}	4.2	$nM^{-1}h^{-1}$
RASGTPGAP → RASGDPP + GAP	k_{44}	8	h^{-1}
RASGTPMAP3K + GAP → RASGDPPByr2GAP	k_{45}	0.00075	$nM^{-1}h^{-1}$
RASGTPMAP3KGAP → RASGDPP + Byr2 + GAP	k_{46}	10	h^{-1}
RASGTP → RASGDPP	k_{47}	10	h^{-1}
RASGDPP → RASGDP + P	k_{48}	1000	h^{-1}
MAPK activation and deactivation			
Byr1 + RASGTPMAP3K→MAP2KP + RASGTPByr2	k_{50}	0.005	$nM^{-1}h^{-1}$
MAP2KP + MAPK → MAP2KP + MAPKP	k_{51}	1	$nM^{-1}h^{-1}$
MAP2KP → MAP2K	k_{52}	8	h^{-1}
MAPKP → MAPK	k_{53}	8	h^{-1}
PhTase + MAPKP → PhTase + MAPK	k_{54}	0.04	$nM^{-1}h^{-1}$

TABLE 3.11: **Reaction scheme for the KR model with Gβγ as the signal transducer.** This model was simulated with the initial conditions from the KR model (Table 3.10).

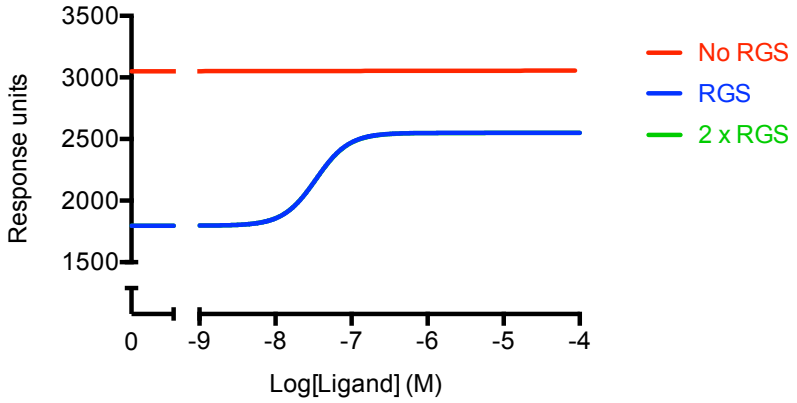

FIGURE 3.25: **Model testing: Gβγ as the signal transducer.** The KR model was modified such that Gβγ was the signal transducer (Table 3.11). The model was simulated with RGS concentration at 0 nM (No RGS), 60 nM (RGS) and 120 nM (2 x RGS). The concentration of ligand was varied over the range 0 nM - 100 µM following 16 h simulated induction. Output from the model shows the accumulation of MAPKP over the duration of the simulated assay.

3.7 Use of the model as a predictive tool

The KR model was developed using experimental data collected both in this study and from the literature. It could qualitatively reproduce all of the end-point (assayed after 16 h of P-factor treatment) experimental data currently available. The consistency between the experimental data and the KR model output increased the confidence in the mechanism proposed in the reactions for signal transduction and regulation. As a consequence, the KR model was used to predict system level signalling behaviour under perturbed conditions of interest.

3.7.1 Removal of GAP causes RGS to act as a sole negative regulator

Rapid hydrolysis of Gpa1 (a G protein), is essential for a maximal transcriptional response in *S. pombe* [190]. Gpa1 and Ras1 (the two known G proteins that act on the transcriptional pathway) are regulated by Rgs1 and Gap1, respectively [86, 87]. The KR model (created in this study) was the first of its kind to include the downstream components Ras1 and Gap1.

In the presence of GAP, the KR model predicts the RGS species has a negative and positive role on signalling response (Figure 3.26a, see maximals), which was confirmed experimentally [190] (Figure 3.24). However, when GAP is absent ([GAP]=0 nM) the KR model predicts that the RGS species acts as a sole negative regulator; where increasing RGS concentration decreases maximal signalling response (Figure 3.26b).

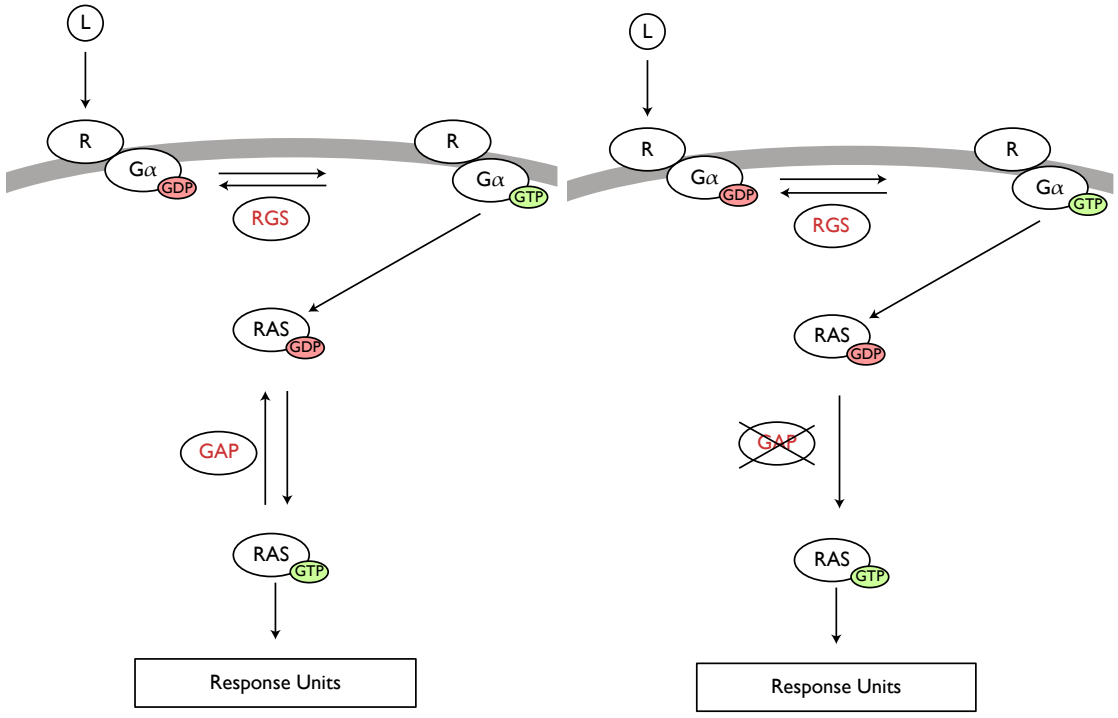

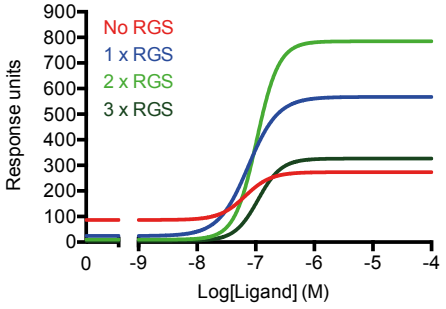

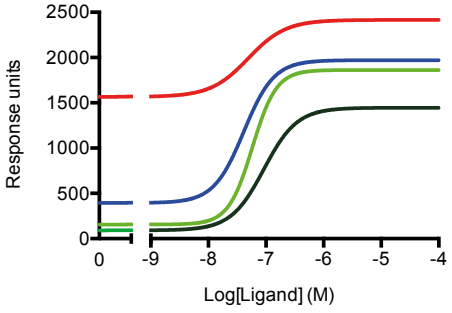

GAP		
RGS	Basal	Maximal
2x •	3	623
1x •	9	517
3x •	2	370
0x •	51	314

ΔGAP		
RGS	Basal	Maximal
0x •	918	1360
1x •	126	1009
2x •	64	966
3x •	43	887

(a) (b)

Figure 3.26: **The KR model predicts that by removing GAP the RGS will act as a sole negative regulator.** Simulations of the KR model with 0 nM (0xRGS), 60 nM (1xRGS), 120 nM (2xRGS) and 180 nM (3xRGS) of RGS species. The concentration of ligand in the simulation was varied over the range 0 µM to 100 µM following 16 h simulated induction. Simulations are the result of (a) GAP being present with initial concentration of 205 nM (b) and in the absence of GAP with initial concentration of 0 nM.

The corresponding basal and maximal simulated values are displayed in the table

To identify whether the KR models' prediction was accurate in terms of signalling behaviour, an equivalent *in vitro* experiment was performed; a *Δrgs1Δgap1 S. pombe* strain (JY1718) was first created by transforming pKS-*gap1::ura4* (JD3535) digested *Eco*RI and *Xba*I, into the *Δrgs1* strain JY630, which inserts a *ura4* cassette into the endogenous ORF of *gap1* (for details see section 2.2.3). *Δgap1* (JY1618) cells were then transformed with pREP3x (JD3386) creating a strain with one endogenous copy of Rgs1 (1xRsg1), pREP3x-Rgs1 (JD2555) containing two copies of Rgs1 (2xRgs1) and both pREP3x-Rgs1 (JD2555) and pREP4x-Rgs1 (JD2388) thus creating a strain with three copies of Rgs1 (3xRgs1). These strains, along with JY1718 (0xRgs1), were grown to mid-exponential growth phase, treated with a range of P-factor concentrations and after 16 h were assayed for β-galactosidase activity (as described in section 2.2.8.1).

In the presence of endogenous Gap1, Rgs1 displayed a negative and positive influence on β-galactosidase activity, consistent with previous observations [190] (Figure 3.27a). However, when Gap1 was absent, deletion of Rgs1 significantly increased basal signalling response in comparison to strains containing endogenous Rgs1 (1xRgs1) (from 2±2 *lacZ* units to 11±2 *lacZ* units, $p<0.0001$ when n=5, Student's t-test). The observed increase in basal activity in *Δrgs1Δgap1* strains was consistent with the *in silico* experiment ([RGSc]=[GAP]=0 nM) from the KR model (Figure 3.26b). The KR model also predicted that increasing RGS concentration reduced basal signalling response however, a significant effect on basal response was not observed *in vitro* ($p>0.05$, when n=3, Student's t-test).

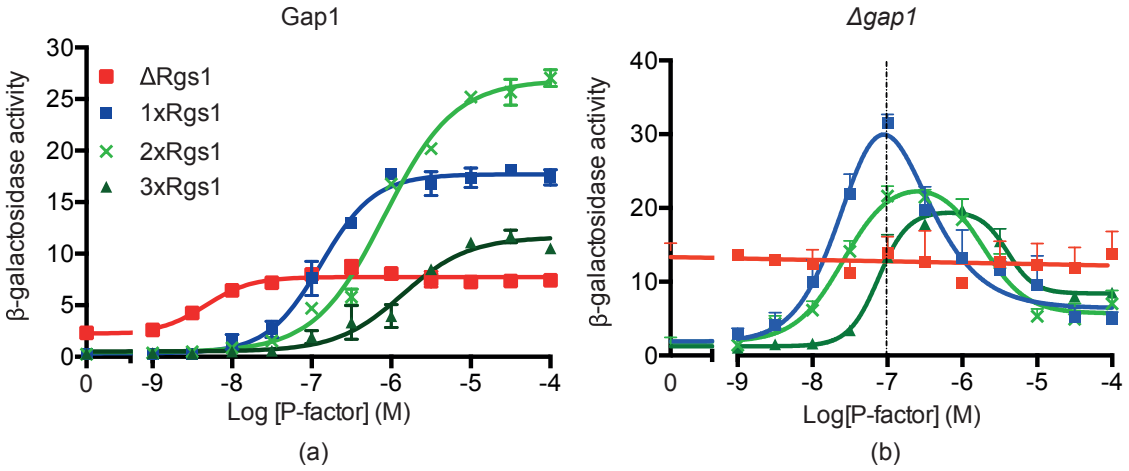

FIGURE 3.27: **Rgs1 acts as a negative regulator.** (a) Experimental data adapted from Smith *et al.* (2009) [190]. (b) *Δgap1 S. pombe* cells (JY1538) were transformed with pREP3x (1xRgs1), pREP3x-Rgs1 (2xRsg1) and finally both pREP4x-Rgs1 and pREP3x-Rgs1 (3xRsg1), these strains and a *Δrgs1Δgap1* strain JY1718 were grown to mid-exponential growth phase before treatment with a range of P-factor concentrations (from 0 µM to 100 µM). Following 16 h stimulation strains were assayed for β-galactosidase activity (as described in section 2.2.8.1). Data shown is the average of three independent experiments ±SEM.

Strains lacking *gap1* but containing Rgs1 displayed a non-monotonic response (Figure 3.27b). Interestingly, the size of the peak (distance from the x-axis) decreased and displayed a horizontal shift (to right) with increasing Rgs1 concentration (Figure 3.27b, see 1xRgs1, 2xRgs1, 3xRgs1). It has been shown that the non-monotonic response observed in *Δgap1* is caused by cell lysis (Figure 3.12). It was also suggested that a plateau in signalling response was observed at ∼100 nM P-factor prior to the reduction in β-galactosidase activity caused by an increase in non-viable cells [223] (Figure 3.27b, dotted line indicates potential maximal response). The reduction in β-galactosidase peak height with increasing Rgs1 concentration may suggest that maximal transcriptional response decreases with increasing Rgs1 concentration. In addition, the horizontal shift in the peak to the right indicates that cell lysis is reduced with Rgs1 concentration. It should be noted that the KR model predicts that maximal transcriptional response decreases with increasing RGSc concentration when [GAP]=0 nM, which is illustrated by the *in vitro* assays.

To verify that cell lysis was indeed reduced in strains lacking *gap1* and containing higher concentration of Rgs1 (2xRgs1 and 3xRgs1), the same strains used in the β-galactosidase described above were assayed for cell viability following treatment with 0 µM to 100 µM P-factor (as described in section 2.2.16). An increase in the basal percentage of non-viable cells was observed between 0xRgs1 and 1xRgs1 at 1±3% to 10±4% non-viable, however this was

not considered statistically significant (p=0.1127 when n=3, Student's t-test) (Figure 3.28). In addition, strains lacking functional Rgs1 and Gap1 did not display a dose-dependent increase in non-viable cells in response to increasing P-factor treatment. Instead, a linear response was observed, consistent with the constant elevated β-galactosidase activity observed in the transcriptional assay (Figure 3.27b).

Δgap1 expressing endogenous Rgs1 (1xRgs1) exhibited the greatest percentage of lysed cells reaching a maximal of 75±4% (Figure 3.28). Increasing the cellular concentration by 2xRgs1 and 3xRgs1 significantly reduced the percentage of non-viable cells to 47±4% and 49±2%, respectively (p=0.0088 and p=0.0038 for n=3, respectively, Student's t-test). A reduction in non-viable cells was not observed between 2xRgs1 and 3xRgs1, even though a reduction and shift in peak size (to the right) in β-galactosidase activity was observed (Figure 3.27b).

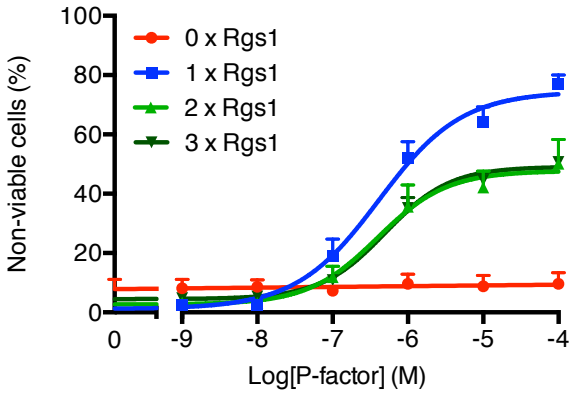

FIGURE 3.28: **Cell lysis is reduced with increasing Rgs1 concentration.** *Δrgs1Δgap1* (JY1718, 0xRgs1) cells and *Δgap1* (JY1618) cells transformed with 1xRgs1, 2xRgs1 and 3xRgs1 were grown to mid-exponential growth phase before treatment with a range of P-factor concentrations (from 0 µM to 100 µM). After 16 h a cell viability assay was performed as described in section 2.2.16. Flow cytometry was used to determine the percentage of non-viable cells within each population. Data presents three independent experiments±SEM.

The increased cell lysis at high (≥1 µM) P-factor concentrations (in comparison to ∼12% non-viable [223]) prevents a dose-dependent transcriptional response, consistent with the results observed in another study [223]. Despite the non-monotonic response, increasing Rgs1 concentration in strains lacking Gap1 reduced maximal signalling response consistent with the KR model prediction. As observed earlier in this chapter (Figure 3.15), removing Scd1 (a GEF for the essential G protein Cdc42) directs signalling to the transcriptional pathway (via Byr2), alleviating the amount of cell lysis. To establish whether increasing

the cellular concentration of Rgs1 reduces maximal transcriptional response, β-galactosidase assays were performed in strains lacking Scd1. Specifically, *Δscd1Δgap1* cells (JY1674) were transformed with 1xRgs1, 2xRgs1 and 3xRgs1, grown to mid-exponential growth phase, treatment with a range of P-factor concentrations (from 0 µM to 100 µM) and after 16 h assayed for β-galactosidase activity and cell viability (as described in section 2.2.8.1 and section 2.2.16). Increasing the cellular concentration of Rgs1 in *Δscd1Δgap1*

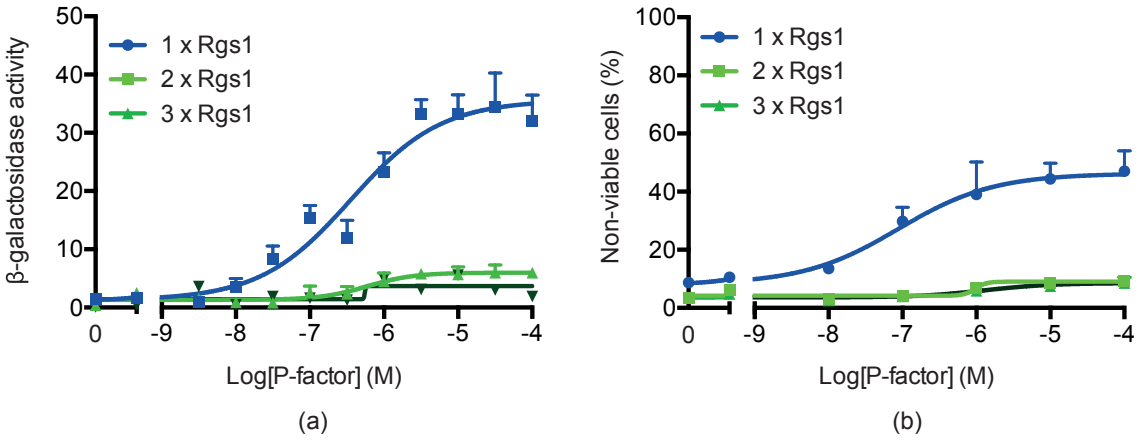

FIGURE 3.29: **Maximal β-galactosidase activity decreases with increasing Rgs1 concentration.** *Δscd1Δgap1* (JY1674) cells transformed with 1xRgs1, 2xRgs1 and 3xRgs1 were grown to mid-exponential growth phase before treatment with a range of P-factor concentrations (from 0 µM to 100 µM). After 16 h cells were assayed for (a) β-galactosidase activity (as described in section 2.2.8.1)and (b) a cell viability assay was performed (as described in section 2.2.16). Flow cytometry was used to determine the percentage of non-viable cells within each population. Data shown is the average of three independent experiments ±SEM.

strains decreases maximal β-galactosidase activity (Figure 3.29a). A significant reduction in β-galactosidase response was observed between *Δscd1Δgap1* cells expressing 1xRgs1 and 2xRgs1 (from 36±3 *lacZ* units to 6±1 *lacZ* units, p=0.0006 when n=3, Student's t-test). Complementary to the reduction in β-galactosidase observed, a significant increase in cell viability was observed with increasing Rgs1 concentration from 1xRgs1 at 46±6% non-viable to 2xRgs1 at 6±2% non-viable (p=0.0028 when n=3, Student's t-test). Further increasing the Rgs1 concentration (to 3xRgs1) did not significantly reduce cell viability (3xRgs1: 9±1% when compared to 2xRgs1, p=0.6899 when n=3, Student's t-test). It should be noted that the percentage of cell lysis displayed in the *Δscd1Δgap1* strains with 1xRgs1 and 2xRgs1 was less than the cell lysis observed in the WT *S. pombe* strain JY544 (12±2%). Together these data support the KR model prediction that Rgs1 behaves as a negative regulator when Gap1 is removed.

3.8 Modelling time-series data

The KR model was validated and could recapitulate all of the end-point data currently available. However, the KR model had not been investigated to determine if it could replicate the signalling behaviour of time-course data. Therefore, a transcriptional time-course assay was performed using the WT (*sxa2>lacZ*) strain JY544. The cells were grown to mid-exponential growth phase, treated with a range of P-factor concentrations from 0 µM to 100 µM and assayed for β-galactosidase activity every 2 h from 0 h to 16 h (as described in section 2.2.8.1). At low (1 nM and 10 nM) P-factor concentrations a negligible increase in transcriptional response in comparison to untreated cells was observed by 16 h (Untreated: 1±1 *lacZ* units compared to 1 nM 2±0.1 *lacZ* units) (Figure 3.30a).

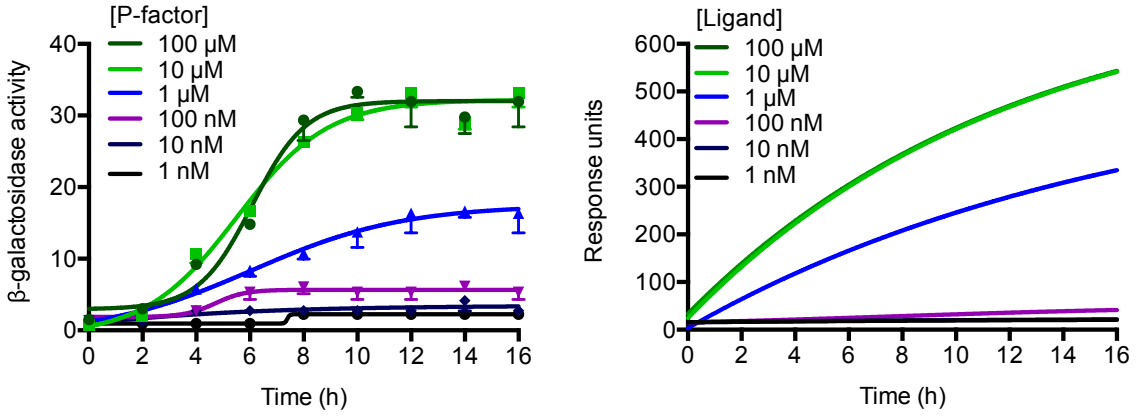

FIGURE 3.30: **The KR model did not recapitulate the plateau in transcriptional response.** (a) The WT strain JY544 was grown to mid-exponential growth phase before treatment with a range of P-factor concentrations (from 0 µM to 100 µM) for 16 h and assayed for β-galactosidase activity (as described in section 2.2.8.1) every 2 h from 0 h to 16 h. Data shown is the average of three independent experiments ±SEM. (b) The equivalent *in silico* experiment was performed using the KR model (Table 3.9). Simulations are of an unmodified system over a simulated 16 h period. The concentration of ligand was varied over the range 0 µM to 100 µM. Output from the model shows the accumulation of MAPKP over the duration of the simulated assay.

β-galactosidase response of cells treated with 100 nM P-factor increased following 0 h and 4 h of treatment and then plateaued between 6 h to 8 h displaying 6±0.3 *lacZ* units from 8 h to 16 h (Figure 3.30a). Following 1 µM P-factor, transcriptional response continued to increase with time until 14 h, where a plateau in response was observed (Figure 3.30a). Cells treated with 10 µM and 100 µM both reached a maximal signalling plateau of 32±1 *lacZ* units by 10 h.

Consistent trends were observed when comparing the *in silico* experiment with the β-galactosidase time-course assays, i.e. by increasing the concentration of ligand increased the number of response units (Figure 3.30). However, the KR *S. pombe* model was unable to capture the plateau in β-galactosidase activity when simulated with >1 µM, instead the response units increased continuously over the 16 h simulated assay. The plateau in response suggested that *lacZ*, the gene that encodes β-galactosidase, was no longer being transcribed.

3.8.1 Internalisation of Mam2

As discussed in the Introduction, numerous mechanisms exist for terminating GPCR signalling, primarily via the removal of the ligand or inactivation of the receptor. **M**-type *S. pombe* cells secrete Sxa2, a serine carboxypeptidase, in response to P-factor stimulation, which hydrolyses the extracellular pheromone and hence, removes the ligand signal [218, 267]. However, the *S. pombe* strains used in this study were *sxa2*$^{-}$ and thus were unable to hydrolyse P-factor, yet still exhibited a transcriptional plateau, suggesting that other mechanisms were responsible for signal termination.

In response to ligand-binding, receptors are often phosphorylated by specific kinases in their intracellular domains to initiate internalisation from the plasma membrane. Mam2, the **M**-type *S. pombe* pheromone receptor is internalised in response to P-factor [173], however the specific kinases that promote internalisation are unknown and there identification is the focus of Chapter 4. To include internalisation of the receptor into the model a generic kinase term, K, was assumed to interact with the ligand-bound receptor and cause it to become inactive (Equation 3.5).

$$RL + K \rightarrow \emptyset + K \qquad k_{56} = 0.05 \ nM^{-1}h^{-1} \tag{3.5}$$

The addition of equation 3.5 to the KR model resulted in the model simulating the plateau in transcriptional response observed with time (compare Figure 3.31a and 3.31b), however the model lacked qualitative agreement with the end-point (following 16 h treatment) transcriptional data when varying the concentration of RGS (compare Figure 3.31d with 3.24b). The rate of receptor desensitisation k_{56}=0.05 $nM^{-1}h^{-1}$ was chosen as this exhibited a plateau in simulated response units by 8 h (when simulated with 100 µM)

as observed in the time-course experiment and appeared to be the best qualitative fit for varying the concentration of RGS for the end-point data.

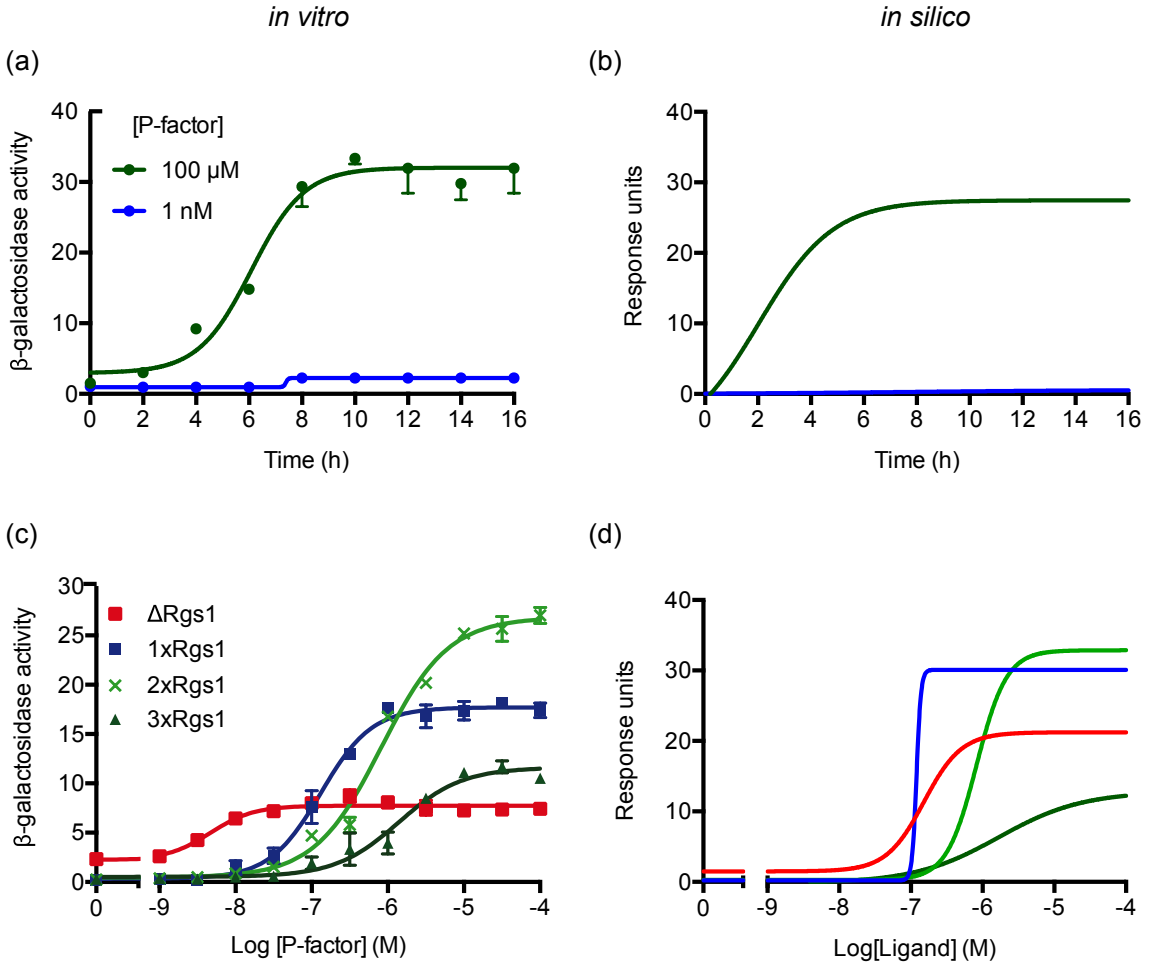

FIGURE 3.31: **The addition of receptor desensitisation into the KR model exhibited a qualitative agreement with the temporal data.** (a) The WT strain JY544 was grown to mid-exponential growth phase treated with 1 nM and 100 μM P-factor for 16 h and assayed for β-galactosidase activity (as described in section 2.2.8.1) every 2 h from 0 h to 16 h. Data shown is the average of three independent experiments ±SEM. (b) The KR model (Table 3.9) with equation 3.5, which includes receptor desensitisation was simulated over a 16 h period with 1 μM and 100 μM P-factor concentration. Output from the model shows the accumulation of MAPKP over the duration of the simulated assay. (c) Experimental data adapted from Smith *et al.* (2009) [190]. (d) The KR model (Table 3.9) with equation 3.5, which includes receptor desensitisation was simulated with varying concentrations of P-factor (from 0 μM to 100 μM P-factor). Output from the model shows the accumulation of MAPKP over the duration of the simulated assay for 16 h.

Equation 3.5 assumes that the ligand-bound receptor is phosphorylated by a single kinase to become inactive. This is a simple way of presenting the process of receptor desensitisation. For example, some GPCRs are multi-phosphorylated by either a single kinase or multiple kinases within their C-terminal domains and hence receptor desensitisation may

not be a binary switch. One example discussed previously is the phosphorylation of the *Sc. cerevisiae* pheromone receptor STE2. This receptor desensitisation event requires both yeast casein kinases YCK1 and YCK2 to phosphorylate the C-terminal tail to promote the same amount of internalisation from the membrane [112]. Perhaps a reason why the KR model simulated with equation 3.5 is unable to show a good qualitative fit is that perhaps receptor desensitisation is a multi-step process which is not incorporated in the model. To incorprate these terms of receptor desensitisation into the model first we must understand which kinases promote internalisation in *S. pombe* and how these kinases control the level or response of receptor inactivation or internalisation in response to pheromone.

3.9 Summary

The previous ODE models of the *S. pombe* mating-response pathway were limited when understanding the pathway as a whole, as only reactions describing the receptor R, Gα and RGS species were included. The transcriptional pathway is more complex than this and therefore, the latest version of the model by Croft *et al.* (2013) was extended to include all downstream signalling components upto and including Spk1 (a MAPK). As a result, a complete model termed the KR model was created, which was developed on experimental data collected both in this study and from the literature. The KR model could qualitatively reproduce the signalling characteristics of the end-point (assayed after 16 h of P-factor treatment) experimental data, which motivated its use as a predictive tool.

When Gap1 was available *in vitro* Rgs1 acts as a negative and positive regulator of signalling [190]. The KR model predicted that by deletion of Gap1 (the negative regulator of Ras1), Rgs1 acts as a sole negative regulator. The equivalent *in vitro* experiment showed that in cells treated with ≤100 nM P-factor, Rgs1 did in fact act as a negative regulator however, the increasing non-viability of cells prevented a typical sigmodal response at higher concentrations. Cell lysis was prevented by deletion of Scd1 (a GEF for CDC42), which transduces signalling via the MAP3K Byr2. In *Δscd1Δgap1* strains cell lysis did not prevent sigmodial response to P-factor and indicated that Rgs1 acted as a sole negative regulator of signalling when treated with >100 nM, consistent with the KR model prediction.

The KR model was also simulated over time and compared with the equivalent *in vitro* time-series β-galactosidase activity experiments. The model displayed qualitative trends with the experimental data; showing that the number of response units increased with ligand concentration. However, the model was unable to capture the plateau in β-galactosidase

activity observed *in vitro*. The plateau in response suggested that *lacZ*, the gene that encodes β-galactosidase, was no longer being transcribed. Attenuation of GPCR signalling occurs if the ligand (P-factor) is removed or the GPCR (Mam2) prevented from activating the G protein. Commonly, GPCRs are internalised following ligand-binding, to prevent continual stimulation and control the amount of activation through the pathway. The KR model was then simulated with a simple receptor desensitisation term that inactivated ligand-bound receptors, which showed a qualitative agreement with the time course data but lacked agreement with the end point data. The kinase(s) or processes involved in receptor desensitisation (including internalisation) are unknown and therefore, the identification of the protein(s) responsible for this process will be the focus of the next chapters.

Chapter 4

The role of Cki1, Cki2 and Cki3 in P-factor signalling

4.1 Background

The KR model developed in chapter 3 was unable to replicate the temporal plateau in β-galactosidase activity produced by WT (*sxa2>lacZ*) cells following treatment with P-factor (Figure 3.30). The plateau in response suggested that *lacZ*, the gene that encodes β-galactosidase, was no longer being transcribed. As stated in the Introduction, numerous mechanisms exist for terminating GPCR signalling, primarily via the removal of the ligand or inactivation of the receptor. **M**-type *S. pombe* cells secrete Sxa2, a serine carboxypeptidase, in response to P-factor stimulation, which hydrolyses the extracellular pheromone [218, 267]. The *sxa2*$^{-}$ strain used in this time-course assay was unable to hydrolyse P-factor, yet still exhibited a transcriptional plateau, suggesting that other mechanisms were responsible for signal termination.

GPCRs are often internalised following phosphorylation of the intracellular receptor domains in response to ligand-binding to prevent further signal transduction via the G protein. Mam2, the **M**-type *S. pombe* pheromone receptor, is internalised in response to P-factor [173]. However, the specific kinase(s) that promote this process have not yet been described. This chapter seeks to identity and characterise potential Mam2 kinase(s) in the **M**-type *S. pombe* pheromone-response pathway.

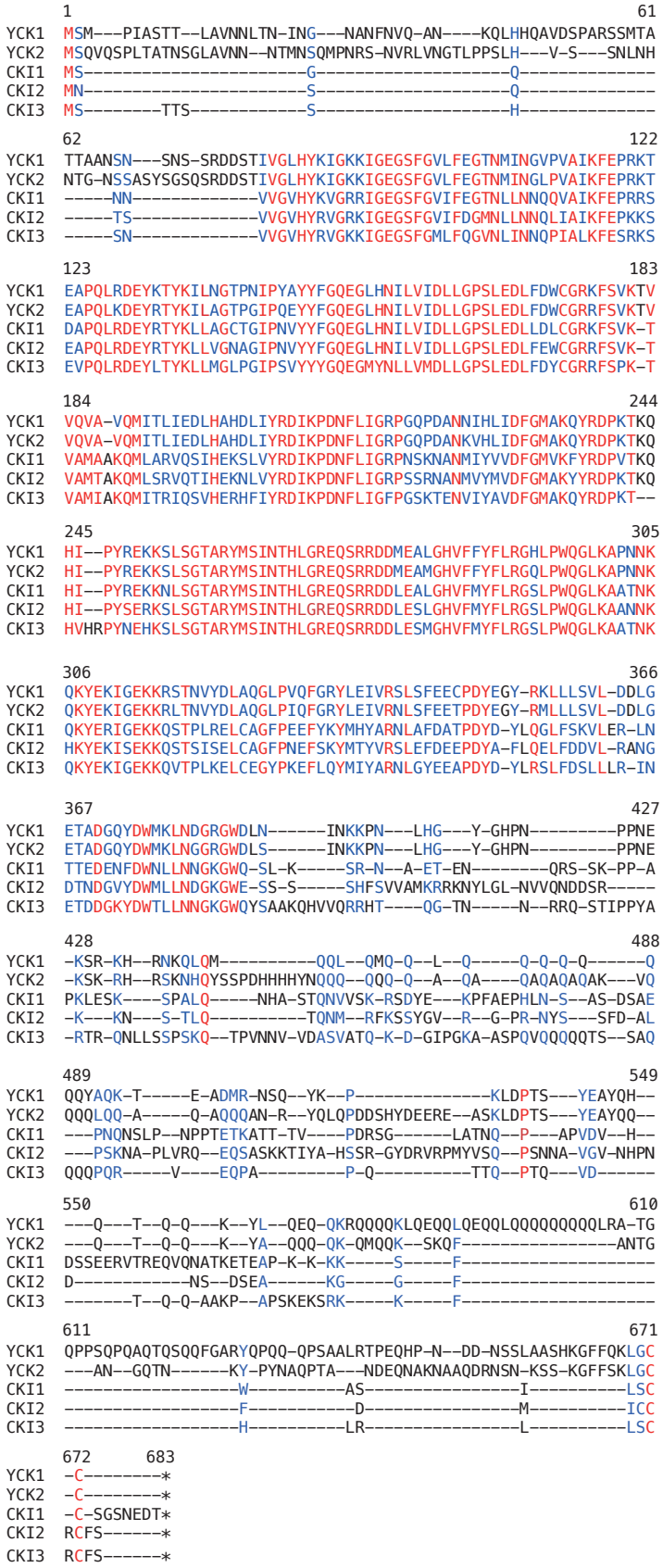

Figure 4.1: **67-69% homology between the *S. cerevisiae* proteins YCK1 and YCK2, with the *S. pombe* proteins Cki1, Cki2 and Cki3.** Sequences were aligned using MutiAlin version 5.4.1 [268]. Gaps (-) were included to optimise the alignment, identical residues are highlighted in red, conservative changes in blue and non-conservative changes have no colouring.

4.2 Identifying potential kinases that promote Mam2 internalisation

In *S. cerevisiae*, two yeast casein kinases YCK1 and YCK2 phosphorylate serine residues in the C-terminal tail of the pheromone GPCR STE2 to promote its internalisation [112, 269, 270]. A protein BLAST search with YCK1 and YCK2 was performed against the 96 protein kinases in *S. pombe* [271] to identify potential candidates that phosphorylate Mam2 in response to P-factor stimulation. Three casein kinase proteins Cki1, Cki2 and Cki3, were identified in the protein BLAST search and displayed a 67-69% sequence homology with YCK1 and YCK2 [272] (Figure 4.1). A previous study showed that Cki1, Cki2 and Cki3 were non-essential, with loss of these proteins exhibiting no observable cellular phenotypes during vegetative growth [272, 273]. However, these kinases' role in the pheromone-induced signalling pathway of *S. pombe* has not yet been investigated.

4.3 Cki1, Cki2 and Cki3 are not essential for mitotic growth

Cki1, Cki2 and Cki3 disruption strains were created from **M**-type *S. pombe* cells that lack both *cyr1* and *sxa2* (for details on how these strains were created see section 2.3.1). *cyr1* encodes adenylyl cyclase, with deletion of this gene enabling sexual differentiation during mitotic growth [53]. *sxa2* produces a serine carboxypeptidase that hydrolyses exogenous P-factor [218, 267], with loss of this gene product, protracting the pheromone-induced signalling response [96]. Five standard analyses were performed with the kinase disruption strains during mitotic growth to verify that any aberrant phenotypes observed during this chapter was the direct result of pheromone treatment.

Wild type (WT) (JY544; *sxa2*$^{-}$ *cyr1*$^{-}$), *Δcki1* (JY1731; *sxa2*$^{-}$ *cyr1*$^{-}$ *cki1::ura4*$^{+}$), *Δcki2* (JY1722; *sxa2*$^{-}$ *cyr1*$^{-}$ *cki2::ura4*$^{+}$) and *Δcki3* (JY1600; *sxa2*$^{-}$ *cyr1*$^{-}$ *cki3::ura4*$^{+}$) strains were grown to mid-exponential growth phase, stained with calcofluor white and imaged to assess cell morphology (as described in section 2.2.12). Calcofluor white is a fluorescent stain that specifically binds linear (1,3)-β-d-glucan, a polysaccharide present in the cell wall that when imaged under UV light can be used to assess cell morphology and deposition of the cell wall material [274]. Microscopy analysis of the kinase disruption strains did not indicate a difference in cell size, shape or cell wall biogenesis in comparison to WT strains (Figure 4.2a).

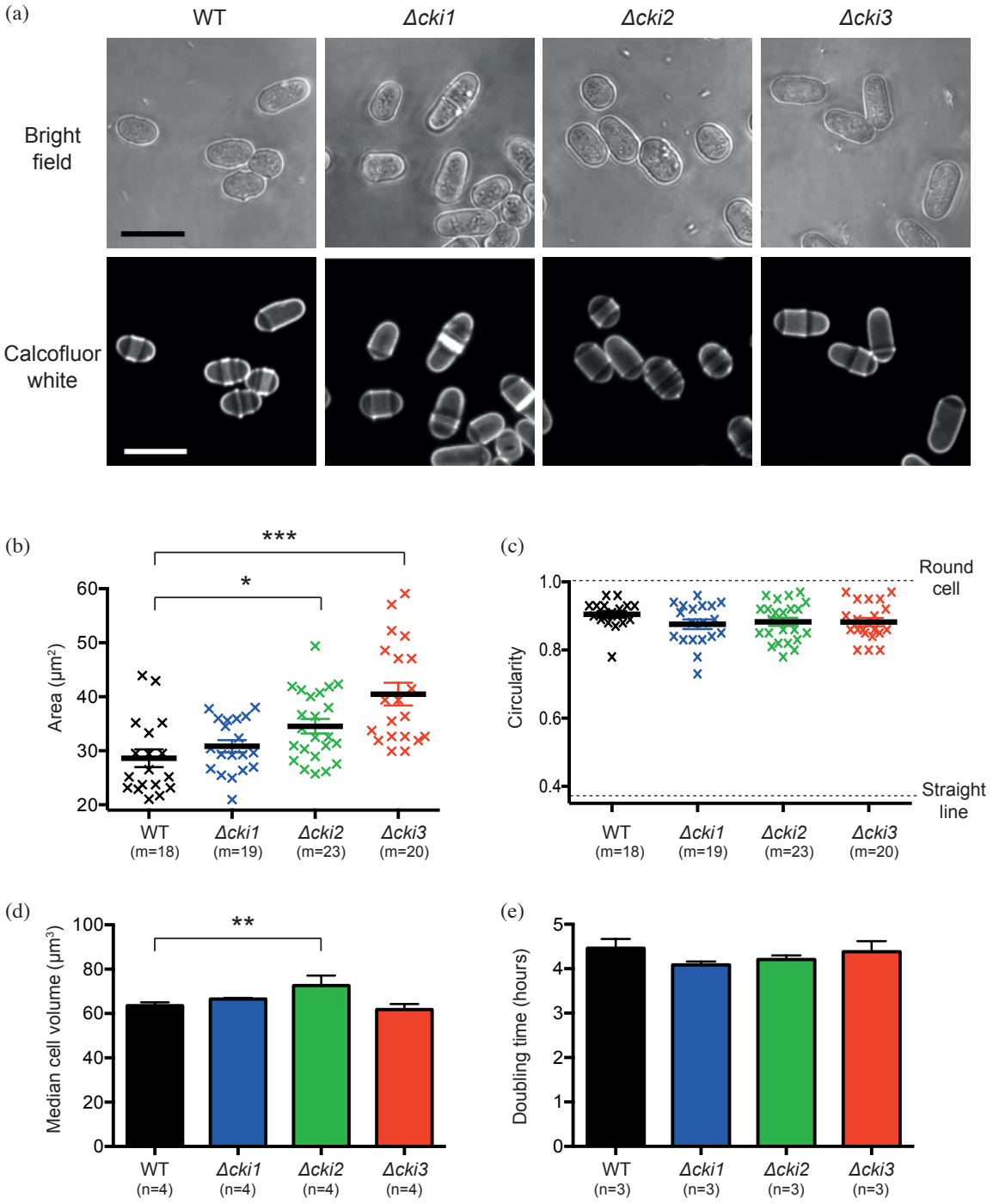

FIGURE 4.2: **Loss of *cki2* increased cell area and volume during vegetative growth.** WT (JY544), *Δcki1* (JY1731), *Δcki2* (JY1722) and *Δcki3* (JY1600) strains were grown to mid-exponential growth phase before (a) staining with calcofluor white and imaged in the bright field and UV channel (section 2.2.12). Scale bar represents 10 μm. The resulting images were analysed using QuimP to quantify (b) area and (c) circularity (section 2.2.18), the figure includes the QuimP output of a circle and straight-line for comparison, here m represents the number of individual cells analysed. During exponential growth phase strains were measured for (d) cell volume (section 2.2.7) and (e) doubling time (section 2.2.9), here n represents the number of independent experiments performed. Statistical significance was calculated using one-way ANOVA. $*p<0.05$, $**p<0.01$ and $***p<0.001$.

QuimP software, a set of plugins for ImageJ, allows segmentation of cells within a fluorescent image and can provide quantitative information regarding morphological variables such as area (cell size) and circularity (cell shape) (for details see section 2.2.18). Individual cells from the calcofluor white images (Figure 4.2a) were analysed using QuimP to detect changes in their area and circularity. *Δcki2* and *Δcki3* strains displayed a significant increase in cell area in comparison to WT strains (WT: 28±2 µm^2 (m=18, where m represents the number of individual cells analysed) compared with *Δcki2*: 35±1 µm^2 (m=23) and *Δcki3*: 41±3 µm^2 (m=20), p=0.0213 and p<0.001 respectively, one-way ANOVA) (Figure 4.2b). The QuimP analysis did not detect a significant difference in circularity between the WT and kinase disruption strains (Figure 4.2c) (p>0.05, one-way ANOVA).

Detecting changes in cell volume of *cki1*, *cki2* and *cki3* disruption strains provides an indirect measure of how these kinases regulate cell size. A cell volume assay (as described in section 2.2.7) was performed with WT, *Δcki1*, *Δcki2* and *Δcki3* cells following their growth to mid-exponential phase. The 64 µm^3 cell volume exhibited by WT (JY544) cells was consistent with those previously observed for the strain JY544 [223]. *Δcki2* strains displayed a significant increase in cell volume in comparison to WT cells (WT at 64±1.5 µm^3 compared with *Δcki2* at 75±2 µm^3, p=0.007 when n=4 using one-way ANOVA, n represents the number of independent experiments performed) (Figure 4.2d). Contrary to the QuimP measurement of cell area (Figure 4.2b), *Δcki3* cells did not display an increase in cell volume.

Proteins that regulate cell cycle progression in *S. pombe* have been identified by measuring the time it takes for the population to grow, measured by the doubling time (DT) [275]. *sxa2*$^+$ *cyr1*$^+$ **M**-type *S. pombe* cells grown in minimal medium have a DT of ∼2.5 h [53, 276]. The WT strain (JY544) used in this thesis was *cyr1*$^-$ and displayed a DT of 4.5±0.4 h, consistent with previously observations for this strain [50]. Disrupting *cki1*, *cki2* and *cki3* (for details on the method see section 2.2.9) did not significantly affect these strains DT in comparison to WT cells (p>0.05, using one-way ANOVA) (Figure 4.2e), suggesting that none of the kinases are required for cell cycle progression during mitotic growth.

Together, the results obtained in section 4.3 suggest a potential role for Cki2 and perhaps Cki3 in regulating cell size during vegetative growth. A critical role of Cki1, Cki2 and Cki3 in regulating cell shape, division or cell wall biogenesis was not observed. Therefore, any aberrant phenotypes observed during this chapter are most likely the result of treatment with P-factor.

4.4 Cki2 and Cki3 regulate mating in *S. pombe*

The function of Cki1, Cki2 and Cki3 within the *S. pombe* mating-response pathway has not yet been investigated. Therefore, four standard mating-response assays were employed to elucidate these kinases' role within the pathway: including the quantification of transcription of mating-responsive genes, the measurement of conjugation tube formation, quantification of the population in G_1 and the measurement of successful mating event by quantifying the production of ascospores (Figure 4.3).

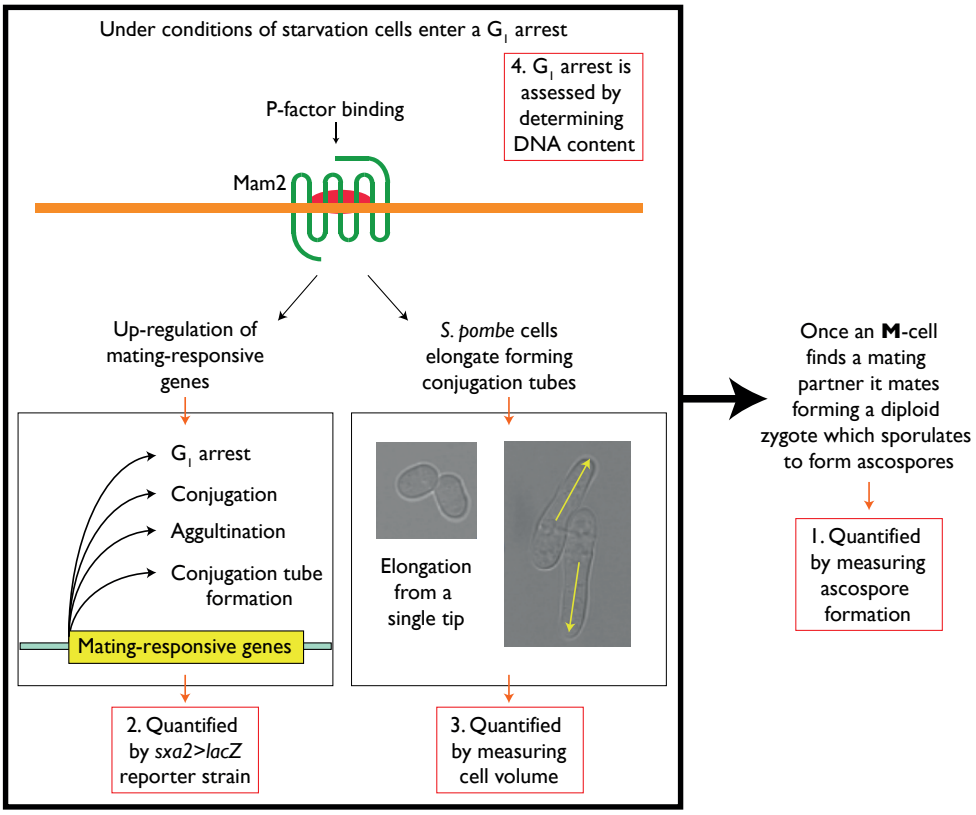

Figure 4.3: **Four assays employed in chapter 4 to measure the pheromone-response pathway in M-type *S. pombe* cells.** Nutrient limitation initiates a G_1 arrest. **P**-type *S. pombe* cells release P-factor, which binds the **M**-type GPCR Mam2. The binding of P-factor initiates a signalling cascade within the cell, resulting in the transcription of mating-responsive genes (including genes required to maintain the cells in a G_1 arrest, conjugation, agglutination and conjugation tube formation) and elongation from a single tip forming a conjugation tube towards a mating partner. When two opposite mating-type cells meet they fuse to form a diploid zygote that sporulates to form ascospores. Prior to mating, three assays can be employed to assess the signalling response (red boxes), these include quantifying signal transduction by utilising a reporter strain *sxa2>lacZ* [11], quantifying conjugation tube formation by measuring cell volume [11] and assessing the percentage of cells that contain one complement of DNA [221, 229]. The mating event its self can be quantified by utilising the heat resistant properties of ascospores [173, 228]. The assays are labelled 1-4 to represent the order at which these are assessed during this chapter.

When two opposite *S. pombe* mating type cells aggregate, they fuse to form a diploid zygote that sporulates to form ascospores [277]. The production of ascospores is the combination of pheromone successfully binding and activating the GPCR, signal transduction to transcribe mating-responsive genes, a G_1 arrest ensuring the cells contain one complement of DNA ready for mating and initiation of conjugation tube formation towards the mating partner (reviewed in [50]). The production of ascospores is therefore the ultimate indicator of a successful mating event (Figure 4.3 assay 1).

Detecting changes in ascospore production in the kinase disruption strains created in section 2.3.1, may indicate whether Cki1, Cki2 and Cki3 play a role in mating. Sxa2, the serine carboxypeptidase that is exogenously secreted in response to P-factor to cleave external pheromone is essential for mating [218]. The kinase disruption strains are *sxa2*$^-$ and therefore constitutive expression of Sxa2 from the pREP41x-Sxa2 vector (JD636, pSxa2) was used to compensate for the lack of endogenous Sxa2 during the mating assays, as described previously [98].

WT (JY544; *sxa2*$^-$ *cyr1*$^-$), *Δcki1* (JY1731; *sxa2*$^-$ *cyr1*$^-$ *cki1::ura4*$^+$), *Δcki2* (JY1722; *sxa2*$^-$ *cyr1*$^-$ *cki2::ura4*$^+$) and *Δcki3* (JY1600; *sxa2*$^-$ *cyr1*$^-$ *cki3::ura4*$^+$) strains containing pSxa2 together with positive (JY444: *sxa2*$^+$ *cyr1*$^+$) and negative (JY544 transformed with pREP41x, JD557) controls were mixed with mating-type stable **P**-cells (JY1025) and grown to mid-exponential growth phase before an iodine staining assay was performed (for details see section 2.2.11.1). This assay utilises the property that iodine stains the starch within the ascospore cell wall, with a brown/black colouration indicating a successful mating event [220]. A qualitative difference in colour intensity between the unmated and mated colonies for each strain was observed (except for the unmated control), suggesting that Cki1, Cki2 and Cki3 were not essential for mating in *S. pombe* (Figure 4.4a).

In addition, to provide a quantitative readout of mating, the same strains were used to assay their ascospore production by utilising the heat-resistant property of ascospores (as detailed in section 2.2.11.2) (Figure 4.3 assay 1). The sporulation assay determines the percentage of colony forming units (CFU) or spore formation following a heat inactivation step at 50 °C for 10 minutes [228]. *Δcki2*+pSxa2 strains displayed a significant reduction in CFU recovery in comparison to WT+pSxa2 cells (a reduction from 29.9±3.7% to 10.2±2.8% was observed, $p=0.0339$ when $n=3$, one-way ANOVA). Conversely, disruption of *cki3* resulted in a significant increase in CFU recovery (an increase from WT at 29.9±3.7% to 54.7±8.1%, $p=0.0089$ when $n=3$, one-way ANOVA).

The reduction in CFU recovery observed in *Δcki2* strains is consistent with previous observations [278] and suggests that Cki2 may have a potentiating role during the mating-response. Whereas, the increase in CFU recovery observed in *Δcki3* strains suggest that Cki3 may negatively regulate the mating-response in *S. pombe*.

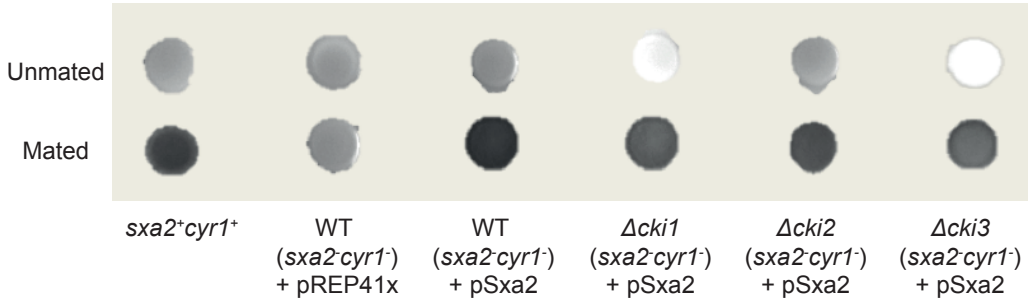

(a)

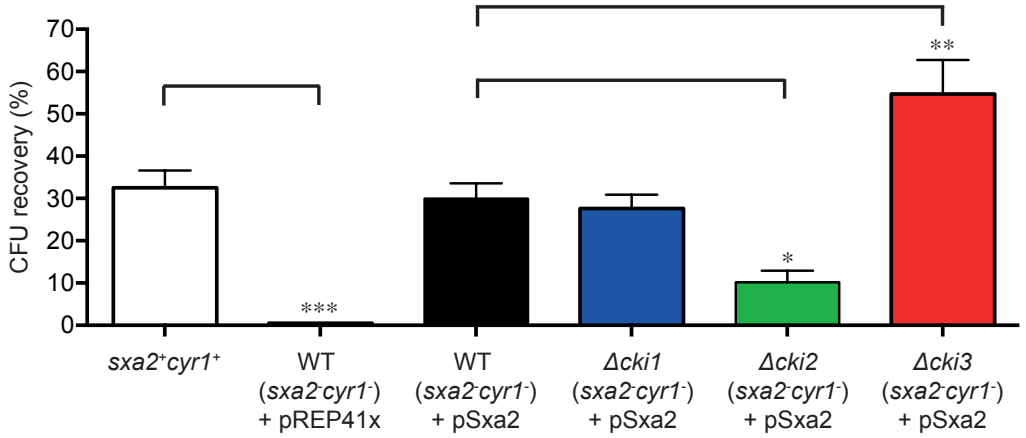

(b)

FIGURE 4.4: **Disruption of *cki2* and *cki3* affected ascospore recovery.** WT (JY544; *sxa2⁻*, *cyr1⁻*), *Δcki1* (JY1731; *sxa2⁻ cyr1⁻ cki1::ura4⁺*), *Δcki2* (JY1722; *sxa2⁻ cyr1⁻ cki2::ura4⁺*) and *Δcki3* (JY1600; *sxa2⁻ cyr1⁻ cki3::ura4⁺*) *S. pombe* **M**-cells containing pREP41x-Sxa2 (JD636, pSxa2) together with positive (JY444: *sxa2⁺ cyr1⁺*) and negative (JY544: *Δsxa2Δcyr1* cells containing pREP41x, JD557) control strains were mixed with mating-type stable **P**-cells (JY1025: *Δsxa2*) and grown to mid-exponential growth phase and mating was assessed using an (a) iodine staining assay where the formation of brown/black colonies indicate successful mating (section 2.2.11.1) and a (b) quantitative sporulation assay, which measures the percentage of colony forming units (CFUs)/spore formation (section 2.2.11.2). Data shown is the average of three independent experiments ±SEM. Statistical significance was calculated using one-way ANOVA, $*p<0.05$, $**p<0.01$ and $***p<0.001$.

4.5 P-factor signalling in *S. pombe*

The mating assays in section 4.4 showed that disruption of Cki2 and Cki3 affected the production of ascospores. This suggests that Cki2 and Cki3 could be affecting the earlier signalling events (prior to ascospore production) such as signal transduction to initiate transcription of mating-responsive genes, the G_1 arrest, the formation of conjugation tubes towards a mating partner or the process of fusion to form a diploid zygote (Figure 4.3) (reviewed in [277]). To determine which mating-responsive processes Cki2 and Cki3 may be influencing in response to P-factor in *S. pombe*, a number of assays which focus on the earlier events of the mating-response were performed (Figure 4.3 assays 2-4)

4.5.1 Cki1 and Cki3 regulate conjugation tube formation

The binding of P-factor to activate Mam2 results in signal transduction via Ras1, an essential G protein required for mating in *S. pombe* [246]. Signal transduction via Ras1 activates the cell polarity pathway, governed by the Rho-like GTPase Cdc42. Enhanced activation of Cdc42 in response to P-factor activation of Mam2 leads to cell growth from a single tip forming a conjugation tube towards a mating partner [97].

To elucidate the role of Cki1, Cki2 and Cki3 during conjugation tube formation WT, *Δcki1*, *Δcki2* and *Δcki3* strains were grown to mid-exponential growth phase before treatment with a range of P-factor concentrations (from 0 µM to 100 µM). After 16 h (at times consistent with other assays [11, 173, 228]) cells were stained with calcofluor white and imaged to assess cell morphology in response to treatment (for details see section 2.2.12). Visualising cells under bright field light can highlight defects in the integrity of membranes, such as the cell, nuclear and vacuola membranes. *Δcki1* and *Δcki2* strains did not show any observable differences in the integrity of membranes in comparison to WT cells.

WT (JY544) cells displayed conjugation tubes following treatment with 100 nM, 1 µM and 10 µM P-factor (Figure 4.5, arrows highlight the tip of the conjugation tube). This was also displayed for *Δcki1* and *Δcki2* strains (Figure 4.6 and 4.7, respectively), however an increase in conjugation tube length was visible in *Δcki1* cells following treatment with 100 nM P-factor in comparison to WT cells.

Following treatment with 10 nM P-factor, *Δcki3* cells display a morphology similar to WT (Figure 4.8). However, following treatment with >10 nM P-factor, cells displayed

hyper-elongated (extended) conjugation tubes, undulating cell structure, septa and aberrant deposition of cell wall material within the cytoplasm. During vegetative growth, cell morphology of *Δcki3* cells was indistinguishable from WT strains (Figure 4.2) and therefore, the adverse morphologies observed here are the most likely result of P-factor treatment.

The microscopy analyses suggested that Cki1 and Cki3 may function as negative regulators of the morphology pathway (that controls conjugation tube formation) in *S. pombe* as disruption of these proteins caused hyper-elongated conjugation tubes and in the case of *Δcki3* aberrant cellular shapes in comparison to WT cells. In addition, *Δcki3* cells displayed septa, suggesting that a loss in function of Cki3 was influencing progression through the cell cycle (Figure 4.8).

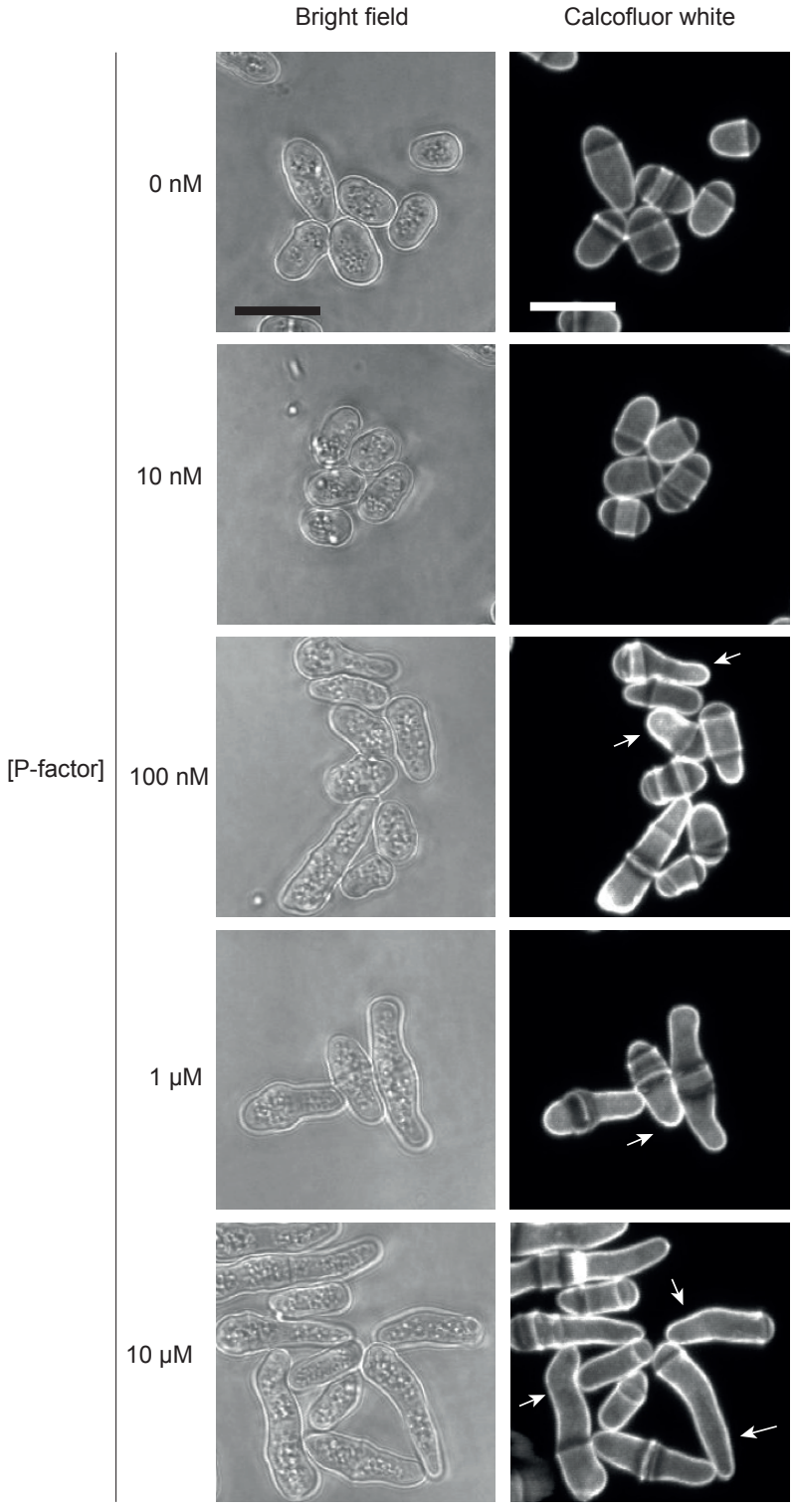

Figure 4.5: **WT (JY544; *sxa2⁻ cyr1⁻*) cells elongated in response to P-factor treatment.** WT *S. pombe* cells were grown to mid-exponential growth phase, treated with a range of P-factor concentrations (from 0 µM to 10 µM) and following 16 h of treatment cells were stained with calcofluor white and imaged under bright field and UV light (section 2.2.12). Bright field images are the projection of the three central Z-stacks. White arrows indicate conjugation tube formation. Scale bars represents 10 µM.

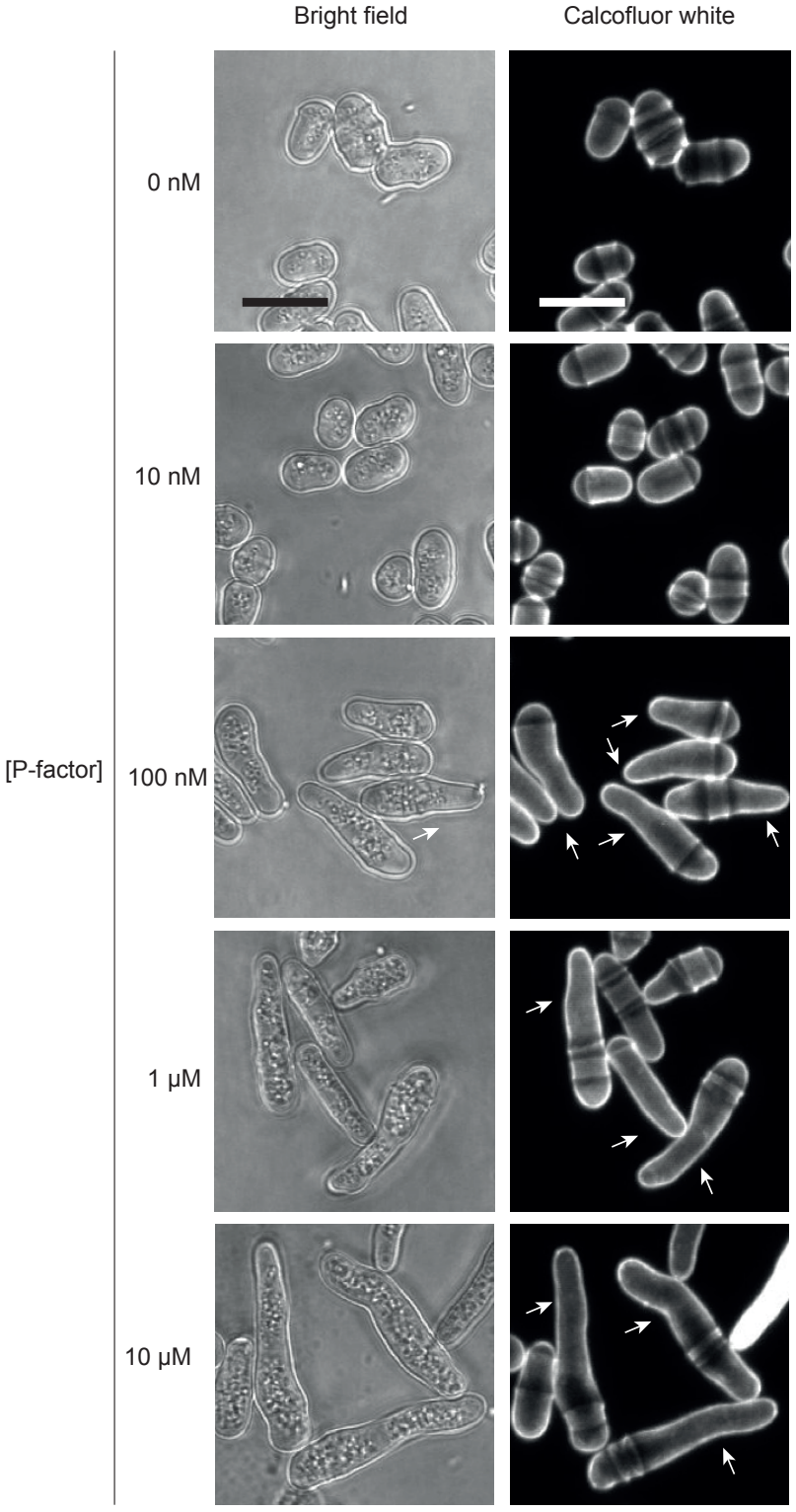

Figure 4.6: ***Δcki1* (JY1731; *sxa2⁻ cyr1⁻ cki1::ura4⁺*) cells were hyper-elongated in response to P-factor treatment.** *Δcki1* cells were grown to mid-exponential growth phase, treated with a range of P-factor concentrations (from 0 µM to 10 µM) and following 16 h of treatment cells were stained with calcofluor white and imaged under bright field and UV light (section 2.2.12). Bright field images are the projection of the three central Z-stacks. White arrows indicate conjugation tube formation. Scale bars represents 10 µM.

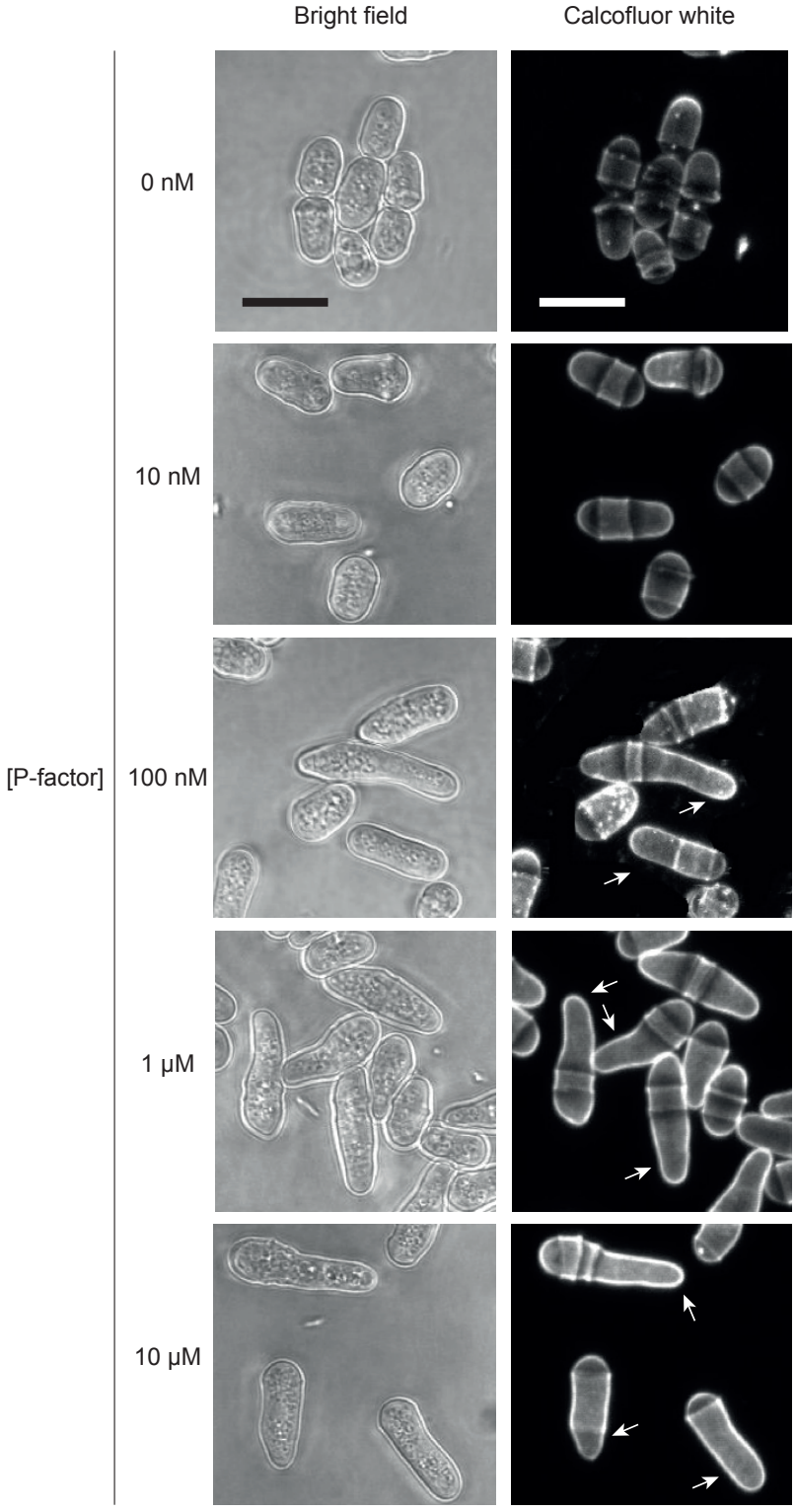

Figure 4.7: ***Δcki2* (JY1722; *sxa2⁻ cyr1⁻ cki2::ura4⁺*) cells elongated in response to P-factor treatment in a similar fashion to WT cells.** *Δcki2* cells were grown to mid-exponential growth phase, treated with a range of P-factor concentrations (from 0 µM to 10 µM) and following 16 h of treatment cells were stained with calcofluor white and imaged under bright field and UV light (section 2.2.12). Bright field images are the projection of the three central Z-stacks. White arrows indicate conjugation tube formation. Scale bars represents 10 µM.

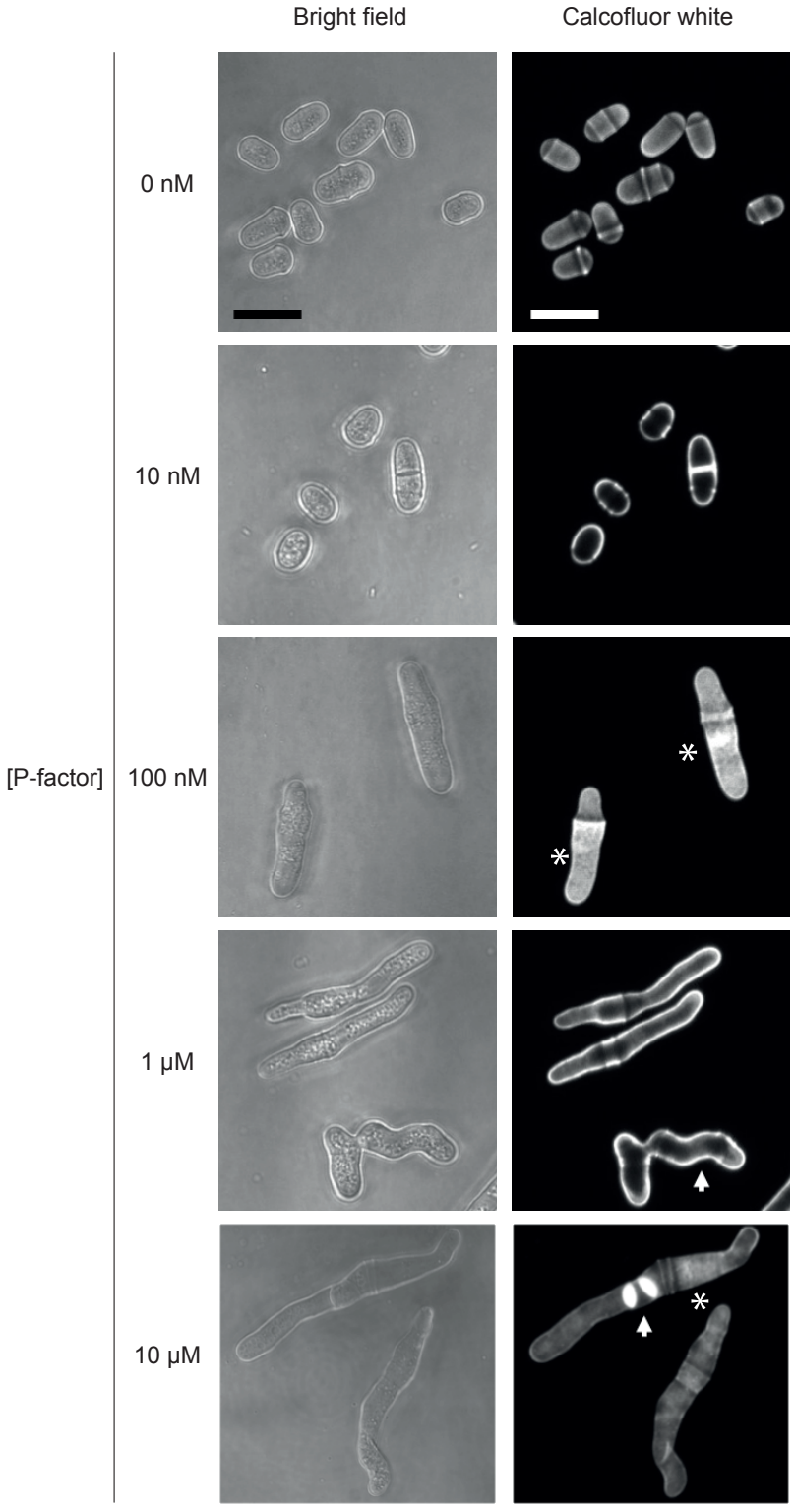

Figure 4.8: ***Δcki3* (JY1600; *sxa2⁻ cyr1⁻ cki3::ura4⁺*) cells displayed adverse morphological defects in response to P-factor treatment.** *Δcki3* cells were grown to mid-exponential growth phase, treated with a range of P-factor concentrations (from 0 µM to 10 µM) and following 16 h of treatment cells were stained with calcofluor white and imaged under bright field and UV light (section 2.2.12). Bright field images are the projection of the three central Z-stacks. Scale bars represents 10 µM. Images were selected to show phenotype; ∗ indicate deposition of the cell wall material and arrows highlight the undulating cell structure and septa.

4.5.2 Cki1 and Cki3 regulate signal transduction of mating-responsive genes and conjugation tube formation in *S. pombe*

A number of mating-responsive genes are upregulated in response to P-factor stimulation [57]. One of these genes is *sxa2*. Replacement of *sxa2* with *lacZ* provides a quantitative measure of signal transduction from activation of the receptor to upregulation of the mating-responsive genes [11] (Figure 4.3 assay 2). In addition to the upregulation of mating-responsive genes, *S. pombe* cells elongate from a single tip towards the source of pheromone (reviewed in [50]) and this elongation event can be indirectly quantified by measuring the median cell volume of the population [11] (Figure 4.3 assay 3).

To ascertain the role Cki1, Cki2 and Cki3 in signal transduction to promote upregulation of mating-responsive genes and conjugation tube formation, WT (JY544: *sxa2>lacZ*), *Δcki1* (JY1731: *sxa2>lacZ*), *Δcki2* (JY1722: *sxa2>lacZ*) and *Δcki3* (JY1600: *sxa2>lacZ*) strains were grown to mid-exponential growth phase, treated with a range of P-factor concentrations (from 0 µM to 100 µM) and after 16 h were assayed for β-galactosidase activity (section 2.2.8.1) and cell volume (section 2.2.7). These are two standard assays for measuring signal transduction in *S. pombe* [173, 190, 223].

Δcki1 and *Δcki3* strains displayed a significant increase in maximal transcriptional response in comparison to WT cells ($p=0.0002$ and $p<0.0001$, when $n=5$, respectively, determined using one-way ANOVA) (Figure 4.9). There was no significant difference in basal β-galactosidase activity or pEC_{50} between WT, *Δcki1*, *Δcki2* and *Δcki3* strains (Figure 4.9b).

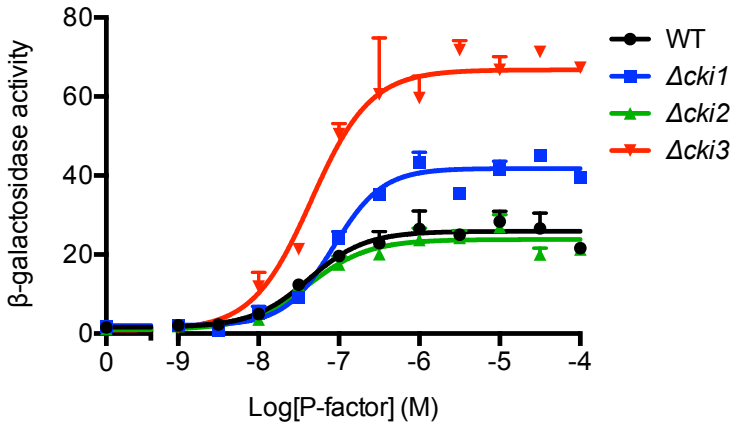

(a)

	Strain			
	WT	*Δcki1*	*Δcki2*	*Δcki3*
Basal (*lacZ* units)	2±1	2±2	1±2	1±3
Maximal (*lacZ* units)	26±1	42±1***	24±1	67±2***
pEC_{50}	7.4±0.1	7.1±0.3	7.4±0.1	7.3±0.2

(b)

FIGURE 4.9: **Disruption of *cki1* and *cki3* increased maximal transcriptional response following P-factor treatment.** WT (JY544), *Δcki1* (JY1731), *Δcki2* (JY1722) and *Δcki3* (JY1600) strains were grown to mid-exponential growth phase before treatment with a range of P-factor concentrations (from 0 µM to 100 µM). After 16 h cells were assayed for β-galactosidase activity (see section 2.2.8.1). Statistical significance was determined using one-way ANOVA, ∗p<0.05, ∗∗p<0.01 and ∗ ∗ ∗p<0.001. Data shown are mean of five independent determinants ±SEM.

A significant increase in basal cell volume was observed in *Δcki2* strains in comparison to WT cells (from 62±1 µm^3 to 73±3 µm^3, p=0.0254 when n=3, one-way ANOVA) (Figure 4.10). The increase in basal cell volume of *Δcki2* was consistent with the assay performed during vegetative growth (section 4.3). This continuity provides supporting evidence that Cki2 regulates cell size, but only during vegetative growth, as *Δcki2* cells did not show an increase in cell volume following treatment with >100 nM P-factor (Figure 4.10b).

In addition to increasing β-galactosidase activity, disruption of *cki1* and *cki3* in *S. pombe* cells significantly increased maximal cell volume in comparison to WT strains (Figure 4.10). WT cells displayed a maximal cell volume of 82±1 µm^3, which increased to 98±3 µm^3 in *Δcki1* strains and more than doubled to 164±3 µm^3 in *Δcki3* cells (p=0.0262 and p<0.0001 when n=3, respectively, one-way ANOVA). The increase in cell volumes observed in *Δcki1* and *Δcki3* strains were consistent with the hyper-elongated conjugation tubes observed

in the microscopy analysis (section 4.5.1), providing further evidence that Cki1 and Cki3 negatively regulate signal transduction prior to conjugation tube formation. In addition to an increase in cell volume following treatment with >100 nM P-factor, *Δcki3* cells also displayed a significant increase in potency of P-factor showing a reduction in pEC_{50} from 7.4±0.1 (WT cells) to 6.9±0.1 ($p=0.0241$ when $n=3$, one-way ANOVA). This increase in potency indicates that less P-factor is required to induce the same conjugation tube length. Together, these data suggest Cki1 and Cki3 negatively regulate signal transduction prior to upregulation of mating-responsive genes and conjugation tube formation.

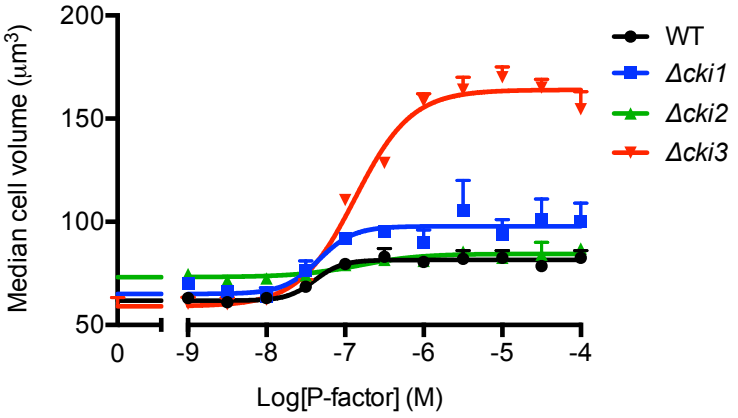

(a)

	WT	*Δcki1*	*Δcki2*	*Δcki3*
Basal (µm^3)	62±1	65±3	73±3*	59±2
Maximal (µm^3)	82±1	98±3*	84±1	164±3***
pEC_{50}	7.39±0.1	7.3±0.2	7.26±0.2	6.9±0.1*

(b)

Figure 4.10: **Disruption of *cki1* and *cki3* increases maximal cell volume following P-factor treatment.** WT (JY544), *Δcki1* (JY1731), *Δcki2* (JY1722) and *Δcki3* (JY1600) strains were grown to mid-exponential growth phase before treatment with a range of P-factor concentrations (from 0 µM to 100 µM). After 16 h cells were assayed for cell volume (see section 2.2.7). Statistical significance was determined using one-way ANOVA with a Dunnett's multiple comparison test, $*p<0.05$, $**p<0.01$ and $***p<0.001$. Data shown is the average of three independent experiments ±SEM.

4.5.3 Cki3 regulates signal transduction directly upstream of transcription of mating-responsive genes

The increase in maximal β-galactosidase activity observed in *Δcki1* and *Δcki3* strains indicates a role for Cki1 and Cki3 in regulating signal transduction prior to upregulation of the mating-responsive genes (section 4.5.2). To assess whether Cki1 and Cki3 regulate proteins involved in the signal transduction pathway directly or whether a delay/feedback-mechanism exists, β-galactosidase expression was analysed over time. WT (*sxa2>lacZ*), *Δcki1* (*sxa2>lacZ*, *cki1::ura4*$^+$), *Δcki2* (*sxa2>lacZ*, *cki2::ura4*$^+$) and *Δcki3* (*sxa2>lacZ*, *cki3::ura4*$^+$) strains were grown to mid-exponential growth phase before treatment with a range of P-factor concentrations (from 0 µM to 100 µM). Strains were assayed for β-galactosidase activity every 2 h from 0 h to 16 h (for details see section 2.2.8.1).

Changes in β-galactosidase activity were detectable following 4 h of treatment with P-factor (Figure 4.11). A previous study has shown that Sxa2 expression is detectable after 1 h [11]. However, the strains used in this thesis are *sxa2>lacZ*, where *lacZ* gene encodes β-galactosidase, which is detectable by cleaving ONPG and hence, it takes longer to detect changes in gene expression in these strains. The time at which changes in β-galactosidase activity is observed (4 h) is consistent with another study that has used *sxa2>lacZ S. pombe* strains [190].

A significant increase in β-galactosidase activity following disruption of *cki1* was only observed from 14 h (WT displayed 30±1 *lacZ* units compared with 37±2 *lacZ* units, p=0.0395 when n=3, Student's t-test), whereas a significant increase in transcriptional response of *Δcki3* was observed following 4 h of P-factor treatment (at 4 h WT displayed 10±1 *lacZ* units compared with 21±2 *lacZ* units displayed by *Δcki3* cells, p=0.0101 when n=3, Student's t-test) (Figure 4.11). WT strains reached a plateau by 10 h, consistent with previous studies [11, 190], suggesting that by this time β-galactosidase was no longer being transcribed. *Δcki2* cells displayed a similar temporal profile to WT strains, reaching a maximal signalling plateau by 10 h, whereas *Δcki1* and *Δcki3* strains did not reach a temporal plateau in β-galactosidase activity until 12 h (Figure 4.11).

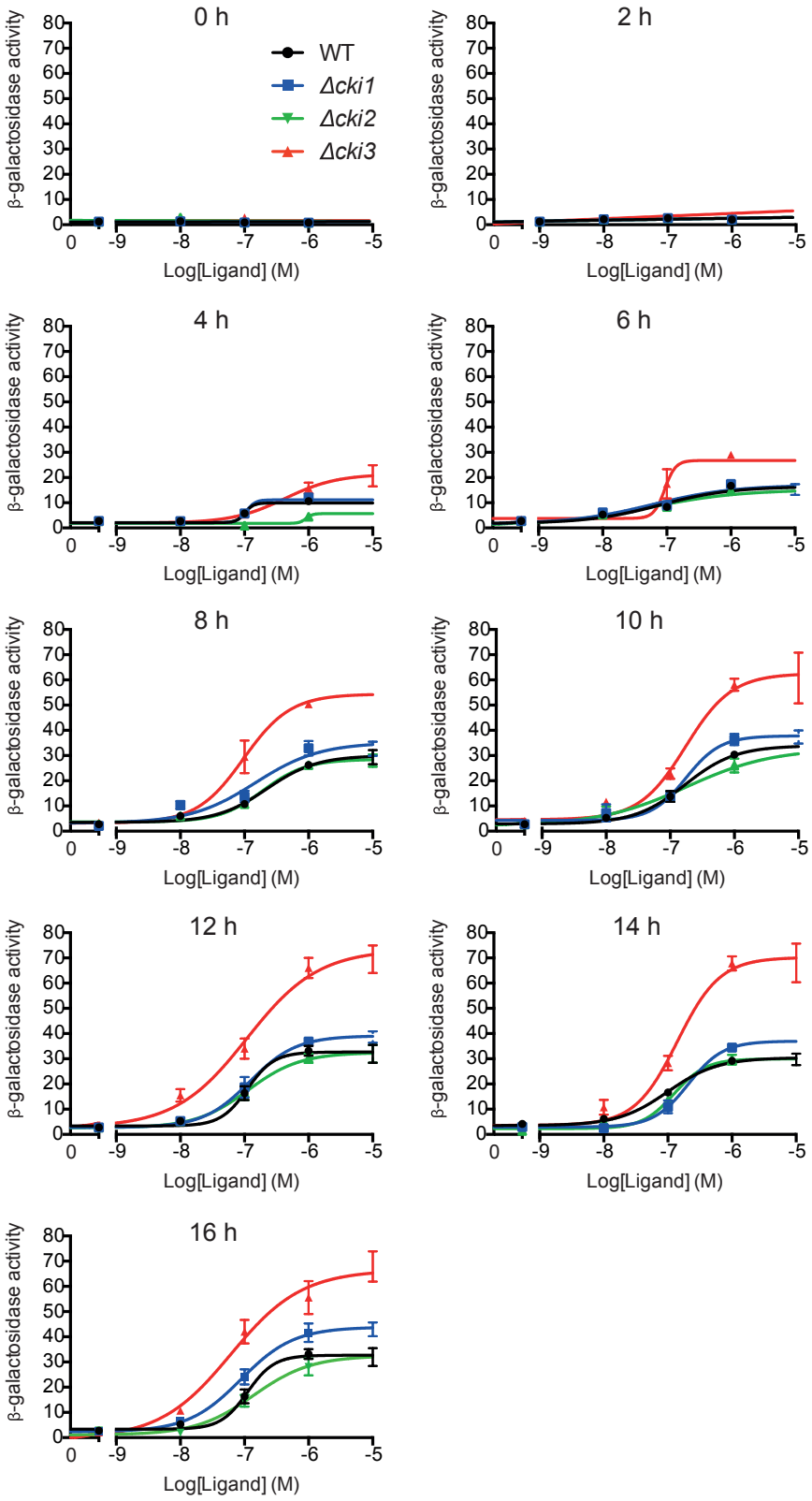

Figure 4.11: **An increased transcriptional response was observed by 14 h and 4 h for *Δcki1* and *Δcki3* strains, respectively.** WT (JY544), *Δcki1* (JY1731), *Δcki2* (JY1722) and *Δcki3* (JY1600) strains were grown to mid-exponential growth phase and treated with a range of P-factor concentrations (from 0 µM to 10 µM). Cells were assayed for β-galactosidase activity every 2 h from 0 h to 16 h as indicated (section 2.2.8.1). Data shown are mean of three independent experiments ±SEM.

The increase in β-galactosidase activity detected in *Δcki1* cells was not observed until 14 h. This suggested that Cki1 may not regulate the proteins involved in signal transduction from the receptor to transcription of the mating-responsive genes, otherwise the increase in β-galactosidase activity would be observed from 4 h. Instead, this suggests that a positive feedback mechanisms exists whereby production of one of the mating-responsive genes may regulate Cki1 activity [11]. Contrary to the *cki1* disruption strains, *Δcki3* cells displayed an increase in transcriptional response from 4 h, indicating that Cki3 may act directly upstream of transcription of mating-responsive genes (i.e. on the proteins involved in signal transduction from Mam2 to the transcription factor Ste11).

4.5.4 Strains lacking Cki3 did not return to mitotic growth following P-factor treatment

WT (*sxa2>lacZ*) *S. pombe* **M**-cells have been shown to increase cell volume following treatment with P-factor, reaching a maximal size following 8 h to 12 h of treatment and then a reduction in cell volume, reaching the size of mitotically growing WT strains by 36 h [11] (Figure 4.12a). This suggests that upon unsuccessfully locating an appropriate mating partner, cells recovered from the response and continued to proliferate via mitosis. Deletion of Pmp1, a dual-specificity phosphatase that is thought to negatively regulate the action of the mating-response MAPK Spk1 [256], showed that cell volume continued to increase over the entire 36 h assay [11] (Figure 4.12a), suggesting that these cells were unable to recover and return to mitotic growth.

Strains lacking Pmp1 (*Δpmp1*) not only displayed hyper-elongated conjugation tubes in response to P-factor but also showed an increase in maximal β-galactosidase activity following 16 h of treatment (Figure 4.12b/c) [11, 221]. The increase in cell volume, β-galactosidase activity and elongated conjugation tubes are all similar phenotypes observed in the *Δcki1* and *Δcki3* strains shown in this study (Figure 4.9 and 4.10) and therefore *Δcki1* and *Δcki3* strains may also be unable to recover from pheromone stimulation and return to mitotic growth. To assess whether the kinase disruption strains were able to recover from P-factor stimulation and return to mitotic growth, cell volume was measured every 0 h, 16 h, 24 h and 36 h (as described in section 2.2.7) with WT (JY544; *sxa2>lacZ*), *Δcki1* (*sxa2>lacZ*, *cki1::ura4*$^+$), *Δcki2* (*sxa2>lacZ*, *cki2::ura4*$^+$) and *Δcki3* (*sxa2>lacZ*, *cki3::ura4*$^+$) strains after growth to mid-exponential growth phase and treatment with 10 μM P-factor.

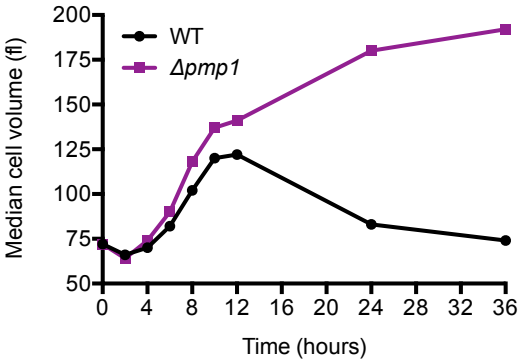

(a)

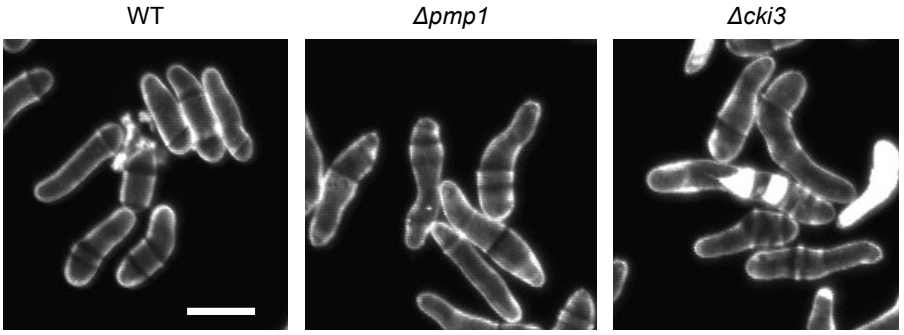

(b)

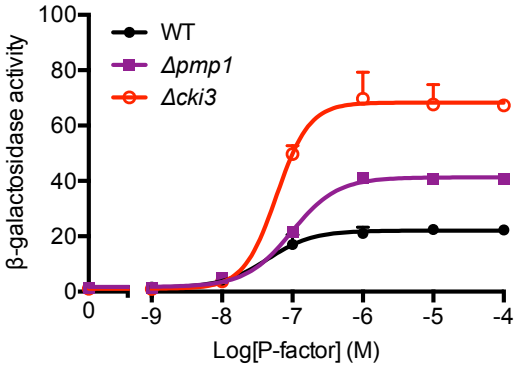

(c)

Figure 4.12: ***Δpmp1* (*sxa2>lacZ*, *pmp1::ura4*$^+$) cell volume increased over the 36 h assay following P-factor treatment.** WT (JY544), *Δpmp1* (JY949) and *Δcki3* (JY1600) strains were grown to mid-exponential growth phase and treated with a range of P-factor concentrations from 0 µM to 100 µM for 16 h (a) *Δpmp1* cell volume data adapted from [11]. (b) Cells were stained calcofluor white and imaged under UV light as described in section 2.2.14. Both *Δcki3* and *Δpmp1* cells displayed hyper-elongated cells. Scale bar represents 10 µm. (c) cells were assayed for β-galactosidase activity: removing Pmp1 shows an increase in transcriptional response.

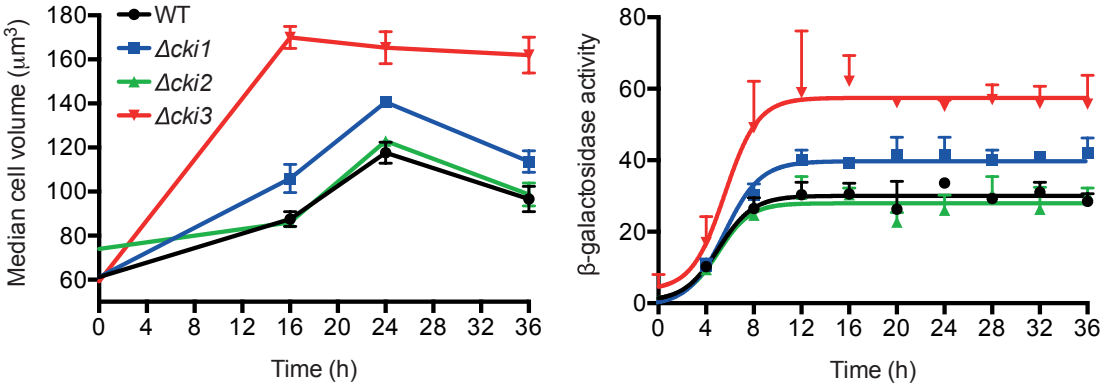

(a) (b)

Figure 4.13: **Strains lacking *cki3* did not show a non-monotonic cell volume distribution over time.** WT (JY544), *Δcki1* (JY1731), *Δcki2* (JY1722) and *Δcki3* (JY1600) strains were grown to mid-exponential growth phase and treated with 10 µM P-factor. (a) Following treatment for 0 h, 16 h, 24 h and 36 h cells were assayed for cell volume (as described in section 2.2.7). (b) Cells were also assayed for β-galactosidase activity every 4 h from 0 h to 36 h (as described in section 2.2.8.1). Data shown is the mean of four independent experiments ±SEM.

The WT strain displayed an increase in cell volume following 0 h to 24 h of treatment with P-factor and then a reduction between 24 h and 36 h (Figure 4.13a). In addition, the WT strains did not reach the cell volume of mitotically growing cells by 36 h. Instead, the population cell volume was still greater than that observed at 16 h (WT at 16 h was 84±2 µm^3 and at 36 h was 96±3 µm^3). This is different to what has previously been observed for the WT strain JY544 by Didmon *et al.* (2002), where a reduction in cell volume was observed following 12 h P-factor treatment [11] (Figure 4.12a). These data suggest that by 36 h WT strains had not recovered from pheromone-stimulation or returned to mitotic growth as expected.

Strains lacking *cki1* and *cki2* maintained the same non-monotonic temporal profile as WT cells, increasing cell volume between 0 h and 24 h and then reducing cell volume between 24 h and 36 h. In comparison to WT strains, *Δcki1* cell volume was increased at 16 h, 24 h and 36 h (Figure 4.13a). *Δcki3* cells reached a maximal cell volume size which was greatly increased in comparison to WT cells at 16 h (rather than at 24 h which was observed by WT cells) and maintained this maximal response over the 36 h assay rather than reducing cell size (Figure 4.13a). These data suggest that cells lacking Cki3 are unable to recover from P-factor stimulation by progressing through the cell cycle to grow mitotically.

The reduction in cell volume between 24 h and 36 h in WT strains suggest that a

proportion of cells within the population had recovered from the G_1 arrest and completed cell division. The converse may be true for strains lacking *cki3*, where the plateau in maximal cell volume suggested that these cells had maintained the G_1 arrest and fail to return to mitotic growth.

Rum1, a cyclin dependent kinase, is upregulated in response to treatment with P-factor [57]. Upregulation of Rum1 maintains the cells in a G_1 arrest by degrading the cyclin Cdc13, a protein essential for the G_1 to S phase transition of the cell cycle [64, 97, 279]. The WT strain JY544 exhibited a plateau in β-galactosidase activity following 10 h of treatment (Figure 3.30a). This suggests that *lacZ*, the gene that encodes β-galactosidase, was no longer being transcribed. If transcription of *lacZ* had been halted during the assay, it is likely that *rum1* transcription had also been halted as the transcription factor Ste11 controls the regulation of both *lacZ* (*sxa2>lacZ*) and *rum1* in response to P-factor. If *rum1* was no longer being transcribed than *S. pombe* cells should have recovered from the G_1 arrest and returned to mitotic growth.

WT cells and strains lacking *cki1* and *cki2* may have began to recover from the G_1 arrest, as a reduction in population cell volume was observed (most likely due to the cells dividing to become smaller in size, Figure 4.13a). However, *Δcki3* cells did not display a reduction in population cell volume. This may be a result of Rum1 still being transcribed in these strains. To determine whether β-galactosidase was still being transcribed following treatment with P-factor and hence, possibly Rum1; β-galactosidase assays were performed with WT, *Δcki1*, *Δcki2* and *Δcki3* strains following growth to mid-exponential growth phase, treatment with 10 µM P-factor, every 2 h from 0 h to 36 h (as detailed in section 2.2.8.1).

All strains reached a plateau in β-galactosidase activity by 12 h (Figure 4.13b). This suggested that by 12 h, *lacZ* and probably *rum1* was no longer being transcribed. If Rum1 was no longer being expressed then all the strains should have began to recover from the G_1 arrest. These results therefore suggest that another mechanism other than Rum1 is maintaining *Δcki3* cells in a G_1 arrest was preventing the cells from dividing.

4.5.5 Strains lacking Cki3 exhibit aberrant morphologies following 36 h treatment with P-factor

To understand why cells lacking *cki3* were unable to divide following prolonged treatment with P-factor, the morphology of the strains was analysed upto 36 h treatment (as only cells following treatment for 16 h had previously been observed, Figure 4.8).

WT, *Δcki1*, *Δcki2* and *Δcki3* strains were grown to mid-exponential growth phase, treated with 10 µM P-factor for 36 h, stained with calcofluor white and imaged to assess cell morphology (as described in section 2.2.12). Strains lacking *cki2* were indistinguishable from WT strains (Figure 4.14), i.e. there was no observable difference in cell shape, size or integrity of the membranes (bright field images). Strains lacking *cki1* and *cki3* exhibited hyper-elongated conjugation tubes in comparison to WT strains. These elongated cells observed in the microscopy images are consistent with the increase in cell volume displayed after 36 h treatment in these cells (Figure 4.13). In the case of *Δcki3* strains, the microscopy analysis revealed septa (Figure 4.14, arrows), aberrant deposition of the cell wall material within the cytoplasm (indicated by the dispersion of calcofluor staining around the septa) and a variation in cytoplasmic texture between septa (Figure 4.14, bright field).

The variation in membrane integrity observed between septa at 36 h in *Δcki3* strains was not observed following 16 h of treatment (Figure 4.8), suggesting that this cellular phenotype becomes exaggerated with time. Therefore, a time-course microscopy analysis was performed with the *Δcki3* strain JY1600 every 4 h from 20 h to 36 h (as described in section 2.2.12) to investigate the changes in integrity of the membranes with time. At 20 h 'nodules' were observed and with increasing time, multiple projection tips were commonplace (Figure 4.15). The frequency of cells displaying a disruption in cell wall biogenesis, indicated by the irregular positioning of calcofluor white staining (cell wall material) within the cytoplasm was pronounced following 24 h treatment (Figure 4.15, $*$'s). The integrity of the cell's membranes were evident following 24/28 h of treatment with P-factor. Septated cells were highly conserved in strains lacking *cki3*, suggesting that cells attempted to divide yet were unable to complete cytokinesis (Figure 4.15, arrows).

It should be highlighted that during vegetative cell growth *Δcki3* strains (JY1600) did not display defects in growth as measured by the DT or defects in cell morphology (Figure 4.2). The adverse morphological defects observed in *Δcki3* cells is therefore a result of treatment with P-factor.

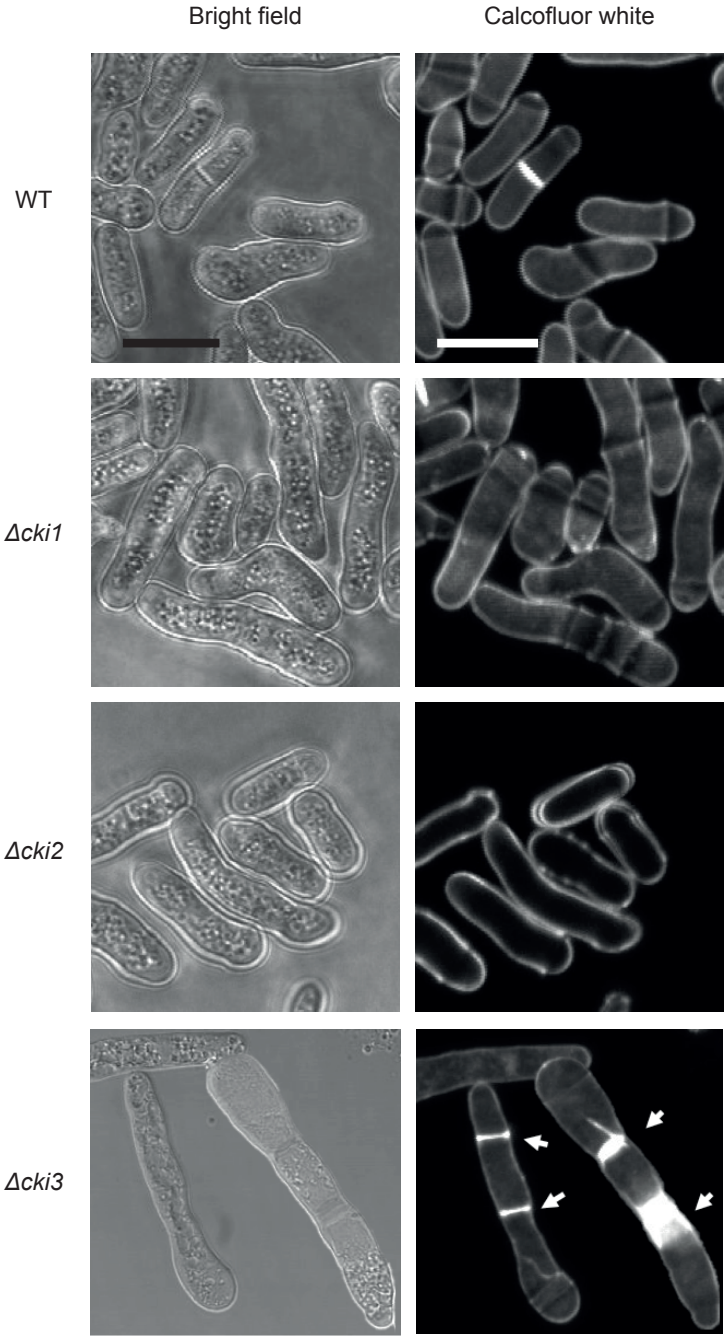

Figure 4.14: **The appearance of septa is a dominant phenotype of *Δcki3* *S. pombe* cells following P-factor treatment for 36 h.** WT (JY544), *Δcki1* (JY1731), *Δcki2* (JY1722) and *Δcki3* (JY1600) strains were grown to mid-exponential growth phase before treatment with 10 µM of P-factor for 36 h. Cells were stained with calcofluor white and imaged under bright field and UV light as described in section 2.2.14. Calcofluor white images are maximal projections of Z-stacks. Scale bar represents 10 µm. Arrows highlight septa in the *Δcki3* strain.

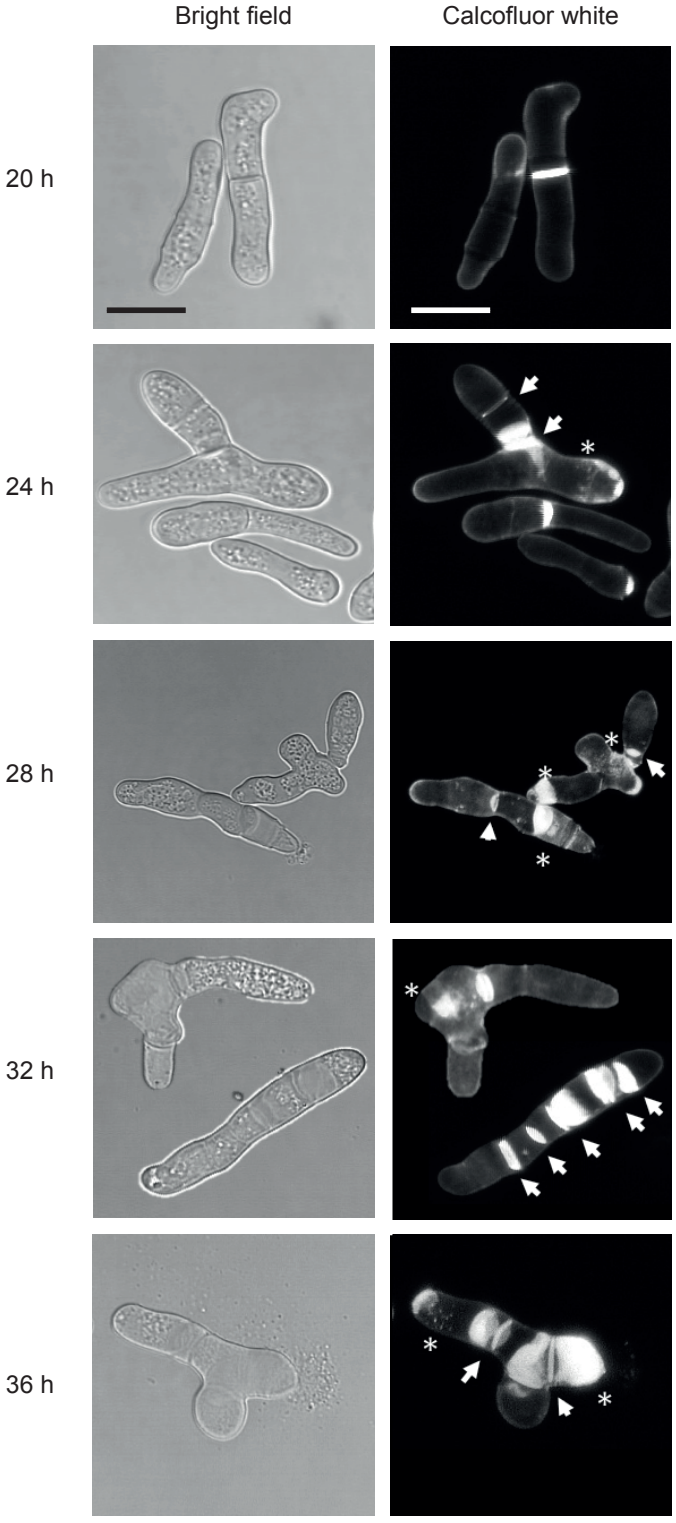

Figure 4.15: ***Δcki3* cells displayed adverse morphological defects in response to P-factor.** The *Δcki3* strain JY1600 was grown to mid-exponential growth phase and treated with 10 µM P-factor. Cells were stained with calcofluor white and imaged with bright field and UV light every 4 h from 20 h to 36 h (as detailed in section 2.2.12). Scale bar represents 10 µm. Images were selected to represent the best example of phenotype; multiple projection tips are visible, arrows and ∗'s highlight septa and aberrant disposition of the cell wall within the cytoplasm, respectively.

4.5.6 The number of cells displaying septa increases with time following P-factor treatment

Δcki3 strains displayed a constant elevated cell size in response to treatment with P-factor that did not begin to recover from treatment as observed with WT cells (Figure 4.13a). Microscopy analysis of *Δcki3* strains in response to P-factor highlighted that septated cells were prominent, indicating that these cells attempted to divide yet where unable to complete cell division (Figure 4.15). To assess how dominant the septa phenotype was in strains lacking *cki3* in response to P-factor, the number of cells displaying septa was quantified following treatment for 16 h and 36 h. WT, *Δcki1*, *Δcki2* and *Δcki3* strains were grown to mid-exponential growth phase before treatment with 10 µM P-factor. Cells were stained with calcofluor white and imaged (as detailed in section 2.2.12) following treatment for 16 h and 36 h. Each cell in the corresponding image was then categorised by the number of septa displayed, either containing no septum, one septum or septa (0, 1 or ≥2, respectively).

No significant difference in the number of cells displaying septa was observed between WT and *Δcki1* or *Δcki2* strains at 16 h or 36 h (Figure 4.16, $p>0.05$ when the number of cells (m)>90 in three experiments, two way ANOVA with a Dunnett's multiple comparison test, for the values see Figure 4.16). However, the percentage of cells displaying septa in *Δcki3* strains was significantly increased following 16 h and 36 h of treatment (16 h: $p=0.002$ and 36 h: $p<0.001$, when the number of cells (m)>90 in three independent experiments, two-way ANOVA with a Dunnett's multiple comparison test, for the values see Figure 4.16). Importantly, the percentage of cells displaying septa at 36 h (50%) was much greater than at 16 h (9%) (Figure 4.16), suggesting the number of *Δcki3* cells that attempt to divide increases with time following treatment with P-factor.

To confirm that the increase in septa observed in *Δcki3* strains was the direct effect of loss of Cki3 function and not a combinatorial effect of disrupting *cyr1* and *cki3*, the number of cells displaying septa was investigated with WT *cyr1*$^+$ (JY448) and *Δcki3*: *cyr1*$^+$ (JY1730) strains. These strains were grown to mid-exponential growth phase in SSL medium (which lacks a nitrogen source), treated with 10 µM P-factor for 36 h and then stained with calcofluor white and imaged (as described in section 2.2.12). Each cell in the corresponding image was categorised by the number of septa displayed (either 0, 1 or ≥2).

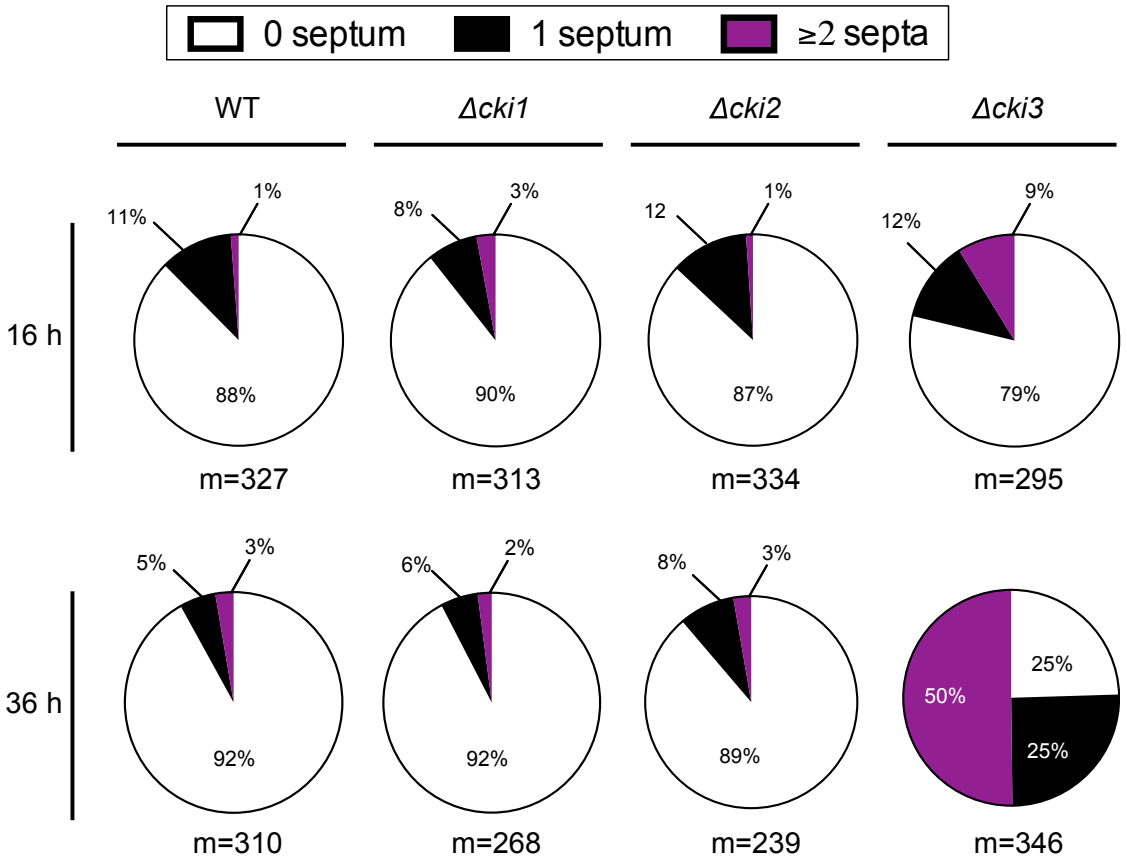

(a)

	WT		*Δcki1*		*Δcki2*		*Δcki3*	
Septum	16 h	36 h	16 h	36 h	16 h	36 h	16 h	36 h
0 (%)	88±2	92±2	90±2	92±2	87±0.1	89±5	79±2***	25±4***
1 (%)	11±1	5±0.6	8±1	6±1	12±1	8±4	12±1	25±2***
≥2 (%)	1±1	3±2	3±1	2±1	1±1	3±1	9±3**	50±2***

(b)

Figure 4.16: **The number of septated *Δcki3* cells increased following treatment with P-factor.** WT (JY544, *sxa2⁻*), *Δcki1* (JY1731, *sxa2⁻*), *Δcki2* (JY1722, *sxa2⁻*) and *Δcki3* (JY1600, *sxa2⁻*) strains were grown to mid-exponential growth phase before treatment with 10 µM P-factor. After 16 h and 36 h cells were stained with calcofluor white and imaged in the UV channel (as described in section 2.2.12) before all the individuals cells in the image were categorised by septum index (0 septum, 1 septum or ≥2 septa). Statistical significance was calculated using two-way ANOVA with a Dunnett's multiple comparison test, where ∗ indicates a p-value<0.05, ∗∗ indicates a p-value<0.01 and ∗ ∗ ∗ indicates a p-value<0.001. Data shown is the average of three independent experiments ±SEM.

A significant increase in the percentage of cells displaying septa between WT and *Δcki3* *cyr1*$^{+}$ strains was observed (from 2±1% to 45±2%, p<0.001 when the number of cells (m)>90 in three independent experiments, two-way ANOVA) (Figure 4.17). Both *cyr1*$^{+}$ and *cyr1*$^{-}$ *Δcki3* strains displayed a significant increase in the percentage of septated cells, suggesting the septa phenotype was the result of disrupting *cki3*.

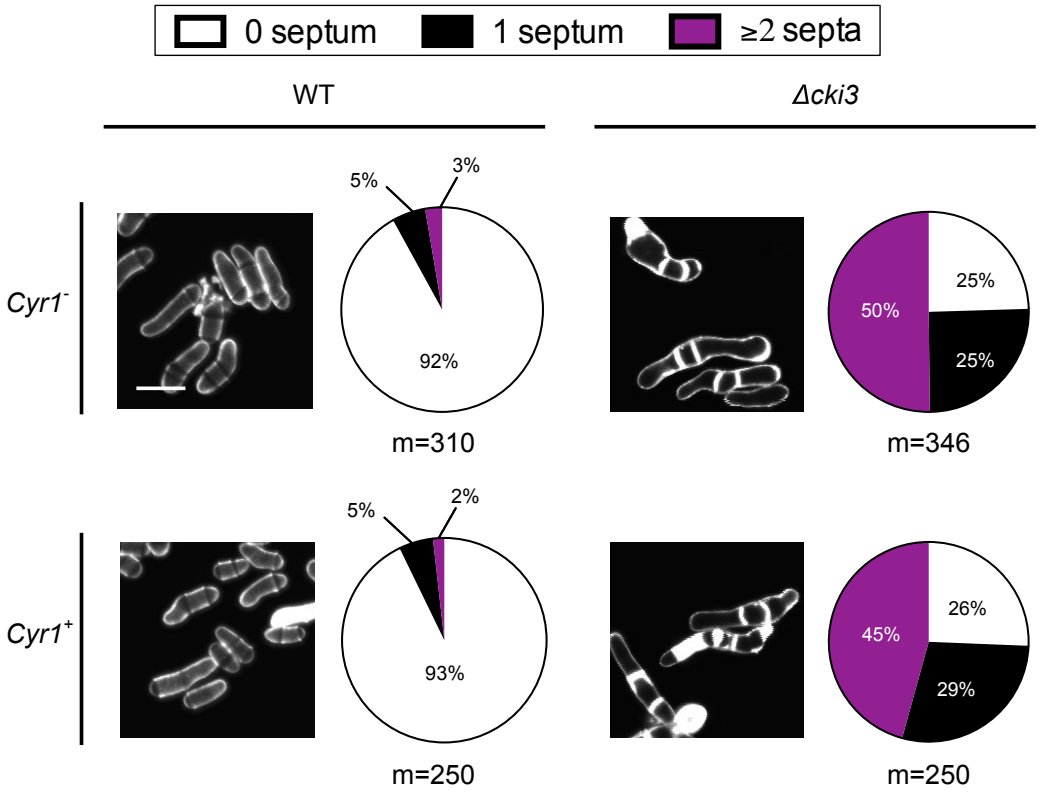

Figure 4.17: **P-factor induced septa is conserved in *cyr1*$^{+}$ *Δcki3* strains.** WT: *cyr1*$^{+}$ (JY448) and *Δcki3*: *cyr1*$^{+}$ (JY1730) strains were grown to mid-exponential growth phase in SSL medium to mimic a nutrient free environment priming the cells for mating. Strains were treated with P-factor for 36 hand then stained with calcofluor white and imaged under UV light (as described in section 2.2.12). Each cell in the image was categorised into the septum index (0 septum, 1 septum or ≥2 septa). The figure includes the data for *cyr1*$^{-}$ strains from Figure 4.16 for comparison. Scale bar represents 10 µm. Data shown is the average of three independent experiments ±SEM.

4.5.7 Cki3 is required to maintain *S.pombe* cells in a G_1 arrest following P-factor treatment

WT cells and strains lacking *cki1* and *cki2* displayed an increase in cell volume following 24 h of treatment with P-factor and then a reduction thereafter (Figure 4.13a). In addition, these strains displayed a plateau in β-galactosidase activity by 12 h (Figure 4.13b), suggesting that *lacZ* and therefore, *rum1* (a gene that encodes Rum1, a protein required to maintain the cells in a G_1 arrest) was no longer being transcribed. Contrary to the WT strains, cells disrupted in *cki3* did not display the reduction in cell volume from 24 h even though a plateau in β-galactosidase activity was observed (Figure 4.13), suggesting that these cells were maintained a G_1 arrest by a different mechanism. Microscopy analysis illustrated that the number of cells displaying septa increased with time (Figure 4.17), demonstrating that *Δcki3* cells attempted to divide yet were unable to complete cell division.

The data collected in this study provide conflicting evidence for whether *Δcki3* cells were maintained in a G_1 arrest or not in response to treatment with P-factor. Therefore, DNA content was measured in these strains to assess what percentage of the cell population was arrested in G_1 phase of the cell cycle following treatment with P-factor (Figure 4.3 assay 4). The assay utilises propidium iodine, a stain that binds stoichiometrically to DNA, which can be used to quantify the DNA content of individual cells in a population via flow cytometry [229]. WT (JY544), *Δcki1* (JY1731), *Δcki2* (JY1722) and *Δcki3* (JY1600) strains were grown to mid-exponential growth phase, treated with 10 µM P-factor and then cell cycle position (or DNA complement) was analysed every 4 h from 0 h to 36 h (as described in section 2.2.15.1).

After 4 h of P-factor treatment all strains displayed a shift from predominantly two complement (2C, G_2 phase) to one complement (1C, G_1 phase) DNA content (Figure 4.18). The shift into G_1 phase was consistent with the detectable changes in Sxa2 expression following treatment with P-factor [190] (Figure 4.11). The number of WT cells arresting in G_1 peaked with 84±3% of the population containing a 1C of DNA by 8 h. After this time, cells began to recover (as a reduction in the number of G_1 arrested cells was observed) reaching a global minimum of 63±5% by 16 h, before tending towards a plateau of ∼67% (oscillating around this value until 36 h). This behaviour was also observed in *Δcki1* and *Δcki2* strains over the 36 h period (Figure 4.18 and 4.19).

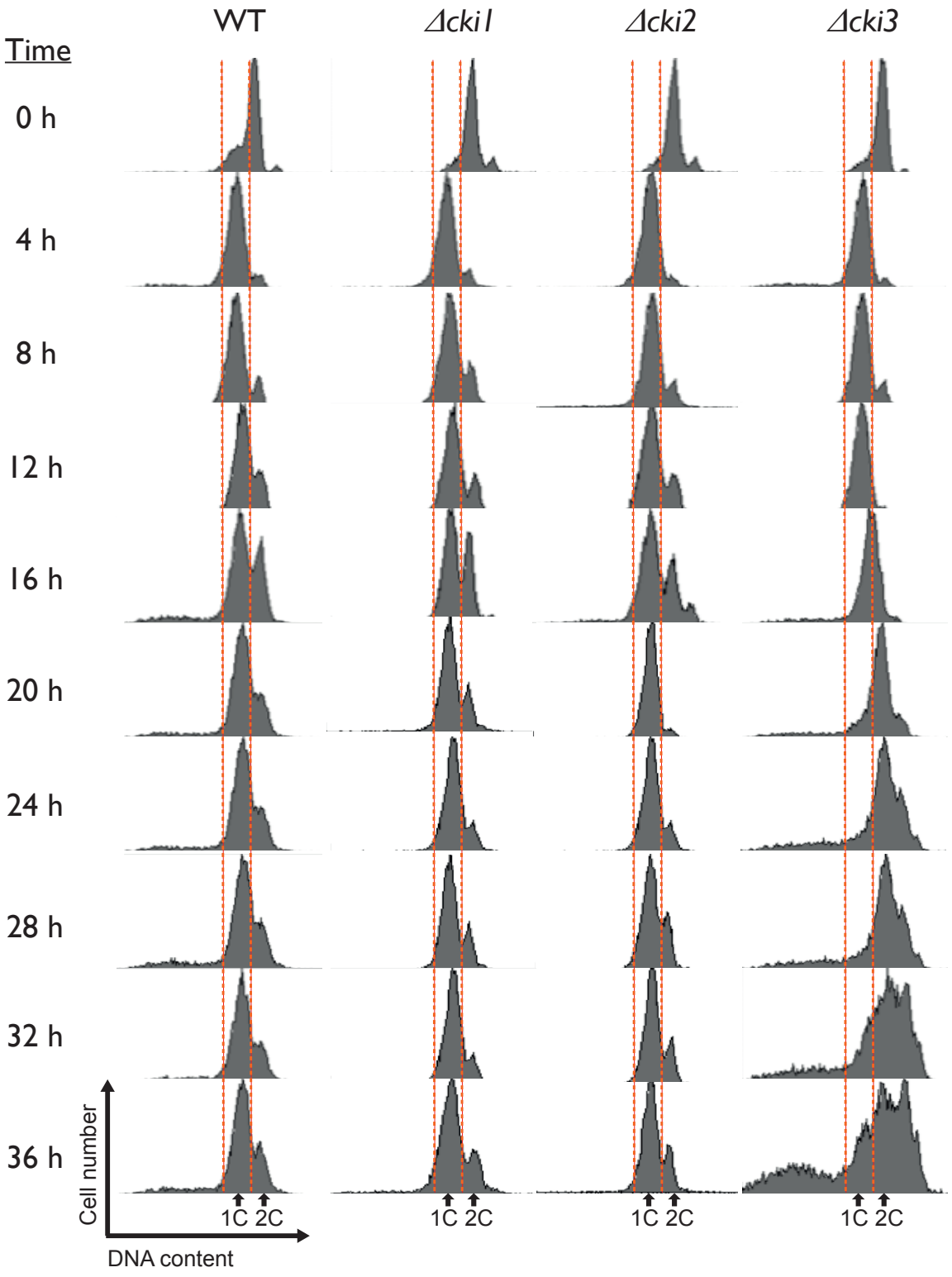

Figure 4.18: ***Δcki3* cells do not contain one complement of DNA following treatment with P-factor for 20 h.** WT (JY544), *Δcki1* (JY1731), *Δcki2* (JY1722) and *Δcki3* (JY1600) strains strains were grown to mid-exponential growth phase and treated with 10 µM P-factor for periods up to 36 h. Cell cycle position (or DNA complement) was analysed every 4 h from 0 h to 36 h (as described in section 2.2.15.1). The two dotted red lines highlight the gating used to identify the number of cells with one complement (1C) of DNA.

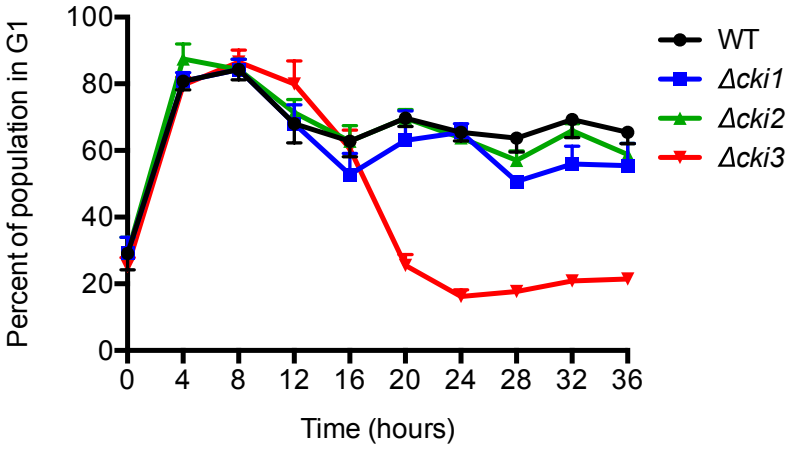

	Time									
Strain	0 h	4 h	8 h	12 h	16 h	20 h	24 h	28 h	32 h	36 h
WT	29±5	83±3	84±3	68±6	63±5	70±3	64±4	64±4	70±5	66±3
Δcki1	29±5	81±3	85±4	70±6	53±6	63±9	65±3	51±2	56±5	56±7
Δcki2	25±4	88±5	82±3	72±4	61±3	68±3	64±1	57±3	66±2	59±3
Δcki3	25±3	80±2	87±4	80±7	61±6	26±3***	16±2***	18± 2***	21±2***	22±2***

Figure 4.19: **G_1 arrest was not maintained in *Δcki3* cells following P-factor treatment from 16 h.** WT (JY544), *Δcki1* (JY1731), *Δcki2* (JY1722) and *Δcki3* (JY1600) strains were grown to mid-exponential growth phase and treated with 10 µM P-factor for periods up to 36 h. Cell cycle position (or DNA complement) was analysed every 4 h from 0 h to 36 h (as described in section 2.2.15.1). Data shown are the average for three independent determinants ±SEM. Statistical significance was calculated using two-way ANOVA with a Dunnett's multiple comparison test, $*p<0.05$, $**p<0.01$ and $***p<0.001$.

Strains disrupted in *cki3* initially followed the same trend as WT strains, displaying a shift from predominately G_2 to G_1 between 0 h to 4 h, reaching a maximal peak of 87±4% in G_1 phase by 8 h. However, following 8 h treatment with P-factor *Δcki3* cells showed a shift from predominantly 1C to predominantly 2C DNA content reaching a global minimum of 16±2% (with 1C of DNA) by 24 h, before tending towards a plateau of ∼20% (until 36 h). The population of *Δcki3* cells in a G_1 arrest was significantly reduced following treatment with P-factor from 20 h onwards in comparison to WT strains (all $p<0.0001$ when $n=3$, one-way ANOVA with a Dunnett's multiple comparison test, Figure 4.19).

The propidium iodide peaks for *Δcki3* cells displayed no defined G_1 peak from 20 h, suggesting that cells had recovered from a G_1 arrest. However, a defined G_2 was not observed either (as seen at 0 h), instead the peaks became progressively dispersed from 20

h. The dispersion of propidium iodide peaks suggested that different sub-populations of cells contained a varied number DNA complements, not just 1C or 2C (Figure 4.18, 24 h to 36 h).

To assess whether the dispersion of propidium iodine peaks observed in *Δcki3* strains following treatment with 10 µM P-factor for a prolonged (>20 h) time was also observed in strains treated with lower (<10 µM) concentrations of P-factor, WT (JY544) and *Δcki3* (JY1600) cells were grown to mid-exponential growth phase and treated with a 1 nM, 100 nM and 10 µM P-factor for periods of up to 36 h. DNA content was determined every 4 h from 0 h to 36 h (as detailed in section 2.2.15.1). In addition to the DNA content profiles, the flow cytometer also measured the forward scatter (FSC) (which correlates to the cell volume) and side scatter (SSC) (which relates to the inner complexity of the cell) of each individual cell.

Following 4 h of treatment with 1 nM P-factor, WT and *Δcki3* cells showed a reduction in the number of G_1 arrested cells (Figure 4.20 and Figure 4.21a). An increase in the population in G_1 was observed in both strains following 4 h treatment with P-factor, reaching a global maximum of 44±3% after 28 h treatment (4.21a). Importantly, these data illustrated that at low (1 nM) P-factor concentrations disruption of *cki3* did not affect cell cycle progression.

WT strains displayed a shift from predominantly 2C (G_2 phase) to predominantly 1C (G_1 phase) DNA content between 8 h and 12 h following treatment with 100 nM P-factor (Figure 4.20). *Δcki3* strains responded quicker to 100 nM P-factor displaying a shift from predominantly 1C to 2C DNA content between 4 h and 8 h (Figure 4.21b). WT strains reached a global maximum (81±2% G_1 arrested cells) at 16 h in comparison to *Δcki3* strains, which reached a global maximum (74±4% G_1 arrested cells) by 12 h (Figure 4.21b). After reaching the maximal peaks both WT strains and cells disrupted in *cki3* showed a reduction in the population of cells showing a G_1 arrest tending towards a plateau of ∼60% (oscillating around this value) (Figure 4.21b). Following 28 h of treatment with 100 nM P-factor, a greater spread in the SSC and FSC of *Δcki3* cells was observed in comparison to WT cells (Figure 4.20).

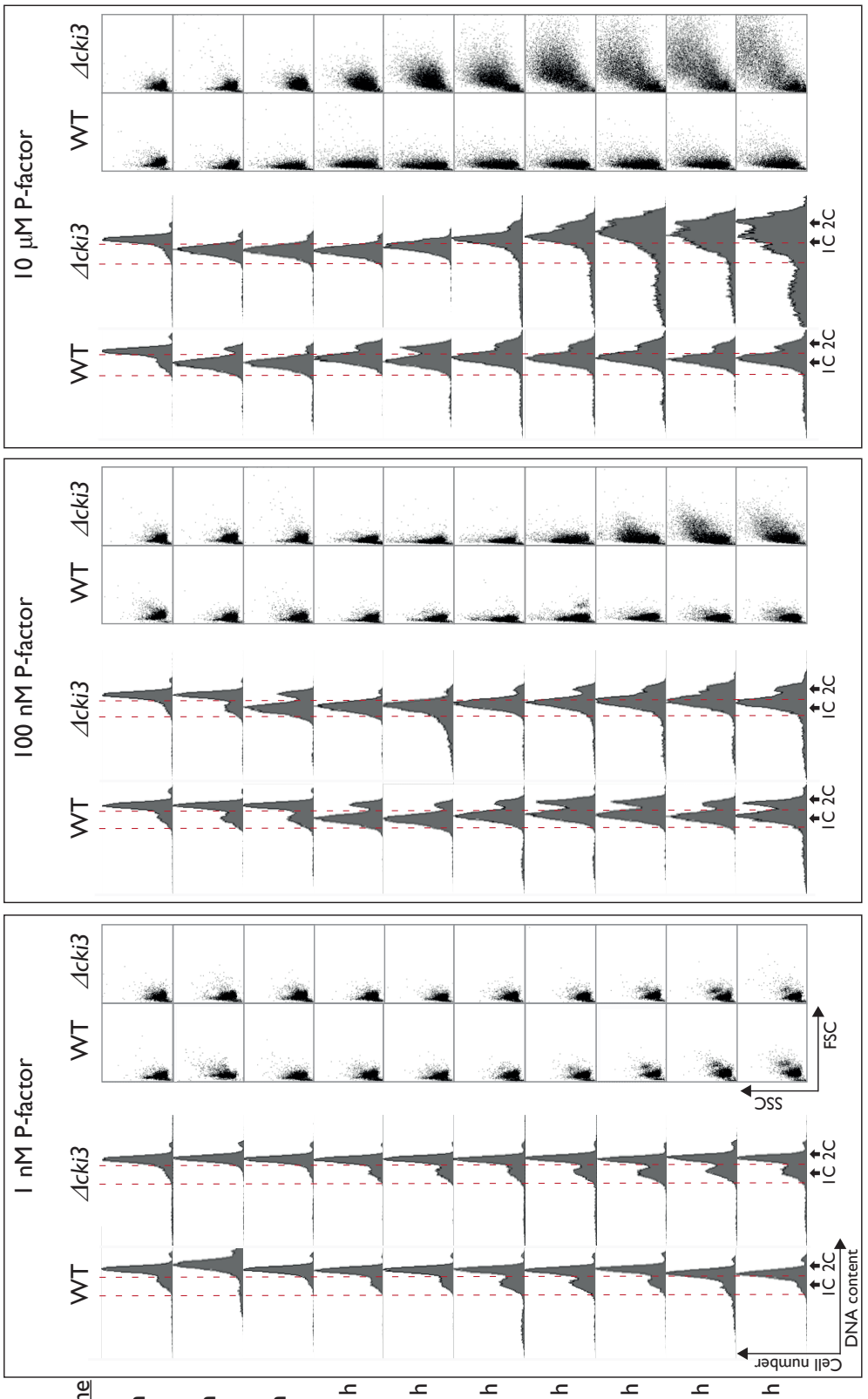

Figure 4.20: **The forward and side scatter of *Δcki3* cells become dispersed following 10 µM P-factor treatment with time.** WT (JY544) and *Δcki3* (JY1600) strains were grown to mid-exponential growth phase and treated with a 1 nM, 100 nM and 10 µM P-factor for periods of up to 36 h. DNA content was determined every 4 h from 20 h to 36 (as detailed in section 2.2.15.1). The scatter plots present the forward scatter (FSC) and side scatter (SSC) correlating to cell volume and inner complexity of the cell, respectively. Histograms indicate the population of cells with propidium iodide staining, the two dotted lines highlight the gating used to identify the number of cells with one complement of DNA.

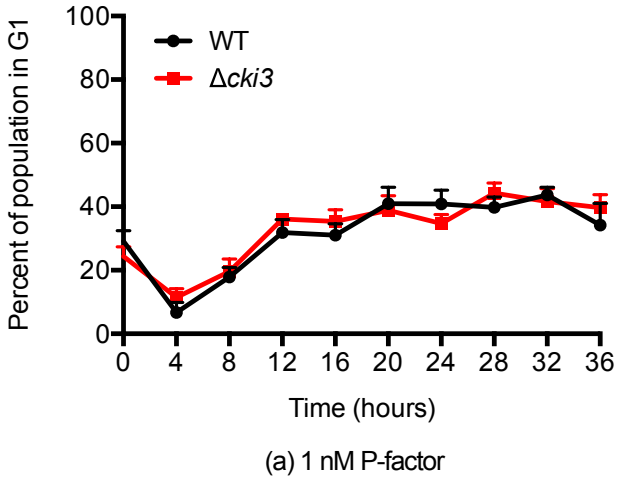

(a) 1 nM P-factor

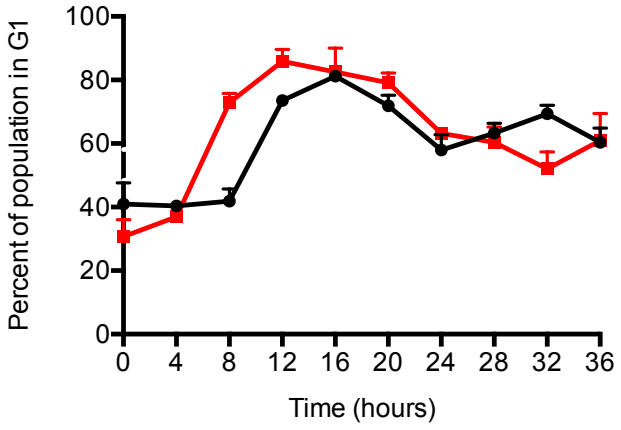

(b) 100 nM P-factor

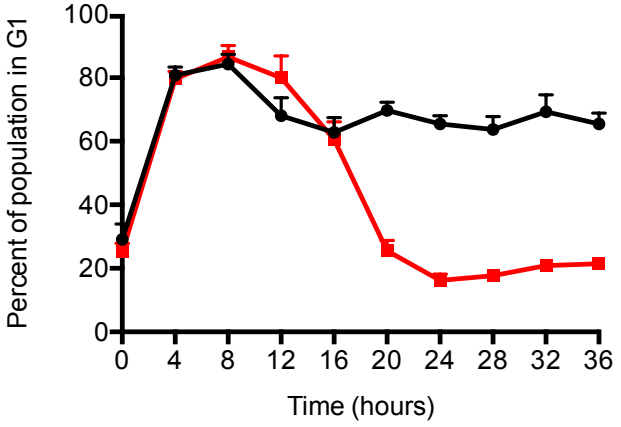

(b) 10 µM P-factor

Figure 4.21: **The reduction in G_1 arrested cells only occurs at high (10 µM) P-factor concentrations.** WT (JY544) and *Δcki3* strains were grown to mid-exponential growth phase before treated with 1 nM, 100 nM and 10 µM P-factor for a period of 36 h. Cell cycle arrest was determined every 4 h from 0 h to 36 h using propidium iodide staining and flow cytometry. Data shown are the average for two independent determinants ±SEM.

As discussed above, strains lacking *cki3* showed a significant reduction in the population of G_1 arrested cells (in comparison to WT cells) following treatment with 10 µM P-factor for 20 h (Figure 4.21c). After 12 h of treatment (with 10 µM P-factor) *Δcki3* cells exhibited a greater spread in FSC in comparison to WT cells that became increasingly dispersed with time (Figure 4.20). The spread in FSC suggested that cell volume increased following treatment with P-factor, which was also demonstrated by the time-course cell volume assay (Figure 4.13). It should be noted that the *Δcki3* cells, which showed a greater FSC also displayed an increase in SSC (greater internal complexity) (Figure 4.20). The increase in internal complexity (represented by the SSC) was consistent with the idea that cells lacking *cki3* attempted to divide and hence replicated internal structures, yet were unable to complete division, resulting in an increased cell volume (represented by FSC).

4.5.8 *Δcki3* cells that display septa also display multiple nuclei

In response to a high (10 µM) concentration of P-factor *Δcki3* strains displayed septa (Figure 4.17), an increase in the frequency of cells displaying a high internal complexity (measured by SSC), an increased cell volume (measured by FCS) (Figure 4.20) and a reduction in the percentage of cells displaying 1C of DNA following 20 h of treatment (Figure 4.21c). Together, these data suggest that in response to P-factor, *Δcki3* strains attempt to divide as the cells progressed from G_1 arrest into S phase (replicating DNA) and entered mitosis (indicated by the formation of the medial ring or septum). However, these cells could not successfully complete cytokinesis, yet still entered into further rounds of division as $\geq$2 septa were displayed in $\sim$50% of the population following 36 h treatment (Figure 4.15).

Formation of the septum occurs in tandem with anaphase B (separation of DNA into daughter cells). To determine whether cells had successfully completed anaphase B by separating the nuclei, the fluorescent stain DAPI, which binds A-T rich regions within DNA was utilised to visualise the nuclei of *S. pombe*. WT (JY544) and *Δcki3* (JY1600) strains were grown to mid-exponential growth phase, treated with 10 µM P-factor and after 36 h cells were stained with DAPI and imaged (as described in section 2.2.13). *Δcki3* cells, which displayed septa also displayed multiple-nuclei (Figure Figure 4.22). This was shown in the pseudocoloured DAPI images (which were used to aid the visualisation of the staining), where DNA is highlighted in yellow (Figure 4.22, arrows highlight multiple nuclei). Multiple-nuclei were not observed in WT cells (Figure 4.22). Together these data

suggest that cells which commit to cell-cycle progression complete anaphase B, indicating that Cki3 is required for cytokinesis.

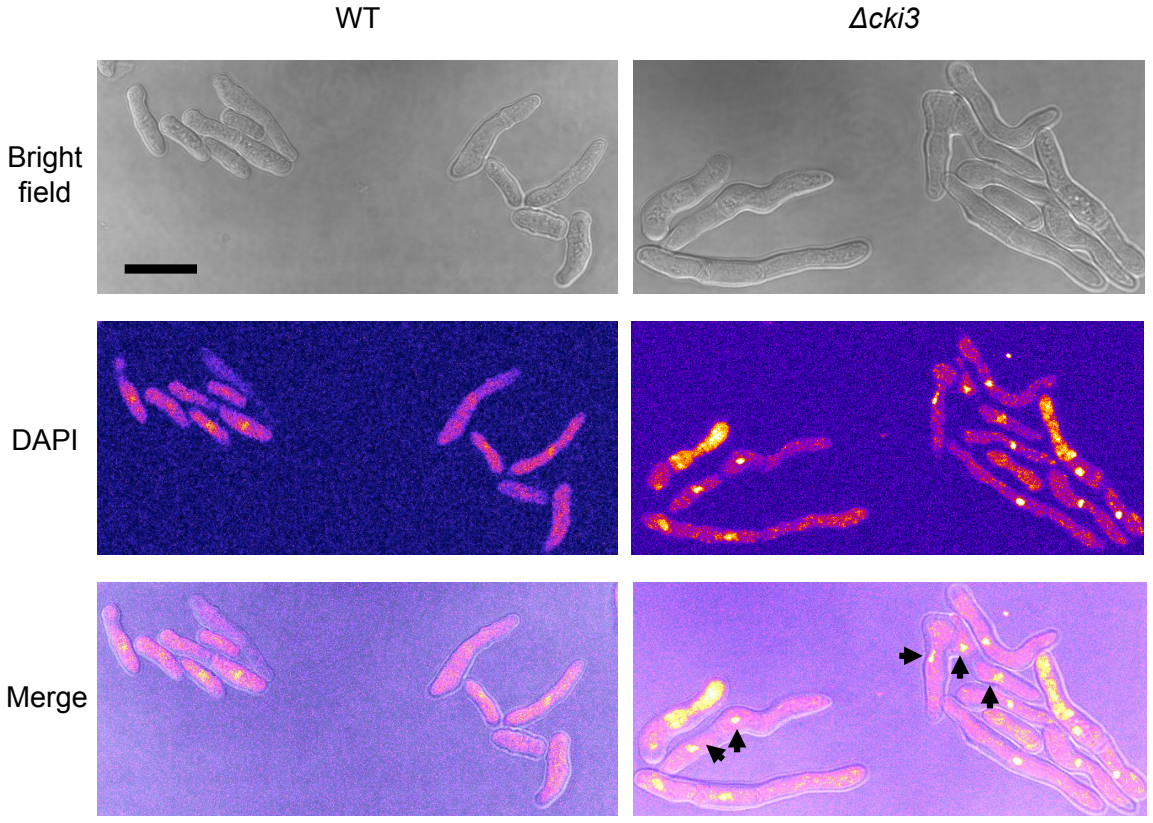

FIGURE 4.22: ***Δcki3* cells that display septa contain multiple nuclei.** WT (JY544) and *Δcki3* (JY1600) strains were grown to mid-exponential growth phase before treated with 10 µM P-factor for 36 h. Cells were stained with DAPI to visualise the DNA and imaged with UV light (as described in section 2.2.13). ImageJ software was used to transform the DAPI images into fire scale for the ease of the reader (this highlights the stained DNA in yellow). Arrows highlight multiple nuclei. Scale bar represents 10 µm.

4.5.9 Constitutive expression of Cki1, Cki2 and Cki3 on the pheromone-response pathway in *S. pombe*

Deletion of the kinases' highlighted a role for Cki1 and Cki3 in regulating signal transduction of the pheromone-responsive pathway (section 4.5). Moreover, Cki2 was shown to play a role in mating (Figure 4.4). Constitutive expression of proteins (by utilising expression plasmids) can provide further information about their role within the mating-response in *S. pombe* [173, 223, 228]. First Cki1, Cki2 and Cki3 were cloned into the expression vector pREP3x (as described in section 2.3.2.1), which allows constitutive expression of exogenous genes at high levels [235].

4.5.9.1 Overexpression of Cki1 partially rescued P-factor-directed responses in strains lacking Cki1

To further investigate the role of Cki1 in pheromone-directed responses, WT (JY544; *sxa2>lacZ*) and *Δcki1* (JY1731; *sxa2>lacZ*, *cki1::ura4*$^+$) strains were transformed with pREP3x (JD3386) and pREP3x-Cki1 (JD3893: pCki1) to increase the cellular concentration of Cki1. The strains were grown to mid-exponential growth phase in the absence of thiamine to induce full plasmid expression and following 16 h of treatment with a range of P-factor concentrations (0 µM - 100 µM P-factor) cells were assayed for β-galactosidase activity and cell volume (as described in section 2.2.8.1 and section 2.2.7, respectively).

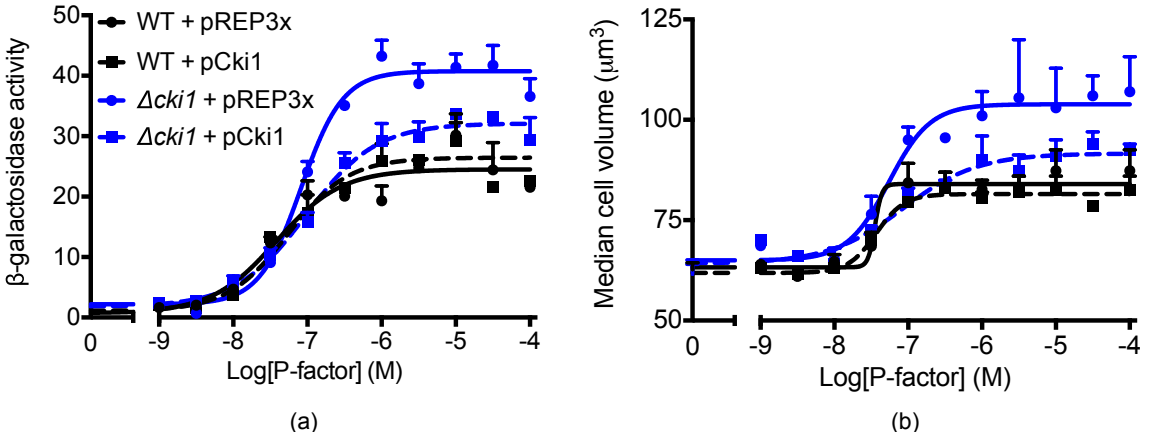

FIGURE 4.23: **Expression of Cki1 in *Δcki1* cells reduced gene transcription and cell volume.** WT (JY544) and *Δcki1* (JY1731) strains expressing pREP3x (JD3386) and pREP3x-Cki1 (JD3893: pCki1) were grown to mid-exponential growth phase before treatment with a range of P-factor concentrations (from 0 µM to 100 µM). After 16 h cells were assayed for (a) β-galactosidase activity and (b) cell volume (as described in section 2.2.8.1 and section 2.2.7, respectively). Scale bar represents 10 µm.

The β-galactosidase and cell volume assay demonstrated that Cki1 overexpression in the WT strain JY544 did not affect the transcription of *lacZ* or conjugation tube formation, as the basal, maximal and pEC_{50} values were not significantly different to WT cells expressing pREP3x ($p>0.05$ when n=3, Student's t-test) (Figure 4.24). However, Cki1 overexpression in *Δcki1* strains significantly but partially reduced maximal β-galactosidase activity (from 40±1 *lacZ* units to 32±1 *lacZ* units, $p=0.0048$ when n=3, Student's t-test) and cell volume (from 104±2 µm^3 to 92±2 µm^3, $p=0.0132$ when n=3, Student's t-test) (Figure 4.24). These data suggest the cellular concentration of Cki1 is not a limiting factor in the *S. pombe* pheromone-response transcriptional pathway.

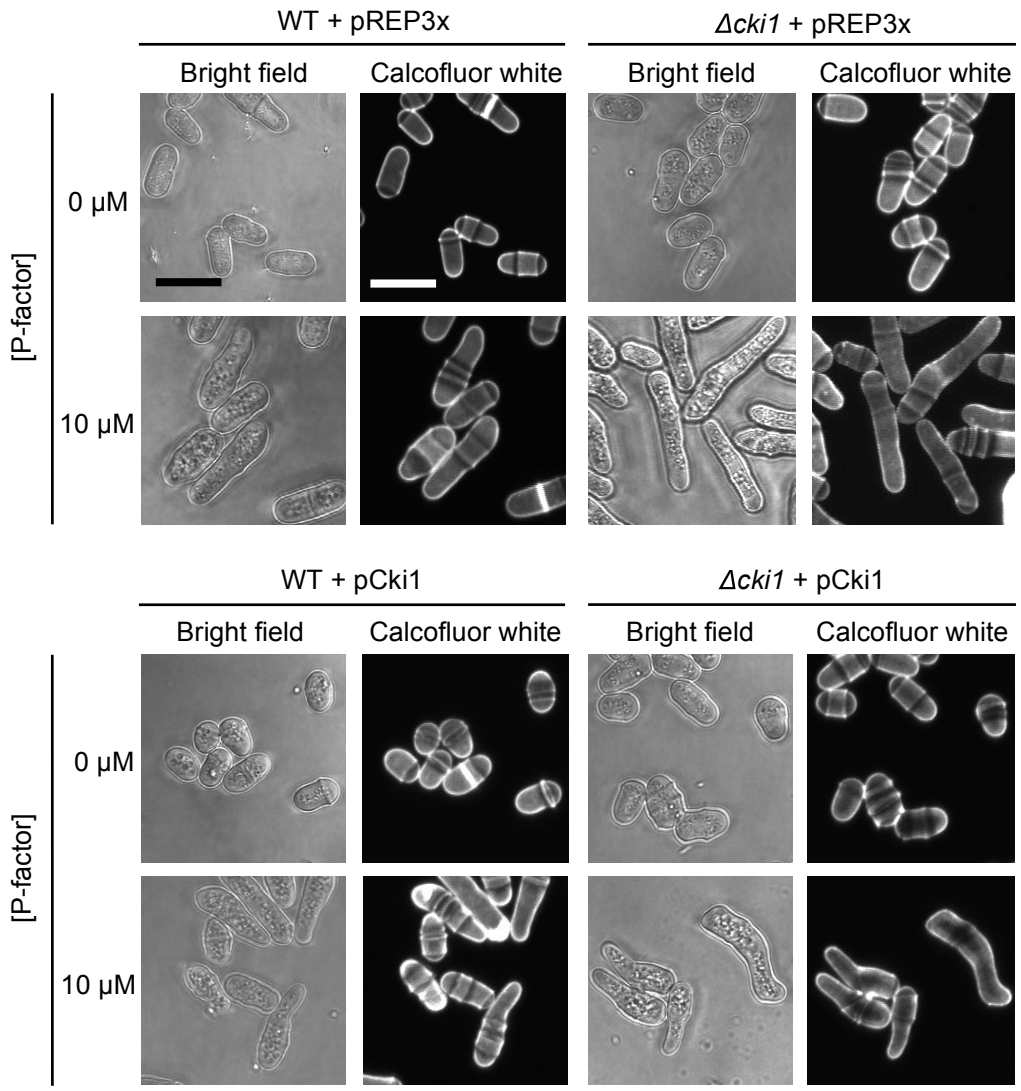

Figure 4.24: **The *Δcki1* hyper-elongated conjugation tube phenotype is rescued with expression of Cki1.** WT (JY544) and *Δcki1* (JY1731) strains expressing pREP3x (JD3386) and pREP3x-Cki1 (JD3893: pCki1) were grown to mid-exponential growth phase before treated with 0 μM and 10 μM P-factor. After 16 h cells were stained with calcofluor white and imaged with bright field and UV light (as described in section 2.2.12). Scale bar represents 10 μm.

The same strains used in the β-galactosidase assay were stained with calcofluor white and imaged to visualise the affect of overexpression of Cki1 on cell size, shape and integrity of the membranes (as described in section 2.2.12). The partial rescue of cell volume observed when overexpresing Cki1 in *Δcki1* strains, in comparison to WT cell volume (Figure 4.23b) was also demonstrated by the reduction in conjugation tube length in the microscopy analysis (Figure 4.24). There was no observed difference in cell elongation following enhanced Cki1 expression in WT cells. The microscopy analysis in combination with the quantitative

cell volume assay suggests that endogenous Cki1 expression levels are not limiting when influencing the morphological response.

4.5.9.2 Overexpression of Cki2 does not affect P-factor-directed responses

A previous study demonstrated that overexpression of Cki2 during vegetative cell growth lead to a pear-shaped cell morphology [272]. To determine the role of Cki2 during the morphological response, WT (*sxa2>lacZ*) and *Δcki2* (JY1722; *sxa2>lacZ*, *cki2::ura4*$^+$) strains expressing pREP3x (JD3386) and pREP3x-Cki2 (JD3766: pCki2) were grown to mid-exponential growth phase before treatment with 0 µM and 100 µM P-factor. After 16 h cells were then stained with calcofluor white and imaged (as described in section 2.2.12). Contrary, to previous observations, overexpression of *cki2* in WT strains in both treated and untreated cells was indistinguishable from WT+pREP3x (Figure 4.26).

To quantify how expression of Cki2 influences the transcriptional and morphological response, WT+pREP3x, WT+pCki2, *Δcki2*+pREP3x and *Δcki2*+pCki2 were grown to mid-exponential growth phase before treatment with a range of P-factor concentrations (from 0 µM to 100 µM). Following 16 h, cells were assayed for β-galactosidase activity and cell volume (as described in section 2.2.8.1 and section 2.2.7, respectively). Expression of Cki2 in WT and *Δcki2* cells did not influence the the transcriptional β-galactosidase expression of cell volume profiles in comparison to cells expressing pREP3x (Figure 4.25). These data provide further evidence that Cki2 does not influence P-factor-directed responses.

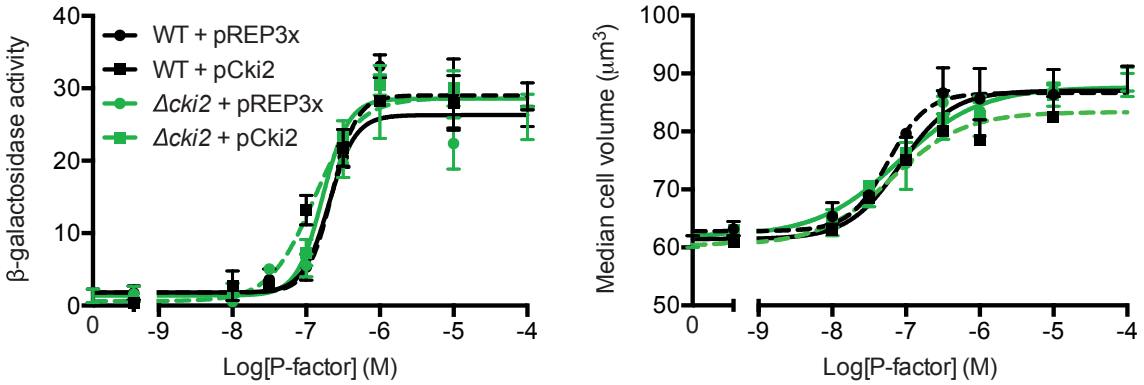

(a) (b)

Figure 4.25: **Expression of Cki2 did not affect gene transcription or cell volume.** WT (JY544) and *Δcki2* (JY1722) strains expressing pREP3x (JD3386) and pREP3x-Cki2 (JD3766: pCki2) were grown to mid-exponential growth phase before treatment with a range of P-factor concentrations (from 0 µM to 100 µM). After 16 h cells were assayed for (a) β-galactosidase activity and (b) cell volume (as described in section 2.2.8.1 and section 2.2.7, respectively). Data shown is the average of three independent experiments ±SEM.

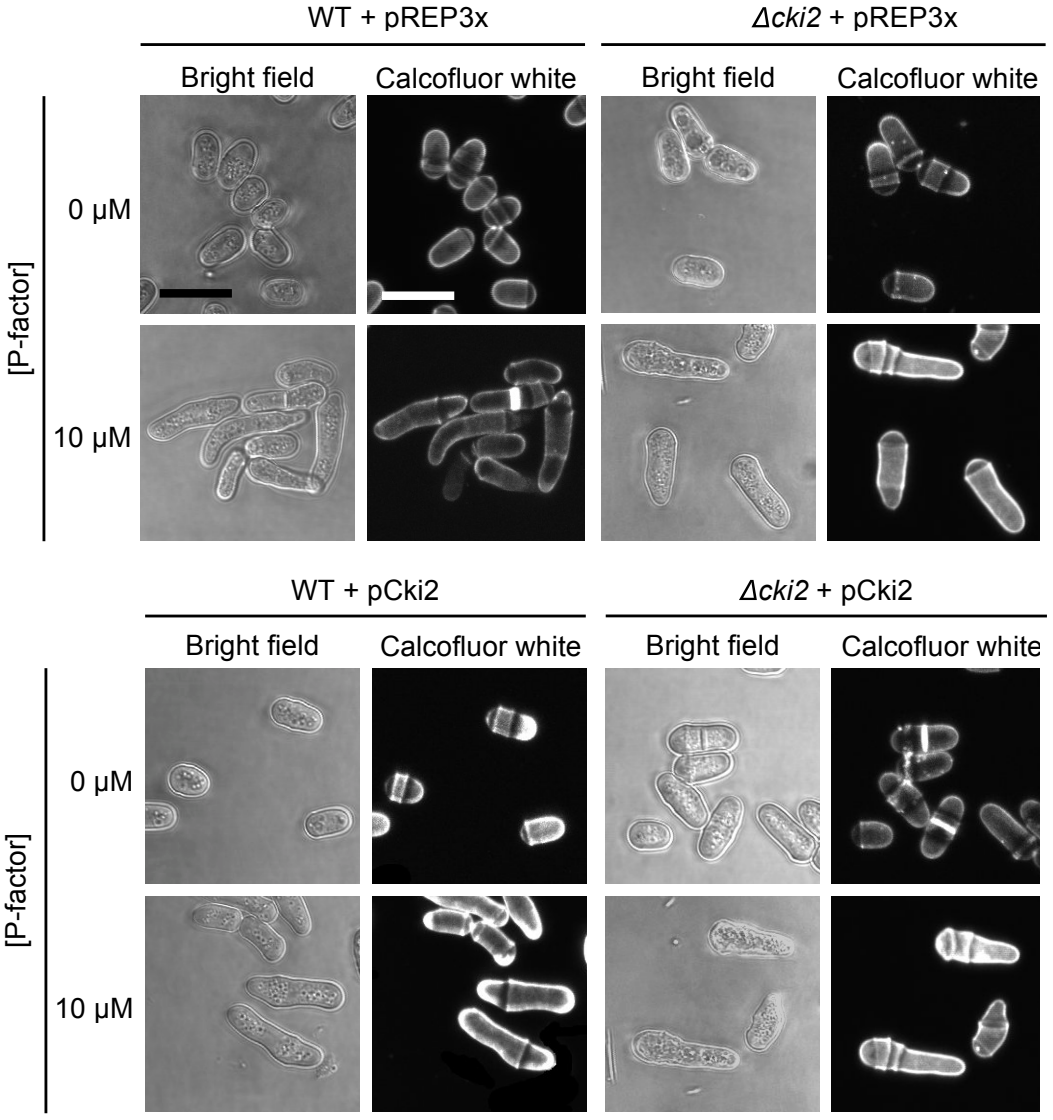

Figure 4.26: **Expression of Cki2 did not influence cell morphology.** WT (JY544) and *Δcki2* (JY1722) strains expressing pREP3x (JD3386) and pREP3x-Cki2 (JD3766: pCki2) were grown to mid-exponential growth phase before treated with 0 µM and 10 µM P-factor. After 16 h cells were stained with calcofluor white and imaged with bright field and UV light (as detailed in section 2.2.12). Scale bar represents 10 µm.

4.5.9.3 Overexpression of Cki3 partially rescued P-factor-directed responses in *Δcki3* strains

To further investigate the role of Cki3 in pheromone-directed responses, WT (JY544; *sxa2>lacZ*) and *Δcki1* (JY1600; *sxa2>lacZ*, *cki3::ura4*$^+$) strains were transformed with pREP3x (JD3386) and pREP3x-Cki3 (JD3782: pCki3) to increase the cellular concentration of Cki3. The strains were were grown to mid-exponential growth phase in the absence of thiamine to induce full plasmid expression and following 16 h of treatment with a range of

P-factor concentrations (0 µM - 100 µM P-factor) the cells were assayed for β-galactosidase activity and cell volume (as described in section 2.2.8.1 and section 2.2.7, respectively).

The β-galactosidase and cell volume assay demonstrated that Cki3 overexpression in the WT strain JY544 did reduce the maximal transcription of *lacZ* and the cell volume of strains, however this was not considered statistically significant in comparison to WT cells expressing pREP3x ($p>0.05$ when n=3, Student's t-test) (Figure 4.27). Cki3 overexpression in *Δcki3* strains did however show a significant partial rescue in maximal β-galactosidase activity (from 58±2 *lacZ* units to 40±2 *lacZ* units, $p=0.0048$ when n=3, Student's t-test) and cell volume (from 145±5 μm^3 to 115±4 μm^3, $p=0.0094$ when n=3, Student's t-test) (Figure 4.27). These data suggest the cellular concentration of Cki3 is a limiting factor in *S. pombe* pheromone-response pathway.

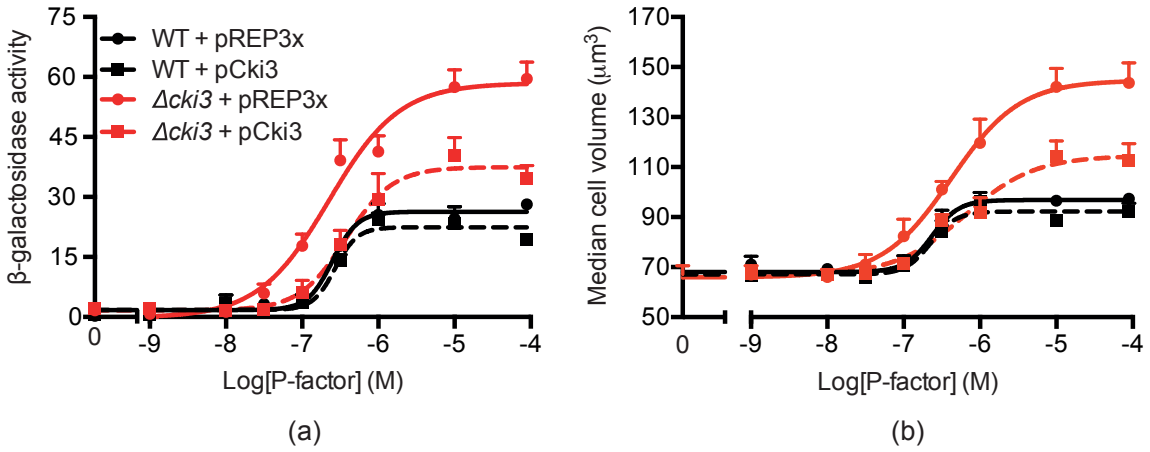

FIGURE 4.27: **Gene transcription and cell volume is reduced following expression of Cki3 in *Δcki3* cells.** WT (JY544) and *Δcki3* (JY1600) strains expressing pREP3x (JD3386) and pREP3x-Cki3 (JD3782: pCki3) were grown to mid-exponential growth phase before treatment with a range of P-factor concentrations (from 0 µM to 100 µM). After 16 h cells were for (a) β-galactosidase activity and (b) cell volume (as described in section 2.2.8.1 and section 2.2.7, respectively). Data shown is the average of three independent experiments ±SEM.

The strains were also stained with calcofluor white and imaged (as described in section 2.2.12) to visually assess the affect of overexpression of Cki3 on cell size, shape and integrity of the membranes. The partial rescue of cell volume observed when overexpresing Cki3 observed in *Δcki3* strains, in comparison to WT cell volume (Figure 4.27b) was also demonstrated by the reduction in conjugation tube length in the microscopy analysis (Figure 4.28). In addition, overexpression of Cki3 prevented the dominant septa phenotype that was observed in *Δcki3* strains (Figure 4.28).

The cell volume assay displayed the same dose-dependent behaviour as the transcriptional assay for all strains; showing that expression of Cki3 in WT and *Δcki3* cells results in no difference and a reduction in cell volume size, respectively.

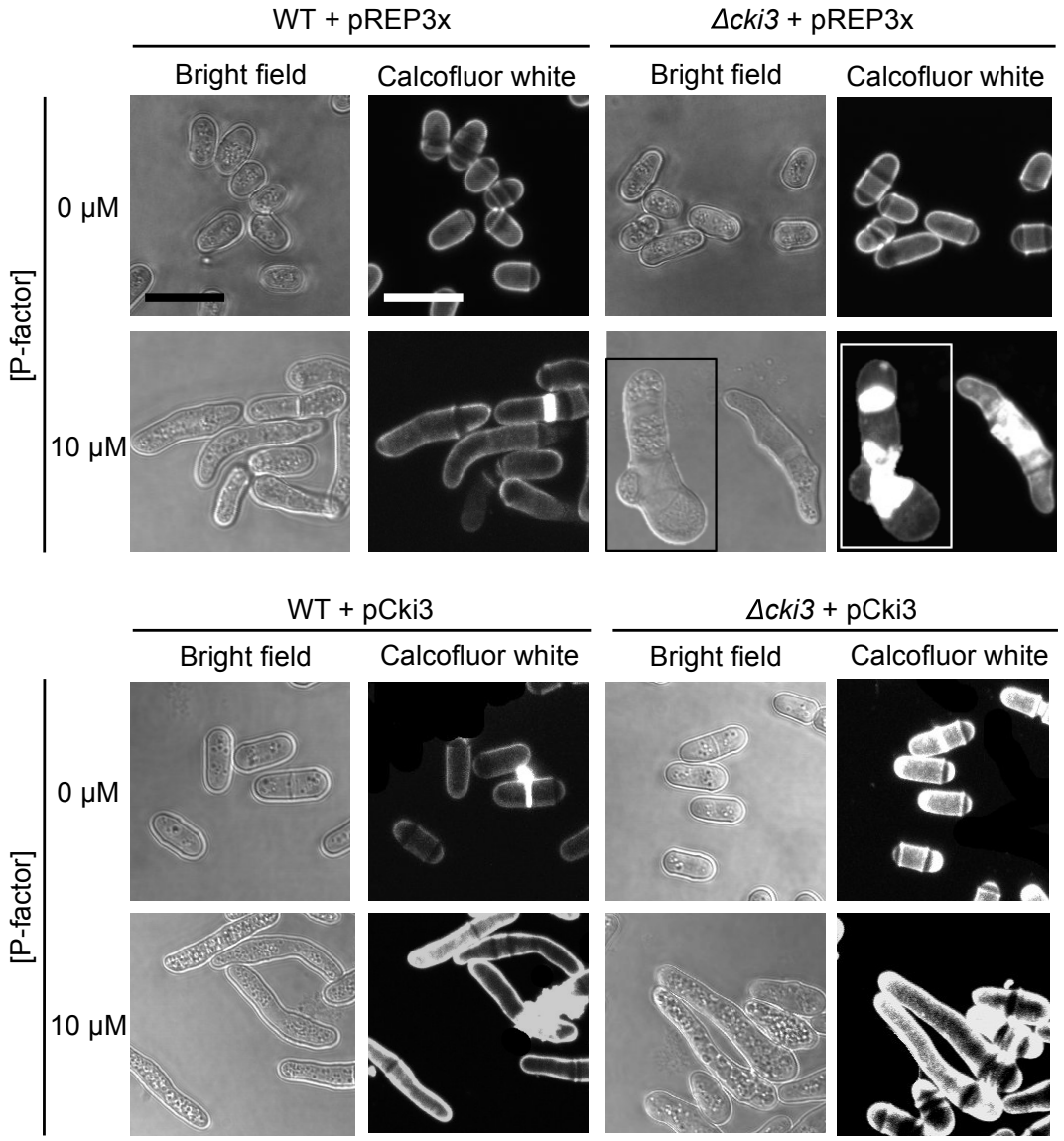

FIGURE 4.28: **The septa phenotype shown in *Δcki3* cells is rescued with expression of Cki3.** WT (JY544) and *Δcki3* (JY1600) strains expressing pREP3x (JD3386) and pREP3x-Cki3 (JD3782: pCki3) were grown to mid-exponential growth phase before treated with 0 μM and 10 μM P-factor. After 16 h cells were stained with calcofluor white and imaged with bright field and UV light (as detailed in section 2.2.12). Composite images were collated for *Δcki3*+pREP3x and are highlighted by a separate box. Scale bar represents 10 μm.

4.6 Summary

This chapter has described the role of Cki1, Cki2 and Cki3 in the pheromone-response pathway of *S. pombe*. To date only two papers have explored these proteins contribution to the pheromone-response, solely via the use of mating assays [273], which has demonstrated a role of Cki2 in regulating the pathway [278]. Deletion strains and constructs for constitutive expression of Cki1, Cki2 and Cki3 were examined (see chapter 2) and four standard mating-response assays were performed. These included quantification of transcription of mating-responsive genes, the measurement of conjugation tube formation, quantification of the population in G_1 and the measurement of successful mating by quantifying the production of ascospores. A summary of the results obtained in this chapter is provided in Table 4.1.

			10 µM P-factor			
Strain		Successful mating	Gene transcription	Conjugation tube formation	Defects in morphology	G_1 arrest
WT	-	✓	✓	✓	×	✓
	+ pCki1	-	✓	✓	×	-
	+ pCki2	-	✓	✓	×	-
	+ pCki3	-	✓	✓	×	-
Δcki1	-	✓	✓✓	✓✓	×	✓
	+ pCki1	-	×✓	×✓	×	-
Δcki2	-	×✓	✓	✓	×	✓
	+ pCki2	-	✓	✓	×	-
Δcki3	-	✓✓	✓✓	✓✓	✓	×
	+ pCki3	-	×✓	×✓	×	-

TABLE 4.1: **A summary of pheromone-induced responses in WT, *Δcki1*, *Δcki2* and *Δcki3* strains.** mating-response, gene transcription, conjugation tube formation, morphological defects (such as multiple projection tips, septa and cell wall deposition) and G_1 arrest following stimulation with 10 µM pheromone are summarised. ✓is used to denote a response, ✓✓indicated an increased response, ×✓= reduced response and ×= no response.

Deletion of *cki1* increased transcriptional response and conjugation tube elongation following treatment with >1 µM P-factor. This behaviour was similar to the phosphatase Pmp1, which is thought to negatively regulate the expression of Spk1 [11, 221] and this therefore indicated that Cki1 could be a negative regulator of the pheromone-response in *S. pombe*. Strains lacking *cki1* arrest in G_1 phase of the cell cycle following treatment with P-factor and were successful at mating since no quantifiable difference in CFU recovery (ascospores) following heat inactivation was observed in comparison to WT strains, suggesting that deletion of *cki1* does not change the cells' ability to mate. This is different to

other known negative regulators of signalling such as Rgs1 [87] and Gap1 [86], which are required for a successful WT mating-response. Constitutive expression of Cki1 in WT *S. pombe* strains did not affect signalling behaviour, however, a partial phenotypic recovery was observed following expression of Cki1 in *Δcki1* cells. Together these data suggested a role for Cki1 in regulating the signalling events prior to conjugation in *S. pombe*.

Previously, Cki2 was shown to be required for successful mating in *S. pombe* [273]. This result was confirmed as *Δcki2* cells showed only a partial increase in CFU recovery when compared to WT cells. Despite this, deletion of *cki2* did not affect transcriptional response, conjugation tube formation or the ability for cells to arrest in G_1 and recover following prolonged treatment with P-factor. However, deletion of *cki2* did significantly increase both the cell area and cell volume during vegetative cell growth. Together these data indicate that Cki2 is required for controlling cell size during vegetative cell growth but is not required for GPCR signalling events prior to agglutination and conjugation, but may be required for the later mating events as the signalling events upstream were unaffected in *Δcki2* cells.

During vegetative cell growth, *Δcki3* cells grow and divide at a normal rate displaying typical morphology. Only in response to P-factor was an increase in transcriptional response and hyper-elongated conjugation tubes observed, displaying multiple-projection tips and septa. In addition to the aberrant morphologies displayed in *cki3* disruption strains, the use of the cell wall marker, calcofluor white, highlighted defects in cell wall biogenesis.

Additional DNA complement assays were performed with *Δcki3*, the resulting propidium iodide peaks (which indicate the DNA complement of cells' within the population) became dispersed following prolonged (from 20 h to 36 h) treatment with P-factor, suggesting that the number of cells containing various complements of DNA, not just one or two complements, increased. Further analysis revealed that the number of *Δcki3* cells displaying septa increased with time in response to high (10 µM) concentrations of P-factor, suggesting that cells attempted to divide yet were unable to complete the process of cytokinesis, as nuclei were observed between septa. Together these data suggest that Cki3 has a negative regulatory role on the pheromone pathway of *S. pombe* and interestingly, Cki3 has an essential role for the progression of cells to complete cytokinesis but only in a P-factor dependent manner.

Chapter 5

The role of Cki1, Cki2 and Cki3 in Mam2 internalisation

5.1 Background

GPCRs are often internalised from the plasma membrane in response to ligand-binding. These internalisation events are typically initiated via phosphorylation of the intracellular receptor domains. Mam2, the **M**-type *S. pombe* pheromone receptor, is internalised in response to P-factor [173]. However, the specific kinase(s) that promote this process have not yet been described. Chapter 4 identified three kinases that potentially promote internalisation of Mam2: Cki1, Cki2 and Cki3 and investigated their role in P-factor-directed responses. This chapter seeks to elucidate whether these kinases initiate the internalisation of Mam2 in response to treatment with P-factor.

5.2 Mam2 does not interact with Cki1, Cki2 or Cki3

To establish whether Cki1, Cki2 and Cki3 interacted with the C-terminal tail of Mam2, a yeast 2-hybrid analysis, which detects a physical interaction between two proteins was performed [280]. The yeast 2-hybrid system utilises the GAL4 transcription factor from *S. cerevisiae*, which is typically involved in the regulation of galactose metabolism [280]. GAL4 consists of two domains; a DNA binding domain (BD) and a DNA activation domain (AD). These domains act in concert to induce the transcription of GAL4 controlled genes. Both the DNA BD and the DNA AD can be fused to two potentially interacting proteins,

with an interaction leading to the reconstitution of the complete functional GAL4 domain and subsequent transcriptional activation of reporter genes.

The *S. cerevisiae* strain AH109 contains three yeast reporter genes *HIS3*, *ADE2*, *MEL1* (which encodes α-galactosidase) and a bacterial reporter gene *lacZ* (which encodes β-galactosidase), all under the control of the GAL4 promoter. Reconstitution of the GAL4 transcription factor by two interacting proteins, enables cell proliferation in the absence of histidine and adenine [281].

5.2.1 Plate-based yeast 2-hybrid assay

To determine whether the kinases interacted with the last 45-residues of Mam2 (the Mam2tail) [173], Cki1, Cki2 and Cki3 were first cloned into the yeast 2-hybrid expression vector pGADT7, which fuses the kinase with the DNA AD (as described in section 2.3.2.2). A yeast 2-hybrid assay was then performed with *S. cerevisiae* strain AH109 transformed with the AD vectors and co-transformed with each BD vector described in Table 5.1. Transformants were grown to mid-exponential growth phase, spotted onto SD-leu-trp plates to confirm the presence of both plasmids and SD-leu-trp-his-ade plates to indicate a protein-protein interaction.

Activating domain (AD)	Binding domain (BD)
pGADT7 (JD2320)	pGBKT7 (JD1170)
pGADT7-Rgs1 (JD3180)	pGBKT7-Mam2tail (JD3221)
pGADT7-Cki1 (JD3770)	pGBKT7-Map3tail (JD3280)
pGADT7-Cki2 (JD3771)	pGBKT7-STE2tail (JD3284)
pGADT7-Cki3 (JD3763)	pGBKT7-Rgs1 (JD3182)

Table 5.1: **The vectors used in the yeast 2-hybrid assay.** The *S. cerevisiae* strain AH109 was transformed with the activating domain vectors and co-transformed with the binding domain vectors.

Vector alone (negative) controls were included to confirm the absence of auto-activation of the promoter and an Rgs1 (positive) control was included as Rgs1 has previously been shown to interact with the last 45-residues of Mam2 [173] (Figure 5.1). The last 54-residues of the **P**-type GPCR Map3 (Map3tail) [282] was also included in the yeast 2-hybrid assay to identify an interaction between Map3 and the kinases. As Cki1, Cki2 and Cki3 are homologous to YCK1 and YCK2, the kinases that phosphorylate the C-terminal domain of STE2 [112], they may confer similar properties. Therefore, the last 133 residues of STE2 (STE2tail) [180] were included in the assay to identify if the kinases interacted with STE2.

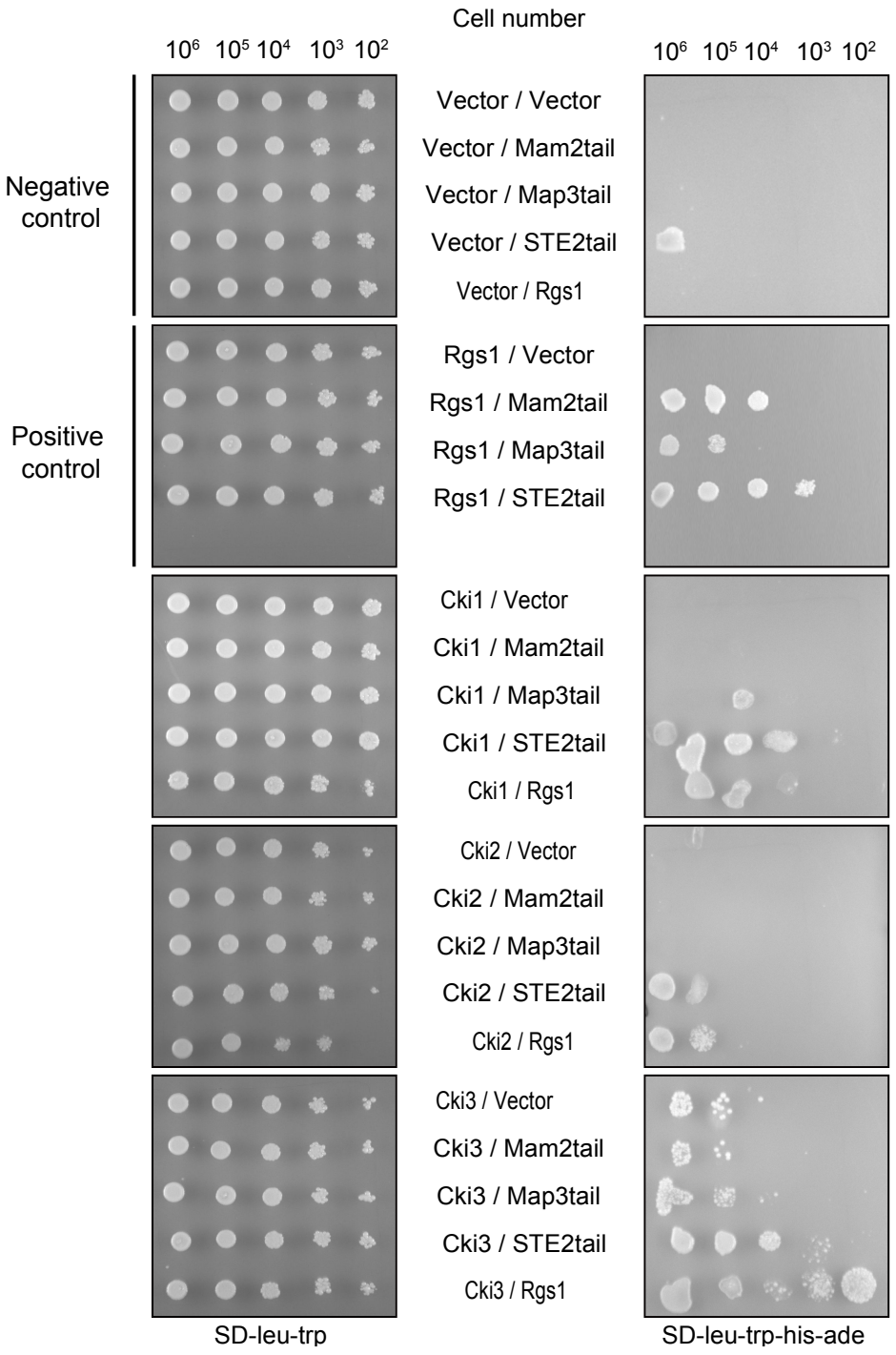

Figure 5.1: **Mam2 does not interact with Cki1, Cki2 or Cki3.** *S. cerevisiae* strains AH109 were transformed with control vector pGADT7 (JD2320), pGADT7-Rgs1 (JD3180), pGADT7-Cki1 (JD3770), pGADT7-Cki2 (JD3771) and pGADT7-Cki3 (JD3763) and were co-transformed with vector pGBKT7 (JD1170), pGBKT7-Mam2tail (JD3221), pGBKT7-Map3tail (JD3280), pGBKT7-STE2tail (JD3284) and pGBKT7-Rgs1 (JD3182). Transformants were grown to mid-exponential growth phase and spotted onto SD-leu-trp (to confirm the presence of both plasmids) and SD-leu-trp-his-ade plates (to indicate a protein-protein interaction). Negative and positive controls (as indicated) were included to confirm the absence of auto-activation of the GAL4 promoter and positive interactions with the the C-terminal tail of Mam2, respectively.

Strains expressing the Mam2tail with Cki1 and Cki2 did not produce colonies on the SD-leu-trp-his-ade plates (Figure 5.1), suggesting that the C-terminal domain of Mam2 does not interact with either kinase. Colony formation was observed on SD-leu-trp-his-ade plates for strains expressing the Mam2tail with Cki3, indicating a potential interaction between these proteins. However, colonies were also observed on the SD-leu-trp-his-ade plates when Cki3 was expressed with the vector control pGBKT7 (Figure 5.1), suggesting that auto-activation of the GAL4 promoter had occurred and hence, it is unlikely that Cki3 interacts with the Mam2tail. Interestingly, colony formation was observed on the SD-leu-trp-his-ade plates between the kinases and STE2 and Rgs1, suggesting a positive interaction between these proteins (Figure 5.1).

5.2.2 Quantitative yeast 2-hybrid assay

lacZ is one of the reporter genes under the control of the GAL4 promoter. *lacZ* encodes β-galactosidase, production of which can be used to quantify the strength or likelihood of any detected interactions between proteins. The plate-based yeast 2-hybrid assays indicated that the kinases did not interact with Mam2 but did interact with *S. pombe* Rgs1 (Figure 5.1). To verify and quantify the results from the growth plate-based experiment the *S. cerevisiae* strain AH109 was transformed with pGADT7-Rgs1, pGADT7-Cki1, pGADT7-Cki2 and pGADT7-Cki3 and co-transformed with vector pGBKT7, pGBKT7-Mam2tail and pGBKT7-Rgs1, grown to mid-exponential growth phase and assayed for β-galactosidase activity as described in section 2.2.8.2. In agreement with the plate-based yeast 2-hybrid experiment, the β-galactosidase assay did not display a difference in reporter activity between strains expressing either kinase with the vector control or Mam2tail ($p>0.05$ when $n=3$ (where n represents the number of independent experiments performed) when calculating one-way ANOVA) (Figure 5.2a). In contrast, a significant increase in β-galactosidase activity was observed between strains expressing Rgs1 with the vector control pGADT7 (0.2 ± 0.1 *lacZ* units) and Rgs1 with Cki1 (1.9 ± 0.4 *lacZ* units), Rgs1 with Cki2 (2.4 ± 0.4 *lacZ* units) and Rgs1 with Cki3 (2.3 ± 0.3 *lacZ* units) (Cki1: $p = 0.0053$, Cki2: $p=0.0006$, Cki3: $p=0.0008$ when $n=3$, one-way ANOVA) (Figure 5.2b). These results suggested that the kinases did not interact with the C-terminal domain of Mam2, but did interact with Rgs1.

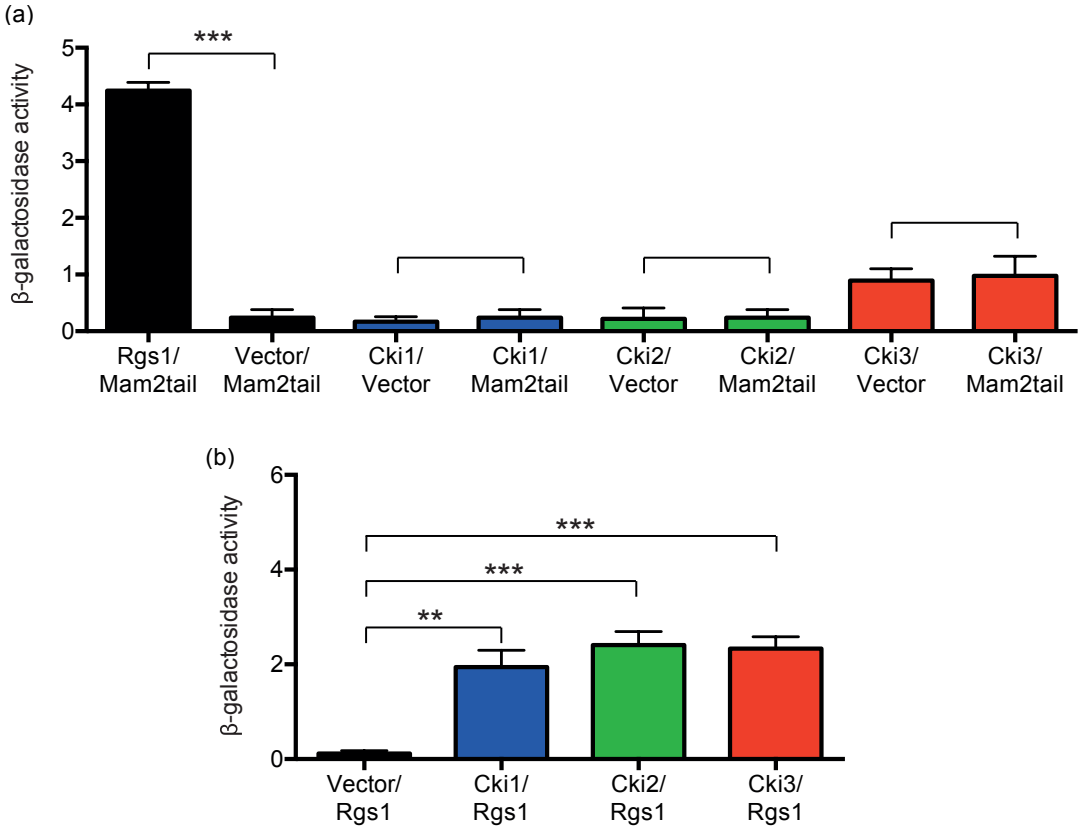

Figure 5.2: **Rgs1 interacts with Cki1, Cki2 and Cki3.** The *S. cerevisiae* strain AH109 was transformed with control pGADT7-Rgs1 (JD3180), pGADT7-Cki1 (JD3770), pGADT7-Cki2 (JD3771) and pGADT7-Cki3 (JD3763) and were co-transformed with vector pGBKT7 (JD1170) and pGBKT7-Mam2tail (JD3221). Transformants were grown to mid-exponential growth phase and a β-galactosidase assay (as described in section 2.2.8.2) was performed. Data shown is the average of three independent experiments ±SEM. Statistical significance was calculated using one-way ANOVA, $*p<0.05$, $**p<0.01$ and $***p<0.001$.

G protein-coupled receptor kinases (GRKs) often phosphorylate ligand-bound GPCRs to initiate the binding of a β-arrestin protein and the subsequent internalisation of the receptor from the plasma membrane (reviewed in [104]). Interestingly, GRKs contain an RGS-like binding domain in their N-terminus and in some instances GRKs have been shown to interact with Gα proteins [132]. An equivalent GRK protein has not yet been identified in *S. pombe* (or any yeast system). As Cki1, Cki2 and Cki3 potentially perform similar roles to GRKs in mammalian cells, it may not be surprising that a positive interaction between these kinases with Rgs1 was observed. However, it should be noted that an RGS-like binding domain has not been identified in Cki1, Cki2 or Cki3.

5.3 Mam2-mCherry could not be utilised to quantify plasma membrane fluorescence

The yeast 2-hybrid assays demonstrated that Cki1, Cki2 and Cki3 did not interact with the C-terminal domain of Mam2. When the C-terminus is transcribed, it would most likely form a conformation that replicates an inactive receptor, as P-factor is not bound promoting the active receptor conformation. If the role of the kinases was to phosphorylate Mam2 in response to P-factor binding, then it is intuitive that if the receptor is in an inactive conformation then the kinases would not interact with Mam2. Therefore, these kinases may still promote Mam2 internalisation in response to P-factor even though an interaction between themselves and the GPCR was not observed.

Some studies, such as in *S. cerevisiae* have quantified GPCR internalisation utilising a radio-labelled ligand [269]. Unfortunately, radio-labelled P-factor was unavailable for this study. The localisation and trafficking of GPCRs can be visualised and also quantified via the addition of a fluorescent protein to the C-terminus of the receptor in combination with confocal microscopy. Previous studies in *S. pombe* have adopted this approach by the addition of a green fluorescent protein (GFP) or mCherry fluorescent protein to the C-terminal tail of Mam2 and have successfully observed the receptor at the plasma membrane and within intracellular vesicles [173, 184]. Therefore, the internalisation of Mam2 was measured in this study by utilising fluorescently labelled Mam2 in combination with cell segmentation software QuimP, which can quantify the cortical fluorescence of individual cells.

5.3.1 Mam2-mCherry was internalised in response to P-factor

The localisation of Mam2 was investigated via the addition of mCherry to the C-terminal domain and expressing this from an inducible plasmid (pREP3x) in combination with confocal microscopy. Visualisation of Mam2 was achieved by utilising an *S. pombe* strain lacking endogenous *mam2* (JY1169; $mam2^{-}$, *sxa2>lacZ*), which was transformed with pREP3x-mCherry (JD3514, pmCh) as a control and pREP3x-Mam2-mCherry (pMam2mCh, JD3590). Strains were grown to mid-exponential growth phase treated with 0 µM and 10 µM P-factor and imaged after 16 h treatment (as described in section 2.2.14).

When untreated Mam2-mCherry was localised in vacuole-like structures within the cell interior (Figure 5.3, red spheres in the cell interior) and at the cell periphery, specifically at

the cell tips (Figure 5.3, arrows). Following treatment with P-factor, cells formed conjugation tubes and Mam2-mCherry was localised within vacuole-like structures in the cytosol, but no longer observed at the cell periphery (Figure 5.3). The lack of visible Mam2-mCherry at the plasma membrane following treatment, suggested the receptor had been internalised (Figure 5.3), in agreement with previous observations [173, 184].

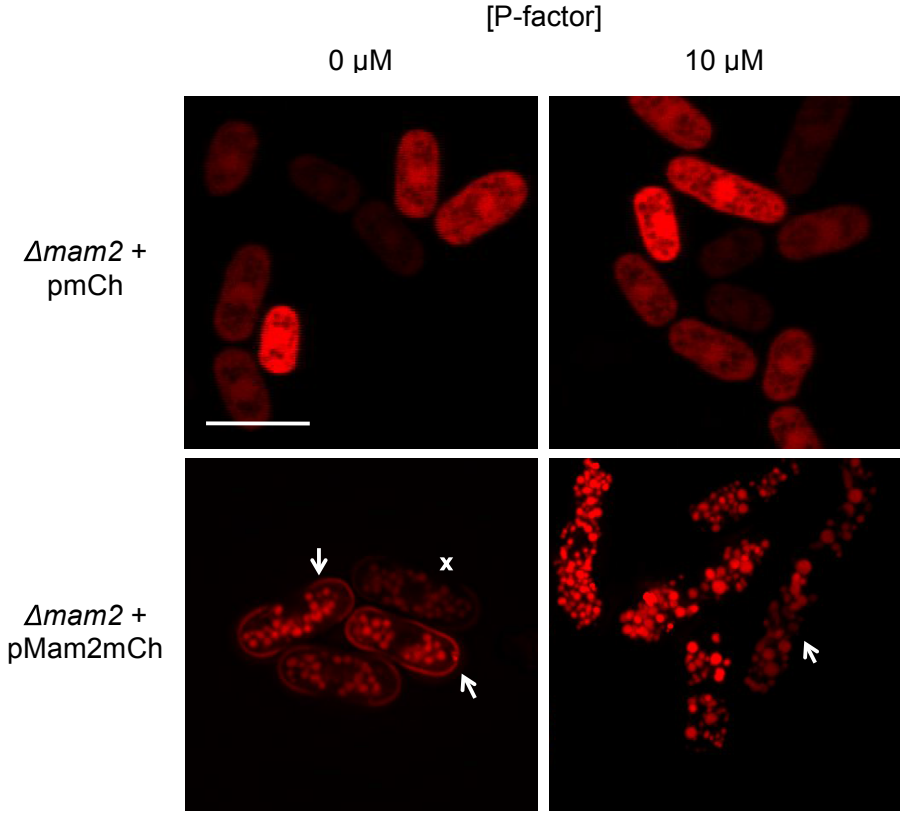

FIGURE 5.3: **Mam2-mCherry is internalised following treatment with P-factor.** *Δmam2* (JY1169) strains were transformed with pREP3x-mCherry (pmCh, JD3514) and pREP3x-Mam2-mCherry (pMam2mCh, JD3590) were grown to mid-exponential growth phase before treatment with a range of P-factor concentrations (from 0 µM to 100 µM). Following 16 h treatment cells were imaged in the mCherry channel (section 2.2.14). Scale bar represents 10 µm. Arrows highlight the receptor is localised to the cell periphery, which we assume is the plasma membrane. The cross highlights that plasma membrane localisation is difficult to identify on some cells.

5.3.2 The mCherry protein did not affect signal transduction via Mam2

The formation of conjugation tubes observed in *S. pombe* strains expressing Mam2-mCherry (Figure 5.3), suggested the addition of the mCherry protein to the C-terminal domain of Mam2 did not hinder signal transduction via the G protein. This was confirmed *in vitro* by performing a β-galactosidase assay. *Δmam2 S. pombe* cells (JY1169) were transformed with

pmCh (JD3514) and pMam2mCh (JD3590) and in addition to the wild type (WT) strain (JY544; *mam2*$^+$, *sxa2>lacZ*) were grown to mid-exponential growth phase, treated with a range of P-factor concentrations (0 µM to 100 µM) for 16 h and assayed for β-galactosidase activity (as described in section 2.2.8.1).

WT strains containing endogenous Mam2 reached a maximum response of 24±1 *lacZ* units (Figure 5.4). Expressing Mam2mCh in *Δmam2* strains from the inducible plasmid pREP3x resulted in a reduction in maximal β-galactosidase activity to 21±1 *lacZ* units (in comparison to WT). However, the reduction in response was not statistically significant (p=0.0779 when n=3, Student's t-test). In addition, no significant change in the potency of P-factor was observed between strains containing endogenous Mam2 and Mam2mCh (Mam2 pEC_{50}: 7.5±0.08 and Mam2mCh pEC_{50}: 7.5±0.13, p=0.7597 when n=3, Student's t-test). Together, the conjugation tube formation observed during the microscopy analysis and similar signalling characteristics exhibited by the β-galactosidase assays suggested that the addition of the mCherry protein to the C-terminal domain of Mam2 did not affect signal transduction via Gpa1 (the G protein) (Figure 5.4).

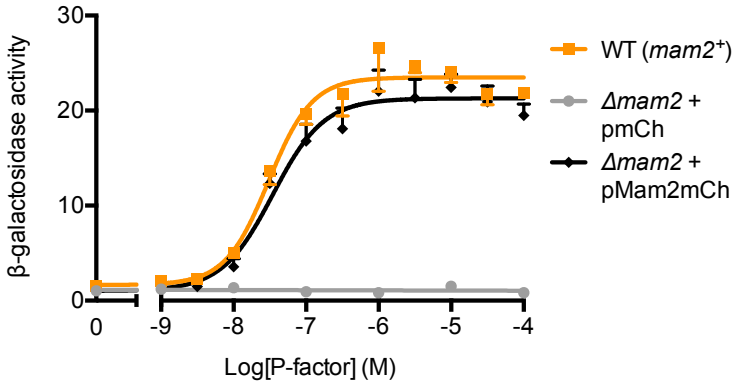

FIGURE 5.4: **Signalling is rescued in *Δmam2* strains expressing Mam2-mCherry.** *Δmam2* (JY1169) strains expressing pmCh (JD3514) and pMam2mCh (JD3590) and the WT strain (JY544, *mam2*$^+$) were grown to mid-exponential growth phase and treated with a range of P-factor concentrations from 0 µM to 100 µM for 16 h before being assayed for β-galactosidase activity (as described in section 2.2.8.1). Data shown is the average of three independent experiments ±SEM.

If Cki1, Cki2 or Cki3 promoted P-factor-induced internalisation of Mam2, then loss of these proteins would retain the receptor at the plasma membrane for longer. To determine whether deletion of the kinases reduces Mam2 internalisation, first **M**-type *S. pombe* strains lacking the endogenous receptor and either Cki1, Cki2 or Cki3 were created (as described in

section 2.3.1). The double knockout strains *Δcki1Δmam2* (JY1727; *sxa2>lacZ*, *Δmam2*, *cki1::ura4*$^+$), *Δcki2Δmam2* (JY1734; *sxa2>lacZ*, *Δmam2*, *cki2::ura4*$^+$) and *Δcki3Δmam2* (JY1720; *sxa2>lacZ*, *Δmam2*, *cki3::ura4*$^+$) had typical cellular morphology and did not respond to P-factor (see Appendix D).

Removing Cki1 and Cki3 from *S. pombe* strains containing endogenous Mam2 exhibited a significant increase in maximal β-galactosidase activity and cell volume following treatment with P-factor (Chapter 4; Figure 4.9 and Figure 4.10, respectively). To verify that these signalling characteristics were maintained with the double-deletion strains expressing Mam2-mCherry, β-galactosidase and cell volume assays were performed. The double deletion strains (*Δcki1Δmam2*, *Δcki2Δmam2* and *Δcki3Δmam2*) and *Δmam2* cells were transformed with pMam2mCh, grown to mid-exponential growth phase, treated with a range of P-factor concentrations (from 0 µM to 100 µM) for 16 h and assayed for β-galactosidase activity and cell volume (as described in section 2.2.8.1 and 2.2.7, respectively).

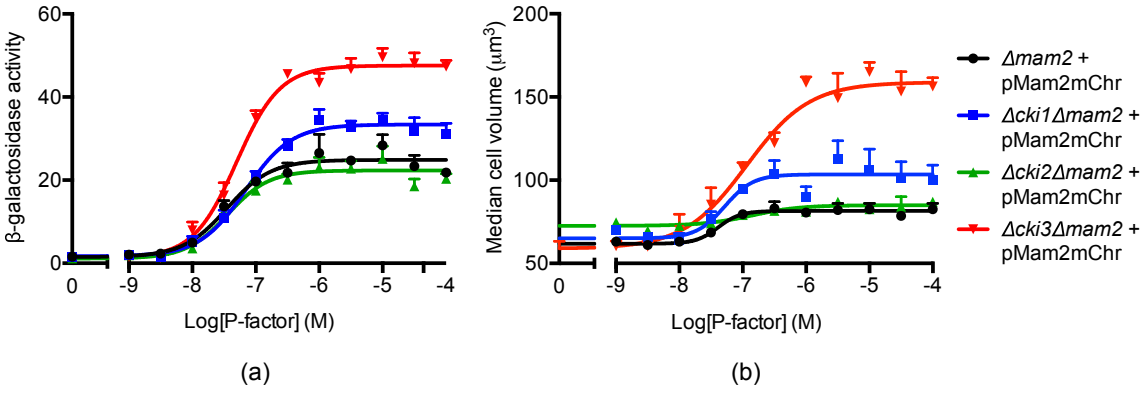

FIGURE 5.5: **The localisation of Mam2-mCherry does not differ in strains lacking Cki1, Cki2 or Cki3.** *Δmam2* (JY1169), *Δcki1Δmam2* (JY1727), *Δcki2Δmam2* (JY1734) and *Δcki3Δmam2* (JY1720) strains expressing pMam2mCh (JD3590) were grown to mid-exponential growth phase and treated with a range of P-factor concentrations from 0 µM to 100 µM for 16 h before being assayed for (a) β-galactosidase activity (section 2.2.8.1) and (b) cell volume (section 2.2.7). Data shown is the average of three independent experiments ±SEM.

Loss of Cki1 and Cki3 in strains expressing Mam2mCh demonstrated a significant increase in β-galactosidase activity, in concert with the previous observations from chapter 4 (Figure 5.5a). Specifically, *Δmam2*+pMam2mCh cells displayed 25±1 *lacZ* units, whereas loss of *cki1* and *cki3* exhibited an increase in maximal response to 33±1 *lacZ* units and 49±2 *lacZ* units, respectively (*Δcki1*: p=0.0048 and *Δcki3*: p=0.0004 when

n=3, Student's t-test) (Figure 5.5a). In addition, *Δcki1Δmam2* and *Δcki3Δmam2* strains expressing Mam2mCh demonstrated a significant increase in maximal cell volume (Figure 5.5b). *cki1*$^{+}$,*cki3*$^{+}$ cells displayed a cell volume of 82±1 µm^3, whereas loss of *cki1* and *cki3* demonstrated an increase in cell volume of 103±3 µm^3 and 159±5 µm^3, respectively (*Δcki1*: p=0.0027 and *Δcki3*: p=0.0001 when n=3, Student's t-test) (Figure 5.5b).

These data illustrate that the signalling characteristics were maintained between strains containing endogenous Mam2 and strains expressing Mam2-mCherry when the kinase ORF's were disrupted (compare Figure 4.9 and Figure 4.10 with Figure 5.5). Therefore, Mam2mCh was utilised to quantify how deletion of Cki1, Cki2 and Cki3 affect plasma membrane localisation of Mam2 in response to P-factor treatment.

5.3.3 Insufficient Mam2 localisation at the plasma membrane

To quantify plasma membrane fluorescence using Mam2-mCherry its expression at the plasma membrane was required to be sufficient enough for the QuimP software to segment the cell periphery. Unfortunately, cells expressing Mam2mCh often did not show a strong association with the cell membrane (as seen in figure 5.3, the cross illustrates a cell with poor receptor membrane expression) and therefore, for many cells the QuimP software was unable to segment the cell perimeter and hence, quantify cortical fluorescence (see Figure 5.6 for an example). The images displayed in Figure 5.6 were achieved using *Δmam2 S. pombe* cells transformed with pMam2mCh, grown to mid-exponential growth phase, treated with 10 µM P-factor for 8 h and imaged every 2 h from 0 h to 8 h (as detailed in section 2.2.14). The fluorescent images were loaded into the QuimP software and an individual cell was selected at random and segmented.

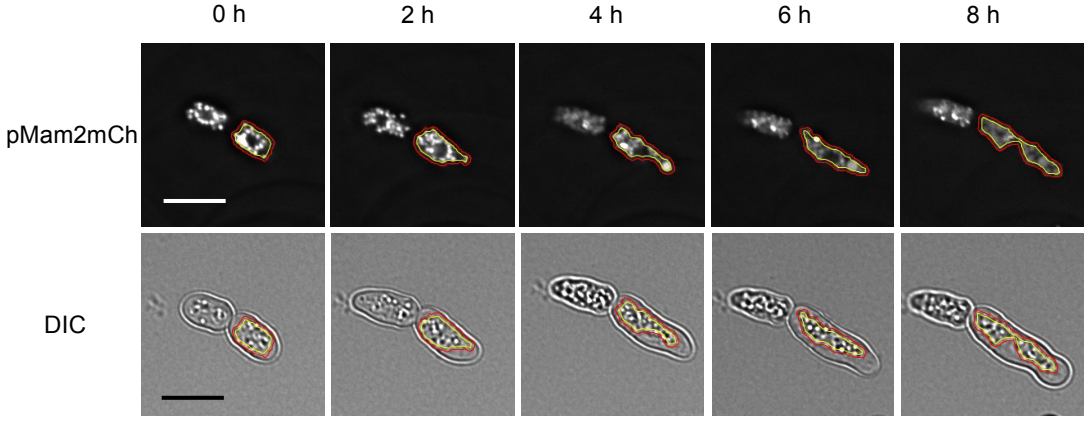

Figure 5.6: **Mam2 tagged mCherry did not localise to the plasma membrane enough for QuimP to segment the cell periphery.** *Δmam2* (JY1169) strains expressing pMam2mCh (JD3590) were grown to mid-exponential growth phase before treatment with 10 µM P-factor for 8 h. Cells were then imaged every 2 h from 0 h to 8 h in the mCherry and differential interference contrast (DIC) channel (or bright field) (as detailed in section 2.2.14). The fluorescent images were loaded into QuimP to segment and measure the plasma membrane fluorescence over time(highlighted by the outer red and inner yellow contours). The DIC channel was shown to illustrate that the software was unable to identify the cell periphery. Scale bar represents 10 µm.

5.4 Characterising the C-terminal domain of Mam2

5.4.1 The C-terminal domain of Mam2 is essential for internalisation

Mam2-mCherry did not associate strongly with the plasma membrane and thus, the QuimP software could not segment the cell periphery. A previous study showed that removing the last 45-residues of Mam2 (as shown in Figure 5.7a) increased receptor plasma membrane concentration [173]. Therefore, *Δmam2* (JY1169) cells expressing pREP3x-Mam2Δtail-

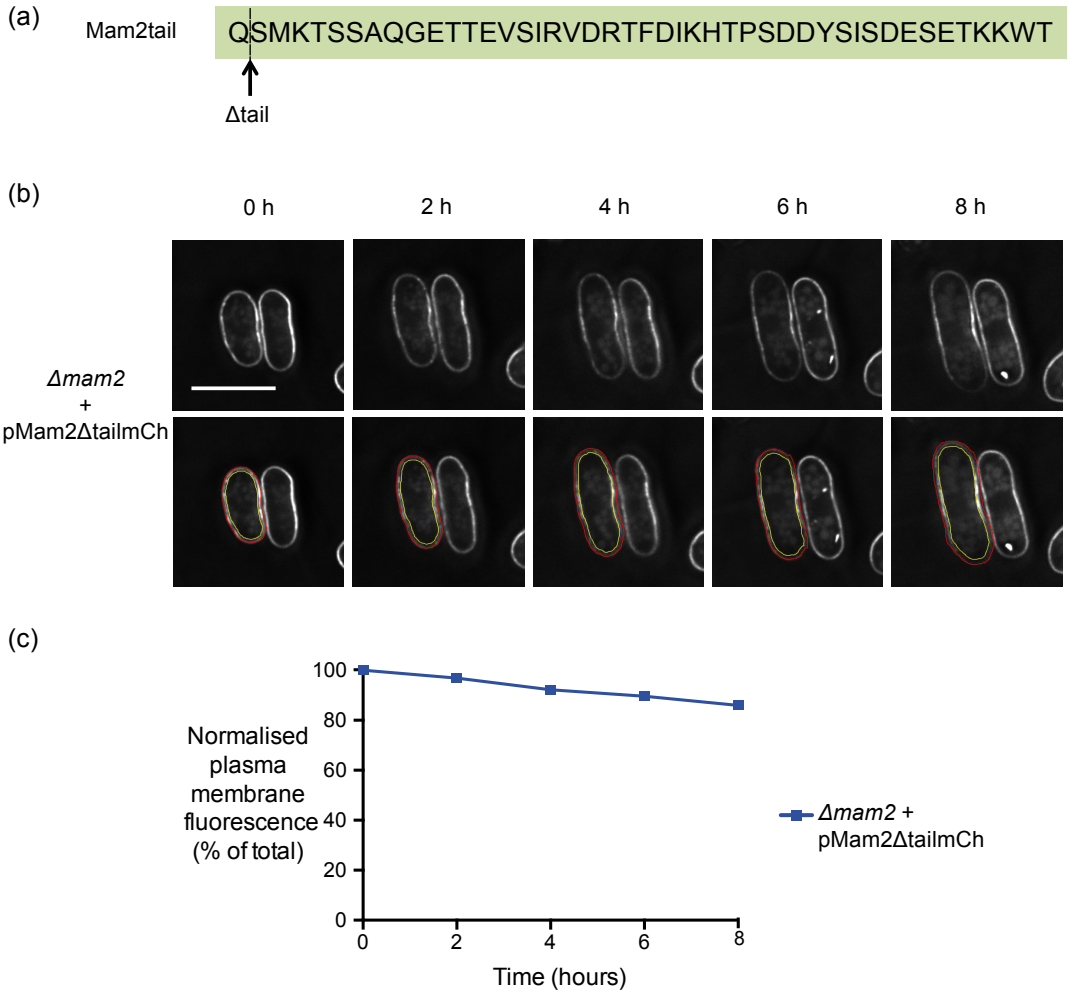

Figure 5.7: **QuimP is able to identify Mam2ΔtailmCh at the plasma membrane.** (a) A schematic representation of of the last 45 amino-acid residues of Mam2, highlighting the truncation point directly downstream of the glutamine (Q) residue used to create pREP3x-Mam2Δtail-mCherry (pMam2ΔtailmCh, JD3621). (b) *Δmam2* (JY1169) cells transformed with pMam2ΔtailmCh were grown to mid-exponential growth phase before treatment with 10 µM P-factor for 8 h. Cells were imaged every 15 min from 0 h to 8 h in the mCherry channel (as described in section 2.2.14). (c) The fluorescent images were loaded into QuimP to segment and measure the plasma membrane fluorescence of individual cells (highlighted by the outer red and inner yellow contours). Scale bar represents 10 µm.

mCherry, which had the last 45-residues removed (Mam2ΔtailmCh, JD3621) were grown to mid-exponential growth phase, treated with 10 µM P-factor and imaged every 15 min from 0 h to 8 h (as described in section 2.2.14). The resulting images were loaded into QuimP to determine whether the concentration of Mam2ΔtailmCh at the plasma membrane was sufficient to segment the cell periphery and hence, quantify cortical fluorescence.

Removing the last 45-residues of Mam2 resulted in a uniform localisation of the receptor at the plasma membrane (Figure 5.7b). As a result, the QuimP software was able to segment the cell periphery and quantify plasma membrane fluorescence over time (Figure 5.7b-c). However, loss of the C-terminal domain prevented both constitutive and ligand-induced internalisation (Figure 5.7b, this can be seen clearly in Figure 5.8a where cells had been treated with P-factor for 16 h, as the receptor was not observed in the vacuole-like structures). Although a reduction in plasma membrane fluorescence was observed between 0 h and 8 h (from 54 % to 47 %) for the cell highlighted in Figure 5.7b, this reduction was most likely the result of continued light exposure during the time-lapse experiment, which causing photobleaching of the fluorescent molecule and hence, a reduction in signal (Figure 5.7c).

Strains expressing Mam2ΔtailmCh did form conjugation tubes in response to P-factor (Figure 5.8). This morphological response (conjugation tube formation) indicated that the C-terminal domain of Mam2 was not essential for signal transduction via the G protein. β-galactosidase assays confirmed the C-terminal tail of Mam2 was not essential for G protein activation. However, it was required for maximal WT (*mam2*$^+$) signalling response (Figure 5.8b). Maximal response was significantly reduced in cells expressing Mam2ΔtailmCh in comparison to strains transformed with pMam2mCh (reduction from 20±0.5 *lacZ* units to 8±1 *lacZ* units , p=0.0001 when n=3, Student's t-test). In addition to the reduction in response, a significant shift in pEC_{50} from Mam2mCh at 6.4±0.1 to Mam2ΔtailmCh at 8±0.2 was observed (p=0.0028 when n=3, Student's t-test).

It has been shown that the C-terminal domain of Mam2 acts as a scaffold for Rgs1 [173]. When the tail is absent Rgs1 is not localised to the plasma membrane and hence, is unable to hydrolyse GTP-bound Gpa1 (a G protein), which is required for a maximal signalling response. The data collected in this section (5.4.1) are in agreement with previous observations [173].

Although removing the C-terminal domain of Mam2 increased plasma membrane localisation such that the QuimP software could segment and quantify cortical fluorescence, the

signalling behaviour was significantly altered and receptor internalisation was prevented (Figure 5.8). Therefore, Mam2ΔtailmCh was not an appropriate receptor to quantify the internalisation of Mam2 in strains lacking Cki1, Cki2 and Cki3. The generation of a receptor that when expressed in untreated cells resembled that of Mam2ΔtailmCh, but internalised and signalled like full length Mam2 would provide a system to enable the quantification of how loss of the kinases affects receptor internalisation.

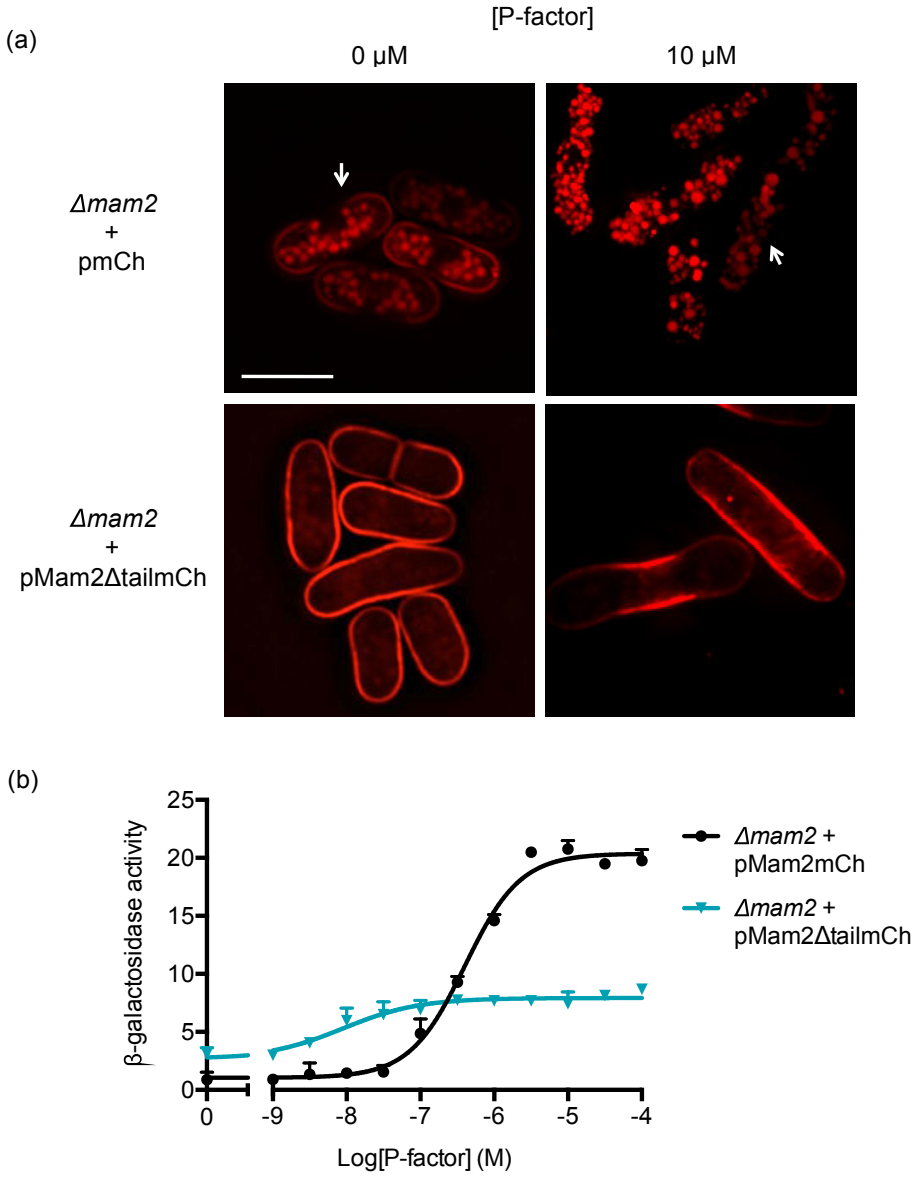

FIGURE 5.8: **The C-terminal tail of Mam2 is essential for internalisation and maximal signalling.** *Δmam2* (JY1169) strains transformed with pMam2mCh (JD3590) and pMam2ΔtailmCh were grown to mid-exponential growth phase before treatment with a range of P-factor concentrations (from 0 µM to 100 µM). Following 16 h (a) cells treated with 0 µM and 10 µM P-factor were imaged in the mCherry channel (as detailed in section 2.2.14) and (b) cells were assayed for β-galactosidase (as described in section 2.2.8.1). Scale bar represents 10 µm. Data shown is the average of three independent experiments ±SEM.

5.4.2 Truncating Mam2 affects receptor localisation and sorting

Truncating the C-terminal tail of Mam2 highlighted that residues within the 45-residue sequence where essential for internalisation and trafficking of the receptor to the vacuoles (Figure 5.8). A previous study suggested that removal of an 8-residue sequence (YSISDESE) from the C-terminal tail of Mam2 increased plasma membrane localisation in untreated cells, yet maintained a maximal signalling response following treatment with P-factor [173]. However, the microscopy images used to make these conclusions were of low-resolution and the localisation and sorting of the receptors in response to treatment with P-factor was not analysed (E. McCann, PhD thesis, 2010).

The localisation and internalisation of Mam2 can now be investigated in greater detail with the aid of higher-resolution microscopy. The sorting of the receptor to the vacuole can be assessed using a lipophilic styryl vacuole dye FM4-64, which binds the plasma membrane of living cells and is endocytosed and trafficked to the vacuole, thereby highlighting the vacuola membranes [283]. FM4-64 is a red fluorescent dye (excitation/emission maxima ~515/640 nm), which can be visualised in the mCherry channel of a DeltaVision system wide-field deconvolution microscope. Therefore, a different coloured fluorescent dye other than mCherry was required for visualising the receptor to co-visualise the receptor with the vacuole dye. A number of truncated versions of Mam2-GFP had previously been created by E. McCann in the inducible plasmid pREP3x and hence, were used to assess the localisation and sorting of the receptors with the vacuole dye (see Figure 5.9 for a list of receptors used in this section).

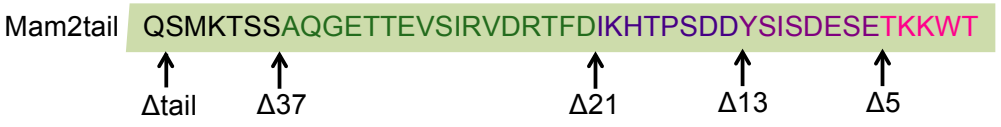

Figure 5.9: **Sequential truncations of the C-terminal tail of Mam2.** Schematic representation of the last 45-amino acid residues of Mam2. The diagram highlights the sequential truncations of Mam2. The resulting DNA fragments were cloned into pREP3x-GFP (pGFP, JD2261) to create pREP3x-Mam2Δ5-GFP (pMam2Δ5GFP, JD2999), pREP3x-Mam2Δ13-GFP (pMam2Δ13GFP, JD3001), pREP3x-Mam2Δ21-GFP (pMam2Δ21GFP, JD3003), pREP3x-Mam2Δ37-GFP (pMam2Δ37GFP, JD3007) and pREP3x-Mam2Δtail-GFP (pMam2ΔGFP, JD3317) (E. McCann, PhD thesis, 2010).

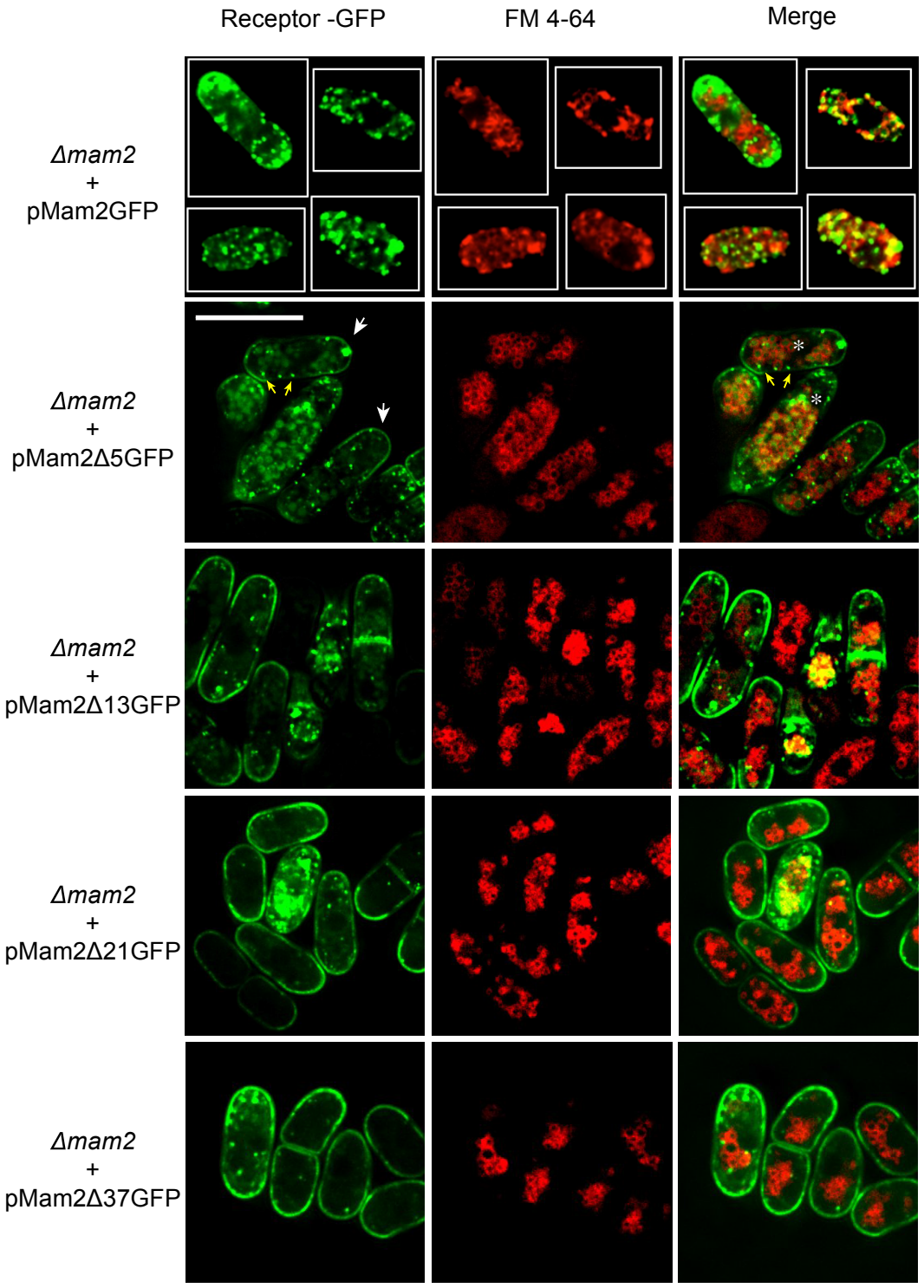

Figure 5.10: **The last 13 residues of Mam2 are essential for constitutive internalisation into the vacuoles.** *Δmam2* strain (JY1169) expressing pMam2GFP (JD2885), pMam2Δ5GFP (JD2999), pMam2Δ13GFP (JD3001), pMam2Δ21GFP (JD3003) and pMam2Δ37GFP (JD3007) were grown to mid-exponential growth phase containing 50 µM of FM 4-64 vacuole staining protein for 16 h [283]. Cells were then imaged in the mCherry and GFP channel as described in section 2.2.14 and the middle 8 stacks were maximally projected to show the cross section of each cell (include vacuole cross section). White arrows highlight the receptor on the plasma membrane, asterisk's indicate cells, which display receptor within the vacuoles and yellow arrows highlight endosomal structures. Composite images were collated into one image for visualisation (marked with a white boarder). Scale bar represents 10 µm.

The *Δmam2 S. pombe* strain JY1169 was transformed with pREP3x-Mam2-GFP (pMam2GFP, JD2885) and those receptors described in Figure 5.9 (each of which contained one GFP molecule at their C-terminus). These strains were grown to mid-exponential growth phase in minimal medium containing 50 µM FM4-64 (vacuole staining protein) for 16 h and imaged as described in section 2.2.14. A previous study illustrated that following growth of *S. pombe* to ~5x10^6 cells/ml and treatment with 50 µM FM4-64 for 1 h was sufficient to identify the vacuola membranes [283]. Therefore, growth with the FM4-64 dye for 16 h was assumed to identify vacuoles (Figure 5.10, FM4-64 panel).

Full length Mam2 (Mam2GFP) and Mam*Δ*5GFP was observed at the plasma membrane, but predominantly within spherical structures in the cell interior (Figure 5.10, arrows). The merged images displayed some green spheres confined by a ring of red FM4-64 staining (Figure 5.10, shown by asterisk's), suggesting that these receptors were contained within the vacuoles. Additional green spherical structures are also observed, but were not encased by FM4-64 staining (Figure 5.10, yellow arrows).

Mam2*Δ*13GFP was visible at the plasma membrane, predominantly at the cell tips and within internal structures in the cytosol (Figure 5.10). The merged image did not show Mam2*Δ*13GFP encased by the red vacuole dye (in comparison to Mam2*Δ*5GFP), suggesting that the last 13-residues of Mam2 were required for receptor sorting to the vacuoles.

Strains expressing Mam2*Δ*21GFP and Mam2*Δ*37GFP exhibited the receptor uniformly distributed at cell perimeter (Figure 5.10), rather than just the cell tips (in comparison to the Mam2*Δ*13GFP receptor). The merged images did not demonstrate any receptors within vacuoles and fewer receptors were observed within internal structures. Truncating the last 21 and 37 residues of Mam2 appeared to increase plasma membrane concentration of the receptor and reduce receptor internalisation.

To investigate the localisation and trafficking of the receptors in response to P-factor, *Δmam2* (JY1169) strains transformed with pMam2GFP, pMam2*Δ*5GFP, pMam2*Δ*13GFP, pMam2*Δ*21GFP and pMam2*Δ*37GFP were grown to mid-exponential growth phase containing 50 µM FM4-64 (vacuole staining protein), treated with a 10 µM P-factor and imaged following 16 h (as detailed in section 2.2.14). The sequential truncations of Mam2 appeared to reduce conjugation tube elongation (Figure 5.11), highlighting that the receptor tail is required for a WT response [173]. This is most likely the result of the predicted Rgs1 binding domain contained within the 16 residue sequence between Mam2*Δ*5GFP

and Mam2Δ21GFP, as Rgs1 interacts with the C-terminal domain stabilising its plasma membrane localisation and G protein hydrolysis [173].

Mam2GFP was not visible at the plasma membrane following treatment with P-factor, instead the receptor was displayed within two types of intracellular spherical structures within the cytosol. One of the spherical structures was encased by the FM4-64 staining (Figure 5.11, merge), suggesting that Mam2 had been internalised and trafficked to the vacuoles. The other structures were not encased by FM4-64 but resided near the cell periphery. Removing the last 5-residues of Mam2 increased plasma membrane localisation as the receptor was observed at the cell periphery following treatment with P-factor in comparison to Mam2GFP (Figure 5.11). Similarly to Mam2GFP, Mam2Δ5GFP was internalised into the cell interior, displaying green spheres encased by FM4-64 staining (vacuoles) and smaller spherical vesicles not encased by the vacuola staining (Figure 5.11, merged).

Removing the last 13 and 21 residues of Mam2 did not increase plasma membrane localisation and these receptors were observed in intracellular compartments that were not vacuoles, as they were not encased by FM4-64 staining (Figure 5.11, merged). Strains expressing Mam2Δ37GFP displayed the receptor predominantly in large intracellular structures positioned near the cell tips and in some cells at the plasma membrane (Figure 5.11). Loss of the 37-residues of Mam2 prevented receptor sorting to the vacuole however, small intracellular structures not encased by FM4-64 were observed near the cell periphery.

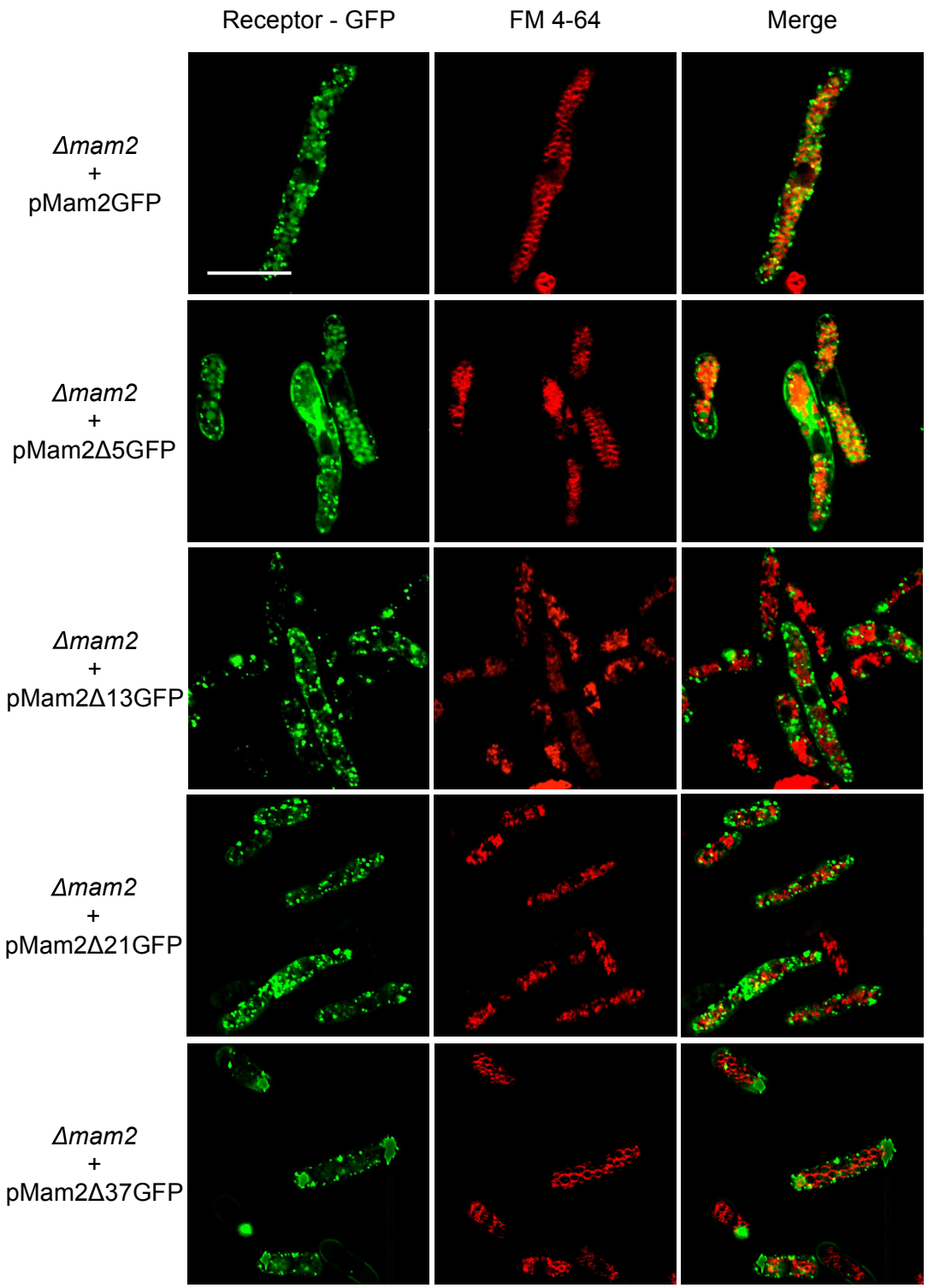

Figure 5.11: **The last 13 residues of Mam2 are essential for trafficking to the vacuoles following endocytosis.** *Δmam2* strain (JY1169) expressing pMam2GFP (JD2885), pMam2Δ5GFP (JD2999), pMam2Δ13GFP (JD3001), pMam2Δ21GFP (JD3003) and pMam2Δ37GFP (JD3007) were grown to mid-exponential growth phase containing 50 µM of FM 4-64 vacuole staining protein before treatment with 10 µM P-factor. After 16 h cells were then imaged in the mCherry and GFP channel as described in section 2.2.14 and the middle 8 stacks were maximally projected to show a cross section of the cell (to include vacuole cross section). Scale bar represents 10 µm.

5.4.3 Truncating Mam2 alters signal transduction in response to P-factor

Mam2Δ21 was uniformly distributed at the cell periphery in untreated cells, yet internalised in response to P-factor (section 5.4.2). Hence, in terms of quantifying plasma membrane fluorescence using QuimP, Mam2Δ21GFP appeared to be an ideal receptor for assessing how loss of Cki1, Cki2 and Cki3 in *S. pombe* strains affects receptor internalisation.

Deleting the last 45-residues of Mam2 reduces maximal signalling response and increases the potency of P-factor (Figure 5.8b). To assess which regions of the tail are essential for a WT (full length Mam2) P-factor-directed transcriptional response and to specifically determine how loss of the 21-residues from the C-terminus of Mam2 changes the signalling characteristics, β-galactosidase assays were performed with the truncated versions of Mam2. *Δmam2* (JY1169; *mam2⁻*, *sxa2>lacZ*) *S. pombe* cells were transformed with pGFP, pMam2GFP, pMam2Δ5GFP, pMam2Δ13GFP, pMam2Δ21GFP and pMam2Δ37GFP, grown to mid-exponential growth phase, treated with a range of P-factor concentrations (from 0 µM to 10 µM P-factor) and assayed for β-galactosidase activity after 16 h (as described in section 2.2.8.1).

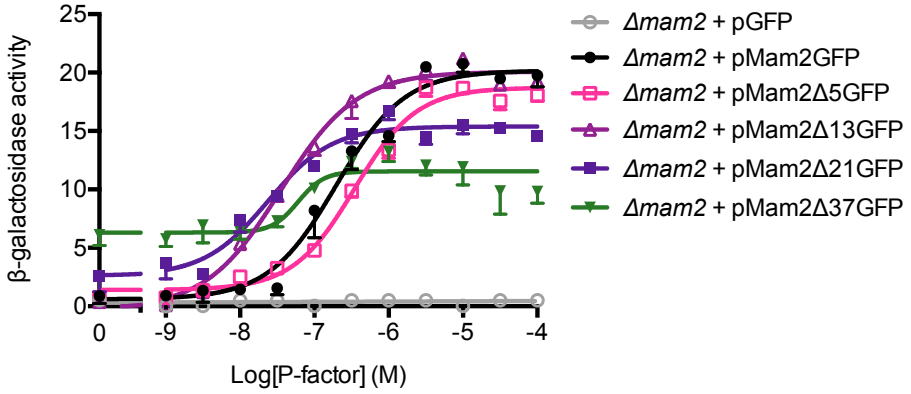

FIGURE 5.12: **Truncating Mam2 caused an increased basal and reduced maximal response following P-factor treatment.** *Δmam2* cells (JY1169) were transformed with pGFP (JD2261), pMam2GFP (JD2885), pMam2Δ5GFP (JD2999), pMam2Δ13GFP (JD3001), pMam2Δ21GFP (JD3003) and pMam2Δ37GFP (JD3007) were grown to mid-exponential growth phase before treated with a range of P-factor concentrations from 0 µM - 100 µM. Following 16 h cells were assayed for β-galactosidase activity (as detailed in section 2.2.8.1). Data shown is the average of three independent experiments ±SEM.

Truncation of the last 5 or 13 residues of Mam2 did not significantly alter the maximal or basal transcriptional signalling responses (Figure 5.12) ($p>0.05$, Student's t-test). However, Mam2Δ13GFP was significantly more potent to P-factor, displaying an increase in

pEC_{50} from 6.8±0.1 to 7.5±0.1, in comparison to full length Mam2 (p=0.0029 when n=3, Student's t-test). Truncating 21 and 37 residues from the C-terminal domain of Mam2 demonstrated an increase in potency of P-factor and basal β-galactosidase activity and a reduction in maximal response (Figure 5.12). Specifically, Mam2Δ21GFP displayed a significant reduction from 20±1 *lacZ* units to at 15±1 *lacZ* units in comparison to full length Mam2 (p=0.0241 when n=3, Student's t-test).

The receptor Mam2Δ13GFP reached the same maximal signalling level as full length Mam2 in response to P-factor (Figure 5.12). However, the receptor did not localise uniformly at the membrane during vegetative growth (only at the tips) (Figure 5.10). In contrast, the receptor Mam2Δ21GFP did localise uniformly at the cell periphery when untreated and would therefore be suitable for segmentation using QuimP (Figure 5.10) but a significant reduction in maximal signalling response was exhibited (Figure 5.12). Together, these data suggest that neither Mam2Δ13GFP or Mam2Δ21GFP are appropriate receptors to access how loss of Cki1, Cki2 and Cki3 affects internalisation of Mam2.

5.5 Characterisation of the lysine deficient C-terminal domain of Mam2

Monoubiquitination of a single lysine residue within the SINNDAKSS sequence of the C-terminal domain of *S. cerevisiae* STE2 is essential for both constitutive and ligand-induced internalisation [174, 284]. However, the investigation of many mammalian GPCRs has revealed that ubiquitination is not required for ligand-induced endocytosis. Some examples are the chemokine CXCR4, β_2AR, DOR and neurokinin (NK1R) receptors [159, 285–288].

Arginine scanning of lysine residues in the *S. cerevisiae* STE3 C-terminal domain prevents ubiquitination-dependent constitutive internalisation of the GPCR, resulting in an increase in plasma membrane concentration, yet the receptor remains sensitive to ligand-induced internalisation [289]. This mechanism of arginine scanning was exploited in order to increase the plasma membrane concentration of Mam2 without altering the ligand-induced internalisation characteristics of the receptor, allowing the QuimP software to successfully segment the cell periphery.

Mam2 contains 4 lysine residues at positions 307, 329, 345 and 346 relative to the ATG (position 1) codon (Figure 5.13). The two latter lysines (345 and 346) are contained within the last 5-residues of Mam2, with truncation of these residues exhibiting no defects in

receptor localisation when compared to full length Mam2 (Figure 5.10 and 5.11). Two potential ubiquitination deficient mCherry tagged receptors were created in plasmids for the expression of proteins under the control of the *nmt1* promoter of pREP3x [235] (for details see section 2.3.2.3 and 2.3.2.4): pREP3x-Mam2^{2K}-mCherry (pMam2^{2K}mCh, JD3802) contains a version of Mam2 with the lysine residues at position 345 and 346 (situated in the last 5-residues) remaining intact but the other lysine residues mutated to arginine and pREP3x-Mam2^{4K}-mCherry (pMam2^{4K}mCh, JD3804) contains a receptor with all four lysine residues either mutated to arginine of deleted (Figure 5.13).

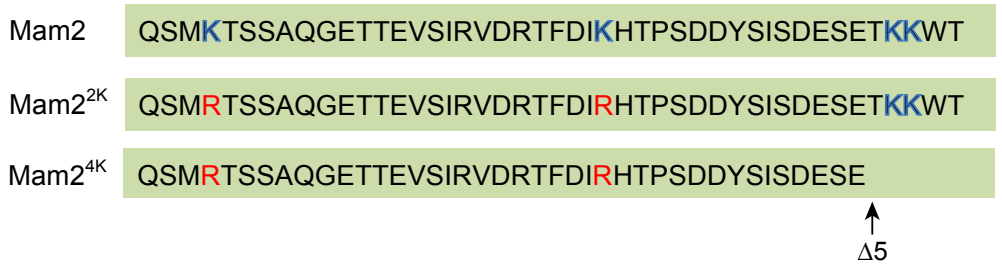

Figure 5.13: **Schematic illustration of the lysine mutations of Mam2.** Schematic representation of the last 45-amino acid residues of Mam2 (Mam2), pREP3x-Mam2^{2K}-mCherry (Mam2^{2K}, JD3802) minus the mCherry tag and pREP3x-Mam2^{4K}-mCherry (Mam2^{4K}, JD3804) minus the mCherry tag. The diagram highlights the lysine (K) residues in blue and the mutation of the lysine to arginine (R) in red. For details on how these Mam2 mutations were created see section 2.3.2.3 and 2.3.2.4.

5.5.1 Mutating the lysine residues of Mam2 does not affect mating in *S. pombe*

Previous studies in *S. pombe* has shown that truncating regions of the C-terminal domain of Mam2 and point mutations within other proteins such as Ras1, can affect the cells' ability to mate ([173]; M. Bond, PhD thesis, 2012). Therefore, mating was assessed for cells expressing the receptors Mam2^{2K}mCh and Mam2^{4K}mCh to verify that mutation of the lysine residues did not affect the cells' ability to mate. *mam2*$^{-}$, *sxa2*$^{+}$ *S. pombe* **M**-type cells (JY1353) were transformed with pmCh, pMam2mCh and pMam2ΔtailmCh as controls for pMam2^{2K}mCh and pMam2^{4K}mCh. In addition, the strain JY1353 was transformed with pREP3x-GFP (pGFP, JD2261), pMam2GFP and pMam2Δ5GFP plasmids for comparison. Strains were mixed with mating-type stable **P**-cells (JY1025: *sxa2*$^{+}$), grown to mid-exponential growth phase and mating was assessed via an iodine staining assay (as described in section 2.2.11.1).

The assay utilises the property that iodine binds the starch within the ascospore cell wall and therefore the production of a brown/black colony colouration indicates a successful

mating event [220]. Cells expressing Mam2mCh, Mam2^{2K}mCh, Mam2^{4K}mCh, Mam2GFP and Mam2Δ5GFP displayed a qualitative difference in colour intensity between the unmated and mated cells (Figure 5.14a), suggesting that strains expressing these receptors were able to mate.

Following these qualitative results, the same strains were assayed for ascospore production by measuring the percentage of colony forming units (CFU) or spore formation after a heat shock step at 50°C for 10 minutes (as detailed in section 2.2.11.2). This quantitative assay utilises the heat resistant property of the spores. A significant difference in CFU recovery was not observed between strains expressing Mam2mCh (35±8%) and Mam2^{2K}mCh (33±4%) or Mam2^{4K}mCh (35±7%) (Figure 5.14b). These data indicate that mating is not affected by the removal or mutation of lysine residues in the C-terminal domain of Mam2 ($p>0.05$, one-way ANOVA) and therefore, further analysis with these receptors could be performed.

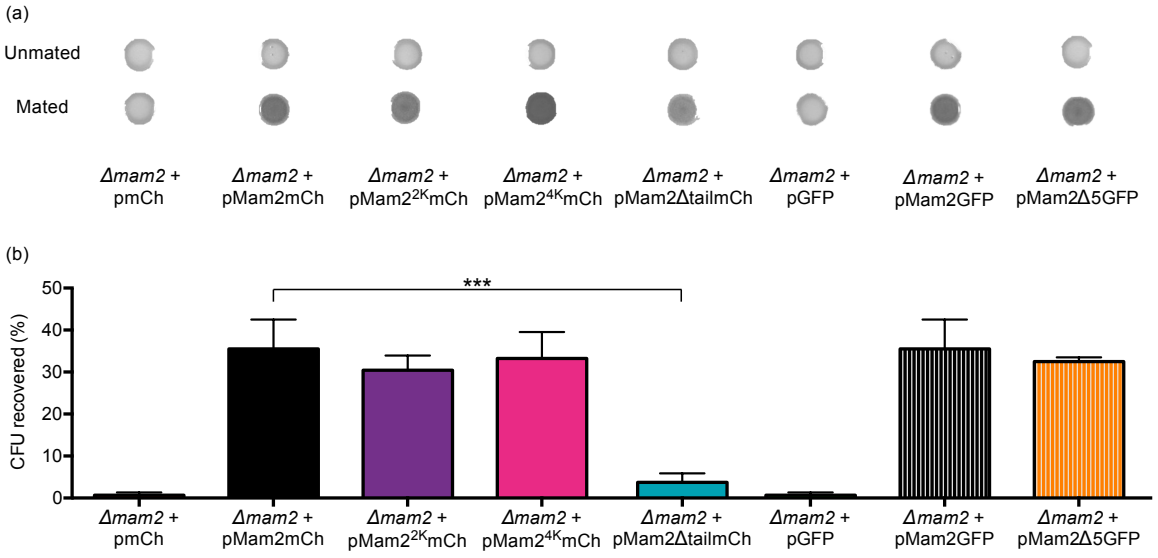

FIGURE 5.14: **CFU recovery is unaffected when removing lysine residues from Mam2.** *mam2⁻ sxa2⁺ S. pombe* **M**-cells (JY1353) were transformed with pmCh (JD3514), pMam2mCh (JD3590), pMam2^{2K}mCh (JD3802), pMam2^{4K}mCh (JD3804), pMam2ΔtailmCh (JD3621), pGFP (JD2261), pMam2GFP (JD2885), pMam2Δ5GFP (JD2999) and mixed with mating-type stable **P**-cells (JY1025: *Δsxa2*). These strains were then grown to mid-exponential growth phase in minimal medium and mating was assessed using an (a) iodine staining assay (brown/black yeast colonies are formed when mating is successful) as described in section 2.2.11.1 and a (b) quantitative sporulation assay, which measures the percentage of colony forming units (CFUs) / spore formation following 10 minutes of heat inactivation at 50°C (for details see section 2.2.11.2). Data shown is the average of three independent experiments ±SEM. Statistical significance was calculated using one-way ANOVA, $*p<0.05$, $**p<0.01$ and $***p<0.001$.

5.5.2 Constitutive internalisation of Mam2 is prevented upon removal of all four lysine residues from its C-terminus

As the lysine deficient receptors did not affected the ability of *S. pombe* cells to mate (Figure 5.14), the localisation of these receptors was investigated. The strain JY1169 (*mam2*$^{-}$, *sxa2>lacZ*) was transformed with the lysine deficient receptors pMam2^{2K}mCh, pMam2^{4K}mCh and pMam2mCh and pMam2ΔtailmCh as controls. Cells were grown to mid-exponential growth phase, treated with 0 µM and 10 µM P-factor and imaged following 16 h of treatment (as described in section 2.2.14).

When untreated Mam2^{2K}mCh was localised uniformly at the plasma membrane, yet was still observed in vacuole-like structures in the cytosol (Figure 5.15). Cells expressing Mam2^{2K}mCh responded to P-factor as conjugation tubes were observed (Figure 5.15). Following treatment, the receptor was localised within intracellular compartments in the cytosol and was not observed at the plasma membrane (Figure 5.15).

Mam2^{4K}mCh was distributed uniformly at the plasma membrane, but was not observed within intracellular compartments in the cytosol, similar to removing the entire C-terminus (Mam2ΔtailmCh) (Figure 5.15). In contrast to Mam2ΔtailmCh P-factor treated receptor, which was localised at plasma membrane only, Mam2^{4K}mCh was observed at the plasma membrane but also within intracellular compartments in the cytosol (Figure 5.15). Cells expressing Mam2^{4K}mCh also formed conjugation tubes in response to treatment.

These microscopy analyses suggest that ligand-induced internalisation of Mam2 is not dependent on ubiquitination. The receptor was internalised and observed in vacuole-like structures in the cytosol when removing of all four lysine residues and thus, sites of ubiquitination in the C-terminal domain of Mam2. The analysis also suggested that removing two lysine residues from the C-terminus of Mam2 (Mam2^{2K}mCh) increased receptor plasma membrane concentration (as the receptor was localised around the cell perimeter). Additional loss of all four lysine residues appeared to enhance receptor membrane association even further (observed by a greater intensity of cortical fluorescence). Quantification of plasma membrane fluorescence using QuimP confirmed that removing the lysine residues from Mam2 increased plasma membrane fluorescence. *Δmam2 S. pombe* (JY1169; *mam2*$^{-}$, *sxa2>lacZ*) strains expressing mCh, Mam2mCh, Mam2^{2K}mCh, Mam2^{4K}mCh and Mam2ΔtailmCh (Figure 5.16). Strains were grown to mid-exponential growth phase imaged and QuimP was used to determine cortical fluorescence (as detailed in section 2.2.14 and 2.2.18, respectively).

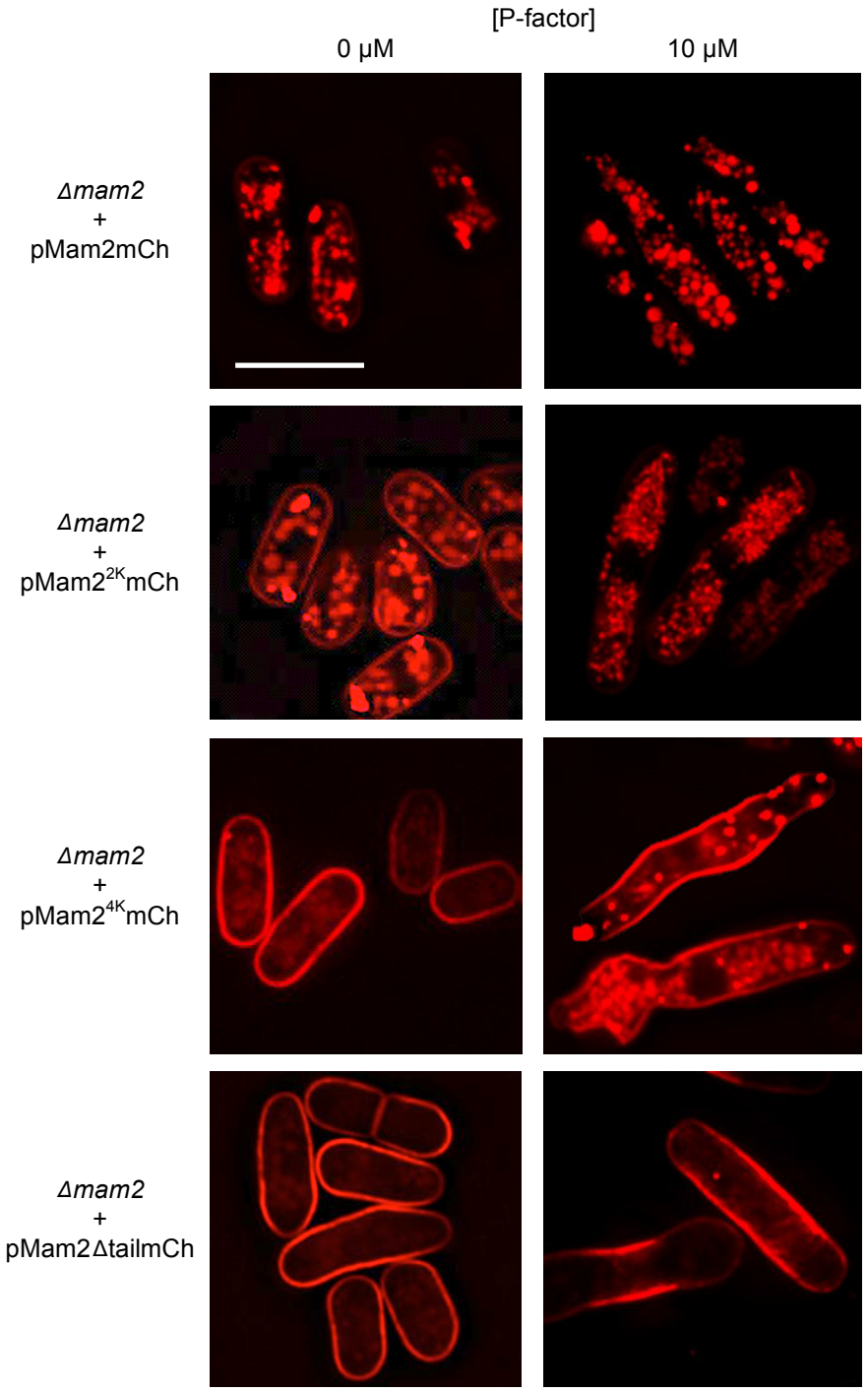

Figure 5.15: **Mam2^{4K}mCh is visible at the plasma membrane following P-factor treatment.** *Δmam2* (JY1169) strains were transformed with pMam2mCh (JD3590), pMam2^{2K}mCh (JD3802), pMam2^{4K}mCh (JD3804) and pMam2ΔtailmCh (JD3621) were grown to mid-exponential growth phase and treated with 0 µM and 10 µM P-factor and imaged in the mCherry channel as described in section 2.2.14. Scale bar represents 10 µm. The videos 3.1 and 3.2 demonstrate that the receptor Mam2^{4K}mCh was internalised into vacuole-like structures.

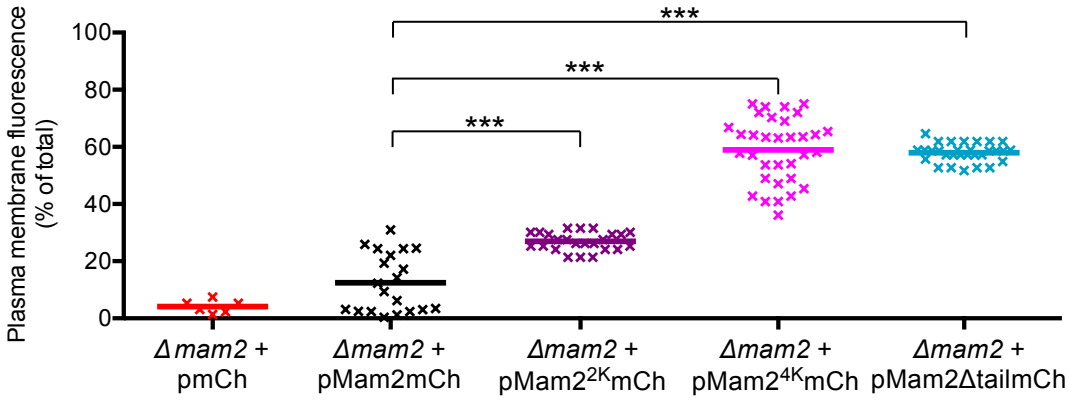

FIGURE 5.16: **Removing lysines from Mam2 increases plasma membrane fluorescence in untreated cells.** *Δmam2 S. pombe* (JY1169) cells were transformed with pmCh (JD3514), pMam2mCh (JD3590), pMam2^{2K}mCh (JD3802), pMam2^{4K}mCh (JD3804) and pMam2*Δ*tailmCh (JD3621), then grown to mid-exponential growth phase before imaging in the mCherry channel. Individual cells (pmCh: m=6, pMam2mCh: m=20 and all others: m=30, where m represents the number of individual cells analysed) were selected at random and their plasma membrane fluorescence was quantified using QuimP (as detailed in section 2.2.18). Statistical significance was determined using one-way ANOVA, $*p<0.05$, $**p<0.01$ and $***p<0.001$.

A significant increase in plasma membrane fluorescence was observed between Mam2mCh at 12% (m=20) and Mam2^{2K}mCh at 27% (m=30, where m represents the number of individual cells analysed) ($p<0.0001$, one-way ANOVA). Removing all four lysine residues increased plasma membrane fluorescence even further to 59% (m=30) of fluorescence (of the total cell) was situated at the membrane, similar to the amount observed when removing the last 45-resides of Mam2 (Mam2*Δ*tail) (58%, when m=30) ($p<0.0001$, one-way ANOVA) (Figure 5.16). Together, these data present Mam2^{4K}mCh as an ideal receptor for assessing how loss of Cki1, Cki2 and Cki3 affects the rate of receptor internalisation. Mainly as its plasma membrane concentration is greatly increased in comparison to Mam2 and hence, QuimP will successfully segment the cell periphery, yet receptor will still remain sensitive to ligand-induced internalisation.

5.5.3 Lysine deficient Mam2 showed an initial sigmodial P-factor-induced transcriptional response like Mam2

Before utilising Mam2^{4K}mCh to measure how loss of the kinases affects receptor internalisation, its signalling behaviour was analysed to ensure that removal of the lysine residues did not alter its signalling characteristics in comparison Mam2. A β-galactosidase assay was performed with *Δmam2* (JY1169; *mam2*$^{-}$, *sxa2>lacZ*) strains transformed with pMam2mCh, pMam2^{2K}mCh and pMam2^{4K}mCh, grown to mid-exponential growth phase

and treated with a range of P-factor concentrations (0 µM-10 µM) for 16 h (as detailed in section 2.2.8.1). Both lysine deficient receptors signalled in a similar fashion to Mam2mCh showing a sigmodial dose-response when treated with 0 µM to 1 µM P-factor (Figure 5.17). However, following treatment with >1 µM P-factor cells expressing Mam2^{2K}mCh and Mam2^{4K}mCh exhibited a reduction in signalling response observed by the bell-shaped (non-monotonic) curves (Figure 5.17).

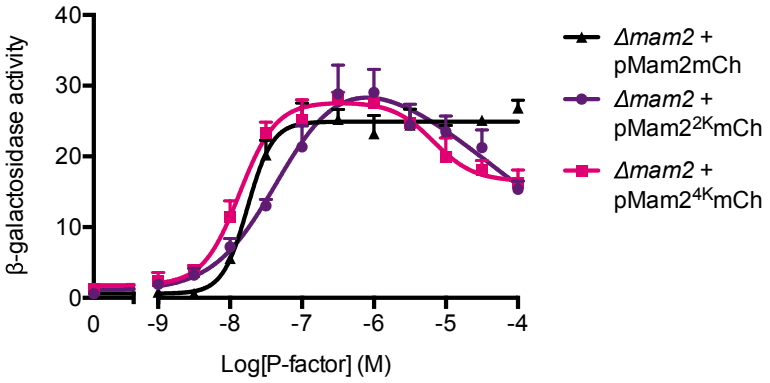

Figure 5.17: **Cells expressing lysine deficient Mam2 showed a reduction in β-galactosidase activity when treated with >1 µM P-factor.** *Δmam2 S. pombe* (JY1169) strains were transformed with pMam2mCh (JD3590), pMam2^{2K}mCh (JD3802), pMam2^{4K}mCh (JD3804) and were grown to mid-exponential growth phase before treatment with a range of P-factor concentrations (0 µM - 100 µM). Cells were assayed for β-galactosidase activity after 16 h as described in section 2.2.8.1. Data shown are the mean of five independent determinants ±SEM.

5.5.4 Lysis is increased in cells expressing C-terminal lysine deficient Mam2 in response to high concentrations of P-factor

Similar bell-shaped β-galactosidase responses have been observed previously, both in this study (Figure 3.11) and in the literature [223]. It has been shown that the reduction in β-galactosidase response was the result of increased cell lysis in response to prolonged (>8 h) treatment with high (>1 µM) concentration of P-factor [223]. In these studies the percentage of non-viable cells in a population was determined using a cell viability assay as described in section 2.2.16, which measures the Förster resonance energy transfer (FRET) signal between two fluorophores, propidium iodide and SYTO®9 [230]. Both dyes are excited using a 488 nm laser on a flow cytometer and emission detected using a 550 nm long pass filter with a 575/26 nm band pass filter for propidium iodide and a 505 nm long pass filter with a 530/30 nm band pass filter for SYTO®9.

A cell viability assay could not be performed with *Δmam2* cells transformed with pMam2^{4K}mCh as the mCherry fluorophore can be excited within the same spectrum of light and hence would affect the results. Instead, cell viability was determined visually from time-lapse microscopy images. *Δmam2* cells were transformed with pMam2mCh and pMam2^{4K}mCh, grown to mid-exponential growth phase, treated with 10 µM P-factor and imaged every 2 h from 0 h to 16 h as described in section 2.2.14. Each cell within the frame was tracked with time to determine its viability (for examples of time-lapse images used to determine cell viability please see the representative images in Appendix F).

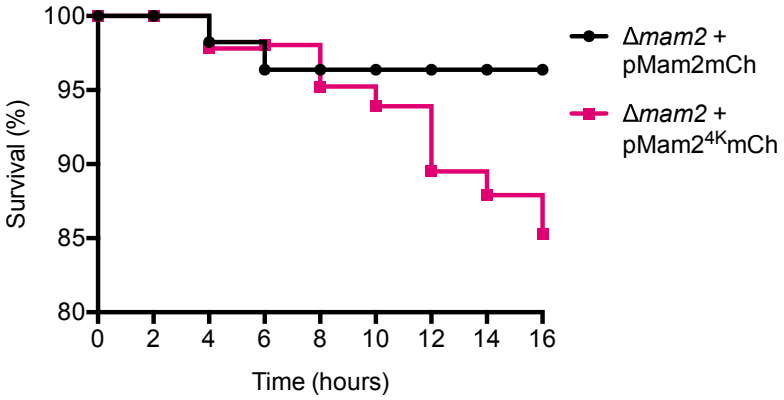

FIGURE 5.18: **Expression of Mam2^{4K}mCh reduces cell-viability with prolonged P-factor treatment.** *Δmam2 S. pombe* cells (JY1169) were transformed with pMam2mCh (JD3590) and pMam2^{4K}mCh (JD3804) grown to mid-exponential growth phase and treated 10 µM P-factor. A randomly selected field of cells (containing ∼30 cells) were chosen and imaged in the mCherry channel every 2 h from 0 h to 16 h as detailed in section 2.2.14. The percentage of non-viable cells in each frame were determined by eye and plotted in a Kaplan-Meier plot. Data shown are the mean of three independent determinants ±SEM.

Mam2 tagged mCherry (Mam2mCh) displayed a 4% reduction in survival following 16 h of treatment (Figure 5.18), whereas Mam2^{4K}mCh showed a 15% reduction in survival from 0 h (100%) to 16 h (85±4%). The difference in survival after 16 h of P-factor treatment between Mam2mCh and Mam2^{4K}mCh was significant (p=0.0135, two-way ANOVA using a Sidak test). These data suggest that removal of all four lysines from the C-terminal domain of Mam2 promotes cell lysis in response to P-factor treatment for periods up to 16 h and hence, provides a possible explanation for the reduction in β-galactosidase activity observed in the transcriptional assay.

5.5.5 Lysine deficient Mam2 alters conjugation tube formation

Cells expressing Mam2^{4K}mCh became increasingly non-viable with time following treatment with 10 µM P-factor (Figure 5.18). Visual analysis of the time-lapse microscopy images exhibited some cells elongating from both tips (rather than one end) to form conjugation tubes in response to treatment. A series of time-lapse images were taken of *mam2*$^{-}$ *S. pombe* cells (JY1169) expressing mCh, Mam2mCh and Mam2^{4K}mCh following treatment with 10 µM P-factor for 16 h. Each cell that responded to P-factor was categorised by whether it had elongated from a single tip or both tips.

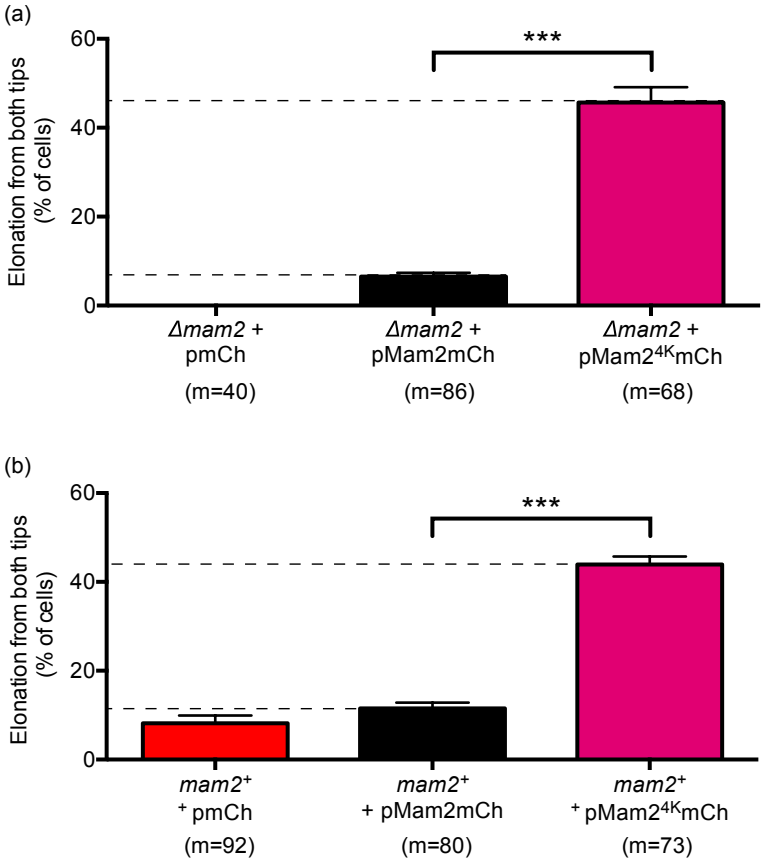

FIGURE 5.19: **Expression of Mam2^{4K}mCh increases the number of cells forming conjugation tubes from both tips.** (a) *Δmam2* (JY1169) and (b) *mam2*$^{+}$ (JY544) *S. pombe* cells were transformed with pmCh (JD3514), pMam2mCh (JD3590) and pMam2^{4K}mCh (JD3804) and were grown to mid-exponential growth phase before treatment with 10 µM P-factor. A frame of cells was selected at random and imaged under bright field light every 15 minutes from 0 h to 16 h. Each cell (that formed conjugation tubes) within that image was then categorised into whether it elongated from a single or both ends. Data shown the average of two independent determinants ±SEM, the total number of cells counted is denoted n. Statistical significance was determined using one-way ANOVA. $*p<0.05$, $**p<0.01$ and $***p<0.001$. The videos 3.3 and 3.4 are representative time-lapse videos showing cells that elongate from a single tip and from both tips, respectively.

46±3% (m=68) of cells expressing Mam2^{4K}mCh formed conjugation tubes from both tips was significantly increased in comparison to 7±1% (m=86) of cells exhibited when expressing Mam2mCh ($p<0.0001$, one-way ANOVA) (Figure 5.19a). Interesting an increase in the number of cells elongating from both tips was also observed in strains expressing both endogenous Mam2 (JY544) and pMam2^{4K}mCh (Figure 5.19b). Indicating that Mam2^{4K}mCh was dominant in terms of signalling preference than endogenous Mam2.

5.5.6 Active Cdc42 was observed at both tips in some cells that formed conjugation tubes from both tips

The G protein Cdc42 is concentrated at the growing tip in *S. pombe* cells [83]. A fluorescent fusion protein Cdc42/Rac interactive binding (CRIB)-GFP binds specifically to activated GTP-bound Cdc42 and can be used as a marker to assess the growing tip of *S. pombe* cells [85, 290, 291]. The strain JY1689 which expresses CRIB-GFP under the control of the Shk1 promoter (a downstream effector of Cdc42) and contains endogenous Mam2, when expressed with additional Mam2-mCherry from the pREP3x vector (pMam2mch, JD3950) was grown to mid-exponential growth phase, plated onto agarose pads contains 10 µM P-factor and imaged every 15 minutes (as described in section 2.2.14) to elucidate the growing tip. Cells transformed with Mam2mCh illustrated that CRIB-GFP was localised to a single elongating tip in response to P-factor (Figure 5.20), consistent with previous studies [223, 290]. Images are shown from 4 h as conjugation tubes are typically observed following 4 h of P-factor treatment and images are shown until 8 h as the direction of growth would be clear by this time.

∼50 % of cells containing endogenous Mam2 and expressing additional Mam2^{4K}mCh elongated from both tips in response to P-factor (Figure 5.19). This elongation from both tips suggested that the receptor Mam2^{4K}mCh was dominant in terms of signalling preference over endogenous Mam2. Therefore, the C-terminal tail lysine deficient receptor was expressed in CRIB-GFP strains (which are *mam2*$^{+}$) to investigate the localisation of active Cdc42. The CRIB-GFP strain JY1689 was transformed with pMam2^{4K}mCh, grown to mid-exponential growth phase, plated onto agarose pads containing 10 µM P-factor and imaged every 15 min from 4 h (as described in section 2.2.14). Some cells expressing Mam2^{4K}mCh that elongated from both ends in response to P-factor exhibited CRIB-GFP at both tips (Figure 5.20). The CRIB-GFP+pMam2^{4K}mCh panel in Figure 5.20 is a representative

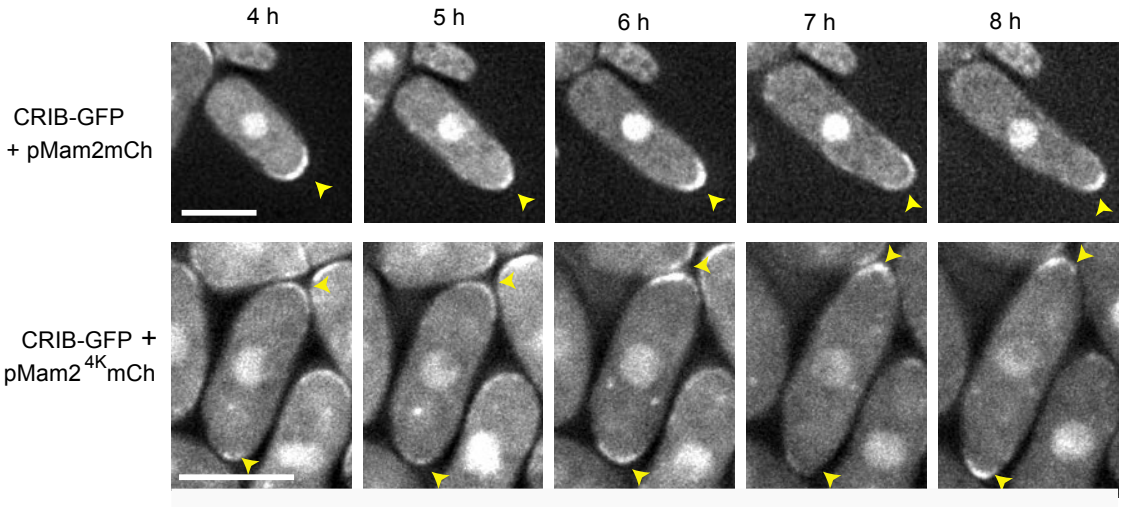

Figure 5.20: **Cells expressing Mam2^{4K}mCh elongate from both tips following P-factor treatment.** *mam2*$^{+}$ strains containing a CRIB-GFP marker for Cdc42-GTP (JY1689) were transformed with pMam2^{4K}mCh (JD3804) and grown to mid-exponential growth phase before treatment with 10 µM P-factor. A randomly selected field of cells were imaged in the GFP channel every 15 minutes from 0 h to 8 h (as described in section 2.2.14). Only 4 h to 8 h are shown here as the majority of cells begin to form conjugation tubes following 4 h of treatment with P-factor. Yellow arrow heads highlight CRIB-GFP at the cell tips. Scale bar represents 10 µm. The video 3.5 is a representative time-lapse image showing that CRIB-GFP was observed at both tips in some cells that elongate from both tips.

image. Not all cells that appeared to elongate from both ends exhibited CRIB-GFP at both tips (see video 3.5).

In mitotically growing cells, following cell division, the daughter cells grow from the tip that existed prior to separation (the 'old' tip). When a minimal size threshold is reached growth is initiated from the opposite tip and period of bipolar growth is established, a process termed new end take off (NETO) [292]. In mitotically growing cells CRIB-GFP has been shown to oscillate by a period of ∼2 minutes during bipolar growth [85]. To obtain time-lapse images of cells every 2 minutes, many factors need to be controlled, such as the photobleaching of the fluorophores and the drift from the microscope. These factors make it incredibly challenging to image these cells over the period of 2 minutes and to observe the conjugation tube formation which can take hours. The images obtained during this study were taken every 15 minutes over a period of ∼5 hours before photobleaching was observed (see video 3.5) and oscillations of CRIB-GFP between each tip was exhibited. These images therefore suggest that conjugation tube formation from both tips may be a result of Cdc42 activation at both tips, suggesting that the Mam2^{4K}mCh influences Cdc42 activation in response to treatment with P-factor.

5.6 Loss of Cki2 reduces receptor internalisation

Cells expressing Mam2^{4K}mCh exhibited an increase in receptor plasma membrane concentration (in comparison to Mam2mCh), as constitutive internalisation was prevented, yet the receptor remained sensitive to P-factor-induced internalisation (Figure 5.15). Strains expressing Mam2^{4K}mCh also demonstrated similar sigmodial responses to P-factor as observed with full length Mam2 when treated with <1 µM P-factor (Figure 5.17). As discussed, cells expressing Mam2^{4K}mCh showed a reduction in β-galactosidase activity as a consequence of the cells becoming increasingly non-viable in response to P-factor. However, this was only significant following 12 h of treatment (Figure 5.18).

These data suggested that the receptor Mam2^{4K}mCh could be utilised to investigate how loss of Cki1, Cki2 and Cki3 alters the rate of receptor internalisation, as the receptor was strongly localised to the cell periphery and could be quantified (prior to the significant cell lysis observed after 12 h of treatment). Therefore, *Δmam2* (JY1169; *mam2⁻*, *sxa2>lacZ*), *Δcki1Δmam2* (JY1727; *mam2⁻*, *cki1::ura4⁺*, *sxa2>lacZ*), *Δcki2Δmam2* (JY1734; *mam2⁻*, *cki2::ura4⁺*, *sxa2>lacZ*) and *Δcki3Δmam2* (JY1720; *mam2⁻*, *cki3::ura4⁺*, *sxa2>lacZ*) *S. pombe* strains were transformed with pMam2^{4K}mCh, grown to mid-exponential growth phase, treated with 0 µM and 10 µM P-factor for 16 h and imaged to assess cell morphology and receptor localisation (as described in section 2.2.14).

When untreated, Mam2^{4K}mCh was predominantly localised to the cell membrane. Vacuole-like structures in the cytosol were observed in *Δcki1Δmam2* and *Δcki3Δmam2* strains (Figure 5.21). In response to P-factor, all strains formed conjugation tubes, localising the receptor at the plasma membrane and within vacuole-like structures within the cytosol, suggesting that some Mam2^{4K}mCh had been internalised from the plasma membrane (Figure 5.21).

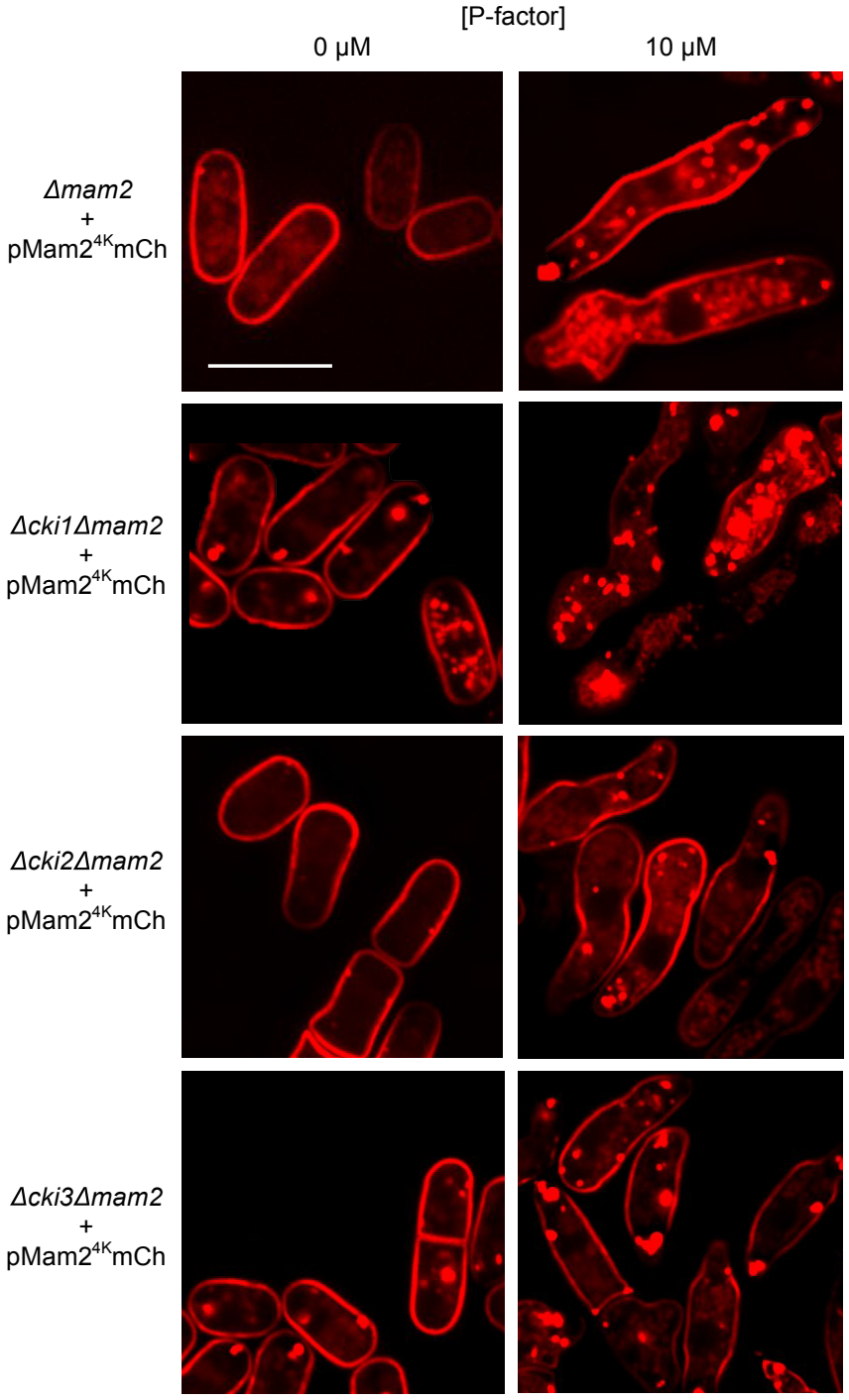

Figure 5.21: **P-factor-induced internalisation of Mam2^{4K}mCh was not prevented by disruption of *cki1*, *cki2* or *cki3*.** *Δmam2* (JY1169), *Δcki1Δmam2* (JY1727), *Δcki2Δmam2* (JY1734) and *Δcki3Δmam2* (JY1720) cells transformed with pMam2Mam2^{4K}mCh (JD3804) were grown to mid-exponential growth phase before treatment with 0 µM and 10 µM P-factor. After 16 h of cells were imaged in the mCherry channel as described in section 2.2.14. Scale bar represents 10 µm.

QuimP was used to analyse the plasma membrane fluorescence of *Δmam2* (JY1169) strains expressing Mam2^{4K}mCh and Mam2*Δ*tailmCh following treatment with P-factor. Strains were grown to mid-exponential growth phase, plated onto agarose gels containing 10 µM P-factor and imaged every 30 minutes from 0 h to 8 h (as described in section 2.2.14). QuimP was used to measure the percentage plasma membrane fluorescence (of the total cell fluorescence) of each cell in every time-lapse frame. Strains expressing Mam2^{4K}mCh and Mam2*Δ*tail displayed a reduction in plasma membrane fluorescence over time (Figure 5.22). However, the reduction displayed by Mam2*Δ*tail (100% to 86%) was not as prominent as Mam2^{4K}mCh (100% to 46%).

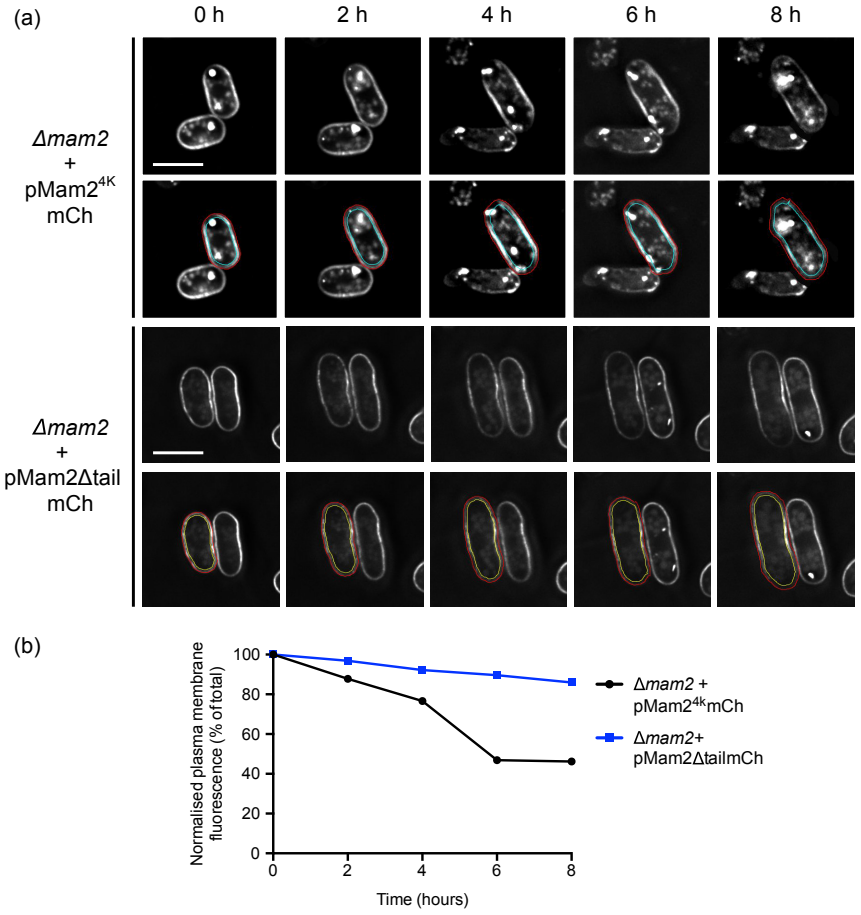

FIGURE 5.22: **Quantifying plasma membrane fluorescence using QuimP.** *Δmam2* (JY1169) cells transformed with pMam2^{4K}mCh (JD3804) and pMam2*Δ*tailmCh (JD3621) were grown to mid-exponential growth phase and plated onto agarose pads containing 10 µM P-factor. Cells were imaged in the mCherry channel every 30 minutes from 0 h to 8 h as detailed in section 2.2.14. QuimP was used to (a) segment the plasma membrane (red and yellow contours define the outer and inner bounds of the membrane, respectively) of a single cell and (b) quantify the the plasma membrane fluorescence as a percentage of the total cell fluorescence (normalised data presented).

To quantify receptor endocytosis following treatment with P-factor in cells disrupted in *cki1*, *cki2* and *cki3* relative to a WT (*cki1*$^+$, *cki2*$^+$ and *cki3*$^+$) strain a combination of microscopy and QuimP analysis was employed. *Δmam2* (JY1169), *Δcki1Δmam2* (JY1727), *Δcki2Δmam2* (JY1734) and *Δcki3Δmam2* (JY1720) strains transformed with pMam2^{4K}mCh were grown to mid-exponential growth phase, plated onto agarose pads containing 10 µM P-factor and a randomly selected field of cells were imaged every 30 minutes from 0 h to 16 h (As described in section 2.2.14). The fluorescent images were loaded into QuimP to determine the plasma membrane fluorescence as a percentage of the total cell fluorescence. Cells were selected provided they did not divide over the time-course or once it had completed a round of division. Each cell was tracked with time and QuimP was used to measure plasma membrane fluorescence every 1 h (from the initial measurement frame) up to 8 h. Individual cell analyses can be found in Appendix E.

Strains lacking functional *cki1* displayed a similar internalisation behaviour to WT cells, where plasma membrane fluorescence decreases following treatment with P-factor over time (Figure 5.23). No significant difference in Mam2^{4K}mCh plasma membrane fluorescence was observed after 8 h of treatment between WT (40±4%, m=21) and *Δcki1Δmam2* cells (47±2%, m=18), where p=0.3598 calculated using two-way ANOVA.

A significant increase in Mam2^{4K}mCh plasma membrane fluorescence was observed in *Δcki2Δmam2* strains following 5 h treatment with P-factor in comparison to *cki2*$^+$ (*Δmam2*+pMam2^{4K}mCh) cells (Figure 5.23). After treatment for 8 h WT strains displayed 47±2% (m=18) whereas *Δcki2Δmam2* cells displayed 65±5% (m=18), which was a significant increase (p=0.0002 calculated using two-way ANOVA).

Strains lacking *cki3* displayed a significant decrease in plasma membrane fluorescence from 4 h to 8 h of treatment (Figure 5.23c), whereas at 8 h WT strains displayed 47±2% (m=18) Mam2^{4K}mCh plasma membrane fluorescence in comparison to *Δcki3Δmam2* cells, which displayed 33±3% (m=16) (p=0.0170 calculated using two-way ANOVA).

These data suggest that Cki2 positively regulates receptor internalisation in response to P-factor, whereas Cki1 and Cki3 did not. In addition, the data collected for *Δcki3* strains indicate that Cki3 may even prevent internalisation, as plasma membrane fluorescence was reduced in comparison to *cki3*$^+$ strains (Figure 5.23).

(a)

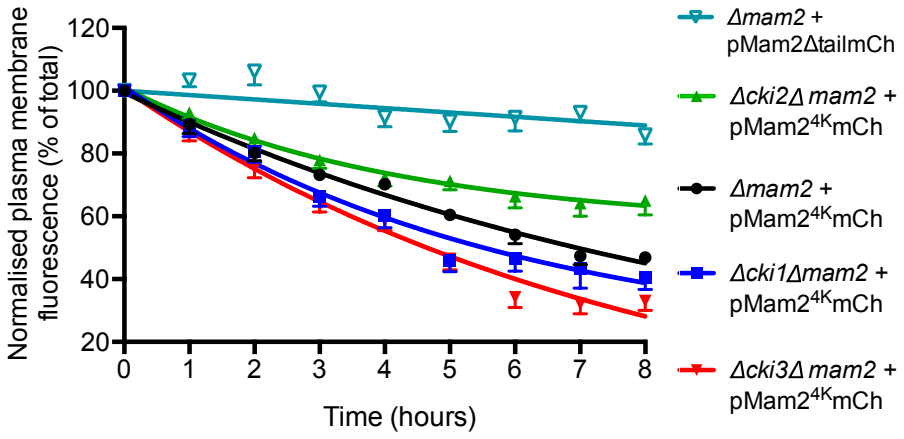

(b)

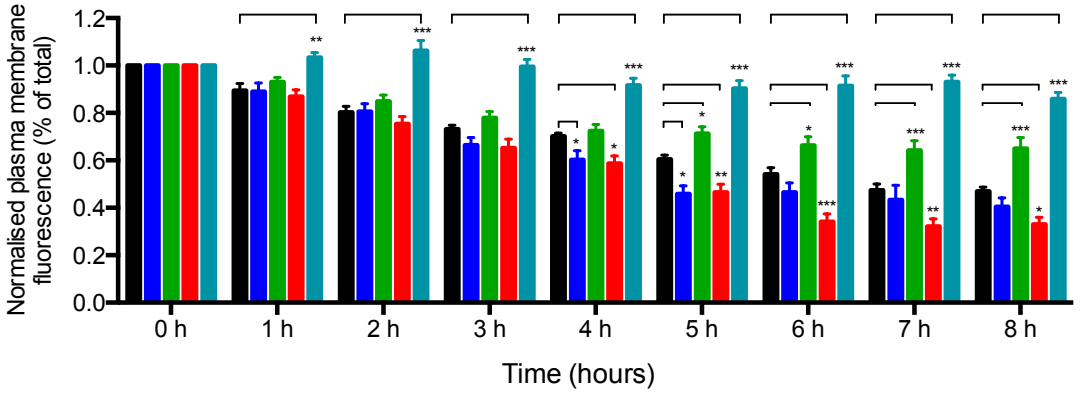

	0 h	1 h	2 h	3 h	4 h	5 h	6 h	7 h	8 h
***Δmam2* + pMam2^{4K}mCh**	100±0	89±3	80±3	73±2	70±3	60±2	54±3	47±3	47±2
***Δcki1Δmam2* + pMam2^{4K}mCh**	100±0	89±4	81±3	66±4	60±4 *	46±3 *	47±4	43±6	40±4
***Δcki2Δmam2* + pMam2^{4K}mCh**	100±0	93±2	85±3	78± 3	72±3	71±3 *	66±4 *	64±4 ***	65±5 ***
***Δcki3Δmam2* + pMam2^{4K}mCh**	100±0	87±3	75±3	65±4	59±3 *	46±3 **	34±3 ***	32±3 **	33±3 *
***Δmam2* + pMam2*Δ*tail**	100±0	103±2 **	106±4 ***	100±3 ***	92±3 ***	90±3 ***	91±4 ***	93±3 ***	86±3 ***

FIGURE 5.23: **Loss of *cki2* reduces the amount of plasma membrane fluorescence over time** *Δmam2* (JY1169) cells transformed with pMam2^{4K}mCh (JD3804) and pMam2*Δ*tailmCh (JD3621) together with *Δcki1Δmam2* (JY1727), *Δcki2Δmam2* (JY1734) and *Δcki3Δmam2* (JY1720) cells transformed with pMam2^{4K}mCh were grown to mid-exponential growth phase before treatment with 10 µM P-factor. A randomly selected field of cells were imaged in the mCherry channel every 30 minutes from 0 h to 8 h as detailed in section 2.2.14. 16 cells or more were quantified for their plasma membrane fluorescence using QuimP (as detailed in section 2.2.18, for exact n numbers see text). The figure displays the (a) mean raw and normalised data ±SEM, (b) the normalised data including statistical significance $*p<0.05$, $**p<0.01$ and $***p<0.001$, following two-way ANOVA (comparing all strains to *Δmam2* + pMam2^{4K}mCh) and (c) the normalised values at each time point.

5.7 Summary

This chapter sought to determine whether Cki1, Cki2 and Cki3 promoted ligand-induced endocytosis of Mam2. Yeast 2-hybrid analysis did not indicate an interaction between Mam2 with either of the kinases however, an interaction with Rgs1 (the RGS protein) was observed (Figure 5.2). Following this, a combination of fluorescent protein markers (mCherry and GFP), microscopy analysis and cell segmentation software was employed to quantify internalisation of Mam2.

Deletion strains that contained the double disruption *mam2* with either *cki1*, *cki2* and *cki3* were created (section 2.3.1) and microscopy analysis and β-galactosidase assays were used to access the localisation and signalling behaviour of Mam2-mCherry expressed from the pREP3x vector (pMam2mCh). Unfortunately, a weak plasma membrane association of Mam2mCh prevented the QuimP software from segmenting the cell periphery and quantifying membrane fluorescence (Figure 5.6). The lack of Mam2 tagged mCherry at the plasma membrane prompted the investigation to create a version of Mam2 that increased the concentration of the receptor at the membrane, yet internalised following treatment with P-factor.

A previous study suggested that sequential truncation of the C-terminal domain of Mam2 increased plasma membrane localisation (E. McCann, PhD thesis, 2010). However, the microscopy images used to make these conclusions were of low-resolution and these receptors localisation had not been investigated in response to P-factor. Previously created truncated versions of Mam2 (Δ5, Δ13, Δ21 and Δ37) tagged with GFP were analysed using high-resolution microscopy in combination with a vacuole staining dye (FM4-64) to assess the receptors localisation and sorting to the vacuole.

Loss of the last 21-residues of Mam2 increased plasma membrane localisation uniformly at the cell perimeter in untreated cells (Figure 5.10) and yet the receptor internalised from the plasma membrane into intracellular structures that were not vacuoles in response to P-factor (Figure 5.11). Therefore, the Mam2Δ21-GFP appeared an ideal receptor for accessing the rate of receptor endocytosis using QuimP. β-galactosidase assays indicated that Mam2Δ21GFP did not signal like full length Mam2 (Mam2GFP) (Figure 5.12), most likely as those residues that were truncated are potential docking sites for Rgs1, an interaction which is essential for a maximal signalling response [173]. As a result of Mam2Δ21-GFP was not used to access internalisation. A summary of the Mam2tail mutant microscopy analysis and β-galactosidase assay results are presented in Table 5.2.

	No P-factor				P-factor			
	Plasma membrane	Internal structures	Vacuole	Basal signalling	Plasma membrane	Internal structures	Vacuole	Maximal signalling
Mam2	✓×	✓	✓		×	✓	✓	
Mam2Δ5	✓	✓	✓	-	×	✓	✓	-
Mam2Δ13	✓	✓	✓×	-	×	✓	×	-
Mam2Δ21	✓	×	×	↑	×	✓	×	↓
Mam2Δ37	✓	×	×	↑	✓×	✓	×	↓
Mam2Δtail	✓	×	×	↑	✓	×	×	↓
$Mam2^{2K}$	✓	✓	✓	-	×	✓	✓	-↓
$Mam2^{4K}$	✓	×	×	-	✓	✓	✓	-↓

TABLE 5.2: **A table summarising the microscopy and β-galactosidase analysis from Chapter 5.** The versions of Mam2 used in this study were analysed using microscopy and β-galactosidase assays to determine whether these receptors were localised to the plasma membrane, internalised and subsequently trafficked to the vacuole and their signalling behaviours, respectively in both a P-factor independent and dependent environment. A ✓ means that this was observed, a × if this was not observed and ✓× if this was observed occasionally. An ↑ indicates an increase, a ↓ indicates a decrease in β-galactosidase signalling compared to Mam2 and a -↓ indicates a reduction in signalling due to cell lysis.

Monoubiquitination of a single lysine residue within C-terminal domain of *S. cerevisiae* STE2 is essential for both constitutive and ligand-induced internalisation [284]. However, for many mammalian GPCRs and the pheromone-type *S. cerevisiae* STE3 ligand-induced endocytosis is not dependent on ubiquitination [287–289]. Therefore, Mam2's dependency on ubiquitination was investigated by mutating the four lysine residues (and hence sites of ubiquitination) contained in the C-terminal tail of Mam2. Two of the four lysine residues were contained within the last five residues of Mam2, which were shown to not be essential for signalling response, internalisation or subsequent receptor sorting to the vacuoles (Table 5.2, see Mam2Δ5GFP). To investigate the involvement of the other two lysine residues (not contained within the last five amino acid residues of Mam2) mutation of the lysine residues to arginine was performed on both Mam2 and Mam2Δ5 (section 2.3.2.3 and 2.3.2.4, respectively).

Mutation of the first two lysine residues with the other two remaining within the last five residues of the Mam2 ($Mam2^{2K}$) increased plasma membrane fluorescence in untreated cells, but did not appear to prevent internalisation and trafficking to the vacuoles. The removal of all four lysine residues ($Mam2^{4K}$) prevented constitutive internalisation and yet receptor endocytosis into the vacuole-like structures was observed in response to P-factor (Figure 5.15). The result suggested that ubiquitination is essential for constitutive internalisation, but not required for P-factor-induced internalisation of Mam2. The C-terminal domain lysine mutated Mam2 receptors β-galactosidase signalling and localisation behaviour are summarised in Table 5.2.

Mam2^{4K}mCh β-galactosidase signalled like full length mam2 (Mam2mCh) following treatment with 0 µM to 1 µM P-factor. However, a reduction of signalling was observed following treatment with >1 µM P-factor. Visual cell viability analysis showed that cells expressing Mam2^{4K}mCh became increasingly non-viable following prolonged (>12 h) treatment with P-factor (Figure 5.18). Further analysis of the microscopy time-lapse images revealed that some cells expressing Mam2^{4K}mCh tended to elongate from both tips than the typical one tip shown by Mam2mCh (Figure 5.19).

Despite the reduction in cell viability following prolonged treatment with P-factor, the receptor was strongly localised at the cell periphery in cells expressing the lysine deficient receptor Mam2^{4K}mCh. Providing the QuimP analysis was performed on cells before the 10 h period (where the percentage of non-viable cells increased), this receptor seemed ideal to access whether Cki1, Cki2 and Cki3 affected P-factor induced internalisation. QuimP analysis on strains lacking *cki1*, *cki2* and *cki3* and expressing Mam2^{4K}mCh suggested that Cki2 promoted receptor internalisation in response to P-factor, where as Cki1 and Cki3 did not. In addition, the data collected for *Δcki3* strains indicate that Cki3 may even prevent internalisation in a P-factor-dependent manner, as plasma membrane fluorescence was reduced in comparison to *cki3*$^{+}$ strains (Figure 5.23).

Chapter 6

Discussion

6.1 Overview

The internalisation of GPCRs has been studied extensively over the last 30 years. The pharmaceutical industry invests billions of dollars each year to discover therapeutic compounds for GPCRs that give desired physiological effects (reviewed in [5]). Many long-term treatments that target these receptors result in the patient becoming tolerant to the drug [293]. This tolerance often results in having to increase the dosage to deliver the same physiological outcome, which can be debilitating for the patient and lead to undesirable side effects. Understanding how these receptors are regulated at the plasma membrane is key to developing appropriate treatments for diseases. In higher eukaryotes, the number of different receptor types expressed on the cell surface at any one time depends on the cell type and as such the cross-talk between these pathways makes it difficult to dissect the role of individual GPCRs in a cellular response.

Despite decades of research on the pheromone-response pathway in fission yeast, the combinatorial process of signal regulation and specifically GPCR internalisation are still unknown. With a greater understanding of GPCR signal regulation in these single celled eukaryotes, this may help to uncover overall processes in higher multi-cellular organisms so that more selective treatments can be designed. This study has identified three potential candidates (Cki1, Cki2 and Cki3) that could promote pheromone-induced internalisation of the **M**-type receptor Mam2 and in doing so has lead to the highly probable discovery that two distinct internalisation pathways exist in fission yeast.

6.2 Development of the KR model

Chapter 3 describes the creation of a fully descriptive model of the pheromone-response pathway in *S. pombe* (called the KR model). The KR model is extended from the pre-existing Croft *et al.* (2013) model [173] to include the downstream signalling components and known regulatory mechanisms of the P-factor-induced *S. pombe* signal transduction pathway. The KR model contains 39 species, 54 reactions and 54 rate constants, which have been heuristically determined to fit the experimental data. Despite the large number of reactions and species, the KR model can qualitatively recapitulate all of the current experimental end-point data (collated form the literature and collected in this study), providing the cells were viable during the assays.

Our confidence in the model reactions prompted its use as a predictive tool for systems level behaviour. Rgs1 (the RGS for Gpa1, the Gα subunit) has previously been shown to have a dual positive and negative role on signalling response [190]. However, upon deletion of Gap1 (the GAP for Ras1) from *S. pombe* the KR model predicts that Rgs1 would now act as a sole negative regulator. The prediction was validated by a series of transcriptional reporter assays [11].

6.2.1 Rgs1 acts as a negative regulator in Gap1 deletion strains

When referring to the model components, GAP represents Gap1 and RGS represents Rgs1. The KR model predicts that setting the initial concentration of GAP to 0 nM ([GAP] = 0 nM) *in silico* results in RGS acting as a negative regulator of signalling (Figure 3.26), i.e. increasing the concentration of RGS decreases the maximal system level output. This was verified *in vitro* by expressing different levels of Rgs1 in Gap1 deletion strains (Figure 3.27.b).

Strains lacking endogenous Rgs1 (*Δrgs1*) exhibit an elevated basal activity [190] (Figure 3.27.b). This increase in basal response suggests that a larger pool of Gpa1 are GTP-bound in comparison to *rgs1*$^+$ strains. The rise in active Gpa1 therefore increases signal transduction to downstream effectors, resulting in an increase in transcription of mating-responsive genes (Figure 3.27.a). Strains lacking endogenous Rgs1 still exhibited a dose-dependent increase in transcriptional response to P-factor, reaching an $\sim\frac{1}{2}$ maximal signalling response in comparison to *rgs1*$^+$ strains [190] (Figure 3.27.a, compare red and blue maximal response levels). Hence, Rgs1 is required for cells to reach a maximal signalling response.

Deleting Gap1 in a *rgs1*$^+$ strain displayed an elevated transcriptional response that did not respond in a dose-dependent manner to P-factor (Figure 3.27.b). Importantly, the level of response in *Δgap1* cells is $\sim\frac{1}{2}$ maximal signalling response of wild type (WT; *rgs1*$^+$*gap1*$^+$) strains and equivalent to the maximal response of *Δrgs1* strains (Figure 3.27, compare the red curves). Therefore, the concentration of GTP-bound Gpa1 becomes a limiting factor in signal transduction in strains lacking *gap1*, i.e. for *Δrgs1Δgap1* the pool of active Gpa1 is already at a maximal level, illustrated by the same transcriptional response level *Δrgs1* in response to P-factor, thus increasing Rgs1 can only have a negative influence on signal transduction.

The *Δrgs1Δgap1* strains created and used in this study are difficult to grow and maintain (data not available). For example, these strains needed to be restricted onto fresh medium plates every week otherwise growth was not observed in liquid culture. In addition, these strains also took longer to reach mid-exponential growth phase than other strains (data not available). The *Δrgs1Δgap1* strains used in the study are *cyr1*$^-$. Deletion of *cyr1* allows *S. pombe* to undergo sexual differentiation during mitotic growth by mimicking nutrient starvation [53]. It is known that nutrient starvation also induces a G_1 arrest [294].

The WT strain JY544 used in this study showed that ∼29% of *S. pombe* cells were arrested in G_1 phase of the cell cycle prior to treatment with P-factor (Figure 4.19, see the WT strain at 0 h), which is consistent with previous studies (M. Bond, PhD Thesis, 2012; C. Weston, PhD thesis, 2013). In combination with ∼29% of the population in G_1 arrest plus the deletion of *rgs1* and *gap1* which enhances basal signalling to $\sim\frac{1}{2}$ maximal response of wild type (WT; *rgs1*$^+$*gap1*$^+$) strains (Figure 3.27), it is most likely that these strains are predominantly in G_1 phase of the cell cycle and hence, growth was significantly reduced. This could be a reason why a dose-dependent response is not observed following treatment with P-factor (Figure 3.27.b), because the cells are already in G_1 phase of the cell cycle. DNA complement could be measured in these strains to assess whether they are predominantly in G_1 phase prior to pheromone stimulation.

6.2.2 Further improving the KR model to show quantitative agreement with empirical data

The KR model is the first model that signals via the Gα subunit, which includes downstream signalling molecules such as the G protein, GAP, a MAPK kinase cascade and phosphatase. Although the KR model can qualitatively recapitulate the vast majority of the experimental

data currently available, a limitation of this work is that it lacks experimentally determined parameters and initial species concentrations.

Many of the initial species concentrations described in the KR model were estimated from known protein expression levels of the components of the *S. cerevisiae* mating-response pathway [241]. It is assumed that the species concentrations or the ratios between the mating-response pathway components were conserved between the two yeasts. To improve the KR model, the protein expression levels of the species involved the *S. pombe* mating-response pathway need to be determined. One study has quantified the protein expression levels of the species in the mating-response pathway of quiescent *S. pombe* cells [295]. *S. pombe* cells arrest in G_1 phase of the cell cycle in response to pheromone stimulation. During the G_1 arrest phase, *S. pombe* cells are in a period of inactivity in terms of cell cycle progression and at this point are most similar to quiescent cells. Therefore, the KR model could be improved by incorporating the potentially more realistic initial species concentrations determined for quiescent *S. pombe* cells.

The KR model is complete in terms of known signalling regulatory mechanisms and is able to reproduce the temporal data (Figure 3.30), however including a term for internalisation into the model hindered the qualitative ability of the model to fit the end-point experimental data as well as it had before. This is most likely because the parameters used in the model are not true parameter values, rather they have been heuristically determined to best fit the experimental data. Although a qualitative agreement is observed between simulations and experimental dose-response data, quantitative agreement is lacking, most likely due to the absence of true parameter values.

Future work should focus on developing the KR model to improve its quantitative accuracy. For example, parameter sensitivity analysis could be performed as a means of improving accuracy. Different parameter values can result in the same model behaviour. Hence it is crucial to estimate the parameter values that are relevant for GPCR signalling in *S. pombe*. One possibility as discussed previously is to experimentally measure each parameter for a specific reaction, however it is often difficult to do such measurements within a biological organism. Another approach is reverse engineering, where model parameters are estimated by fitting model output to available experimental data. This type of analysis is often used to assess how changes in model parameters affect the model output and can provide valuable information on which parameters are crucial to determine experimentally and which, if any, can be discarded. In addition, by fitting a model to the experimental

data, a set of parameter values can be determined, which do not need to be measured experimentally. The disadvantage with fitting such a model is that it may not offer any explanatory power; for example, a high order polynomial can be fitted to almost any data set, however this is not biologically accurate.

6.3 Characterisation of Cki1, Cki2 and Cki3

The yeast casein kinase proteins YCK1 and YCK2 are required for the phosphorylation of serine residues within the C-terminal tail of the *S. cerevisiae* pheromone receptor STE2 and its subsequent internalisation in response to treatment with pheromone [112, 269, 270]. The aim of chapter 4 was to identify and characterise the role of the proteins homologous to YCK1 and YCK2 in the *S. pombe* mating-response pathway, Cki1, Cki2 and Cki3. Four standard mating-response assay were employed, with the kinase disruption strains or overexpression plasmids, which indicated a role of each kinase (Cki1, Cki2 and Cki3) within the mating-response of *S. pombe* (discussed in more detail below).

6.3.1 Cki1 negatively regulates the pheromone-response pathway in *S. pombe*

This thesis provides evidence that Cki1 negatively regulates the transcriptional and morphological response of the pheromone-response pathway in *S. pombe*. Disruption of Cki1 showed a significant increase in maximal transcriptional reporter activity (Figure 4.9), cell volume (Figure 4.10) and hyper-elongated conjugation tubes (Figure 4.6). Removing a negative regulator of pheromone-signalling typically results in an increase in P-factor-directed responses. For example, Pmp1, the phosphatase that is thought to negatively regulate the action of the MAPK Spk1, when deleted also displays elongated-conjugation tubes, an increase in transcriptional response and an increase in cell volume following 16 h treatment with P-factor [11, 221] (Figure 4.12).

A significant increase (in comparison to WT) in transcriptional activity is only observed in Cki1 deletion strains following 14 h treatment with P-factor (Figure 4.11). This delay in the increase of transcriptional activity suggests that Cki1 may not directly regulate the components of the transcriptional pathway (described in Figure 1.7), but may influence pheromone-signalling by a feedback mechanism initiated by pheromone activation.

Additional evidence to support this, is that unlike other negative regulators of pheromone-signalling, such as Rgs1 [87] and Gap1 [86], deletion of Cki1 does not reduce the number of successful mating events (CFU recovery) (Figure 4.4).

It is known that Cki1 phosphorylates and inactivates phosphatidylinositol 4-phosphate 5-kinase (PIP_5K), a protein kinase that catalyses the last step in the synthesis of PIP_2 [296]. As discussed in the introduction, PIP_2 is a precursor of DAG and IP_3 (second messenger signalling molecules) and is involved in the regulation of actin cytoskeleton remodelling, membrane trafficking [297] and vesicle transport [298]. PIP_2 has a specific role in binding Sec3 and Exo70 components of the exocyst complex (which is transported along actin cables in a myosin V manner) and provides positional information for localisation of the entire complex at the cell tip [80, 299, 300]. A previous study has shown that overexpression of Cki1 reduces plasma membrane localisation and activity of PIP_5K (by ~48% [296]), ultimately reducing the synthesis of PIP_2. Overexpression of Cki1 in this study did not alter cell morphology or influence pheromone-signalling suggesting that despite the potential reduction and inactivation of PIP_2 at the plasma membrane, this was not a limiting factor for cellular processes, even if overexpression of Cki1 reduced its localisation at the membrane.

Further work investigating Cki1's role in pheromone-signalling should be investigated, as this may reveal an additional feedback mechanism/regulation that has not yet been identified. Casein kinases have numerous roles within the cell and can target many regulatory proteins [110, 301]. Therefore, to uncover which proteins Cki1 is targeting and to understand how this feedback effects pheromone signalling, a yeast 2-hybrid screen could be performed to identify proteins that potentially interact with Cki1.

6.3.2 Cki2 plays a role in regulating cell size during vegetative growth

A previous study has shown that overexpression of Cki2 causes pear-shaped cells that separate poorly following septation, suggesting a potential role of Cki2 in regulating cell morphology [272]. Pear-shaped cells or cells that were unable to separate following septation were not observed in this study, instead the results show that deletion of Cki2 increases cell size during vegetative growth, yet not in response to P-factor.

Previous studies have coupled vegetative cell size to entry into mitosis, through a spatial intracellular gradient of Pom1, a dual-specificity Yak-related kinase (DYRK) [302]. DYRKs self-catalyse via multiple autophosphorylation reactions within their activation loop [303].

When the cells are small, Pom1 is located across the entire cell and inhibits transition into mitosis (via inhibition of the kinase Cdr2, enabling the M phase inhibitor protein kinase Wee1 to inhibit Cdc2, thereby preventing cell cycle progression), but as the cells elongate the source of the Pom1 gradient at cell tips is moved further apart and thus the concentration of Pom1 in the cell centre is reduced, removing inhibition of mitosis, resulting in cell division [304] (Figure 6.1).

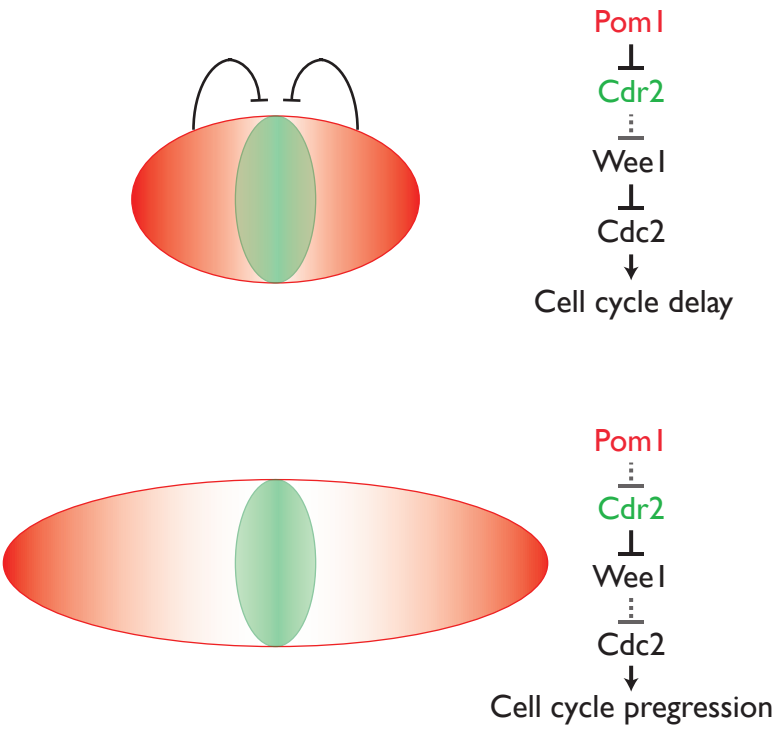

FIGURE 6.1: **A model describing how *S. pombe* cells monitor their length to control entry into mitosis.** A gradient of Pom1 from cell tips overlaps significantly with Cdr2 at the centre of small cells, leading to Cdr2 inhibition and cell cycle delay. As the cells grow and become longer in size, the concentration of Pom1 at the cell centre is no longer sufficient for significant Cdr2 inhibition, allowing cell cycle progression. Figure adapted from [302].

The Pom1 gradient is maintained by microtubules, which amongst other proteins such as Tea1 [305] and Tea4 [306], traffic Pom1 to the cell tips to mark the sites of actin nucleation and consequently cell growth [307]. A basic domain within Pom1 associates with lipids in the plasma membrane and this affinity is lost with increasing autophosphorylation, which ultimately results in Pom1's release into the cytoplasm. Concomitantly to this process of Pom1 autophosphorylation and cytoplasmic release, Tea4 recruits the protein phosphatase

Dis2 [308], which dephosphorylates Pom1 at cell tips leading to a greater membrane association [309].

Cki2 may regulate the association of Pom1 with the plasma membrane, for example by modulating the activity of Dis2, such that loss of Cki2 would result in a reduction in Dis2 phosphatase activity, leading to an increase in cytoplasmic Pom1. Dis2 has been shown to have multiple phosphorylation sites [310]. As a result, the cells would grow to a larger size before the reduction in Pom1 in the center of the cell would be reduced enough to promote cell cycle progression (Figure 6.2). In response to P-factor the Pom1 gradient sensing machinery is overridden by Cdc42 activation, which promotes elongation from a single tip and therefore, would explain why loss of Cki2 only increases vegetative cell size and not conjugation length/cell volume in response to P-factor.

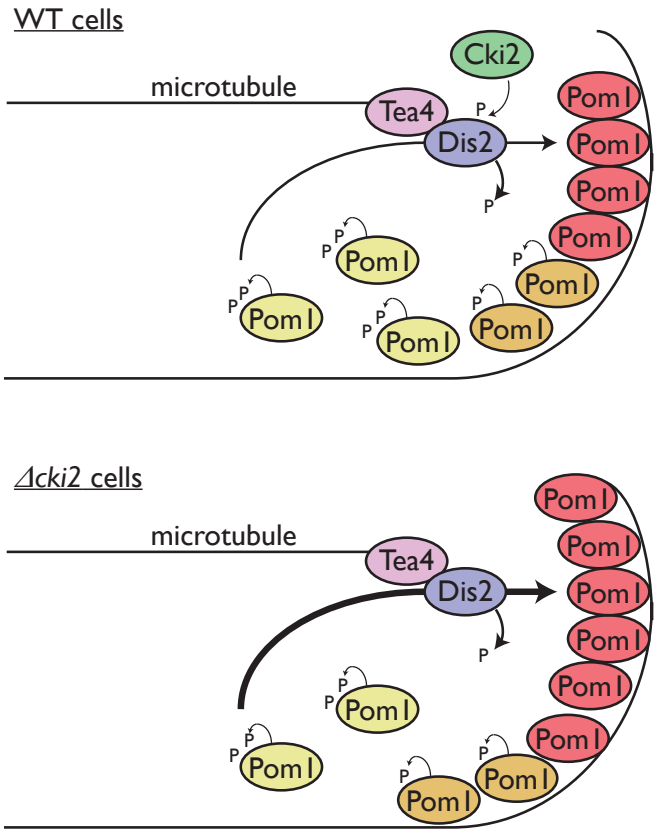

FIGURE 6.2: **A model for the modulation of intracellular Pom1 gradients.** Tea4 traffics Dis2 upto the cell tips via microtubules. Dephosphorylation of Pom1 is mediated via the phosphatase Dis2 and results in a strong membrane association. Autophosphorylation of Pom1 reduces its affinity for the cell membrane, which increase the probability of Pom1 detaching from the membrane. Cki2 may be acting, by phosphorylation of Dis2, to regulate Dis2's activity. Figure adapted from [309].

6.3.3 Cki3 is a negative regulator of the pheromone-response in *S. pombe*

A previous study has shown that deletion or overexpression of Cki3 exhibit no characteristic phenotypes during vegetative growth [273]. This thesis confirms that overexpression or deletion of Cki3 does not result in cell morphological defects however, an increase in cell area was observed with loss of Cki3 (Figure 4.2). This result could be an experimental outlier because a cell volume assay was also performed on these strains but did not exhibit a significant increase in cell volume.

The results indicate that loss of Cki3 increases P-factor-directed transcriptional and morphological responses. Specifically, an increase in cell volume (Figure 4.9 and 4.10) measured by a quantitative assay and hyper-elongated conjugation tubes determined visually from the microscopy analysis (Figure 4.8) were observed. The increase in transcriptional response and cell volume displayed by *Δcki3* cells is observed following 4 h of P-factor treatment (Figure 4.11 and Figure 4.13, respectively), suggesting that Cki3 may directly regulate the morphological and transcriptional response in *S. pombe*.

Ras1 mediates both the morphological and transcriptional pathway in response to P-factor. Therefore, Cki3 may act to regulate Ras1 activation or the components of the pathway directly upstream of Ras1. The YCK1 and YCK2 *S. cerevisiae* kinases were shown to phosphorylate STE2 (the pheromone GPCR) in response to α-factor, to promote its internalisation from the plasma membrane [112]. Cki3 is 67-69% homologous to YCK1 and YCK2 (Figure 4.1) and therefore, may perform a similar cellular role in *S. pombe*. Given Mam2 (the pheromone GPCR in *S. pombe*) acts upstream of Ras1 and that loss of Cki3 enhances signal propagation via Ras1, the data collected in this study may suggest that Cki3 is phosphorylating Mam2 to promote its internalisation.

6.3.4 Cki3 is required for the completion of cytokinesis, but only in *S. pombe* cells that have responded to P-factor

Loss of the negative regulators Rgs1 and Gap1 in *S. pombe* reduces the cells' ability to mate successfully [86, 87]. This study identified Cki3 as a negative regulator of signalling however, rather than exhibiting a reduction in successful mating events, loss of Cki3 shows an increase in CFU recovery/successful mating events (Figure 4.4).

Deletion of other proteins such as the cyclin Cig2 [311] and Cpc2 (the receptor for activated C kinase 1 (RACK1) orthologue) [221] have also been shown to exhibit an increase in

successful mating events. Interestingly, both Cig2 and Cpc2 proteins have been implicated in regulating cell cycle progression [312, 313]. It is clear that Cki3 also plays a role in cell cycle progression as septa were found in *Δcki3* cells following treatment with P-factor.

As previously discussed, during mitotic growth, *S. pombe* cells spatially sense their size through an intracellular gradient of Pom1 [302]. In response to P-factor, Cdc42 activation is enhanced and this is thought to override this sensing machinery and initiate elongation from a single tip forming conjugation tubes towards a mating partner [223]. Following prolonged (∼8 h) treatment with P-factor *S. pombe* cells can undertake two successive rounds of divisions and then continue to respond to P-factor forming conjugation tubes (W. Croft, Doctoral thesis). This novel mechanism of cell division in response to prolonged treatment suggests that either the gradient sensing machinery overrides the Cdc42 activation mechanism to promote cell division or another mechanism that has not yet been described initiates this cell division process.

The septa and multi-nucleated *Δcki3* cells observed in this study suggest that cells are able to complete anaphase B; the event of segregating nuclei into daughter cells, yet are unable to separate the daughter cells. Although strains lacking *cki3* are unable to complete cell separation, they still enter into additional rounds of division, as more than two septa were displayed in ∼50% of cells following 36 h of P-factor treatment. To further support the theory that Cki3 is involved in cell cycle progression, the dispersion of propidium iodide peaks, FCS and SSC scatter plots collected during this study all indicate that a sub-population of cells contain more than two complements of DNA.

The septa and multiple projection phenotype observed in *Δcki3* cells in response to P-factor are similar to those observed for the temperature-sensitive *YCK1* and *YCK2* mutant strain in *S. cerevisiae*. The double mutant cells yck^{ts} (*yck1-Δ1::ura3 yck2-2*^{ts}) are viable at the permissive temperature of 24 °C but become lethal at the restrictive temperature of 36 °C, which after several aberrant rounds of cell division form multiple elongated septated buds containing multiple nuclei [314, 315]. At the permissive temperature yck^{ts} cells grow and divide normally however, in response to pheromone cells become hyper-elongated and form conjugation tubes which display morphological abnormalities that become exaggerated over time, eventually resembling the morphologies of vegetative cells at at the restrictive temperature [316].

S. cerevisiae **a**-cells that have a reduction in YCK1 and YCK2 activity also exhibit elongated conjugation tubes in response to treatment with α-factor [316], similar to the loss of

Cki3 in *S. pombe* illustrated in this study. The localisation of YCK2 also changes throughout the cell cycle. YCK2 is situated at the growing tip during conjugation tube formation and vegetative growth, but is then positioned at the bud neck. This data suggested that YCK1 and YCK2 proteins are involved in cell polarity [316]. As cells lacking Cki3 exhibit similar behaviours to the YCK1 and YCK2 mutant cells this may suggest that Cki3 is also involved in cell polarity in *S. pombe*.

6.3.4.1 A potential role for Cki3 in regulating septins

To understand the relevance of the Cki3's potential role for regulating septin organisation during cytokinesis, an overview of the *S. pombe* cell cycle is described here. The onset of mitosis is characterised by a rearrangement of the actin cytoskeleton. F-actin patches delocalise from cell tips and reorganise in the centre by forming an actomyosin-based contractile ring overlying the nucleus. Once formed, four *S. pombe* septin proteins (Spn1, Spn2, Spn3 and Spn4) organise to the cell centre forming a septin ring adjacent to the actomyosin ring. Septins are conserved GTP-binding proteins that form hetero-oligomeric complexes, which assemble into higher-order structures, such as filaments and rings [317]. Septin complexes provide a scaffold to which many proteins bind (reviewed in [318]) and/or diffusion barriers to affect a range of cellular functions, including: cytokinesis, mitosis, exocytosis and apoptosis [319].

As the nuclei are segregated during anaphase B, the actomyosin ring constricts guiding the closure of the plasma membrane. Concomitant with this process, the primary septum flanked by two secondary septa develops behind the constricting ring, which splits the septin ring in two. The association of the septin ring with a protein Mid2, maintains the integrity and stability of the septin ring during the contractile ring closure [320]. Formation of the septin-Mid2 ring guides a multi-protein exocyst complex, which transports vesicles in a myosin V dependent-manner via actin cables to the cell centre [321]. The exocyst complex is thought to transport and secrete the enzymes Eng1 and Agn1, to cleave the primary septum and the cell wall [322], thereby separating the two daughter cells (reviewed by [323]).

Loss of any or all of the septins or Mid2 in *S. pombe* causes a chained cell phenotype [317, 320, 324, 325]. In *S. cerevisiae*, the septin CDC12 was mislocalised in yck^{ts} mutant cells [316], suggesting that YCK1 and YCK2 activity could regulate the site or process of assembling the septins at the bud neck. The *S. cerevisiae* mutant yck^{ts} and *Δcki3 S.*

pombe cells show a similar phenotypic behaviour in response to pheromone stimulation and therefore, Cki3 may function in a similar role in *S. pombe* by regulating septin assembly during the cell cycle.

In *S. cerevisiae* the septin ring is regulated via phosphorylation of the septins, by several protein kinases, including CDK1 and CLA4 [326, 327]. Specifically, loss of CLA4 resulted in elongated cells and mislocalisation of the septins to the cell tips rather than the bud neck [328]. This study also suggests that CLA4 is activated by CDC42, to phosphorylate the septins at the division site, stabilising the septin ring formation [328]. The CDK1 and CLA4 homologues in *S. pombe* are Cdr1 and Cdr2, however these proteins have not been shown to phosphorylate Spn1, Spn2, Spn3 or Spn4 [329] or have not been identified in influencing septin ring formation. The data collected in this study suggests that Cki3 kinase is required for cell division in response to P-factor. Given that CLA4 may be activated in a CDC42-dependent manner in *S. cerevisiae* and given that CDC42 is assumed to perform an equivalent role to Cdc42 in *S. pombe*, which is activated in response to P-factor, Cki3 activity could be enhanced by activation of Cdc42 and could be the kinase that phosphorylates the septins to promote their organisation during cytokinesis.

6.4 Cki1, Cki2 and Cki3 as potential targets for pheromone-induced internalisation of Mam2

Chapter 5 investigated and discussed the role of Cki1, Cki2 and Cki3 in the internalisation of Mam2. Microscopy analysis of mCherry-tagged Mam2 in combination with the QuimP software to allow the analysis of cortical fluorescence [231, 232] was employed to quantify the levels of plasma membrane localisation in strains lacking either Cki1, Cki2 and Cki3. Due to the weak plasma membrane expression levels of WT mCherry-tagged Mam2 the QuimP software was unable to segment the cell periphery. A receptor lacking all four lysines within the 45 residue C-terminal tail was created, which enhanced plasma membrane localisation as a result of preventing constitutive internalisation, yet still internalised in response to treatment with pheromone. The QuimP segmentation and fluorescence software was used to quantify plasma membrane fluorescence following treatment with P-factor in strains lacking Cki1, Cki2 and Cki3.

6.4.1 Sorting of Mam2 following its internalisation

Microscopy analysis of the GFP tagged truncated Mam2 receptors showed that the last five residues of Mam2 were not essential for constitutive and pheromone-induced internalisation, or subsequent trafficking of the receptor to the vacuoles, as the localisation of the receptor was indistinguishable from full length Mam2. The FM4-64 vacuole staining dye in combination with the loss of the five residues of GFP tagged Mam2 revealed two pockets of receptors: ones that were encased by the red dye indicating that these receptor were in the vacuoles and ones that were not encased by the dye. There are two possible explanations for these vesicles of receptors not encased by the vacuole dye. They could either be newly synthesised receptors that are being trafficked to the plasma membrane or they could have been recently endocytosed from the plasma membrane into the endosomes/MVBs and have yet to be trafficked to the vacuoles.

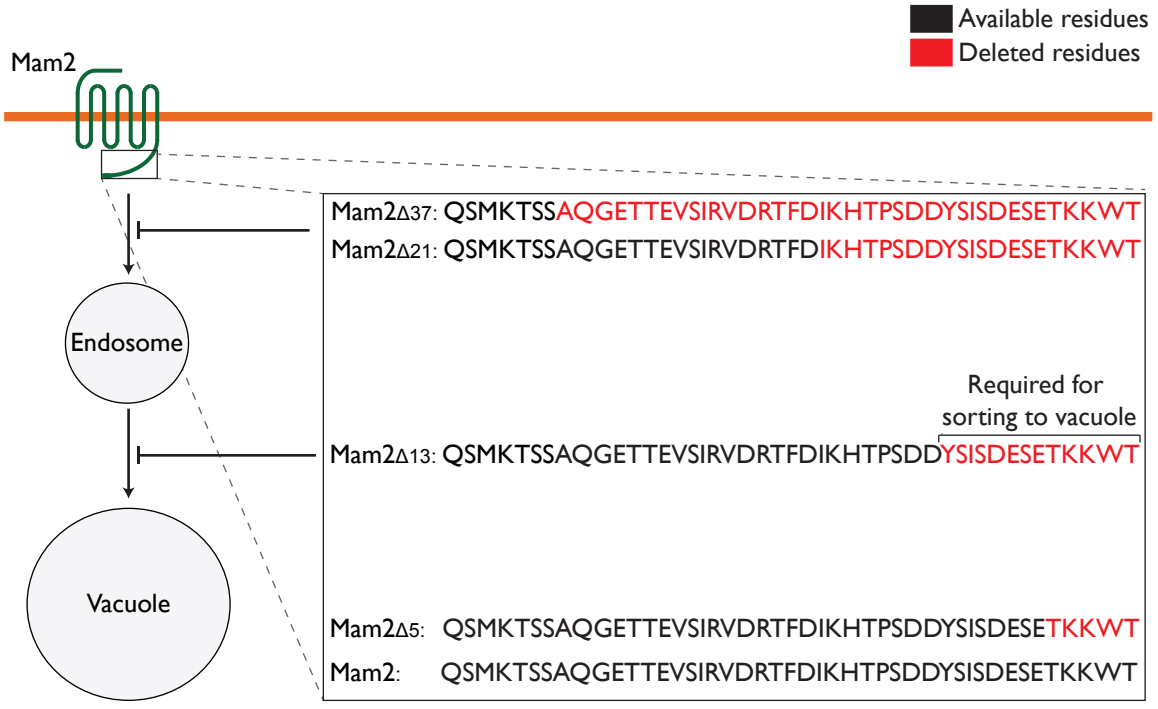

FIGURE 6.3: **Specific regions within the C-terminal domain of Mam2 control its internalisation and subsequent sorting.** A model that illustrates how truncation of specific regions of Mam2 alters its internalisation and subsequent trafficking to the vacuole.

Loss of the 13 residue sequence (YSISDESETKKWT) significantly reduced receptor

trafficking to the vacuoles and further truncation of the Mam2 removing 21 residues prevented receptor sorting into the vacuoles (Figure 6.3). Ubiquitination of lysine residues typically targets proteins to the vacuoles/lysosome as ESCRT proteins contain ubiquitin binding domains that recognise the ubiquitinated receptors and mediate there invagination into MVBs and transport to the vacuole [160]. Loss of the last 5-residues (TKKWT), which contain two (Lys345 and Lys346) of the four (Lys307, Lys329, Lys345 and Lys346) lysines within the C-terminal tail of Mam2, did not prevent sorting to the vacuole. This therefore suggests that specific residues within the 16-residue sequence IKHTPSDDYSISDESE (between the Δ21 and Δ5 Mam2 truncations) are essential for receptor vacuole localisation. Significantly, Lys329 is contained within the 16-residue sequence however, the lysine deficient mutant Mam2^{2K}-mCherry receptor where Lys307 and Lys329 are mutated to arginine but still contain intact Lys345 and Lys346 (from TKKWT Δ5) appeared to be trafficked to vacuoles following internalisation (Figure 5.15). This suggests that receptor sorting to the vacuole is not lysine specific, i.e. it does not matter which lysine residue is ubiquitinated to promote trafficking to the vacuole.

Mutation of the lysine residues (Lys307, Lys329, Lys345 and Lys346) prevents constitutive receptor internalisation, yet in response to P-factor the receptor is internalised and appears to be trafficked to the vacuole-like structures. Some GPCRs are sorted to the lysosome independently of ubiquitination. For example, the δ-opioid receptor (DOR) is trafficked to the lysosome in response to ligand-binding, like WT DOR even when all intracellular lysine residues are mutated to arginine [287].

The last 37-residues of Mam2 appear essential for constitutive internalisation, as the receptor was only observed at the plasma membrane (Figure 5.10). Whereas the last 37-residues of Mam2 did not appear essential for P-factor-induced Mam2 internalisation as the receptors were observed within the cytosol, in large structures positioned at the cell tips and within smaller spheres situated in close proximity to the cell periphery (Figure 5.11). This suggests that there are two distinct internalisation pathways within *S. pombe* **M**-type cells.

6.4.2 Two distinct receptor internalisation pathways in *S. pombe*

This study provides evidence that the receptor Mam2 can be internalised via two distinct pathways. The removal of all four lysine residues from the C-terminal domain of Mam2

(ubiquitination deficient receptor) prevented constitutive internalisation yet remained sensitive to ligand-induced internalisation. This is similar to observations made of STE3 (a pheromone GPCR) [289] but different to STE2 (another pheromone receptor) where ubiquitination is required for all internalisation mechanisms in *S. cerevisiae* [112]. This could suggest that the pheromone-induced endocytotic pathway in *S. pombe* may be a more representative pathway for studying the general principles of mammalian GPCR ligand-induced internalisation, as most mammalian GPCRs can be internalised via distinct pathways. Promoting pheromone-induced internalisation of Mam2, like mammalian cells and *S. cerevisiae* is most likely the result of phosphorylation of the intracellular regions of the GPCR following P-factor stimulation.

6.4.3 *S. pombe* cells elongate from both tips when expressing ubiquitination deficient Mam2

During mitotic growth, Cdc42 is activated in a Ras1-independent manner (via Gef1, a GEF [330]) and a Ras1-dependent manner (via Scd1). Following cell division, the daughter cells grow from the tip that existed prior separation (the 'old' tip). When a minimal size threshold is reached growth is initiated from the opposite tip and period of bipolar growth is established, a process termed new end take off (NETO). Gef1 establishes growth at the 'new' tip during NETO [330], potentially via regulation of myotonic dystrophy like-kinase Orb6 [331], which spatial maintains Gef1 at the cell tips. Scd1 and Cdc42 have been observed to have oscillatory behaviour during this period of bipolar growth [85]. Both Gef1 and Scd1 are recruited to the cell centre at the end of growth phase where Cdc42 activity then directs the formation of the actomyosin ring. P-factor stimulation is thought to seize control of this process, by increasing Ras1 activation and thus coordinating Cdc42 activation at a single tip.

In response to treatment with P-factor, some cells expressing the C-terminal tail lysine deficient Mam2 were shown to form conjugation tubes by initiating growth from both tips (section 5.5.5). The use of CRIB-GFP marker for Cdc42 activation showed that Cdc42 activation was present at both tips in these cells rather than at the single growing tip in typical *S. pombe* cells. Overexpression of Mam2 in *S. pombe* cells did not demonstrate a significant increase in the number of cells that elongate from both tips, whereas preventing constitutive internalisation promoted elongation from both tips. This suggests that it is the increase in receptor concentration at the membrane that causes Cdc42 activation at both

tips. This could be investigated further by analysing the percentage of cells that elongate from both tips when removing the C-terminal domain (45-residues) of Mam2.

6.4.4 Cki2 and Cki3 may both be required for Mam2 desensitisation

The results from Chapter 4 indicate that deletion of Cki3 enhances P-factor-directed signalling responses. One possible explanation for these results could be that when Cki3 is absent the receptor Mam2 remains active at the cell membrane for longer and thus protracts signalling response. If this was the case it would suggest that Cki3 may regulate the activity of Mam2 or its localisation in response to P-factor. The QuimP analysis performed on *Δcki3* strains in Chapter 5 revealed that rather than reducing receptor internalisation, removal of Cki3 actually enhanced the ability of the receptor to be removed from the plasma membrane. Interestingly, deletion of Cki2, which was shown to have no effect on signalling responses, significantly reduces the rate at which Mam2 was internalised from the plasma membrane. Perhaps unexpectedly suggesting that Cki2 rather than Cki3 may positively regulate the internalisation of Mam2 in response to treatment.

In *S. cerevisiae* both YCK1 and YCK2 are required to phosphorylate the C-terminal tail of STE2 (a pheromone GPCR) to promote endocytosis and in fact deletion of both kinases is lethal to the cell. A possible explanation for the results obtained in this study is that like in *S. cerevisiae*, perhaps Cki2 and Cki3 are both required for efficient Mam2 desensitisation in response to pheromone stimulation. Perhaps Cki3 is required to phosphorylate Mam2 to prevent further G protein activation, whilst Cki2 is required to initiate the internalisation of the receptor. The creation of a double deletion strain of Cki2 and Cki3 were attempted in this study however it was unsuccessful, perhaps as this double deletion may be lethal to *S. pombe*. To truly test this hypothesis a temperature sensitive mutant with Cki2 and Cki3 strains should be created and the localisation and internalisation of the receptor could be investigated.

Another possible explanation that has not yet been considered for why deletion of Cki2 reduces Mam2 internalisation is that perhaps following internalisation, the receptor it is being increasingly recycled back to the plasma membrane. Perhaps phosphorylation of the receptor or the internalisation machinery by Cki2 is necessary for an interaction with another protein of the degradation pathway. Hence when Cki2 is unavailable the receptor is not being trafficked into the degradation pathway and hence is being recycle back to the plasma membrane. Recycling of yeast GPCRs has not yet been described, but this could

still be occurring. In addition, Cki2 could have a role in the secretory pathway of newly synthesis Mam2 and that perhaps when Cki2 is removed this enhances receptor trafficking to the membrane.

6.5 Limitations and Future work

This work investigates three potential candidates for promoting receptor internalisation. Our analysis has revealed that Cki2 may play a role in pheromone-induced Mam2 internalisation. However, these findings are not conclusive and further work needs to be undertaken to clarify whether Cki1, Cki2 and/or Cki3 promote pheromone-induced desensitisation of Mam2. Future study could explore the use of mass-spectrometry to identify whether loss of Cki1, Cki2 or Cki3 would alter the amount of Mam2 phosphorylation in response to P-factor. In addition, the use of two-dimensional gel electrophoresis can be used to identify different phosphorylation states of Mam2. Furthermore, quantitative Western blotting could be used to clarify whether Cki1, Cki2 and Cki3 would affect receptor internalisation from the plasma membrane. The QuimP analysis does not take into account the production of trafficking of newly synthesised receptors to the plasma membrane, therefore more QuimP analysis should be performed using cycloheximide to inhibit new receptor synthesis.

This study identified novel roles of Cki1, Cki2 and Cki3 in the pheromone-response pathway of *S. pombe*. It has demonstrated that deletion of Cki3 has severe affects on cell morphology and for the first time has implicated Cki3 in regulating cell cycle progression. The morphologies displayed in Cki3 disrupted cells are similar to those observed upon deletion of YCK2 from *S. cerevisiae*, which show a displacement of septin CDC12 localisation during cell division [316]. Further investigation into the role of Cki3 in cell cycle progression and an investigation into its potential role in regulating septin localisation during cell division should be performed. The use of fluorescently tagged septin in Cki3 disrupted strains would aid this investigation.

6.6 Advances and conclusions

Many challenges remain in understanding GPCR signal transduction and desensitisation and specifically the role of casein kinases in promoting internalisation, ubiquitination and GPCR sorting following internalisation both in general and in the mating-response pathway in *S. pombe*. This project has advanced the pre-existing mathematical models of the

S. pombe pheromone-response to include all downstream components and regulatory mechanisms of GPCR signalling in *S. pombe*.

Novel roles for Cki1, Cki2 and Cki3 were identified in regulating the pheromone-response in *S. pombe*, specifically with regard to Cki3 in regulating cell cycle progression and Cki2 was shown to promote ligand induced internalisation in response to P-factor.

Appendix A

DNA construct design

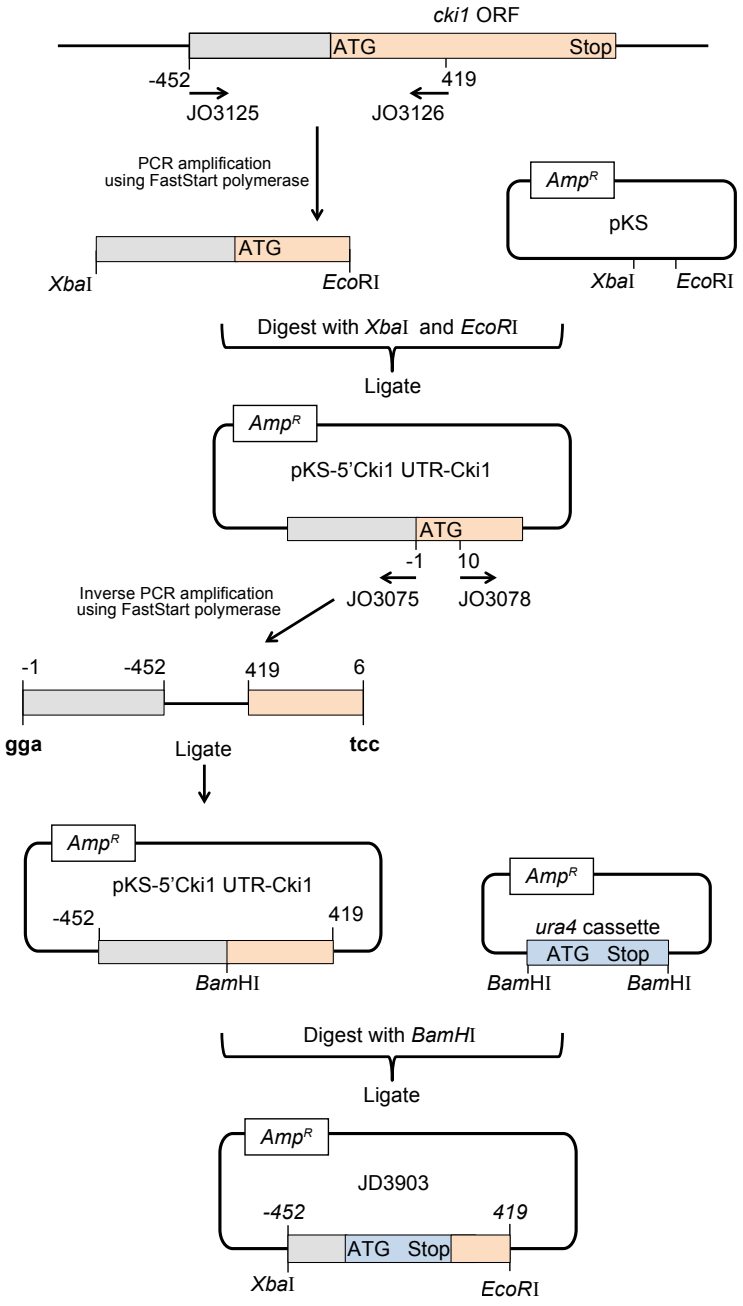

Oligonucleotide	Sequence
JO3125	ggg**tctaga**GACTGCAAAATGATTCTATTATTTAAGAATGCACCTTGCATATG
JO3126	ccc**gaattc**GCCAAAGTCTACTACGTAGATCATATTAGCATTTTTACTGTTTGG
JO3075	**tcc**TATCTTTGAACGATTTGTGCTGGAGATTTGTC
JO3078	**tcc**CAAAACAATGTAGTCGGTGTCCACTACAAAGTTGGAAGAAGAATTGGCG

Figure A.1: **Construction of *cki1::ura4*$_+$ disruption cassette.** To drive integration of the *ura4* cassette into the first 9 bp region of the *cki1* ORF (from position 1 from the ATG) a 452 bp fragment containing the 5' UTR and the first 419 bp of the *cki1* ORF was amplified to introduce *Xba*I and *Eco*RI restriction sites. The PCR product was ligated into the pKS vector (JD1776) and inverse PCR performed to introduce a *Bam*HI site allowing insertion of the *ura4* cassette to produce JD3903. An *Xba*I/*Eco*RI digest releases a fragment suitable to generate *cki1::ura4* strains through homologous recombination. Restriction sites within oligonucleotides are highlighted in bold and non-endogenous bases are denoted in lower case.

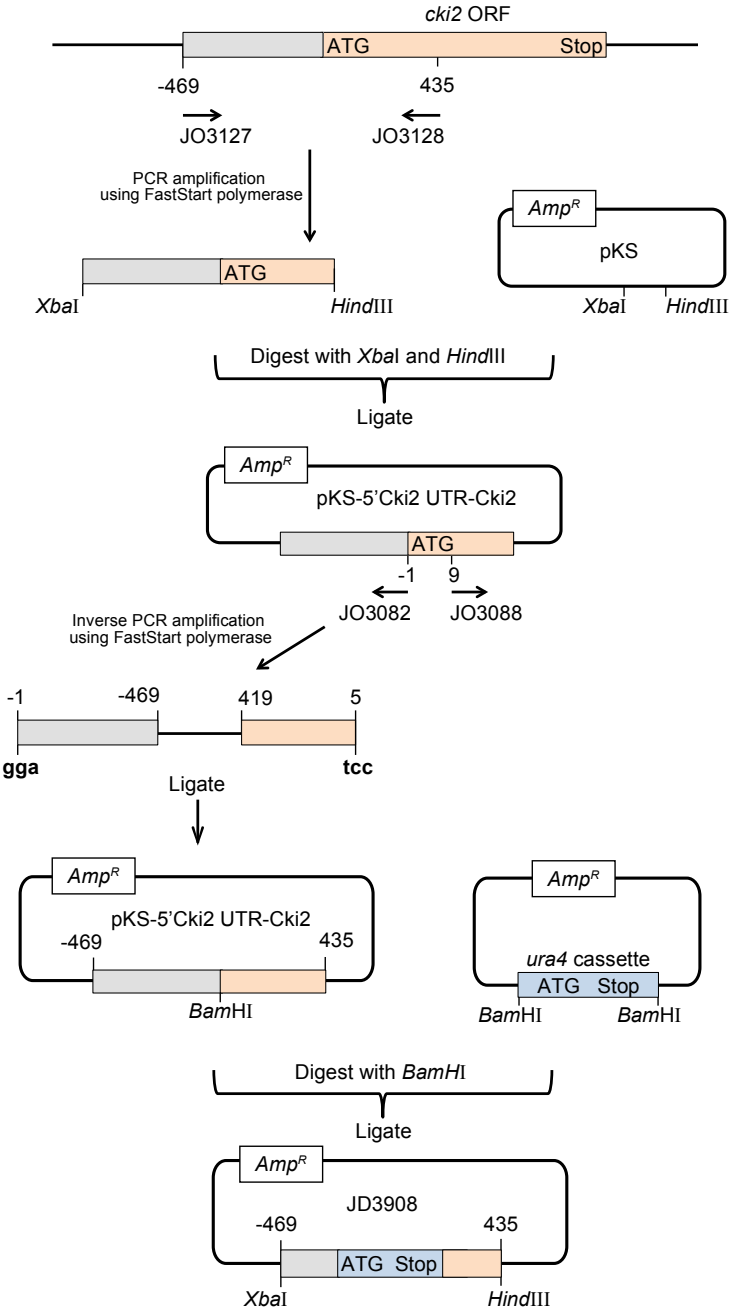

Oligonucleotide	Sequence
JO3127	ggg**tctaga**GTTTGTATAATCTATCGTATAGCCTCAGCTCCGACAACTCCGTTTTTACGATGG
JO3128	ccc**aagctt**CCTTATAGGAACAACTTAGGAAACTTACCATCTGTTTCGCCGTCATAGCCACC
JO3082	**tcc**CCAAACGAGCGTAGTAGGGGTTCACTATCGCGTGGG
JO3088	**tcc**GATAAATAACCCTGTCACAAGGAATTGACCG

Figure A.2: **Construction of *cki2::ura4* disruption cassette.** To drive integration of the *ura4* cassette into the first 8 bp region of the *cki2* ORF (from position 1 from the ATG) a 904 bp fragment containing a 469 bp 5' UTR and 435 bp of the *cki2* ORF was amplified to introduce *Xba*I and *Hind*III restriction sites. The PCR product was ligated into pKS vector (JD1776) and inverse PCR performed to introduce a *Bam*HI site allowing insertion of the *ura4* cassette to produce JD3808. *Xba*I/*Hind*III digest releases a fragment suitable to generate *cki2::ura4* strains through homologous recombination. Restriction sites within oligonucleotides are highlighted in bold and non-endogenous bases are denoted in lower case.

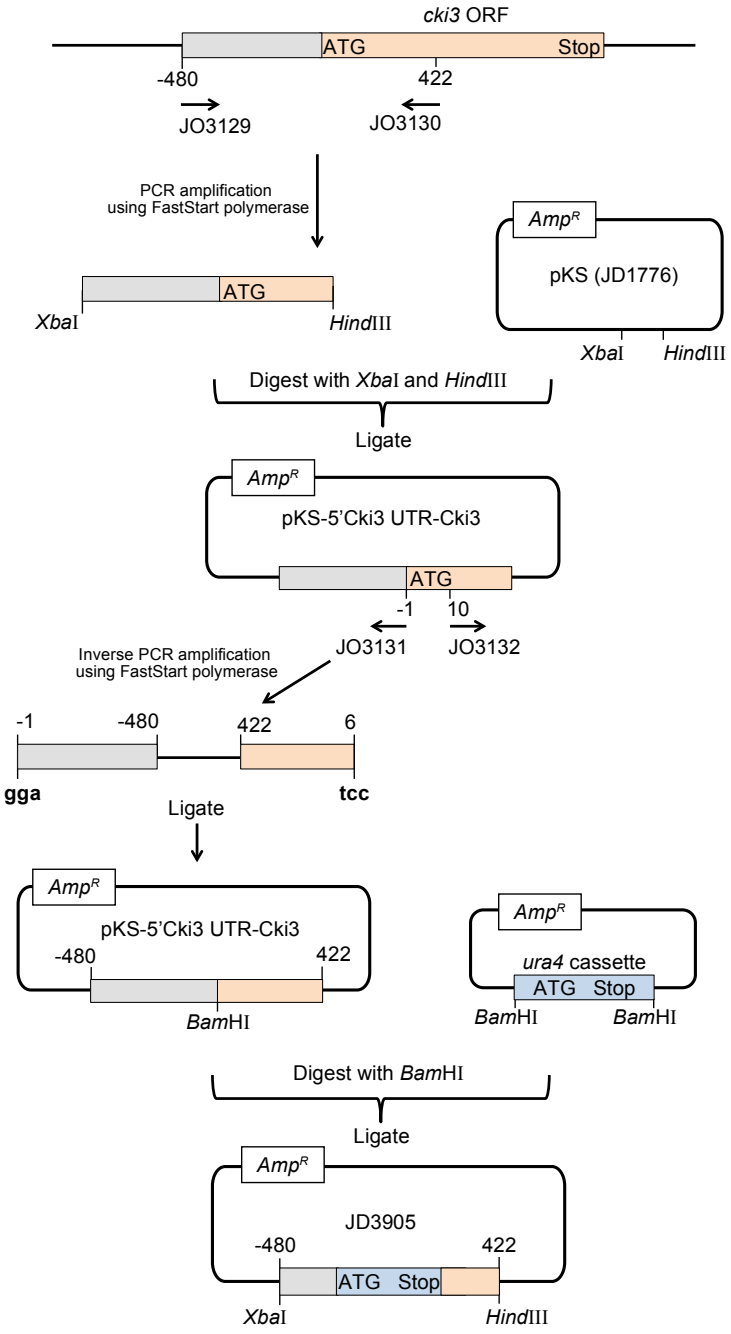

Oligonucleotide	Sequence
JO3129	ggg**tctaga**ACTTGCTATATTAGTATGTGTTTAAGTTGCGATACGATTTAACCTTTATCTTAATC
JO3130	ccc**aagctt**GCAATCATGGCAACGGTTTTAGGACTAAAACGTCTGCCACAATAATC
JO3032	**tcc**CTTCGTCTCACTCCAACGTCGTTGGTGTTCATTACCG
JO3031	**tcc**GATGGTCTTTTAAATATTCCACTATGTTAAATGC

Figure A.3: **Construction of *cki3::ura4* disruption cassette.** To drive integration of the *ura4* cassette into the first 9 bp region of the *cki3* ORF (from position 1 from the ATG), a 902 bp fragment containing 480 bp of the 5' UTR and 422 bp of the *cki3* ORF was amplified to introduce *Xba*I and *Hind*III restriction sites. The PCR product was ligated into pKS vector (JD1776) and inverse PCR performed to introduce a *Bam*HI site allowing insertion of the *ura4* cassette to produce JD3905. *Xba*I/*Hind*III digest releases a fragment suitable to generate *cki3::ura4* strains through homologous recombination. Restriction sites within oligonucleotides are highlighted in bold and non-endogenous bases are denoted in lower case.

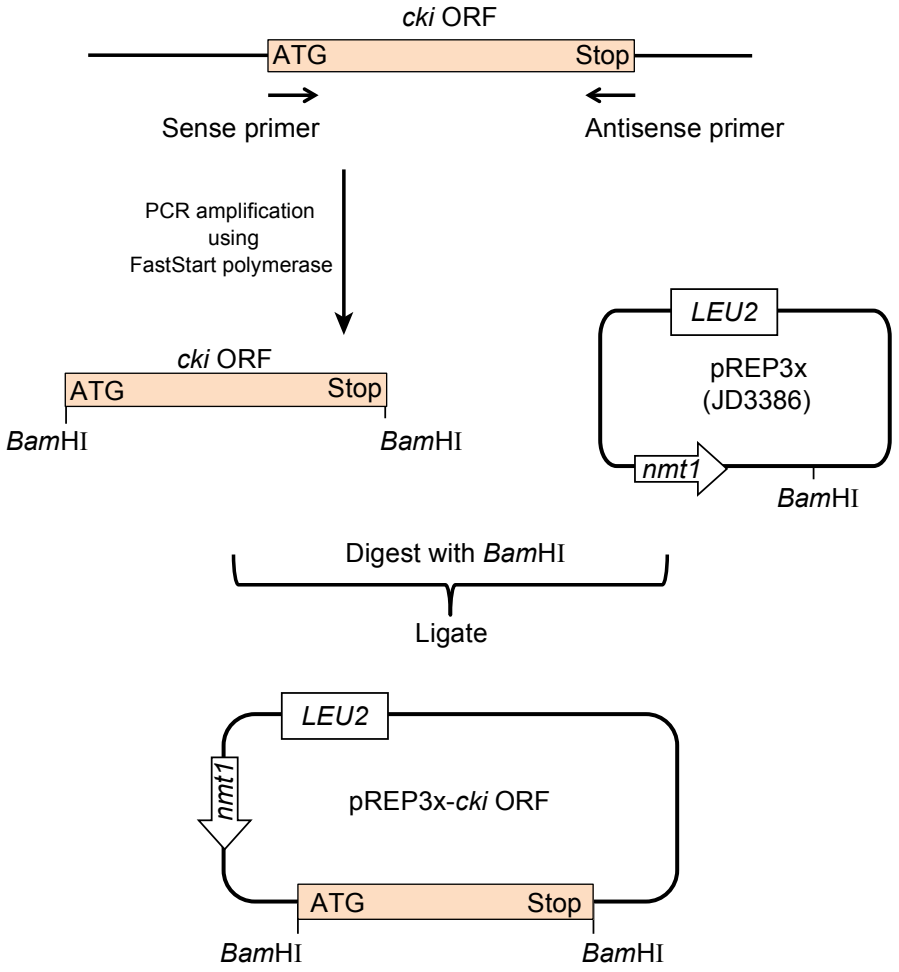

cki ORF	Sense oligonucleotide	Antisense oligonucleotide
*cki*1	gg**ggatcc**ATGAGTGGACAAAACAATGTAGTCGGT	gg**ggatcc**TCATGTGTCTTCATTGGAGCCA
cki2	gg**ggatcc**ATGAATTCCCAAACGAGCGTAGTA	gg**ggatcc**CTAAGAAAAGCAACGACAGCATATCATATC
cki3	gg**ggatcc**ATGTCAACTACTTCGTCTCACTCC	gg**ggatcc**CTATTCTTGTTTCGATATGCAGCAAGAC

Figure A.4: **Cloning of Cki1, Cki2 and Cki3 ORFs into pREP3x.** The Cki1, Cki2 and Cki2 ORFs were amplified on a cDNA library using the oligonucleotides listed. This introduced a *Bam*HI site at either end of the PCR product, which along with pREP3x (JD3386) vector were digested with *Bam*HI and ligated to create pREP3x-Cki1 (JD3893), pREP3x-Cki2 (JD3766) and pREP3x-Cki3 (JD3782). Restriction sites within oligonucleotides are highlighted in bold and non-endogenous bases are denoted in lower case.

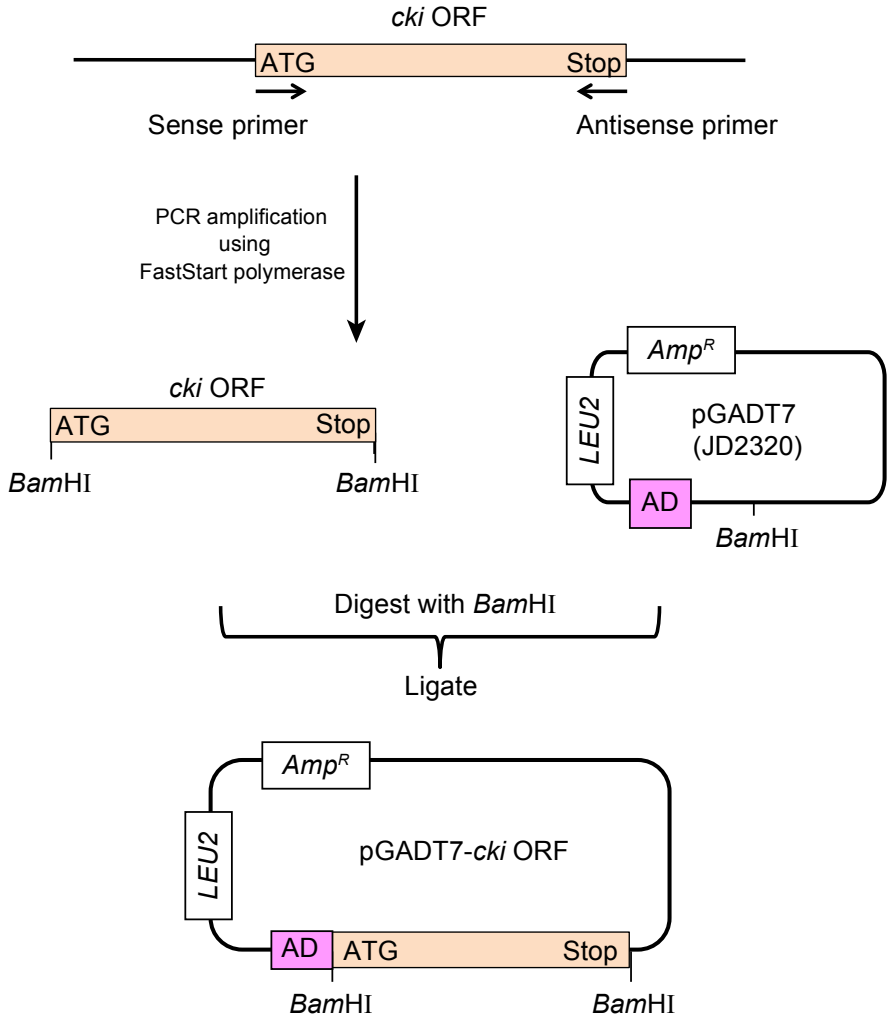

cki ORF	Sense oligonucleotide	Antisense oligonucleotide
*cki*1	gg**ggatcc**ATGAGTGGACAAAACAATG TAGTCGGT	gg**ggatcc**TCATGTGTCTTCATTGGAG CCA
cki2	gg**ggatcc**ATGAATTCCCAAACGAGCG TAGTA	gg**ggatcc**CTAAGAAAAGCAACGACAG CATATCATATC
cki3	gg**ggatcc**ATGTCAACTACTTCGTCTC ACTCC	gg**ggatcc**CTATTCTTGTTTCGATATGC AGCAAGAC

Figure A.5: **Cloning of Cki1, Cki2 and Cki3 ORFs into pGADT7.** The *cki* ORFs were amplified using a cDNA library using the oligonucleotides listed. This introduced a *Bam*HI site at either end of the PCR product, which along with the pGADT7 (JD2320) vector were digested with *Bam*HI and ligated to create pGADT7-Cki1 (JD3770), pGADT7-Cki2 (JD3771) and pGADT7-Cki3 (JD3763). Restriction sites within oligonucleotides are highlighted in bold and non-endogenous bases are denoted in lower case.

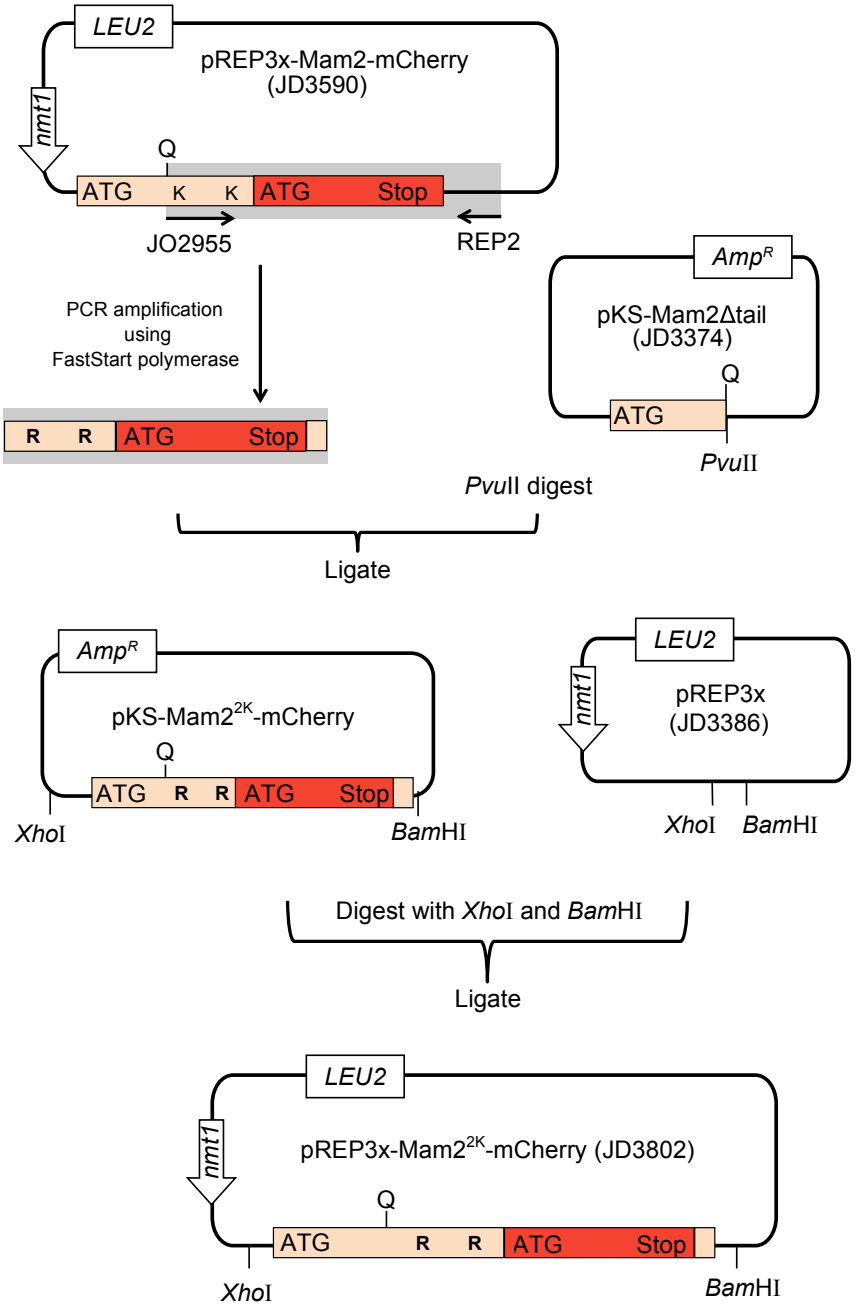

Oligonucleotide	Sequence
JO2955	CAAAGCATG**AgA**ACTTCATCTGCGCAAGGAGAAACCACCGAGGTTTCGA
	TTAGAGTTGATAGAACGTTTGATATC**AgA**CATACT
REP2	GCAGCTTGAATGGGCTTCC

Figure A.6: **Creation of pREP3x-Mam2^{2K}-mCherry.** Mam2 tagged mCherry was amplified from pREP3x-Mam2-mCherry (JD3590) using a mutagenic sense oligonucleotide and an antisense oligonucleotide (REP2) (grey region). This introduced a mutation at the 307^{th} and 329^{th} codons of Mam2 changing a lysine (AAA) to arginine (AgA). The product was ligated into *Pvu*II digested pKS-Mam2Δtail and the small fragment produced from a *Xho*I/*Bam*HI digest was ligated into *Xho*I/*Bam*HI digested pREP3x (JD3386) to produce pREP3x-Mam2^{2K}-mCherry (JD3802). Codon mutations are highlighted in bold and non-endogenous bases are denoted in lower case.

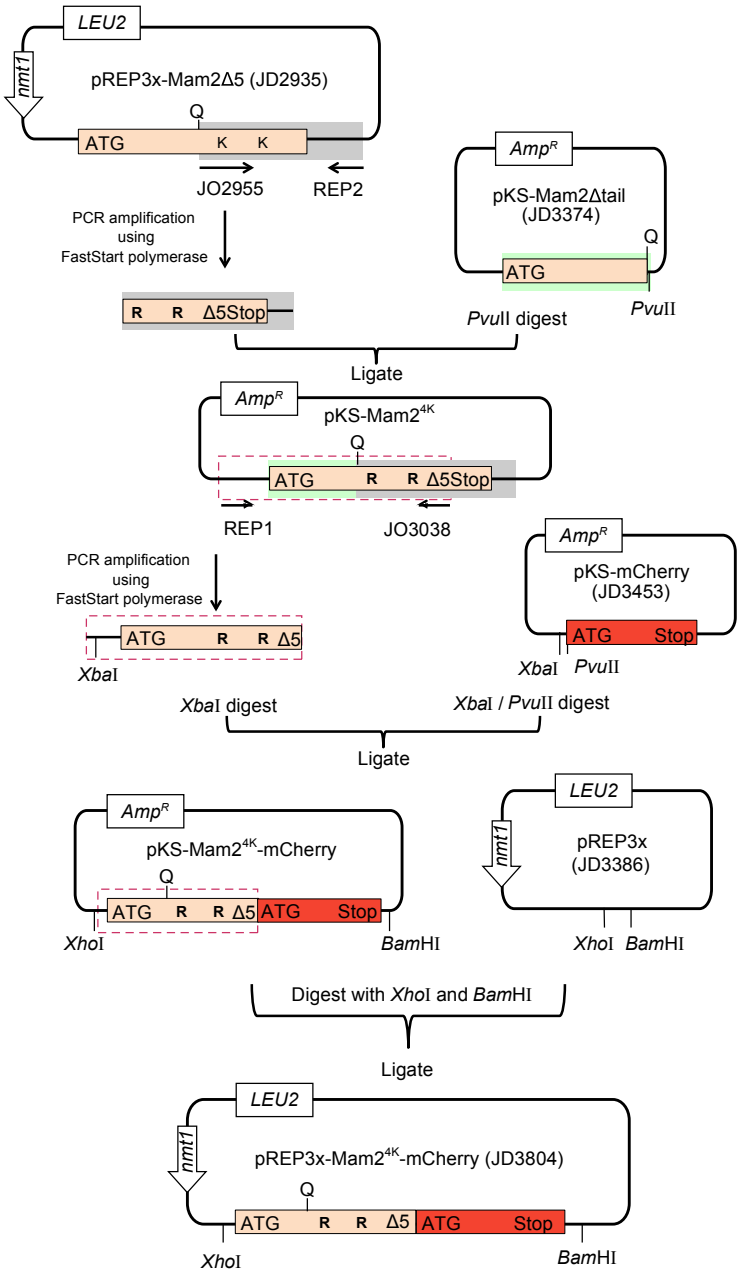

Oligonucleotide	Sequence
JO2955	CAAAGCATG**Ag**A**A**CTTCATCTGCGCAAGGAGAAACCACCGAGGTTTCGATT AGAGTTGATAGAACGTTTGATATC**Ag**A**A**CATACT
REP2	GCAGCTTGAATGGGCTTCC
REP1	ATCCGATTGTCATTCGGC
JO3038	TTCAGATTCATCAGAAATCG

Figure A.7: **Creation of Mam2^{4K}-mCherry.** The Mam2Δ5-tail was amplified using a mutagenic sense (JO2955, initiated directly downstream of the Glutamate (Q) codon, introducing a mutation at the 307^{th} and 329^{th} codons of Mam2) and antisense (REP2) oligonucleotide and the product was ligated into *Pvu*II digested pKs-Mam2Δtail. The stop codon was removed through amplification of the resulting vector (pKS-Mam2^{4K}) with sense (REP1) and antisense (JO3038) oligonucleotides. The product was digested with *Xba*I and ligated into *Xba*I/*Pvu*II digested pKS-mCherry. Finally, the small fragment produced from *Xho*I/*Bam*HI digested pKS-Mam2^{4K}-mCherry was ligated into *Xho*I/*Bam*HI digested pREP3x. Codon mutations are highlighted in bold and non-endogenous bases are denoted in lower case.

Appendix B

Model reaction schemes developed in Chapter 3

Species	Initial concentration (nM)
L	0 - 100,000
R	205
GαGDP	205
G$\beta\gamma$	205
RGSc	60
Gef	205
RasGDP	205
Gap	205
All other species were set to 0 nM	

Table B.1: **Initial concentrations for species in the Ras model.** For simulation of WT cells when simulated with the Ras model from Table B.2.

Ligand / G protein signalling			
L + R → LR	k_1	0.0025	$nM^{-1}h^{-1}$
G$\alpha\beta\gamma$ + R → RG$\alpha\beta\gamma$	k_2	0.005	$nM^{-1}h^{-1}$
G$\alpha\beta\gamma$ + LR → LRG$\alpha\beta\gamma$	k_3	0.02	$nM^{-1}h^{-1}$
L + RG$\alpha\beta\gamma$ → LRG$\alpha\beta\gamma$	k_4	0.005	$nM^{-1}h^{-1}$
L + RRGSm → LRRGSm	k_5	0.005	$nM^{-1}h^{-1}$
G$\alpha\beta\gamma$ + RRGSm → RRGSmG$\alpha\beta\gamma$	k_6	0.005	$nM^{-1}h^{-1}$
G$\alpha\beta\gamma$ + LRRGSm → LRRGSmG$\alpha\beta\gamma$	k_7	0.02	$nM^{-1}h^{-1}$
L + RRGSmG$\alpha\beta\gamma$ → LRRGSmG$\alpha\beta\gamma$	k_8	0.005	$nM^{-1}h^{-1}$
G protein activation			
LRG$\alpha\beta\gamma$ → GαGTP + G$\beta\gamma$ + LR	k_9	50	h^{-1}
G$\alpha\beta\gamma$ → GαGTP + G$\beta\gamma$	k_{10}	0.2	h^{-1}
LRRGSmG$\alpha\beta\gamma$ → GαGTP + G$\beta\gamma$ + LRRGSm	k_{11}	40	h^{-1}
RGS trafficking			
RRGSc → RRGSm	k_{12}	0.0005	h^{-1}
RRGSm → RRGSc	k_{13}	0.005	h^{-1}
R + RRGSc → RRGSm	k_{14}	0.1	$nM^{-1}h^{-1}$
RRGSm → R + RRGSm	k_{15}	100	h^{-1}
LR + RRGSc → LRRGSm	k_{16}	0.1	$nM^{-1}h^{-1}$
LRRGSm → LR + RRGSm	k_{17}	100	h^{-1}
RG$\alpha\beta\gamma$ + RRGSc → RRGSmG$\alpha\beta\gamma$	k_{18}	0.1	$nM^{-1}h^{-1}$
RRGSmG$\alpha\beta\gamma$ → RG$\alpha\beta\gamma$ + RRGSm	k_{19}	0.1	h^{-1}
LRG$\alpha\beta\gamma$ + RRGSc → LRRGSmG$\alpha\beta\gamma$	k_{20}	0.1	$nM^{-1}h^{-1}$
GαGTP + RRGSc → RRGSmGαGTP	k_{21}	60	$nM^{-1}h^{-1}$
RRGSmGαGTP → GαGTP + RRGSc	k_{22}	0.05	h^{-1}
Switching off / recycling G protein			
GαGTP → GαGDP	k_{23}	0.005	h^{-1}
GαGTP + RRGSm → RRGSmGαGTP	k_{24}	500	$nM^{-1}h^{-1}$
RRGSmGαGTP → GαGDPP + RRGSc	k_{25}	2.5	h^{-1}
GαGTP + LRRGSm → LRRGSmGαGTP	k_{26}	100	$nM^{-1}h^{-1}$
LRRGSmGαGTP → GαGDPP + LRRGSm	k_{27}	2.5	h^{-1}
GαGTP + RRGSm → RRGSmGαGTP	k_{28}	0.5	$nM^{-1}h^{-1}$
RRGSmGαGTP → GαGDPP + RRGSm	k_{29}	0.5	h^{-1}
GαGDPP → GαGDP + P	k_{30}	1000	h^{-1}
GαGDP + G$\beta\gamma$ → G$\alpha\beta\gamma$	k_{31}	1000	$nM^{-1}h^{-1}$
P → ∅	k_{32}	10	h^{-1}
RAS activation			
GEF + GαGTP → GαGTPGEF	k_{33}	13	$nM^{-1}h^{-1}$
GαGTPGEF + RASGDP → inertGαGTPGEFRASGTP	k_{41}	50	$nM^{-1}h^{-1}$
inertGαGTPGEFRASGTP → inertGαGTPGEF + RASGTP	k_{42}	4	h^{-1}
GαGTP + RASGDP → GαGTP + RASGTP	k_{50}	0.00034	$nM^{-1}h^{-1}$
Recycling of G protein / GEF complex			
inertGαGTPGEF + RRGSc → RRGSminertGαGTPGEF	k_{34}	0.0001	$nM^{-1}h^{-1}$
inertGαGTPGEF → GαGDPP + GEF	k_{36}	0.005	h^{-1}
inertGαGTPGEF + RRGSm → RRGSminertGαGTPGEF	k_{37}	0.3	$nM^{-1}h^{-1}$
RRGSminertGαGTPGEF → RGαGDPP + RRGSc + GEF	k_{38}	0.3	h^{-1}
inertGαGTPGEF + LRRGSm → LRRGSminertGαGTPGEF	k_{39}	50	$nM^{-1}h^{-1}$
LRRGSm inertGαGTPGEF → GαGDPP + LRRGSm + GEF	k_{40}	0.3	h^{-1}
Regulation of RAS by GAP			
RASGTP + GAP → RASGTPGAP	k_{44}	4.2	$nM^{-1}h^{-1}$
RASGTPGAP → RASGDPP + GAP	k_{45}	8	h^{-1}
RASGTP → RASGDPP	k_{48}	10	h^{-1}
RASGDPP → RASGDP + P	k_{49}	1000	h^{-1}

Table B.2: **RAS model.** Includes reactions for activation of RAS via GEF and GαGTP, and regulation of RAS by GAP. to be simulated with initial conditions displayed in Table B.1.

Appendix C

Validation of the KR model

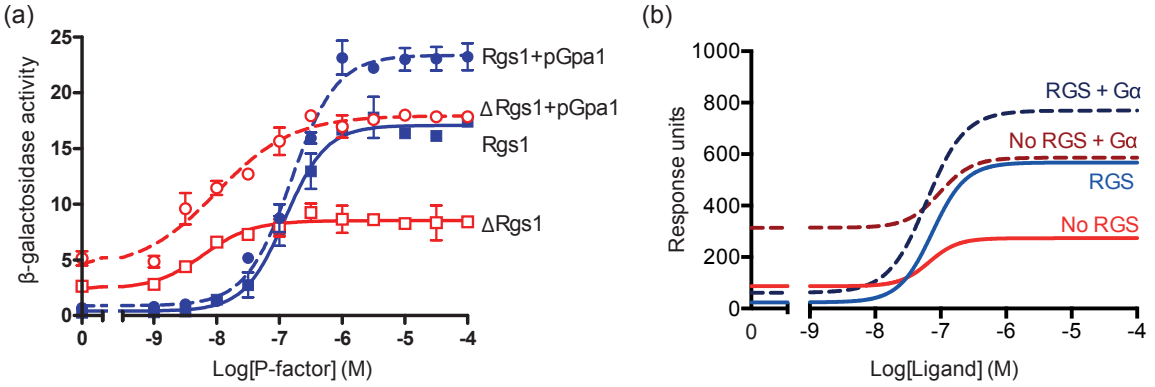

FIGURE C.1: **Model testing: Dependence on Gpa1 concentration.** (a) The WT strain was transformed with pREP3x (JD3386) and pREP3x-Gpa1 (JD2332) to create Rgs1 and Rgs1+pGpa1, respectively. Also, the *Δrgs1* (JY630) strain was transformed with pREP3x (JD3386) and pREP3x-Gpa1 (JD2332) to create *Δ*Rgs1 and *Δ*Rgs1+pGpa1 respectively. Cells were grown to mid-exponential growth phasebefore treatment with a range of P-factor concentrations (from 0 µM to 100 µM). After 16 h cells were assayed for β-galactosidaseactivity (as described in section 2.2.8.1). Data shown is the average of three independent experiments ±SEM. Data adapted from Smith *et al.* (2009) [190]. (b) The equivalent *in silico* experiment was simulated using the KR model (Table 3.9). Simulations are of an unmodified system (RGS), when Gα concentration is doubled to 410 nM (RGS+Gα), when the concentration of RGS is 0 nM (No RGS) and simulating a system when the concentration of RGS=0 nM and the concentration of Gα was doubled to 420 nM (No RGS+Gα). The concentration of ligand was varied over the range 0 to 100 µM following 16 h simulated induction. Output from the model shows the accumulation Spk1P complexes over the duration of the simulated assay.

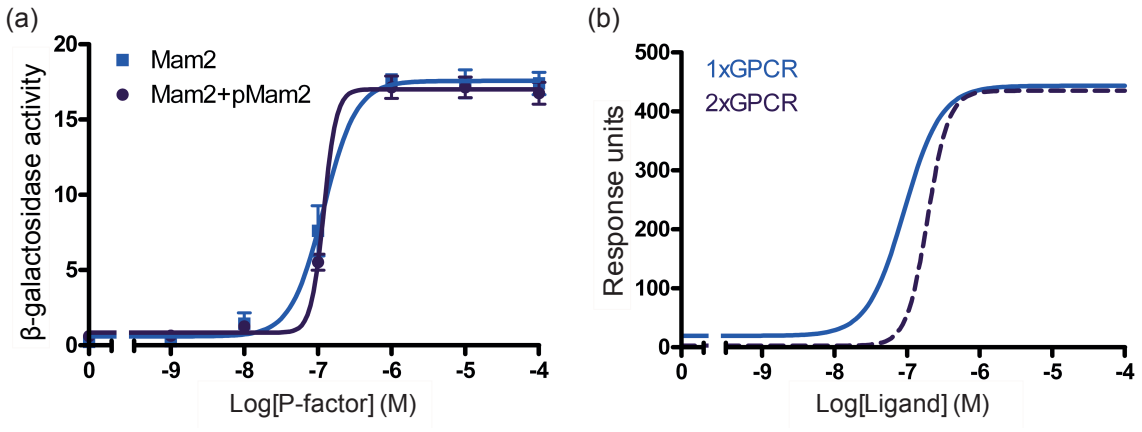

FIGURE C.2: **Model testing: Overexpression of Mam2.** (a) The WT strain (JY544), which contains endogenous Mam2 was transformed with pREP3x (JD3386) and pREP3x-Mam2 (JD2880) to create Mam2 and Mam2+pMam2 respectively. Cells were grown to mid-exponential growth phasebefore treatment with a range of P-factor concentrations (from 0 µM to 100 µM). After 16 h cells were assayed for β-galactosidaseactivity (as described in section 2.2.8.1). Data shown is the average of three independent experiments ±SEM. Data was adapted from W. Croft, PhD thesis, 2012. (b) The equivalent *in silico* experiment was simulated using the KR model (Table 3.9). Simulations are of an unmodified system (1xGPCR) and a system initialised with double the concentration of receptor (2xGPCR). The concentration of ligand was varied over the range 0 to 100 µM following 16 h simulated induction. Output from the model shows the accumulation Spk1P complexes over the duration of the simulated assay.

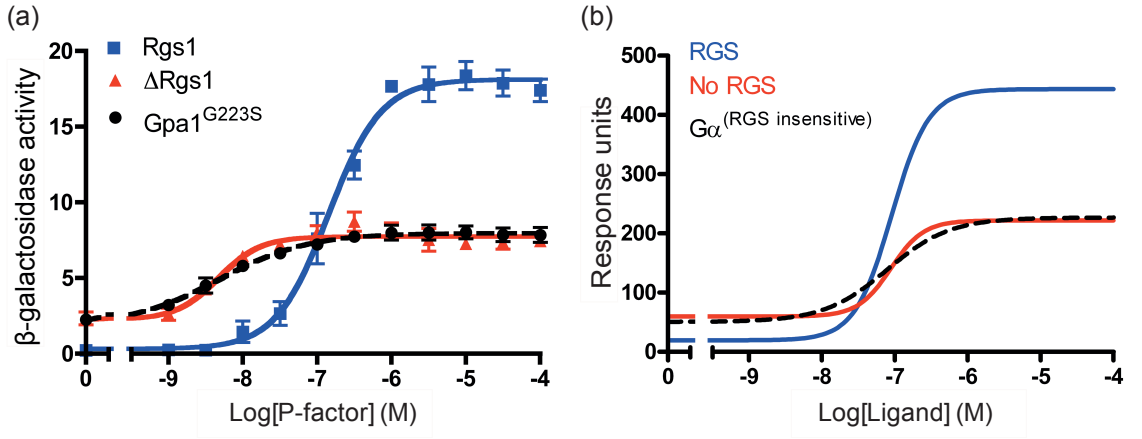

FIGURE C.3: **Model testing: Overexpression of Mam2.** ((a) WT (JY544), which contains endogenous Rgs1 (Rgs1), *Δrgs1* strain (JY630), which lacks endogenous Rgs1 (ΔRgs1) and *Δgpa1* (JY1285) transformed with pREP3x-Gpa1^{G223S} (JD2673) (Gpa1^{G223S}) were grown to mid-exponential growth phasebefore treatment with a range of P-factor concentrations (from 0 µM to 100 µM). After 16 h cells were assayed for β-galactosidaseactivity (as described in section 2.2.8.1). Data shown is the average of three independent experiments ±SEM. Data was adapted from Smith *et al.* (2009) [190]. (b) The equivalent *in silico* experiment was simulated using the KR model (Table 3.9). Simulations are of an unmodified system (RGS), a system initialised with the concentration of RGS=0nM (No RGS) and a system where all Gα-RGS interactions are blocked (Gα^{RGSinsensitive}). The concentration of ligand was varied over the range 0 µM to 100 µM following 16 h simulated induction. Output from the model shows the accumulation Spk1P complexes over the duration of the simulated assay.

Appendix D

Mam2 is essential for pheromone-induced signalling

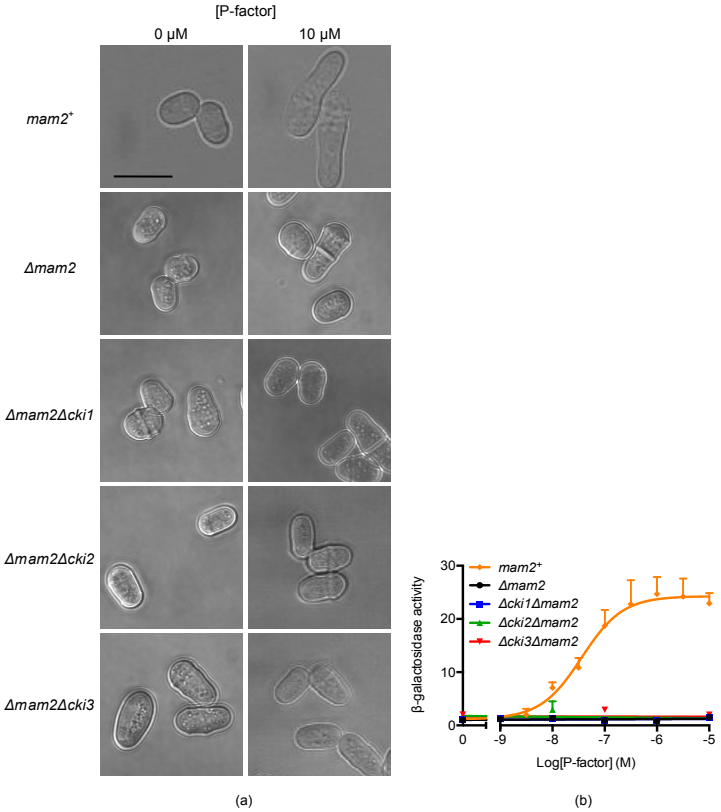

FIGURE D.1: **Mam2 is essential for P-factor induced transcriptional response and cell elongation.** WT (*mam2*$^{+}$, JY544), *Δmam2* (JY1169), *Δcki1Δmam2* (JY1727), *Δcki2Δmam2* (JY1734) and *Δcki3Δmam2* (JY1720) strains were grown to mid-exponential growth phasebefore treatment with a range of P-factor concentrations (from 0 µM to 100 µM). After 16 h cells (a) treated with 0 µM and 10 µM P-factor were imaged under brightfield light as described in section 2.2.14 and (b) assayed for β-galactosidase activity as detailed in section 2.2.8.1. Scale bar represents 10 µm. Data shown is the average of three independent experiments ±SEM.

Appendix E

QuimP internalisation data

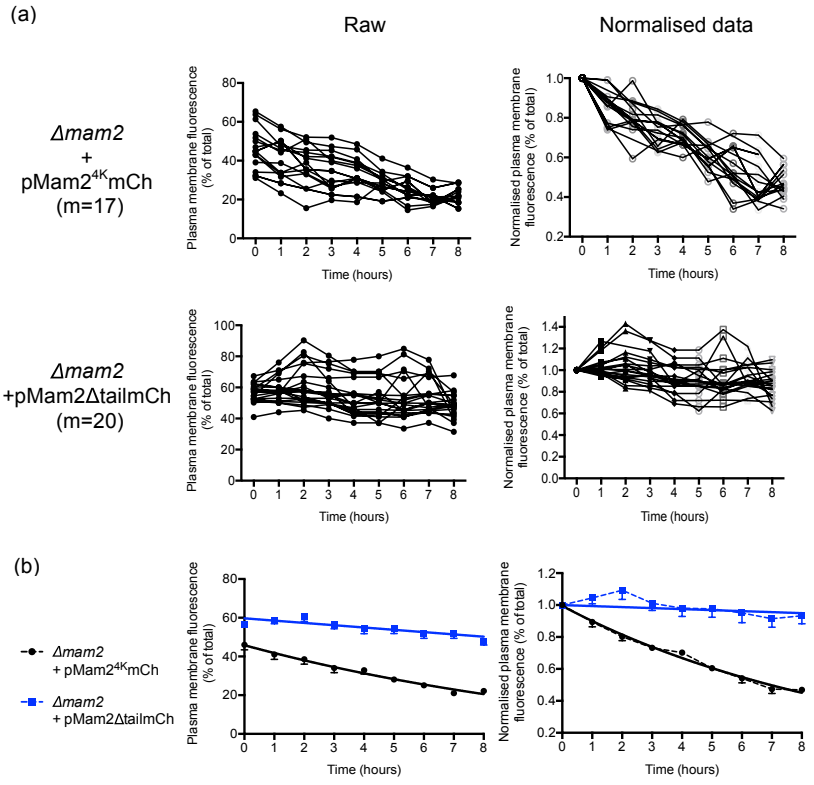

FIGURE E.1: **Mam2^{4K}mCh and Mam2ΔtailmCh plasma membrane fluorescence data from QuimP.** *Δmam2* (JY1169) cells transformed with pMam2^{4K}mCh (JD3804) and pMam2ΔtailmCh (JD3621) were grown to mid-exponential growth phasebefore treatment with 10 µM P-factor. Cells were imaged in the mCherry as described in section 2.2.14. A single cell was selected at random and quantified for their plasma membrane fluorescence using QuimP (as detailed in section 2.2.18). The figure shows the raw and normalised (a) individual data and (b) mean data ±SEM. The mean data for cells expressing Mam2^{4K}mCh was fitted using an exponential decay model fit and cell expressing Mam2ΔtailmCh was fitted using linear regression.

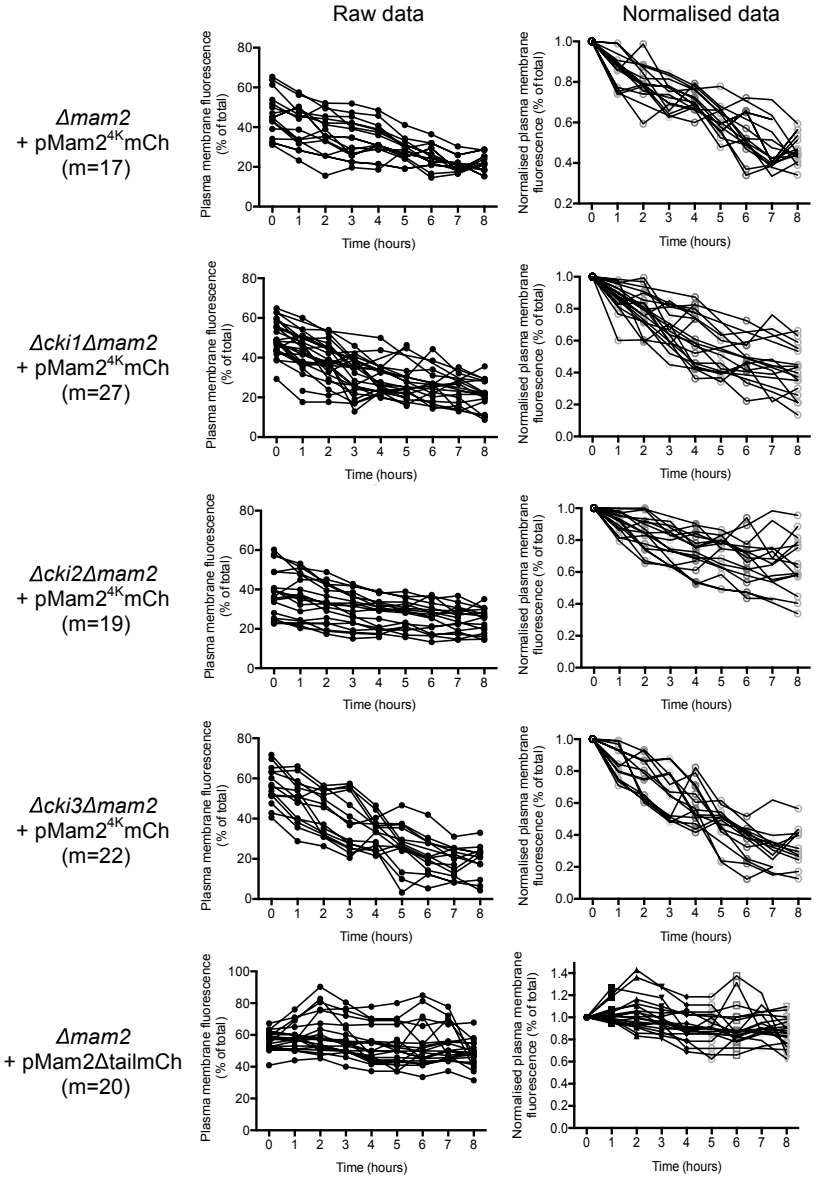

Figure E.2: **Raw and normalised plasma membrane fluorescence data from QuimP for *cki1*, *cki2* and *cki3* disruption strains.** *Δmam2* (JY1169), *Δcki1Δmam2* (JY1727), *Δcki2Δmam2* (JY1734) and *Δcki3Δmam2* (JY1720) *Sz. pombe* transformed Mam2^{4K}-mCherry and *Δmam2* (JY1169) transformed Mam2Δtail were grown to mid-exponential growth phasebefore treatment with 10 µM P-factor. Cells were imaged in the mCherry as described in section 2.2.14. A single cell was selected at random and quantified for their plasma membrane fluorescence using QuimP (as detailed in section 2.2.18).

Appendix F

Determining cell lysis

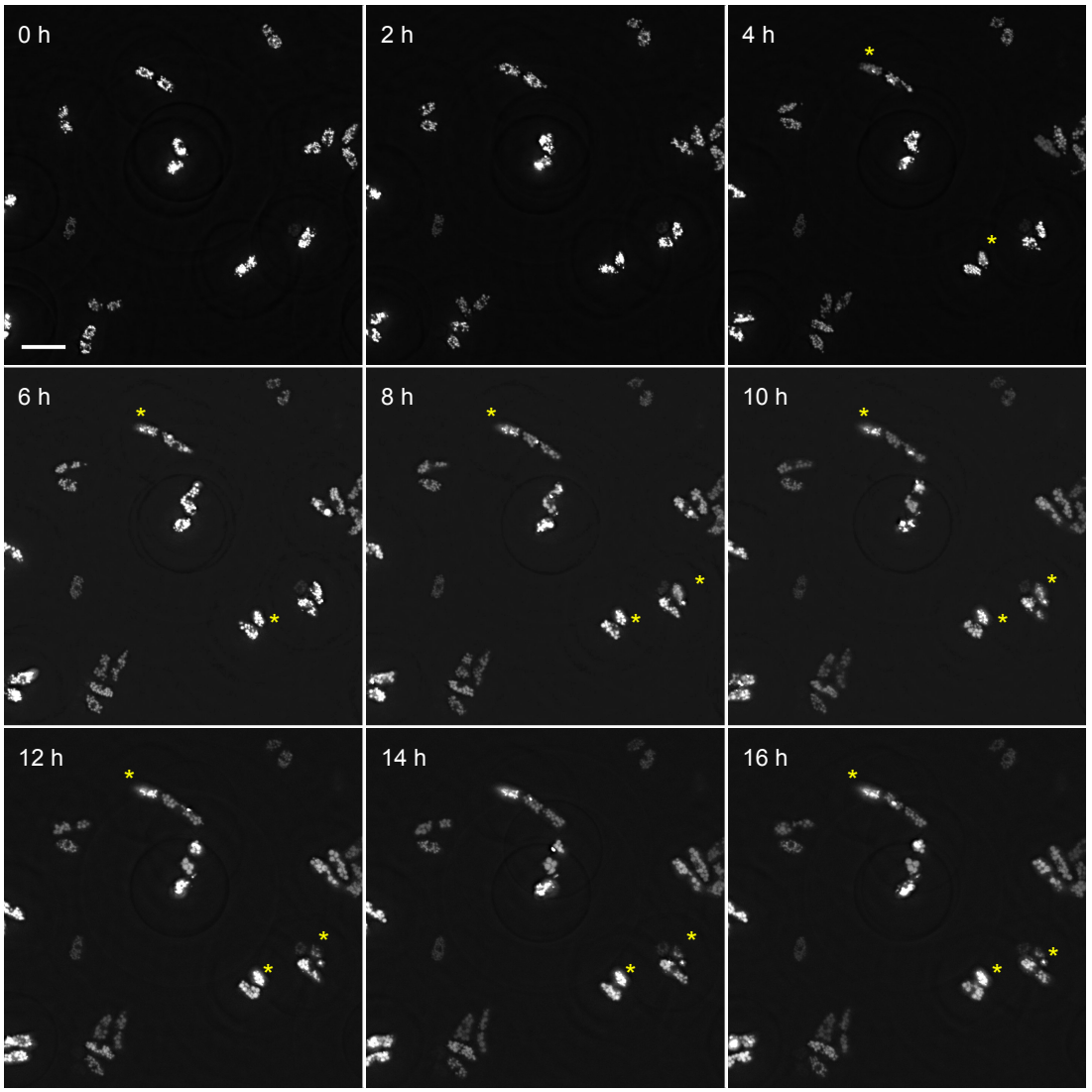

FIGURE F.1: **Time-lapse images of Mam2-mCherry.** *Δmam2* cells were transformed with pMam2mCh, grown to mid-exponential growth phase, treated with 10 µM P-factor and imaged every 2 h from 0 h to 16 h as described in section 2.2.14. Each cell within the frame was tracked with time to determine its viability heuristically. Yellow asterisk's indicate the lysed cells in each frame.

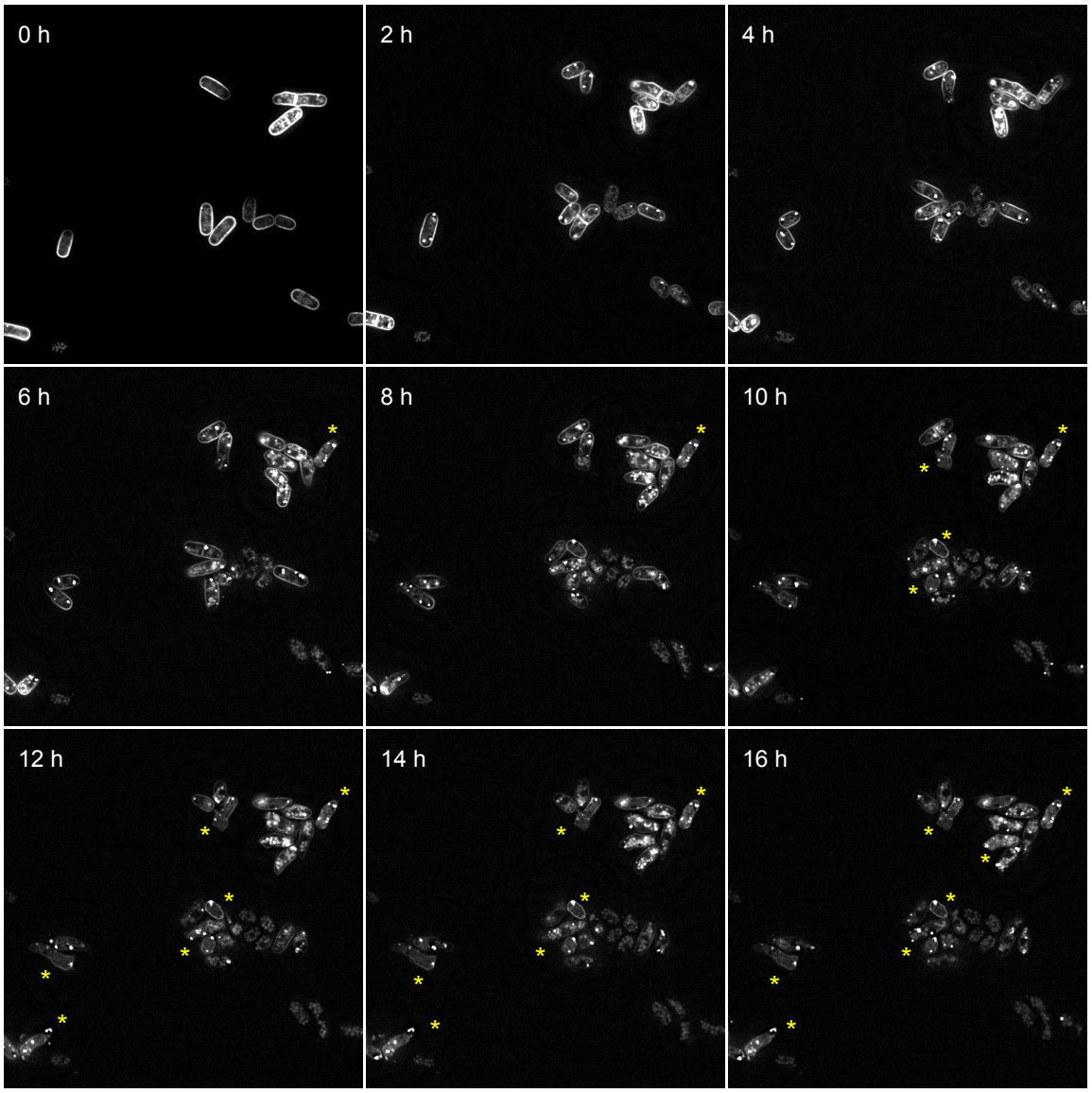

Figure F.2: **Time-lapse images of C-terminal lysine deficient Mam2.** *Δmam2* cells were transformed with pMam2^{4K}mCh, grown to mid-exponential growth phase, treated with 10 µM P-factor and imaged every 2 h from 0 h to 16 h as described in section 2.2.14. Each cell within the frame was tracked with time to determine its viability heuristically. Yellow asterisk's indicate the lysed cells in each frame. For the actual video see video 3.1 (this is a representative video used to determine the percentage of lysed cell in each frame following treatment with P-factor for 16 h).

Appendix G

Publication: Mos *et al.* (2013)

This appendix contains: **Mos M, Esparza-Franco MA, Godfrey EL, Richardson K, Davey J, Ladds G.** The role of the RACK1 ortholog Cpc2p in modulating pheromone-induced cell cycle arrest in fission yeast'. PLoS One. 2013 Jul 3; 8

OPEN ACCESS Freely available online

PLOS ONE

The Role of the RACK1 Ortholog Cpc2p in Modulating Pheromone-Induced Cell Cycle Arrest in Fission Yeast

Magdalena Mos[1]*, Manuel A. Esparza-Franco[2], Emma L. Godfrey[1], Kathryn Richardson[2], John Davey[1], Graham Ladds[1]

1 Division of Biomedical Cell Biology, Warwick Medical School, University of Warwick, Coventry, United Kingdom, **2** Systems Biology Doctoral Training Centre, University of Warwick, Coventry, United Kingdom

Abstract

The detection and amplification of extracellular signals requires the involvement of multiple protein components. In mammalian cells the receptor of activated C kinase (RACK1) is an important scaffolding protein for signal transduction networks. Further, it also performs a critical function in regulating the cell cycle by modulating the G_1/S transition. Many eukaryotic cells express RACK1 orthologs, with one example being Cpc2p in the fission yeast *Schizosaccharomyces pombe*. In contrast to RACK1, Cpc2p has been described to positively regulate, at the ribosomal level, cells entry into M phase. In addition, Cpc2p controls the stress response pathways through an interaction with Msa2p, and sexual development by modulating Ran1p/Pat1p. Here we describe investigations into the role, which Cpc2p performs in controlling the G protein-mediated mating response pathway. Despite structural similarity to Gβ-like subunits, Cpc2p appears not to function at the G protein level. However, upon pheromone stimulation, cells overexpressing Cpc2p display substantial cell morphology defects, disorientation of septum formation and a significantly protracted G_1 arrest. Cpc2p has the potential to function at multiple positions within the pheromone response pathway. We provide a mechanistic interpretation of this novel data by linking Cpc2p function, during the mating response, with its previous described interactions with Ran1p/Pat1p. We suggest that overexpressing Cpc2p prolongs the stimulated state of pheromone-induced cells by increasing *ste11* gene expression. These data indicate that Cpc2p regulates the pheromone-induced cell cycle arrest in fission yeast by delaying cells entry into S phase.

Citation: Mos M, Esparza-Franco MA, Godfrey EL, Richardson K, Davey J, et al. (2013) The Role of the RACK1 Ortholog Cpc2p in Modulating Pheromone-Induced Cell Cycle Arrest in Fission Yeast. PLoS ONE 8(7): e65927. doi:10.1371/journal.pone.0065927

Editor: Takashi Toda, Cancer Research UK London Research Institute, United Kingdom

Received November 19, 2012; **Accepted** May 4, 2013; **Published** July 3, 2013

Funding: This work was supported by the Biotechnology and Biological Sciences Research Council (BBSRC) (grant BB/G01227X/1 to MM and GL), University Hospitals of Coventry and Warwickshire NHS Trust (GL), Birmingham Science City Research Alliance (GL), a BBSRC pre-doctoral traineeship (KR), and the National Council on Science and Technology of Mexico (CONACYT) (MAE-F). The funders had no role in study design, data collection and analysis, decision to publish, or preparation of the manuscript.

Competing Interests: The authors have declared that no competing interests exist.

* E-mail: m.mos@warwick.ac.uk

Introduction

Eukaryotic cells are constantly exposed to different stimuli and are therefore required to both interpret and integrate their response to these signals in order to modulate their behavior. Many external signals are detected through cell surface G protein-coupled receptors (GPCRs), which couples to heterotrimeric G proteins consisting of a Gα, Gβ and a Gγ. In the inactive state, a Gα subunit is bound to a molecule of GDP. Upon agonist stimulation of a GPCR, nucleotide exchange occurs upon the Gα subunit such that GDP is lost and replaced by GTP. This promotes disassociation of Gα-GTP from the Gβγ dimer. Each can then regulate the activity of effector proteins thereby bringing about changes in cellular behavior [1]. Signaling is terminated when Gα-GTP is hydrolyzed to GDP through the intrinsic GTPase activity of the Gα subunit leading to the re-association of the heterotrimer.

The Gβγ-dimer can function at different levels to regulate G protein signaling. Most Gβγ-dimers recruit Gα-subunits to the plasma membrane facilitating interactions with agonist-bound receptors. However, they can also act as guanine nucleotide disassociation inhibitors (GDIs) by blocking the spontaneous exchange of GTP for GDP on the Gα subunit. Finally, Gβα-subunits can act as signal transducers within their own right by activating proteins such as adenylate cyclases and specific G protein-inward rectifying potassium channels [2]. A number of specific Gβγ-modulating/activating proteins have been identified including the activator of G protein signaling (AGS) superfamily [3–5].

In recent times it has become evident that G protein-mediated signaling cascades do not always require classical Gβγ-subunits. One such example is the glucose-sensing pathway in the budding yeast *Saccharomyces cerevisiae* where a number of Gβ-structural mimics have been reported. These include two kelch-repeat containing proteins Krh1p/Gpb1p and Krh2p/Gpb1p (however these proteins are now known to act further downstream of the Gα subunit [6–9]) and more recently a WD-repeat protein, Asc1p [10] an ortholog of mammalian receptor of activated protein C kinase (RACK1). It has been speculated that Gα subunits in other GPCR-mediate systems may interact with non-classical Gβγ-like proteins, and one such example is the pheromone-response pathway of fission yeast [11].

During the mating response *Schizosaccharomyces pombe* cells exchange pheromones that bind to cell surface GPCRs [12],

and transduce their signals via Gpa1p (Gα subunit) through a classical mitogen-activated protein (MAP) kinase cascade, resulting in activation of the transcription factor Ste11p. Critical for efficient mating of the cells, is their resultant entry into a transient G_1 arrest following pheromone stimulation [13]. Based upon sequence and structural comparison of typical G protein subunits within the *S. pombe* genome, there appears to be only one canonical Gβγ-subunit (Git5p/Git11p). Early research suggested that Git5p/Git11p could function on the pheromone cascade [14], however this now appears to be incorrect [15]. We have recently reported, through the use of a yeast 2–hybrid screen to identify interacting partners of Gpa1p, the isolation of a Gβ-like subunit, Gnr1p [16]. Both disruption and overexpression of Gnr1p demonstrated its role as a negative regulator of Gpa1p but it was not required for signaling [16]. As part of the same screen, we identified a second weak interacting partner of Gpa1p, Cpc2p.

Cpc2p is a Trp-Asp (WD)-repeat protein, and is the *S. pombe* ortholog of both RACK1 and Asc1p [17,18]. RACK1 is highly conserved among eukaryotic species [18,19], and it was originally described for its ability to interact with specific protein kinase C isoforms. In addition, it has become apparent that RACK1 is involved in complex cellular signal transduction pathways and chromatin organization [18,19]. Further, it also plays a role in mitotically growing cells by delaying entry into S phase [20,21].

Analogous to RACK1, Cpc2p appears to regulate a wide range of responses within *S. pombe*. It has also been suggested that Cpc2p modulates sexual development though its action on Ran1p/Pat1p, so regulating the transition from mitosis to meiosis [17,22]. In addition, Cpc2p controls the stress response pathway through regulation of Atf1p via an interaction with Msa2p [18] although the precise nature of this modulation remains unknown. It has however, been demonstrated that deletion of *cpc2* is epistatic to an *msa2* deletion suggesting that Msa2p may negatively regulate Cpc2p [22]. Further, Msa2p performs a number of cellular roles including modulating the stability of *cdc4* mRNA, (Cdc4p encodes an essential light chain of myosin and plays a crucial role in cytokinesis) [23], and regulates the onset of sexual differentiation by repressing Ste11p-regulated genes [24]. The interplay between Msa2p and Ste11p regulated genes appears complex since, Msa2p is itself, negatively regulated by pheromone. Upon pheromone-stimulation activated Spk1p (the MAP kinase of the mating response) reduces Msa2p activity, allowing an increase in Ste11p translation [25]. Cpc2p appears to have a number of other cellular roles including; modulating the cell cycle of mitotically growing cells by regulating the G_2/M transition [26] and a documented association with the 40S ribosomal subunit [27], that suggests a role in modulating the level of translation for many other genes.

Here we describe a novel and distinct role for Cpc2p within the *S. pombe* pheromone-response pathway. Despite initially isolating Cpc2p as a structural Gβ-mimic for Gpa1p, we now suggest that, Cpc2p also performs an important role in modulating *S. pombe* cells entry into S phase following pheromone-induced cell cycle arrest. We attempt to provide a molecular explanation for this data by linking Cpc2p modulation of Ran1p/Pat1p to pheromone signaling and also highlight a potential role for Msa2p in this process.

Results

Sequence and structural comparisons of typical G protein subunits within the fission yeast genome have identified a single canonical Gβγ (Git5p/Git11p). Evidence has been presented suggesting that Git5p and Git11p do not function on the pheromone-response pathway but solely act to module Gpa2p from the glucose-sensing pathway [15]. In a previous study, we described our use of the yeast-2 hybrid system to identify Gpa1p-binding partners [16]. From this screen we isolated a number of interactants, including the WD-repeat protein, Gnr1p. Quantitative characterization (Figure S1) [16] using previously described reporter strains (JY546; h^-, *cyr1*$^-$, *sxa2>lacZ*) where the bacterial enzyme β-galactosidase transcription is linked to the promoter of the Ste11p-regulated pheromone-responsive gene *sxa2* (Sxa2p is a carboxypeptidase that is only expressed after pheromone stimulation [28,29]) confirmed Gnr1p as a negative modulator of the pheromone-response pathway in fission yeast.

A second Gpa1p-binding partner identified in our yeast-2 hybrid screen [16], but not extensively characterized was Cpc2p. Deletion of the *cpc2* ORF from our Ste11p-regulated pheromone-responsive *sxa2>lacZ* reporter strains (JY1628; h^-, *cyr1*$^-$, *sxa2>lacZ*, *cpc2*$^-$) resulted in cells displaying a reduced sensitivity to pheromone (Wild type (JY546) - $pEC_{50} = 7.3 \pm 0.07$; *cpc2*$^-$ (JY1628) - $pEC_{50} = 6.9 \pm 0.03$) and a two-fold decrease in the extent of the maximal response (Wild type (JY546) - $E_{max} = 24.45 \pm 0.73$ units; *cpc2*$^-$ (JY1628) - $E_{max} = 10.82 \pm 0.22$ units) (Figure 1A). These defects were rescued upon expression of Cpc2p from an inducible plasmid. Overexpression of Cpc2p in cells containing an endogenous copy of *cpc2*, did not significantly alter their sensitivity or maximal response to pheromone. These results are in contrast to that observed for Gnr1p (Figure S1), and suggest that Cpc2p is not a negative modulator of pheromone signaling, despite its potential interaction with Gpa1p. Attempts to validate a potential *in vivo* interaction between Gpa1p and Cpc2p using co-immunoprecipitation have proven to be unsuccessfully (data not shown) and indicate a potential weak interaction between these two proteins. Subsequent mutational analysis of the N-terminal 40 amino acids of Gpa1p suggested that these residues alone are necessary and sufficient to enable Gpa1p association with plasma membrane structures in the absence of either Cpc2p or Gnr1p (Figure S2). These results would suggest that Gpa1p does not directly require the presence of a classical Gβ-like subunit for its regulation.

Cpc2p is a WD-repeat protein and an ortholog of the *S. cerevisiae* protein Asc1p. *cpc2* encodes a 314 amino acids peptide, with a predicted molecular mass of 34.6 kDa and, analogous to Asc1p and Gnr1p, contains 7 predicted WD-repeats. Using EMBOSS Needle [30], we determined that Cpc2p-Asc1p share 67% similarity, while Cpc2p-Gnr1p only share 28%. Further, relatively high sequence alignment (64%) was also identified between Cpc2p and mammalian RACK1. For a more detailed structural analysis, we used *SWISS-MODEL Repository* [31,32] to illustrate the multi-domain nature of the Cpc2p peptide, highlighting the 7 WD repeats (Figure 1B). Interestingly, many WD-repeat proteins contain a specific (up to 600 amino acids) C-terminal extension [33] although this motif does not seem to be present in Cpc2p.

Despite Cpc2p not appearing to be a negative regulator of pheromone signaling, it clearly performs a role in modulating the response. We therefore sought to determine what role Cpc2p may play upon both mitotically growing wild type (JY448; *cyr1*$^+$, *sxa2*$^-$) and pheromone-responsive (JY546; h^-, *cyr1*$^-$, *sxa2>lacZ*) cells. It should be noted that to enable quantitative characterization of the extent of pheromone-responsiveness we use strains defective for Cyr1p, which generates a genotype that mimics starvation and produces a more diminished cell size [34,35] (Figure 1C).

For wild type mitotically growing Cyr1p expressing cells, disruption of the *cpc2* ORF resulted in cells displaying a slightly decreased size at the point of cell division (Wild type (JY448) $= 12.16 \pm 0.44$ μm; *cpc2*$^-$ (JY1712) $= 11.32 \pm 0.21$ μm) although this was not statistically significant ($p > 0.5$; $n = 400$). A more

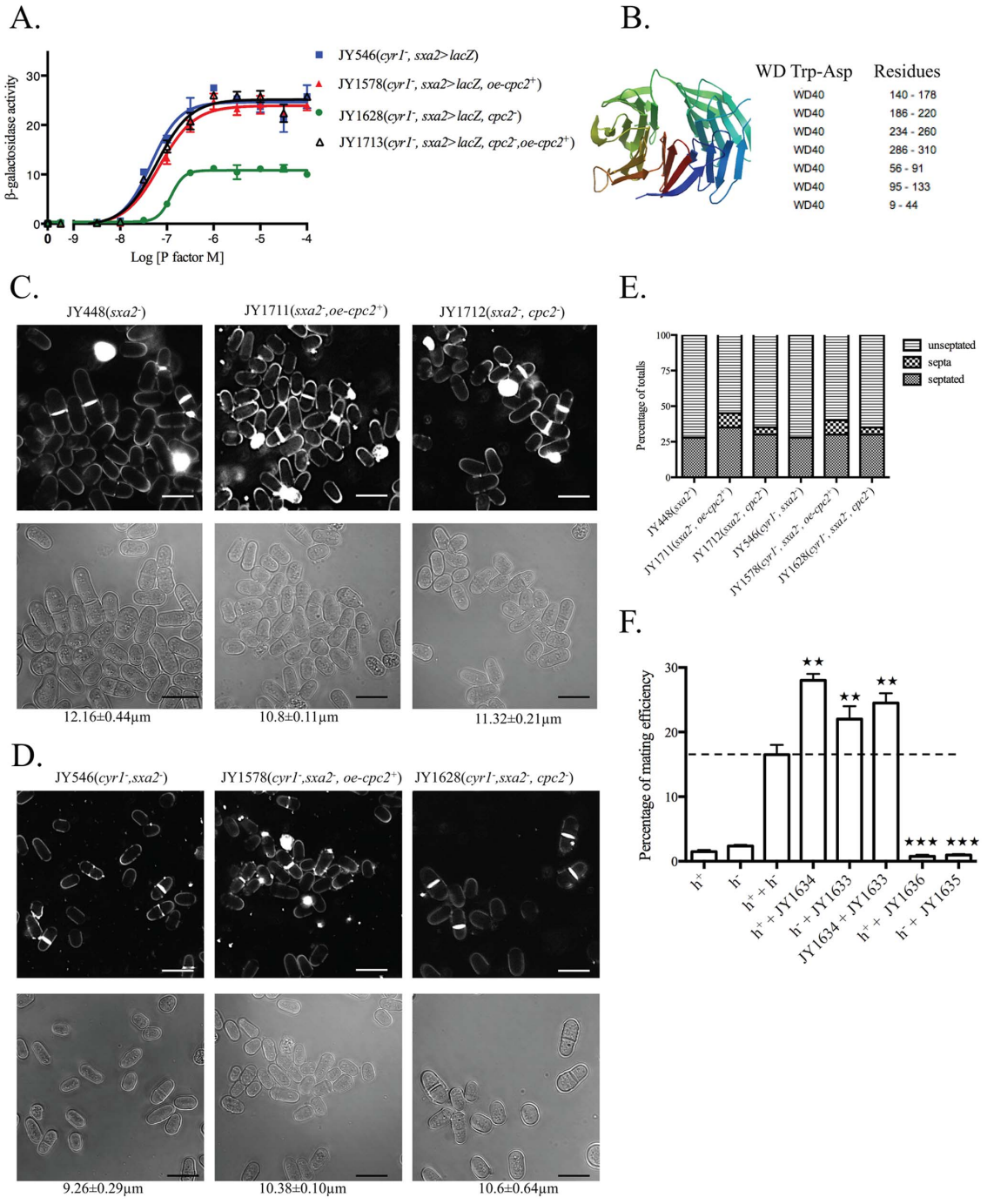

Figure 1. Characterization of potential Gβ-subunit mimic in the pheromone-response pathway. (A) Pheromone-dependent transcription for the strains JY546 (h^-, $cyr1^-$, sxa2>lacZ), JY1578 (h^-, $cyr1^-$, sxa2>lacZ+oe-$cpc2^+$), JY1628 (h^-, $cyr1^-$, sxa2>lacZ, $cpc2^-$) and JY1713 (h^-, $cyr1^-$, sxa2>lacZ, $cpc2^-$+oe-$cpc2^+$) was determined using the sxa2>lacZ reporter. Values are means of triplicate determinations ± S.E.M. (B) Molecular structure as determined using the SWISS-MODEL Repository for Cpc2p. Cpc2p contains seven WD-40 repeat domains with positions of residues as indicated by colors on the molecular structure. (C) Cell morphology and size, at division (micrometers ± S.D.) for strains JY448 (h^-, $cyr1^-$, $sxa2^-$), JY1711 (h^-, $sxa2^-$+oe-$cpc2^+$), JY1712 (h^-, $sxa2^-$, $cpc2^-$), grown in minimal medium at 29°C and stained with calcofluor white (top panel) or imaged

through using bright field microscopy on agar pads (bottom panel). Scale bars 10 μm. (D) As for C except strains JY546 (h^-, $cyr1^-$, sxa2>lacZ), JY1578 (h^-, $cyr1^-$, sxa2>lacZ+oe-cpc2$^+$), and JY1628 (h^-, $cyr1^-$, sxa2>lacZ, $cpc2^-$) were used. (E) Numbers of non-septated, septated and multiple septa containing cells for the strains in C and D were determined from 400 individual cells. Values shown correspond to the percentages of the total population. Cells were stained with calcofluor white, to enable visualization of septum material. (F) Mating efficiency was quantitated for cells overexpressing (JY1634, h^-, +oe-cpc2$^+$; JY1633 h^+, +oe-cpc2$^+$) or lacking Cpc2p (JY1636, h^-, $cpc2^-$; JY1635 h^+, $cpc2^-$) compared to M (JY402, h^-) and P (JY383, h^+) control cells. Statistical significance determined compared to M (h^-) and P (h^+) using a one-way Anova with a tukey multiple comparison post test where ★★★ represents $p \leq 0.001$, ★★ represents $p \leq 0.01$, and ★ represents $p \leq 0.1$.
doi:10.1371/journal.pone.0065927.g001

significant effect ($p<0.1$, $n = 400$) was observed upon overexpression of Cpc2p (*oe-cpc2p*$^+$) with cells displaying a decreased size at the point of cell division (*oe-cpc2*$^+$ (JY1711) $= 10.8 \pm 0.11$ μm). As mentioned above cells lacking Cyr1p display a smaller size at division (Figure 1D). Both the deletion or overexpression of the *cpc2* ORF from these strains increased the overall cell size (Wild type (JY546) $= 9.26 \pm 0.29$ μm; *cpc2*$^-$ (JY1628) $= 10.6 \pm 0.64$ μm; *oe-cpc2*$^+$ (JY1578) $= 10.38 \pm 0.10$ μm) however these changes were not found to be statistically significant (*cpc2*$^-$ (JY1628) = $p>0.5$, $n = 400$; *oe-cpc2*$^+$ (JY1578) = $p>0.5$, $n = 400$). Some of these sizes are different to what maybe predicted from previous studies [18] but may arise due to the genetic backgrounds we have used compared to others. Indeed while all of the cell sizes at division in this study appear to be slightly smaller than accepted within the field (*S. pombe* cells generally undergo cell division at a size of between 13-14 μm), it should be noted that the growth media used in our assays is a variant of the classical EMM as described by Davey *et al.*, 1995 [36]. This media places a higher nutritional demand on the cells and as a result causes the cells to undergo division at a smaller size. Indeed it has been documented that nutritional reduction of growth rate results in decreased cell size [37].

We next sought to determine the effects upon the cell cycle of deleting, or overexpressing Cpc2p, using the previously described strains (Figure 1E). Deletion of Cpc2p slightly increased the percentage of cells within a population contain multiple-septa (regardless of the presence or absence of Cyr1) and is consistent with previous reports [26]. Interestingly, and somewhat counter-intuitive, this effect was more pronounced upon overexpression of Cpc2p regardless of the presence (Wild type (JY448) = <0.1%; *oe-cpc2*$^+$ (JY1711) $= 10 \pm 0.2\%$ - $p = <0.0001$, $n = 4$) or absence of Cyr1p (Wild type (JY546) = <0.1%; *oe-cpc2*$^+$ (JY1578) $= 10 \pm 0.15\%$ - $p = <0.0001$, $n = 4$). These results are consistent with Cpc2p inhibiting the activity of Ran1p/Pat1p resulting in an increase in Ste11p activity. Further, Cpc2p and Msa2p activity are tightly coordinated and thus increased Cpc2p expression may reduce the ability of Msa2p to stabilize *cdc4* mRNA, causing defects in cell division.

Deletion of *cpc2* renders cells of both mating types sterile (Figure 1F). It should be noted that all strains used in the quantitative mating assays express *sxa2* since strains lacking Sxa2p are sterile [28]. Significantly, increasing Cpc2p expression leads to a ~1.5 fold increase in mating efficiency (observed for both mating types).

Having established a role for Cpc2p during the mating response, we next sought to provide a molecular explanation for these effects. During mating cells undergo a unidirectional elongation towards a potential partner (termed a shmoo) [38]. Our strains (either expressing or deleted for *cyr1*) lack Sxa2p and therefore display abnormally long conjugation tubes following prolonged exposure (>8 h) to high pheromone concentrations (10 μM) in the absence of a sufficient nutrient source (Figure 2A) [28]. After approximately 10-12 h these cells appear to resume mitotic division, before generating a second pheromone dependent-response. Strains deleted for *cpc2* failed to generate any morphological response to the presence of the pheromone and continued mitotic growth (Figure 2B). Strains overexpressing Cpc2p, when grown in the absence of nitrogen and treated with pheromone, initially generated conjugation tubes of equivalent size to wild type cells however, they failed to undergo division. Instead, after >16 h, cells displayed very specific cell branching activity (Figure 2C - arrows) but did not appear to lose viability. Moreover, following prolonged pheromone exposure (>30 h) many cells contained an increased number of septa, suggesting an inability to efficiently divide. As described previously, these data are consistent with Cpc2p having pleiotropic effects on the ability of Msa2p to regulate *cdc4* mRNA.

The observation that cells overexpressing Cpc2p appear to elongate from multiple tips when exposed, for prolonged periods to pheromone, led us to hypothesize that these strains may exhibit a protracted pheromone-induced G_1 cell cycle arrest. To address this, we used flow cytometry to analyze the response of cells when stimulated with pheromone. As mentioned previously, the strain JY546 lacks adenylate cyclase [34], and this results in an increased number of cells, within a population (~20-25%) containing a single 1C content of DNA when analyzed using flow cytometry reflecting modification of the mitotic cell cycle in these strains (Figure 3C). Deletion of *cpc2* from strains lacking *cyr1* reduces the percentage of cells within a population containing a single 1C content of DNA, while overexpression did not have a significant effect ($p>0.5$, $n = 3$).

Following exposure to 10 μM pheromone, the proportion of wild type (JY546) cells with a 1C content of DNA steadily increased reaching a maximum (after 8 h) before decreasing over the subsequent 8 h time-frame. This cycle was repeated for the following 16 h time period. These two phases reflect the morphological images shown in Figure 2A and confirm that cells lacking Cyr1p only respond for a fixed period (~10–12 h) before resuming mitotic division. In contrast, overexpression of Cpc2p results in an accelerated (compared to wild type) increase in the percentage of cells exhibiting a 1C content of DNA (90%, $n = 3$) following exposure to pheromone (Figure 3B and 3C). Consistent with the morphological data presented in Figure 2C, these cells failed to regain a 2C DNA content over the time frame analyzed. Interestingly, the strain lacking *cpc2* (JY1628) did show an increase (from 10% to 55%) in the percentage of cells containing a single 1C content of DNA following pheromone stimulation. This did not however coincide with an increase in cell size (Figure 2B) suggesting these cells can detect the presence of the pheromone, undergo an arrest but fail to initiate shmoo formation.

We next sought to observe if similar effects upon cell cycle regulation was observed for strains expressing Cyr1p, when nitrogen starved and exposed to pheromone (Figure 3D). Significantly, cells overexpressing Cpc2p appeared to increase the number of cells entering and remaining in a G_1 arrest. Unlike the strains lacking *cyr1*, nitrogen starvation prevents cells from regaining their 2C complement and therefore they remain arrested in G_1 (reviewed [13]). Overexpression of Cpc2p increased the percentage of cells within the population that contained a single 1C content following pheromone stimulation. Interestingly however, strains lacking *cpc2* did not appear to display any significant arrest in G_1. This is in contrast to the data observed with *cyr1*$^-$

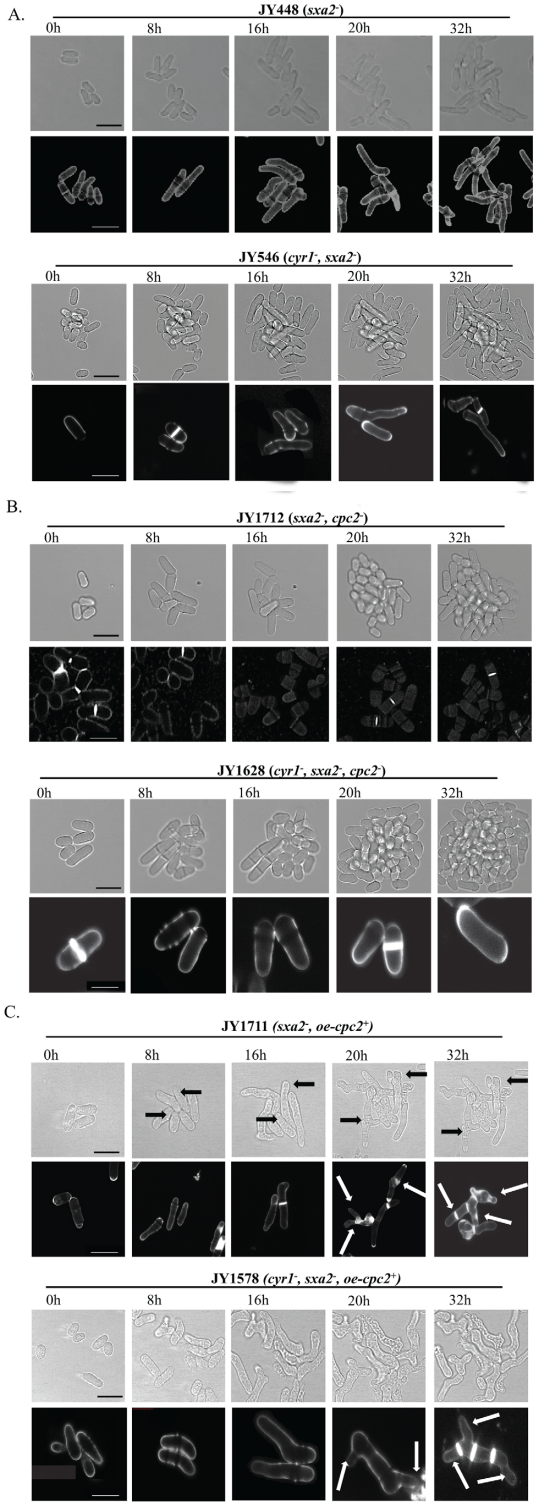

Figure 2. Cpc2p has profound morphological effects upon pheromone-stimulated cells. The strains (A) JY448 (h^-, $sxa2^-$) and JY546 (h^-, $cyr1^-$, sxa2>lacZ); (B) JY1712 (h^-, $sxa2^-$, $cpc2^-$) and JY1628 (h^-, $cyr1^-$, sxa2>lacZ, $cpc2^-$); (C) JY1711 (h^-, $sxa2^-$+oe-$cpc2^+$), JY1578 (h^-, $cyr1^-$, sxa2>lacZ+oe-$cpc2^+$), were grown to mid-exponential phase over 32 h in minimal media. Cells were then imaged using bright field microscopy on pads containing 10 μM of pheromone (see methods). Cells were also stained with calcofluor white (lower panels A-C) to visualize septation. Scale bars 10 μm. Prolonged exposure to pheromone for cells overexpressing Cpc2p (oe-$cpc2^+$) results in multiple projection tips and a failure to undergo cytokinesis. Cells lacking Cpc2p fail to generate the classical shmoo formation as observed for control cells.
doi:10.1371/journal.pone.0065927.g002

strains and highlights potential differences that this nutritional selection may enforce on *S. pombe* cells. Moreover the data would suggest that the regulatory mechanism utilized by Cpc2p and Cyr1p to control G_1 arrest are different. It is entirely probable that the increased percentage of cells that initially contain a 1C content in a *cyr1*$^-$ background amplifies any potential arrests observed for strains following pheromone stimulation.

Overall, these data suggest that Cpc2p proactively induces the pheromone-dependent G_1 arrest and following prolonged exposure, cells overexpressing Cpc2p are unable to become desensitized to pheromone and remain arrested in the G_1 phase of the cell cycle although the precise mechanism for this protracted G_1 arrest is unknown but maybe due, in part, to Cpc2p partially inhibiting Ran1p/Pat1p. Cells lacking *cpc2* do not appear to generate a typical pheromone-induced G_1 arrest and this is consistent with the lack of shmoo formation observed previously (Figure 2B).

Mammalian RACK1 has been reported to, in mitotically growing cells mouse NIH3T3 cells, delay their entry into S phase [21,39]. Further, it has been suggested that RACK1 suppresses *cpc2* defects in *S. pombe* cells [17]. We therefore sought to determine the effects on pheromone-induced responses in our strains expressing mammalian RACK1. Cells lacking an endogenous copy of the *cpc2* were transformed with an inducible plasmid expressing mammalian RACK1 and their dose-dependent response to pheromone determined using the *sxa2>lacZ* reporter. As has previously been suggested [17], mammalian RACK1 was able to functionally complement for the loss of Cpc2p, with cells generating a near normal pheromone-dependent response profile (Figure S3A). Further, upon investigation of the DNA content of cells expressing RACK1, when exposed to 10 μM pheromone, we observed a prolonged G_1 arrest (Figure S3B) analogous to that described for increased Cpc2p expression (compare Figure 3C and 3D with Figure S3B). Taken together, these data highlight the functional similarities between Cpc2p and RACK1 in modulating the cells ability to exit pheromone-induced G_1 phase of the cell cycle.

Having established that pheromone treated cells overexpressing Cpc2p display a protracted G_1 arrest, we sought to determine if this was as a direct result of cells failing to enter S phase. *S. pombe* relies on a single cyclin-dependent kinase (CDK) Cdc2p, to regulate and control mitotic cell-cycle events. Cdc2p is controlled by association with B-type cyclins such that, Cdc2p-Cdc13p act as the mitotic kinase [40,41], and Cdc2p-Cig2p the G_1-S kinase [42]. In *S. pombe* cells, Rum1p, the sole cyclin-dependent kinase inhibitor (CKI), plays an important role in regulating both Cdc2p-Cig2p and Cdc2p-Cdc13p (over expression of Rum1p induces polyploidy due to the bypass of M-phase [43]). During anaphase, Rum1p starts to accumulate, becomes stable and consistent during G_1, and diminishes in S-phase [43]. In addition, its expression is increased upon exposure to pheromone (http://www.pombase.org/). Via its regulating activity of Cdc2p-Cig2p,

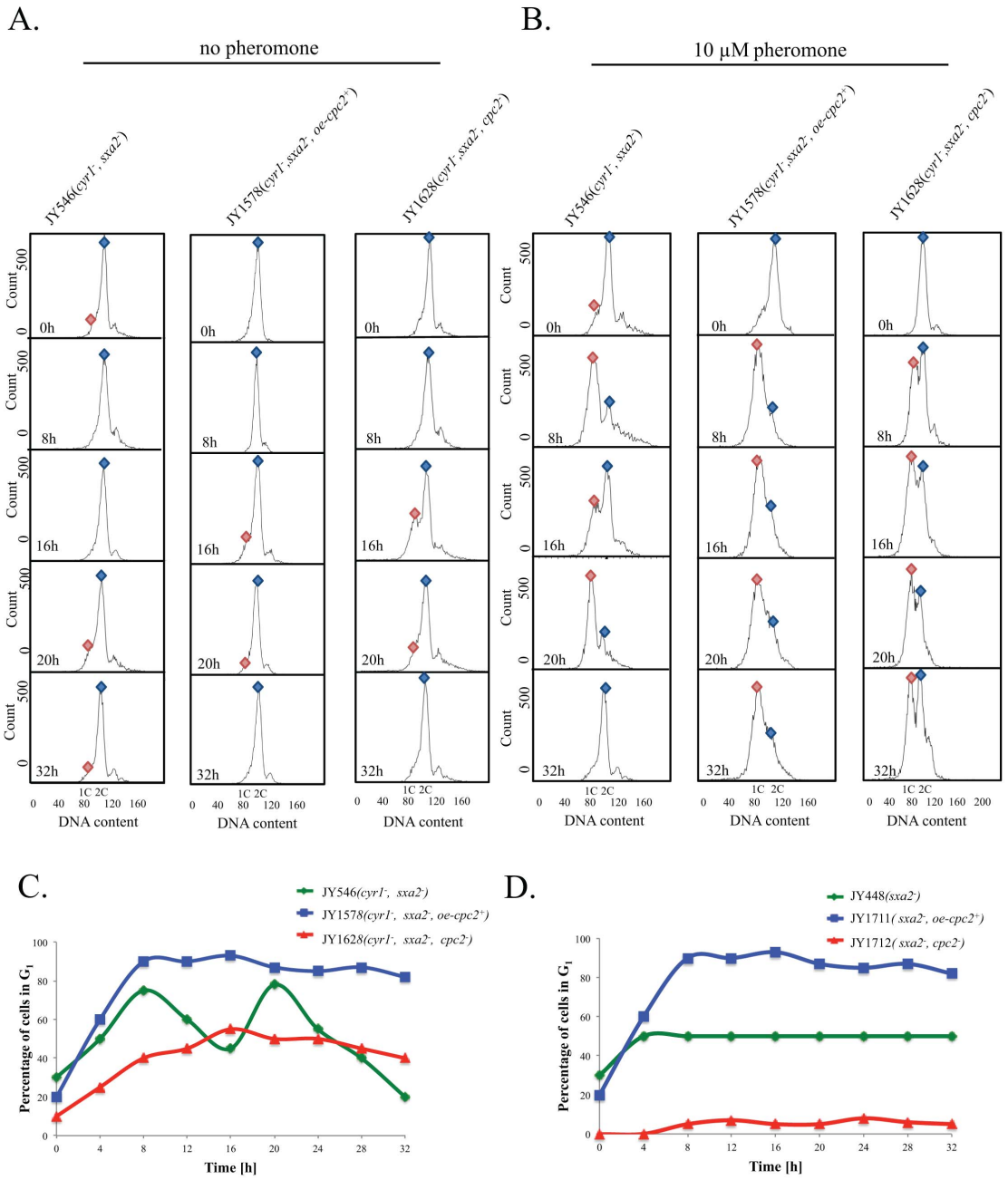

Figure 3. Cpc2p control the G1/S transition in pheromone-stimulated cells. (A) The strains JY546 (h^-, $cyr1^-$, sxa2>lacZ), JY1578 (h^-, $cyr1^-$, sxa2>lacZ, +oe-$cpc2^+$) and JY1628 (h^-, $cyr1^-$, sxa2>lacZ, $cpc2^-$) were grown in minimal medium and (B) minimal media containing 10 μM of pheromone for the times indicated. Cells were harvested and fixed prior to staining with propidium iodide prior to analysis using flow cytometry (see methods). The proportion of cells exhibiting 1C or 2C DNA content was determined using FACSDiva v4.1 software for the assigned gates indicated by the blue and red shapes. (C) The percentage of cells containing a 1C content (arrested in G_1) as determined from B. Cells containing an additional content of Cpc2 fail to desensitize following pheromone stimulation and remain arrested for the time frame analyzed. Cells lacking Cpc2p fail to generate a significant arrest in G_1 following exposure to 10 μM pheromone. (D) The percentage of cells from the strains JY448 (h^-, $sxa2^-$), JY1711 (h^-, $sxa2^-$+oe-$cpc2^+$), JY1712 (h^-, $sxa2^-$, $cpc2^-$) containing a 1C content (arrested in G_1) following nitrogen starvation and stimulation with 10 μM pheromone.

doi:10.1371/journal.pone.0065927.g003

Rum1p functions as the main controlling agent for maintaining the G_1 phase of the cell cycle [40-42,44]. We therefore generated a pheromone-responsive reporter strain lacking Rum1p (JY1520; h^-, *cyr1*$^-$, *sxa2>lacZ, rum1*$^-$) capable of overexpressing Cpc2p.

Cells lacking Rum1p displayed a smaller size (irrespective of the expression of Cyr1p) than wild type strains (Figure 4A), although their morphology appeared normal. Further, there were no observable defects in the levels of septation (Figure 4B) and/or growth rates for the strain lacking Rum1p. Overexpression of Cpc2p in strains lacking Rum1p resulted in a slight increase in cell size (Figure 4A) and a 7-fold increase in the occurrence of multiple septa (Figure 4B).

We next investigated the pheromone-dependent responses of cells lacking Rum1p with and without additional Cpc2p (Figure 4C). Cells lacking Rum1p failed to generate a dose-dependent response to stimulation with pheromone and this was not recovered by the overexpression of Cpc2p (JY1637). Flow cytometry analysis revealed that both these populations (JY1520 (*rum1*$^-$) and JY1637 (*rum1*$^-$+*oe-cpc2*$^+$)) contained a 2C content of DNA regardless of the presence of 10 μM pheromone (Figure 4D), suggesting that cells failing to reside in the G_1 phase of the cell cycle for an extended period, are not subjected to pheromone-induced Cpc2p regulation of the G_1/S transition.

Significantly, bright field microscopy images of our Rum1p deleted strains overexpressing Cpc2p, following exposure to 10 μM pheromone (for 32 h) indicate the presence of elongated cells compared to the non-stimulated populations (Figure 4E). These effects were not observed in a strain lacking both Rum1p and Cpc2p (JY1710; h^-, *cyr1*$^-$, *sxa2>lacZ, cpc2*$^-$, *rum1*$^-$). The pheromone-induced elongate cells in the *rum1* deleted strain overexpressing Cpc2p showed considerable similarity to the classical shmoo morphology described in Figure 2A. The presence of pheromone-induced elongated cells in a strain lacking Rum1p strain suggests the possibility that *S. pombe* cells can generate a G_1-independent morphological response to pheromone. This data would suggest that pheromone induces shmoo formation at the same time as a G_1 arrest. To the best of our knowledge, these observations represent the first demonstration of a pheromone-induced cell elongation for an *S. pombe* population that fails to enter G_1.

Following our observations that Cpc2p may play a role in modulate cells passage into S phase, we sought to provide a mechanistic interpretation to our data. The failure of cells lacking Rum1p to enter a protracted G_1 arrest suggests that Cpc2p performs its role by over-activation of the Ste11p-regulated pheromone-response pathway. Following pheromone activation of cell surface receptors, Gpa1p propagates the response by activating Ras1p. This leads to stimulation of a MAP kinase cascade and activation of Ste11p. Further, Spk1p also phosphorylates an unknown negative regulator of Msa2p [25], reducing it's activity leading to an increase in Ste11p translation therefore reinforcing the response.

The promiscuous dual-specificity phosphatase Pmp1p, has among other roles, been suggested to negatively modulate the action of Spk1p [45]. Deletion of Pmp1p results in Spk1p remaining activate for longer so prolonging Ste11p activation [45]. Thus, we sought to determine if similar cellular defects were observed in Pmp1p deleted cells to that observed for cells overexpressing Cpc2p. Morphological analysis of a strain lacking Pmp1p, (JY948; h^-, *cyr1*$^-$, *sxa2>lacZ, pmp1*$^-$ and JY1716; h^-, *sxa2*$^-$, *pmp1*$^-$) when stimulated with 10 μM pheromone for 32 h, reveals cells that displayed extended conjugation tubes and multiple projection tips (Figure 5A and 5B). Further, Pmp1p depleted cells exhibit an elevated maximal response to pheromone (Figure 5F), and flow cytometry analysis suggests that these cells fail to exit from a pheromone-induced G_1 arrest (Figure 5C). These results are consistent with that observed for overexpression of Cpc2p, and would suggest that Cpc2p could be acting to increase MAP kinase/Ste11p activity in response to pheromone.

It is of interested to note that Cpc2p does not perform a direct role in modulating the expression levels of Pmp1p but in contrast, it has been reported that Cpc2p regulates the activity of two other MAP kinase phosphatases Pyp1p and Pyp2p [18]. To date, little information has been published relating to potential roles of Pyp1p and Pyp2p in relation to pheromone signaling. Based upon our results with deletion of *pmp1* we sought to evaluate the role of Cpc2p modulation of these two phosphatases with respect to pheromone transduction. Unfortunately, despite numerous attempts the concurrent deletion of *pyp1* and *cyr1* appears synthetically lethal (Didmon and Davey unpublished). As a result we have only been able to investigate the role of Pyp2p.

Cells lacking Pyp2p (JY709; h^-, *cyr1*$^-$, *sxa2>lacZ, pyp2*$^-$) and (JY710; h^-, *sxa2,*$^-$ *pyp2*$^-$) have a slightly reduced size (Figure 5D) that is not significantly increase upon overexpression of Cpc2p. Interestingly, and in contrast to all other strains tested within this study, overexpression of Cpc2p did not induce an increase in septa formation (Figure 5E). It has been reported that cells overexpressing Pyp2p exhibit a delay in mitosis [46], and which appears analogous to the overexpression of Cpc2p [18]. Since Cpc2p has been documented to modulate the expression of Pyp2p, the removal of *pyp2* renders Cpc2p activity redundant. Finally, irrespective of the presence of excess Cpc2p, cells lacking Pyp2p fail to respond to pheromone (Figure 5F) and appear to contain a 2C DNA content at all times (Figure 5G and 5H). These results are similar to the Rum1p disruption, however cells lacking Pyp2p fail to generate a G_1-independent morphological response to the presence of the pheromone.

Discussion

The eukaryotic scaffold protein RACK1 (a WD-repeat protein) is involved in a wide range of signal transduction pathways including cell cycle progression. The fission yeast ortholog Cpc2p has been reported to modulate the stress-response pathway and positively regulates the G_2/M transition at the ribosomal level [26]. Here we have described the role of Cpc2p in modulating the pheromone-response pathway. In a previously described yeast 2-hybid screen for interacting partners of Gpa1p, we identified Cpc2p [16]. Based upon the similarity of Cpc2p to the Asc1p (a Gβγ-like subunit for Gpa2p involved in the glucose-sensing pathway from budding yeast) [10] we investigate the potential for Cpc2p to act as the Gβγ-subunit within the pheromone-response pathway in fission yeast. Despite performing a significant role in pheromone-mediated signaling, Cpc2p does not appear to regulate Gpa1p and attempts to validate this interaction *in vivo* proved unsuccessful. Indeed, it is highly probable that Gpa1p does not require a chaperone to target it to the plasma membrane. Gpa1p contains a consensus MG_2XXXS_6 myristoylation sequence [47], and a downstream cysteine, which is likely to be a target for palmitoylation, so facilitating association with membranes. Moreover, mutational analysis suggests that the N-terminal first 40 amino acids of Gpa1p are necessary and sufficient to enable its association with membrane structures (Figure S2).

Our data has confirmed that Cpc2p performs a role in regulating sexual differentiation in *S. pombe*. Cells lacking Cpc2p display little change in the transcription levels of *ste11* mRNA despite but are sterile [25]. Interestingly, *cpc2* depleted cells do however, display decreased reduce protein concentration of

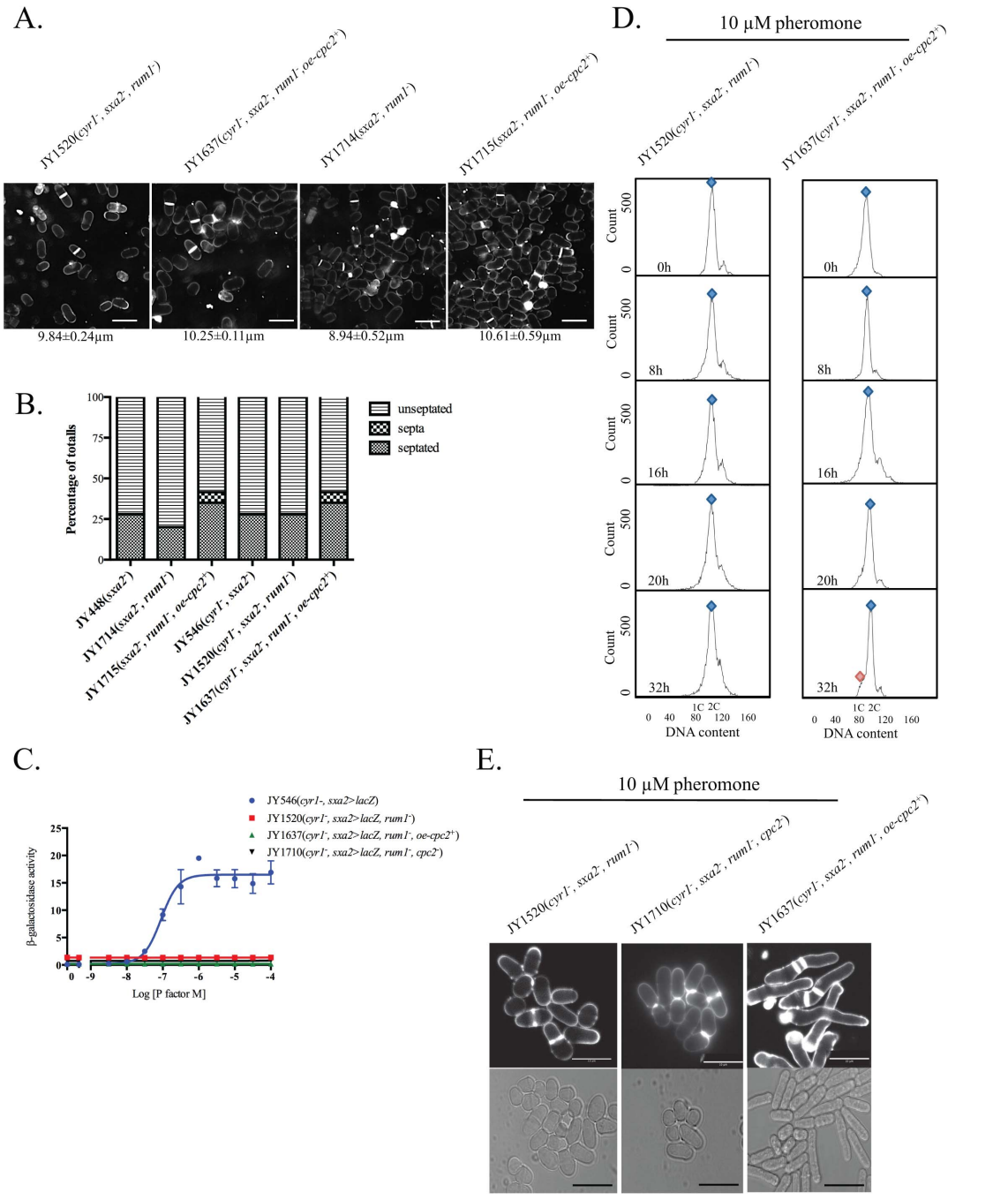

Figure 4. Overexpression of cpc2 mediates its pheromone effects in a G1-dependent manner. (A) Cell morphology and size, at division (micrometers ± S.D.) for strains JY1520 (h^-, $cyr1^-$, sxa2>lacZ, $rum1^-$), JY1637 (h^-, $cyr1^-$, sxa2>lacZ, $rum1^-$+ oe-$cpc2^+$), JY1714 (h^-, $sxa2^-$, $rum1^-$) and JY1715 (h^-, $sxa2^-$, $rum1^-$+oe-$cpc2^+$) grown in minimal medium at 29°C and stained with calcofluor. Scale bars 10 μm. (B) Number of non-septated, septated and multiple septa containing cells for the strains JY448 (h^-, $sxa2^-$), JY1714 (h^-, $sxa2^-$, $rum1^-$), JY1715 (h^-, $sxa2^-$, $rum1^-$+oe-$cpc2^+$), JY546 (h^-, $cyr1^-$, sxa2>lacZ), JY1520 (h^-, $cyr1^-$, sxa2>lacZ, $rum1^-$) and JY1637 (h^-, $cyr1^-$, sxa2>lacZ, $rum1^-$+oe-$cpc2^+$) were determined from 400 individual cells. Values shown correspond to the percentage of the total population. Cells were stained with calcofluor white, to enable visualization of septum material. (C) Pheromone-dependent transcription for the strains JY546, JY1520, JY1637 and JY1710 (h^-, $cyr1^-$, sxa2>lacZ,

rum1$^-$, cpc2$^-$) was determined using the sxa2>lacZ reporter. Cells were stimulated with pheromone for 16 h in minimal media and assayed for β-galactosidase production using ONPG. Activity is expressed as OD_{420} units per 10^6 cells. Values are means of triplicate determinations ± S.E.M. (D) The strains JY1520 and JY1637 were grown in minimal medium containing 10 μM of pheromone for the times indicated. Cells were harvested and fixed prior to staining with propidium iodide prior to analysis using flow cytometry (see methods). The proportion of cells exhibiting 1C or 2C DNA content was determined using FACSDiva v4.1 software for the assigned gates indicated by the blue and red shapes (E) The strains JY1520, JY1710 and JY1637 were grown to mid-exponential phase over 32 h in minimal media. Cells were then stained with calcofluor white to visualize septation (top panel) and imaged bright field microscopy (bottom panel) after 32 h exposure to pheromone. Scale bars 10 μm.
doi:10.1371/journal.pone.0065927.g004

Ste11p that is insufficient to induce downstream targets. Our studies have utilized a pheromone-reporter strain (*sxa2>lacZ*) under the direct control of Ste11p (Figure 1A) so validating the notion that *cpc2*$^-$ cells have reduced Ste11p activity.

Although Cpc2p does not appear to function as a Gβ-like subunit in *S. pombe*, our results suggest that in a pheromone-stimulated environment, overexpression of Cpc2p causes significant cellular effects including; defects in cell integrity, increased mating efficiency, increased septum formation, reduced cell cycle progression and increased cell morphological defects. Significantly, Cpc2p appears to actively promote and prolong the pheromone-induced G_1 arrested state, preventing cells from adapting to the presence of the pheromone and resuming mitotic growth. Moreover, cells expressing RACK1 display the same cell cycle progression defect when subjected to pheromone stimulation, confirming functional similarity between these two orthologs.

The precise mechanism by which Cpc2p protracts the G_1 arrest upon pheromone stimulation remains to be determined. Initially, it was tempting to speculate that this effect was due to the Cpc2p interaction with Msa2p. Indeed, upon pheromone stimulation Spk1p phosphorylates a negative regulator of Msa2p allowing production of Ste11p. However, Msa2p is expected to negatively regulate Cpc2p since it has been demonstrated that the *cpc2* null strain is phenotypically epistatic to an *msa2* deleted strain [22]. It is more plausible that the effects we observe following overexpression of Cpc2p are due to its role as an inhibitor of the essential kinase, Ran1p/Pat1p which has been reported to act by phosphorylating Mei2p so regulating sexual differentiation [48,49]. Cpc2p has been demonstrated to bind to Ran1p/Pat1p resulting in a change in its cellular localization causing a loss of activity [17]. The partial inhibition of Ran1p/Pat1p in starved haploid cells leads to a G_1 cell cycle arrest. This is consistent with our observations for cells lacking Cpc2p, which are sterile and fail to exhibit a pheromone-induced G_1 arrest. Moreover, it has been demonstrated that Ran1p/Pat1p phosphorylates Ste11p to down regulate its activity [50]. Thus overexpression of Cpc2p will lead to enhanced inhibition of Ran1p/Pat1p so preventing negative regulation of Ste11p [51] and prolonging the G_1 arrest. Further experimental work will be required to fully dissect the precise role that Cpc2p performs in modulating Ran1p/Pat1p activity and consequently Ste11p.

The pheromone-induced effects of Cpc2p are potentially re-enforced through the action of Msa2p. It has been suggested that upon pheromone stimulation, Spk1p phosphorylates an, as yet, unidentified negative regulator of Msa2p, so allowing increased production of Ste11p [25]. Overexpression of Cpc2p results in enhanced activation of Ste11p and coincides with abnormal morphologies and defects in cytokinesis (probably relating from reduced Cdc4p activity). Both these effects are consistent with a reduction in Msa2p activity since it negatively regulates Ste11p translation and also stabilizes *cdc4* mRNA [22]. Cpc2p modulates the activity of Atf1p and acts as a positive translational regulator of mRNA for Pyp1p and Pyp2p activity so reducing Pmk1p activity. This consequently decreases Msa2p activity.

Further to its roles in regulating sexual development through modulating Ran1p/Pat1p activity, Cpc2p has been described as being associated with the 40S ribosomal subunit so modulating gene transcription [27]. Paul and colleagues provided evidence to suggest that Cpc2p, through association with Moc2p and Rpl32-2p, may act to increase sexual differentiation [52]. Specifically, Rpl32-2p expression was shown to increase upon nitrogen starvation, analogous to Ste11p levels. In addition, deletion of *moc1* or *moc3* results in reduced *ste11* expression. Indeed it has been suggested that all Moc proteins and Cpc2p might act as a translational regulator involved in controlling sexual differentiation. Thus it is apparent that Cpc2p may play numerous roles in regulating the pheromone response by modulating *ste11* gene expression.

Previous investigations of Cpc2p activity within *S. pombe* have suggested that, in contrast to a role in modulating the G_1/S transition, that Cpc2p acts to positively regulate the G_2/M transition for mitotically growing cells [26]. However, as the authors themselves highlight, *S. pombe* cells spend most of their time (about three-quarters of the cell cycle) in G_2 whereas for mammalian cells the longest phase of the cell cycle is G_1 [26]. However, the addition of pheromone to *S. pombe* cells (subjected to nutrient limitation or removal of *cyr1*) causes them to initiate the meiotic mating-response pathway, resulting in cells remaining in the G_1 phase of the cell cycle for longer. Under these conditions addition of exogenous RACK1/Cpc2p results in a protraction of the G_1 arrest and prevents a return to mitotic growth. By the addition of pheromone to nitrogen starved *S. pombe* cells these now mimic mammalian cells by exhibiting an extended G_1 so enabling RACK1/Cpc2p to suppress G_1/S transition. These observations were confirmed by removal of Rum1p (the single CKI in fission yeast) or Pyp2p (MAPK phosphatases) both of which results in cells failing to enter G_1 and consequently, were unaffected by the addition of exogenous Cpc2p. By manipulating the duration of the G_1 phase of the cell cycle we have uncovered a subtle role that Cpc2p plays in *S. pombe*.

Materials and Methods

Strains, Reagents and General Methods

Fission yeast strains used in this study are listed in Table 1. Culture media used was YE - yeast extract for routine cell growth, amino acid (AA) medium for auxotrophic selection and DMM – a defined minimal medium for selective growth and all the assays. DMM is a variant of EMM and contains little nutritional supplement for the yeast. As a consequence cells can appear slightly more rounded than wild type strains. Nutritional limitation has previously been described as reducing the rate of cell growth and size [37]. As described previously lithium acetate was used for transformation of yeast [29,36]. Cell concentrations were determined using a Coulter Channelyser (Beckman Coulter, Luton, UK). DNA manipulations were performed by standard methods. Oligonucleotides were synthesized by Invitrogen Ltd. (Paisley, Scotland, UK). Amplification by the polymerase chain reaction (PCR) used *Pwo* DNA polymerase (from *Pyrococcus woesei*) according to the supplier's instructions (Boehringer–Mannheim Biochemicals, Lewes, East Sussex, UK). All constructs generated by PCR were confirmed by sequencing.

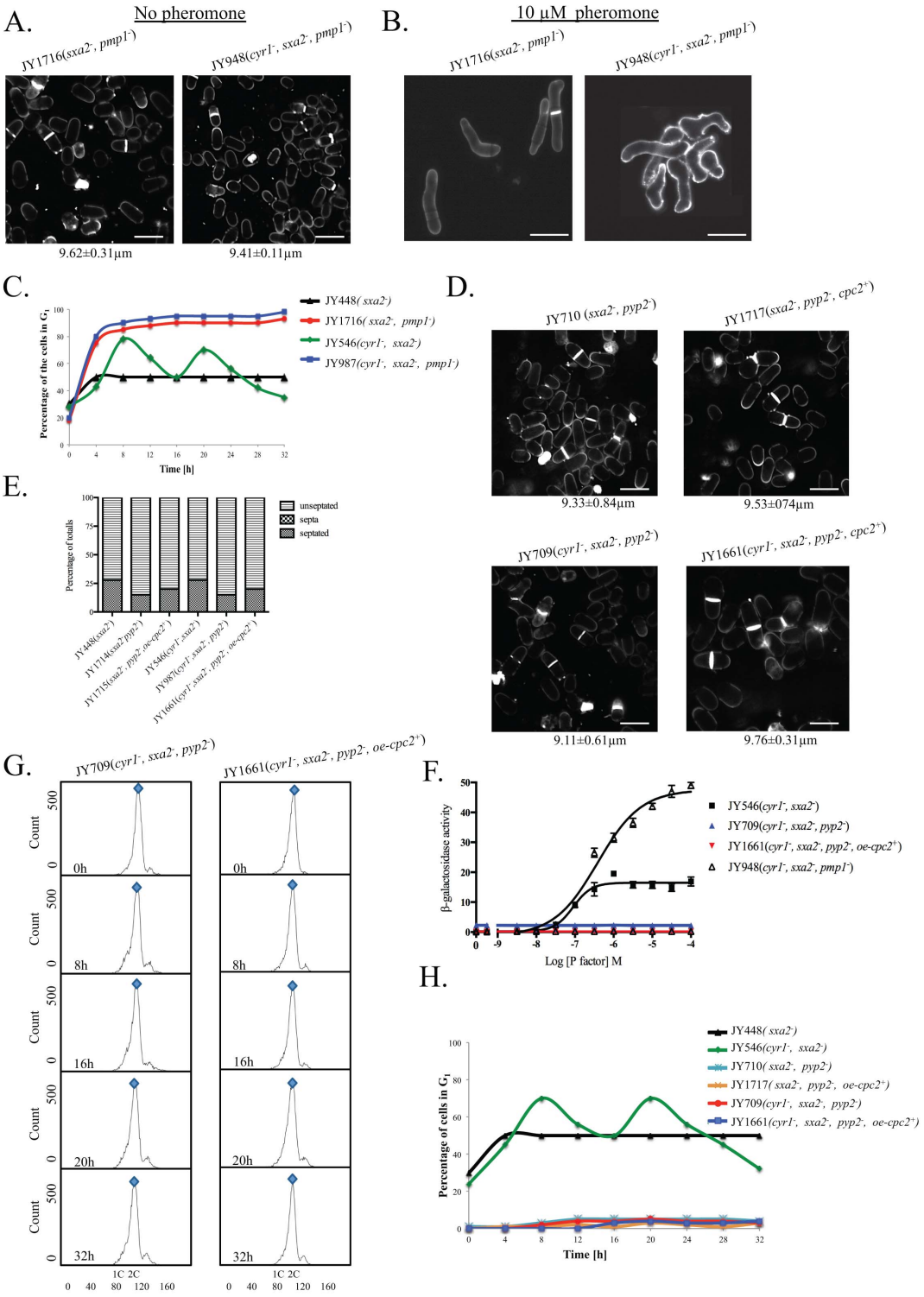
A.
No pheromone
JY1716(sxa2-, pmp1-)
JY948(cyr1-, sxa2-, pmp1-)
9.62±0.31μm
9.41±0.11μm
B.
10 μM pheromone
JY1716(sxa2-, pmp1-)
JY948(cyr1-, sxa2-, pmp1-)
C.
Percentage of the cells in G1
Time [h]
JY448(sxa2-)
JY1716(sxa2-, pmp1-)
JY546(cyr1-, sxa2-)
JY987(cyr1-, sxa2-, pmp1-)
D.
JY710 (sxa2-, pyp2-)
JY1717(sxa2-, pyp2-, cpc2+)
9.33±0.84μm
9.53±074μm
JY709(cyr1-, sxa2-, pyp2-)
JY1661(cyr1-, sxa2-, pyp2-, cpc2+)
9.11±0.61μm
9.76±0.31μm
E.
Percentage of totalls
unseptated
septa
septated
JY448(sxa2-)
JY1714(sxa2-pyp2-)
JY1715(sxa2-, pyp2-,oe-cpc2+)
JY546(cyr1-,sxa2-)
JY987(cyr1-,sxa2-, pmp1-)
JY1661(cyr1-,sxa2-, pyp2-, oe-cpc2+)
F.
β-galactosidase activity
Log [P factor] M
JY546(cyr1-, sxa2-)
JY709(cyr1-, sxa2-, pyp2-)
JY1661(cyr1-, sxa2-, pyp2-, oe-cpc2+)
JY948(cyr1-, sxa2-, pmp1-)
G.
JY709(cyr1-, sxa2-, pyp2-)
JY1661(cyr1-, sxa2-, pyp2-, oe-cpc2+)
Count
0h
8h
16h
20h
32h
1C 2C
H.
Percentage of cells in G1
Time [h]
JY448(sxa2-)
JY546(cyr1-, sxa2-)
JY710(sxa2-, pyp2-)
JY1717(sxa2-, pyp2-, oe-cpc2+)
JY709(cyr1-, sxa2-, pyp2-)
JY1661(cyr1-, sxa2-, pyp2-, oe-cpc2+)

Figure 5. Overexpression of Cpc2 in pheromone stimulated cells mimics prolonged pheromone stimulation. (A) Cell morphology and size, at division (micrometers ± S.D.) for the strains JY1716 (h^-, $sxa2^-$, $pmp1^-$) and JY948 (h^-, $cyr1^-$, sxa2>lacZ, $pmp1^-$) grown in minimal medium at 29°C and stained with calcofluor white. (B) Strains from A strains were exposure to 10 μM of pheromone for 32 h and stained with calcofluor white. (C) The percentage of cells containing a 1C content (arrested in G_1) for the strains JY448, JY1716, JY546 and JY948 as determined using flow cytometry. Cells lacking Pmp1p show a failure to exit from a G_1 arrest analogous to strains where the cpc2 ORF has been deleted. (D) Cell morphology and size, at division (micrometers ± S.D.) for strains JY710 (h^-, $sxa2^-$ $pyp2^-$) and JY1717 (h^-, $sxa2^-$, $pyp2^-$+oe-$cpc2^+$) grown in minimal medium at 29°C and stained with calcofluor white (top panel). Cell morphology and size at division (micrometers ± S.D.) for the strains JY709 (h^-, $cyr1^-$, sxa2>lacZ, $pyp2^-$) and JY1661 (h^-, $cyr1^-$, sxa2>lacZ, $pyp2^-$+oe-$cpc2^+$) grown in minimal medium at 29°C and stained with calcofluor white (bottom panel). (E) Numbers of non-septated, septated and multiple septa containing cells for the strains JY448, JY1714, JY1715, JY546, JY987 and JY1661 were determined from 400 individual cells. Values shown correspond to the percentages of the total population. Cells were stained with calcofluor white, to enable visualization of septum material. (F) Pheromone-dependent transcription for the strains JY546, JY709, JY1661 and JY948 was determined using the sxa2>lacZ reporter. Cells were stimulated with pheromone for 16 h in minimal media and assayed for β-galactosidase production using ONPG. Activity is expressed as OD_{420} units per 10^6 cells. Values are means of triplicate determinations ± S.E.M. (G) The strains JY709 and JY1661 were grown in minimal medium containing 10 μM of pheromone for the times indicated. Cells were harvested and fixed prior to staining with propidium iodide prior to analysis using flow cytometry (see methods). The proportion of cells exhibiting 1C or 2C DNA content was determined using FACSDiva v4.1 software for the assigned gates indicated by the blue and red shapes. (H) The percentage of cells containing a 1C content (arrested in G_1) as determined for the strains JY448, JY546, JY710, JY1717, JY709 and JY1661.
doi:10.1371/journal.pone.0065927.g005

Table 1. *S. pombe* strains used in this study.

Strain	Genotype	Source/reference
JY383	*mat1-P, Δmat2/3::LEU2⁻, leu1-32, ade6-M216, ura4-D18*	[56]
JY402	*mat1-M, Δmat2/3::LEU2⁻, ade6-M216, leu1-32 ura4-D18*	[57]
JY448	*mat1-M, Δmat2/3::LEU2⁻, leu1-32⁻, ade6-M216, ura4-D18, sxa2-D15*	[57]
JY546	*mat1-M, Δmat2/3::LEU2⁻, leu1-32, ade6-M216, ura4-D18, cyr1-D51, sxa2>lacZ*	[45]
JY709	*mat1-M, Δmat2/3::LEU2⁻, leu1-32, ade6-M216, ura4-D18, cyr1-D51, sxa2>lacZ, pyp2::ura4⁻*	This study
JY710	*mat1-M, Δmat2/3⁻::LEU2⁻, leu1-32, ade6-M216, ura4-D18, sxa2-D15, pyp2::ura4⁻*	This study
JY948	*mat1-M, Δmat2/3::LEU2⁻, leu1-32, ade6-M216, ura4-D18, cyr1-D51, sxa2>lacZ, pmp1::ura4⁻*	This study
JY1034	*mat1-M, Δmat2/3::LEU2⁻, leu1-32, ade6-M216, ura4-D18, cyr1-D51, sxa2>lacZ,* pREP3x-$^{1-40}$Gpa1-GFP	This study
JY1314	*mat1-M, Δmat2/3::LEU2⁻, leu1-32, ade6-M216, ura4-D18, cyr1-D51, sxa2>lacZ, gnr1::ura4⁻*	[12]
JY1315	*mat1-M, Δmat2/3::LEU2⁻, leu1-32, ade6-M216, ura4-D18, cyr1-D51, sxa2>lacZ, gnr1::ura4⁻*, pREP3x-$^{1-40}$Gpa1-GFP	This study
JY1316	*mat1-M, Δmat2/3::LEU2⁻, leu1-32, ade6-M216, ura4-D18, cyr1-D51, sxa2>lacZ,* pREP3x-Gnr1	This study
JY1317	*mat1-M, Δmat2/3::LEU2⁻, leu1-32, ade6-M216, ura4-D18, cyr1-D51, sxa2>lacZ, gnr1::ura4⁻*, pREP3x-Gnr1	This study
JY1520	*mat1-M, Δmat2/3::LEU2⁻, leu1-32, ade6-M216, ura4-D18, cyr1-D51, sxa2>lacZ, rum1::ura4⁻*	This study
JY1578	*mat1-M, Δmat2/3::LEU2⁻, leu1-32, ade6-M216, ura4-D18, cyr1-D51, sxa2>lacZ,* pREP3x-Cpc2	This study
JY1628	*mat1-M, Δmat2/3::LEU2⁻, leu1-32, ade6-M216, ura4-D18, cyr1-D51, sxa2>lacZ, cpc2::ura4⁻*	This study
JY1629	*mat1-M, Δmat2/3::LEU2⁻, leu1-32, ade6-M216, ura4-D18, cyr1-D51, sxa2>lacZ, cpc2::ura4⁻*, pREP3x-$^{1-40}$Gpa1-GFP	This study
JY1633	*mat1-P, Δmat2/3::LEU2⁻, leu1-32, ade6-M216, ura4-D18,* pREP3x-Cpc2	This study
JY1634	*mat1-M,Δmat2/3::LEU2⁻, leu1-32, ade6-M216, ura4-D18,* pREP3x-Cpc2	This study
JY1635	*mat1-P, Δmat2/3::LEU2⁻, leu1-32, ade6-M216, ura4-D18, cpc2::ura4⁻*	This study
JY1636	*mat1-M,Δmat2/3::LEU2⁻, leu1-32, ade6-M216, ura4-D18, cpc2::ura4⁻*	This study
JY1637	*mat1-M, Δmat2/3::LEU2⁻, leu1-32, ade6-M216, ura4-D18, cyr1-D51, sxa2>lacZ, rum1::ura4⁻*, pREP3x-Cpc2	This study
JY1661	*mat1-M, Δmat2/3::LEU2⁻, leu1-32, ade6-M216, ura4-D18, cyr1-D51, sxa2>lacZ, pyp2::ura4⁻*, pREP3x-Cpc2	This study
JY1662	*mat1-M, Δmat2/3::LEU2⁻, leu1-32, ade6-M216, ura4-D18, cyr1-D51, sxa2>lacZ, cpc2::ura4⁻*, pREP3x-RACK1	This study
JY1663	*mat1-M, Δmat2/3::LEU2⁻, leu1-32, ade6-M216, ura4-D18, cyr1-D51, sxa2>lacZ,* pREP3x-RACK1	This study
JY1710	*mat1-M, Δmat2/3::LEU2⁻, leu1-32, ade6-M216, ura4-D18, cyr1-D51, sxa2>lacZ, rum1::ura4⁻, cpc2::ura4⁻*	This study
JY1711	*mat1-M, Δmat2/3::LEU2⁻, leu1-32, ade6-M216, ura4-D18, sxa2-D15,* pREP3x-Cpc2	This study
JY1712	*mat1-M, Δmat2/3::LEU2⁻, leu1-32, ade6-M216, ura4-D18, sxa2-D15, cpc2::ura4⁻*	This study
JY1713	*mat1-M, Δmat2/3::LEU2⁻, leu1-32, ade6-M216, ura4-D18, cyr1-D51, sxa2>lacZ, cpc2::ura4⁻*, pREP3x-Cpc2	This study
JY1714	*mat1-M, Δmat2/3::LEU2⁻, leu1-32, ade6-M216, ura4-D18, sxa2-D15, rum1::ura4⁻*	This study
JY1715	*mat1-M, Δmat2/3::LEU2⁻, leu1-32, ade6-M216, ura4-D18, sxa2-D15, rum1::ura4⁻*, pREP3x-Cpc2	This study
JY1716	*mat1-M, Δmat2/3::LEU2⁻, leu1-32, ade6-M216, ura4-D18, sxa2-D15, pmp1::ura4⁻*	This study
JY1717	*mat1-M, Δmat2/3::LEU2⁻, leu1-32, ade6-M216, ura4-D18, sxa2-D15, pyp2::ura4⁻*, pREP3x-Cpc2	This study

doi:10.1371/journal.pone.0065927.t001

Disruption of Endogenous S. pombe cpc2

The upstream region of *cpc2* locus was amplified from *S. pombe* genomic DNA using sense oligonucleotide JO2836 (aaaTCTAGACTAGAGCATTATTCAAGATAAATTTC; position 954 to 928 relative to *cpc2* ATG, *Xba*I site underlined) and antisense oligonucleotide JO2837 (aaaGGATCCCCCCTTCACTGGTCGGGATGTC; position 35 to 3 relative to *cpc2* ATG, *Bam*HI site underlined). The downstream region of *cpc2* locus was amplified from *S. pombe* genomic DNA using sense oligonucleotide JO2838 (aaaGGATCCGGGAAA*TAA*GATTTTAATTGTTGTCCC; position 4 to 40 relative from *cpc2* STOP anticodon, *Bam*HI site underlined) and antisense oligonucleotide JO2839 (aaaCCCGGGGAACAACAACT*ATT*CAGCCACCCCCAGCGAAGG; position 444 to 485 relative from *cpc2* STOP anticodon (italics), *Sma*I site underlined). A 1.8 kb fragment of the *S. pombe ura4*$^+$ cassette was amplified using sense oligonucleotide JO1049 (CTGGATCCACCATGTAGCTACAAATCC) and antisense oligonucleotide JO1050 (CTGGATCCACCATGTAGTGATATTGAC). Both up and downstream PCR products were cloned respectively into pKS$^+$ Bluescript (Stratagene) digested with *Bam*HI. The *ura4*$^+$ cassette (JD3725) was cloned into the unique *Bam*HI site within the *cpc2* ORF to create *cpc2*::*ura4*$^+$. The strains JY448 (h$^-$, *sxa2*$^-$) and JY546 (h$^-$, *cyr1*$^-$, *sxa2*>*lacZ*) were transformed with the *Xba*I/*Sma*I fragment from JD3725 and integration of the *ura4* cassette selected by growth on medium lacking uracil. To enable consistent comparison with the parent strains, which were *ura4*$^-$, the Ura4 ORF was subsequently deleted from the *cpc2* locus using a *Bam*HI digest of JD437 (pKS$^+$ Bluescript containing the 5′ and 3′ un-translated regions of the *ura4* cassette separated by an *Eco*RV site). We have used similar techniques for disruption of other members of the *S. pombe* pheromone-response pathway [11]. Transformants were selected by growth on minimal media supplemented with 5-fluoro-orotic acid (FOA). The resultant strains produced were JY1712 (h$^-$, *sxa2*$^-$, *cpc2*$^-$) and JY1628 (h$^-$, *cyr1*$^-$, *sxa2*>*lacZ*, *cpc2*$^-$).

Disruption of Endogenous Rum1

A similar two-step technique as described for *cpc2* was used for the disruption of *rum1*. Briefly, the *rum1* locus was amplified from *S. pombe* genomic DNA using sense oligonucleotide JO2658 (gggACTAGTTTTTAAATTCTAACATTAG; position -569 to -545 relative to *rum1* ATG, *Spe*I site underlined) and antisense oligonucleotide JO2659 (cccACTAGTTATTGAGAATAACAGAC; position 550 to 568 relative from *rum1* STOP anticodon, *Spe*I site underlined). This product was cloned into pKS$^+$ Bluescript digested with *Pvu*II. The ORF was removed from this construct and replaced with a unique *Bgl*II site by inverse PCR to generate JD3674 using the antisense oligonucleotide JO2661 (AGATCTAGCGAACTGACAATCC; position -1 to -16 relative to *rum1* ATG, *Bgl*II site underlined) and sense oligonucleotide JO2660 (AGATCTCGCATTTTGTAATTGTGTTTG; position 10 to 31 relative from *rum1* STOP anticodon, *Bgl*II site underlined). The 1.8 kb *ura4*$^+$ cassette was cloned into the unique *Bgl*II site of JD3674 to create the *rum1*::*ura4*$^+$ contained within pKS$^+$ Bluescript (JD3675). The strains JY1628 (h$^-$, *cyr1*$^-$, *sxa2*>*lacZ*, *cpc2*$^-$) and JY546 (h$^-$, *cyr1*$^-$, *sxa2*>*lacZ*) were transformed with the *Spe*I fragment from JD3675 and integration of the *ura4* cassette selected by growth on medium lacking uracil. Removal of the Ura4 ORF from the locus of *rum1* was achieved as described for *cpc2*. The resultant strains produced were JY1710 (h$^-$, *sxa2*$^-$, *cpc2*$^-$, *rum1*$^-$), JY1520 (h$^-$, *cyr1*$^-$, *sxa2*>*lacZ*, *rum1*$^-$).

Disruption of Endogenous pmp1 and pyp2

We have previously described the generation of the strain JY723 that lacks *pmp1* (h$^-$, *cyr1*$^-$, *sxa2*>*lacZ*, *pmp1::ura4*$^+$) [45]. Removal of the Ura4 ORF from this strain generated JY948 (h$^-$, *cyr1*$^-$, *sxa2*>*lacZ*, *pmp1::ura4*$^-$). A similar two-step method was used to disrupt *pmp1* from JY448 (h$^-$, *sxa2*$^-$) generating JY1716 (h$^-$, *sxa2*$^-$, *pmp1::ura4*$^-$). Disruption of *pyp2* was again accomplished using a two-step integration strategy. The *pyp2* locus was amplified using sense oligonucleotide JO842 (gggcagCTGTTCAACATCAATAGGCAA; position -528 to -508 relative to *pyp2* ATG, *Pvu*II site underlined) and antisense oligonucleotide JO843 (gggcagCTGGTAACAATGCAAATCAAC; position 531 to 551 relative from *pyp2* STOP anticodon) and cloned into pKS$^+$ Bluescript digested with *Pvu*II. The Pyp2 ORF was removed from this construct and replaced with a unique *BamH*I site by inverse PCR to generate JD970 using the antisense oligonucleotide JO844 (ggggatccTTGAAAACACCTTGGAAGATG; position -16 to -36, relative to *pyp2* ATG, *Bam*HI site underlined) and sense oligonucleotide JO845 (ggggatccGATGACTTAACGAAACGACTG; position -7 to 14 relative from *pyp2* STOP anticodon). The 1.8 kb *ura4*$^+$ cassette was cloned into the unique *Bam*HI site of JD970 to create the *pyp2*::*ura4*$^+$ contained within pKS$^+$ Bluescript (JD978). The strains JY448 (h$^-$, *sxa2*$^-$) and JY546 (h$^-$, *cyr1*$^-$, *sxa2*>*lacZ*) were transformed with the *Pvu*II fragment from JD978 and integration of the *ura4* cassette selected by growth on medium lacking uracil. Removal of the Ura4 ORF from the locus of *pyp2* was achieved as described for *cpc2*. The resultant strains produced were JY709 (h$^-$, *cyr1*$^-$, *sxa2*>*lacZ*, *pyp2*$^-$) and JY710 (h$^-$, *sxa2*$^-$, *pyp2*$^-$). All gene replacements were confirmed by PCR from genomic DNA.

The Mating-response Assay

Cells were cultured in liquid DMM to a density of 5x10^6 cells/ml. 200 µl of each mating type strain were mixed and harvested by centrifugation (2000 rpm for 3 min). Cells were suspended in 10 µl of sterile water and spotted onto low nitrogen containing DMM plates. Non-mixed controls were also spotted onto the plates. Following 72 h incubation at 29°C, each colony was collected from the spots and suspended in 1 ml of sterile water. Two separate 1 in 100 dilutions were then made from each 1 ml culture. One of these was plated onto separate YE plates at final dilution factors of 1 in 1,000 and 1 in 10,000 respectively. The other was placed in a 55°C heat block for 10 min to heat-inactivate everything except spores formed from mating events. This heat-treated sample was then also plated onto separate YE plates at final dilution factors of 1 in 1,000 and 1 in 10,000. Following 72 h incubation, the number of colonies on each plate was counted using a G-Box iChemi gel documentation system with GeneTool analysis software (Syngene, Cambridge, UK). The number of colonies as a percentage of the total (colony survival) can then be calculated for mated strains and controls, then the mating efficiency calculated as colony survival (mated strains) - colony survival (non-mated control strain).

pREP Expression Constructs

pREP series of *S. pombe* vectors allows expression of genes under the control of the thiamine-repressible *nmt1* promoter [53]. pREP3x-Cpc2 has been kindly offered by Jose Cansado (University of Murcia, Spain). The ORF of mammalian RACK1 was amplified from a plasmid donated by Dorit Ron (University of California, USA) using the sense primer JO2996 (GCCACCATGGATTACAAGGAT), and the antisense primer JO1606 (*TTA*GCGGGTACCAATAGTCACCT) which contains the stop anticodon (italics). The PCR product was cloned into the unique

*Eco*RV site of a modified pREP3x vector to generate (pREP3x-RACK1).

$^{1-40}$Gpa1 was first amplified using a sense oligonucleotide beginning at the initiating ATG (JO1605) (ATGGGATG-CATTCGAGTAAATACGC) and an antisense oligonucleotide containing half an *Eco*RV site (underlined) (JO2684) (atcTG-GAACTCGAGCGTTTTG). The PCR product was cloned into the unique *Eco*RV site of a modified pREP3x vector containing GFP.

Assay of β-galactosidase Activity

Assays were performed using a method modified from Dohlman *et al.* (1995) [45,54]. *S. pombe* cells were cultured to a density of ~5x10^6 cells/ml in DMM and 500µl aliquots transferred to 2 ml Safe-Lock tubes (Eppendorf, Hamburg, Germany) containing 5 µl of the appropriate ligand (in HPLC-grade methanol). Tubes were incubated at 29°C for 16 h on a rotating wheel, and 50 µl transferred to 750 µl Z-buffer containing 2.25 mM o-nitrophenyl-β-D-galactopyranoside (ONPG). Reactions were stopped after 90 min by adding 200 µl of 2 M Na_2CO_3 and β-galactosidase activity calculated as optical density at 420 nm (OD_{420}) per 10^6 cells (determined using a Coulter Channelyzer).

Confocal Microscopy

In order to measure cell size at division and percentage of multi-septated cells, strains were grown in low nitrogen containing DMM medium to an ~5x10^6 cells/ml and stained with calcofluor white (Sigma), which specifically stains cell wall and septum [54,55]. Minimums of 200 cells, chosen at random, were used in calculating septation rate for each mutant. For life cell imaging cells were placed on a solid DMM (2% agarose) pad on a CoverWell^{TM} imaging chamber (Grace Bio-Labs, Oregon, USA) coverslip was placed over the cells on the agar pad and sealed with a Vaseline, Lanolin and Paraffin equal parts by weight mixture to prevent drying of the sample. Images were then obtained using a True Confocal Scanner Leica TCS SP5 microscope (Leica Microsystems Ltd., Milton Keynes, UK). Series of images were taken using Z stacks at time = 0 h and subsequently every 15 min for a period of 16 h. The imaging procedure was set up such that cells were focused at 0 h and the Z position noted (Z_{focus}). The Z-stack was then defined such that 20 Z-slice images would be obtained from Z_{focus} - 10 µm to Z_{focus} +10 µm to allow for drift in the focal plane over the course of the experiment. The time-series experiment was setup such that both bright field and fluorescence images were generated, and imported into ImageJ (http://rsb.info.nih.gov/ij/). Following analysis the image in the z–stack with the highest intensity was chosen.

Flow Cytometry

Flow cytometry was performed using a Becton, Dickinson and Company (BD) LSR II flow cytometer (BD Biosciences, Oxford, UK). For cell cycle progression analysis, cells were grown under standard conditions and following sonication, harvested by centrifugation and fixed in 1 ml of ice cold 70% ethanol overnight. 300 µl of fixed cells were then washed in 3 ml of fresh 50 mM sodium citrate and re-suspended in 500 µl of fresh 50 mM sodium citrate containing 0.1 mg/ml RNase A. Cells were incubated at 37°C for 2 h before the addition of 500 µl of 50 mM sodium citrate containing 8 g/ml propidium iodide (Sigma). Up to 30,000 particles per sample were then analyzed using the flow cytometer, measuring the intensities of staining with propidium iodide. Excitation was achieved using a 488 nm laser, and emission detected using a 575/26 nm band pass filter with a 550 nm long pass filter. All analysis was performed using FACSDiva v4.1 (BD Biosciences).

Data analysis. Data were analyzed using linear and non-linear regression as appropriate using GraphPad Prism v6.0b (GraphPad Software Inc, San Diego, CA). Statistical significance was determined using a one-way ANOVA with a Tukey multiple comparison post-test or an un-paired Student's t test.

Supporting Information

Figure S1 Characterization of Gnr1p a potential Gβ-subunit mimic in the pheromone-response pathway. Pheromone-dependent transcription for cells either lacking or overexpressing (using the thiamine repressible nmt1 promoter) Gnr1p, was determined using the sxa2>lacZ reporter. Cells were stimulated with pheromone for 16 h in minimal media and assayed for β-galactosidase production using ONPG. Activity is expressed as OD_{420} units per 10^6 cells (see methods).
(TIF)

Figure S2 The N-terminal domain alone of Gpa1 is sufficient to ensure correct plasma membrane localization. The strains JY546 (h$^-$, cyr1$^-$, sxa2>lacZ), JY1314 (h$^-$, cyr1$^-$, sxa2>lacZ, gnr1$^-$) and JY1628 (h$^-$, cyr1$^-$, sxa2>lacZ, cpc2$^-$) containing pGFP or p$^{1-40}$Gpa1-GFP were imaged using fluorescence microscopy. Scale bars 10 µm. The N-terminal 40 amino acids of Gpa1 are sufficient to promote plasma membrane localization of GFP. This suggests that Gpa1p does not have a requirement for a classical Gβγ to enable plasma membrane localization.
(TIF)

Figure S3 Pheromone-dependent transcription for the strains JY546 (h$^-$, cyr1$^-$, sxa2>lacZ), JY1662 (h$^-$, cyr1$^-$, sxa2>lacZ, cpc2$^-$, +oe-RACK1$^+$) and JY1663 (h$^-$, cyr1$^-$, sxa2>lacZ, +oe-RACK1$^+$) was determined using the sxa2>lacZ reporter (A). Mammalian RACK1 was expressed using the thiamine repressible nmt1 promoter and cells were cultured in the absence of thiamine to ensure maximal levels of transcription. Cells were stimulated with pheromone for 16 h in minimal media and assayed for β-galactosidase production using ONPG. Activity is expressed as OD_{420} units per 10^6 cells (see methods). (B) The strains JY546 and JY1663 were treated described in Figure 3, and the number of cells containing a 1C content of DNA (expressed as a percentage of total cells) determined. Consistent with overexpression of Cpc2, RACK1 containing cells fail to desensitize from pheromone stimulation and remain arrested for the time frame analyzed.
(TIF)

Acknowledgments

We thank Jose Cansado for Cpc2 plasmids, Dorit Ron for providing the RACK1 mammalian plasmid, Michael Bond for generation of the Rum1 deletion strain, and Cathryn Weston for providing images of $^{1-40}$Gpa1-GFP localization.

Author Contributions

Conceived and designed the experiments: MM GL. Performed the experiments: MM MAE-F. Analyzed the data: MM GL. Contributed reagents/materials/analysis tools: MM GL. Wrote the paper: MM GL. Performed part of the experiments: ELG KR. Research advisor: JD.

References

1. Gilman AG (1987) G proteins: transducers of receptor-generated signals. Annu Rev Biochem 56: 615–649.
2. Dupré DJ, Robitaille M, Rebois RV, Hébert TE (2009) The Role of Gβγ Subunits in the Organization, Assembly, and Function of GPCR Signaling Complexes. Annu Rev Pharmacol Toxicol 49: 31–56.
3. Hill C, Goddard A, Ladds G, Davey J (2009) The cationic region of Rhes mediates its interactions with specific Gbeta subunits. Cell Physiol Biochem 23: 1–8.
4. Hiskens R, Vatish M, Hill C, Davey J, Ladds G (2005) Specific in vivo binding of activator of G protein signalling 1 to the G [beta] 1 subunit. Biochem Biophy Res Commun 2;337:1038–1046.
5. Blumer JB, Cismowski MJ, Sato M, Lanier SM (2005) AGS proteins: receptor-independent activators of G-protein signaling. Trends Pharmacol Sci 26: 470–476.
6. Batlle M, Lu A, Green DA, Xue Y, Hirsch JP (2003) Krh1p and Krh2p act downstream of the Gpa2p G(alpha) subunit to negatively regulate haploid invasive growth. J Cell Sci 116: 701–710.
7. Peeters T, Louwet W, Geladé R, Nauwelaers D, Thevelein JM, et al. (2006) Kelch-repeat proteins interacting with the G protein Gpa2 bypass adenylate cyclase for direct regulation of protein kinase A in yeast. Proc Natl Acad Sci 35: 13034–13039.
8. Niranjan T, Guo X, Victor J, Lu A, Hirsch JP (2007) Kelch Repeat Protein Interacts with the Yeast G Subunit Gpa2p at a Site That Couples Receptor Binding to Guanine Nucleotide Exchange. J Biol Chem 282: 24231–24238.
9. Harashima T, Heitman J (2005) Galpha subunit Gpa2 recruits kelch repeat subunits that inhibit receptor-G protein coupling during cAMP-induced dimorphic transitions in Saccharomyces cerevisiae. Mol Biol Cell 16: 4557–4571.
10. Zeller CE, Parnell SC, Dohlman HG (2007) The RACK1 ortholog Asc1 functions as a G-protein beta subunit coupled to glucose responsiveness in yeast. J Biol Chem 282: 25168–25176.
11. Ladds G, Goddard A, Hill C, Thornton S, Davey J (2007) Differential effects of RGS proteins on G alpha(q) and G alpha(11) activity. Cell Signal 19: 103–113.
12. Ladds G, Goddard A, Davey J (2005) Functional analysis of heterologous GPCR signalling pathways in yeast. Trends Biotechnol 23: 367–373.
13. Davey J (1998) Fusion of a fission yeast. Yeast 14: 1529–1566.
14. Kim DU, Park SK, Chung KS, Choi MU, Yoo HS (1996) The G protein beta subunit Gpb1 of Schizosaccharomyces pombe is a negative regulator of sexual development. Mol Gen Genet 252: 20–32.
15. Landry S, Pettit MT, Apolinario E, Hoffman CS (2000) The fission yeast git5 gene encodes a Gbeta subunit required for glucose-triggered adenylate cyclase activation. Genetics 154: 1463–1471.
16. Goddard A, Ladds G, Forfar R, Davey J (2006) Identification of Gnr1p, a negative regulator of Gα signalling in Schizosaccharomyces pombe, and its complementation by human Gβ subunits. Fungal Genet Biol 43: 840–851.
17. McLeod M, Shor B, Caporaso A, Wang W, Chen H, et al. (2000) Cpc2, a fission yeast homologue of mammalian RACK1 protein, interacts with Ran1 (Pat1) kinase To regulate cell cycle progression and meiotic development. Mol Cell Biol 20: 4016–4027.
18. Núñez A, Franco A, Madrid M, Soto T, Vicente J, et al. (2009) Role for RACK1 orthologue Cpc2 in the modulation of stress response in fission yeast. Mol Biol Cell 20: 3996–4009.
19. McCahill A, Warwicker J, Bolger G, Houslay M, Yarwood S (2002) The RACK1 scaffold protein: A dynamic cog in cell response mechanisms. Mol Pharmacol 62: 1261–1273.
20. Mamidipudi V, Miller LD, Mochly-Rosen D, Cartwright CA (2007) Peptide modulators of Src activity in G1 regulate entry into S phase and proliferation of NIH 3T3 cells. Biochem Biophys Res Commun 352: 423–430.
21. Mamidipudi V, Zhang J, Lee KC, Cartwright CA (2004) RACK1 regulates G1/S progression by suppressing Src kinase activity. Mol Cell Biol 24: 6788–6798.
22. Jeong HT, Oowatari Y, Abe M, Tanaka K, Matsuda H, et al. (2004) Interaction between a Negative Regulator (Msa2/Nrd1) and a Positive Regulator (Cpc2) of Sexual Differentiation in Schizosaccharomyces pombe. Biosci Biotechnol Biochem 68: 1621–1626.
23. Balasubramanian M, McCollum D, Chang L (1998) Isolation and characterization of new fission yeast cytokinesis mutants. Genetics 149: 1265–1275.
24. Tsukahara K, Yamamoto H, Okayama H (1998) An RNA binding protein negatively controlling differentiation in fission yeast. Mol Cell Biol 18: 4488–4498.
25. Oowatari Y, Jeong H, Tanae K, Nakagawa T, Kawamukai M (2011) Regulation and role of an RNA-binding protein Msa2 in controlling the sexual differentiation of fission yeast. Current Genetics 57: 191–200.
26. Núñez A, Franco A, Soto T, Vicente J, Gacto M, et al. (2010) Fission yeast receptor of activated C kinase (RACK1) ortholog Cpc2 regulates mitotic commitment through Wee1 kinase. J Biol Chem 285: 41366–41373.
27. Shor B, Calaycay J, Rushbrook J, McLeod M (2003) Cpc2/RACK1 is a ribosome-associated protein that promotes efficient translation in Schizosaccharomyces pombe. J Biol Chem 278: 49119–49128.
28. Imai Y, Yamamoto M (1992) Schizosaccharomyces pombe sxa1+ and sxa2+ encode putative proteases involved in the mating response. Mol Cell Biol 12: 1827–1834.
29. Ladds G, Rasmussen EM, Young T, Nielsen O, Davey J (1996) The sxa2-dependent inactivation of the P-factor mating pheromone in the fission yeast Schizosaccharomyces pombe. Mol Microbiol 20: 35–42.
30. Lipman D, Pearson W (1985) Rapid and sensitive protein similarity searches. Science 227: 1435–1441.
31. Kiefer F, Arnold K, Künzli M, Bordoli L, Schwede T (2009) The SWISS-MODEL Repository and associated resources. Nucleic Acids Res 37: D387–D392.
32. Kopp J (2004) The SWISS-MODEL Repository of annotated three-dimensional protein structure homology models. Nucleic Acids Res 32: D230–234.
33. Neer EJ, Schmidt CJ, Nambudripad R, Smith TF (1994) The ancient regulatory-protein family of WD-repeat proteins. Nature 371: 297–300.
34. Maeda TT, Mochizuki NN, Yamamoto MM (1990) Adenylyl cyclase is dispensable for vegetative cell growth in the fission yeast Schizosaccharomyces pombe. Proc Natl Acad Sci USA 87: 7814–7818.
35. Jin M, Fujita M, Culley BM, Apolinario E, Yamamoto M, et al. (1995) sck1, a high copy number suppressor of defects in the cAMP-dependent protein kinase pathway in fission yeast, encodes a protein homologous to the Saccharomyces cerevisiae SCH9 kinase. Genetics 140: 457–467.
36. Davey J, Egel R, Nielsen O (1995) Methods in Molecular Genetics. Elsevier. 17 pp.
37. Fantes P, Nurse P (1977) Control of cell size at division in fission yeast by a growth-modulated size control over nuclear division. Exp Cell Res 107:377–386.
38. Davey J (1992) Mating pheromones of the fission yeast Schizosaccharomyces pombe: purification and structural characterization of M-factor and isolation and analysis of two genes encoding the pheromone. EMBO J 11: 951.
39. Mamidipudi V, Dhillon NK, Parman T, Miller LD, Lee KC, et al. (2007) RACK1 inhibits colonic cell growth by regulating Src activity at cell cycle checkpoints. Oncogene 26: 2914–2924.
40. C Martin-Castellanos, Labib K, Moreno S(1996) B-type cyclins regulate G1 progression in fission yeast in opposition to the p25rum1 cdk inhibitor. EMBO J 15: 839.
41. Correa-Bordes J, Nurse P (1995) p25rum1 orders S phase and mitosis by acting as an inhibitor of the p34cdc2 mitotic kinase. Cell 83: 1001–1009.
42. Moreno S, Nurse P (1994) Regulation of progression through the Gl phase of the cell cycle by the rum1+ gene. Nature 367: 236–242.
43. Benito J, Martín-Castellanos C, Moreno S (1998) Regulation of the G1 phase of the cell cycle by periodic stabilization and degradation of the p25rum1 CDK inhibitor. EMBO J 17: 482–497.
44. Moreno S, Labib K, Correa J, Nurse P (1994) Regulation of the cell cycle timing of Start in fission yeast by the rum1+ gene. J Cell Sci Suppl 18: 63–68.
45. Didmon M, Davis K, Watson P, Ladds G, Broad P, et al. (2002) Identifying regulators of pheromone signalling in the fission yeast Schizosaccharomyces pombe. Curr Genet 41: 241–253.
46. Hanning G, Ottilie S, Erikson R (1994) Negative Regulation of Mitosis in Fission Yeast by Catalytically Inactive Pyp1 and Pyp2 Mutants. Proc Natl Acad Sci USA 91: 10084–10088.
47. Johnson DR, Knoll LJ, Levin DE, Gordon JI (1994) Saccharomyces cerevisiae contains four fatty acid activation (FAA) genes: an assessment of their role in regulating protein N-myristoylation and cellular lipid metabolism. J Cell Biol 127: 751–762.
48. Kitamura K, Katayama S, Dhut S, Sato M, Watanabe Y, et al. (2001) Phosphorylation of Mei2 and Ste11 by Pat1 kinase inhibits sexual differentiation via ubiquitin proteolysis and 14–3-3 protein in fission yeast. Dev Cell 1: 389–399.
49. Watanabe Y, Shinozaki-Yabana S, Chikashige Y, Hiraoka Y, Yamamoto M (1997) Phosphorylation of RNA-binding protein controls cell cycle switch from mitotic to meiotic in fission yeast. Nature 386: 187–190.
50. Li P, McLeod M (1996) Molecular mimicry in development: identification of ste11+ as a substrate and mei3+ as a pseudosubstrate inhibitor of ran1+ kinase. Cell 87: 869–880.
51. Kjaerulff S, Lautrup-Larsen I, Truelsen S, Pedersen M, Nielsen O (2005) Constitutive activation of the fission yeast pheromone-responsive pathway induces ectopic meiosis and reveals ste11 as a mitogen-activated protein kinase target. Mol Cell Biol 25: 2045–2059.
52. Paul SK, Oowatari Y, Kawamukai M (2009) A large complex mediated by Moc1, Moc2 and Cpc2 regulates sexual differentiation in fission yeast. FEBS J 276:5076–5093.
53. Maundrell K (1993) Thiamine-Repressible Expression Vectors Prep and Prip for Fission Yeast. Gene 123: 127–130.
54. Ladds G, Davis K, Hillhouse EW, Davey J (2003) Modified yeast cells to investigate the coupling of G protein-coupled receptors to specific G proteins. Mol Microbiol 47: 781–792.
55. Ladds G, Davey J (2000) Identification of proteases with shared functions to the proprotein processing protease Krp1 in the fission yeast Schizosaccharomyces pombe. Mol Microbiol 38: 839–853.
56. Watson P, Davis K, Didmon M, Broad P (1999) An RGS protein regulates the pheromone response in the fission yeast Schizosaccharomyces pombe. Mol Microbiol 33:623–634.
57. Egel R, Willer M, Kjærulff S, Davey J, Nielsen O (1994) Assessment of pheromone production and response in fission yeast by a halo test of induced sporulation. Yeast 10:1347–1354.

Bibliography

[1] J. C. Venter, M. D. Adams, E. W. Myers, H. O. Smith, and et al., "The sequence of the human genome," *Science*, vol. 291, pp. 1304–51, Feb 2001.

[2] R. Fredriksson, M. C. Lagerström, L.-G. Lundin, and H. B. Schiöth, "The G-protein-coupled receptors in the human genome form five main families. phylogenetic analysis, paralogon groups, and fingerprints," *Mol Pharmacol*, vol. 63, pp. 1256–72, Jun 2003.

[3] K. L. Pierce, R. T. Premont, and R. J. Lefkowitz, "Seven-transmembrane receptors," *Nat Rev Mol Cell Biol*, vol. 3, pp. 639–50, Sep 2002.

[4] S. J. Hill, "G-protein-coupled receptors: past, present and future," *Br J Pharmacol*, vol. 147 Suppl 1, pp. S27–37, Jan 2006.

[5] R. Lappano and M. Maggiolini, "G protein-coupled receptors: novel targets for drug discovery in cancer," *Nat Rev Drug Discov*, vol. 10, pp. 47–60, Jan 2011.

[6] S. Tugendreich, D. E. Bassett, V. A. McKusick, M. S Boguski, and P. Hieter, "Genes conserved in yeast and humans," *Hum Mol Genet*, vol. 3 Spec No, pp. 1509–17, Jan 1994.

[7] T. Kataoka, S Powers, S Cameron, O. Fasano, M. Goldfarb, J. Broach, and M. Wigler, "Functional homology of mammalian and yeast Ras genes," *Cell*, vol. 40, pp. 19–26, Jan 1985.

[8] M. G. Lee and P. Nurse, "Complementation used to clone a human homologue of the fission yeast cell cycle control gene cdc2," *Nature*, vol. 327, pp. 31–5, Jan 1987.

[9] A. H. Zetterberg, R. F. Pettersson, and S G Lindahl, "Hartwell, Hunt and Nurse share the 2001 Nobel Prize in physiology or medicine. CDK and cyclin–molecular motors of cell cycle," *Lakartidningen*, vol. 98, pp. 4544–50, Oct 2001.

[10] M. A. Dickson and G. K. Schwartz, "Development of cell-cycle inhibitors for cancer therapy," *Curr Oncol*, vol. 16, pp. 36–43, Mar 2009.

[11] M. Didmon, K. Davis, P. Watson, G. Ladds, P. Broad, and J. Davey, "Identifying regulators of pheromone signalling in the fission yeast *Schizosaccharomyces pombe*," *Curr Genet*, vol. 41, pp. 241–53, Jul 2002.

[12] A. Krishnan, M. Sällman Almén, R. Fredriksson, and H. B. Schiöth, "The origin of GPCRs: identification of mammalian like Rhodopsin, Adhesion, Glutamate and Frizzled GPCRs in fungi," *PLoS ONE*, vol. 7, p. e29817, Jan 2012.

[13] J. Wess, Sung Jun Han, Soo Kyung Kim, K. A. Jacobson, and J. H. Li, "Conformational changes involved in G-protein-coupled-receptor activation," *Trends Pharmacol Sci*, vol. 29, pp. 616–25, Dec 2008.

[14] M. Conner, M. R. Hicks, T. Dafforn, T. J. Knowles, C. Ludwig, Susan Staddon, M. Overduin, U. L. Günther, J. Thome, M. Wheatley, D. R. Poyner, and A. C. Conner, "Functional and biophysical analysis of the C-terminus of the CGRP-receptor; a family B GPCR," *Biochemistry*, vol. 47, pp. 8434–44, Aug 2008.

[15] B. Chini and M. Parenti, "G-protein-coupled receptors, cholesterol and palmitoylation: facts about fats," *J Mol Endocrinol*, vol. 42, pp. 371–9, May 2009.

[16] M. Saraste, P. R. Sibbald, and A. Wittinghofer, "The P-loop–a common motif in ATP- and GTP-binding proteins," *Trends Biochem Sci*, vol. 15, pp. 430–4, Nov 1990.

[17] S. R. Sprang, "G protein mechanisms: insights from structural analysis," *Annu Rev Biochem*, vol. 66, pp. 639–78, Jan 1997.

[18] D. G. Lambright, J. P. Noel, H. E. Hamm, and P. B. Sigler, "Structural determinants for activation of the alpha-subunit of a heterotrimeric G protein," *Nature*, vol. 369, pp. 621–8, Jun 1994.

[19] J. L. Bos, H. Rehmann, and A. Wittinghofer, "GEFs and GAPs: critical elements in the control of small G proteins," *Cell*, vol. 129, pp. 865–77, Jun 2007.

[20] E. C. Stites, P. C. Trampont, Z. Ma, and K. S Ravichandran, "Network analysis of oncogenic Ras activation in cancer," *Science*, vol. 318, pp. 463–7, Oct 2007.

[21] T. Y. Shih, S Hattori, D. J. Clanton, L. S Ulsh, Z. Q. Chen, J. A. Lautenberger, and T. S Papas, "Structure and function of p21 Ras proteins," *Gene Amplif Anal*, vol. 4, pp. 53–72, Jan 1986.

[22] J. B. Gibbs and M. S Marshall, "The Ras oncogene–an important regulatory element in lower eucaryotic organisms," *Microbiol Rev*, vol. 53, pp. 171–85, Jun 1989.

[23] P. Chardin, "The Ras superfamily proteins," *Biochimie*, vol. 70, pp. 865–8, Jul 1988.

[24] A. Hall, "The cellular functions of small GTP-binding proteins," *Science*, vol. 249, pp. 635–40, Aug 1990.

[25] J. Colicelli, "Human Ras superfamily proteins and related GTPases," *Sci STKE*, vol. 2004, p. RE13, Sep 2004.

[26] K. Wennerberg, K. L. Rossman, and C. J. Der, "The Ras superfamily at a glance," *J Cell Sci*, vol. 118, pp. 843–6, Mar 2005.

[27] A. Aronheim, D. Engelberg, N. Li, N. al Alawi, J. Schlessinger, and M. Karin, "Membrane targeting of the nucleotide exchange factor Sos is sufficient for activating the Ras signaling pathway," *Cell*, vol. 78, pp. 949–61, Sep 1994.

[28] C. S Hill, J. Wynne, and R. Treisman, "The Rho family GTPases Rhoa, Rac1, and CDC42Hs regulate transcriptional activation by SRF," *Cell*, vol. 81, pp. 1159–70, Jun 1995.

[29] J. M. Lambert, Q. T. Lambert, G. W. Reuther, A. Malliri, D. P. Siderovski, J. Sondek, J. G. Collard, and C. J. Der, "Tiam1 mediates Ras activation of Rac by a PI(3)K-independent mechanism," *Nat Cell Biol*, vol. 4, pp. 621–5, Aug 2002.

[30] S. I. J. Ellenbroek and J. G. Collard, "Rho GTPases: functions and association with cancer," *Clin Exp Metastasis*, vol. 24, pp. 657–72, Jan 2007.

[31] J. R. Hepler and A. G. Gilman, "G proteins," *Trends Biochem Sci*, vol. 17, pp. 383–7, Oct 1992.

[32] J. A. Javitch, D. Fu, G. Liapakis, and J. Chen, "Constitutive activation of the beta2 adrenergic receptor alters the orientation of its sixth membrane-spanning segment," *J Biol Chem*, vol. 272, pp. 18546–9, Jul 1997.

[33] J. A. Ballesteros, A. D. Jensen, G. Liapakis, S G Rasmussen, L. Shi, U. Gether, and J. A. Javitch, "Activation of the beta 2-adrenergic receptor involves disruption of an ionic lock between the cytoplasmic ends of transmembrane segments 3 and 6," *J Biol Chem*, vol. 276, pp. 29171–7, Aug 2001.

[34] R. T. Dorsam and J. Silvio Gutkind, "G-protein-coupled receptors and cancer," *Nat Rev Cancer*, vol. 7, pp. 79–94, Feb 2007.

[35] S. R. Neves, P. T. Ram, and R. Iyengar, "G protein pathways," *Science*, vol. 296, pp. 1636–9, May 2002.

[36] R. Taussig and G. Zimmermann, "Type-specific regulation of mammalian adenylyl cyclases by G protein pathways," *Adv Second Messenger Phosphoprotein Res*, vol. 32, pp. 81–98, Jan 1998.

[37] S. Peleg, D. Varon, T. Ivanina, C. W. Dessauer, and N. Dascal, "G(alpha)(i) controls the gating of the G protein-activated K(+) channel, GIRK," *Neuron*, vol. 33, pp. 87–99, Jan 2002.

[38] N. Wettschureck and Stefan Offermanns, "Mammalian G proteins and their cell type specific functions," *Physiol Rev*, vol. 85, pp. 1159–204, Oct 2005.

[39] G. Iwami, J. Kawabe, T. Ebina, P. J. Cannon, C. J. Homcy, and Y. Ishikawa, "Regulation of adenylyl cyclase by Protein Kinase A," *J Biol Chem*, vol. 270, pp. 12481–4, May 1995.

[40] L. Birnbaumer, J. Abramowitz, and A. M. Brown, "Receptor-effector coupling by G proteins," *Biochim Biophys Acta*, vol. 1031, pp. 163–224, May 1990.

[41] M. Bronfman, M. N. Morales, and A. Orellana, "Diacylglycerol activation of Protein Kinase C is modulated by long-chain acyl-Coa," *Biochem Biophys Res Commun*, vol. 152, pp. 987–92, May 1988.

[42] D. E. Clapham and E. J. Neer, "G protein beta gamma subunits," *Annu Rev Pharmacol Toxicol*, vol. 37, pp. 167–203, Jan 1997.

[43] C. L. Huang, P. A. Slesinger, P. J. Casey, Y. N. Jan, and L. Y. Jan, "Evidence that direct binding of g beta gamma to the GIRK1 G protein-gated inwardly rectifying K+ channel is important for channel activation," *Neuron*, vol. 15, pp. 1133–43, Nov 1995.

[44] C. He, X. Yan, H. Zhang, T. Mirshahi, T. Jin, A. Huang, and D. E. Logothetis, "Identification of critical residues controlling G protein-gated inwardly rectifying K(+) channel activity through interactions with the beta gamma subunits of G proteins," *J Biol Chem*, vol. 277, pp. 6088–96, Feb 2002.

[45] K. L. Pierce, L. M. Luttrell, and R. J. Lefkowitz, "New mechanisms in heptahelical receptor signaling to mitogen activated Protein Kinase Cascades," *Oncogene*, vol. 20, pp. 1532–9, Mar 2001.

[46] O. Kranenburg and W. H. Moolenaar, "Ras-MAP kinase signaling by lysophosphatidic acid and other G protein-coupled receptor agonists," *Oncogene*, vol. 20, pp. 1540–6, Mar 2001.

[47] V. L. Lowes, N. Y. Ip, and Y. H. Wong, "Integration of signals from receptor tyrosine kinases and G protein-coupled receptors," *Neurosignals*, vol. 11, pp. 5–19, Jan 2002.

[48] Z. Naor, O. Benard, and R. Seger, "Activation of MAPK cascades by G-protein-coupled receptors: the case of gonadotropin-releasing hormone receptor," *Trends Endocrinol Metab*, vol. 11, pp. 91–9, Apr 2000.

[49] S. Tsang, A. Y.-H. Woo, W. Zhu, and R.-P. Xiao, "Deregulation of Rgs2 in cardiovascular diseases," *Front Biosci (Schol Ed)*, vol. 2, pp. 547–57, Jan 2010.

[50] J. Davey, "Fusion of a fission yeast," *Yeast*, vol. 14, pp. 1529–66, Dec 1998.

[51] R. M. Welton and C. S Hoffman, "Glucose monitoring in fission yeast via the Gpa2 Galpha, the git5 Gbeta and the git3 putative glucose receptor," *Genetics*, vol. 156, pp. 513–21, Oct 2000.

[52] F. D. Ivey and C. S Hoffman, "Direct activation of fission yeast adenylate cyclase by the Gpa2 Galpha of the glucose signaling pathway," *Proc Natl Acad Sci USA*, vol. 102, pp. 6108–13, Apr 2005.

[53] T. Maeda, N. Mochizuki, and M. Yamamoto, "Adenylyl cyclase is dispensable for vegetative cell growth in the fission yeast *Schizosaccharomyces pombe*," *Proc Natl Acad Sci USA*, vol. 87, pp. 7814–8, Oct 1990.

[54] M. Yamamoto, "Regulation of meiosis in fission yeast," *Cell Struct Funct*, vol. 21, pp. 431–6, Oct 1996.

[55] M. Nocero, T. Isshiki, M. Yamamoto, and C. S Hoffman, "Glucose repression of fbp1 transcription of *Schizosaccharomyces pombe* is partially regulated by adenylate cyclase activation by a G protein alpha subunit encoded by Gpa2 (git8)," *Genetics*, vol. 138, pp. 39–45, Sep 1994.

[56] C. S Hoffman, "Glucose sensing via the Protein Kinase A pathway in *Schizosaccharomyces pombe*," *Biochem Soc Trans*, vol. 33, pp. 257–60, Feb 2005.

[57] J. Mata and J. Bähler, "Global roles of Ste11p, cell type, and pheromone in the control of gene expression during early sexual differentiation in fission yeast," *Proc Natl Acad Sci USA*, vol. 103, pp. 15517–22, Oct 2006.

[58] O. Mondesert, C. H. McGowan, and P. Russell, "Cig2, a B-type cyclin, promotes the onset of S in *Schizosaccharomyces pombe*," *Mol Cell Biol*, vol. 16, pp. 1527–33, Apr 1996.

[59] M. Yanagida, Y. M. Yamashita, H. Tatebe, K. Ishii, K. Kumada, and Y. Nakaseko, "Control of metaphase-anaphase progression by proteolysis: cyclosome function regulated by the Protein Kinase A pathway, ubiquitination and localization," *Philos Trans R Soc Lond, B, Biol Sci*, vol. 354, pp. 1559–69; discussion 1569–70, Sep 1999.

[60] Y. M. Yamashita, Y. Nakaseko, I. Samejima, K. Kumada, H. Yamada, D. Michaelson, and M. Yanagida, "20S cyclosome complex formation and proteolytic activity inhibited by the cAMP/PKA pathway," *Nature*, vol. 384, pp. 276–9, Nov 1996.

[61] K. Kitamura and C. Shimoda, "The *Schizosaccharomyces pombe* mam2 gene encodes a putative pheromone receptor which has a significant homology with the *Saccharomyces cerevisiae* Ste2 protein," *EMBO J*, vol. 10, pp. 3743–51, Dec 1991.

[62] K. Tanaka, J. Davey, Y. Imai, and M. Yamamoto, "*Schizosaccharomyces pombe* map3+ encodes the putative M-factor receptor," *Mol Cell Biol*, vol. 13, pp. 80–8, Jan 1993.

[63] T. Obara, M. Nakafuku, M. Yamamoto, and Y. Kaziro, "Isolation and characterization of a gene encoding a G-protein alpha subunit from *Schizosaccharomyces pombe*: involvement in mating and sporulation pathways," *Proc Natl Acad Sci USA*, vol. 88, pp. 5877–81, Jul 1991.

[64] B. Stern and P. Nurse, "Cyclin B proteolysis and the cyclin-dependent kinase inhibitor rum1p are required for pheromone-induced G1 arrest in fission yeast," *Mol Biol Cell*, vol. 9, pp. 1309–21, Jun 1998.

[65] G. Ladds, M. Rasmussen, and J. Davey, "Characterisation of Sxa2, a protease involved in pheromone communication in fission yeast," *Biochem Soc Trans*, vol. 23, p. 565S, Nov 1995.

[66] G. Ladds and J. Davey, "Characterisation of Sxa2, a carboxypeptidase involved in pheromone recovery in fission yeast," *Biochem Soc Trans*, vol. 24, p. 210S, May 1996.

[67] J. Petersen, O. Nielsen, R. Egel, and I. M. Hagan, "F-actin distribution and function during sexual differentiation in *Schizosaccharomyces pombe*," *J Cell Sci*, vol. 111 (Pt 7), pp. 867–76, Apr 1998.

[68] D. A. Hughes, Y. Fukui, and M. Yamamoto, "Homologous activators of Ras in fission and budding yeast," *Nature*, vol. 344, pp. 355–7, Mar 1990.

[69] T. Toda, M. Shimanuki, and M. Yanagida, "Fission yeast genes that confer resistance to staurosporine encode an AP-1-like transcription factor and a protein kinase related to the mammalian ERK1/MAP2 and budding yeast FUS3 and KSS1 kinases," *Genes Dev*, vol. 5, pp. 60–73, Jan 1991.

[70] S. Kjaerulff, I. Lautrup-Larsen, Søren Truelsen, M. Pedersen, and O. Nielsen, "Constitutive activation of the fission yeast pheromone-responsive pathway induces ectopic meiosis and reveals ste11 as a mitogen-activated protein kinase target," *Mol Cell Biol*, vol. 25, pp. 2045–59, Mar 2005.

[71] S. Rincon, P. M. Coll, and P. Perez, "Spatial regulation of Cdc42 during cytokinesis," *Cell Cycle*, vol. 6, pp. 1687–91, Jul 2007.

[72] B. Onken, H. Wiener, M. R. Philips, and E. C. Chang, "Compartmentalized signaling of Ras in fission yeast," *Proc Natl Acad Sci USA*, vol. 103, pp. 9045–50, Jun 2006.

[73] E. C. Chang, M. Barr, Y. Wang, V. Jung, H. P. Xu, and M. H. Wigler, "Cooperative interaction of *S. pombe* proteins required for mating and morphogenesis," *Cell*, vol. 79, pp. 131–41, Oct 1994.

[74] S. Marcus, A. Polverino, E. Chang, D. Robbins, M. H. Cobb, and M. H. Wigler, "Shk1, a homolog of the *Saccharomyces cerevisiae* Ste20 and mammalian p65PAK

protein kinases, is a component of a Ras/Cdc42 signaling module in the fission yeast *Schizosaccharomyces pombe*," *Proc Natl Acad Sci USA*, vol. 92, pp. 6180–4, Jun 1995.

[75] T. Niccoli and P. Nurse, "Different mechanisms of cell polarisation in vegetative and shmooing growth in fission yeast," *J Cell Sci*, vol. 115, pp. 1651–62, Apr 2002.

[76] H. Tu, M. Barr, D. L. Dong, and M. Wigler, "Multiple regulatory domains on the Byr2 protein kinase," *Mol Cell Biol*, vol. 17, pp. 5876–87, Oct 1997.

[77] M. Toya, Y. Iino, and M. Yamamoto, "Fission yeast Pob1p, which is homologous to budding yeast Boi proteins and exhibits subcellular localization close to actin patches, is essential for cell elongation and separation," *Mol Biol Cell*, vol. 10, pp. 2745–57, Aug 1999.

[78] S. G. Martin, Sergio A Rincón, R. Basu, P. Pérez, and F. Chang, "Regulation of the formin for3p by cdc42p and bud6p," *Mol Biol Cell*, vol. 18, pp. 4155–67, Oct 2007.

[79] S. A. Rincón, Y. Ye, M. A. Villar-Tajadura, B. Santos, Sophie G Martin, and P. Pérez, "Pob1 participates in the Cdc42 regulation of fission yeast actin cytoskeleton," *Mol Biol Cell*, vol. 20, pp. 4390–9, Oct 2009.

[80] F. O. Bendezú and Sophie G Martin, "Actin cables and the exocyst form two independent morphogenesis pathways in the fission yeast," *Mol Biol Cell*, vol. 22, pp. 44–53, Jan 2011.

[81] M. Estravís, Sergio A Rincón, B. Santos, and P. Pérez, "Cdc42 regulates multiple membrane traffic events in fission yeast," *Traffic*, vol. 12, pp. 1744–58, Dec 2011.

[82] G. Ladds, A. Goddard, C. Hill, Steven Thornton, and J. Davey, "Differential effects of Rgs proteins on G alpha(q) and G alpha(11) activity," *Cell Signal*, vol. 19, pp. 103–13, Jan 2007.

[83] H. Tatebe, K. Nakano, Rachel Maximo, and K. Shiozaki, "Pom1 DYRK regulates localization of the Rga4 GAP to ensure bipolar activation of Cdc42 in fission yeast," *Curr Biol*, vol. 18, pp. 322–30, Mar 2008.

[84] F. D. Kelly and P. Nurse, "Spatial control of Cdc42 activation determines cell width in fission yeast," *Mol Biol Cell*, vol. 22, pp. 3801–11, Oct 2011.

[85] M. Das, T. Drake, D. J. Wiley, P. Buchwald, D. Vavylonis, and F. Verde, "Oscillatory dynamics of Cdc42 GTPase in the control of polarized growth," *Science*, vol. 337, pp. 239–43, Jul 2012.

[86] Y. Imai, S Miyake, D. A. Hughes, and M. Yamamoto, "Identification of a GTPase-activating protein homolog in *Schizosaccharomyces pombe*," *Mol Cell Biol*, vol. 11, pp. 3088–94, Jun 1991.

[87] P. Watson, K. Davis, M. Didmon, P. Broad, and J. Davey, "An Rgs protein regulates the pheromone response in the fission yeast *Schizosaccharomyces pombe*," *Mol Microbiol*, vol. 33, pp. 623–34, Aug 1999.

[88] L. L. Baggio and D. J. Drucker, "Biology of incretins: GLP-1 and GIP," *Gastroenterology*, vol. 132, pp. 2131–57, May 2007.

[89] T. J. Kieffer, C. H. McIntosh, and R. A. Pederson, "Degradation of glucose-dependent insulinotropic polypeptide and truncated glucagon-like peptide 1 in vitro and in vivo by dipeptidyl peptidase IV," *Endocrinology*, vol. 136, pp. 3585–96, Aug 1995.

[90] R. Mentlein, B. Gallwitz, and W. E. Schmidt, "Dipeptidyl-peptidase IV hydrolyses gastric inhibitory polypeptide, glucagon-like peptide-1(7-36)amide, peptide histidine methionine and is responsible for their degradation in human Serum," *Eur J Biochem*, vol. 214, pp. 829–35, Jun 1993.

[91] D. Yabe and Y. Seino, "Two incretin hormones glp-1 and gip: comparison of their actions in insulin secretion and cell preservation," *Prog Biophys Mol Biol*, vol. 107, pp. 248–56, Nov 2011.

[92] V. L. MacKay, S K Welch, M. Y. Insley, T. R. Manney, J. Holly, G. C. Saari, and M. L. Parker, "The *Saccharomyces cerevisiae* bar1 gene encodes an exported protein with homology to pepsin," *Proc Natl Acad Sci USA*, vol. 85, pp. 55–9, Jan 1988.

[93] C. B. Xue, E. Eriotou-Bargiota, D. Miller, J. M. Becker, and F. Naider, "A covalently constrained congener of the *Saccharomyces cerevisiae* tridecapeptide mating pheromone is an agonist," *J Biol Chem*, vol. 264, pp. 19161–8, Nov 1989.

[94] V. L. MacKay, J. Armstrong, C. Yip, S Welch, K. Walker, S Osborn, P. Sheppard, and J. Forstrom, "Characterization of the Bar proteinase, an extracellular enzyme

from the yeast *Saccharomyces cerevisiae*," *Adv Exp Med Biol*, vol. 306, pp. 161–72, Jan 1991.

[95] R. K. Chan and C. A. Otte, "Physiological characterization of *Saccharomyces cerevisiae* mutants supersensitive to G1 arrest by a factor and alpha factor pheromones," *Mol Cell Biol*, vol. 2, pp. 21–9, Jan 1982.

[96] Y. Imai and M. Yamamoto, "*Schizosaccharomyces pombe* sxa1+ and sxa2+ encode putative proteases involved in the mating response," *Mol Cell Biol*, vol. 12, pp. 1827–34, Apr 1992.

[97] J. Davey and O. Nielsen, "Mutations in cyr1 and pat1 reveal pheromone-induced G1 arrest in the fission yeast *Schizosaccharomyces pombe*," *Curr Genet*, vol. 26, pp. 105–12, Aug 1994.

[98] G. Ladds and J. Davey, "Sxa2 is a Serine carboxypeptidase that degrades extracellular P-factor in the fission yeast *Schizosaccharomyces pombe*," *Mol Microbiol*, vol. 36, pp. 377–90, Apr 2000.

[99] M. Hughes and J. Davey, "The role of Sxa1 in pheromone recovery in *Schizosaccharomyces pombe*," *Biochem Soc Trans*, vol. 25, p. 229S, May 1997.

[100] J. Davey, "Mating pheromones of the fission yeast *Schizosaccharomyces pombe*: purification and structural characterization of M-factor and isolation and analysis of two genes encoding the pheromone," *EMBO J*, vol. 11, pp. 951–60, Mar 1992.

[101] O. Nielsen, J. Davey, and R. Egel, "The Ras1 function of *Schizosaccharomyces pombe* mediates pheromone-induced transcription," *EMBO J*, vol. 11, pp. 1391–5, Apr 1992.

[102] J. Davey, P. U. Christensen, and O. Nielsen, "Identification of the transporter for the M-factor mating pheromone in fission yeast," *Biochem Soc Trans*, vol. 25, p. 224S, May 1997.

[103] F. Jean-Alphonse and A. C. Hanyaloglu, "Regulation of GPCR signal networks via membrane trafficking," *Mol Cell Endocrinol*, vol. 331, pp. 205–14, Jan 2011.

[104] C. A. C. Moore, Shawn K Milano, and J. L. Benovic, "Regulation of receptor trafficking by GRKs and arrestins," *Annu Rev Physiol*, vol. 69, pp. 451–82, Jan 2007.

[105] S. S Ferguson, "Evolving concepts in G protein-coupled receptor endocytosis: the role in receptor desensitization and signaling," *Pharmacol Rev*, vol. 53, pp. 1–24, Mar 2001.

[106] J. L. Benovic, L. J. Pike, R. A. Cerione, C. Staniszewski, T. Yoshimasa, J. Codina, M. G. Caron, and R. J. Lefkowitz, "Phosphorylation of the mammalian beta-adrenergic receptor by cyclic AMP-dependent protein kinase. regulation of the rate of receptor phosphorylation and DEPhosphorylation by agonist occupancy and effects on coupling of the receptor to the stimulatory guanine nucleotide regulatory protein," *J Biol Chem*, vol. 260, pp. 7094–101, Jun 1985.

[107] R. J. Lefkowitz, W. P. Hausdorff, and M. G. Caron, "Role of phosphorylation in desensitization of the beta-adrenoceptor," *Trends Pharmacol Sci*, vol. 11, pp. 190–4, May 1990.

[108] J. Benovic, L. Pike, and R. Cerione..., "Phosphorylation of the mammalian beta-adrenergic receptor by cyclic AMP-dependent protein kinase. regulation of the rate of receptor phosphorylation and ...," *Journal of Biological ...*, Jan 1985.

[109] H. Qian, L. Pipolo, and W. G. Thomas, "Identification of Protein Kinase C phosphorylation sites in the angiotensin ii (AT1A) receptor," *Biochem J*, vol. 343 Pt 3, pp. 637–44, Nov 1999.

[110] M. A. Price, "Cki, there's more than one: casein kinase i family members in Wnt and hedgehog signaling," *Genes Dev*, vol. 20, pp. 399–410, Feb 2006.

[111] H. R. Panek, J. D. Stepp, H. M. Engle, K. M. Marks, P. K. Tan, S K Lemmon, and L. C. Robinson, "Suppressors of yck-encoded yeast casein kinase 1 deficiency define the four subunits of a novel clathrin AP-like complex," *EMBO J*, vol. 16, pp. 4194–204, Jul 1997.

[112] L. Hicke, B. Zanolari, and H. Riezman, "Cytoplasmic tail phosphorylation of the alpha-factor receptor is required for its ubiquitination and internalization," *J Cell Biol*, vol. 141, pp. 349–58, Apr 1998.

[113] A. F. Roth and N. G. Davis, "Ubiquitination of the yeast A-factor receptor," *J Cell Biol*, vol. 134, pp. 661–74, Aug 1996.

[114] Y. Feng and N. G. Davis, "Akr1p and the type I casein kinases act prior to the ubiquitination step of yeast endocytosis: Akr1p is required for kinase localization to the plasma membrane," *Mol Cell Biol*, vol. 20, pp. 5350–9, Jul 2000.

[115] H. Ohguro, M. Rudnicka-Nawrot, J. Buczyłko, X. Zhao, J. A. Taylor, K. A. Walsh, and K. Palczewski, "Structural and enzymatic aspects of Rhodopsin phosphorylation," *J Biol Chem*, vol. 271, pp. 5215–24, Mar 1996.

[116] M. G. Waugh, R. A. Challiss, G. Berstein, S R Nahorski, and A. B. Tobin, "Agonist-induced desensitization and phosphorylation of M1-muscarinic receptors," *Biochem J*, vol. 338 (Pt 1), pp. 175–83, Feb 1999.

[117] L. Mou, A. Gates, V. A. Mosser, A. Tobin, and D. A. Jackson, "Transient hypoxia induces sequestration of M1 and M2 muscarinic acetylcholine receptors," *J Neurochem*, vol. 96, pp. 510–9, Jan 2006.

[118] A. B. Tobin, N. F. Totty, A. E. Sterlin, and S R Nahorski, "Stimulus-dependent phosphorylation of G-protein-coupled receptors by casein kinase 1alpha," *J Biol Chem*, vol. 272, pp. 20844–9, Aug 1997.

[119] D. C. Budd, J. E. McDonald, and A. B. Tobin, "Phosphorylation and regulation of a Gq/11-coupled receptor by casein kinase 1alpha," *J Biol Chem*, vol. 275, pp. 19667–75, Jun 2000.

[120] A. B. Tobin, "G-protein-coupled receptor phosphorylation: where, when and by whom," *Br J Pharmacol*, vol. 153 Suppl 1, pp. S167–76, Mar 2008.

[121] A. C. Hanyaloglu, M. Vrecl, K. M. Kroeger, L. E. Miles, H. Qian, W. G. Thomas, and K. A. Eidne, "Casein kinase II sites in the intracellular C-terminal domain of the thyrotropin-releasing hormone receptor and chimeric gonadotropin-releasing hormone receptors contribute to beta-arrestin-dependent internalization," *J Biol Chem*, vol. 276, pp. 18066–74, May 2001.

[122] I. Torrecilla, E. J. Spragg, B. Poulin, P. J. McWilliams, Sharad C Mistry, A. Blaukat, and A. B. Tobin, "Phosphorylation and regulation of a G protein-coupled receptor by Protein Kinase CK2," *J Cell Biol*, vol. 177, pp. 127–37, Apr 2007.

[123] H. Rebholz, A. Nishi, Sabine Liebscher, A. C. Nairn, M. Flajolet, and P. Greengard, "CK2 negatively regulates Galphas signaling," *Proc Natl Acad Sci USA*, vol. 106, pp. 14096–101, Aug 2009.

[124] G. Davidson, W. Wu, J. Shen, J. Bilic, U. Fenger, P. Stannek, A. Glinka, and C. Niehrs, "Casein kinase 1 gamma couples Wnt receptor activation to cytoplasmic signal transduction," *Nature*, vol. 438, pp. 867–72, Dec 2005.

[125] S. Amit, A. Hatzubai, Y. Birman, J. S Andersen, E. Ben-Shushan, M. Mann, Y. Ben-Neriah, and I. Alkalay, "Axin-mediated CKI phosphorylation of beta-catenin at Ser 45: a molecular switch for the Wnt pathway," *Genes Dev*, vol. 16, pp. 1066–76, May 2002.

[126] C. Liu, Y. Li, M. Semenov, C. Han, G. H. Baeg, Y. Tan, Z. Zhang, X. Lin, and X. He, "Control of beta-catenin phosphorylation/degradation by a dual-kinase mechanism," *Cell*, vol. 108, pp. 837–47, Mar 2002.

[127] S. ichi Yanagawa, Y. Matsuda, J.-S. Lee, H. Matsubayashi, Sonoka Sese, T. Kadowaki, and A. Ishimoto, "Casein kinase I phosphorylates the Armadillo protein and induces its degradation in Drosophila," *EMBO J*, vol. 21, pp. 1733–42, Apr 2002.

[128] N. Inestrosa and L. Varela-Nallar, "Wnt Signaling roles on the Structure and function of the central Synapses: Involvement in alzheimer's disease," *intechopen.com*, Jan 2013.

[129] V. Karoor and C. C. Malbon, "Insulin-like growth factor receptor-1 stimulates phosphorylation of the beta2-adrenergic receptor in vivo on sites distinct from those phosphorylated in response to insulin," *J Biol Chem*, vol. 271, pp. 29347–52, Nov 1996.

[130] V. Karoor, L. Wang, H. Y. Wang, and C. C. Malbon, "Insulin stimulates sequestration of beta-adrenergic receptors and enhanced association of beta-adrenergic receptors with grb2 via tyrosine 350," *J Biol Chem*, vol. 273, pp. 33035–41, Dec 1998.

[131] S. Doronin, E. Shumay, H. yu Wang, and C. C. Malbon, "Akt mediates sequestration of the beta(2)-adrenergic receptor in response to insulin," *J Biol Chem*, vol. 277, pp. 15124–31, Apr 2002.

[132] P. W. Day, P. B. Wedegaertner, and J. L. Benovic, "Analysis of G-protein-coupled receptor kinase Rgs homology domains," *Meth Enzymol*, vol. 390, pp. 295–310, Jan 2004.

[133] E. V. Gurevich, J. J. G. Tesmer, A. Mushegian, and V. V. Gurevich, "G protein-coupled receptor kinases: more than just kinases and not only for GPCRs," *Pharmacol Ther*, vol. 133, pp. 40–69, Jan 2012.

[134] K. Palczewski, J. Buczyłko, M. W. Kaplan, A. S Polans, and J. W. Crabb, "Mechanism of Rhodopsin kinase activation," *J Biol Chem*, vol. 266, pp. 12949–55, Jul 1991.

[135] C. Y. Chen, S B Dion, C. M. Kim, and J. L. Benovic, "Beta-adrenergic receptor kinase. Agonist-dependent receptor binding promotes kinase activation," *J Biol Chem*, vol. 268, pp. 7825–31, Apr 1993.

[136] S. J. Perry and R. J. Lefkowitz, "Arresting developments in heptahelical receptor signaling and regulation," *Trends Cell Biol*, vol. 12, pp. 130–8, Mar 2002.

[137] R. J. Lefkowitz and E. J. Whalen, "beta-arrestins: traffic cops of cell signaling," *Curr Opin Cell Biol*, vol. 16, pp. 162–8, Apr 2004.

[138] K. L. Pierce and R. J. Lefkowitz, "Classical and new roles of beta-arrestins in the regulation of G-protein-coupled receptors," *Nat Rev Neurosci*, vol. 2, pp. 727–33, Oct 2001.

[139] S. M. DeWire, Seungkirl Ahn, R. J. Lefkowitz, and Sudha K Shenoy, "Beta-arrestins and cell signaling," *Annu Rev Physiol*, vol. 69, pp. 483–510, Jan 2007.

[140] O. B. Goodman, J. G. Krupnick, F. Santini, V. V. Gurevich, R. B. Penn, A. W. Gagnon, J. H. Keen, and J. L. Benovic, "Beta-arrestin acts as a clathrin adaptor in endocytosis of the beta2-adrenergic receptor," *Nature*, vol. 383, pp. 447–50, Oct 1996.

[141] F. T. Lin, K. M. Krueger, H. E. Kendall, Y. Daaka, Z. L. Fredericks, J. A. Pitcher, and R. J. Lefkowitz, "Clathrin-mediated endocytosis of the beta-adrenergic receptor is regulated by phosphorylation/dephosphorylation of beta-arrestin1," *J Biol Chem*, vol. 272, pp. 31051–7, Dec 1997.

[142] S. A. Laporte, R. H. Oakley, J. Zhang, J. A. Holt, S S Ferguson, M. G. Caron, and L. S Barak, "The beta2-adrenergic receptor/betaarrestin complex recruits the clathrin

adaptor AP-2 during endocytosis," *Proc Natl Acad Sci USA*, vol. 96, pp. 3712–7, Mar 1999.

[143] T. Shiina, K. Arai, S Tanabe, N. Yoshida, T. Haga, T. Nagao, and H. Kurose, "Clathrin box in G protein-coupled receptor kinase 2," *J Biol Chem*, vol. 276, pp. 33019–26, Aug 2001.

[144] J. Allen and R. Halverson-Tamboli. . . , "Lipid raft microdomains and neurotransmitter signalling," *Nature Reviews . . .*, Jan 2006.

[145] J. L. Benovic, R. H. Strasser, M. G. Caron, and R. J. Lefkowitz, "Beta-adrenergic receptor kinase: identification of a novel protein kinase that phosphorylates the agonist-occupied form of the receptor," *Proc Natl Acad Sci USA*, vol. 83, pp. 2797–801, May 1986.

[146] M. J. Lohse, "Molecular mechanisms of membrane receptor desensitization," *Biochim Biophys Acta*, vol. 1179, pp. 171–88, Nov 1993.

[147] A. M. Zamah, M. Delahunty, L. M. Luttrell, and R. J. Lefkowitz, "Protein kinase A-mediated phosphorylation of the beta 2-adrenergic receptor regulates its coupling to Gs and Gi. demonstration in a reconstituted system," *J Biol Chem*, vol. 277, pp. 31249–56, Aug 2002.

[148] M. Nishida, M. Ogushi, R. Suda, M. Toyotaka, Shota Saiki, N. Kitajima, M. Nakaya, K.-M. Kim, T. Ide, Y. Sato, K. Inoue, and H. Kurose, "Heterologous down-regulation of angiotensin type 1 receptors by purinergic P2Y2 receptor stimulation through S-nitrosylation of NF-kappaB," *Proc Natl Acad Sci USA*, vol. 108, pp. 6662–7, Apr 2011.

[149] T. T. Chuang, L. Iacovelli, M. Sallese, and A. D. Blasi, "G protein-coupled receptors: heterologous regulation of homologous desensitization and its implications," *Trends Pharmacol Sci*, vol. 17, pp. 416–21, Nov 1996.

[150] J. Trejo and S R Coughlin, "The cytoplasmic tails of protease-activated receptor-1 and substance P receptor specify sorting to lysosomes versus recycling," *J Biol Chem*, vol. 274, pp. 2216–24, Jan 1999.

[151] T. T. Cao, H. W. Deacon, D. Reczek, A. Bretscher, and M. von Zastrow, "A kinase-regulated PDZ-domain interaction controls endocytic sorting of the beta2-adrenergic receptor," *Nature*, vol. 401, pp. 286–90, Sep 1999.

[152] G. Innamorati, H. M. Sadeghi, N. T. Tran, and M. Birnbaumer, "A Serine cluster prevents recycling of the V2 vasopressin receptor," *Proc Natl Acad Sci USA*, vol. 95, pp. 2222–6, Mar 1998.

[153] J. N. Hislop and M. V. Zastrow, "Role of ubiquitination in endocytic trafficking of G-protein-coupled receptors," *Traffic*, vol. 12, pp. 137–48, Feb 2011.

[154] K. Cadwell and L. Coscoy, "Ubiquitination on nonlysine residues by a viral E3 ubiquitin ligase," *Science*, vol. 309, pp. 127–30, Jul 2005.

[155] T. Woelk, Sara Sigismund, L. Penengo, and Simona Polo, "The ubiquitination code: a signalling problem," *Cell Div*, vol. 2, p. 11, Jan 2007.

[156] D. Mukhopadhyay and H. Riezman, "Proteasome-independent functions of ubiquitin in endocytosis and signaling," *Science*, vol. 315, pp. 201–5, Jan 2007.

[157] J. D. Schnell and L. Hicke, "Non-traditional functions of ubiquitin and ubiquitin-binding proteins," *J Biol Chem*, vol. 278, pp. 35857–60, Sep 2003.

[158] M. H. Glickman and A. Ciechanover, "The ubiquitin-proteasome proteolytic pathway: destruction for the sake of construction," *Physiol Rev*, vol. 82, pp. 373–428, Apr 2002.

[159] A. Marchese and J. L. Benovic, "Agonist-promoted ubiquitination of the G protein-coupled receptor CXCR4 mediates lysosomal sorting," *J Biol Chem*, vol. 276, pp. 45509–12, Dec 2001.

[160] C. Raiborg and H. Stenmark, "The ESCRT machinery in endosomal sorting of ubiquitylated membrane proteins," *Nature*, vol. 458, pp. 445–52, Mar 2009.

[161] N. P. Martin, R. J. Lefkowitz, and Sudha K Shenoy, "Regulation of V2 vasopressin receptor degradation by agonist-promoted ubiquitination," *J Biol Chem*, vol. 278, pp. 45954–9, Nov 2003.

[162] C. Jacob, G. S Cottrell, D. Gehringer, F. Schmidlin, E. F. Grady, and N. W. Bunnett, "c-Cbl mediates ubiquitination, degradation, and down-regulation of human protease-activated receptor 2," *J Biol Chem*, vol. 280, pp. 16076–87, Apr 2005.

[163] R. P. Kommaddi and Sudha K Shenoy, "Arrestins and protein ubiquitination," *Prog Mol Biol Transl Sci*, vol. 118, pp. 175–204, Jan 2013.

[164] D. T. Chalmers and D. P. Behan, "The use of constitutively active GPCRs in drug discovery and functional genomics," *Nat Rev Drug Discov*, vol. 1, pp. 599–608, Aug 2002.

[165] M. Scarselli and J. G. Donaldson, "Constitutive internalization of G protein-coupled receptors and G proteins via clathrin-independent endocytosis," *J Biol Chem*, vol. 284, pp. 3577–85, Feb 2009.

[166] R. Seifert, K. Wenzel-Seifert, T. W. Lee, U. Gether, E. Sanders Bush, and B. K. Kobilka, "Different effects of Gsalpha splice variants on beta2-adrenoreceptor-mediated signaling. the Beta2-adrenoreceptor coupled to the long splice variant of Gsalpha has properties of a constitutively active receptor," *J Biol Chem*, vol. 273, pp. 5109–16, May 1998.

[167] B. L. Wolfe, A. Marchese, and J. Trejo, "Ubiquitination differentially regulates clathrin-dependent internalization of protease-activated receptor-1," *J Cell Biol*, vol. 177, pp. 905–16, Jun 2007.

[168] M. Canals, D. J. Scholten, Sabrina de Munnik, M. K. L. Han, M. J. Smit, and R. Leurs, "Ubiquitination of CXCR7 controls receptor trafficking," *PLoS ONE*, vol. 7, p. e34192, Jan 2012.

[169] J. Bockaert, G. Roussignol, C. Bécamel, S Gavarini, L. Joubert, A. Dumuis, L. Fagni, and P. Marin, "GPCR-interacting proteins (gips): nature and functions," *Biochem Soc Trans*, vol. 32, pp. 851–5, Nov 2004.

[170] S. E. Craven and D. S Bredt, "PDZ proteins organize synaptic signaling pathways," *Cell*, vol. 93, pp. 495–8, May 1998.

[171] H.-C. Wong, A. Bourdelas, A. Krauss, H.-J. Lee, Y. Shao, D. Wu, M. Mlodzik, D.-L. Shi, and J. Zheng, "Direct binding of the PDZ domain of dishevelled to a conserved internal sequence in the C-terminal region of frizzled," *Mol Cell*, vol. 12, pp. 1251–60, Nov 2003.

[172] A. A. Roy, K. E. Lemberg, and P. Chidiac, "Recruitment of Rgs2 and Rgs4 to the plasma membrane by G proteins and receptors reflects functional interactions," *Mol Pharmacol*, vol. 64, pp. 587–93, Sep 2003.

[173] W. Croft, C. Hill, E. McCann, M. Bond, M. Esparza-Franco, J. Bennett, D. Rand, J. Davey, and G. Ladds, "A physiologically required g protein-coupled receptor (GPCR)-regulator of G protein Signaling (RGS) interaction that compartmentalizes Rgs activity," *J Biol Chem*, vol. 288, pp. 27327–42, Sep 2013.

[174] D. R. Ballon, P. L. Flanary, D. P. Gladue, J. B. Konopka, H. G. Dohlman, and J. Thorner, "DEP-domain-mediated regulation of GPCR signaling responses," *Cell*, vol. 126, pp. 1079–93, Sep 2006.

[175] M. Abramow-Newerly, A. A. Roy, C. Nunn, and P. Chidiac, "RGS proteins have a signalling complex: interactions between Rgs proteins and GPCRs, effectors, and auxiliary proteins," *Cell Signal*, vol. 18, pp. 579–91, May 2006.

[176] K. L. Neitzel and J. R. Hepler, "Cellular mechanisms that determine selective Rgs protein regulation of G protein-coupled receptor signaling," *Semin Cell Dev Biol*, vol. 17, pp. 383–9, Jun 2006.

[177] Z. Georgoussi, L. Leontiadis, G. Mazarakou, M. Merkouris, K. Hyde, and H. Hamm, "Selective interactions between G protein subunits and Rgs4 with the C-terminal domains of the mu- and delta-opioid receptors regulate opioid receptor signaling," *Cell Signal*, vol. 18, pp. 771–82, Jun 2006.

[178] H. Boudin, A. Doan, J. Xia, R. Shigemoto, R. L. Huganir, P. Worley, and A. M. Craig, "Presynaptic clustering of mGluR7a requires the PICK1 PDZ domain binding site," *Neuron*, vol. 28, pp. 485–97, Nov 2000.

[179] T. Seck, R. Baron, and W. C. Horne, "Binding of filamin to the C-terminal tail of the calcitonin receptor controls recycling," *J Biol Chem*, vol. 278, pp. 10408–16, Mar 2003.

[180] J. B. Konopka, D. D. Jenness, and L. H. Hartwell, "The C-terminus of the *S. cerevisiae* alpha-pheromone receptor mediates an adaptive response to pheromone," *Cell*, vol. 54, pp. 609–20, Aug 1988.

[181] T. Galvez, B. Duthey, J. Kniazeff, J. Blahos, G. Rovelli, B. Bettler, L. Prézeau, and J. P. Pin, "Allosteric interactions between GB1 and GB2 subunits are required for optimal GABA(b) receptor function," *EMBO J*, vol. 20, pp. 2152–9, May 2001.

[182] S. Grünewald, B. J. Schupp, Stephen R Ikeda, R. Kuner, F. Steigerwald, H.-C. Kornau, and G. Köhr, "Importance of the gamma-aminobutyric acid(b) receptor C-termini for G-protein coupling," *Mol Pharmacol*, vol. 61, pp. 1070–80, May 2002.

[183] A. M. Pooler, A. G. Gray, and R. A. J. McIlhinney, "Identification of a novel region of the GABA(b2) C-terminus that regulates surface expression and neuronal targeting of the GABA(b) receptor," *Eur J Neurosci*, vol. 29, pp. 869–78, Mar 2009.

[184] G. Ladds, K. Davis, A. Das, and J. Davey, "A constitutively active GPCR retains its G protein specificity and the ability to form dimers," *Mol Microbiol*, vol. 55, pp. 482–97, Jan 2005.

[185] D. D. Jenness, A. C. Burkholder, and L. H. Hartwell, "Binding of alpha-factor pheromone to *Saccharomyces cerevisiae* a cells: dissociation constant and number of binding sites," *Mol Cell Biol*, vol. 6, pp. 318–20, Jan 1986.

[186] K. A. Schandel and D. D. Jenness, "Direct evidence for ligand-induced internalization of the yeast alpha-factor pheromone receptor," *Mol Cell Biol*, vol. 14, pp. 7245–55, Nov 1994.

[187] E. M. Ross, "Coordinating speed and amplitude in G-protein signaling," *Curr Biol*, vol. 18, pp. R777–R783, Sep 2008.

[188] J. J. Tesmer, D. M. Berman, A. G. Gilman, and S R Sprang, "Structure of Rgs4 bound to alf4–activated g(i alpha1): stabilization of the transition state for GTP hydrolysis," *Cell*, vol. 89, pp. 251–61, Apr 1997.

[189] P. S Pereira and N. C. Jones, "The Rgs domain-containing fission yeast protein, Rgs1p, regulates pheromone signalling and is required for mating," *Genes Cells*, vol. 6, pp. 789–802, Sep 2001.

[190] B. Smith, C. Hill, E. L. Godfrey, D. Rand, H. van den Berg, Steven Thornton, M. Hodgkin, J. Davey, and G. Ladds, "Dual positive and negative regulation of GPCR signaling by GTP hydrolysis," *Cell Signal*, vol. 21, pp. 1151–60, Jul 2009.

[191] H. Resat, T. P. Straatsma, D. A. Dixon, and J. H. Miller, "The arginine finger of Rasgap helps Gln-61 align the nucleophilic water in GAP-stimulated hydrolysis of GTP," *Proc Natl Acad Sci USA*, vol. 98, pp. 6033–8, May 2001.

[192] D. R. Alexander, "The role of phosphatases in signal transduction," *New Biol*, vol. 2, pp. 1049–62, Dec 1990.

[193] P. Cohen, "The structure and regulation of protein phosphatases," *Annu Rev Biochem*, vol. 58, pp. 453–508, Jan 1989.

[194] Y. Yamaguchi, H. Katoh, K. Mori, and M. Negishi, "Galpha(12) and Galpha(13) interact with Ser/thr protein phosphatase type 5 and stimulate its phosphatase activity," *Curr Biol*, vol. 12, pp. 1353–8, Aug 2002.

[195] D. Zhu, K. S. Kosik, T. E. Meigs, V. Yanamadala, and B. M. Denker, "Galpha12 directly interacts with PP2A: evidence FOR Galpha12-stimulated PP2A phosphatase activity and dehosphorylation of microtubule-associated protein, tau," *J Biol Chem*, vol. 279, pp. 54983–6, Dec 2004.

[196] Z. G. Goldsmith and D. N. Dhanasekaran, "G protein regulation of MAPK networks," *Oncogene*, vol. 26, pp. 3122–42, May 2007.

[197] M. A. Rowland, W. Fontana, and E. J. Deeds, "Crosstalk and competition in signaling networks," *Biophys J*, vol. 103, pp. 2389–98, Dec 2012.

[198] J. B. Millar, V. Buck, and M. G. Wilkinson, "Pyp1 and Pyp2 PTPases DEPhosphorylate an osmosensing MAP kinase controlling cell size at division in fission yeast," *Genes Dev*, vol. 9, pp. 2117–30, Sep 1995.

[199] K. Shiozaki and P. Russell, "Counteractive roles of protein phosphatase 2c (pp2c) and a MAP kinase kinase homolog in the osmoregulation of fission yeast," *EMBO J*, vol. 14, pp. 492–502, Feb 1995.

[200] R. Sugiura, T. Toda, H. Shuntoh, M. Yanagida, and T. Kuno, "pmp1+, a suppressor of calcineurin deficiency, encodes a novel MAP kinase phosphatase in fission yeast," *EMBO J*, vol. 17, pp. 140–8, Jan 1998.

[201] T. Toda, S Dhut, G. Superti Furga, Y. Gotoh, E. Nishida, R. Sugiura, and T. Kuno, "The fission yeast pmk1+ gene encodes a novel mitogen-activated protein kinase

homolog which regulates cell integrity and functions coordinately with the Protein Kinase C pathway," *Mol Cell Biol*, vol. 16, pp. 6752–64, Dec 1996.

[202] A. S Sengar, N. A. Markley, N. J. Marini, and D. Young, "Mkh1, a MEK kinase required for cell wall integrity and proper response to osmotic and temperature stress in *Schizosaccharomyces pombe*," *Mol Cell Biol*, vol. 17, pp. 3508–19, Jul 1997.

[203] R. Sugiura, T. Toda, S Dhut, H. Shuntoh, and T. Kuno, "The MAPK kinase Pek1 acts as a phosphorylation-dependent molecular switch," *Nature*, vol. 399, pp. 479–83, Jun 1999.

[204] R. Loewith, A. Hubberstey, and D. Young, "Skh1, the mek component of the mkh1 signaling pathway in *Schizosaccharomyces pombe*," *J Cell Sci*, vol. 113 (Pt 1), pp. 153–60, Jan 2000.

[205] J. J. Linderman, "Modeling of G-protein-coupled receptor signaling pathways," *J Biol Chem*, vol. 284, pp. 5427–31, Feb 2009.

[206] T. Kenakin, "Drug efficacy at G protein-coupled receptors," *Annu Rev Pharmacol Toxicol*, vol. 42, pp. 349–79, Jan 2002.

[207] P. S H Park, D. T. Lodowski, and K. Palczewski, "Activation of G protein-coupled receptors: beyond two-state models and tertiary conformational changes," *Annu Rev Pharmacol Toxicol*, vol. 48, pp. 107–41, Jan 2008.

[208] J. M. Weiss, P. H. Morgan, M. W. Lutz, and T. P. Kenakin, "The cubic ternary complex receptor-occupancy model. III. resurrecting efficacy," *J Theor Biol*, vol. 181, pp. 381–97, Aug 1996.

[209] J. W. Black and P. Leff, "Operational models of pharmacological agonism," *Proc R Soc Lond, B, Biol Sci*, vol. 220, pp. 141–62, Dec 1983.

[210] A. Christopoulos and T. Kenakin, "G protein-coupled receptor allosterism and complexing," *Pharmacol Rev*, vol. 54, pp. 323–74, Jun 2002.

[211] J. MONOD, J. P. CHANGEUX, and F. JACOB, "Allosteric proteins and cellular control systems," *J Mol Biol*, vol. 6, pp. 306–29, Apr 1963.

[212] K. Leach, P. M. Sexton, and A. Christopoulos, "Allosteric GPCR modulators: taking advantage of permissive receptor pharmacology," *Trends Pharmacol Sci*, vol. 28, pp. 382–9, Aug 2007.

[213] N. Hao, N. Yildirim, Y. Wang, T. C. Elston, and H. G. Dohlman, "Regulators of G protein signaling and transient activation of signaling: experimental and computational analysis reveals negative and positive feedback controls on G protein activity," *J Biol Chem*, vol. 278, pp. 46506–15, Nov 2003.

[214] T.-M. Yi, H. Kitano, and M. I. Simon, "A quantitative characterization of the yeast heterotrimeric G protein cycle," *Proc Natl Acad Sci USA*, vol. 100, pp. 10764–9, Sep 2003.

[215] B. Kofahl and E. Klipp, "Modelling the dynamics of the yeast pheromone pathway," *Yeast*, vol. 21, pp. 831–50, Jul 2004.

[216] J. Schaber, B. Kofahl, A. Kowald, and E. Klipp, "A modelling approach to quantify dynamic crosstalk between the pheromone and the starvation pathway in baker's yeast," *FEBS J*, vol. 273, pp. 3520–33, Aug 2006.

[217] A. J. Klar and L. M. Miglio, "Initiation of meiotic recombination by double-strand DNA breaks in *S. pombe*," *Cell*, vol. 46, pp. 725–31, Aug 1986.

[218] G. Ladds, E. M. Rasmussen, T. Young, O. Nielsen, and J. Davey, "The sxa2-dependent inactivation of the P-factor mating pheromone in the fission yeast *Schizosaccharomyces pombe*," *Mol Microbiol*, vol. 20, pp. 35–42, Apr 1996.

[219] J. L. Brown, M. Jaquenoud, M. P. Gulli, J. Chant, and M. Peter, "Novel Cdc42-binding proteins Gic1 and Gic2 control cell polarity in yeast," *Genes Dev*, vol. 11, pp. 2972–82, Nov 1997.

[220] R. Egel, M. Willer, S Kjaerulff, J. Davey, and O. Nielsen, "Assessment of pheromone production and response in fission yeast by a halo test of induced sporulation," *Yeast*, vol. 10, pp. 1347–54, Oct 1994.

[221] M. Mos, M. A. Esparza-Franco, E. L. Godfrey, K. Richardson, J. Davey, and G. Ladds, "The role of the Rack1 ortholog cpc2p in modulating pheromone-induced cell cycle arrest in fission yeast," *PLoS ONE*, vol. 8, p. e65927, Jan 2013.

[222] G. Ladds and J. Davey, "Analysis of human GPCRs in fission yeast," *Curr Opin Drug Discov Devel*, vol. 7, pp. 683–91, Sep 2004.

[223] C. Weston, M. Bond, W. Croft, and G. Ladds, "The coordination of cell growth during fission yeast mating requires Ras1-GTP hydrolysis," *PLoS ONE*, vol. 8, p. e77487, Jan 2013.

[224] J. Sambrook, E. Fritsch, and T. Maniatis, "Molecular cloning: A laboratory manual," *NY: Cold Spring Harbour Labortary Press*, vol. 2nd Edition, 1989.

[225] K. Okazaki, N. Okazaki, K. Kume, S Jinno, K. Tanaka, and H. Okayama, "High-frequency transformation method and library transducing vectors for cloning mammalian cDNAs by trans-complementation of *Schizosaccharomyces pombe*," *Nucleic Acids Res*, vol. 18, pp. 6485–9, Nov 1990.

[226] C. S Hoffman and F. Winston, "A ten-minute DNA preparation from yeast efficiently releases autonomous plasmids for transformation of escherichia coli," *Gene*, vol. 57, pp. 267–72, Jan 1987.

[227] H. G. Dohlman, D. Apaniesk, Y. Chen, J. Song, and D. Nusskern, "Inhibition of G-protein signaling by dominant gain-of-function mutations in Sst2p, a pheromone desensitization factor in *Saccharomyces cerevisiae*," *Mol Cell Biol*, vol. 15, pp. 3635–43, Jul 1995.

[228] M. Bond, W. Croft, R. Tyson, T. Bretschneider, J. Davey, and G. Ladds, "Quantitative analysis of human Ras localization and function in the fission yeast *Schizosaccharomyces pombe*," *Yeast*, vol. 30, pp. 145–56, Apr 2013.

[229] S. Sazer and S W Sherwood, "Mitochondrial growth and DNA synthesis occur in the absence of nuclear DNA replication in fission yeast," *J Cell Sci*, vol. 97 (Pt 3), pp. 509–16, Nov 1990.

[230] T. Zhang and H. H. P. Fang, "Quantification of *Saccharomyces cerevisiae* viability using BacLight," *Biotechnol Lett*, vol. 26, pp. 989–92, Jun 2004.

[231] D. Dormann, T. Libotte, C. J. Weijer, and T. Bretschneider, "Simultaneous quantification of cell motility and protein-membrane-association using active contours," *Cell Motil Cytoskeleton*, vol. 52, pp. 221–30, Aug 2002.

[232] L. Bosgraaf, P. J. M. van Haastert, and T. Bretschneider, "Analysis of cell movement by simultaneous quantification of local membrane displacement and fluorescent intensities using quimp2," *Cell Motil Cytoskeleton*, vol. 66, pp. 156–65, Mar 2009.

[233] R. Tyson, D. Epstein, and K. Anderson. . . , "High resolution tracking of cell membrane dynamics in moving cells: an electrifying approach," *Math Model Nat . . .*, Jan 2010.

[234] L. Bosgraaf and P. V. Haastert, "Quimp3, an automated pseudopod-tracking algorithm," *Cell adhesion & migration*, Jan 2010.

[235] K. Maundrell, "Thiamine-repressible expression vectors pREP and pRIP for fission yeast," *Gene*, vol. 123, pp. 127–30, Jan 1993.

[236] Y. Kikuchi, Y. Kitazawa, H. Shimatake, and M. Yamamoto, "The primary structure of the leu1+ gene of *Schizosaccharomyces pombe*," *Curr Genet*, vol. 14, pp. 375–9, Oct 1988.

[237] S. L. Forsburg, "Comparison of *Schizosaccharomyces pombe* expression systems," *Nucleic Acids Res*, vol. 21, pp. 2955–6, Jun 1993.

[238] C. Grimm, J. Kohli, J. Murray, and K. Maundrell, "Genetic engineering of *Schizosaccharomyces pombe*: a system for gene disruption and replacement using the ura4 gene as a selectable marker," *Mol Gen Genet*, vol. 215, pp. 81–6, Dec 1988.

[239] C. Bai and S J Elledge, "Gene identification using the yeast two-hybrid system," *Meth Enzymol*, vol. 273, pp. 331–47, Jan 1996.

[240] H. Zhong, Susan M Wade, P. J. Woolf, J. J. Linderman, J. R. Traynor, and R. R. Neubig, "A spatial focusing model for G protein signals. regulator of G protein signaling (rgs) protien-mediated kinetic scaffolding," *J Biol Chem*, vol. 278, pp. 7278–84, Feb 2003.

[241] N. Yildirim, N. Hao, H. G. Dohlman, and T. C. Elston, "Mathematical modeling of Rgs and G-protein regulation in yeast," *Meth Enzymol*, vol. 389, pp. 383–98, Jan 2004.

[242] S. J. Bornheimer, M. R. Maurya, M. G. Farquhar, and Shankar Subramaniam, "Computational modeling reveals how interplay between components of a GTPase-cycle module regulates signal transduction," *Proc Natl Acad Sci USA*, vol. 101, pp. 15899–904, Nov 2004.

[243] I. Tratner, A. Fourticq-Esqueöute, J. Tillit, and G. Baldacci, "Cloning and characterization of the *S. pombe* gene efc25+, a new putative guanine nucleotide exchange factor," *Gene*, vol. 193, pp. 203–10, Jul 1997.

[244] P. Papadaki, V. Pizon, B. Onken, and E. C. Chang, "Two Ras pathways in fission yeast are differentially regulated by two Ras guanine nucleotide exchange factors," *Mol Cell Biol*, vol. 22, pp. 4598–606, Jul 2002.

[245] J. W. Erickson and R. A. Cerione, "Structural elements, mechanism, and evolutionary convergence of Rho protein-guanine nucleotide exchange factor complexes," *Biochemistry*, vol. 43, pp. 837–42, Feb 2004.

[246] Y. Fukui, Y. Kaziro, and M. Yamamoto, "Mating pheromone-like diffusible factor released by *Schizosaccharomyces pombe*," *EMBO J*, vol. 5, pp. 1991–3, Aug 1986.

[247] K. Scheffzek, A. Lautwein, W. Kabsch, M. R. Ahmadian, and A. Wittinghofer, "Crystal structure of the GTPase-activating domain of human p120GAP and implications for the interaction with Ras," *Nature*, vol. 384, pp. 591–6, Dec 1996.

[248] P. Gideon, J. John, M. Frech, A. Lautwein, R. Clark, J. E. Scheffler, and A. Wittinghofer, "Mutational and kinetic analyses of the GTPase-activating protein (gap)-p21 interaction: the C-terminal domain of GAP is not sufficient for full activity," *Mol Cell Biol*, vol. 12, pp. 2050–6, May 1992.

[249] P. J. Miller and D. I. Johnson, "Cdc42p GTPase is involved in controlling polarized cell growth in *Schizosaccharomyces pombe*," *Mol Cell Biol*, vol. 14, pp. 1075–83, Feb 1994.

[250] K. Nakano, T. Mutoh, and I. Mabuchi, "Characterization of GTPaseactivating proteins for the function of the Rhofamily small GTPases in the fission yeast *Schizosaccharomyces pombe*," *Genes to Cells*, Jan 2001.

[251] T. Masuda, K. Kariya, M. Shinkai, T. Okada, and T. Kataoka, "Protein kinase byr2 is a target of Ras1 in the fission yeast *Schizosaccharomyces pombe*," *J Biol Chem*, vol. 270, pp. 1979–82, Feb 1995.

[252] P. Bauman, Q. C. Cheng, and C. F. Albright, "The Byr2 kinase translocates to the plasma membrane in a Ras1-dependent manner," *Biochem Biophys Res Commun*, vol. 244, pp. 468–74, Mar 1998.

[253] R. Seger and E. G. Krebs, "The MAPK signaling cascade," *FASEB J*, vol. 9, pp. 726–35, Jun 1995.

[254] P. Bauman and C. F. Albright, "Functional analysis of domains in the Byr2 kinase," *Biochimie*, vol. 80, pp. 621–5, Jul 1998.

[255] Y. Wang, H. P. Xu, M. Riggs, L. Rodgers, and M. Wigler, "*byr2*, a *Schizosaccharomyces pombe* gene encoding a Protein Kinase Capable of partial suppression of the Ras1 mutant phenotype," *Mol Cell Biol*, vol. 11, pp. 3554–63, Jul 1991.

[256] Y. Gotoh, E. Nishida, M. Shimanuki, T. Toda, Y. Imai, and M. Yamamoto, "*Schizosaccharomyces pombe* Spk1 is a tyrosine-phosphorylated protein functionally related to xenopus mitogen-activated protein kinase," *Mol Cell Biol*, vol. 13, pp. 6427–34, Oct 1993.

[257] S. A. Nadin-Davis and A. Nasim, "*Schizosaccharomyces pombe* Ras1 and byr1 are functionally related genes of the ste family that affect starvation-induced transcription of mating-type genes," *Mol Cell Biol*, vol. 10, pp. 549–60, Feb 1990.

[258] S. A. Nadin-Davis and A. Nasim, "A gene which encodes a predicted Protein Kinase Can restore some functions of the Ras gene in fission yeast," *EMBO J*, vol. 7, pp. 985–93, Apr 1988.

[259] A. M. Neiman, B. J. Stevenson, H. P. Xu, G. F. Sprague, I. Herskowitz, M. Wigler, and S Marcus, "Functional homology of protein kinases required for sexual differentiation in *Schizosaccharomyces pombe* and *Saccharomyces cerevisiae* suggests a conserved signal transduction module in eukaryotic organisms," *Mol Biol Cell*, vol. 4, pp. 107–20, Jan 1993.

[260] K. Y. Choi, B. Satterberg, D. M. Lyons, and E. A. Elion, "Ste5 tethers multiple protein kinases in the MAP kinase cascade required for mating in S. cerevisiae," *Cell*, vol. 78, pp. 499–512, Aug 1994.

[261] M. Good, G. Tang, J. Singleton, A. Reményi, and W. A. Lim, "The Ste5 scaffold directs mating signaling by catalytically unlocking the Fus3 MAP kinase for activation," *Cell*, vol. 136, pp. 1085–97, Mar 2009.

[262] L. J. Flatauer, Sheena F Zadeh, and L. Bardwell, "Mitogen-activated protein kinases with distinct requirements for Ste5 scaffolding influence signaling specificity in *Saccharomyces cerevisiae*," *Mol Cell Biol*, vol. 25, pp. 1793–803, Mar 2005.

[263] J. G. Zalatan, Scott M Coyle, Saravanan Rajan, Sachdev S Sidhu, and W. A. Lim, "Conformational control of the Ste5 scaffold protein insulates against MAP kinase misactivation," *Science*, vol. 337, pp. 1218–22, Sep 2012.

[264] M. A. Schwartz and H. D. Madhani, "Principles of MAP kinase signaling specificity in *Saccharomyces cerevisiae*," *Annu Rev Genet*, vol. 38, pp. 725–48, Jan 2004.

[265] H. G. Dohlman, "G proteins and pheromone signaling," *Annu Rev Physiol*, vol. 64, pp. 129–52, Jan 2002.

[266] S. A. Chasse, P. Flanary, Stephen C Parnell, N. Hao, J. Y. Cha, D. P. Siderovski, and H. G. Dohlman, "Genome-scale analysis reveals Sst2 as the principal regulator of mating pheromone signaling in the yeast *Saccharomyces cerevisiae*," *Eukaryotic Cell*, vol. 5, pp. 330–46, Feb 2006.

[267] G. Ladds and J. Davey, "Sxa2, a carboxypeptidase that degrades extracellular pheromone in fission yeast," *Biochem Soc Trans*, vol. 25, p. 228S, May 1997.

[268] F. Corpet, "Multiple sequence alignment with hierarchical clustering," *Nucleic Acids Res*, vol. 16, pp. 10881–90, Nov 1988.

[269] J. Terrell, S Shih, R. Dunn, and L. Hicke, "A function for monoubiquitination in the internalization of a G protein-coupled receptor," *Mol Cell*, vol. 1, pp. 193–202, Jan 1998.

[270] J. Y. Toshima, J. ichi Nakanishi, K. Mizuno, J. Toshima, and D. G. Drubin, "Requirements for recruitment of a G protein-coupled receptor to clathrin-coated pits in budding yeast," *Mol Biol Cell*, vol. 20, pp. 5039–50, Dec 2009.

[271] V. Wood, M. A. Harris, M. D. McDowall, K. Rutherford, B. W. Vaughan, D. M. Staines, M. Aslett, A. Lock, J. Bähler, P. J. Kersey, and Stephen G Oliver, "PomBase: a comprehensive online resource for fission yeast," *Nucleic Acids Res*, vol. 40, pp. D695–9, Jan 2012.

[272] P. C. Wang, A. Vancura, A. Desai, G. Carmel, and J. Kuret, "Cytoplasmic forms of fission yeast casein kinase-1 associate primarily with the particulate fraction of the cell," *J Biol Chem*, vol. 269, pp. 12014–23, Apr 1994.

[273] K. Kitamura and I. Yamashita, "Identification of a novel casein kinase-1 homolog in fission yeast *Schizosaccharomyces pombe*," *Gene*, vol. 214, pp. 131–7, Jul 1998.

[274] J. C. G. Cortés, M. Konomi, I. M. Martins, J. Muñoz, M. B. Moreno, M. Osumi, A. Durán, and J. C. Ribas, "The (1,3)beta-D-glucan synthase subunit Bgs1p is responsible for the fission yeast primary septum formation," *Mol Microbiol*, vol. 65, pp. 201–17, Jul 2007.

[275] S. hei Yoshida, H. Al-Amodi, T. Nakamura, C. J. McInerny, and C. Shimoda, "The *Schizosaccharomyces pombe* cdt2(+) gene, a target of G1-s phase-specific transcription factor complex DSC1, is required for mitotic and premeiotic DNA replication," *Genetics*, vol. 164, pp. 881–93, Jul 2003.

[276] R. S Kao, E. Morreale, L. Wang, F. D. Ivey, and C. S Hoffman, "*Schizosaccharomyces pombe* Git1 is a C2-domain protein required for glucose activation of adenylate cyclase," *Genetics*, vol. 173, pp. 49–61, May 2006.

[277] K. Tanaka and A. Hirata, "Ascospore development in the fission yeasts *Schizosaccharomyces pombe* and *S. japonicus*," *J Cell Sci*, vol. 56, pp. 263–79, Aug 1982.

[278] M. Onishi, Y. Nakamura, T. Koga, K. Takegawa, and Y. Fukui, "Isolation of suppressor mutants of phosphatidylinositol 3-phosphate 5-kinase deficient cells in *Schizosaccharomyces pombe*," *Biosci Biotechnol Biochem*, vol. 67, pp. 1772–9, Aug 2003.

[279] Y. Imai and M. Yamamoto, "The fission yeast mating pheromone P-factor: its molecular structure, gene structure, and ability to induce gene expression and G1 arrest in the mating partner," *Genes Dev*, vol. 8, pp. 328–38, Feb 1994.

[280] S. Fields and O. Song, "A novel genetic system to detect protein-protein interactions," *Nature*, vol. 340, pp. 245–6, Jul 1989.

[281] G. G. Toby and E. A. Golemis, "Using the yeast interaction trap and other two-hybrid-based approaches to study protein-protein interactions," *Methods*, vol. 24, pp. 201–17, Jul 2001.

[282] K. Hirota, K. Tanaka, Y. Watanabe, and M. Yamamoto, "Functional analysis of the C-terminal cytoplasmic region of the M-factor receptor in fission yeast," *Genes Cells*, vol. 6, pp. 201–14, Mar 2001.

[283] T. A. Vida and S D Emr, "A new vital stain for visualizing vacuolar membrane dynamics and endocytosis in yeast," *J Cell Biol*, vol. 128, pp. 779–92, Mar 1995.

[284] L. Hicke and H. Riezman, "Ubiquitination of a yeast plasma membrane receptor signals its ligand-stimulated endocytosis," *Cell*, vol. 84, pp. 277–87, Jan 1996.

[285] A. C. Hanyaloglu, E. McCullagh, and M. V. Zastrow, "Essential role of Hrs in a recycling mechanism mediating functional resensitization of cell signaling," *EMBO J*, vol. 24, pp. 2265–83, Jul 2005.

[286] S. K. Shenoy, P. H. McDonald, T. A. Kohout, and R. J. Lefkowitz, "Regulation of receptor fate by ubiquitination of activated beta 2-adrenergic receptor and beta-arrestin," *Science*, vol. 294, pp. 1307–13, Nov 2001.

[287] M. Tanowitz and M. V. Zastrow, "Ubiquitination-independent trafficking of G protein-coupled receptors to lysosomes," *J Biol Chem*, vol. 277, pp. 50219–22, Dec 2002.

[288] G. S Cottrell, B. Padilla, Stella Pikios, D. Roosterman, M. Steinhoff, D. Gehringer, E. F. Grady, and N. W. Bunnett, "Ubiquitin-dependent down-regulation of the neurokinin-1 receptor," *J Biol Chem*, vol. 281, pp. 27773–83, Sep 2006.

[289] L. Chen and N. G. Davis, "Ubiquitin-independent entry into the yeast recycling pathway," *Traffic*, vol. 3, pp. 110–23, Feb 2002.

[290] F. O. Bendezú and Sophie G Martin, "Cdc42 explores the cell periphery for mate selection in fission yeast," *Curr Biol*, vol. 23, pp. 42–7, Jan 2013.

[291] W. Croft, C. Elliott, G. Ladds, and B. Stinner. . . , "Parameter identification problems in the modelling of cell motility," *arXiv preprint arXiv: . . .*, Jan 2013.

[292] J. M. Mitchison and P. Nurse, "Growth in cell length in the fission yeast *Schizosaccharomyces pombe*," *J Cell Sci*, vol. 75, pp. 357–76, Apr 1985.

[293] A. DuPen, D. Shen, and M. Ersek, "Mechanisms of opioid-induced tolerance and hyperalgesia," *Pain Manag Nurs*, vol. 8, pp. 113–21, Sep 2007.

[294] R. Egel and M. Egel-Mitani, "Premeiotic dna synthesis in fission yeast," *Exp Cell Res*, vol. 88, pp. 127–34, Sep 1974.

[295] S. Marguerat, A. Schmidt, Sandra Codlin, W. Chen, R. Aebersold, and J. Bähler, "Quantitative analysis of fission yeast transcriptomes and proteomes in proliferating and quiescent cells," *Cell*, vol. 151, pp. 671–83, Oct 2012.

[296] I. Vancurova, J. H. Choi, H. Lin, J. Kuret, and A. Vancura, "Regulation of phosphatidylinositol 4-phosphate 5-kinase from *Schizosaccharomyces pombe* by casein kinase i," *J Biol Chem*, vol. 274, pp. 1147–55, Jan 1999.

[297] T. Terui, R. A. Kahn, and P. A. Randazzo, "Effects of acid phospholipids on nucleotide exchange properties of ADP-ribosylation factor 1. evidence for specific interaction with phosphatidylinositol 4,5-bisphosphate," *J Biol Chem*, vol. 269, pp. 28130–5, Nov 1994.

[298] K. Zhou, K. Takegawa, S D Emr, and R. A. Firtel, "A phosphatidylinositol (PI) kinase gene family in Dictyostelium discoideum: biological roles of putative mammalian p110 and yeast Vps34p PI 3-kinase homologs during growth and development," *Mol Cell Biol*, vol. 15, pp. 5645–56, Oct 1995.

[299] X. Zhang, K. Orlando, B. He, F. Xi, J. Zhang, A. Zajac, and W. Guo, "Membrane association and functional regulation of Sec3 by phospholipids and Cdc42," *J Cell Biol*, vol. 180, pp. 145–58, Jan 2008.

[300] F. O. Bendezú, V. Vincenzetti, and Sophie G Martin, "Fission yeast Sec3 and Exo70 are transported on actin cables and localize the exocyst complex to cell poles," *PLoS ONE*, vol. 7, p. e40248, Jan 2012.

[301] N. A. St Denis and D. W. Litchfield, "Protein kinase CK2 in health and disease: From birth to death: the role of Protein Kinase Ck2 in the regulation of cell proliferation and survival," *Cell Mol Life Sci*, vol. 66, pp. 1817–29, Jun 2009.

[302] S. G. Martin and M. Berthelot-Grosjean, "Polar gradients of the DYRK-family kinase pom1 couple cell length with the cell cycle," *Nature*, vol. 459, pp. 852–6, Jun 2009.

[303] P. A. Lochhead, G. Sibbet, N. Morrice, and V. Cleghon, "Activation-loop autophosphorylation is mediated by a novel transitional intermediate form of DYRKs," *Cell*, vol. 121, pp. 925–36, Jun 2005.

[304] J. B. Moseley, A. Mayeux, A. Paoletti, and P. Nurse, "A spatial gradient coordinates cell size and mitotic entry in fission yeast," *Nature*, vol. 459, pp. 857–60, Jun 2009.

[305] J. M. Glynn, R. J. Lustig, A. Berlin, and F. Chang, "Role of bud6p and tea1p in the interaction between actin and microtubules for the establishment of cell polarity in fission yeast," *Curr Biol*, vol. 11, pp. 836–45, Jun 2001.

[306] S. G. Martin, W. H. McDonald, J. R. Yates, and F. Chang, "Tea4p links microtubule plus ends with the formin for3p in the establishment of cell polarity," *Dev Cell*, vol. 8, pp. 479–91, Apr 2005.

[307] T. Niccoli, M. Arellano, and P. Nurse, "Role of Tea1p, Tea3p and Pom1p in the determination of cell ends in *Schizosaccharomyces pombe*," *Yeast*, vol. 20, pp. 1349–58, Dec 2003.

[308] I. Alvarez-Tabarés, A. Grallert, J.-M. Ortiz, and I. M. Hagan, "*Schizosaccharomyces pombe* protein phosphatase 1 in mitosis, endocytosis and a partnership with Wsh3/Tea4 to control polarised growth," *J Cell Sci*, vol. 120, pp. 3589–601, Oct 2007.

[309] O. Hachet, M. Berthelot-Grosjean, K. Kokkoris, V. Vincenzetti, J. Moosbrugger, and Sophie G Martin, "A phosphorylation cycle shapes gradients of the DYRK family kinase Pom1 at the plasma membrane," *Cell*, vol. 145, pp. 1116–28, Jun 2011.

[310] H. Yamano, K. Ishii, and M. Yanagida, "Phosphorylation of dis2 protein phosphatase at the C-terminal cdc2 consensus and its potential role in cell cycle regulation," *EMBO J*, vol. 13, pp. 5310–8, Nov 1994.

[311] T. Obara-Ishihara and H. Okayama, "AB-type cyclin negatively regulates conjugation via interacting with cell cycle 'start' genes in fission yeast," *EMBO J*, vol. 13, pp. 1863–72, Apr 1994.

[312] C. Martin-Castellanos, K. Labib, and S Moreno, "B-type cyclins regulate G1 progression in fission yeast in opposition to the p25rum1 cdk inhibitor," *EMBO J*, vol. 15, pp. 839–49, Feb 1996.

[313] M. McLeod, B. Shor, A. Caporaso, W. Wang, H. Chen, and L. Hu, "Cpc2, a fission yeast homologue of mammalian Rack1 protein, interacts with ran1 (pat1) kinase to regulate cell cycle progression and meiotic development," *Mol Cell Biol*, vol. 20, pp. 4016–27, Jun 2000.

[314] L. C. Robinson, E. J. Hubbard, P. R. Graves, A. A. DEPaoli Roach, P. J. Roach, C. Kung, D. W. Haas, C. H. Hagedorn, M. Goebl, and M. R. Culbertson, "Yeast casein kinase I homologues: an essential gene pair," *Proc Natl Acad Sci USA*, vol. 89, pp. 28–32, Jan 1992.

[315] L. C. Robinson, M. M. Menold, S Garrett, and M. R. Culbertson, "Casein kinase I-like protein kinases encoded by YCK1 and YCK2 are required for yeast morphogenesis," *Mol Cell Biol*, vol. 13, pp. 2870–81, May 1993.

[316] L. C. Robinson, C. Bradley, J. D. Bryan, A. Jerome, Y. Kweon, and H. R. Panek, "The Yck2 yeast casein kinase 1 isoform shows cell cycle-specific localization to sites of polarized growth and is required for proper septin organization," *Mol Biol Cell*, vol. 10, pp. 1077–92, Apr 1999.

[317] M. S Longtine, D. J. DeMarini, M. L. Valencik, O. S Al-Awar, H. Fares, C. D. Virgilio, and J. R. Pringle, "The septins: roles in cytokinesis and other processes," *Curr Opin Cell Biol*, vol. 8, pp. 106–19, Feb 1996.

[318] M. Kinoshita, "Diversity of septin scaffolds," *Curr Opin Cell Biol*, vol. 18, pp. 54–60, Feb 2006.

[319] Y. Oh and E. Bi, "Septin structure and function in yeast and beyond," *Trends Cell Biol*, vol. 21, pp. 141–8, Mar 2011.

[320] A. Berlin, A. Paoletti, and F. Chang, "Mid2p stabilizes septin rings during cytokinesis in fission yeast," *J Cell Biol*, vol. 160, pp. 1083–92, Mar 2003.

[321] H. Wang, X. Tang, J. Liu, Susanne Trautmann, D. Balasundaram, D. McCollum, and M. K. Balasubramanian, "The multiprotein exocyst complex is essential for cell separation in *Schizosaccharomyces pombe*," *Mol Biol Cell*, vol. 13, pp. 515–29, Feb 2002.

[322] A. B. Martín-Cuadrado, J. L. Morrell, M. Konomi, H. An, C. Petit, M. Osumi, M. Balasubramanian, K. L. Gould, F. D. Rey, and C. R. V. de Aldana, "Role of septins and the exocyst complex in the function of hydrolytic enzymes responsible for fission yeast cell separation," *Mol Biol Cell*, vol. 16, pp. 4867–81, Oct 2005.

[323] M. Sipiczki, "Splitting of the fission yeast septum," *FEMS Yeast Res*, vol. 7, pp. 761–70, Sep 2007.

[324] J. J. Tasto, J. L. Morrell, and K. L. Gould, "An anillin homologue, Mid2p, acts during fission yeast cytokinesis to organize the septin ring and promote cell separation," *J Cell Biol*, vol. 160, pp. 1093–103, Mar 2003.

[325] H. An, J. L. Morrell, J. L. Jennings, A. J. Link, and K. L. Gould, "Requirements of fission yeast septins for complex formation, localization, and function," *Mol Biol Cell*, vol. 15, pp. 5551–64, Dec 2004.

[326] M. S Longtine, H. Fares, and J. R. Pringle, "Role of the yeast Gin4p protein kinase in septin assembly and the relationship between septin assembly and septin function," *J Cell Biol*, vol. 143, pp. 719–36, Nov 1998.

[327] M. Schmidt, A. Varma, T. Drgon, B. Bowers, and E. Cabib, "Septins, under cla4p regulation, and the chitin ring are required for neck integrity in budding yeast," *Mol Biol Cell*, vol. 14, pp. 2128–41, May 2003.

[328] M. Versele and J. Thorner, "Septin collar formation in budding yeast requires GTP binding and direct phosphorylation by the PAK, Cla4," *J Cell Biol*, vol. 164, pp. 701–15, Mar 2004.

[329] J. L. Morrell, C. B. Nichols, and K. L. Gould, "The GIN4 family kinase, Cdr2p, acts independently of septins in fission yeast," *J Cell Sci*, vol. 117, pp. 5293–302, Oct 2004.

[330] P. M. Coll, Y. Trillo, A. Ametzazurra, and P. Perez, "Gef1p, a new guanine nucleotide exchange factor for Cdc42p, regulates polarity in *Schizosaccharomyces pombe*," *Mol Biol Cell*, vol. 14, pp. 313–23, Jan 2003.

[331] P. Perez and Sergio A Rincón, "Rho GTPases: regulation of cell polarity and growth in yeasts," *Biochem J*, vol. 426, pp. 243–53, Mar 2010.